Durham E-Theses

Determination of aquifer properties from tidal influences on pore pressures

Carrington, Rachel Elizabeth

Determination of Aquifer Properties from Tidal Influences on Pore Pressures

Rachel Elizabeth Carrington

Abstract

This project involved investigation of the tidal analysis technique, defined by Ferris (1951), for determining the aquifer properties of permeability, storage and leakage. The approach included laboratory experimental work using a physical model of a semi-confined aquifer. In addition, field work was undertaken to record groundwater levels in a coastal aquifer.

The laboratory work concluded with results of amplitude decay and time lag. Numerical analysis illustrated the significant effects of reflection and leakage on the results of amplitude decay and time lag. Therefore, Ferris' theory was advanced to incorporate both reflection from an impermeable boundary and leakage. This theory was applied to the laboratory results, to conclude an estimate for the coefficient of permeability of 8×10^{-3} m/s. In addition, a range of values for the leakage coefficient were evaluated: 0 to 4×10^{-5} s^{-1}. These values compared well with earlier work using the Durham Model Aquifer where similar results were obtained.

Ferris' theory was applied to the field data for instances where tidal influence on groundwater behaviour was observed. Estimates for aquifer properties based on the tidal technique compared well with those based on soil grading methods.

The analytical theory, developed within this programme of work, incorporated three unknown parameters, transmissivity, storage and leakage. The value of one of these parameters must be assumed in order to then compute estimates for the remaining two aquifer properties. When a semi-confined aquifer is under investigation, application of this theory provides increased accuracy for the estimates of aquifer properties when compared with results based on Ferris' equations.

Tidal analysis incorporates the heterogeneity of the aquifer over a wider area than alternative methods available for determining aquifer properties. The method may be used to supplement and verify estimates of aquifer properties derived from alternative techniques.

Determination of Aquifer Properties from Tidal Influences on Pore Pressures

Rachel Elizabeth Carrington
BSc (Hons) Dunelm
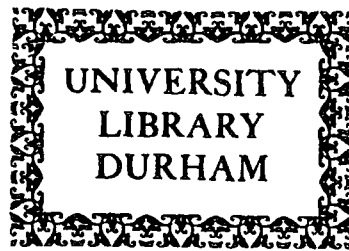
Thesis submitted for Degree of
Master of Science

School of Engineering
University of Durham

October 1995

Table of Contents

Table of Figures

Table of Tables

Declaration of Original Work

I confirm that, unless otherwise stated, no part of the material offered has previously been submitted by me for a degree in this or in any other University.

Copyright

Acknowledgements

Nomenclature

Symbol	Parameter	Dimensions
K	Coefficient of Permeability	$[LT^{-1}]$
T	Transmissibility/Transmissivity	$[LT^{-2}]$
S	Storage Coefficient	[non-dimensional]
S_s	Specific Storage	$[L^{-1}]$
S_Y	Specific Yield	[non-dimensional]
β	Coefficient of Leakage	$[T^{-1}]$
σ'	Effective Stress	$[ML^{-1}T^{-2}]$
σ	Total Stress	$[ML^{-1}T^{-2}]$
u_w	Pore Water Pressure	$[ML^{-1}T^{-2}]$
W	Darcy Velocity	$[LT^{-1}]$
i	Hydraulic Gradient	[non-dimensional]
b	Thickness of Aquifer	[L]
K'	Coefficient of Permeability of Confining Layer/Aquitard	$[LT^{-1}]$
b'	Thickness of Aquitard	[L]
h	Rise or Fall of Peizometric Level with Reference to Mean	[L]
h*	Fixed Hydraulic Head in Aquitard	[L]
t	Time	[T]
h_0	Amplitude of Tidal Wave	[L]
ω	Angular Velocity	$[T^{-1}]$
t_0	Period of Wave	[T]
t_l	Time Lag	[T]
x	Horizontal Distance Inshore from Tidal Boundary	[L]
L	Length of Aquifer	[L]
h_{amp}	Amplitude of Wave at Distance x inshore	[L]
C_z	Coefficient of Curvature	[non-dimensional]
C_u	Coefficient of Uniformity	[non-dimensional]
D_{10}	Effective Size	[L]
λ	Wavelength	[L]
a	Wave Number	$[L^{-1}]$
ϕ	Phase angle	[non-dimensional]

Chapter 1

Introduction

1.1. Determination of Aquifer Properties

Determination of aquifer properties is important for construction, environmental management and water resources planning. In summary, knowledge of aquifer properties is necessary for predictive analyses of:

- Groundwater resources available

- Temporary Effects of Construction on Groundwater Behaviour - Water Flow into Excavations

- Migration of Contamination

- Groundwater Level Variations due to Tidal Fluctuations

- Permanent Effects of Construction on Groundwater Behaviour

- Water Table Lowering Inducing Settlement

1.1.1.   Groundwater Resources Available

The term *groundwater* is usually used to denote subsurface water that occurs beneath the water table in the pores of saturated soils and rock formations, existing at pressures greater than or equal to atmospheric pressure.

Groundwater is especially important as a resource in arid regions e.g. the Hararghe Region of Ethiopia, where surface resources are limited due to minimal precipitation and rapid evaporation. In other cooler climatic areas, such as the U.K., groundwater has become important since surface resources are often polluted and insufficient to meet high demands. In the U.K. in the past, heavy industry warranted use of large quantities of fresh water which was often exploited from river resources. With the recent reduction of heavy industry and cessation of water extraction, river levels and water tables have risen dramatically, sometimes resulting in problems of extensive and damaging flooding. This was experienced in the Tees estuary as well as in the

Thames vicinity and was in part, reason for the construction of barrages across the respective rivers coupled with the desire to limit surface water pollution.

Groundwater is an important source of fresh water. In England and Wales approximately one-third of fresh water comes from groundwater sources. As groundwater development intensifies to meet the high demands for fresh water made by an increasing world population, aquifers and their response to heavy pumping become vital in detailing the availability of water for a specific area.

1.1.2. Water Flow into Excavations

Engineers faced with construction projects beneath the water table (e.g. tunnels, excavations) require details of aquifer properties to predict induced water flow into excavated areas. Once sufficiently accurate volumetric flowrates are calculated, suitable drainage procedures can be designed and incorporated.

1.1.3. Migration of Contamination

Induced water flow can also cause migration of contamination. Alteration of water tables (due to commencement or cessation of water extraction) causes variations in groundwater flow. If a contaminant source exists within the zone of influence, migration of contamination will commence or change as groundwater flow varies and originally fresh water resources may become polluted. An example illustrating this problem is in the Czech Republic where a hydraulic barrier was created to prevent groundwater flow from an area containing a radioactive contaminant source. Maintaining this hydraulic barrier (which consists of several pumps introducing water and reversing the hydraulic gradient) is proving expensive. Predictive analyses of contaminant migration following cessation of pumping is in progress. These analyses are wholly dependent on aquifer and aquitard properties and require accurately determined values (particularly with regard to permeability) so that the necessary precautions can be taken in an attempt to contain the pollution.

Another case of migration of contamination exists here in the U.K. The recent cessation of many of the deep coal mining activities has resulted in the switching off of

drainage pumps and groundwater recovery has been allowed to occur. Groundwater flow has transported contaminants from the mine workings polluting both groundwater and surface water.

1.1.4. Groundwater Level Variations due to Tidal Fluctuations

In coastal areas, the tide influences groundwater behaviour. The effects of tidal fluctuation are dependent on the properties of the aquifer of interest and whether it is *confined* or *unconfined*. An aquifer is confined if the pore water completely fills the aquifer formation (saturation) which is overlain by an impervious confining bed. An aquifer is unconfined where the water only partially fills the aquifer formation and the water table can rise and fall within the stratum.

For the case of the unconfined aquifer, tidal fluctuations may cause a cyclic rise and fall of the water table, and at depth changes in pore water pressure will be experienced.

The tidal effects on a confined aquifer will be to induce variations in pore water pressure, with consequential changes in soil strength (illustrated by eqtn 1.1 below):

$$\sigma' = \sigma_T - u_w \longrightarrow eqtn(1.1) \qquad \text{(Terzaghi 1923)}$$

where σ' = effective stress experienced by the soil - an indication of soil strength

σ_T = total stress placed on the formation

u_w = pore water pressure

1.1.5. Construction Effects on Groundwater Behaviour

In addition to *confined* and *unconfined* aquifers (described in section 1.1.4), there also exist *semi-confined* aquifers. An aquifer is semi-confined (leaky) when it can lose or gain water through an overlying or underlying semi-pervious formation.

Construction can result in substitution of the semi-impervious formation with a relatively impermeable layer (e.g. concrete), thus preventing leakage from or into the semi-confined aquifer (reducing the vertical permeability). The effect of this is to alter

groundwater flow. Predictive analyses are necessary to prevent problems by implementing suitable design procedures.

1.1.6.   Water Table Lowering Inducing Settlement

When a load is applied to saturated soil material, it is supported by both the pore water and soil matrix. When the water table is lowered the pore water is drained from the soil material and hence any applied load now has to be carried by the soil matrix alone. If the effective strength of the soil, as defined by Terzaghi and quoted above in eqtn (1.1), is insufficient to cope with the extra load, the soil will deform and settlement will occur. Lowering of the water table can be the result of groundwater resource exploitation, construction dewatering or natural drought. In September 1995, following one of the driest summers on record, there were several reports of building subsidence following natural drought.

Accurate determination of aquifer properties is necessary to try to avoid settlement by predicting the extent of water table lowering due to these effects. A recharging process can then be outlined if applicable. This procedure was adopted for excavation for the Tower Latino Americana in Mexico City, in order to avoid serious settlement of neighbouring streets and buildings.

1.2. Definition of Aquifer Properties

The hydraulic properties of any aquifer are dependent on its geological characteristics which can be subdivided into four sections:

1. Geological evolution of the ground, e.g. due to sedimentation or volcanic behaviour.

2. Progressive geological events, such as plate tectonics resulting in folding fissures and faults.

3. Chemical processes, especially in limestones.

4. The grading analyses of the soil i.e. constituent materials.

4

Particular Properties of interest are:

- Coefficient of Permeability[1]
- Coefficient of Specific Storage
- Coefficient of Leakage

1.2.1. Coefficient of Permeability

Darcy found specific discharge (flowrate per cross-sectional area) to be proportional to the hydraulic gradient. The constant of proportionality, the coefficient of permeability, is a property both of the porous medium and of the water flowing through that medium, and details the *rate* at which water flows through the formation. Darcy's equation is given in eqtn (1.2) below.

$$W = -Ki \longrightarrow eqtn(1 \cdot 2)$$

where W = Darcy velocity [L/T]

K = coefficient of permeability [L/T]

i = hydraulic gradient [non-dimensional]

The grading of the soil material governs permeability. The effective size, D_{10} (sieve size through which 10% of the soil material passes) can be used to provide an estimate for this aquifer property. In addition to the soil material itself, the coefficient of permeability of an aquifer is largely influenced by fissures in the soil strata.

Throughout this report, the 'coefficient of permeability' may be abbreviated to the term 'permeability', which has the meaning as described above.

Transmissivity (also referred to as transmissibility) represents the flow per unit width of the aquifer, and is defined as:

$$T = Kb \longrightarrow eqtn(1 \cdot 3)$$

where T = transmissivity [L²/T]

K = coefficient of permeability [L/T]

b = thickness of saturated aquifer [L]

---

[1] The coefficient of permeability is also known as the hydraulic conductivity.

1.2.2. Coefficient of Specific Storage

This parameter details the amount of water that can be released from a unit volume of the aquifer for a unit change of head. Specific storage is dependent on both the compressibility of the soil skeleton and that of the pore water, and applies to confined aquifers. A similar parameter, specific yield, is used for unconfined aquifers to detail the amount of water available by pumping exploitation of the formation.

The storage coefficient is related to specific storage by the relationship below:

$$S = S_s b \longrightarrow eqtn(1 \cdot 4)$$

where S = storage coefficient [non-dimensional]

S_s = specific storage [L^{-1}]

b = thickness of saturated aquifer [L]

1.2.3. Coefficient of Leakage

The coefficient of leakage details the rate at which groundwater flows into or out of an aquifer system and frequently occurs due to precipitation percolating the soil overlying the aquifer formation. Coefficient of leakage is dependent on both the permeability of the confining layer and its corresponding thickness. It is also dependent on the head difference over the confining layer. These relationships are indicated below in equation (1.5).

$$\beta = \frac{K'}{b'} = \frac{q}{(h - h^*)} \longrightarrow eqtn(1 \cdot 5)$$

where β = coefficient of leakage [T^{-1}]

K' = coefficient of permeability of confining layer (aquitard) [L/T]

b' = thickness of aquitard [L]

q = leakage flowrate [L/T]

h = piezometric level in aquifer [L]

h* = fixed hydraulic head in aquitard [L]

1.3. Methods Available to Determine Aquifer Properties

Aquifer tests encompass all the effects of the geological characteristics described in section 1.2, and provide average estimates for aquifer properties over a region. The impact of geological irregularities is reduced.

Deviations between analytical methods and field results will occur due to:

1. The heterogeneity of the ground, e.g. impermeable lenses, sudden variations in local permeability.

2. Problems due to measurement devices and instrumentation errors.

3. The effects of geological structures, e.g. well design and interference, hydraulic boundaries

Various tests are available for determining aquifer properties. The tests provide estimates for aquifer characteristics to relative degrees of accuracy depending largely on the cost of performing the test and analysing the results. Typical test methods in practice are:

- Pump Tests

- Slug Tests

- Falling Head Tests

- Soil Sampling

- Tracer Tests

- Monitoring of cyclic changes in groundwater due to influence of a periodically changing water surface, e.g. tidal effects on groundwater behaviour

The method chosen to determine aquifer properties depends both on the options available at the site and also on the reason for determining aquifer properties.

Pump tests are the most common and rigorous methods for determination of aquifer properties. A single pump test provides a range of values for permeability as the test progresses. Estimates founded on information recorded at the start of the test (with minimal drawdown) can be used for determination of pollution migration, when no drawdown is anticipated. Estimates based on measurements much later in the test, when a steady state condition of drawdown is observed, provide much more

7

satisfactory values for an aquifer which is to be exploited for water resources (when drawdown conditions are the norm).

Pump tests rely on information from surrounding observation piezometers in addition to borehole information and so provide an estimate of aquifer properties over a large region of the aquifer. Semi-pervious layers, impermeable lenses and barrier effects are averaged out.

Falling head and slug tests provide estimates for aquifer properties that are fairly localised to the observation borehole.

Soil sampling tests, unlike others mentioned, are not performed *in situ* and therefore do not provide such accurate estimates of aquifer properties when compared to alternative methods.

1.4. Analyses of Cyclic Fluctuations in Groundwater Level for Determination of Aquifer Properties - Ferris' Technique.

Ferris' technique for determining aquifer properties is summarised below. This summary is based on the paper by Ferris (1951), entitled "Cyclic Fluctuations of Water Level as a Basis for Determining Aquifer Transmissibility".

1.4.1. Introduction

A technique for determining aquifer diffusivity (transmissivity/storage coefficient) was developed by Ferris (1951) who investigated cyclic fluctuations of groundwater level. This technique has applications to a stream, lake or sea that undergoes periodic changes in stage, generally sinusoidal fluctuations. A continuous data record of groundwater head changes and corresponding variations in stage of the surface-water source can be used to estimate diffusivity of the aquifer. Ferris assimilated the dependence of groundwater head on the source stage with Angstrom's work (documented by Carslaw in 1945) to determine the thermal conductivity of various

solids. Two formulae were concluded which incorporate, respectively, time lag and attenuation differences between the source stage and groundwater head at various distances from the boundary. Diffusivity can be calculated from these equations, which can then assist in providing estimates for coefficients of permeability and storage.

1.4.2. Assumptions

The theory presented by Ferris assumes an ideal homogeneous aquifer of uniform thickness, extending an infinite distance from the hydraulic source. This theory is based upon the governing equations of one-dimensional transient groundwater flow in a confined and saturated porous medium as developed by Theiss (1935). This equation is as follows:

$$\frac{\partial}{\partial x}\left(T\frac{\partial h}{\partial x}\right) = S\frac{\partial h}{\partial t} \qquad \ldots\ldots\ldots\ldots\ldots\ldots\ldots eqtn(1.6)$$

where T = Transmissivity

S = Storage coefficient

This equation has been used widely in practice and is based on two key concepts:-

1.   Conservation of mass within a compressible porous medium

2.   Darcy's law that the average seepage velocity is proportional to the head gradient.

The work by Ferris (1951) was to solve the above equation subject to the external conditions of a sinusoidal hydraulic head boundary condition. The application of this equation to such cyclic conditions was validated against field conditions. Ferris assumed that the aquifer was fully hydraulically connected to the linear surface-water source propagating cyclic fluctuating waves. For the cases where the aquifer is not fully connected to the surface-water source, tidal analyses will provide useful estimates of aquifer properties, provided the aquifer is unaffected by vertical components of flow.

Limitations to Ferris Theory

Previous analytical solutions of groundwater behaviour under harmonic conditions have been limited to solving the equation governing transient groundwater flow in a non-leaky confined aquifer. This is not, however, the case in most aquifers where, as the pressure rises, a proportion of the water will leak out of the upper or lower confining layers. Similarly, when water pressure falls, this will induce water from outside into the aquifer. Based on the assumption that the inflow and outflow to the aquifer is proportional to the head fall or rise, Jacob (1946) developed the governing equation for flow in such a leaky aquifer as:-

$$\frac{\partial}{\partial x}\left(T\frac{\partial h}{\partial x}\right) = S\frac{\partial h}{\partial t} + \beta h \quad \ldots\ldots\ldots\ldots\ldots\ldots eqtn(1.7)$$

where ß = Leakage coefficient

The solution to this equation under the condition of a fixed pumping rate was further developed by Hantush and Jacob (1955) with regard to understanding the transient behaviour of a leaky aquifer when subjected to a period of pumping at constant rate.

The work by Hantush and Jacob on leaky aquifers was further developed to incorporate well storage and non-linear leakage. However, no analytical solution has been produced to solve the leaky aquifer equation (eqtn 1.7 above). Such a solution has been developed as part of this project thesis and is included in chapter 5.

Model Verification

Although no analytical solution has been developed to solve eqtn(1.7) above, for sinusoidal boundary conditions, the numerical model CVM (Thomas et. al, 1994) solves this equation using a finite element numerical technique. This CVM model has been well documented with various other analytical and numerical solutions under transient and leaky aquifer conditions.

Since the CVM model is based on the equation of Jacob (1946), any analytical solution developed in this thesis to solve eqtn(1.7) above has therefore the capability of being verified by application of the CVM model.

1.4.3. Theoretical Equations for Tidal Analyses Derived by Ferris

The governing equation for flow in a one-dimensional, homogeneous, confined aquifer is

$$\frac{\partial^2 h}{\partial x^2} = \frac{S}{T}\frac{\partial h}{\partial t} \quad \dots\dots\dots\dots\dots\dots\dots\dots\text{eqtn(1.8)}$$

where h = rise of piezometric level with reference to mean level

S = Storage coefficient of the aquifer

t = time

T = Transmissivity of the aquifer

t = time

x = distance

Ferris derived a solution to eqtn(1.8), designating the amplitude of the tide as h_0, and applying the following boundary conditions

$$h = h_0 \sin \omega t \text{ at } x = 0 \text{ and } h = 0 \text{ at } x = \infty$$

where angular velocity = $\omega = \dfrac{2\pi}{t_0}$ and t_0 = period of tidal oscillation.

Ferris solved the governing eqtn(1.8) applying the above boundary conditions to give

$$h = h_0 \exp\left(-x\sqrt{\pi S / t_0 T}\right) \sin\left(\frac{2\pi t}{t_0} - x\sqrt{\pi S / t_0 T}\right) \dots\dots\dots\dots\text{eqtn(1.9)}$$

The solution in eqtn(1.6) illustrates that tidal pressure waves remain sinusoidal as they travel through the aquifer from the sea with a time lag and an exponential decrease in amplitude with distance from the sea.   This is illustrated in Figure 1.1.   The magnitudes of the time lag, t_L and amplitude variations, h_x, are

$$t_L = x\sqrt{\frac{t_0 S}{4\pi T}} \dots\dots\dots\dots\text{eqtn(1.10)}$$

$$h_x = h_0 \exp\left(-x\sqrt{\frac{\pi S}{t_0 T}}\right) \dots\dots\dots\dots\text{eqtn(1.11)}$$

Eqtn(1.11) can be rearranged thus:

$$\ln\left(\frac{h_x}{h_0}\right) = -x\sqrt{\frac{\pi S}{t_0 T}} \dots\dots\dots\dots\text{eqtn(1.12)}$$

11

This theory is documented in several textbooks including Todd (1980).

1.4.4. Validation of Theory

Ferris validated the formulae to a certain extent with specific examples. Field data was presented for three riverside observation wells at the Ashland station, City of Lincoln, Nebr. Groundwater levels were studied at three observation wells at distances of 42, 106 and 252 feet from the River Platte. The ratio of groundwater fluctuation to river stage was computed for the rising and falling limb of each cycle. Data was recorded for the duration of a week and the period of the river fluctuation was found to average 24 hours.

A semi-logarithmic plot of $(\ln h_x/h_0)$ versus horizontal distance from the observation well, x, was drawn up from the results. A line of best-fit was drawn through the results and diffusivity was then calculated from the gradient of this line using eqtn(1.12) above. Ferris stated that reasonable estimates of storage coefficient, S, can be determined if it is known whether the aquifer is locally confined or unconfined based on observation of water level records. Hence, a range of appropriate values of storage coefficient for unconfined conditions for the Nebr. aquifer were assumed. A range of transmissivity values were then calculated. It was concluded that the results were affected by:

1. Pumping from municipal wells, the rate and distribution of which varied slightly during the weekly period of testing.

2. Variations in the screen resistance of each observation well.

Time lag versus distance from the observation well was also plotted. From the gradient of this plot, a second value for diffusivity was determined. Several values of transmissivity were then calculated by substituting in the selected range of storage coefficients.

A significant difference between estimates of transmissivity based on time lag methods and amplitude methods was observed. This was attributed to the effects of local pumping, and Ferris recommended that future field work should be in an area not subject to heavy pumping.

Ferris concluded by suggesting that use of the theory could also be made for the response of aquifers to a single flood crest in a hydraulically connected stream.

1.5. Literature Review Detailing Application and Verification of Ferris' Technique

Since Ferris' technique is not common practice, a detailed literature review was executed to outline its application and evaluate its relative merits over standard pump tests procedures.

Application and validation of Ferris theory has been discussed by a range of authors. These include Carr and Van Der Kamp (1969), Erskine (1991), Pandit et al (1991), Crowe (1994) and White and Roberts (1994).

1.5.1. Carr and Van Der Kamp (1969)

1.5.1.1. Summary

Specific storage and coefficient of permeability were determined from fluctuating groundwater levels. Tidal efficiency was calculated and used to compute an estimate of specific storage by considering porosity of the rock and compressibility of the aquifer and water (Jacob, 1950). Application of Ferris' theory then led to an estimate for the coefficient of permeability. The approach was verified by field work in Prince Edward Island, Canada. Results from tidal analyses compared well with those based on pump test methods.

1.5.1.2. Tidal Efficiency

In a confined subsea aquifer, change in load on the aquifer due to tidal variations is carried by both the soil skeleton and the pore water. Therefore, the amplitudes of tidal fluctuation will be smaller in the subsea aquifer than in the ocean. The *true* tidal efficiency is defined as the ratio of amplitudes of groundwater fluctuation, in a subsea portion of an aquifer, to tidal fluctuation. It was possible to obtain *apparent* tidal efficiency which is the ratio of groundwater fluctuation in the aquifer *inland* compared to tidal fluctuation. The pressure wave has progressed inland and become damped by

movement through the aquifer. True tidal efficiency is the special case of apparent tidal efficiency at the boundary of the sea. Tidal efficiency can therefore be incorporated into Ferris amplitude decay equation as shown below:

$$TE_{true} = TE_{app} \exp\left(-x\sqrt{\frac{\pi S}{t_0 T}}\right)$$ ....eqtn (1.13)

1.5.1.3. Field Work

Prince Edward Island is underlain by sandstone and siltstone sediments with small amounts of clay and conglomerate. The strata are thin and groundwater was known to flow mainly through fractures rather than pores in soil material. Pump test data showed the aquifer to be semi-confined.

Measurements of groundwater level fluctuations were obtained for eleven piezometers covering a range of distances from the sea from 180 feet to 527 feet. Tidal efficiency was calculated by comparing the observed rise or fall in groundwater level with the respective rise or fall in sea level. Time lag was determined by comparing times between maximum and minimum groundwater levels and corresponding high and low tides. Average values of tidal efficiency and time lag for each borehole were then computed. The effects of lag due to the observation hole and time taken for surrounding groundwater changes to affect piezometric head were considered and Hvorslev's theory (1951) applied to results. This was found to have significant effect on observed time lags, which were then adjusted accordingly. The damping effect of the piezometer was also calculated (Hvorslev 1951) and found to have a small effect on results. Specific storage was calculated by considering compressibility of water and mean value of porosity determined from forty rock samples. The coefficient of permeability was then calculated from Ferris theory.

Pump test methods were used for comparison since they provide estimates of permeability for a large portion of the aquifer, similar to tidal analyses methods. It was not possible to perform pump tests at any of the peizometers used for tidal tests, however pump test data were available from investigations on local, similar soil

14

material. Mean values of specific storage obtained were in good agreement. Coefficients of permeability based on pump tests compared reasonably well with those from tidal analyses methods.

Errors in estimates based on tidal analyses were thought to occur due to discontinuities in the strata, reflection effects and inaccuracies in measurements. Applications of Ferris' theory were thought to be limited because a straight shoreline is assumed with little or no vertical leakage. Inaccuracies due to approximations of tidal period were also outlined.

1.5.2. Erskine (1991)

1.5.2.1. Summary

Tidal fluctuations affected groundwater in the coastal aquifer around Sizewell 'B' Nuclear Power Station, East Anglia, U.K. Construction of the new power station warranted extensive dewatering during construction. Detailed monitoring of groundwater was made to avoid disturbing effects on the existing and operating Sizewell 'A' Power Station. Tidal effects were eliminated so that the effects of dewatering could be carefully monitored.

1.5.2.2. Field Work and Tidal Analysis of Results.

The geology of the site consisted of high permeability sand overlying clay bedrock. Piezometers were located in the highly permeable unconfined aquifer at various distances of between 50 and 400 metres from the sea. Data of groundwater levels was collected from 39 piezometers over a 24 hour period. A standard deviation method was applied to determine the amplitude decay from results. The time lag was measured from results using the least squares fit method. The data was filtered to compensate for tidal effects. It was stated that atmospheric pressure and meteorological changes will affect both the aquifer and tides. At small values of amplitude decay, the accuracy of both time lag and amplitude decay was significantly reduced. At distances from the sea exceeding 350 metres, efficiencies were down to 4% or less. Scattering of results was attributed to variations in geology of the area

and design of piezometers. Erskine stated that results illustrated a clear tendency for deeper piezometers to have smaller lags and larger tidal efficiencies. He attributed this to the unconfining nature of the aquifer close to the phreatic surface. Pressure waves tended to be damped in this area because the storage coefficient used was unconfined, whereas at depth confined storage governs pressure changes. Erskine performed regression analysis on data points to get best fit lines.

Time lags observed appeared to be larger than expected. The time taken for the piezometer to respond to changes in groundwater pressure was calculated from Hvorslev's theory, and found to be negligible. Application of Ferris' theory was questioned since the aquifer may not come into contact with the sea until a considerable distance from the beach. Furthermore, if this was the case, characteristics of the sea bed may interfere with transmission of oscillations from sea water to aquifer.

Erskine assumed a value for transmissivity based on pump test results, and hence derived estimates for storage coefficient from both time lag and amplitude decay formulae. He found these estimates to lie between the confined and unconfined storage of the aquifer as estimated from the pump test. He concluded that this illustrated that the aquifer was not acting as a confined or unconfined aquifer, but exhibiting a combination of the two. Erskine also discussed Ferris' assumption that variations in transmissivity resulting from fluctuations in the level of the phreatic surface were negligible. Erskine concluded that his results would not correspond exactly because of unconfined aquifer behaviour. The damping effect of the phreatic surface was suggested to have more effect on the amplitude decay of tidal oscillations than time lags. Erskine mentioned the work of Reynolds (1987) who found that by matching time lag rather than amplitude decay, his simulated diffusivity tended to correspond with parameters for confined aquifers.

1.5.3. Pandit, El-Khazen and Sivaramapillai (1991)

The main objective of their work was to determine the ratio of the vertical to horizontal components of the coefficient of permeability of an aquifer using a finite element

model. In addition to this, the horizontal component of coefficient of permeability was estimated by studying tidal effects on groundwater in a coastal aquifer at Port St. Lucie, Florida.

The aquifer was in the most part unconfined, however confined conditions were recorded where discontinuous clay lenses acted as confining units.

Groundwater levels were monitored hourly on two separate days. It was found that groundwater levels were fluctuating in response to tidal variations in the Indian River Lagoon, as opposed to the sea itself. Ferris theory was applied to data from one observation well. It was found that significant changes in specific yield had little effect on groundwater levels, however a value of storage coefficient was assumed that predicted groundwater levels close to those measured. From this, a value for the coefficient of permeability was estimated. This value was found to be in good agreement with a range of values obtained from alternative methods.

1.5.4.   Crowe (1994)

1.5.4.1.   Summary

Crowe investigated the tidal method for determining aquifer properties. Information was gathered from a site in Humberside, U.K., and comparisons made between estimates of aquifer properties determined by a variety of techniques. Computer models were used to simulate observed behaviour of groundwater in response to tidal fluctuations.

1.5.4.2.   Geology

The geology of the site consisted of alluvial material and made ground overlying glacial deposits, including till; sand and gravels; glacial lake deposits. Underlying the region was Cretaceous chalk.

There were two aquifers in the area. The upper aquifer, was in the granular alluvial and glacial deposits. The lower aquifer, lay in the chalk.

17

1.5.4.3. Analysis of Earlier Site Investigation Results

Earlier site investigation results, including packer permeability tests, were available and Crowe analysed this data. He found that permeability estimates depended largely on test method, with results spanning four orders of magnitude. Significant discrepancies were found between estimates from pump in and pump out tests. It was suggested that this was due to the washing out of fines contained in fissures, implying that most groundwater flow occurred through such fissures.

1.5.4.4. Field Work - Manual Recording of Data

At the Humberside site, Crowe manually recorded measurements of groundwater level from nine boreholes over a period of six hours.

Amplitude results were plotted on a graph of $\ln(h_x/h_0)$ versus horizontal distance, x. From the plot, the distance from the riverside to the submarine outcrop was estimated at 160 metres. The gradient of the best-fit line was measured and hence diffusivity was estimated to be 9×10^5 m^2/day (applying Ferris' theory). It was assumed that pump tests and tidal analyses resulted in an estimate of the same mean permeability. Substitution of the mean value of permeability obtained from packer tests into the diffusivity result, provided an estimate for specific storage. Using this value, Crowe calculated the mean permeability for each of his data points.

The range of permeability estimates obtained from packer tests was compared with those from tidal analyses. It was noted that the packer test data, based on pump-out tests, ignored variations in permeability with depth. Crowe found that the range of results for permeability from the tidal analyses method was much smaller than that from pump test analyses. Figure 1.2 illustrates Crowe's results from this comparison.

Crowe also estimated time lag from the data. It was anticipated (as predicted from Ferris' theory) that a time lag versus distance plot should produce a straight line. The results were extremely scattered and there was no indication of a straight line pattern. Diffusivity could not be estimated from the manual time lag results.

On close analysis of the manual data, Crowe found periodic variation in the wave.

Crowe suggested several reasons for discrepancies in estimates of permeability based on the manual data and tidal analysis. These included:

1. Effect of flood waves and weather conditions in the Humber catchment.

2. Atmospheric variations. It was thought that this effect could cause variations in sea level of ±0.25 metres.

3. Associated British Ports pump water into the docks to maintain water levels for three hours either side of high tide. It was thought that this would artificially influence the period and time lag without significantly affecting amplitudes.

4. Variations in groundwater flows due to weather conditions.

1.5.4.5. Field Work - Data Loggers

Pressure transducers and data loggers were installed in three boreholes to record groundwater levels. Measurements were taken every five minutes for 14 days. Amplitude results were plotted on a graph of $\ln(h_x/h_0)$ versus horizontal distance, x. A best-fit line was drawn through the points. The gradient of the line was measured and diffusivity calculated to be 5×10^5 m^2/day. This compared well with the estimate from data gathered manually .

Time lag was calculated and plotted versus horizontal distance. A best-fit line was drawn through points on the graph and from the gradient of the line, diffusivity was calculated to be 6×10^6 m^2/day (applying Ferris' theory).

There was clear discrepancy in the estimate of diffusivity (an order of magnitude) between amplitude and time lag techniques. Crowe suggested that this may be due to leakage, instigated by removal of some of the confining material when the dock foundations were constructed. He concluded that leakage would have the effect of damping oscillations, whilst time lags remained unchanged.

No variation in period was observed in the data logger results.

1.5.4.6. Fourier Analysis

Fourier analysis was carried on tidal data to establish predominant wave forms. These were concluded to sine waves of periods ½, 1 and 14 days.

1.5.4.7.   Atmospheric Pressure

Results from atmospheric monitoring were considered inconclusive particularly because of the effects of heating of the metal casing. The mean value of the data from one borehole varied by around 150mm which may have been the result of atmospheric effects. This value was greater than the amplitude of oscillations in that hole.

1.5.4.8.   Computer Models

Two different software programmes were used to model the situation at Humberside. Results from both models were consistent with amplitude results given by Ferris' theory, and with data from the earlier site investigation. Crowe investigated the effects of leakage on amplitude decay using one of the computer models. Whilst other aquifer properties are kept constant, Crowe found leakage had significant effect on amplitude decay. It was not possible to measure time lags accurately using the computer models.

1.5.4.9.   Conclusions

Crowe concluded that tidal analyses methods produced results of permeability with less scatter than those obtained by pump tests. He also suggested that it may be possible to obtain an estimate of leakage from the aquifer by comparing amplitude and time lag methods. It was recommended that both amplitude and time lag methods be used to estimate diffusivity since the presence of leakage may reduce apparent diffusivity as calculated form the amplitude method, leading to incorrect conclusions.

1.5.5.   White and Roberts (1994)

The causes and transmission mechanisms of tidal influences were discussed and estimates of aquifer properties based on tidal analyses compared with those expected at a variety of sites around the United Kingdom. White and Roberts questioned the viability of Ferris' theory, particularly since the effective location of the source could be

significantly further than the distance as measured from the observation borehole. This could be the case for two reasons:

1. If a narrow zone of lower permeability material sealed the source from the aquifer, this would have the effect of reducing the fluctuation at all positions by a factor. It was suggested that to avoid this type of confusion, a minimum of two observations of groundwater level should be made at different locations and the results compared, before analyses with tidal fluctuations was performed.

2. A confined aquifer may not be directly connected to the source. This would affect tidal efficiency, as the full tidal loading would not be transmitted to underlying pore pressure response. It was concluded that Ferris' theory discounts overlying strata hence reducing tidal efficiency.

Analysis of results from the six case studies produced a variety of conclusions.

Site 1. Estimates of diffusivity from pump test data at Port Solent were in good agreement with estimates based on tidal analyses.

Site 2. Data collected from a single piezometer located in an unconfined aquifer at a site near Folkestone was used to compute an estimate of diffusivity and permeability. The results compared reasonably well with particle size distribution data.

Site 3. Estimates of aquifer properties at a site at Blackwall were based on borehole investigations and particle size distribution data. Tidal analyses estimates were found to be unexpectedly low. This was thought to be due to differences between effective distances and actual distances.

Site 4. Estimated parameters based on soil material at the Medway site were significantly different to those obtained from tidal analyses methods. It was suggested that the aquifer was partially confined and effective distances much greater than actual distances.

Site 5. Comparisons of confined aquifer properties at Limehouse from both site investigation and tidal analyses compared well.

<u>Site 6.</u> Diffusivity estimated from tidal analyses at the Conwy site was larger than expected. The reason for this was attributed to the anisotropic nature of Lake deposits which have a higher horizontal permeability.

Underestimates of tidal response induced by the 19mm diameter piezometer were suggested to be as large as 25% for permeabilities of 10^{-6} m/s.

White and Roberts concluded that tidal response data could not be used to determine aquifer properties such as permeability with any useful accuracy. It was suggested that it could provide a useful supplement to a site investigation but would never rival rigorous methods such as pump tests in accuracy of determining aquifer properties.

1.6. Literature Review Detailing Groundwater Behaviour and Determination of Aquifer Properties from Tidal Efficiencies

Studies of groundwater behaviour and determination of aquifer properties with regard to tidal efficiencies have been discussed by Gregg (1966) and Money (1986).

1.6.1. Gregg (1966)

1.6.1.1. Summary

The formulae to determine tidal and barometric efficiencies when both are changing simultaneously were derived. Gregg also discussed changes in tidal efficiency with depth and distance from the sea. Coefficient of storage was calculated from tidal efficiency measured at a site in Glynn County, Georgia, U.S.A.

1.6.1.2. Details

Tidal efficiency is defined as:

$$\text{Tidal efficiency} = \frac{\text{well water level change}}{\text{tidal level change}} \longrightarrow \text{eqtn}(1\cdot14)$$

This is analogous with amplitude decay as described by Ferris (1951).

22

Discrepancies in tidal efficiencies were thought to occur due to variations in thickness of sedimentary materials overlying the aquifer. Conditions of greater thickness would reduce the effect of damping of tidal waves. Larger coefficients of storage were suggested to cause higher tidal efficiency. Tidal efficiencies of wells at the site were found to decrease with depth and also with distance from the influencing tidal body. Decrease in tidal efficiency with depth was attributed to heterogeneity of materials and increase in the number of hard, dense beds with depth. It was suggested that tidal efficiency increased during spring tides due to an increase in the total load on the aquifer.

Tidal efficiency was used to determine the bulk modulus of elasticity and compression and the coefficient of storage of the aquifer (Jacob, 1950). The estimate of storage coefficient obtained by this method compared well with those based on alternative techniques.

1.6.2.   Money (1986)

Type curves were constructed from Ferris theory to predict piezometric response. A field site in the Tees estuary was selected for validation of the theoretical plots. Discrepancy was found between field results and predicted theory. This was attributed to the net coastward flow of groundwater.

1.7. Discussion of Ferris Technique for Determination of Aquifer Properties

It can be concluded from field work analysed to verify Ferris' theory (referenced and detailed above) that the method provides an approximate estimate of aquifer properties. The technique does not appear to provide such reliable estimates as pump test methods. It is limited to a certain extent by the assumptions made by Ferris, particularly with regard to negligible vertical flow. Difficulty in measurement of distance from the observation well to the sub-sea outcrop also leads to significant

discrepancies in results. Further problems have been noted due to coastward flow of groundwater.

Ferris' technique incorporates the heterogeneity of the aquifer formation and therefore gives more accurate representation of a wider area than alternative methods. Semi-pervious layers, impermeable lenses and barrier effects are incorporated to provide average estimates for aquifer properties over a wide coastal area.

1.8. The Importance of Determining Aquifer Properties in Coastal Areas

Nearly two thirds of the world's population now inhabit coastal areas and numbers are growing (United Nations Environment Programme). Consequently, there is demand for fresh water resources and construction services and in addition, problems of pollution are inherent. Therefore, determination of aquifer properties, as outlined in section 1.1, is important for predictive analyses in meeting people's needs whilst avoiding environmental problems.

Particular problems occur due to high demand for fresh water resources. Rivers in coastal areas are frequently polluted and groundwater has become an important source of fresh water supply. Excessive pumping of coastal aquifers can lead to saline intrusion and pollution of the source. This then incurs the expense of desalination if the groundwater resource is to continue to be exploited. In order to avoid this unnecessary expense, coastal aquifer properties require to be accurately determined so that the effects of heavy pumping can be predicted.

1.9. Physical Modelling of Coastal Aquifers to Improve Methods for Accurately Determining Aquifer Properties

Accurate determination of aquifer properties in coastal area is therefore essential. Ferris' method is particularly suitable for estimates of coastal aquifer properties,

however, as explained in section 1.7. above, the theory is somewhat limited, and requires further validation.

Investigation and development of engineering techniques to estimate aquifer properties includes field work, numerical modelling, physical modelling or mathematical development of existing theory. The validity of any technique in the long term is greatly enhanced by research covering the full repertoire of these activities. There are few examples in geotechnical engineering that involve physical modelling as a means of research and development. Subsurface features are often too large and influenced by a number of external factors which are difficult and impractical to simulate in the laboratory.

The objective of this research project was to further investigate the application of Ferris' technique. This involved field work in addition to physical modelling of a coastal aquifer constructed in the laboratory at Durham University.

Figure 1.1. Ferris Tidal Method
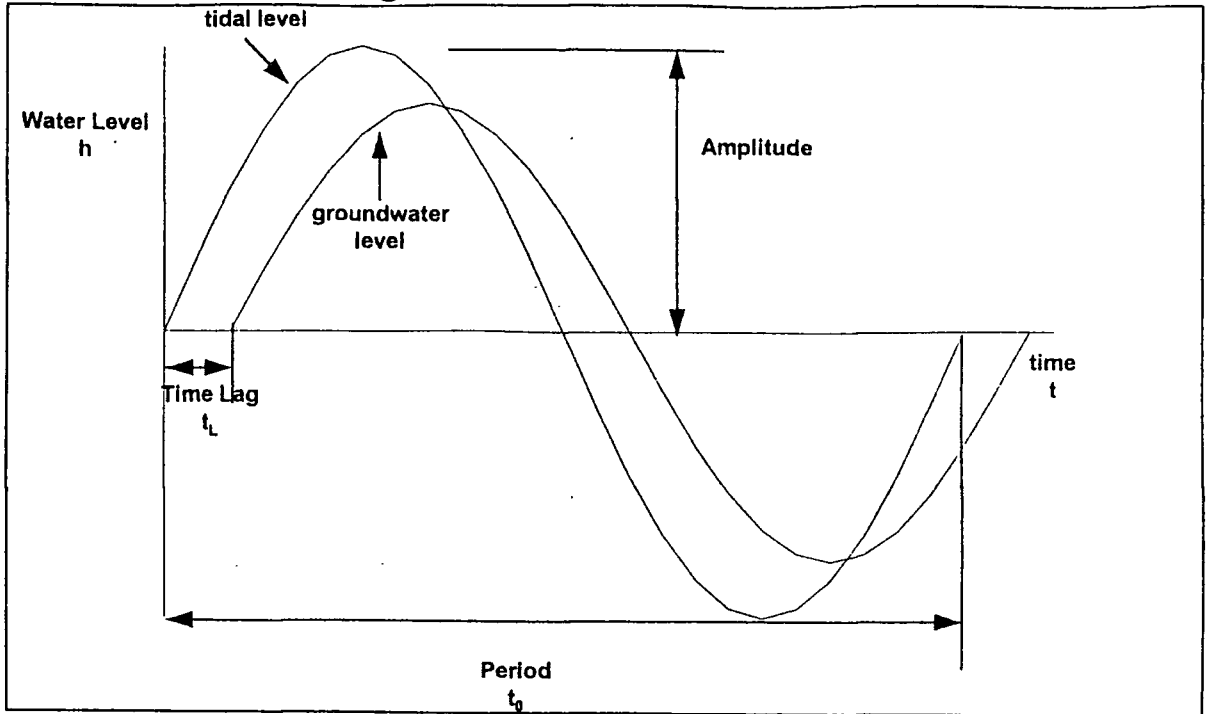
Figure 1.2. Comparison of Pump Tests and Tidal Monitoring
Frequency Distribution

_ _ _ _ Field data from Tidal Monitoring ___ Field data from Pump Test Data
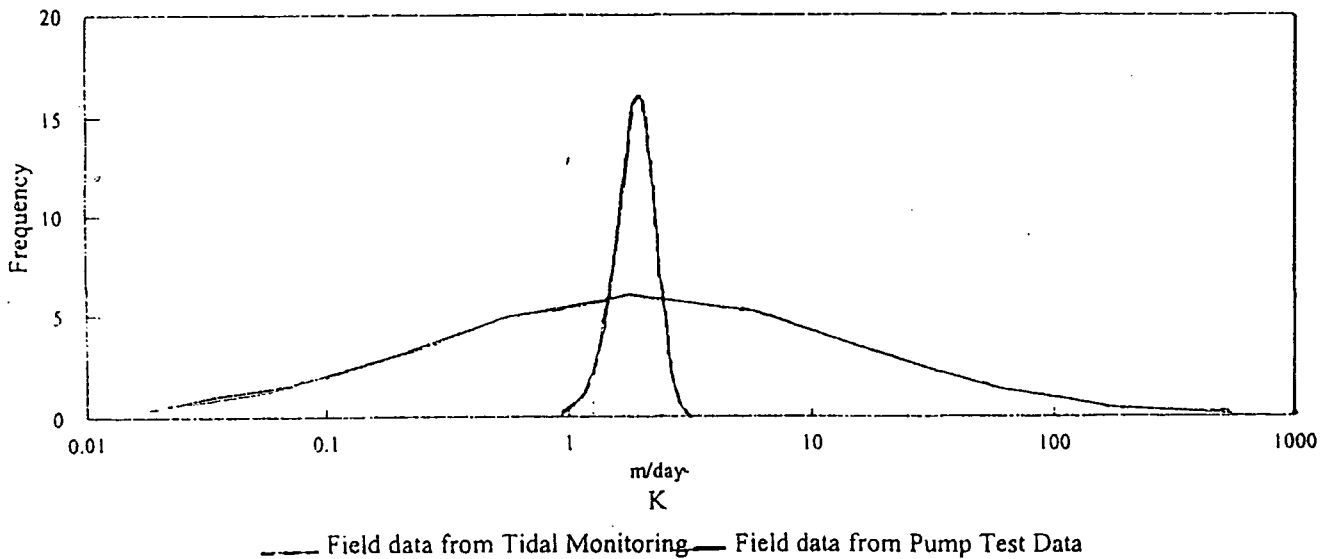
Tidal data has been multiplied by 2.6 to give equivalent sample sizes.

From Crowe, C.G. (1994). Tidal Variations in Groundwater. University of Durham, Submission Thesis for the Degree of Master of Science.

Chapter 2

The Durham Model Aquifer

2.1. Introduction

As part of an undergraduate project, Carrington (1994) constructed a basic laboratory model of a coastal aquifer. The objective of this work was to further investigate Ferris' theory for the estimation of aquifer properties in coastal areas. The viability of the physical model was determined from experimental work. This was essential before tidal tests could be performed. Analysis of these results concluded estimates of values for aquifer properties.

Within the current programme of work, which formed the post-graduate research project, the tidal system for the Durham Model Aquifer was installed. Two preliminary tests were performed under steady state conditions followed by sixteen series of tidal tests.

This chapter describes concepts leading to construction of the Durham Model Aquifer and describes the equipment. A summary of results from undergraduate experimental work (Carrington, 1994) is also included.

Details are then given regarding installation of the tidal system as part of the post-graduate research.

2.2. Model Concepts

The conceptual requirements for the physical model were as follows:

- Permeable soil material, submerged in water - the aquifer, with specific storage and permeability.

- Horizontal flow of water within the soil material - groundwater flow.

○ A periodical wave applied at one boundary - simulated tide.

○ An overburden - simulating weight of overlying strata.

○ Accurate Instrumentation to measure pore pressures in order to determine *time lag* variations and *amplitude decay* of the applied wave at a number of horizontal distances from the harmonically varying boundary.

2.3. Model Size

The size of the model required to be such as to provide realistic estimates of aquifer properties. Small data values were thought to be significantly affected by experimental errors, and yet size of the model was obviously limited due to physical constraints and expense. A balance had to be obtained.

Figure 2.1 provides an indication of the size of the influential zone of existing aquifer tests when compared with the field.
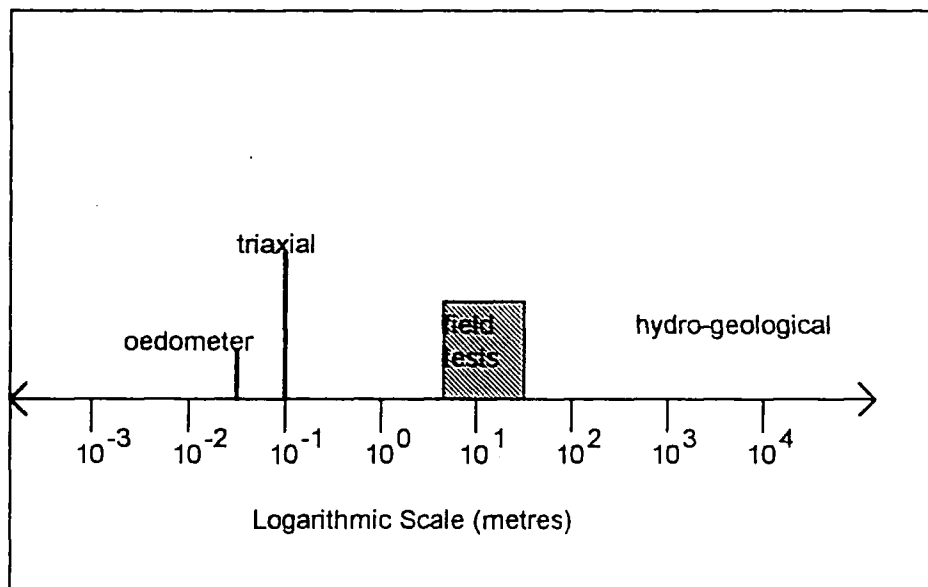
Figure 2.1. Indication of Influential Zone of Existing Aquifer Tests

From Figure 2.1, it can be seen that aquifer testing in the past has been limited to small soil samples (of the order of centimetres) or to much larger areas with application of field methods such as pump tests (of the order of tens of metres). Little experimental work has been performed covering regions of the order of metres.

Investigation into determining aquifer properties for influential regions of between one and ten metres could improve available techniques for accurately measuring aquifer properties, such as permeability, specific storage and leakage.

2.4. Model Overview

This section describes the equipment constructed in an undergraduate project by Carrington (1994).

The Durham Model Aquifer was designed and constructed from consideration of the required concepts and size as outlined above. A schematic diagram of the constructed model is shown in Figure 2.2.

A descriptive overview of the physical model is outlined below.

The model consisted of a container (4.8m long, 0.25m wide and 0.25m deep), filled with sand submerged in water. The head was varied in a water tank, linked to the laboratory aquifer at one end, whilst pore water pressure measurements were recorded at various positions along the base of the aquifer container, the density of measurements being greatest nearer the water tank where larger pressure variations were anticipated.

A detailed diagram of the Durham Model Aquifer together with a photograph of the equipment before the tidal system was installed are presented in Figures 2.3 and 2.4 (Photograph A). The aquifer container was constructed from wood in a double layer to help prevent leakage and to give strength. Variations of head within the water tank resulted in flow into the semi-confined model aquifer. The water tank was linked to the model aquifer by a length of pipe. At the end of this pipe a perspex plate secluded a grid

of holes and series of grooves between these holes. Water was filtered along the grooves because the plate was fixed flush with a solid lamina. After passing along some of these grooves, water flowed through the holes to porous material (Dupont typar®) attached to the other face of the perspex plate which prevented sand from the aquifer entering the water tank. The water filtered through this material into the sandy aquifer bed where it became 'pore water'. Water remained in this bed under pressure from an overburden of compressed air (equivalent to 1.20m head of water) within a rubber bag. The rubber bag was constrained from rising by a series of metal bars bridged by a wooden support above the air bag. Water leakage from the aquifer occurred along the sides of the container, between the rubber bag and wooden panels. This free water surface was maintained at constant head using a drain positioned above the rubber bag at the far end of the aquifer container.

The water level in the tank was altered as testing proceeded. Pore water pressure was measured at twelve different positions in the system, eleven in the base of the aquifer container and one in the base of the water tank (these twelve positions were individually connected with piping to a brass manifold). The locations of each of the pore water measurement positions are outlined in table 2.1. below.

Pore Water Measurement Position	Distance from Tidal Aquifer Boundary (m)
1	N/A Base of Tidal Tank
2	0.05
3	0.145
4	0.420
5	0.780
6	1.210
7	1.720
8	2.280
9	2.810
10	3.425
11	4.095
12	4.795

Table 2.1. Locations of Pore Water Measurement Positions from Aquifer Boundary Nearest Tidal Tank.

At each of these twelve positions, porous discs in brass tappings prevented larger sand particles migrating from the aquifer and blocking peripheral equipment. Twelve solenoid switches, located at the entrances to the manifold, were controlled by computer to open sequentially. The opening of each of these switches linked water at the corresponding position in the base of the aquifer model with that in the manifold. A transducer, connected to the manifold, was programmed by computer to measure water pressure eighty seconds subsequent to switch-opening, after which time the pressure within the manifold was anticipated to have reached equilibrium with that in the base of the Durham Model Aquifer. This pressure measurement was recorded together with the corresponding position in the aquifer. To minimise external influences, such as atmospheric effects, on pore water pressure measurements, a single transducer was used, and therefore variations in pore water pressure were comparable for each of the twelve positions. The accuracy of the transducer was found to be ± 1 mbar.

It was necessary to ensure minimal air in the Durham Model Aquifer system because this would distort pore water pressure measurements. The system was therefore regularly flushed through with water. Leakage also continually occurred from the upper surface of the aquifer aiding the reduction of trapped air in the system.

2.5. Soil Material Details

Sherburn Quarry Sand was used to form a homogeneous aquifer of suitable permeability. The properties of local Sherburn Quarry Sand, listed below in Table 2.2, were determined by particle size analysis, applying sedimentation by pipette analysis for differentiation of fines.

Coefficient of Curvature (C_z)	1.11
Coefficient of Uniformity (C_u)	4.44
Effective Size (D_{10})	90×10^{-3}mm

Table 2.2. Properties of Sherburn Quarry Sand

The grading curve for the sample is shown in Figure 2.5.

2.6. Estimates of Aquifer Properties from Previous Experimental Work

Experimental work was performed as part of the undergraduate project, Carrington (1994), using the Durham Model Aquifer. This work concluded with estimates for the coefficients of permeability and leakage.

In summary, the coefficient of permeability of the Durham Model Aquifer was estimated to be 3×10^{-3} m/s. This result is within a range of estimates of permeability for sand

material (Freeze and Cherry, 1979). The leakage coefficient was estimated to be 7×10^{-6} s^{-1}.

In addition to the above tests, Carrington (1994) performed experimental work to determine the specific storage of the Durham Model Aquifer. Results from Carrington's work were analysed by Lourenco (1994) who concluded values for storage and leakage coefficient of 0.1 and 8×10^{-6} s^{-1} respectively. This estimate for the storage coefficient was higher than anticipated. This was attributed to the fact that the definition of storage coefficient is based on compressibility of the soil and pore water, and ignores the presence of any air within the system. The significant amount of air present in the Durham Model Aquifer system was therefore thought to be the reason for an unusually large estimate for this aquifer property.

The results are summarised in table 2.3 below.

Aquifer Property	Estimated Value
Coefficient of Permeability	3×10^{-3} m/s
Coefficient of Leakage	7.5×10^{-6} s^{-1}
Storage Coefficient	0.1

Table 2.3. Summary of Estimates for Aquifer Properties from Preliminary tests.

2.7. Repair and Modification of Equipment

The Durham Model Aquifer was not used for seven months prior to commencement of the MSc post-graduate research project. Before further testing was possible, certain repairs and improvements had to be made to the equipment. These repairs formed part of the current programme of work and are outlined below.

1. It was anticipated that sand material constituting the model aquifer had become dry during the seven month period and therefore had to be re-saturated with water. This

involved repeatedly filling the tidal tank with water and allowing time for this water to dissipate into the model aquifer. Leakage from the upper surface of the aquifer ensured that the system was flushed through with fresh water.

2. Air had entered the system over the seven month period. Therefore, as much air had to be expelled as was physically possible. Filling the tidal tank as described in 1. above aided this process, eliminating some entrapped air. In addition to this method, water was also injected into the base of aquifer through three of the brass tappings (located for pore water pressure measurement). Water was injected for lengths of time not exceeding one hour.

3. Leaks had occurred at seals in the aquifer container and these had to be repaired by sealing with silicone sealant.

4. Silt material had become trapped in the piping linking the solenoid switches to the base of the aquifer. This had to be removed along with any air bubbles that had become trapped in the pipe work. This was done by two methods. Firstly, detaching pipework from solenoids and enabling water to flow (due to head difference) from the aquifer. If this was insufficient to clear the pipe, the second method of water injection (similar to that described in 2. above) was used. This forced silt and air back into the aquifer. It was hoped that most of this air would be cleared as the aquifer was repeatedly flushed through with water.

5. Silt material had also become trapped in the plastic pipe linking the tidal tank and model aquifer and had to be cleared out.

5. A new air regulator had to be bought and installed to more accurately control the air pressure within the rubber bag overlying the model aquifer.

6. The existing computer programme designed to control the solenoid switches and record transducer measurements had to be improved. Time between readings had to be as short as possible and data had to be stored in a more convenient form for subsequent analyses. The required time between pore water pressure measurements was found to be at least 100 seconds. This allowed the necessary

time for the water pressure in the manifold to reach steady state. This 100 second time interval was required due to silting in pipes and around pore water pressure measurement areas. The transducer also took time to adjust to new pressures in the manifold.

7. The rubber bag had to be re-filled with air.

8. Existing overlying wood had become rotten due to continuous saturation in water. New suitably-sized wood had to be obtained to replace the existing wood overlying the rubber bag.

9. The rubber bag had to be constrained from rising so that the overburden pressure was exerted down onto the model aquifer.

10. The electronic system for opening and closing the solenoids (controlled by the computer programme) required improvement. On switching on the computer system, all the switches were automatically opened. This was changed so that all the switches remained closed when the computer was turned on. As a consequence of this work some of the commands within the computer programme had to be negated.

Once all the above work was completed, work began to install the tidal system.

2.8. Installation of Tidal System

The tidal system was a method of producing a harmonically varying water head in the tidal tank, the period of which could be controlled. This system was designed and constructed as part of the current research project.

The design included a control system regulating two central heating pumps: one pumping water *into* the tidal tank, the other pumping water *from* the tidal tank. Central heating pumps were used as they were relatively inexpensive and easily obtainable. Figure 2.6 below presents a schematic diagram of the tidal arrangement.
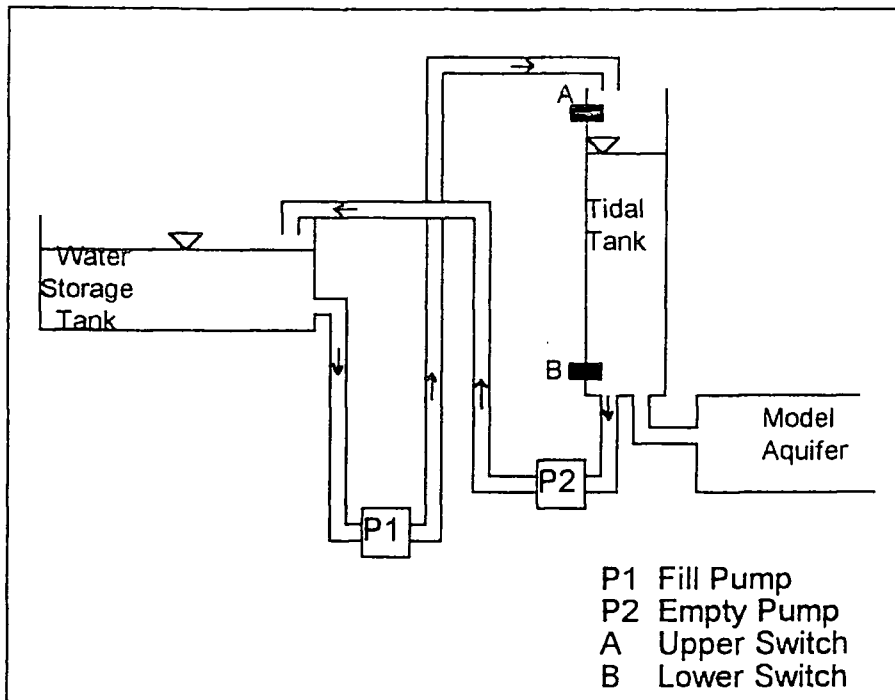
Figure 2.6. Tidal Arrangement.

Water was pumped from the water storage tank into the tidal tank by use of pump P1, until the level reached switch A. Pumping was then paused for a controlled length of time, after which pump P2 pumped water from the tidal tank back to the water storage tank, until the level reached switch B. Once more, pumping was paused for a controlled length of time, after which pump P1 again began pumping water from the storage tank to the tidal tank as before. This cycle was repeated for durations of up to four days.

The electrical control mechanism included a programmable Timer Base which enabled the period of the cycle to be altered by specifying the pausing times between the action of pumps P1 and P2. Details of the programmable timer base are given in Appendix 2.1. In addition to this, the central heating pumps had three speed settings, and thus the rate of water flow into and out of the tidal tank could also be adjusted. The period range available was 20 to 45 minutes. The detailed electrical design of the control system was outwith the scope of this project.

The arrangement selected for the system, as illustrated in Figure 2.6, ensured that non-return valves were not required. Piping was arranged so that the head ensured that

water flowed only when the pumps were in operation (with the exception of minimal flow into the model aquifer due to aquifer leakage effects). Therefore when pump P1 stopped, water flow also stopped since the pipe outlet was higher than the water level in the storage tank. This was also the case for pump P2. Once pump P2 stopped and the water level in the tidal tank was at switch B, the height of the outlet of the pipe was higher than the water level in the tidal tank thus water flow also stopped.

Installation of the tidal system required the following:

1. Design of supports for the central heating pumps and a board so that they could be conveniently attached to the wall, adjacent to the tidal tank.

2. Obtaining suitable fittings so that 8mm diameter piping could be attached to the central heating pumps. These components were then connected with care taken to seal joints.

3. Ordering a suitable polythene water storage tank, and provision of a platform to support the weight of this water tank when full.

4. Drilling a hole in the water storage tank for the 8mm pipe connection to the central heating pump.

5. Obtaining suitable screws and rawl plugs and attaching the central heating pumps on their mounts to the wall.

6. Obtaining and installing a replacement for switch B in the tidal tank. The existing switch B (installed when the tidal tank was constructed in November 1994), did not have a switching mechanism suitable for the control system.

The entire tidal system was controlled electrically. Due to the fact that there was a small amount of water flow into the model aquifer, a continuous water flowrate was applied to the water storage tank from an external source to compensate for this loss. This flowrate was determined by monitoring flowrate from the drain overlying the model aquifer.

A diagram illustrating the tidal arrangement in relation to the rest of the Durham Model Aquifer Equipment is shown in Figure 2.7. A photograph of the equipment is shown in Figure 2.4 (photograph B). This shows the central heating pumps attached to the wall

and the black plastic water storage tank situated above the model aquifer. The white electrical control box can also be seen in this photograph, situated on the wall to the right of the tidal tank.

The tidal system was set to run whilst water pressure measurements were recorded from the base of the tidal tank. The graph showing this harmonic variation is given in Figure 2.8. It can be seen that the waveform is largely representative of a sawtooth wave. Fast Fourier Transform analysis of this wave established two major sinusoidal constituents. These are illustrated graphically in Figure 2.9.

In order to establish the viability of the tidal system, it was set to run whilst measurements of pore water pressure were recorded from the twelve different positions: eleven in the base of the aquifer, one in the base of the tidal tank (indicating simulated tidal variations). Analyses of the data illustrated that the harmonic pressure wave was transmitted through the aquifer with an observed amplitude decay and increase in time lag as horizontal distance from the tidal boundary also increased.

Following this preliminary investigation, more detailed laboratory tests were performed using the Durham Model Aquifer. Experimental methods and results from these tests are outlined in chapter 3.

Figure 2.2. Schematic Diagram of Constructed Model

Tidal Tank

Air Bag

Aquifer

4.8m

Computer
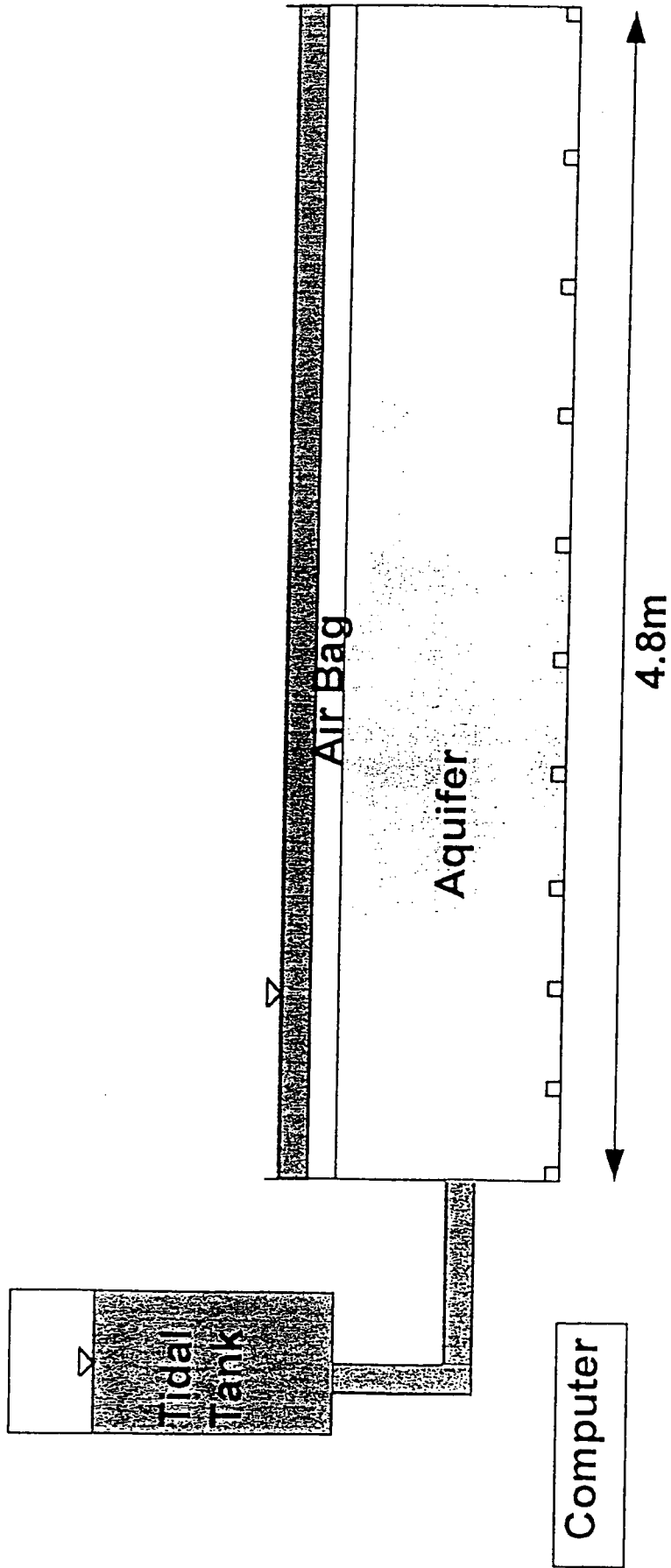
Figure 2.3. Detailed Diagram of Durham Model Aquifer
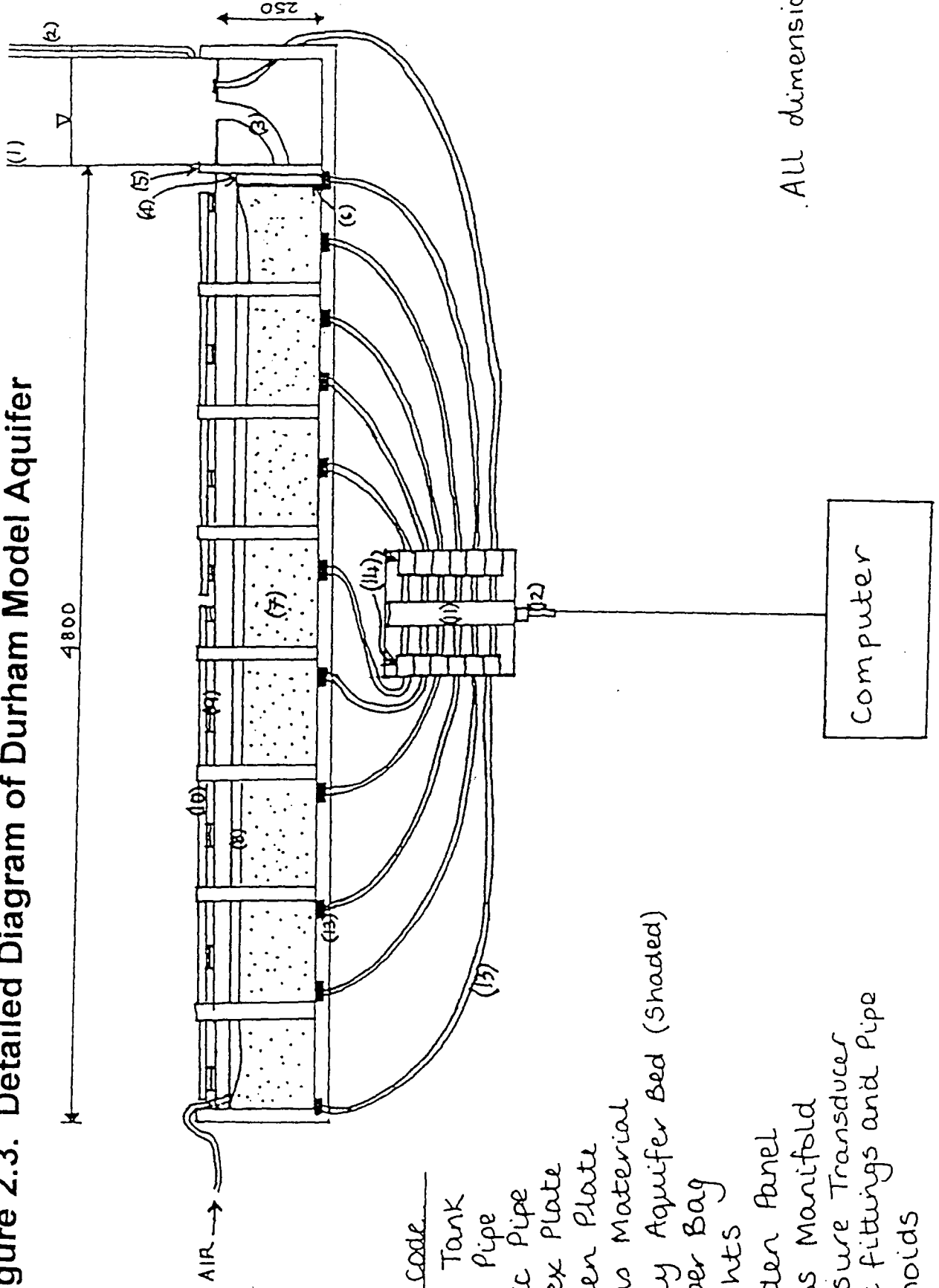
Number Code
1) Water Tank
2) Glass Pipe
3) Plastic Pipe
4) Perspex Plate
5) Wooden Plate
6) Porous Material
7) Sandy Aquifer Bed (Shaded)
8) Rubber Bag
9) Weights
10) Wooden Panel
11) Brass Manifold
12) Pressure Transducer
13) Enot Fittings and Pipe
14) Solenoids

All dimensions in mm.

Photograph A of Model

Photograph B of Model
(Illustrating water storage tank and control pumps for tidal system)
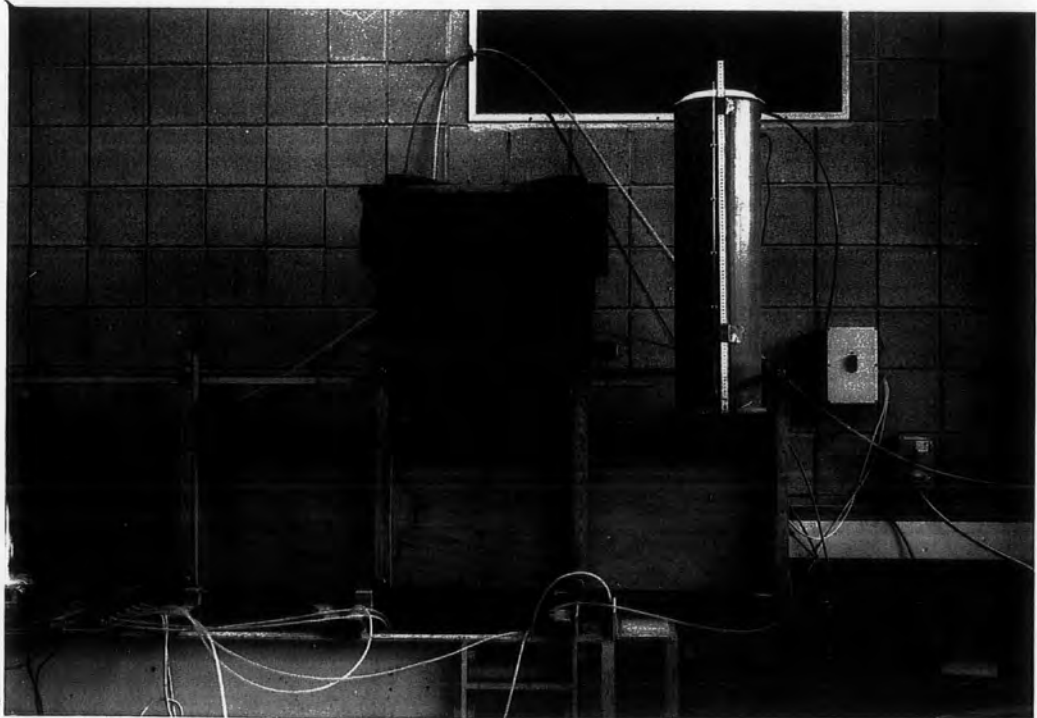
Figure 2.4. Photographs of Durham Model Aquifer

Figure 2.5. Sherburn Sand Grading Curve
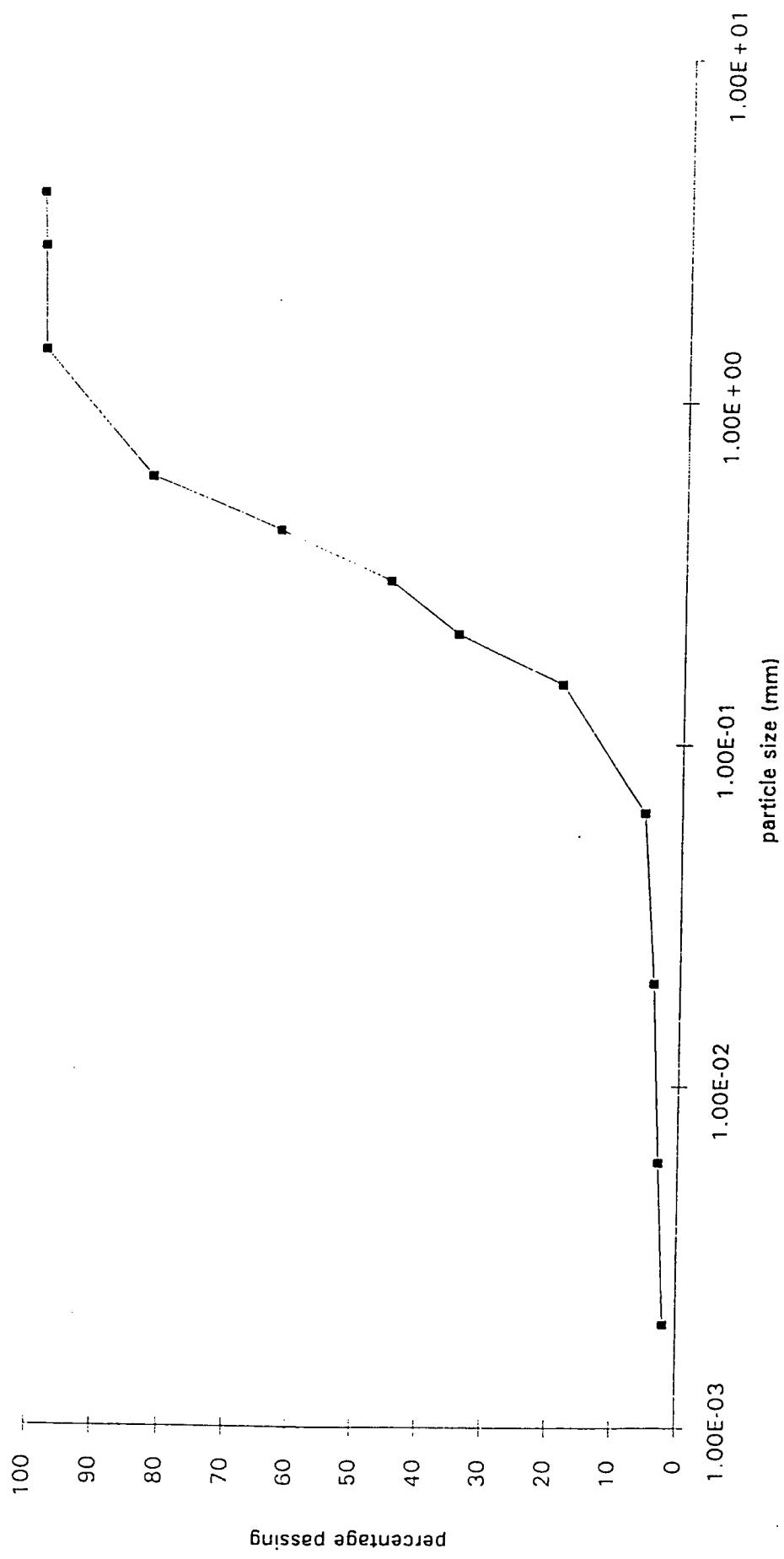
Figure 2.7. Constructed Aquifer System Illustrating Tidal Arrangement

PUMP/
SWITCH
CONTROL

TIDAL
TANK

WATER
STORAGE
TANK

CENTRAL
HEATING
PUMPS

A   B

COMPUTER

4800

250

250

AIR
IN
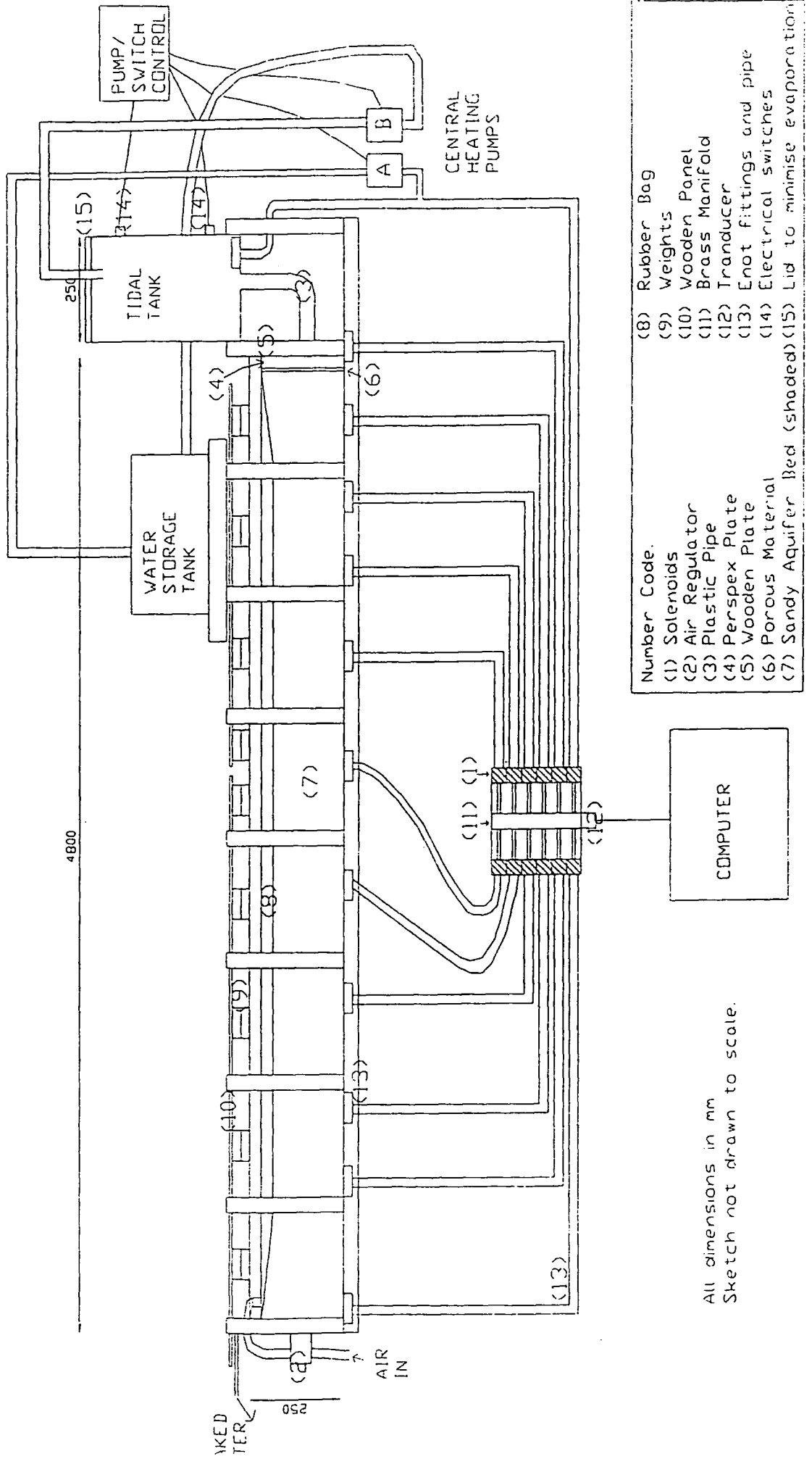
Number Code.
(1) Solenoids
(2) Air Regulator
(3) Plastic Pipe
(4) Perspex Plate
(5) Wooden Plate
(6) Porous Material
(7) Sandy Aquifer Bed (shaded)

(8) Rubber Bag
(9) Weights
(10) Wooden Panel
(11) Brass Manifold
(12) Tranducer
(13) Enot fittings and pipe
(14) Electrical switches
(15) Lid to minimise evaporation

All dimensions in mm
Sketch not drawn to scale.

Figure 2.8. Electrical Tidal Simulation. Water Pressure Variation at Position 1 (in base of tidal tank).
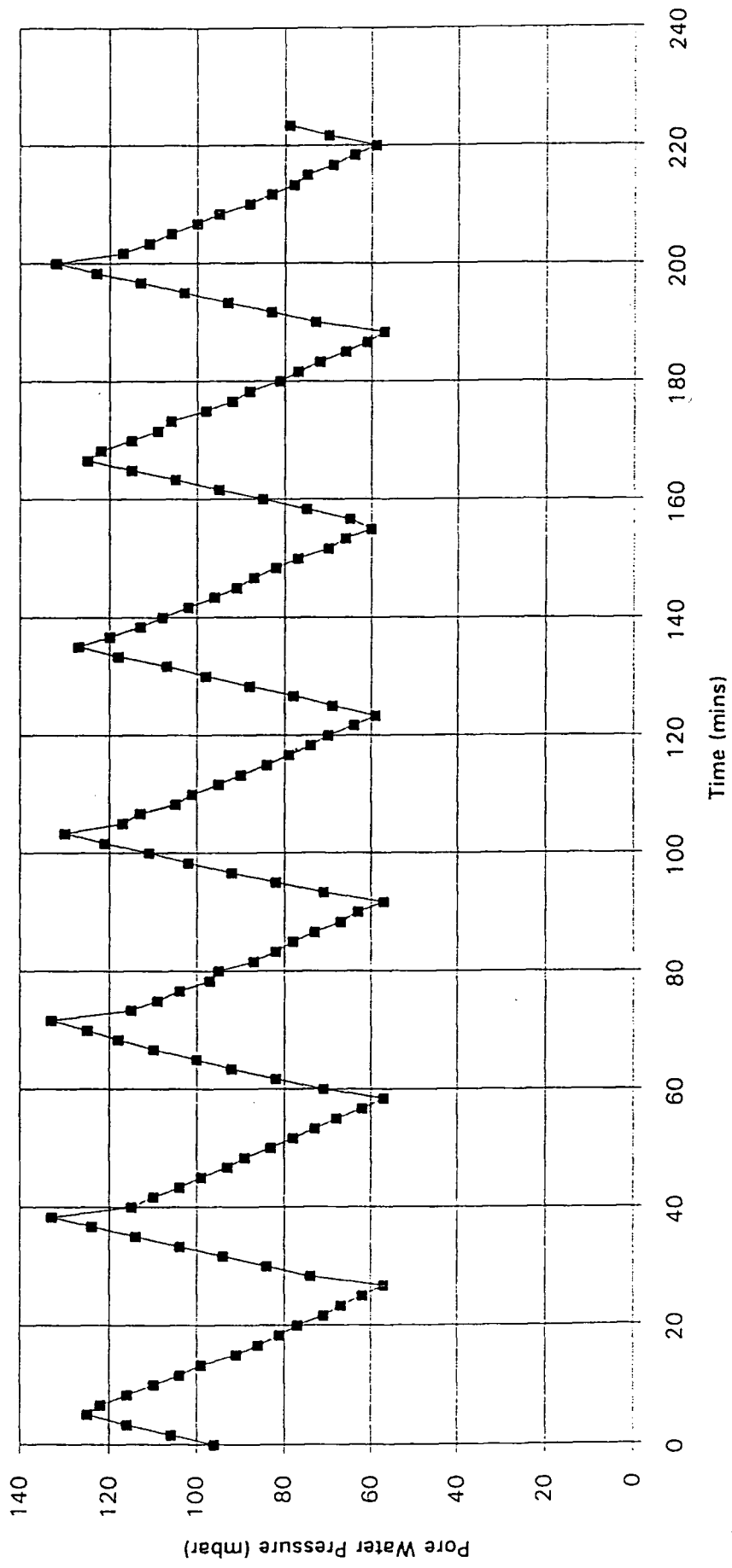
Figure 2.9. Wave Spectra from Fast Fourier Transform Analysis of Results from Position 1 (in base of tidal tank).
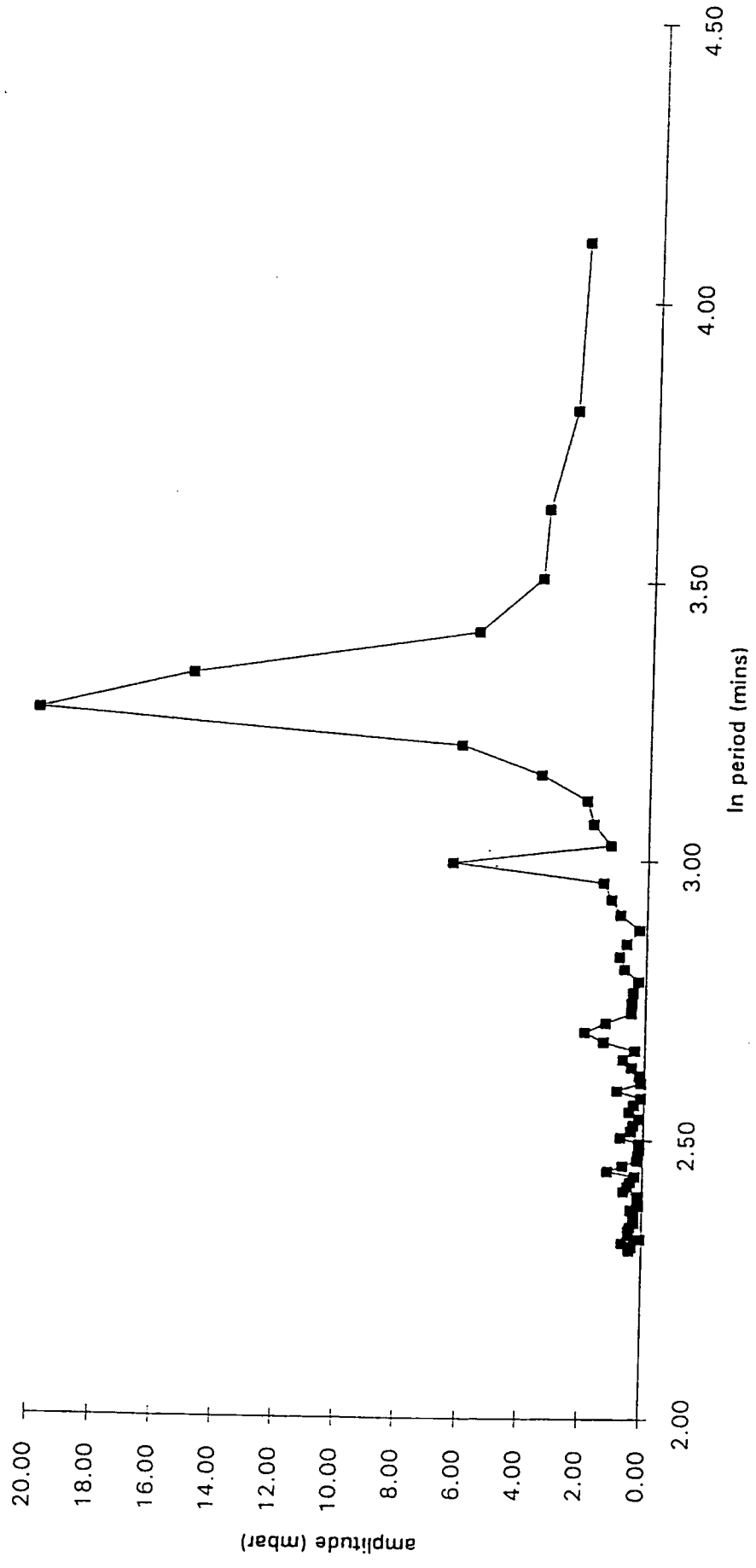
Chapter 3

Laboratory Experimental Work

3.1. Introduction

All work outlined in this chapter formed part of the current programme of post-graduate research.

The purpose of the laboratory work was to investigate tidal effects on the Durham Model Aquifer. However, before tidal testing began, two preliminary tests at steady state were performed using the model. Analyses of results from these tests concluded with estimates for aquifer properties: coefficients of permeability and leakage.

A single tidal test was then carried out on the Durham Model Aquifer whilst controlling the water level in the tidal tank manually. Continual series of pore water pressure measurements were obtained from five different positions in the base of the aquifer container. Recorded data from this test were arranged into graphical form illustrating amplitude decay of the tidal wave with horizontal distance.

Following installation of the tidal system, four tidal tests were performed with the water level in the tidal tank controlled electrically using the system outlined in chapter 2. The period of the simulated tidal cycle was varied slightly between tests. Continual series of pore pressure measurements were obtained from all twelve positions in the base of the aquifer container and tidal tank.

At this point in the testing schedule, essential repairs had to be carried out on the Durham Model Aquifer before further experimental work could be performed. The reason for these repairs and details of their nature is outlined in this chapter.

Once repair work was complete, eleven further tidal tests were carried out. Once again, the period of the simulated tidal cycle was varied slightly between tests.

Continual series of pore pressure measurements were obtained from eleven positions in the base of the aquifer container and tidal tank.

Recorded data from all fifteen electrically-controlled tidal tests were arranged into graphical result form. These graphs illustrate the amplitude decay and time lag of the harmonic wave (initiated in the tidal tank) as it penetrated through the model aquifer. This chapter outlines all experimental work and intervening repairs performed on the Durham Model Aquifer. In addition, a summary of laboratory work results is presented.

3.2. Preliminary Experiments

3.2.1. Introduction

Leakage from the model aquifer was in practice not uniform, but tended to occur through weak points or zones of high permeability in the overlying confining bed. It was beneficial to obtain a mean parameter for the leakage coefficient which could initially be used within a mathematical model to validate the Durham Model Aquifer, and then later as a comparison with results obtained by tidal analyses. This being the case, a test was designed to obtain the average value of permeability and leakage coefficient over the entire length of the model aquifer. The test required applying a flow rate to the water tank (in later tests known as the 'tidal' tank) at a constant rate. Pore water pressure was measured along the length of the model aquifer once steady state conditions were achieved. Results from two such tests are outlined in section 2.6 above and, further to these, as part of the MSc research, two additional tests were performed since the equipment had been out of use for seven months. Any significant changes in model aquifer parameters over the intervening period could therefore be determined. Since these experiments were performed under steady state conditions, when the water pressure did not vary with time, the value of specific storage was irrelevant.

3.2.2. Test One - Constant Flowrate 0.675 litres/min.

3.2.2.1. Method

The computer programme recorded pore water pressure at specified positions in the base of the aquifer model whilst a constant flowrate of 0.675 litres/min was applied to the water tank. A steady state condition was observed once the flowrate into the water tank equalled the leakage rate from the aquifer.

3.2.2.2. Results

Results were arranged in graphical form (pressure head above datum versus horizontal distance from the water tank). This graph is shown in Figure 3.1.

3.2.2.3. Analysis of Results

Average head (h') was calculated from the results shown in Figure 3.1 using the mathematical trapezoidal rule and found to be 0.40 metres. A pressure head change was observed between the base of the aquifer and the free water surface above the rubber bag. This was assumed to have occurred solely between the lower and upper surfaces of the rubber membrane. Application of this assumption resulted in an estimate for the leakage coefficient, β (theory detailed in appendix 3A).

Area of leakage surface, A_S = width of aquifer x length.

$$A_s = (0 \cdot 25 \times 4.8) = 1 \cdot 2 \text{ m}^2$$

leakage flowrate per unit area $= q_L = \dfrac{Q}{A_s} = \dfrac{1 \cdot 1 \times 10^{-5} \text{ m}^3 / \text{s}}{1 \cdot 2 \text{ m}^2} = 9 \times 10^{-6} \text{ m} / \text{s}$

where Q = input flowrate applied to the water tank. At steady state, this is equal to the leakage from the upper surface of the model aquifer.

$$\beta = \frac{q}{h'} = \frac{9 \times 10^{-6}}{0 \cdot 40} = 2 \times 10^{-5} \text{ s}^{-1}$$

The leakage coefficient was estimated to be $2 \times 10^{-5} \text{ s}^{-1}$.

Theory detailed in appendix 3B was applied for the steady state condition, using the following results:

h_1 = 0.475 metres

48

h_2 = 0.375 metres

These values were substituted into equations (3.17) and (3.18) in Appendix 3B. Four reflective waves were considered, since effects further to this were found to be negligible. An iterative process was applied to obtain two distinct relationships between the leakage coefficient and the coefficient of permeability.

The finite element computer model, Curved Valley Model (CVM), was also used to obtain a distinct value for leakage coefficient and permeability for corresponding flow rates and heads, h_1 and h_2. Head h_1 was fixed as also was β, based on the earlier estimate. The coefficient of permeability was then varied until a value for h_2 was produced which compared well with the experimental result.

The relationship between permeability and leakage obtained from the analytical theory and numerical modelling is shown graphically in Figure 3.2. The leakage coefficient resulting from the h_2 analytical solution falls to zero sharply once the coefficient of leakage reaches a 2.2×10^{-5} s^{-1} as illustrated by Figure 3.2. If the coefficient of leakage exceeds this value all the input water leaks from the upper surface of the aquifer before reaching the far end, thus resulting in a value of zero for h_2.

The intersection of the two lines produced from analytical solutions for h_1 and h_2 provided a unique value for the coefficient of permeability of the model aquifer. For this particular test, the unique value for coefficient of permeability was 3×10^{-3} m/s. The unique value for permeability obtained from CVM numerical modelling was 5×10^{-3} m/s, together with a leakage coefficient of 2×10^{-5} s^{-1}. This estimate of leakage coefficient compared well with the earlier estimate. Errors between estimates for the coefficient of permeability were attributed to the sharp fall in the analytical solution for h_2. This effect resulted in a wide range of possible values for permeability within a significantly small leakage range.

Study of Figure 3.2 once more, concluded an estimate for leakage coefficient (intersection of the two analytical solutions) of 2×10^{-5} s^{-1}.

3.2.2.4. Conclusions

For an input flow rate of 0.675 litres/min, the analytical and numerical solutions correlate to give a unique value for the coefficient of permeability for the Durham Model Aquifer of 4 x 10^{-3} m/s; and a unique value for the leakage coefficient of 2 x 10^{-5} s^{-1}.

3.2.3. Test Two - Constant Flowrate 0.5 litres/min.

3.2.3.1. Method

This test was performed in a similar manner to test one outlined above, however a lower flowrate of 0.5 litres/min was applied to the water tank.

3.2.3.2. Results

Results from this second test were dealt with in a similar manner to the first test. A graph of head above the datum versus distance from the water tank was plotted and this is shown in Figure 3.3.

3.2.3.3. Analysis of Results

The average head, h', was calculated from Figure 3.3 by applying the mathematical trapezoidal rule.

h' = 0.31 metres

Once more, following the same procedures as above, the leakage coefficient was estimated to be 2 x 10^{-5} s^{-1}.

Theory outlined in appendix 3B, particularly equations (3.14) and (3.15), were applied for the steady state condition using the following values of h_1 and h_2:

h_1 = 0.43 metres

h_2 = 0.30 metres

The iterative process was repeated to determine a relationship between coefficient of permeability and leakage. This is shown graphically in Figure 3.4. The numerical modelling approach was applied to obtain a distinct value for the coefficient of

permeability corresponding with the experimental results for h_1 and h_2 and the earlier estimate of leakage coefficient.

Figure 3.4 illustrates that the leakage coefficient resulting from the h_2 analytical solution falls to zero sharply once the coefficient of leakage reaches a specific value suggested to correspond with all input water leaking from the upper surface of the aquifer before reaching the second boundary.

3.2.3.4.   Conclusions

For an input flow rate of 0.5 litres/min, the analytical and numerical solutions correlate to give a unique value for the coefficient of permeability for the Durham Model Aquifer of 4×10^{-3} m/s; and a unique value for the leakage coefficient of 2×10^{-5} s^{-1}.

3.2.4.   Summary of Results

Table 3.1 below summarises the data and results from the analysis procedure for the two preliminary experiments.

Test No.	1	2
Flowrate	0.675 litres/min $1.1 \times 10^{-5} m^3/s$	0.5 litres/min $8.3 \times 10^{-6} m^3/s$
Average Head (m)	0.40	0.31
Estimated Leakage Coefficient (s^{-1})	2×10^{-5}	2×10^{-5}
Head at Water Tank h_1 (m)	0.475	0.43
Head at Aquifer end Boundary h_2 (m)	0.375	0.30
Coefficient of Permeability (ms^{-1})	4×10^{-3}	4×10^{-3}
Coefficient of Leakage (s^{-1})	2×10^{-5}	2×10^{-5}

Table 3.1. Summary of Data and Results from Two Preliminary Tests Under Steady State Conditions.

3.2.5. Conclusions

Analysis of the results concluded estimates for the coefficients of permeability and leakage as follows:

Coefficient of permeability: 4×10^{-3} m/s

Coefficient of leakage: $2 \times 10^{-5} s^{-1}$

3.2.6. Discussion

Earlier work, summarised in chapter 2.6, concluded with estimates for the coefficients of permeability and leakage of 3×10^{-3} m/s and $7 \times 10^{-6} s^{-1}$ respectively. The coefficient of permeability based on the later experimental work was of the same order of magnitude as that documented from analysis of earlier tests, although slightly

increased. It was concluded that this small increase was negligible and insignificant. The range of values of permeability for a given soil material is large. Values for this property can vary by several orders of magnitude. Therefore, the two estimates of permeability from these tests can be concluded to compare very well. The experimental work indicated that the leakage coefficient had increased over the seven month period. This significant increase was attributed to the likelihood that, with time, further weak points and zones of high permeability had occurred in the overlying confining bed. This enabled water to leak more easily from the upper surface of the model aquifer.

In summary, it was concluded that the coefficient of permeability of the Durham Model Aquifer had not changed significantly over the seven month period of disuse, whilst the leakage coefficient was slightly increased due to a higher number of weak points in the overlying confining bed, enabling water to flow more easily from the model aquifer.

3.3. Manual Tidal Simulation Experiment

3.3.1. Introduction

The electrical tidal simulation system, described in chapter 2.8, took considerable time to set up. This delay was partly due to time taken for specific components to arrive. Whilst awaiting arrival of necessary equipment, it was decided to use the time constructively by performing a single tidal test on the Durham Model Aquifer whilst controlling the water level in the tidal tank manually.

The form of the input wave in the tidal tank was designed such that it was closely analogous to a sinusoidal waveform in an attempt to simulate tidal waves as accurately as was physically possible. With this in mind, a suitable input wave was selected following experimental work investigating ease and relative accuracy of manually filling the tidal tank. The period of the wave was dependent on the above

experimental work and also chosen to correlate with the range of periods obtainable using the timer base designed for the electrical tidal system. The input wave selected is compared with a sine wave of corresponding period 24.5 minutes in Figure 3.5.

Five of the eleven positions for pore water pressure measurement, located in the base of the aquifer, were selected for the manual tidal simulation experiment. These were positions 3, 5, 8, 10 and 12. The exact locations of these pore water measurement positions is indicated in Table 2.3 in chapter 2 and are recalled below in Table 3.2.

Position	Distance from Position 3 (m)
3	0
5	0.635
8	2.135
10	3.280
12	4.650

Table 3.2. Locations for Pore Water Pressure Measurement for Manual Tidal Simulation Experiment.

3.3.2. Method

The entire series of tidal tests obtained by manual tidal simulation comprised five sub-tests, one for each of the respective pore water pressure measurement positions.

The first sub-test performed was at position 3. The computer was set to continually record measurements of pore water pressure every 100 seconds together with the corresponding time of measurement. Meanwhile, the water level in the tidal tank was controlled manually to closely follow the pattern outlined in Figure 3.5. The water level in the tank was recorded every time a manual alteration was made to the tidal system, together with the corresponding time of that alteration. The test was continued for approximately four tidal cycles which inferred a sub-test duration equivalent to four periods (approximately 100 minutes).

The experimental procedure was repeated four times, whilst measurements of pore water pressure were recorded from each of positions 5, 8, 10 and 12 respectively.

3.3.3. Results

The pressure head was plotted versus time and compared with the head variation of the input wave in the tidal tank. Results from these five sub-tests are shown in Figures 3.6, 3.7, 3.8, 3.9 and 3.10 corresponding to positions 3, 5, 8, 10 and 12 respectively.

3.3.4. Analysis of Results - Part One

The objective of this first part of the analysis procedure was to arrange the recorded data into a form suitable for subsequent tidal analyses. This would enable determination of aquifer properties considering analytical theory (the second part of the analysis procedure). As suggested from tidal analyses work by previous authors, results were arranged to illustrate amplitude decay of the simulated tidal (input) wave with horizontal distance. This comprised the first part of the analysis procedure. The time lag was not calculated from this manual test because it was anticipated that measurement errors would be so significant as to render the results meaningless.

In order to accurately determine the amplitude decay of the simulated tidal wave (or input wave), it was necessary to split the wave into its sinusoidal constituents.

Therefore, Fast Fourier Transform Analysis, using WAVETRAN[1], was carried out, both of the simulated tidal wave and also of the pressure waves it initiated.

Figures 3.6 to 3.10 illustrate that there was a time delay before the pore water responded to the input wave with a regular pattern (i.e. fluctuated about a constant mean value). Results before a steady tidal pattern was observed were ignored. Subsequent results were extrapolated to provide sufficient data (four periods) for fast fourier transform (FFT) analysis.

---

[1] WAVETRAN - software designed by Dr. Stephen Thomas for Fast Fourier Transform Analysis.

Appendix 3C illustrates the wave spectra produced as a result of the analyses.

From the wave spectra, the amplitude and period of the governing, primary sinusoidal component of the wave was established. Secondary sinusoidal constituents of the waveform were unclear.

Table 3.3 below summarises the amplitude and period of the governing sinusoidal component of the input wave and of the wave observed at each of the pore water pressure measurement locations.

Location of Pore Water Pressure Measurement	Amplitude of Governing Sine Wave Constituent (mbar)	Period of Governing Sine Wave Constituent (mins)
Position 3:- 0.3 m	15.752	26.7
Position 5:- 1.08 m	11.479	26.7
Position 8:- 2.58 m	12.058	22.9
Position 10:- 3.725 m	15.968	26.7
Position 12:- 5.095 m	7.089	26.7

Table 3.3. Summary of Fast Fourier Transform Analyses of Results from Manual Tidal Simulation Tests.

From Table 3.3, it can be seen that period of the governing waveform at position 8 is lower than those at other positions. The amount of data available implied that FFT analysis allowed distinction between periods of 2133s, 1600s and 1280s indicating that the accuracy to which the period of a governing waveform could be detected was limited. Therefore a discrepancy between the period at position 8 and those at alternative positions is insignificant, considering the accuracy of the analyses method. Similarly, from the wave spectra in Appendix 3C, the period of the governing sine wave and that at the corresponding pore pressure measurement location appears to vary slightly. This suggests a possible change in the period of the wave as it is transmitted through the pore water of the model aquifer. However, with the minimal

56

amount of data available for analyses, the results will inevitably show inaccuracies. It should also be remembered that the manual system of controlling the tidal wave implied that the input wave was not particularly regular due to human response times and variation in tap pressures.

The results of Table 3.3. were summarised to form a decay curve. Due to the unknown permeability of the silt within the plastic pipe linking the tidal tank and model aquifer, results were considered with respect to position 3. It was assumed that the aquifer soil material beyond position 3 was homogenous. Material close to the tidal boundary was likely to be affected by the simulated tide causing silting and heterogeneities making the permeability of the aquifer significantly different to that further from the tidal boundary. The amplitude decay curve is shown in Figure 3.11. These results will be discussed further in chapter 6 of the thesis.

3.4. Four Tidal Experiments Using Electrical Tidal Arrangement

3.4.1. Introduction

Once the electrical tidal system was completely established following the work outlined in chapter 2.8, electrically simulated tidal tests were performed. The long-term objective of these tests was to investigate the tidal analysis method for determining aquifer properties. In order to make this possible, the amplitude decay and time lag of a simulated tidal wave were determined at various horizontal positions from a tidal boundary. The experimental procedure and arrangement of data to determine amplitude decay and time lag for the first four electrical tidal tests is outlined below.

3.4.2. Method

The following experimental method was carried out for each of the four series of tests. The period of the simulated tidal cycle was varied slightly between the four tests and was set using the timer base. This equipment proved difficult to calibrate and it was found that alterations of the fine scale for period adjustment were not always significant. Therefore, the exact period of a specific tidal test was established from the recorded data once a test was complete.

The water tank was emptied and filled repeatedly under the control of the electrical tidal system. The equipment was left to run for four hours, during which time it was anticipated that effects of the simulated tide would be fully realised within the model aquifer. After this time, pore water pressure was measured and recorded from each of the twelve positions in both the base of the aquifer model and tidal tank. The time of each measurement was also recorded. Measurements were recorded at each position at approximately 100 second intervals, for periods of 5.3 hours, after which point the designed computer software switched the system to measuring pore water pressure from the next consecutive position in the base of the model aquifer. Earlier experimental work showed that a time interval of 100 seconds between readings was required for the water pressure in the brass manifold to reach equilibrium with that in the pipe linked to the aquifer model. A total of 192 pore water pressure measurements were recorded for each of the individual positions.

The above procedure was repeated for three further series of tests whilst the period of the tidal cycle was varied slightly between series of tests.

3.4.3. Results

Results of pore water pressure and their corresponding time were plotted for each of the twelve different measurement locations. These results were arranged graphically for series 1 and 2 and are contained within Appendix 3D of the report. Results for series 3 and 4 are presented in slightly less detail in Appendix 3E.

The results for position 10 did not illustrate tidal behaviour, but a very gradual decrease in pore water pressure. To investigate the reason for this, solenoid 10 was tested and operation was found to be temperamental. After each of the test series, attempts were made to solve this problem whilst avoiding significant amounts of air becoming entrapped within the system. Once the switch was thought to be repaired, a further series of tests would be performed. Results illustrated that the switch was still not functioning correctly. It was thought that silt from the model aquifer was preventing correct operation of the switch. Apart from this fault at position 10, the equipment seemed to be running well. Solving the fault at position 10 would take considerable time and would inevitably result in further air entrapment in the system. Results from other measurement positions were deemed satisfactory, and therefore it was decided to continue the test programme without the use of solenoid 10 and measurements of pore water pressure from this position.

Results from series 3 and 4 indicated a lower amplitude of wave at position 2 than those at later positions in the aquifer (up to position 11). It was thought that this was due to lower permeability silt material in the vicinity, brought about by the nearness of position 2 to the boundary with the tidal tank.

3.4.4. Analysis of Results - Part One

As was the case with the manual tidal simulation experiment, the objective of this first part of the analysis procedure was to arrange the recorded data into a form suitable for subsequent tidal analyses. Results were arranged to illustrate amplitude decay and time lag of the simulated tidal wave with horizontal distance. This comprised the first part of the analysis procedure.

3.4.4.1. Amplitude Decay

Fast Fourier Transform (FFT) Analysis, using WAVETRAN, was carried out, both of the simulated tidal wave and also of the pressure waves it initiated. This analysis concluded the amplitude and period of the governing sinusoidal components of each 'tidal' wave in series 1, 2, 3 and 4.

59

It was found that 194 data points were required for detailed fourier transform analysis and therefore results were extrapolated to provide sufficient data. Appendix 3F illustrates the wave spectra produced for series 1, 2, 3, and 4 as a result of the analyses.

From the wave spectra, the amplitude and period of the primary sinusoidal component of the wave was established. The amount of data available implied that FFT analysis allowed distinction between periods of 2743s, 2400s, 2133s, 1920s, 1745s and 1600s. This was significantly more detailed than analysis of manual tidal data. The FFT analysis also indicated a clear *secondary* sinusoidal component of the 'tidal' wave with a smaller period and amplitude than the primary constituent. Thus, from a single test series, amplitude decay of primary *and* secondary components could be concluded.

Due to results of low amplitude at position 2, thought to be the result of low permeability material in that area, and the silted pipe between the tidal tank and aquifer, amplitude decay of the 'tidal' wave was calculated with respect to position 3. At and beyond this location, the effects of the tidal boundary where thought to be negligible.

Details of the horizontal distances of measurement positions with respect to position 3 are detailed in Table 3.4 below.

Position	Horizontal Distance from Position 3 (m)
3	0
4	0.275
5	0.635
6	1.065
7	1.575
8	2.135
9	2.665
10	3.280
11	3.950
12	4.65

Table 3.4. Relative Locations of Measurement Positions with Reference to Position 3.

The periods of the primary and secondary constituents of series 1, 2, 3 and 4 are outlined below in table 3.5.

	Series 1	Series 2	Series 3	Series 4
Primary Period (s)	1920	2133	2133	2400
Secondary Period (s)	960	1010	1067	1200

Table 3.5. Periods of Primary and Secondary Constituents for Series 1, 2, 3, and 4.

The graphs of amplitude decay with horizontal distance for the primary constituent are indicated for series 1, 2, 3 and 4 in Figures 3.12, 3.13, 3.14 and 3.15 respectively. Graphs illustrating amplitude decay of the secondary component for series 1, 2, 3 and 4 are in Figures 3.16, 3.17, 3.18 and 3.19 respectively.

3.4.4.2. Time Lag

The objective was to determine time lag of the pressure wave at various horizontal distances with respect to position 3. The reason that position 3 was selected as the reference position was outlined in section 3.4.4.1 above.

Several alternative methods were investigated for determining the time lag. These included:

1. Approximating a sine wave of suitable period and amplitude to the pore water pressure variation pattern at position 3. This was then extrapolated to overlie pore water pressure variation patterns for later positions. The mean pore pressure about which the data varied was established, as was the mean of the superimposed sine wave. Intersections of the data pattern and sine wave with the corresponding mean pressure were compared. From this, the time lag between the sine wave and data variation was ascertained. This approach proved to be long-winded and over-detailed in comparison to the accuracy to which the time lag could be established.

2. Investigating the use of WAVETRAN software to determine time lag. The software only proved useful if results were recorded simultaneously. This was not the case for the tidal results. Altering the programme to suit would be difficult and therefore this approach was considered unsatisfactory.

3. Writing a new programme to determine time lag. Input data for the programme included (a) *times* for four peaks of the reference pressure wave i.e. position 3, (b) two *data values* for all consecutive positions which represented peaks in the harmonic wave. Errors in this approach were large due to the small amount of input data. Lack of useful results for position 10 also posed a problem.

4. A similar approach to 1. above, but less detailed. This involved relating pressure variations to those at a previous position. A graph was produced which illustrated, in detail, the link between consecutive positions (e.g. positions 3 and 4). The mean pore pressure about which the data varied at both positions was established. The average period of the wave at the earlier position was calculated by physically measuring the distances between points where the data

crossed that mean, and relating this to the scale on the x-axis. Points of intersection were then projected for late time. The time of these projected points was compared with times of mean-intersection, based on data from the next consecutive measurement position. From this the time lag was established. It was appreciated that this method induced large errors in the computation of time lag. However, it was thought that the effect of these errors would be averaged out when considering several series of results.

Approach 4. was deemed the most suitable and convenient. It was the easiest method and incorporated a suitable amount of data points.

The time lag for position 1 was not established since the measurement of pore pressures was paused mid-way through the series. The reason for this momentary pause was to download data to monitor whether this, the first electrically simulated tidal test, was proceeding correctly.

Appendix 3G provides detailed graphs illustrating the method of calculation for time lag for series 2 results. This same method was used for results from series 3 and 4. Figures 3.20, 3.21 and 3.22 illustrate time lag with respect to position 3 for series 2, 3 and 4 respectively.

3.5. Essential Repair Work of the Durham Model Aquifer

During the Christmas and New Year period, the equipment was left unattended. Following the break, operation of the equipment was observed to cause large vigorous air bubbling in the plastic pipe linking the tidal tank and model aquifer. This effect was particularly strong when the water level in the tidal tank was low. It caused significant waves in the tidal tank resulting in incorrect operation of switch B. Air bubbles were also observed in the water overlying the model aquifer. It was concluded that a significant quantity of air was leaking from the rubber bag, possibly in a number of places. The air pressure in the rubber bag was reduced to a minimum

considering that it had to at least balance the effect of water head in the tidal tank. This reduced bubbling in the tidal tank, however it was not eliminated and it was probable that air was also leaking into the model aquifer itself. It was anticipated that this would significantly affect pore water pressure measurements thus distorting results.

Therefore, it was necessary to dismantle the upper part of the model aquifer to investigate the source of the problem. Water that had leaked from the aquifer was overlying the wood to the level of the drain. As much water as possible was siphoned off before the dismantling process began. A water and solids vacuum cleaner was also used to remove water and silts that had reached the upper surface of the aquifer in the leaked water. The wooden panels overlying the rubber bag were removed and upper side panels illustrated in Figure 3.23 were unscrewed. Once again water and silts were removed before the air bag was lifted out of place. The 5 metre long rubber bag was filled with air and tested for leaks in a large water filled tank. Two significant leaks were observed and their locations marked. It was decided to repair these leaks by covering them with small rubber patches. The rubber bag was removed from the tank and dried thoroughly. Patches were constructed from thin rubber material. Wire-tack adhesive was used to stick these patches over the marked holes. Once the adhesive was set, the rubber bag was further tested for air leaks following the same procedure described earlier. All observed air leaks were carefully repaired. On completion of this work, the model aquifer was able to be reconstructed.

It was decided to modify the method of attachment of the upper side panels. Whilst leakage from around the edges of the rubber bag was required, it was anticipated that existing holes may incur more leakage than had earlier been recorded due to wear and tear during the renovation work. In an attempt to avoid this foreseen problem, the former method of brass attachment screws was replaced by zinc coated bolts which passed right through the walls of the wooden container. These would be easier to tighten than the screws, and a better seal could be obtained. Holes were drilled into the sides of the wooden container in the locations of the existing screw holes. The model aquifer was then reconstructed using bolts.

Following this repair work, the tidal system was set to run for three days to verify that the model was functioning correctly.

3.6. Eleven Further Tidal Experiments Using Electrical Tidal Arrangement

3.6.1. Introduction

Following the repair work, eleven further tidal tests were performed. Fast fourier transform analysis of the results concluded graphs illustrating primary and secondary amplitude decay of the 'tidal' wave with horizontal distance. The time lag of the pressure wave as it penetrated through the model aquifer was also determined for each of the eleven series of results.

3.6.2. Method

The computer programme was altered to record 195 pore water pressure measurements from each position. This avoided the need to extrapolate results for fast fourier transform analysis.

Apart from this minor alteration, the experimental method for each of the eleven series exactly followed the procedure outlined in section 3.4.2 above.

3.6.3. Results

Results were dealt with in a exactly the same manner to that outlined in section 3.4.3 above.

3.6.3.1. Amplitude Decay

Fast fourier transform analysis using software, WAVETRAN, allowed results of amplitude decay to be determined. Figures 3.24 to Figure 3.34 illustrate primary

amplitude decay for series 5 to 15 inclusive. Secondary amplitude decay is illustrated in Figures 3.35 to 3.45 for series 5 to 15 inclusive.

3.6.3.2. Time Lag

The time lag of the tidal waves for series 5 to 15 was determined by the same method as that outlined in section 3.4.4.2 above. Time lag of the tidal waves with horizontal distance is illustrated in Figures 3.46 to 3.56 for series 5 to 15 inclusive.

3.7. Discussion of Results from Tidal Experiments

The primary and secondary amplitude decay graphs from all tidal experiments were compared. Time Lag graphs were also compared. It was realised, however, that the variety in periods meant that direct comparison was unhelpful, and therefore merely general trends were noted.

Ferris' theory detailed a straight line relationship between time lag and horizontal distance. Time lag graphical results suggested the possibility of such a relationship. Time lag was deduced to an accuracy of ± 50s. Points on the graph close to the tidal boundary would therefore incorporate a larger percentage error than those toward the far end of the aquifer.

Ferris' theory outlined an exponential relationship between amplitude decay and horizontal distance. Study of the decay graphs suggested the possibility of such a relationship. Amplitude decay appeared less rapid in the region close to the tidal tank. This region was possibly significantly affected by water flow into the aquifer from the tidal tank and therefore soil material may be finer and less permeable. In addition, the aquifer is likely to have suffered invasion of bacterial growth. This may have affected some regions of the aquifer more than others, thus leakage from the aquifer was unlikely to have been uniform over the entire length. The seal around the

upper surface and confining bag was also non-uniform, resulting in varying leakage over the length of the aquifer.

In a few cases the amplitude decay exceeded 100% at considerable distance from the tidal tank. Also, the amplitude decay appeared to rise as distance from the tidal boundary increased. These irregularities were attributed to air trapped in soil pores and pipework, and impermeable lenses bounding pore pressure measurement locations.

In addition to the problems outlined above, errors in measurements will occur due to the occasional irregularities in the behaviour of the tidal system. This was observed in data for series 2, position 6 (Appendix 3D-18), and caused a deviation in the harmonic pattern.

The fourier transform analysis would also induce errors since the sensitivity of procedure was such that periods were detected to the nearest 2 minutes. These errors were not considered significant.

The percentage error in the large amplitude of the primary sinusoidal waveform is likely to be considerably less than the percentage error in the smaller amplitude of the secondary constituent. Therefore, primary amplitude decay results were thought to be more accurate than the secondary decay results.

In conclusion, the general pattern of graphical results was similar for all tidal test series.

3.8. Summary of Tidal Test Results

The test schedule is summarised in Tables 3.6 and 3.7 overleaf. In addition, the periods of the primary and secondary constituents of the tidal wave for each of the tests is outlined.

Primary and Secondary amplitude decay in addition to timelag graphs were obtained from results.

Graphical results of similar period are compared and discussed in detail in chapter 6.

Table 3.6. Summary of Tidal Experimental Work Prior to Repair Work.

	Manual	Series 1	Series 2	Series 3	Series 4
Start Date	17/11/94	30/11/94	2/12/94	6/12/94	9/12/94
End Date	22/11/94	2/12/94	6/12/94	9/12/94	12/12/94
Primary Period (s)	1600	1920	2133	2133	2400
Secondary Period (s)	NONE	960	1010	1067	1200

Table 3.7. Summary of Tidal Experimental Work Following Repairs.

	Series 5	Series 6	Series 7	Series 8	Series 9	Series 10	Series 11	Series 12	Series 13	Series 14	Series 15
Start Date	6/3/95	10/3/95	16/3/95	22/3/95	28/3/95	30/3/95	5/4/95	25/4/95	28/4/95	5/5/95	10/5/95
End Date	9/3/95	13/3/95	19/3/95	26/3/95	30/3/95	3/4/95	8/4/95	28/4/95	2/5/95	9/5/95	13/5/95
Primary Period (s)	2400	2743	2400	1600	1920	1920	1746	1920	1920	1920	1920
Secondary Period (s)	1200	1371	1200	533.3	662	662	873	914	619	960	960

Figure 3.1.

Test 1 - Applied Flowrate 0.675 litres/min. Pressure Head versus Horizontal Distance (from Water Tank) at Steady State Conditions.
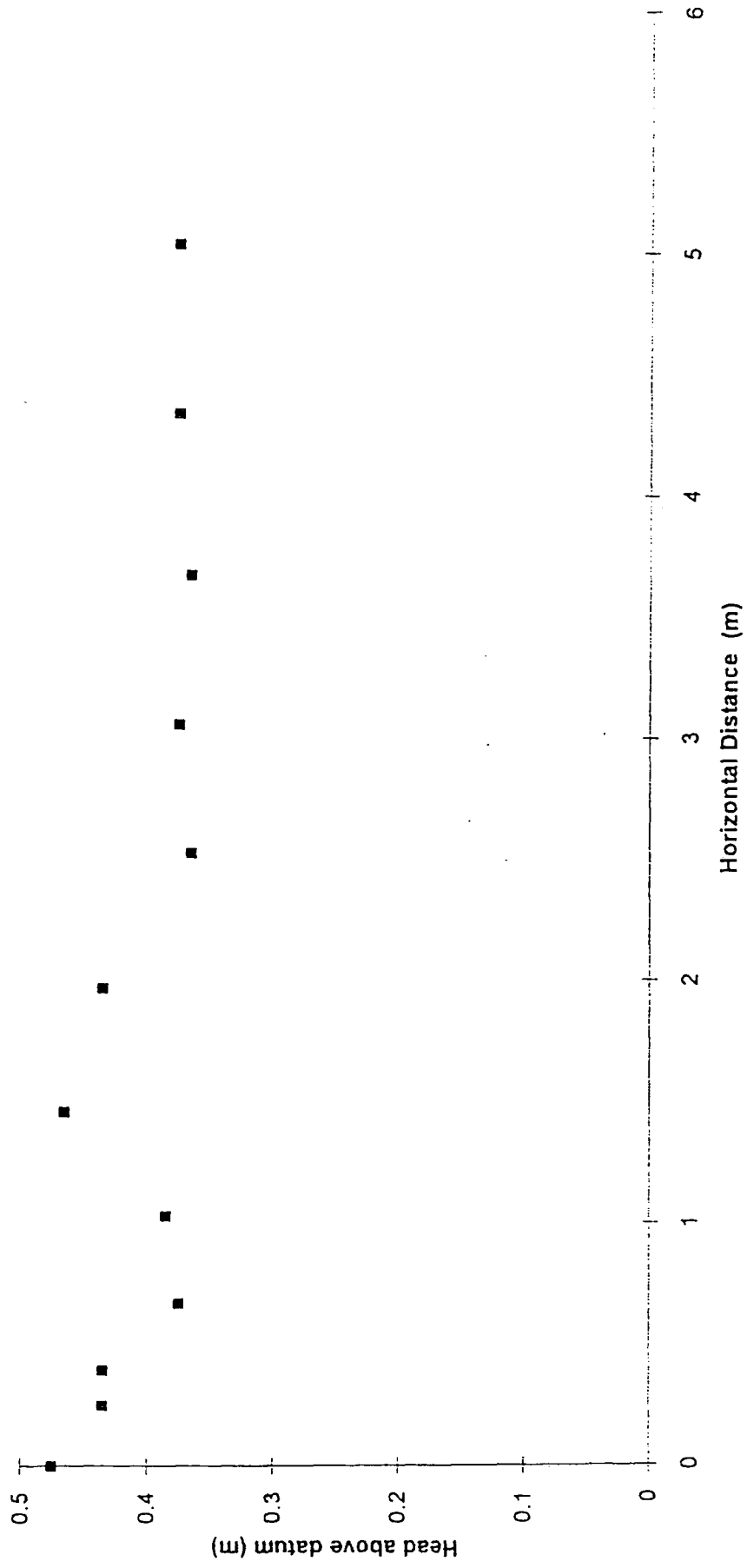
Figure 3.2.

Test 1 - Applied Flowrate 0.675 litres/min. KB Relationship from Infinite Image Well Theory.

K=coefficient of permeability (m/s)

B=leakage coefficient (/s)

——— analytical soln for h1   – – – – analytical soln for h2   ■   numerical result
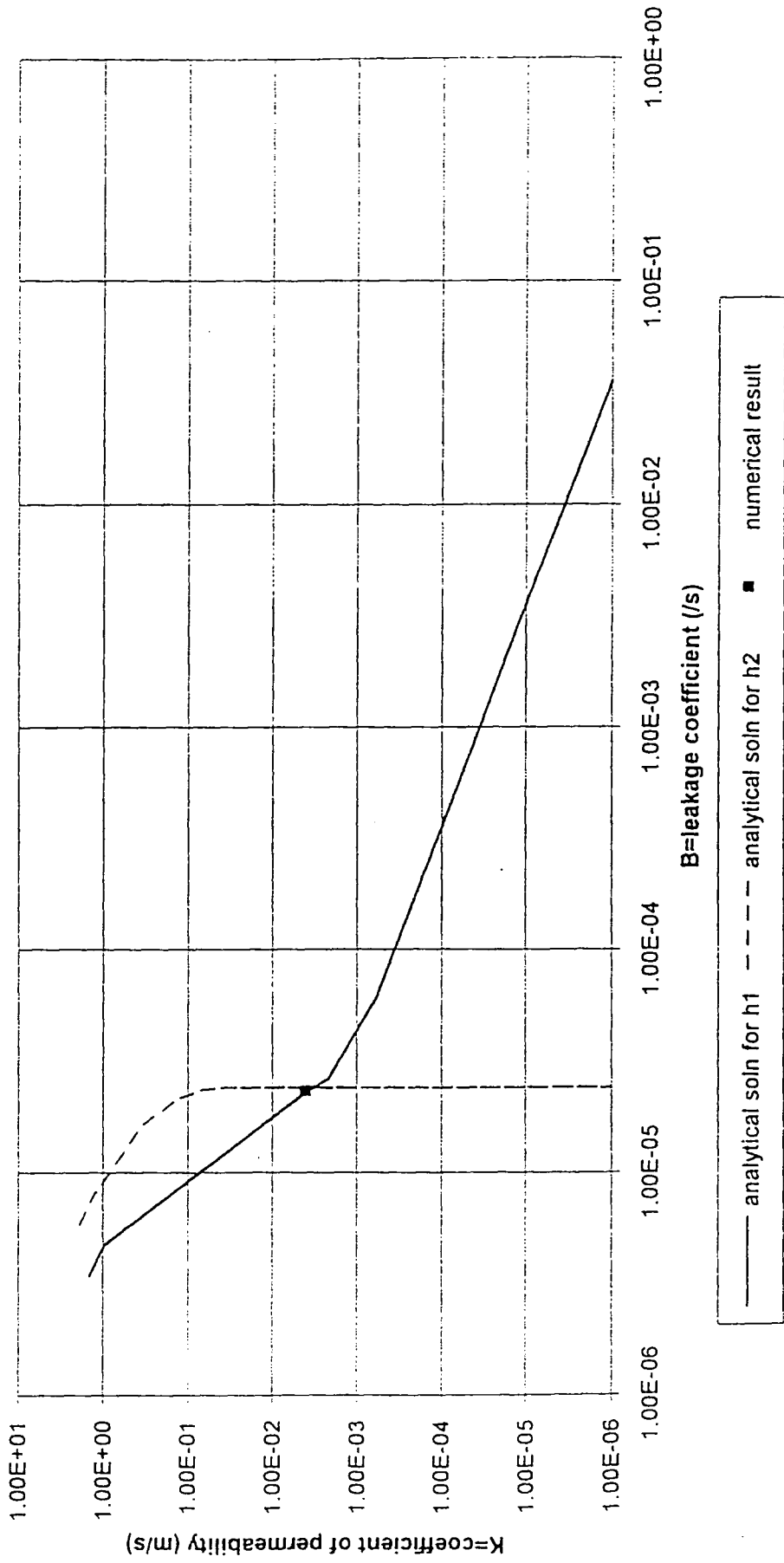
Figure 3.3.

Test 2 - Applied Flowrate **0.5** litres/min. Pressure Head versus Horizontal Distance (from Water Tank) at Steady State Conditions.
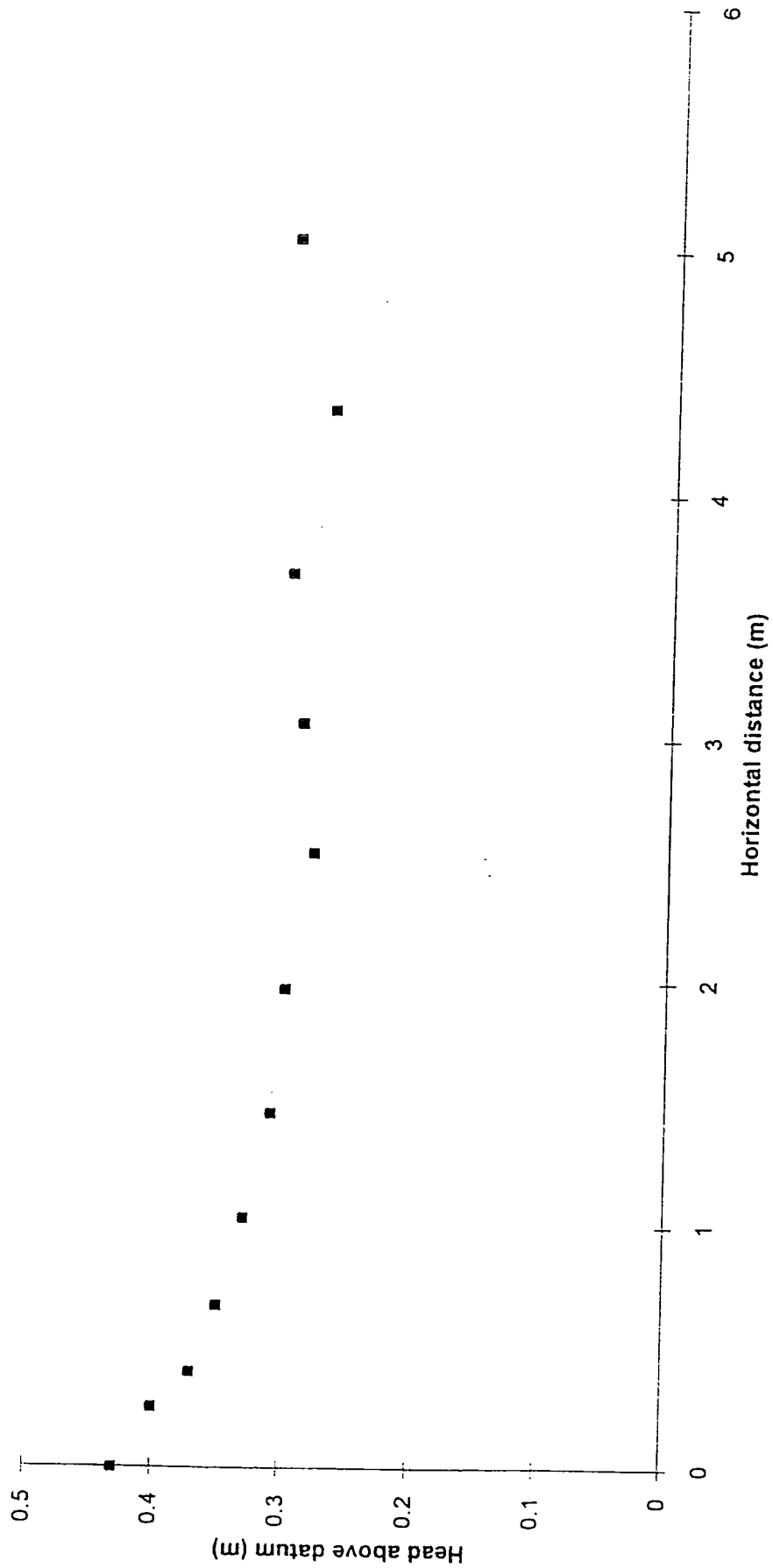
Figure 3.4.

Test 2 - Applied Flowrate 0.5 litres/min. KB Relationship from Infinite Image Well Theory.
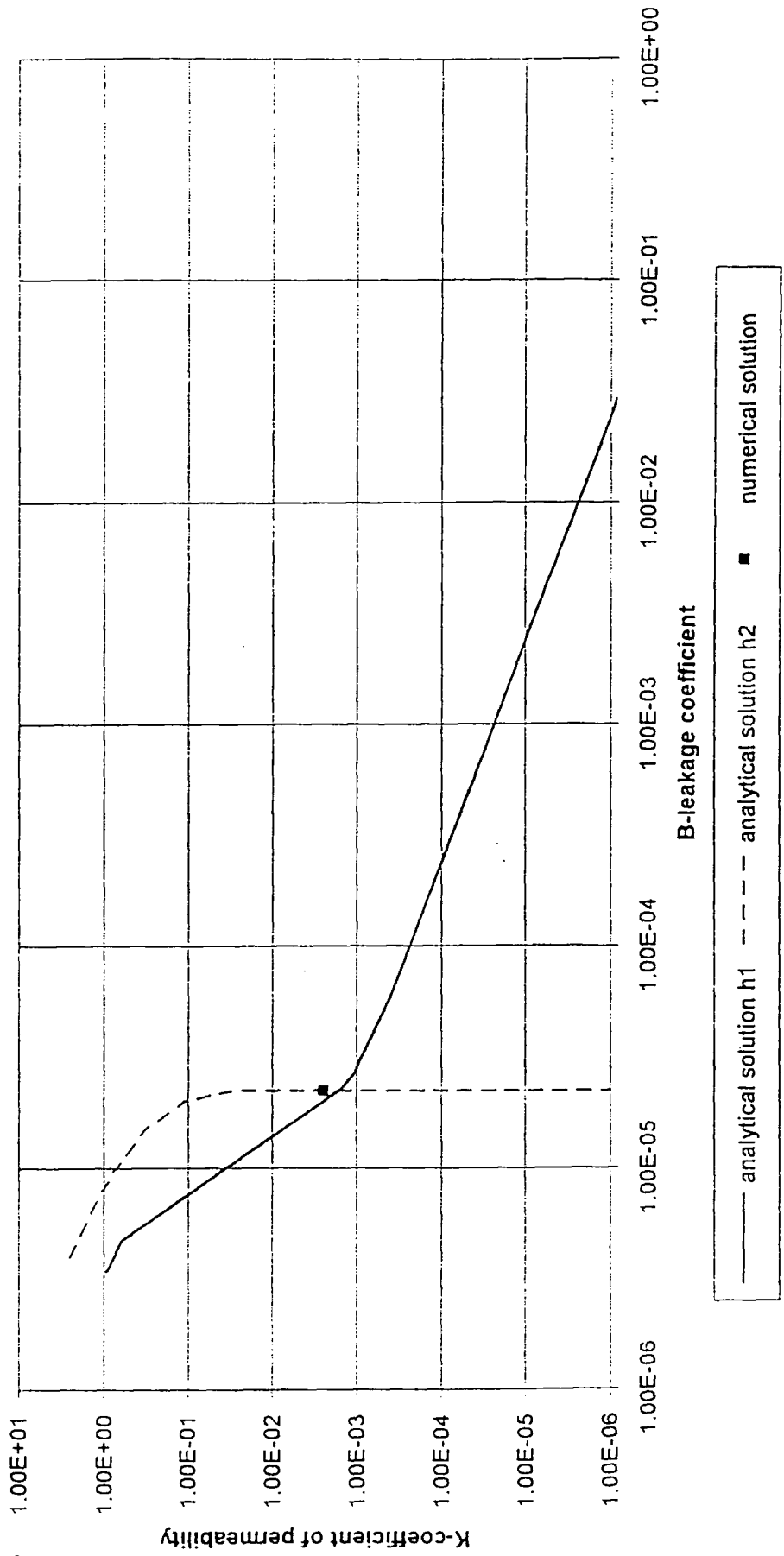
Figure 3.5. Comparison of Manually Controlled Water Level in Tidal Tank with Sine Wave of Corresponding Period.
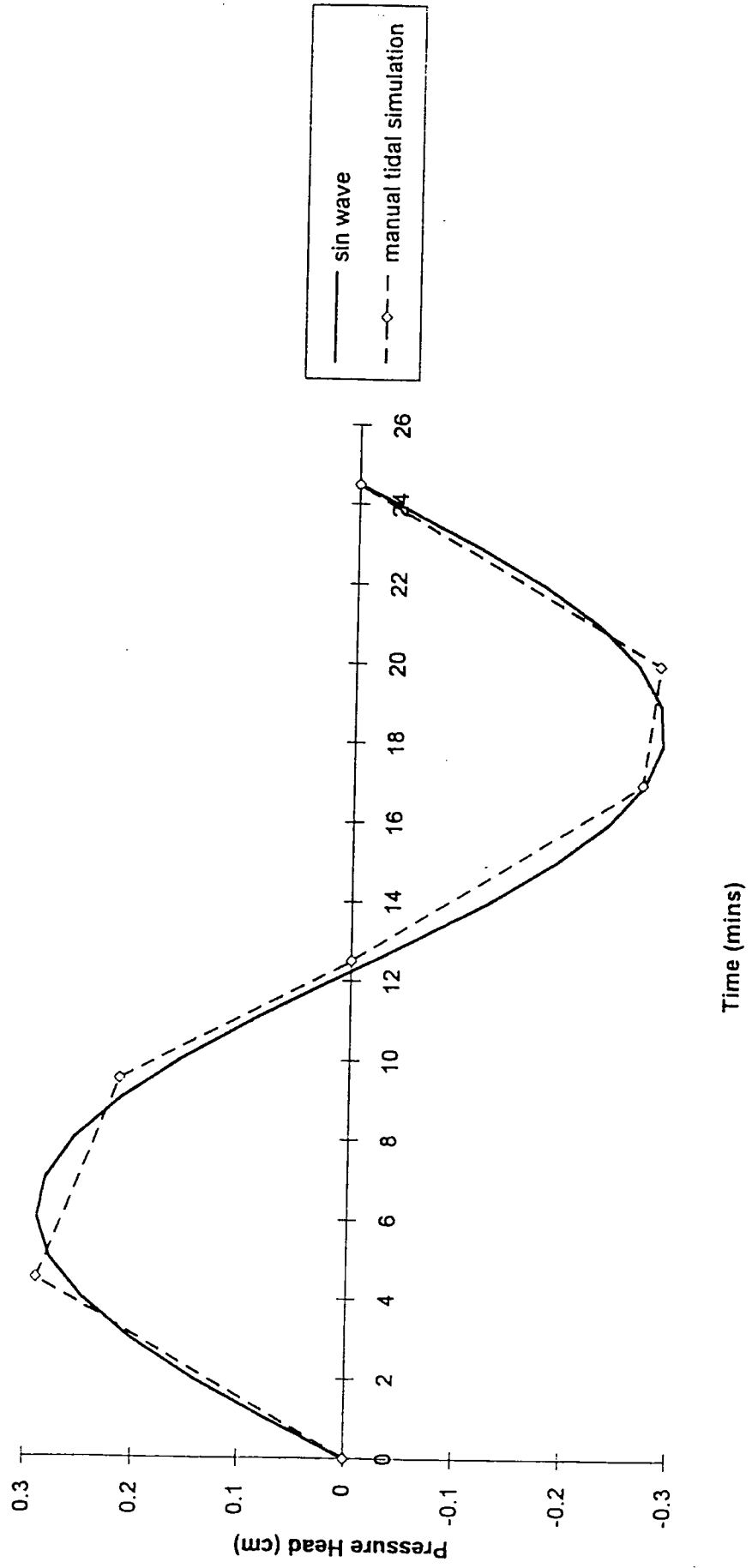
Figure 3.6. Variation of Pore Water Pressure at Position 3 and Corresponding Simulated Tidal Fluctuation (Input Wave).
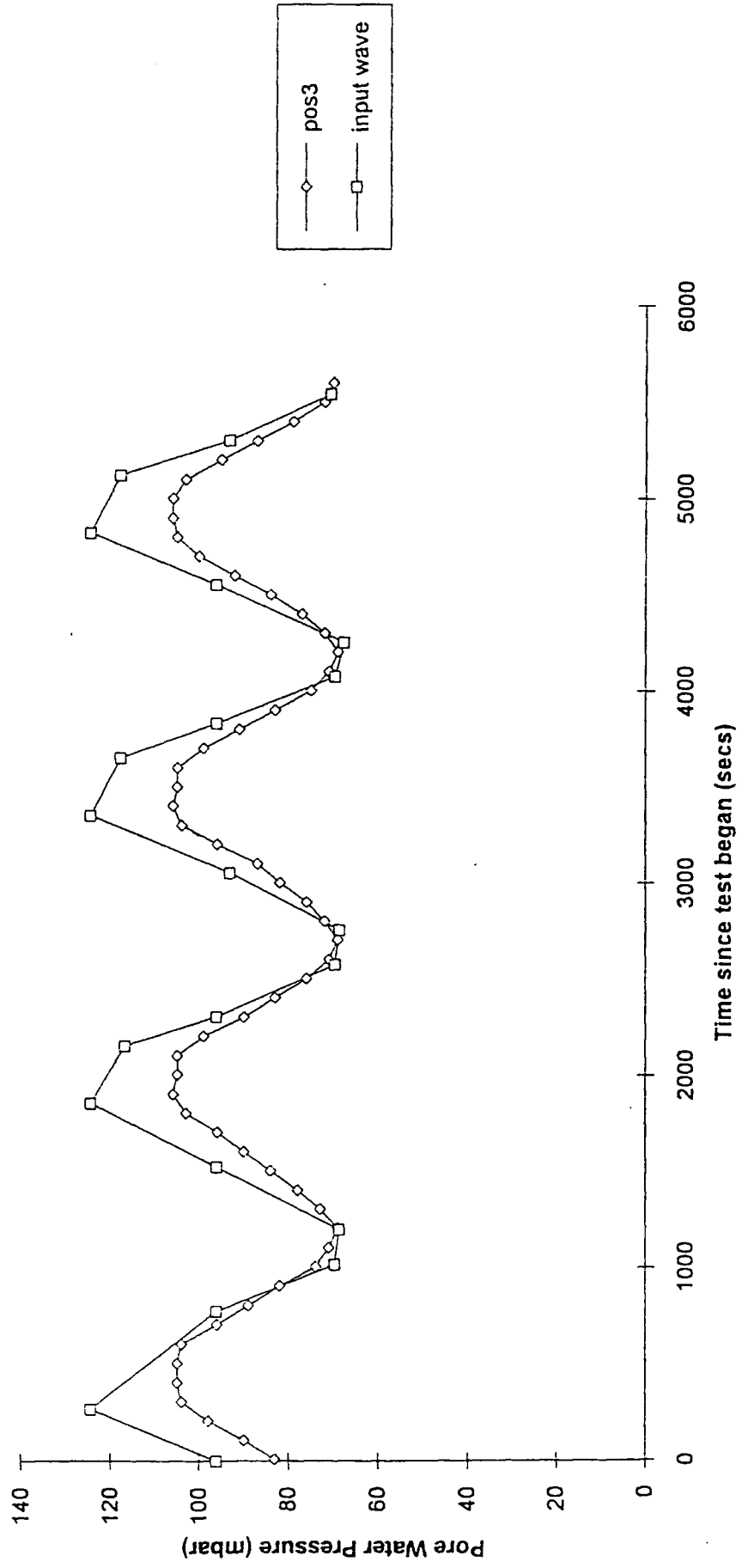
Figure 3.7. Variation of Pore Water Pressure at Position 5 and Corresponding Simulated Tidal Fluctuation (Input Wave).
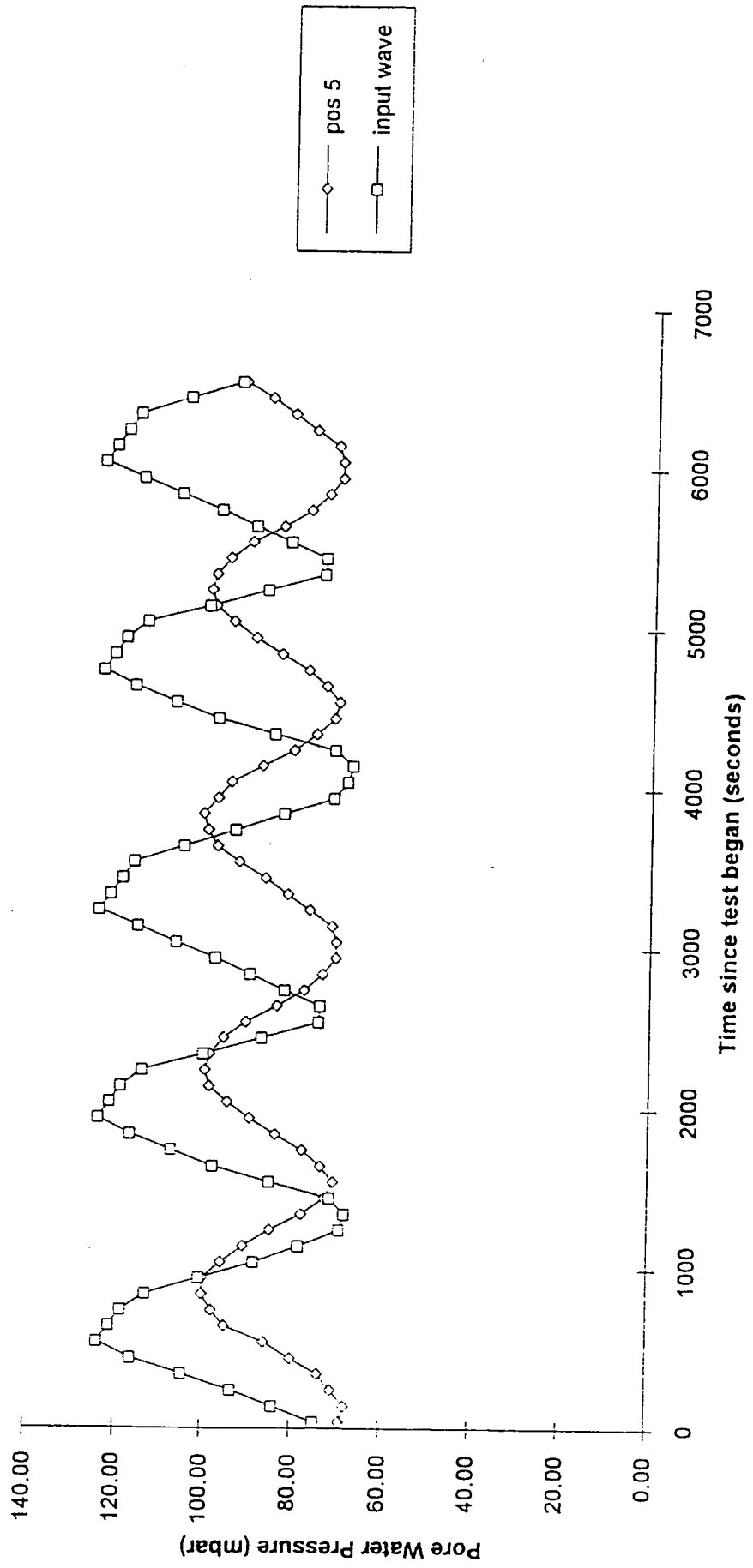
Figure 3.8. Variation of Pore Water Pressure at Position 8 and Corresponding Simulated Tidal Fluctuation (Input Wave).
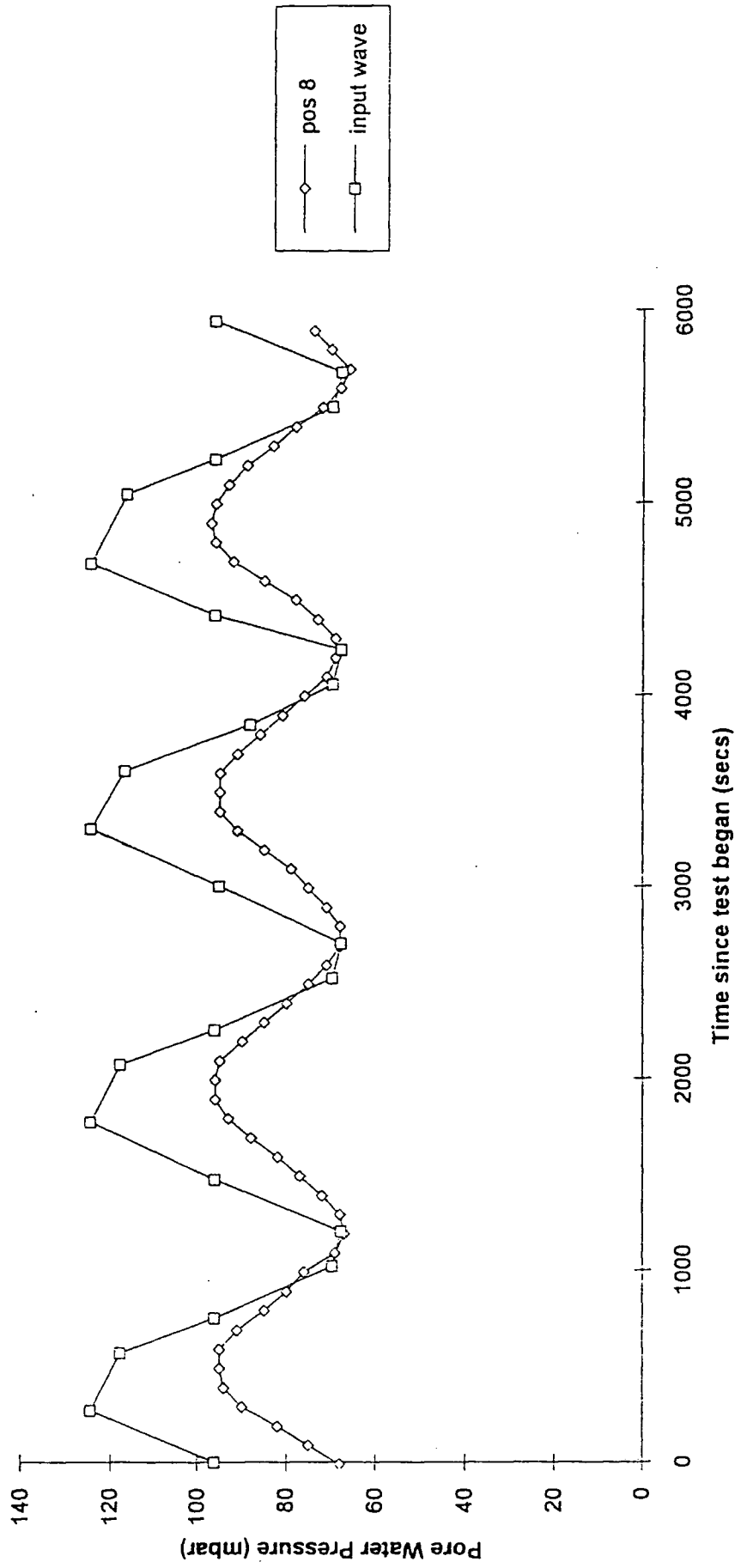
Figure 3.9. Variation of Pore Water Pressure at Position 10 and Corresponding Simulated Tidal Fluctuation (Input Wave).
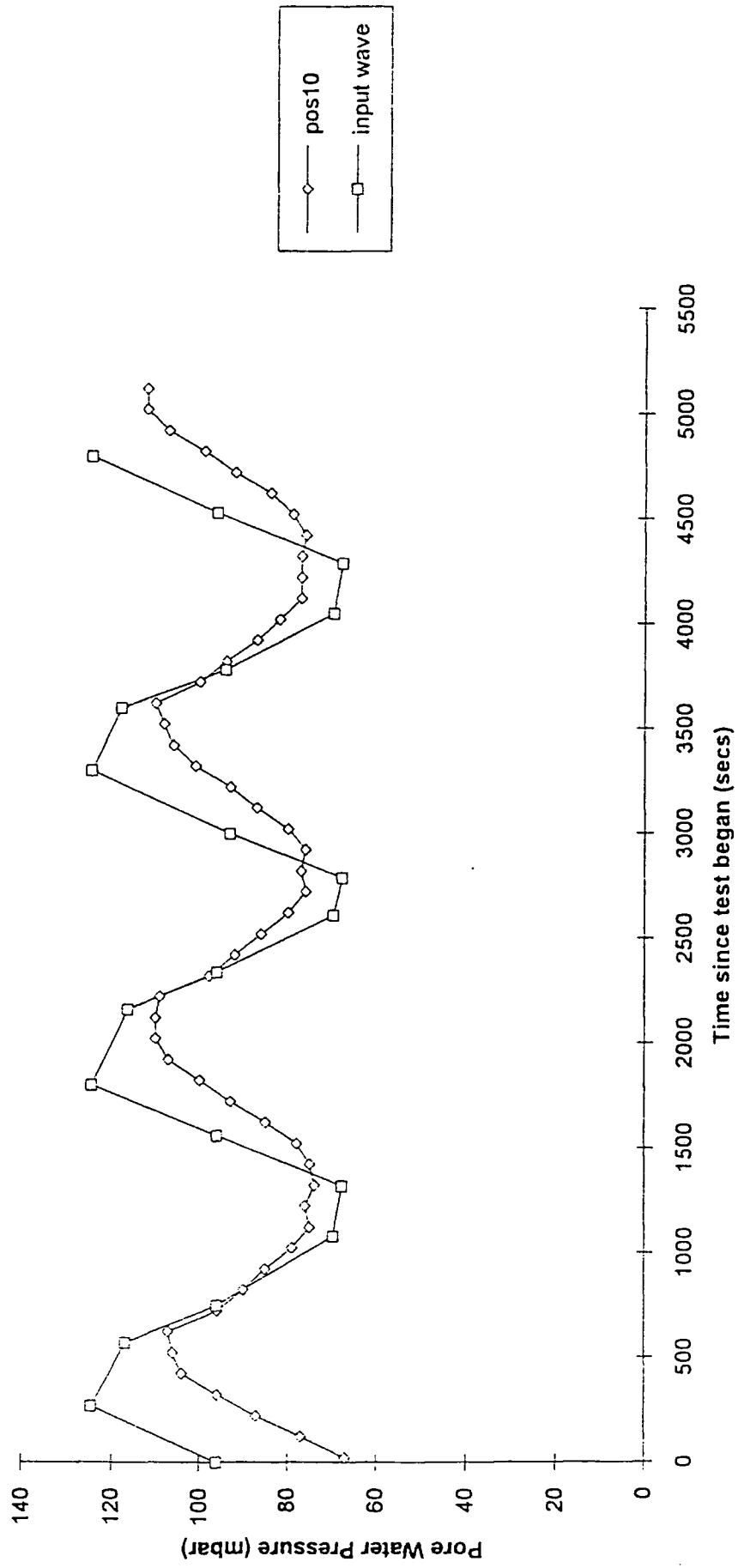
Figure 3.10. Variation of Pore Water Pressure at Position 12 and Corresponding Simulated Tidal Fluctuation (Input Wave).
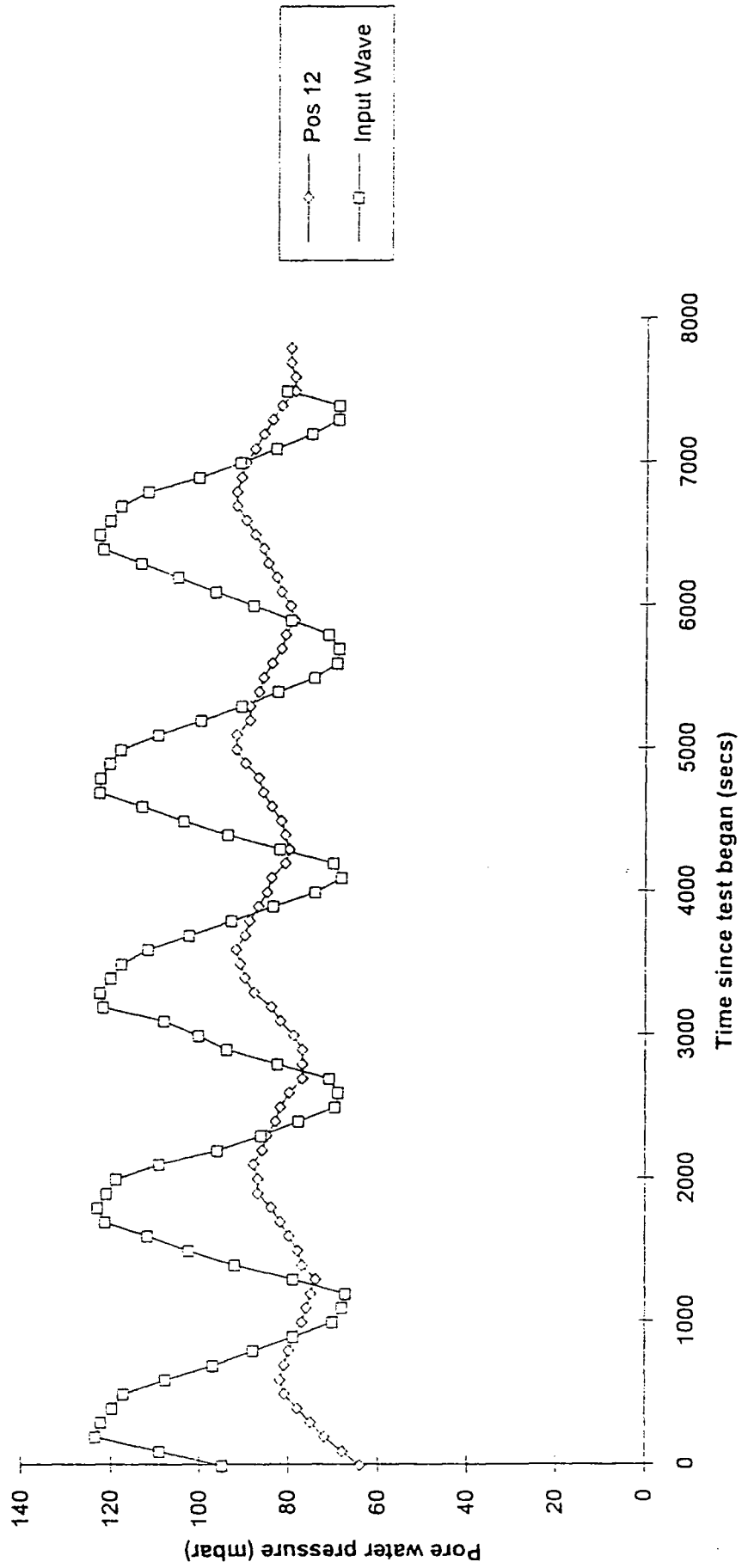
Figure 3.11. Manual Tidal Simulation - Amplitude Decay of Input Pressure Wave with Horizontal Distance from Tidal Tank.
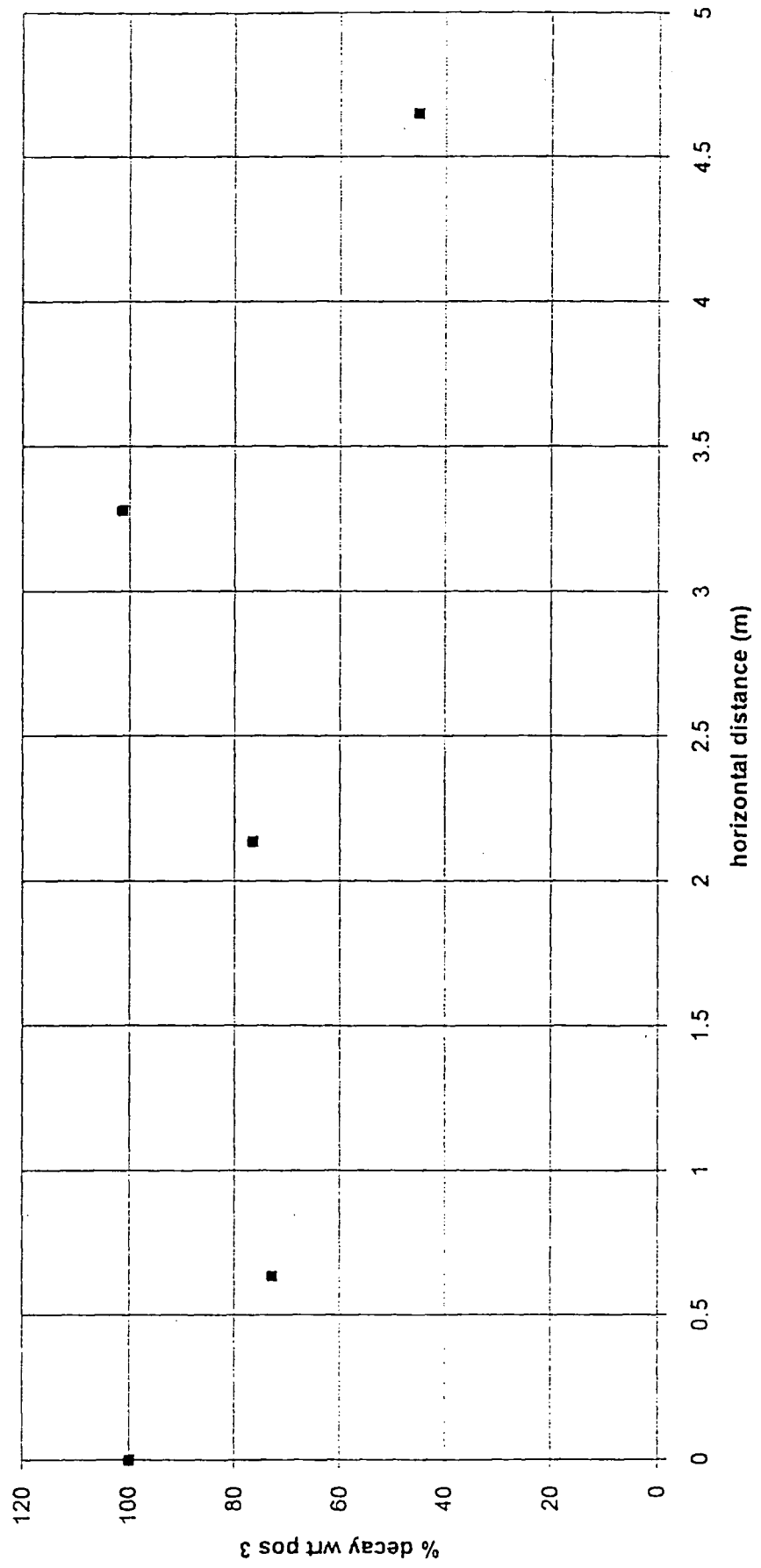
Figure 3.12. Series 1. Primary Amplitude Decay Curve.
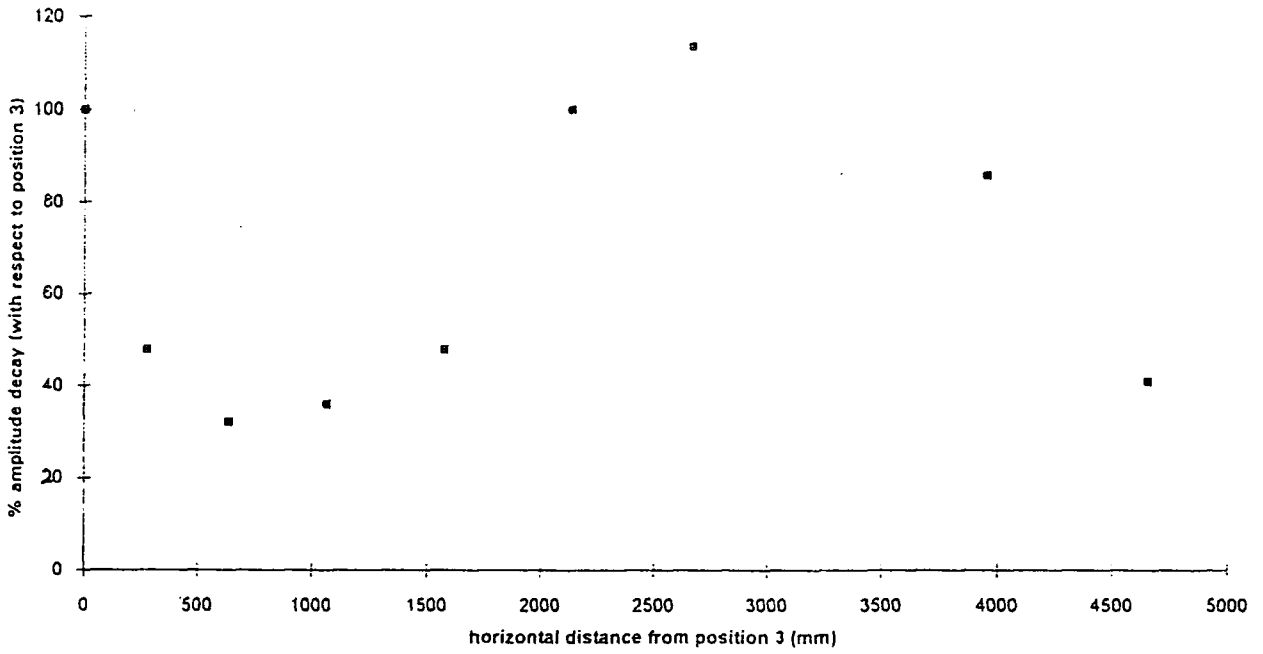
Figure 3.13. Series 2. Primary Amplitude Decay Curve.
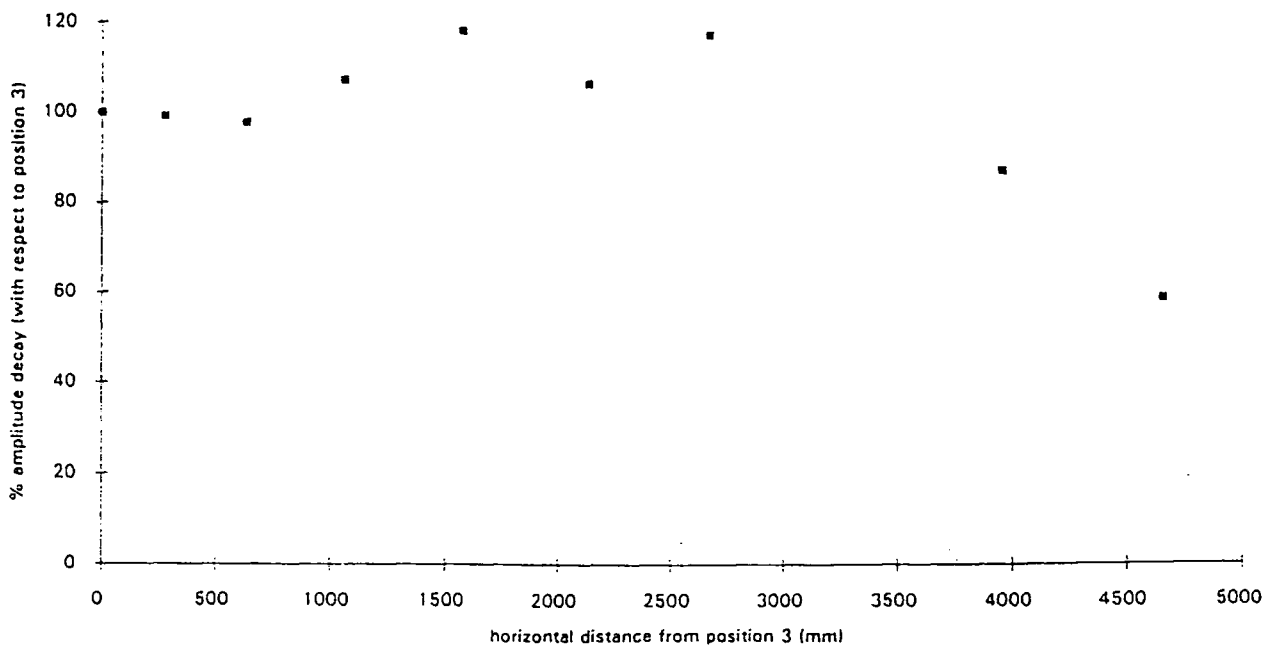
Figure 3.14. Series 3. Primary Amplitude Decay Curve.
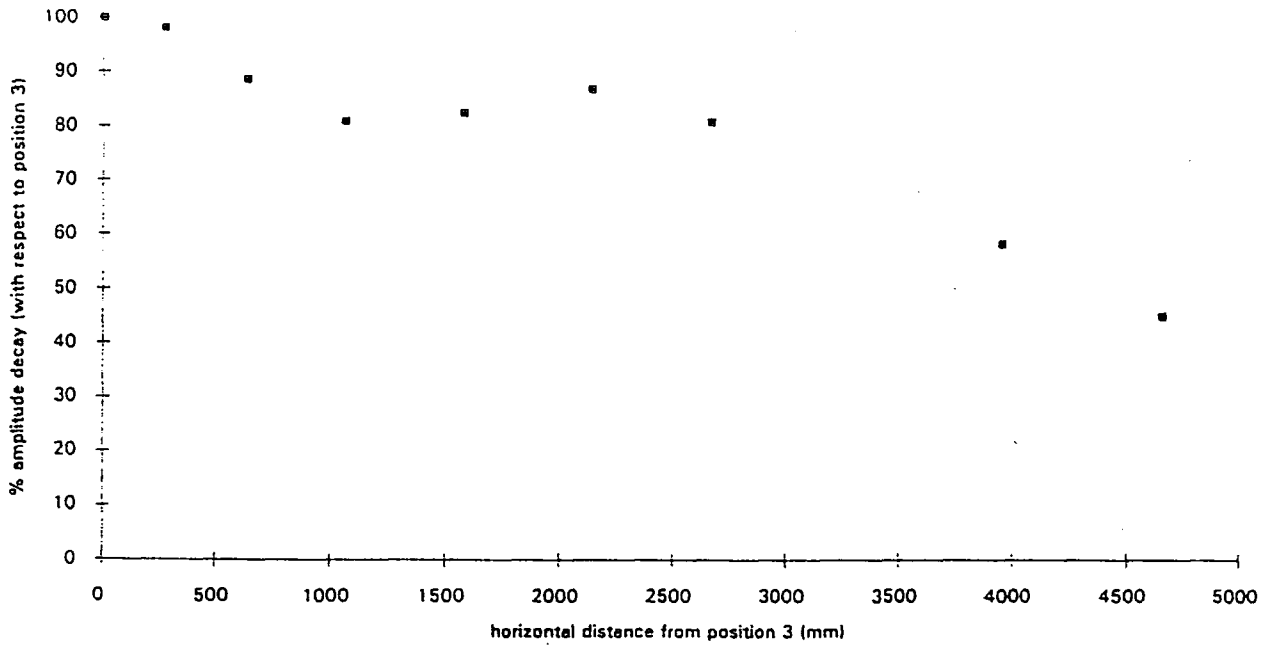
Figure 3.15. Series 4. Primary Amplitude Decay Curve.
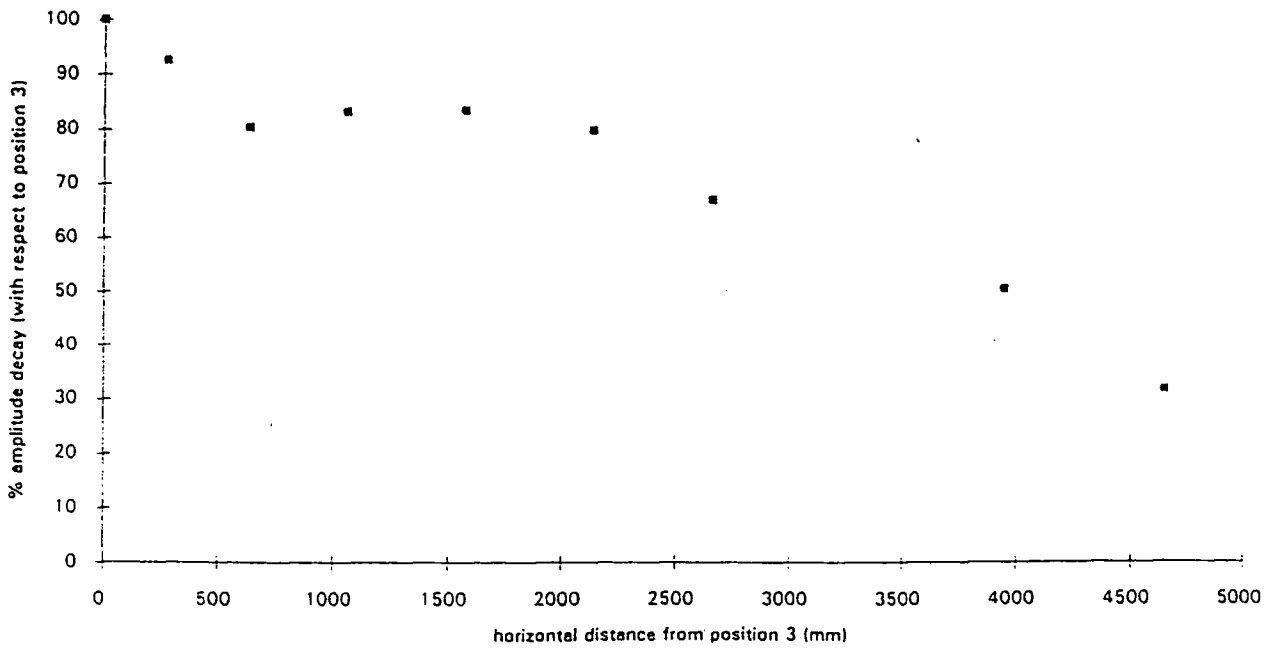
Figure 3.16. Series 1. Secondary Amplitude Decay Curve.
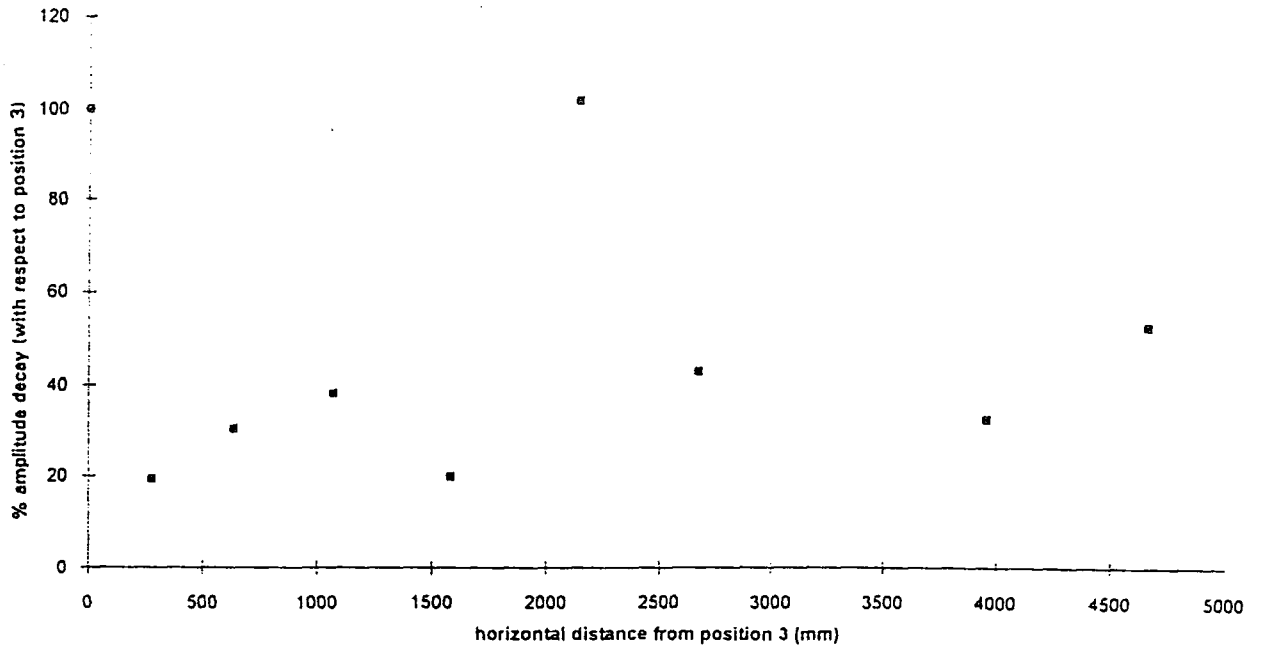
Figure 3.17. Series 2. Secondary Amplitude Decay Curve.
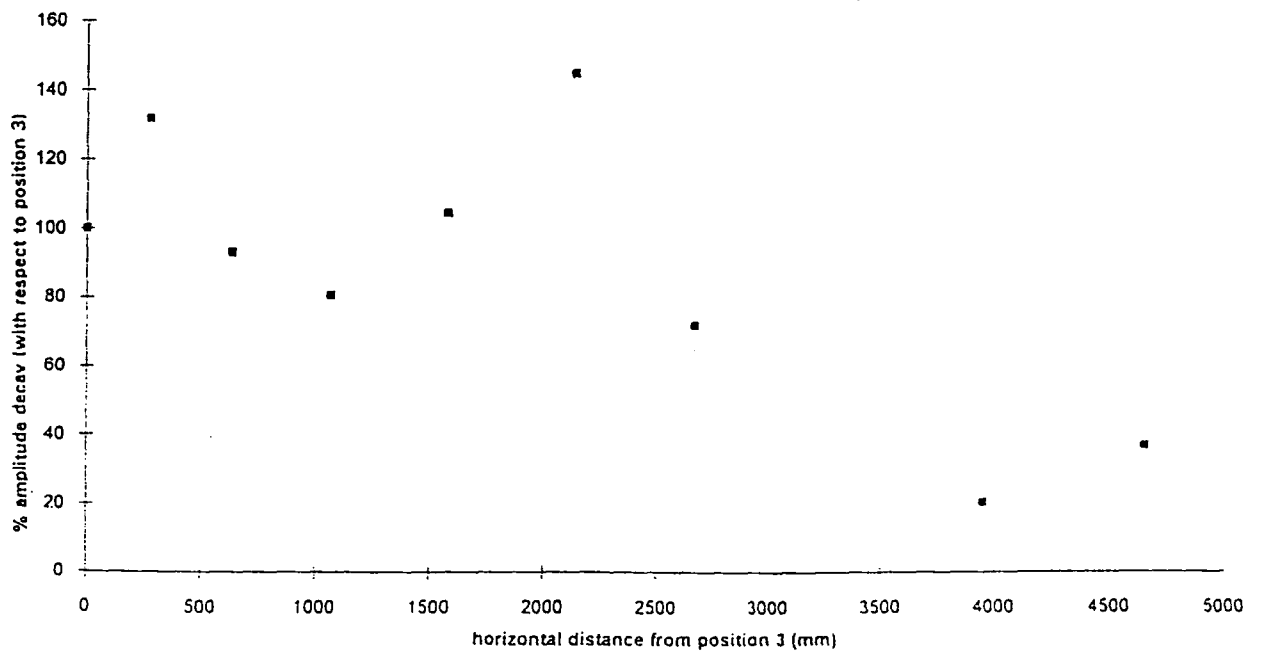
Figure 3.18. Series 3. Secondary Amplitude Decay Curve.
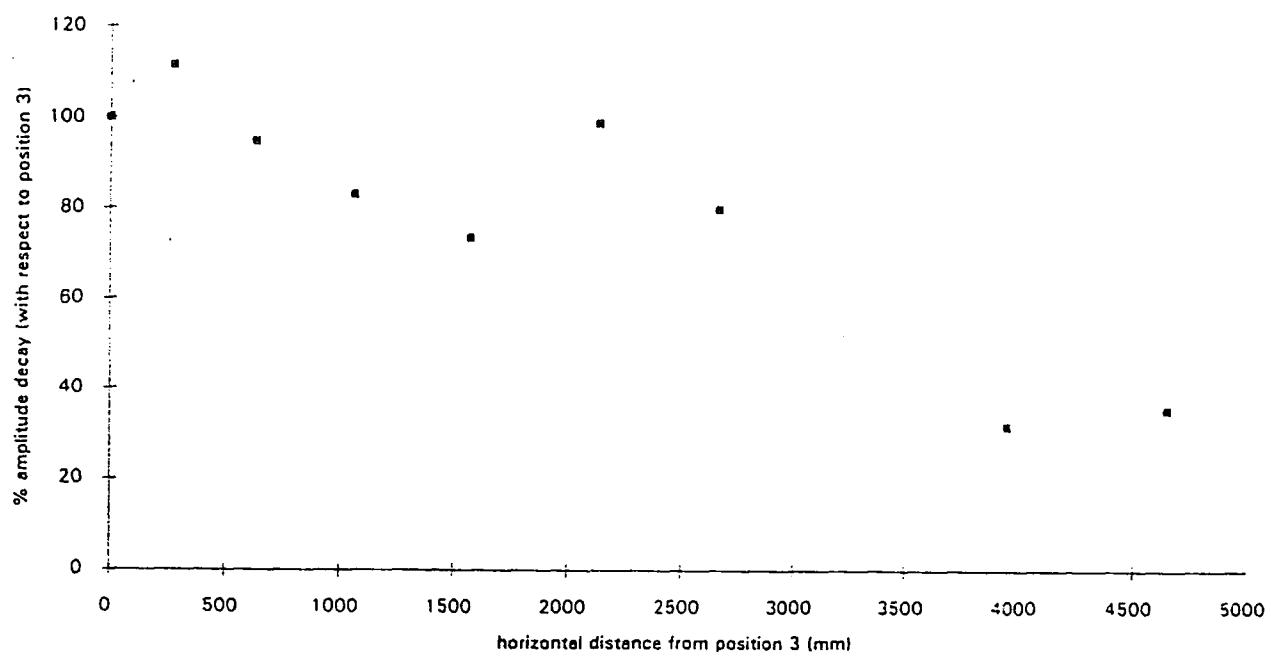
Figure 3.19. Series 4. Secondary Amplitude Decay Curve.
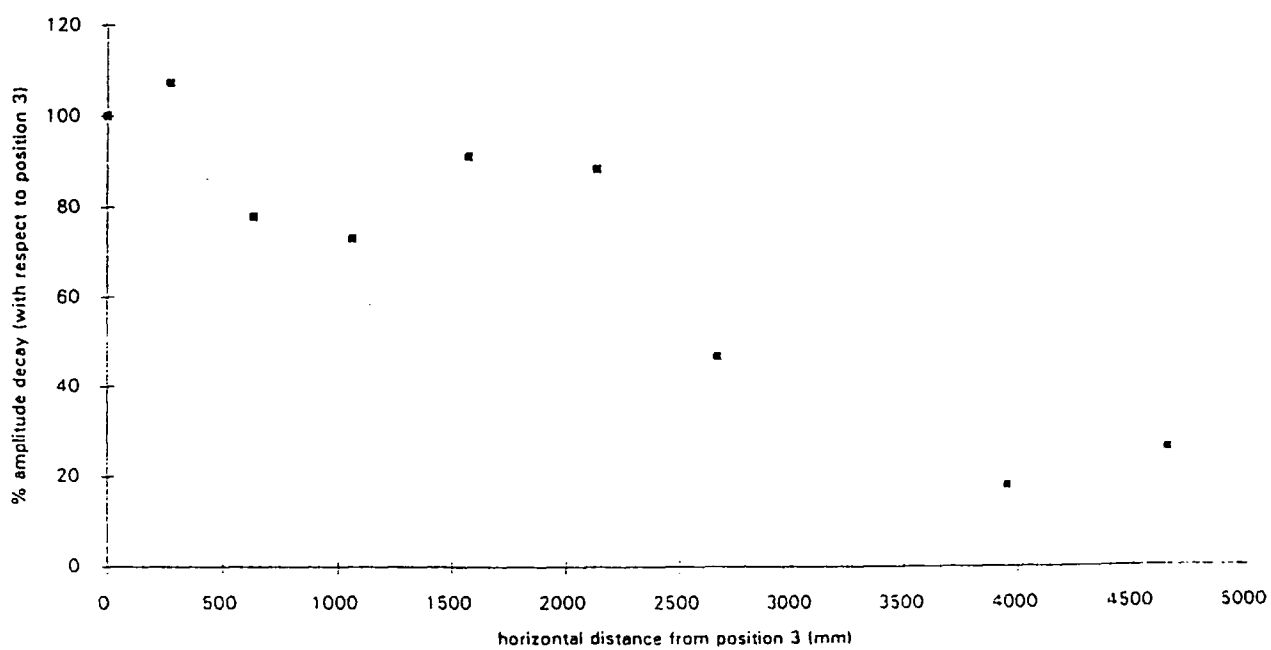
Figure 3.20.

Series 2. Timelag
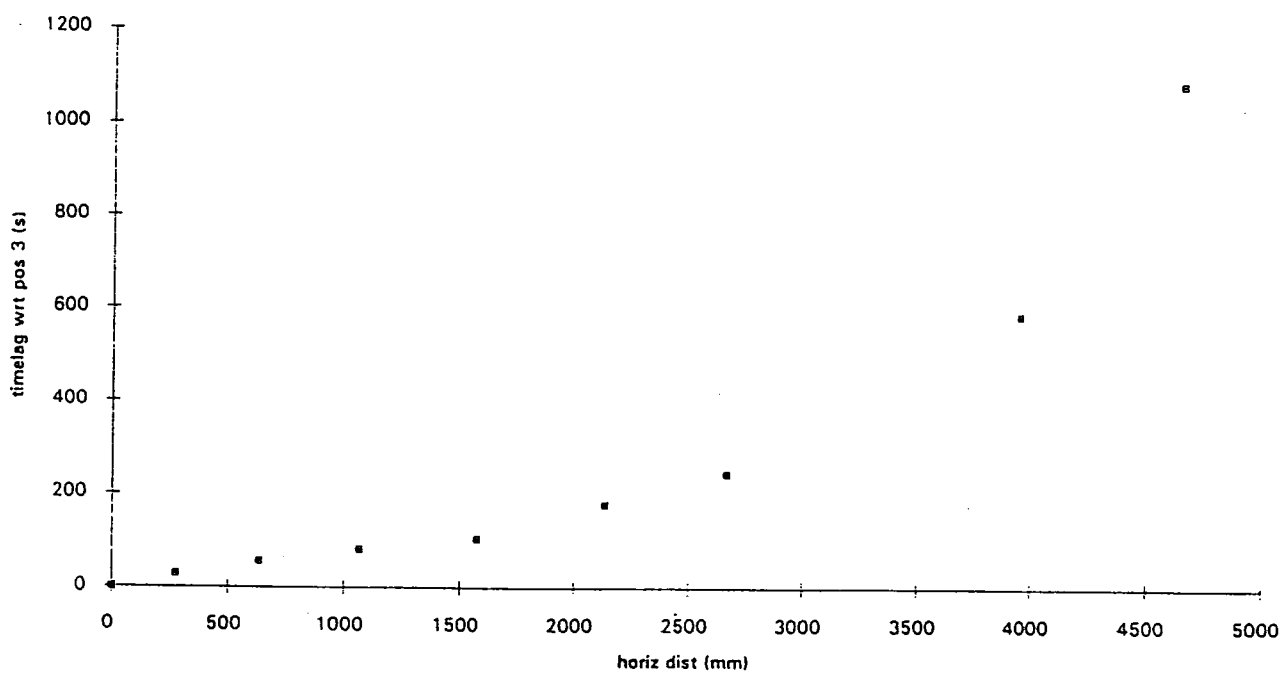
Figure 3.21.

Series 3. Timelag

Figure 3.22.

Series 4. Timelag
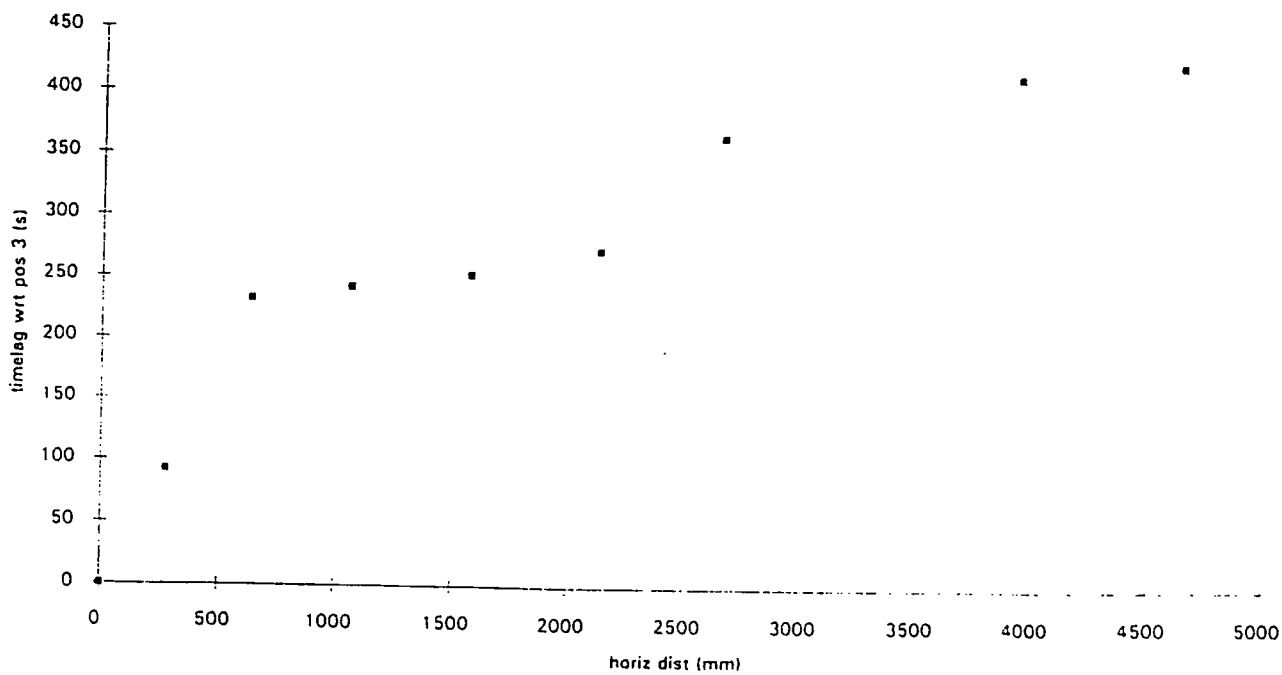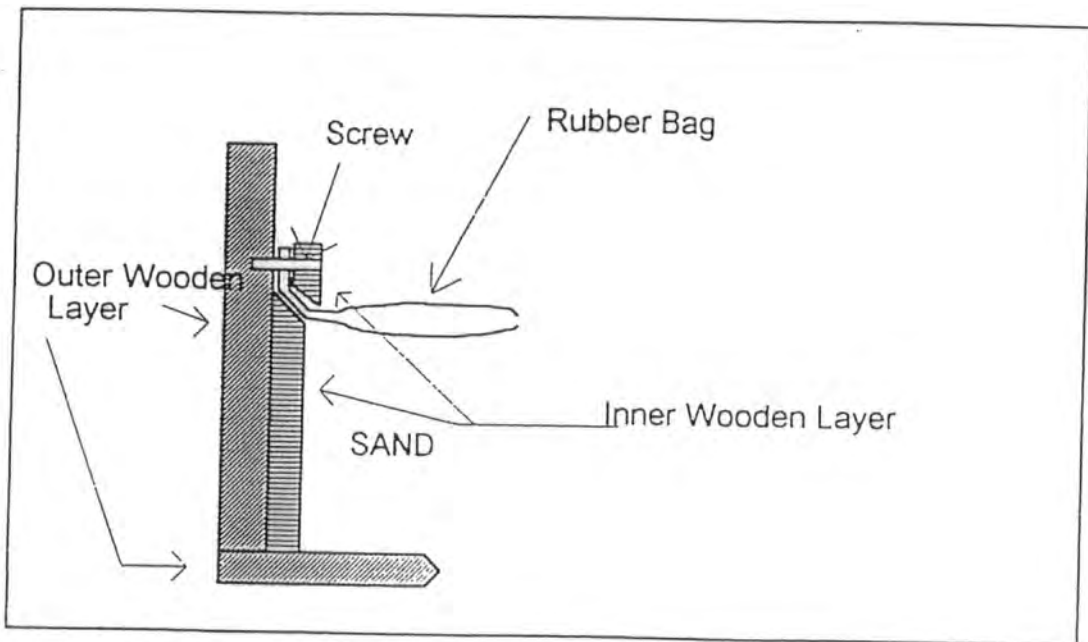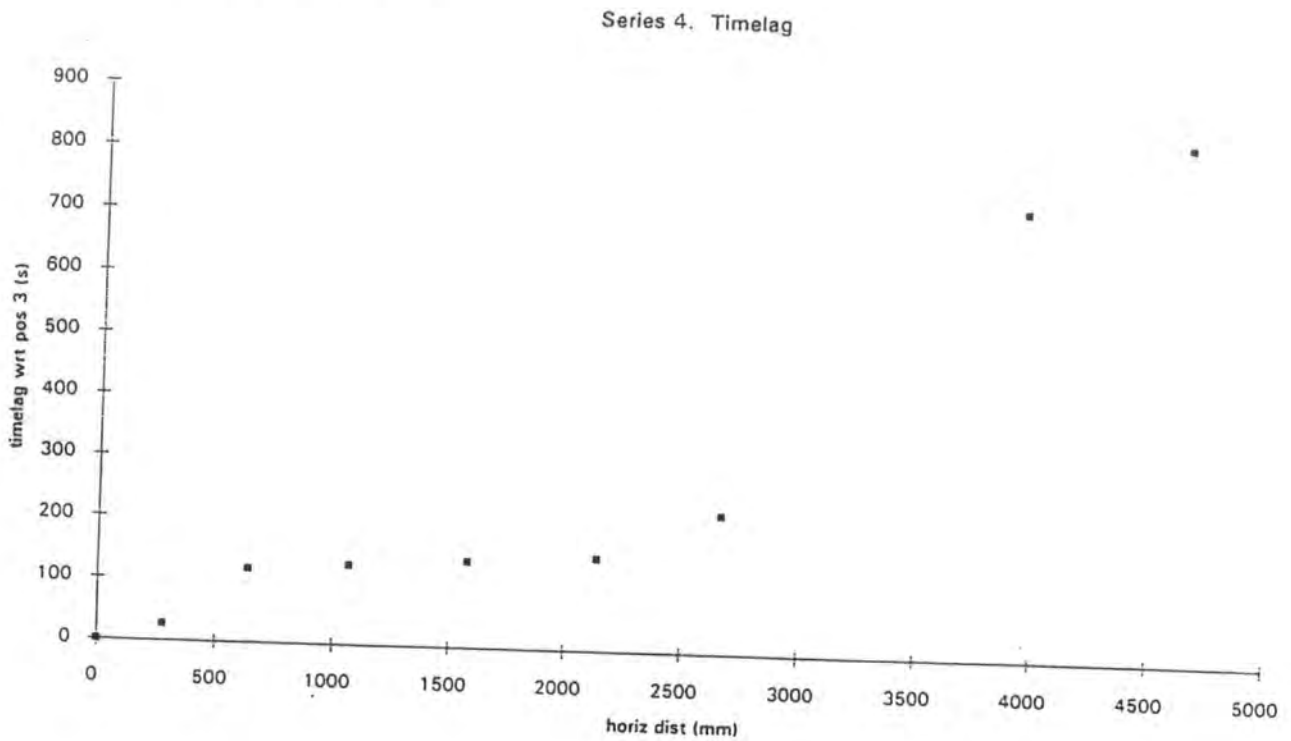
Figure 3.23.

Detail Illustrating Attachment of Rubber Membrane

Figure 3.24   Series 5. Primary Amplitude Decay Curve.
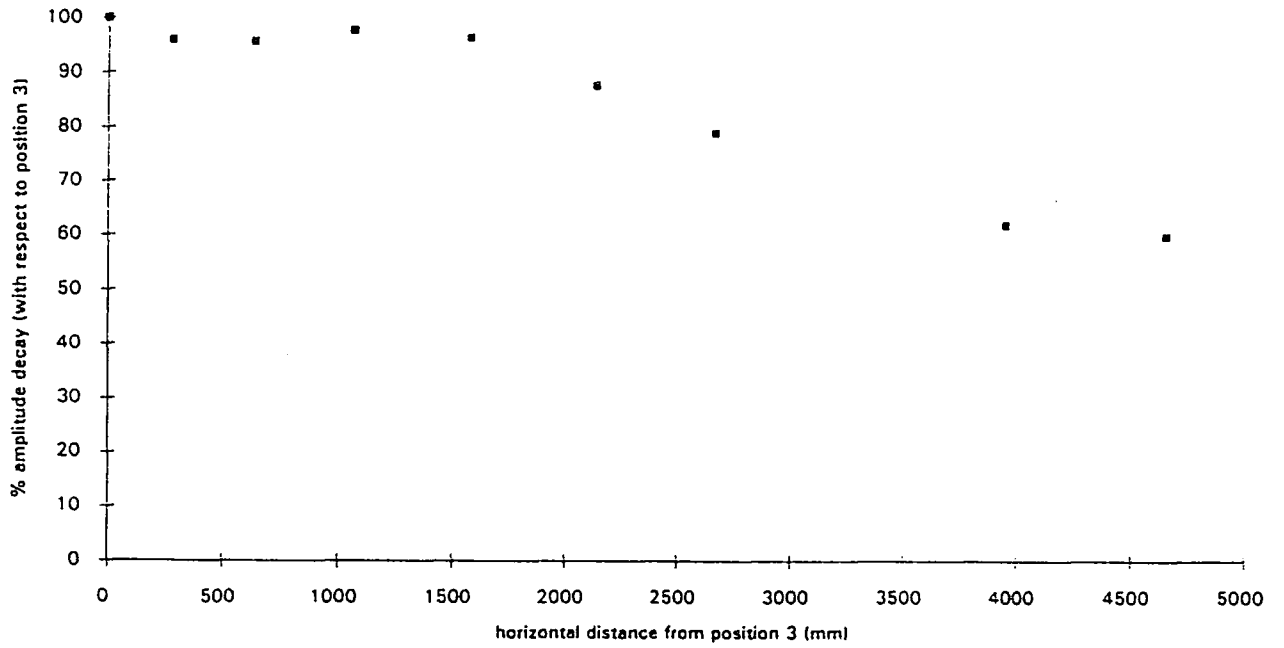
Figure 3.25. Series 6. Primary Amplitude Decay Curve.
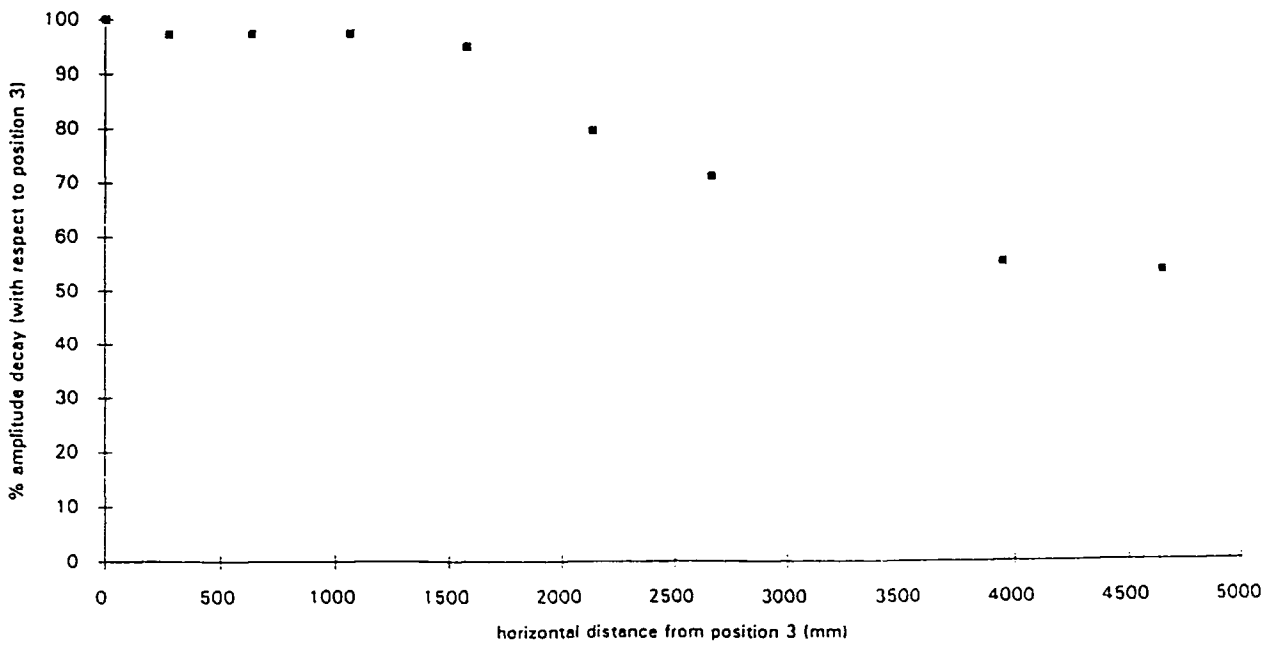
Figure 3.26. Series 7. Primary Amplitude Decay Curve.
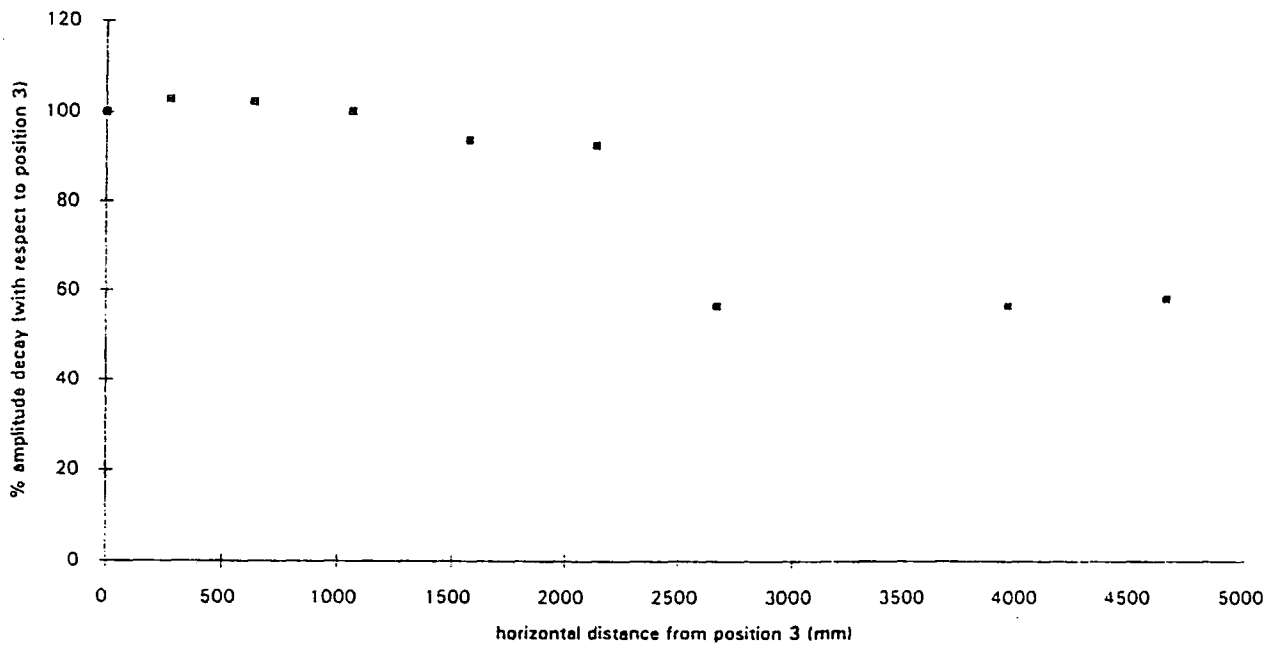
Figure 3.27. Series 8. Primary Amplitude Decay Curve.
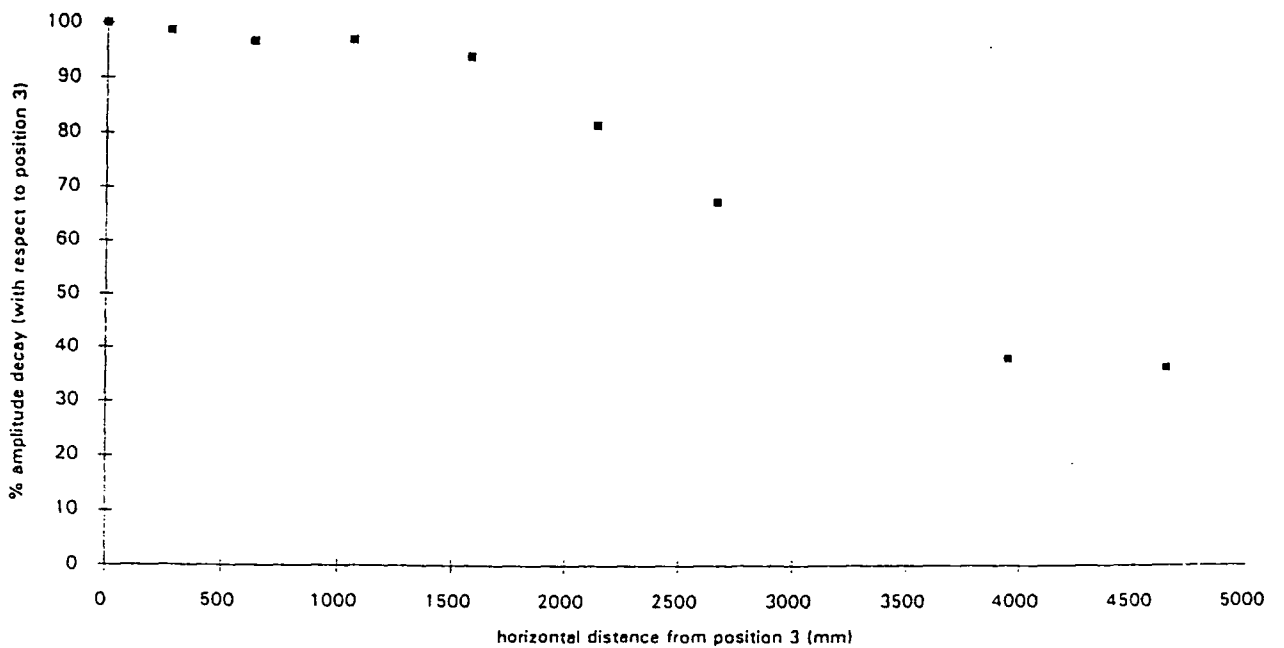
Figure 3.28. Series 9. Primary Amplitude Decay Curve.
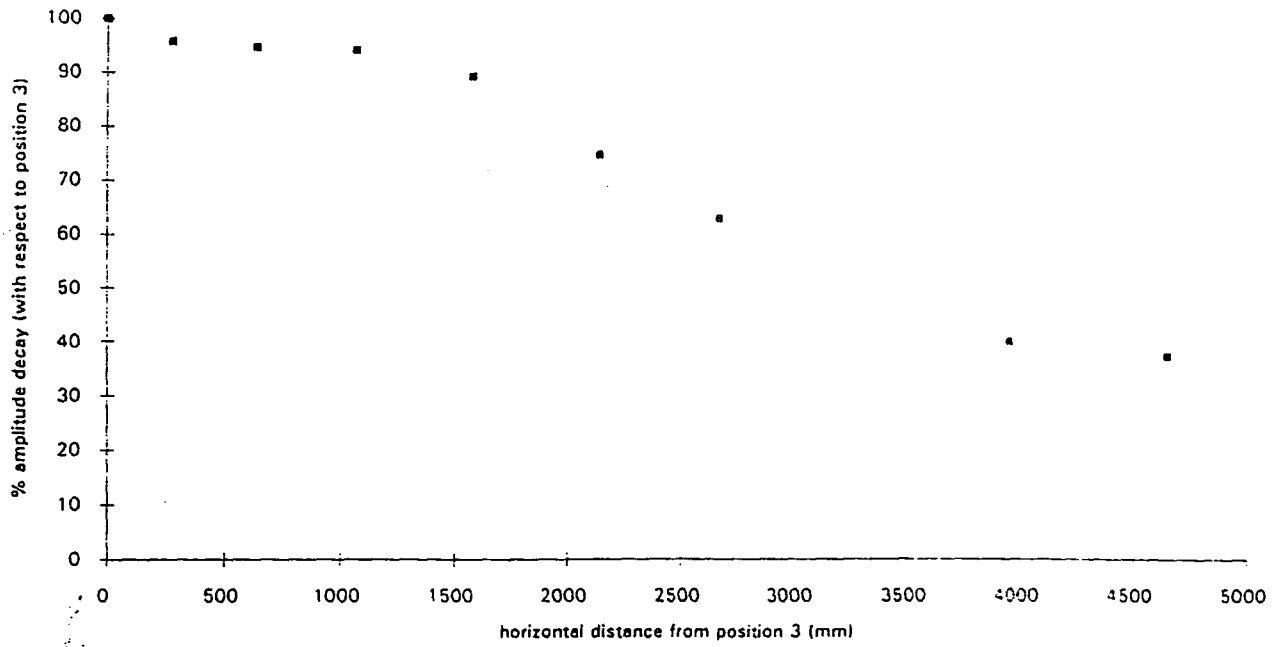
Figure 3.29. Series 10. Primary Amplitude Decay Curve.
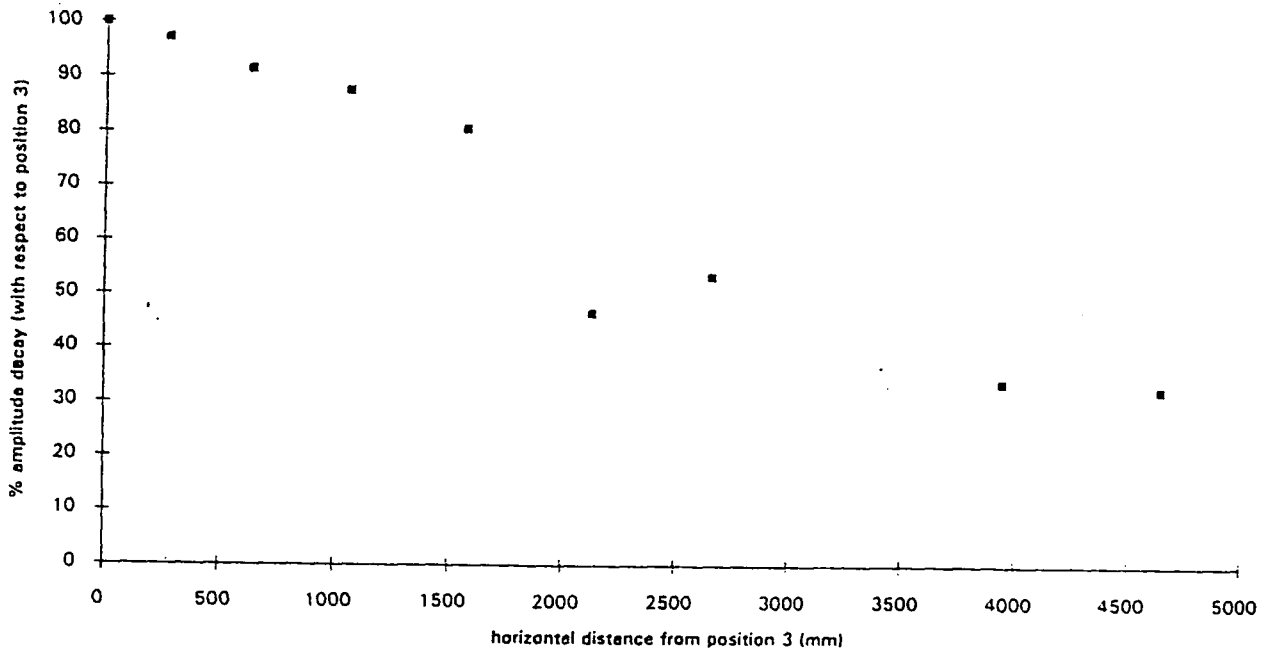
Figure 3.30. Series 11. Primary Amplitude Decay Curve.
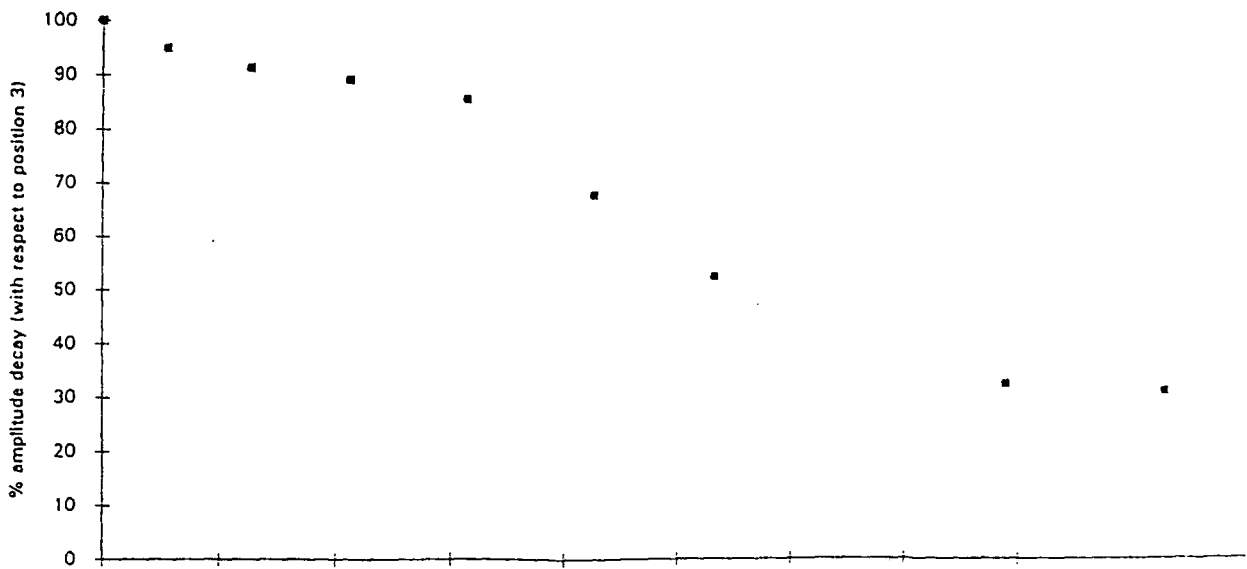
Figure 3.31. Series 12. Primary Amplitude Decay Curve.

horizontal distance from position 3 (mm)
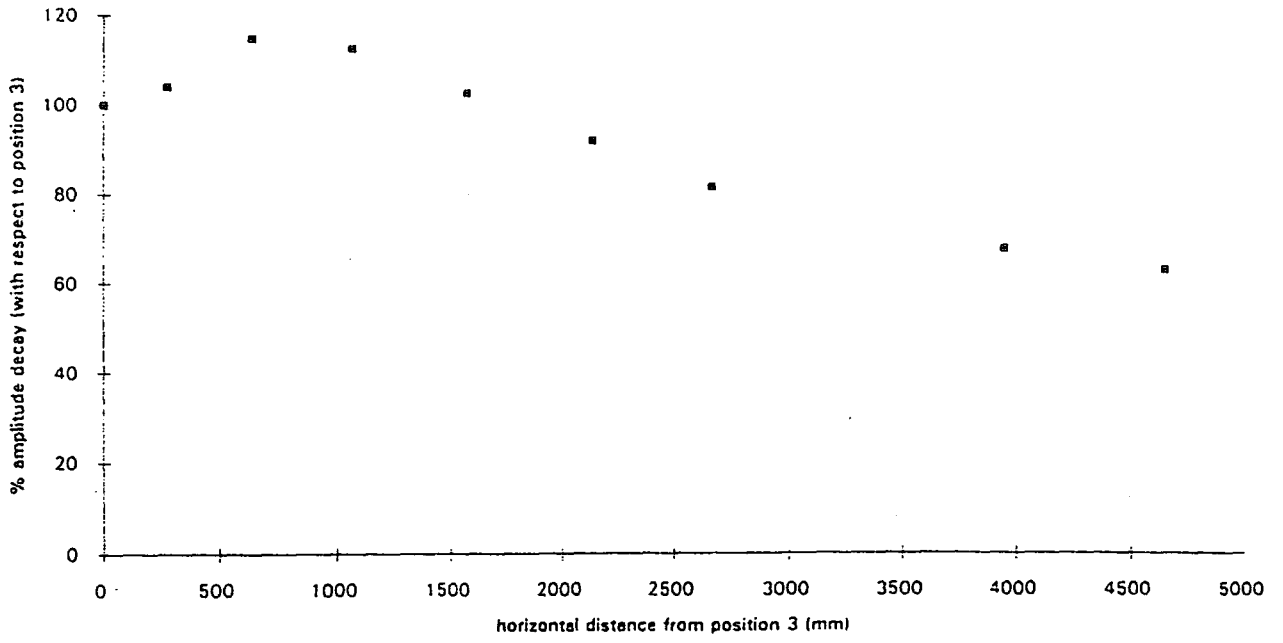
Figure 3.32. Series 13. Primary Amplitude Decay Curve.

horizontal distance from position 3 (mm)
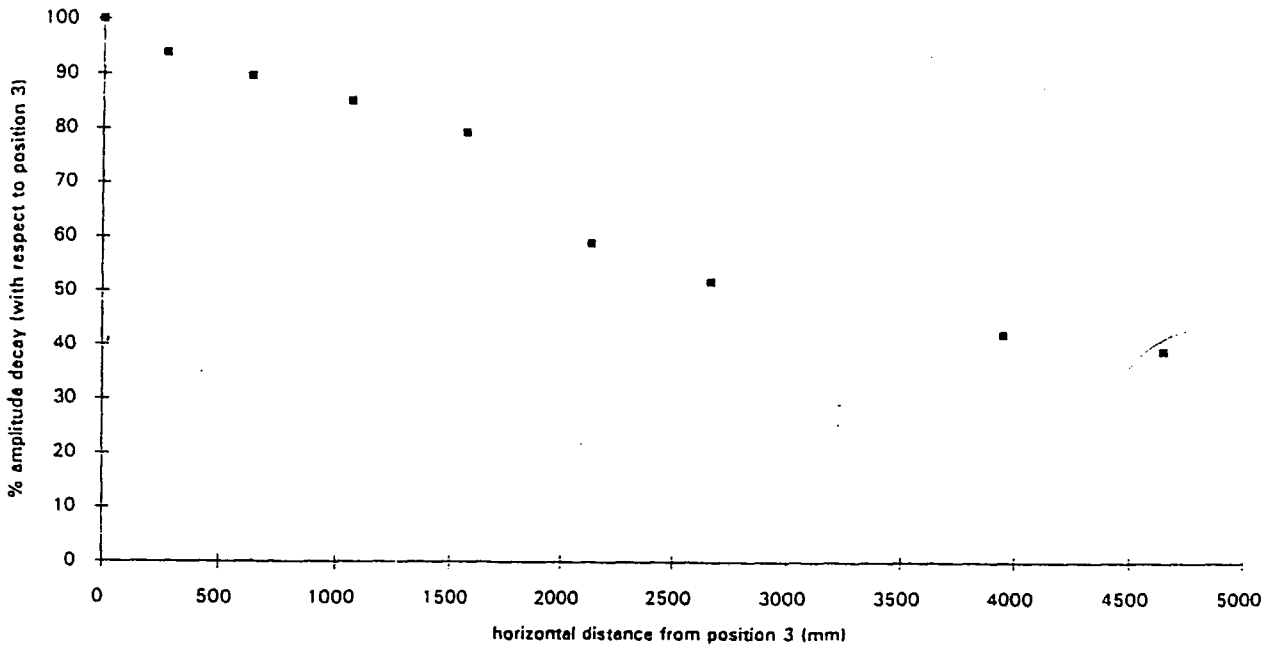
Figure 3.33. Series 14. Primary Amplitude Decay Curve.
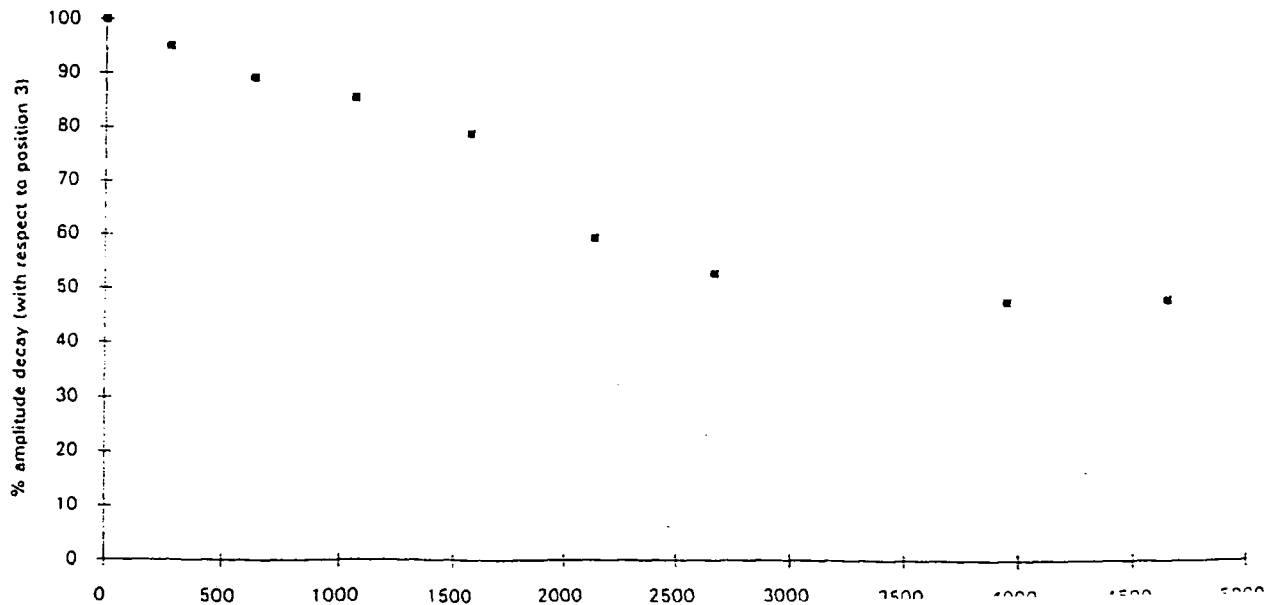
Figure 3.34. Series 15. Primary Amplitude Decay Curve.

horizontal distance from position 3 (mm)
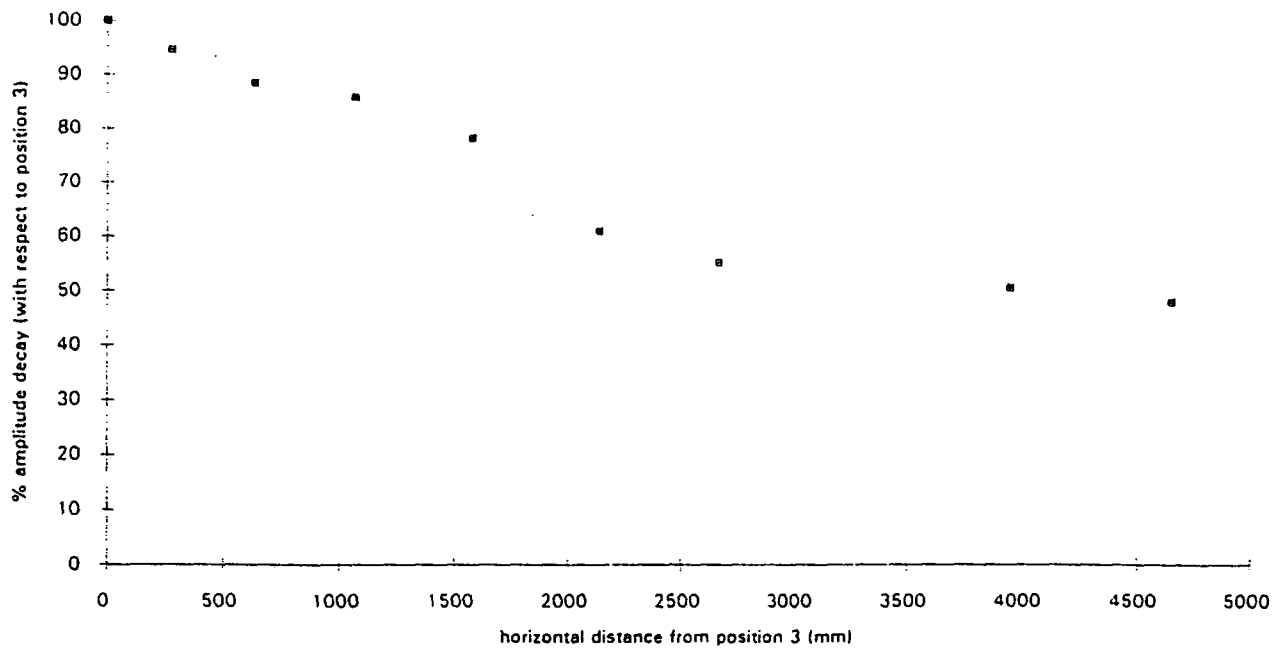
Figure 3.35. Series 5. Secondary Amplitude Decay Curve.

horizontal distance from position 3 (mm)
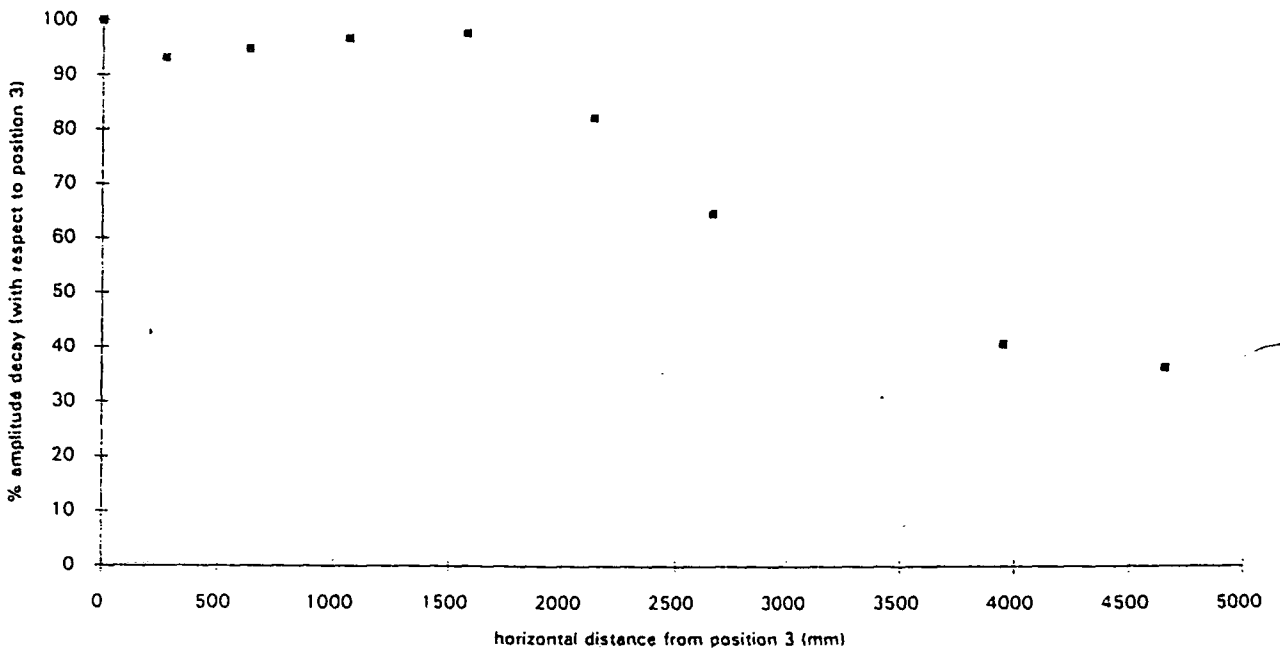
Figure 3.36. Series 6. Secondary Amplitude Decay Curve.
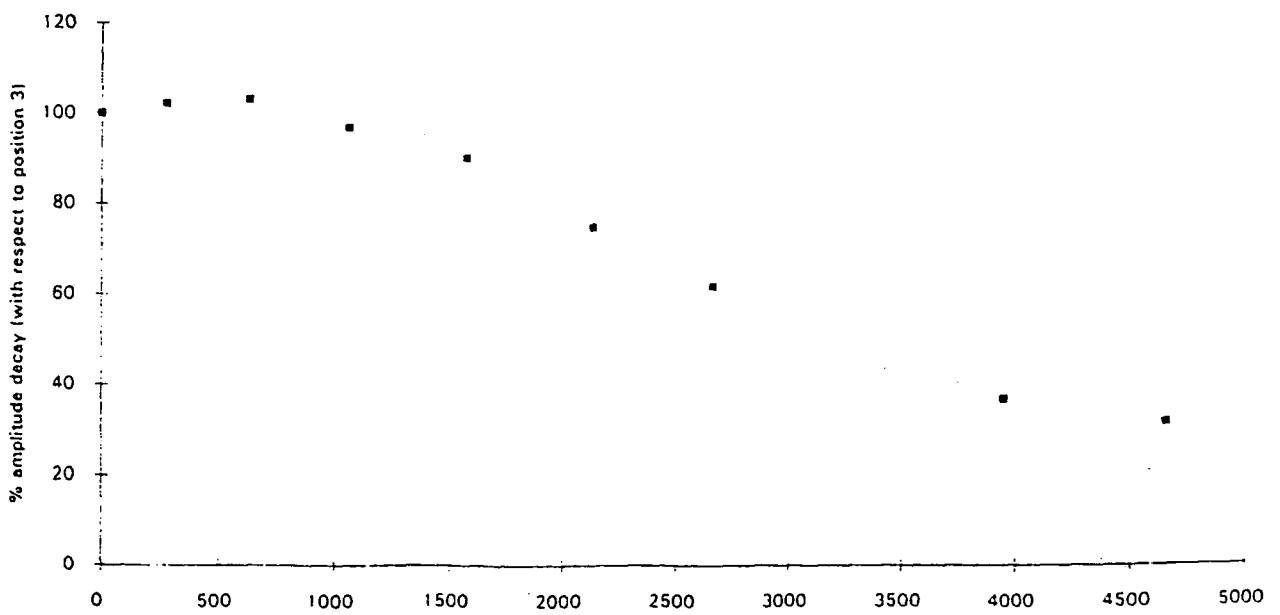
Figure 3.37. Series 7. Secondary Amplitude Decay Curve.

horizontal distance from position 3 (mm)
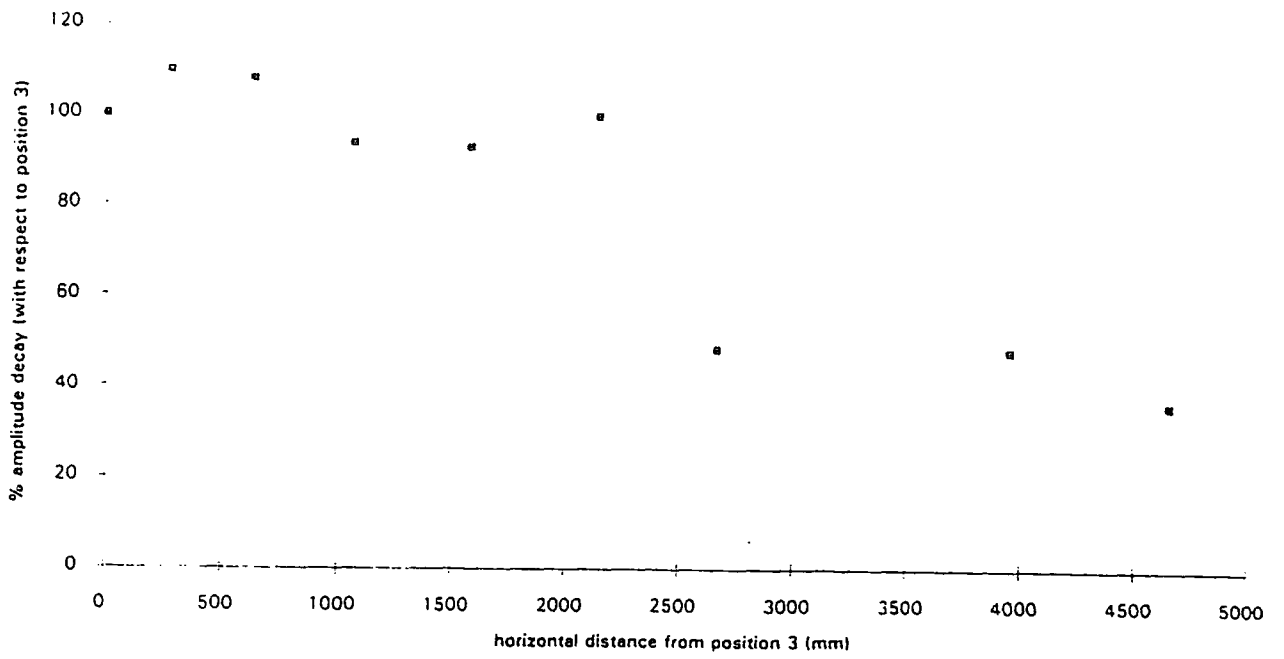
Figure 3.38. Series 8. Secondary Amplitude Decay Curve.

horizontal distance from position 3 (mm)
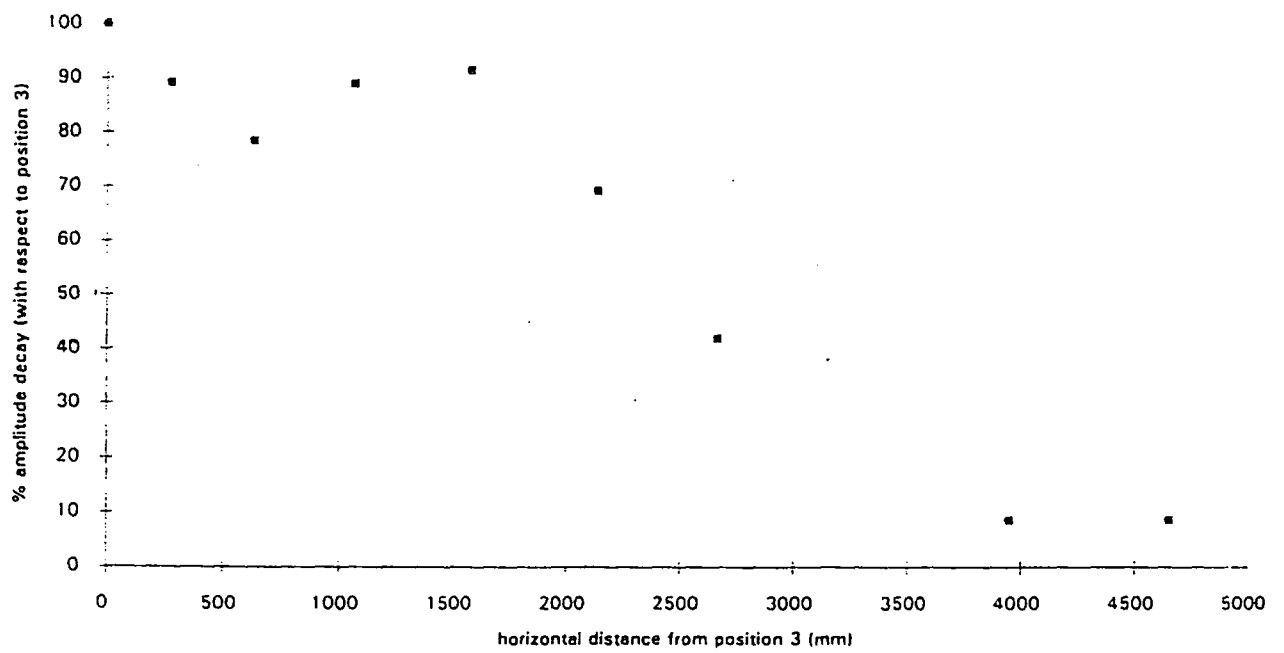
Figure 3.39. Series 9. Secondary Amplitude Decay Curve.
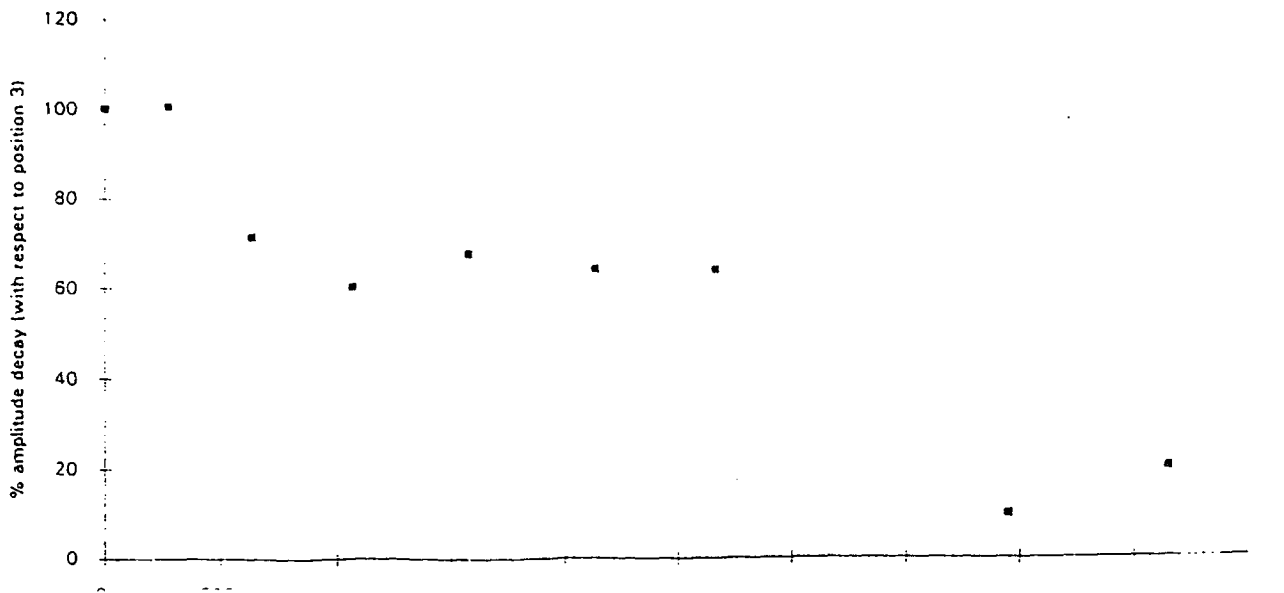
Figure 3.40. Series 10. Secondary Amplitude Decay Curve.
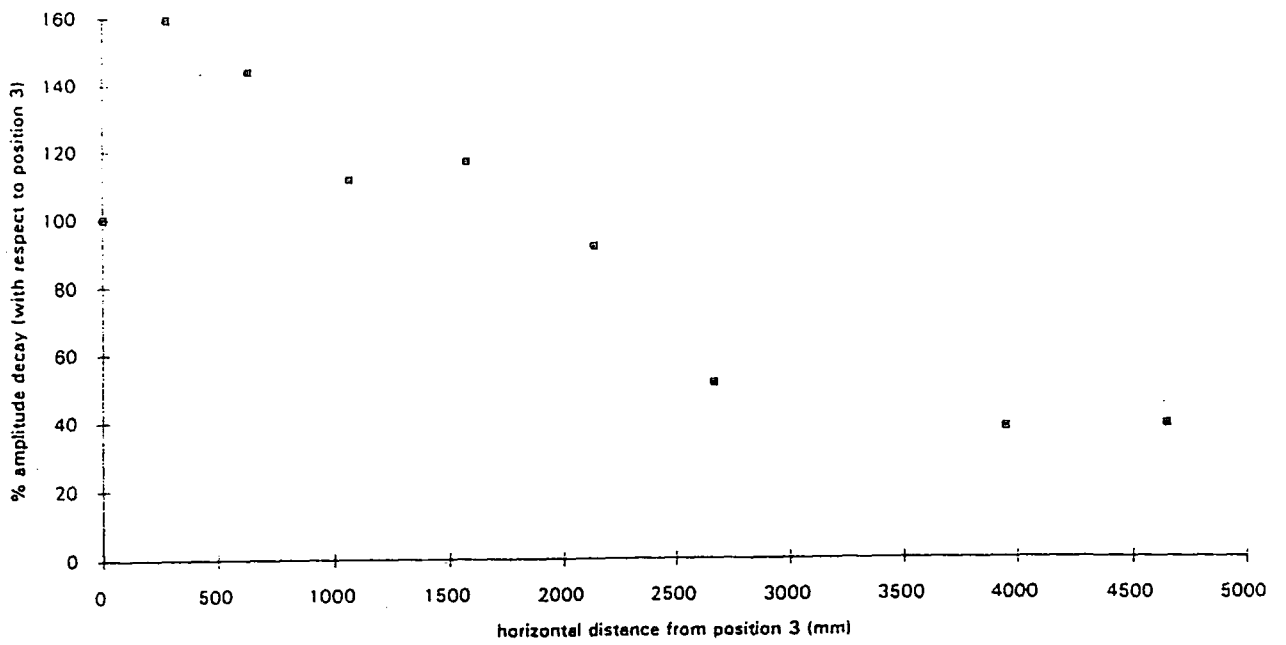
Figure 3.41. Series 11. Secondary Amplitude Decay Curve.
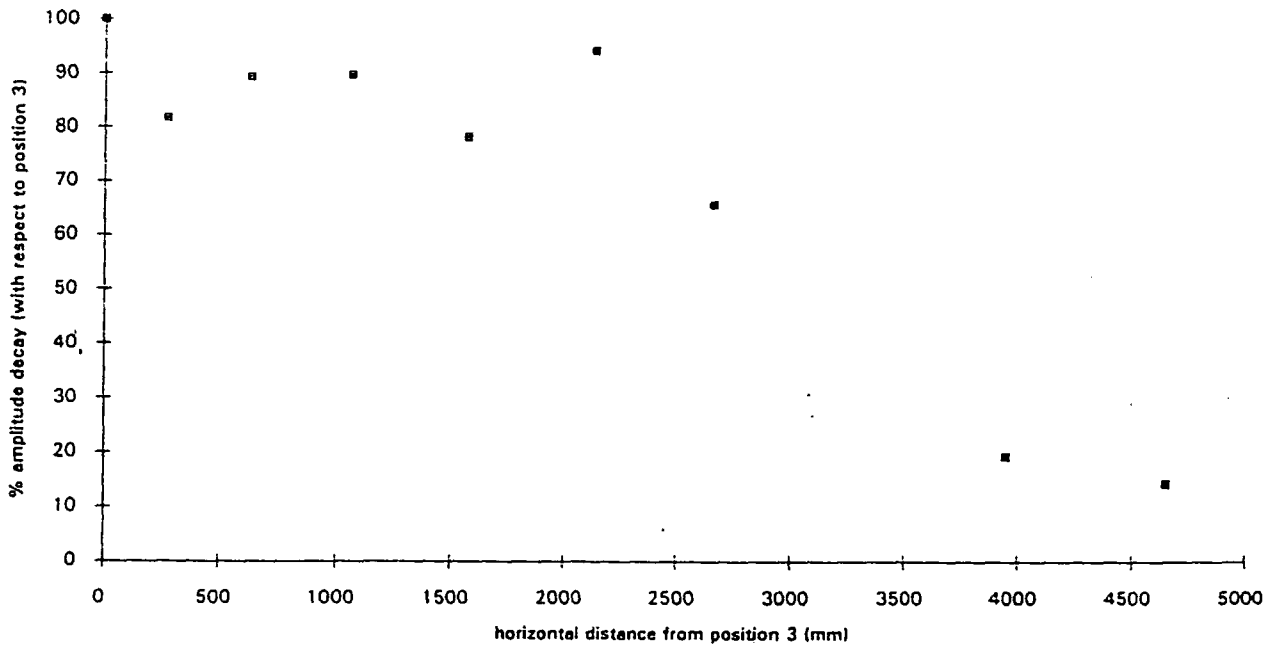
Figure 3.42. Series 12. Secondary Amplitude Decay Curve.
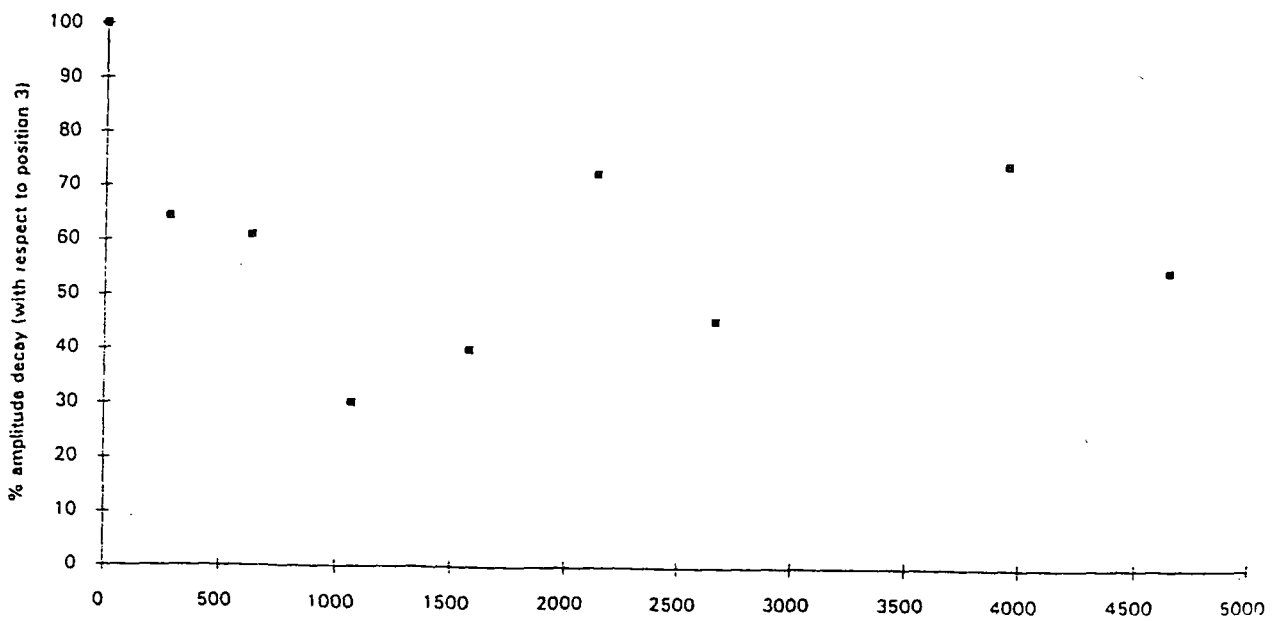
Figure 3.43. Series 13. Secondary Amplitude Decay Curve.
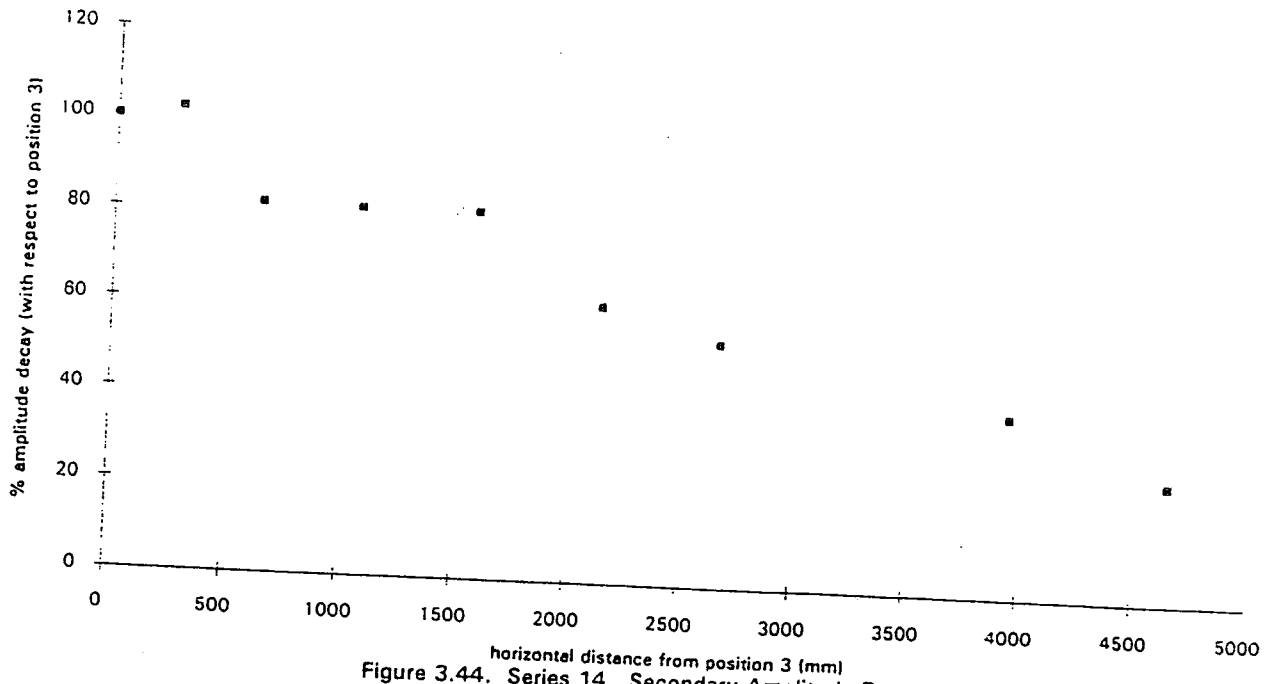
Figure 3.44. Series 14. Secondary Amplitude Decay Curve.
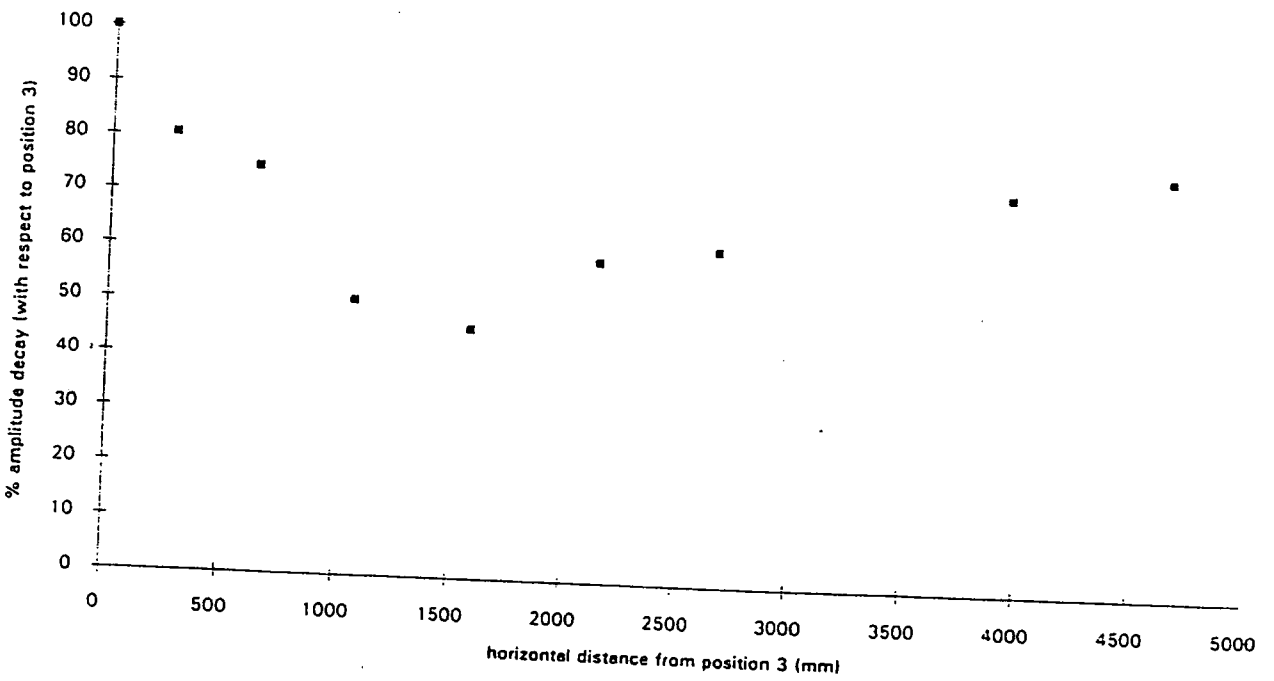
Figure 3.45. Series 15. Secondary Amplitude Decay Curve.
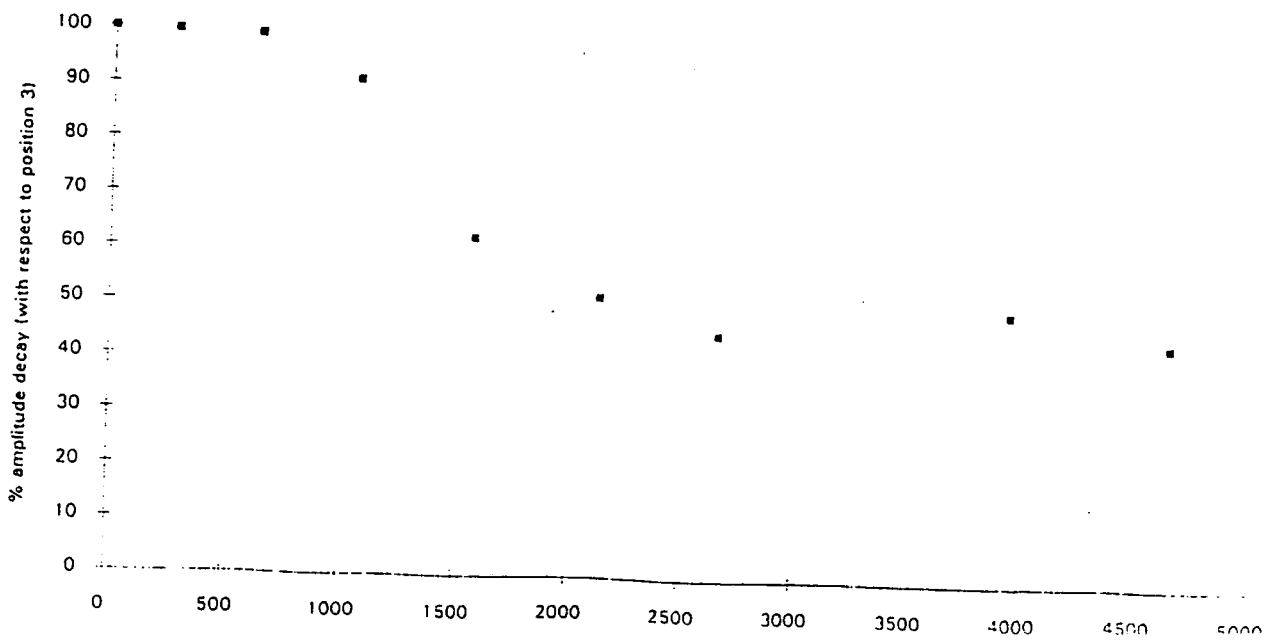
Figure 3.46. Series 5. Timelag
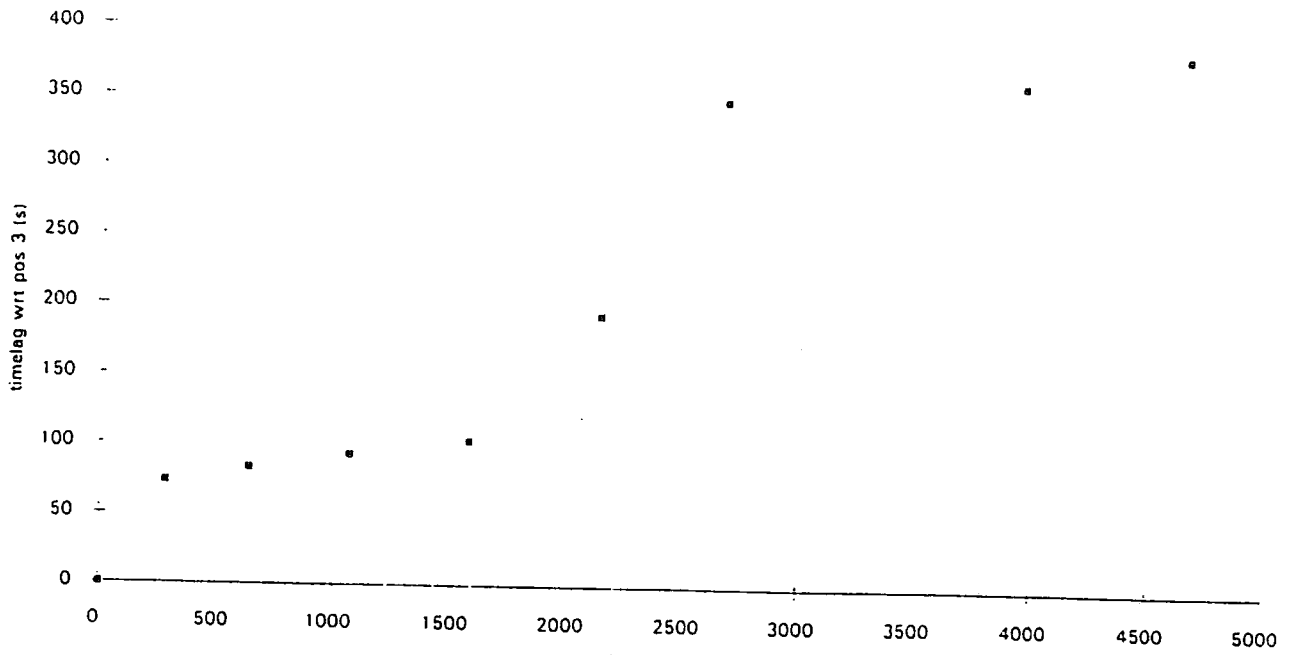
Figure 3.47. Series 6. Timelag
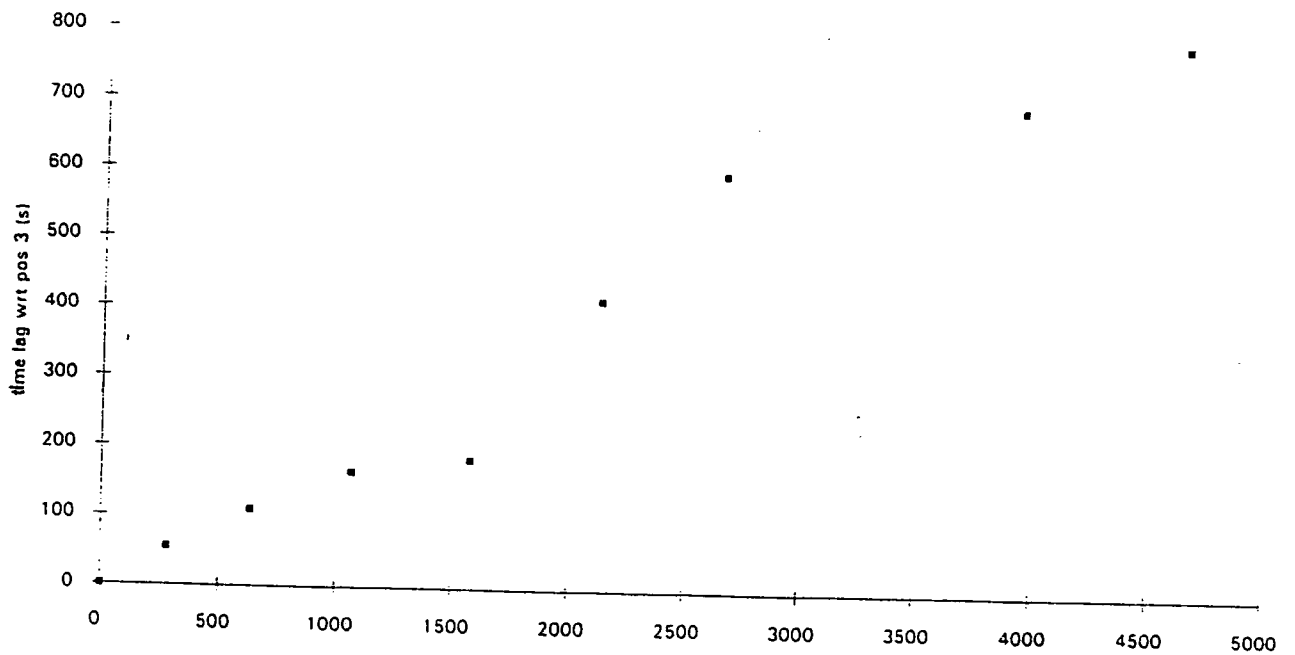
Figure 3.48. Series 7. Timelag
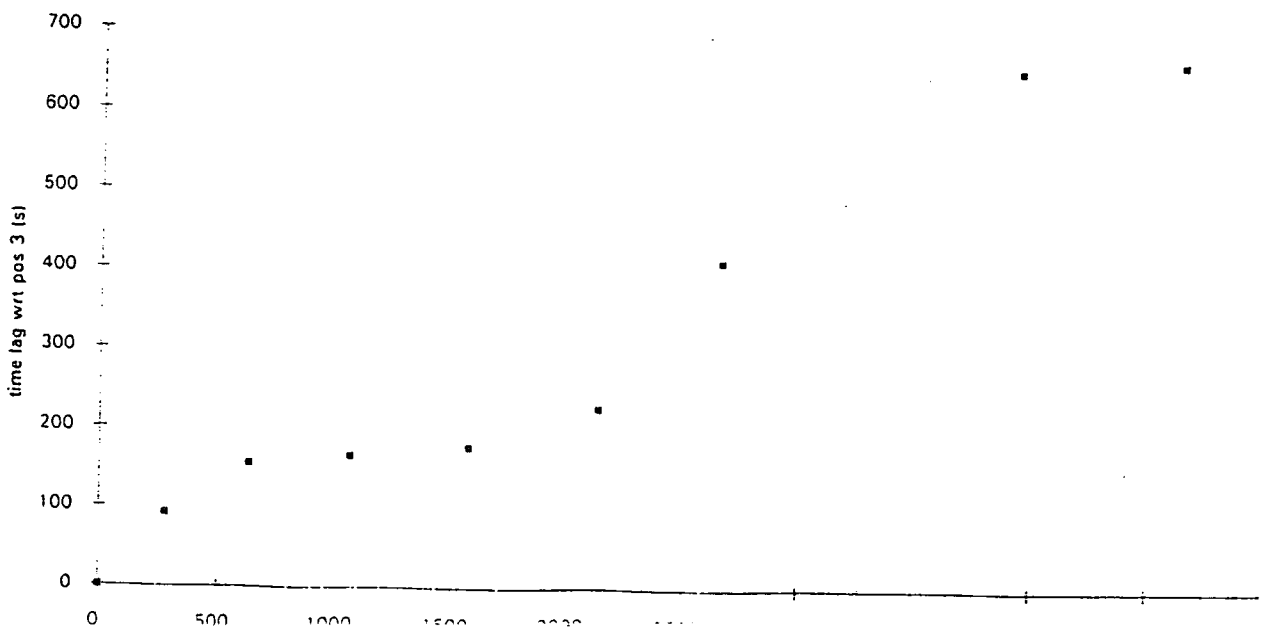
Figure 3.49. Series 8. Timelag
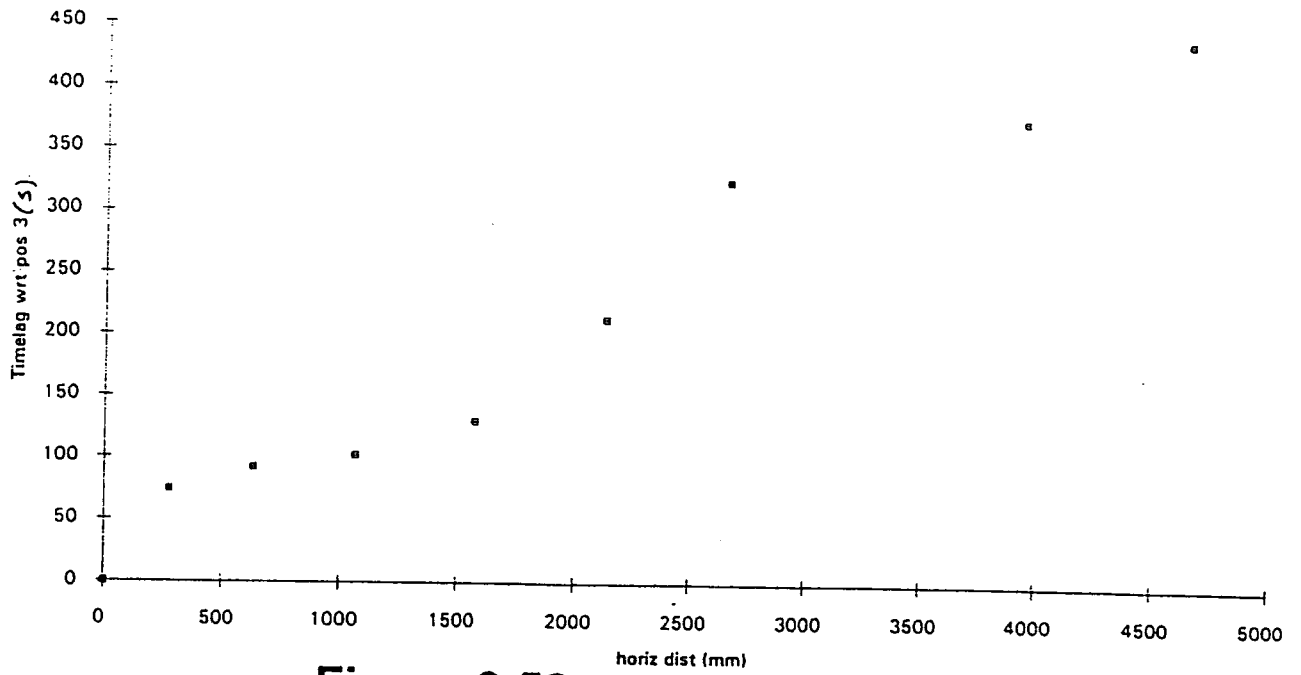
Figure 3.50. Series 9. Timelag
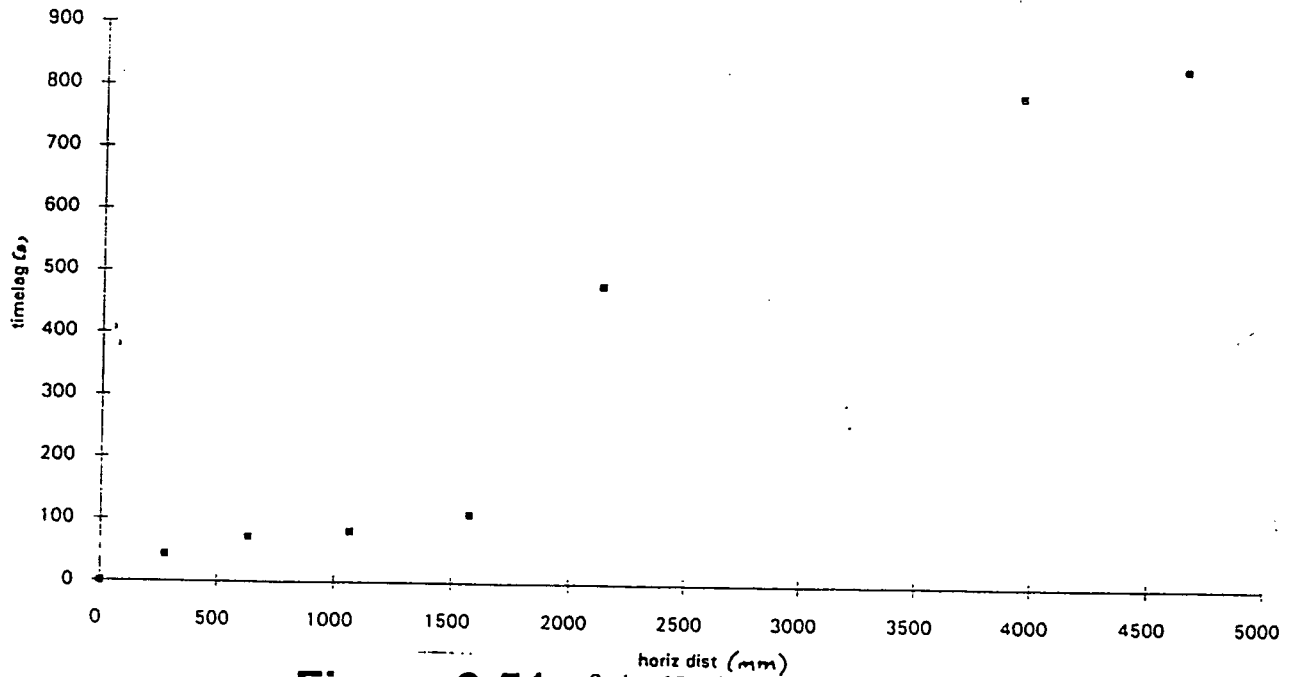
Figure 3.51. Series 10. timelag
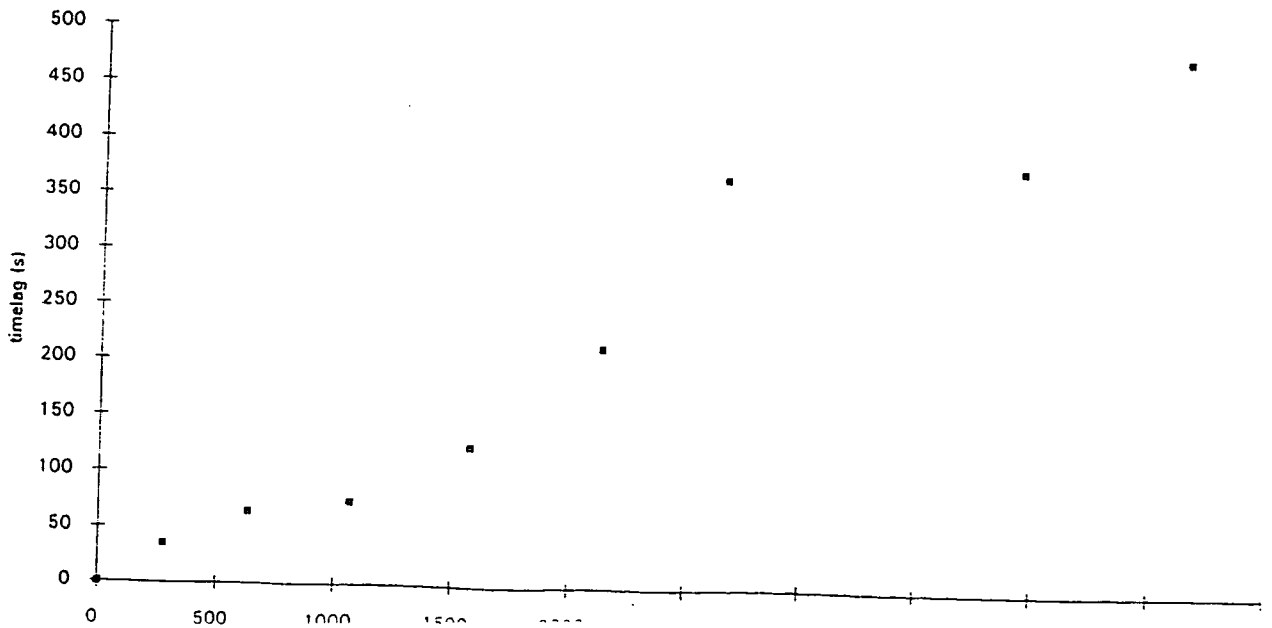
Figure 3.52. Series 11. Timelag
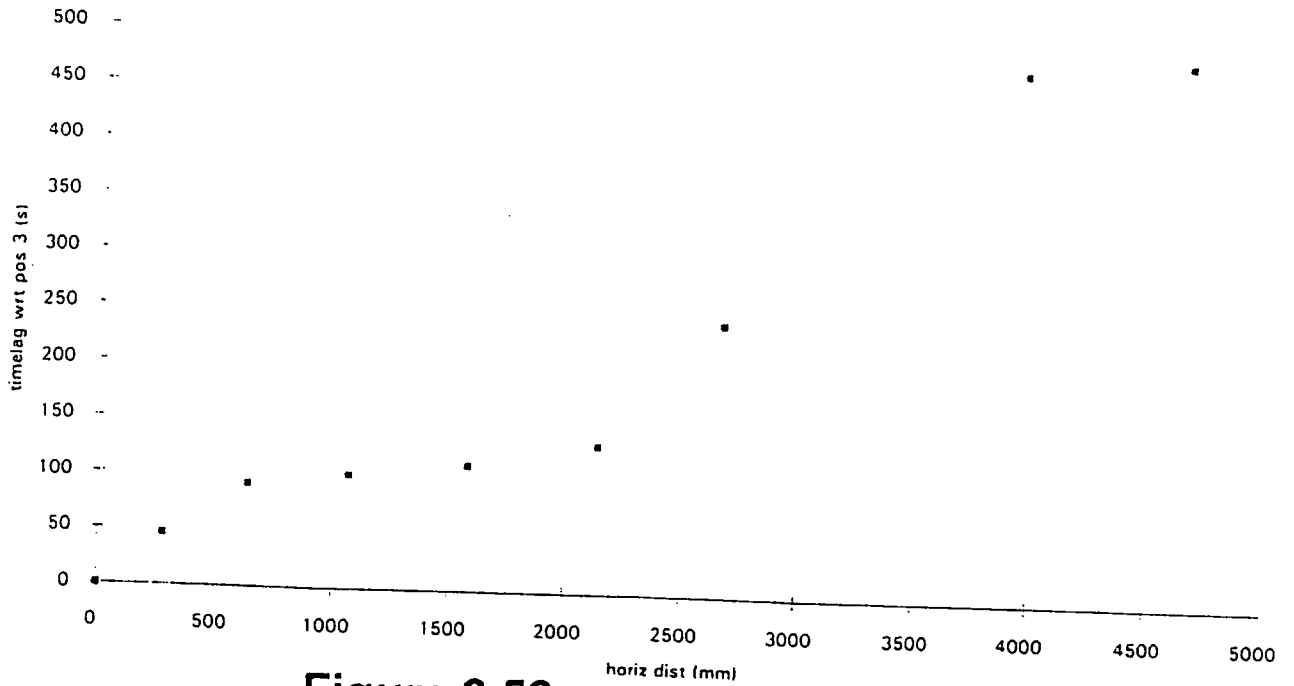
Figure 3.53. Timelag Series 12
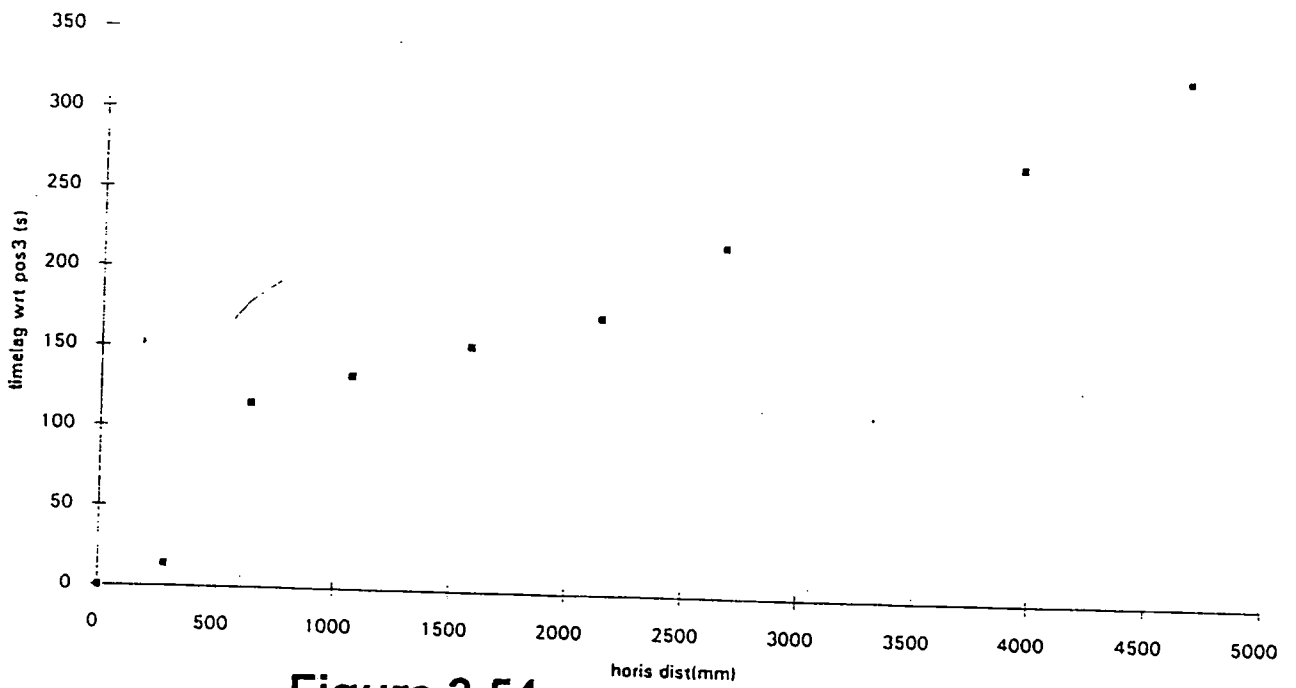
Figure 3.54. Series 13. Timelag
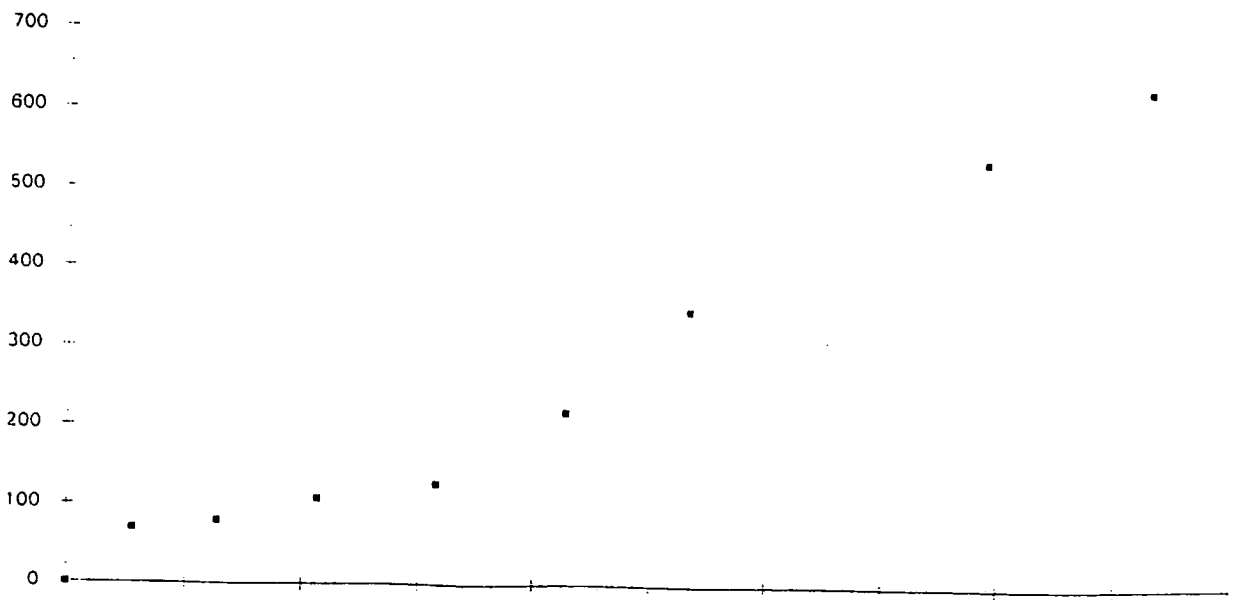
Figure 3.55. Series 14. Timelag
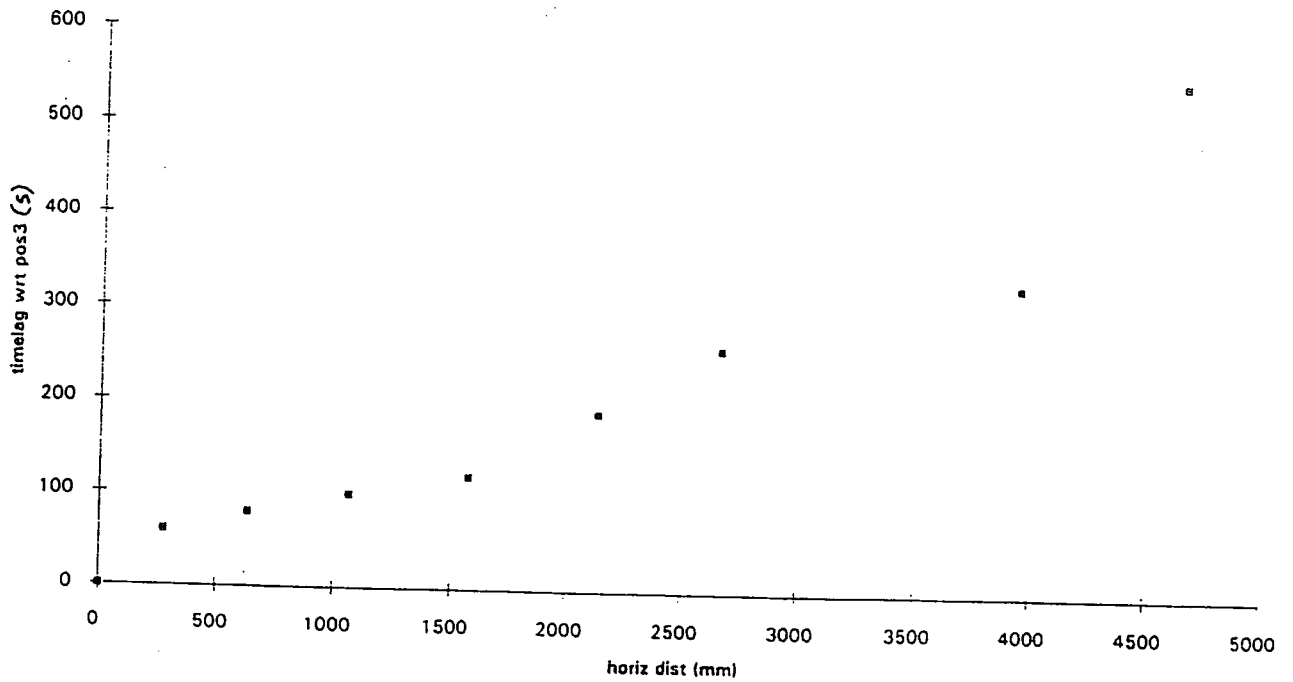
Figure 3.56. Series 15. Timelag
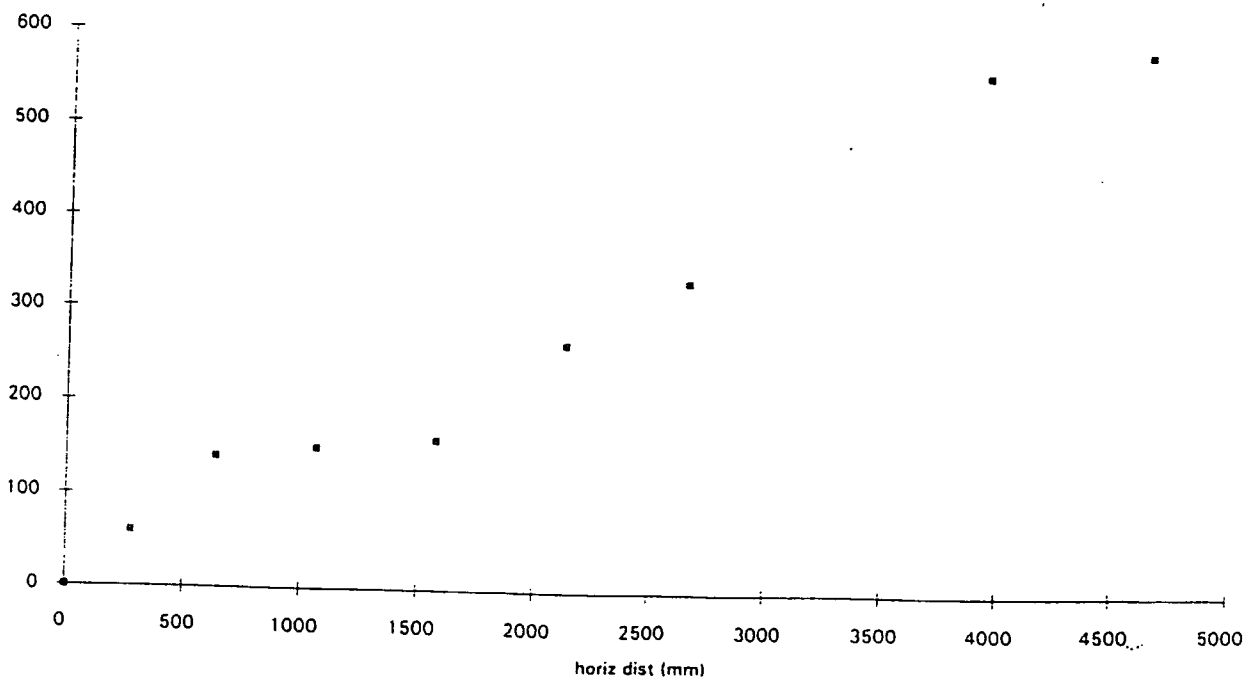
Chapter 4
Numerical Modelling

4.1. Introduction

The Laboratory experimental work outlined in chapter 3 concluded with graphs representing primary and secondary amplitude decay and time lag. The objective of this project was to apply these results to determine the model aquifer properties:- coefficients of permeability, leakage and storage.

Ferris developed two equations which incorporate time lag and attenuation differences between source stage and groundwater head at various distances from the tidal boundary. These formulae can be applied to results from which diffusivity (transmissivity/storage coefficient) can be determined. Ferris' assumptions in developing the theory are outlined in detail in section 1.4.2. Two of these assumptions were:

1. The aquifer extends an infinite distance shoreward from the harmonically varying source.

2. Vertical flow considered negligible, i.e. leakage from or into the aquifer is insignificant.

This chapter outlines the model concepts and details numerical modelling with a view to whether Ferris theory, which incorporates the above assumptions, can be applied to results obtained from the Durham Model Aquifer. In addition, the effects on results of amplitude decay and time lag due to variation of the tidal period were ascertained.

4.2. Conceptual Model

The design concepts for the model were outlined in section 2.2 of the thesis and a schematic diagram of the constructed model was presented in Figure 2.2.

In addition to the design concepts, the model aquifer was semi-confined (thus allowing vertical leakage) and also constrained by a finite length. The consequences of these effects were:

(a) Leakage from the upper surface of the aquifer.

(b) Reflection from the end of the aquifer - an impermeable boundary.

This is illustrated in Figure 4.1 below.
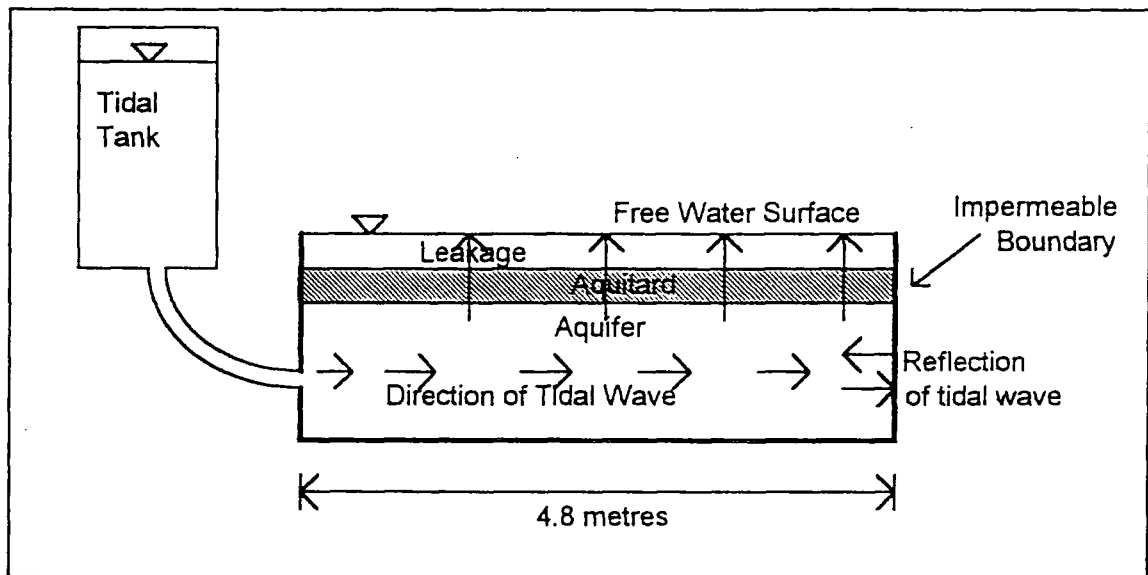
Figure 4.1. Schematic Diagram Illustrating Finite Length and Semi-confined Nature of the Durham Model Aquifer.

The leakage effect was quantified in preliminary work when an estimate for the leakage coefficient of 2×10^{-5} s^{-1} was concluded. The effects of leakage on amplitude decay and time lag of the tidal wave were uncertain.

The effects of the impermeable boundary and reflection of the tidal wave were also uncertain.

Due to the above two characteristics, it was not known whether Ferris' assumptions could be reasonably applied to represent the case of the Durham Model Aquifer

Therefore, it was decided to investigate the extent the influence of these characteristics on (a) amplitude decay and (b) time lag.

From this investigation, it could be concluded whether the effects were significant and therefore whether application of Ferris' theory to the tidal test results on the Durham Model Aquifer was justified.

4.3. Programme of Numerical Analyses

The purpose of the numerical modelling work was to investigate the effects of leakage, reflection and period variation on amplitude decay and time lag of the tidal wave. Amplitude decay and time lag were the results from the experimental work on the physical model.

The software, CVM (OGI, 1994) was applied for this work.

The structure of the investigation is outlined below:

Case Study A. Confined Aquifer of Infinite Length.

The concepts of leakage and reflection were not incorporated in the numerical model for case study A.

1. Ferris' theory. Graphical results of time lag and amplitude decay.

2. Numerical modelling. Application of CVM software concluded graphical results of time lag and amplitude decay.

3. Comparison of Ferris and CVM results.

4. Examination of effects of different periods on amplitude decay and time lag. Normalisation of period influence, so that results of varying periods can be compared.

Case Study B. Confined Aquifer of Finite Length.

Reflection was incorporated in the numerical model whilst the concept of leakage was ignored. Three periods were selected for investigation.

1. Amplitude decay and time lag were deduced from numerical modelling, applying CVM.

2. Results from application of CVM were compared with solutions derived from Ferris' theory.

3. Image Well Theory was described to aid explanation of reflective effects.

Case Study C. Semi-confined Aquifer of Infinite Length.

The concept of leakage was incorporated in the numerical model whilst reflection was ignored.

The CVM solution was then compared with Ferris' solution.

Case Study D. Semi-confined Aquifer of Finite Length.

The concepts of leakage and reflection were both incorporated in the numerical model.

1. Amplitude decay and time lag from application of CVM were compared with solutions derived using Ferris' theory.

2. Attempts were made to normalise results so that different periods could be compared.

These Case Studies together with graphical results are outlined in more detail below.

4.4. Design of the Numerical Model

The Curved Valley Model (CVM) software was prepared by Oxford Geotechnica International, and was modified by Crowe (1994) to incorporate a harmonic boundary. Conclusive results from numerical modelling were derived by running the CVM software three times:

Run 1. This involved establishing a decay envelope to minimise the number of time steps required before a regular harmonic pattern was observed. The software is designed to iterate results until they fall within a specified tolerance. The number of iterations is reduced if input heads are relatively close to expected results. The aquifer was designed with a fixed head at one boundary. The programme was then run for steady state conditions, producing results illustrating exponential head decay with distance. These results were later returned to the input file for future restart. Running the

software with an input file designed for steady state conditions, produced an exponential decay curve. This curve was the decay envelope for harmonic variations of head. These head values were inserted into the file for Run 2.

Run 2. As yet harmonic parameters cannot be incorporated in the visual basic part of the CVM programme. Run 2 is therefore required to define a transient situation. In addition, the heads from Run 1. are incorporated as a starting point for head calculations.

Run 3. The input file from Run 2. was edited to incorporate tidal wave parameters. The modified version of CVM (CVMWAVE) was then run to conclude harmonic head variations with time.

Details of the design of the numerical model are provided below.

4.4.1. Aquifer Modelling

A finite element model was designed to represent the physical Durham Model Aquifer. This involved setting boundary conditions and defining aquifer properties. For numerical analyses purposes, the aquifer properties were assumed values estimated from preliminary laboratory work with the Durham Aquifer. These properties are listed below.

Coefficient of permeability 4×10^{-3} m/s

Coefficient of leakage 2×10^{-5} s^{-1}

Coefficient of storage   0.1

In addition to the aquifer properties, the size of the model had to be prescribed. The CVM software was designed with no-flow boundaries at either end of the aquifer. The length of the aquifer was defined as the distance from position 3 to the boundary farthest from the tidal tank i.e. 4.7 metres. This was to comply with the experimental results of amplitude decay and time lag which were calculated with reference to this position. The no-flow boundary farthest from the tidal tank constituted an

102

impermeable boundary. Therefore definition of an aquifer length of 4.7 metres would include the concept of reflection.

A schematic diagram for explanatory purposes is presented below in Figure 4.2.
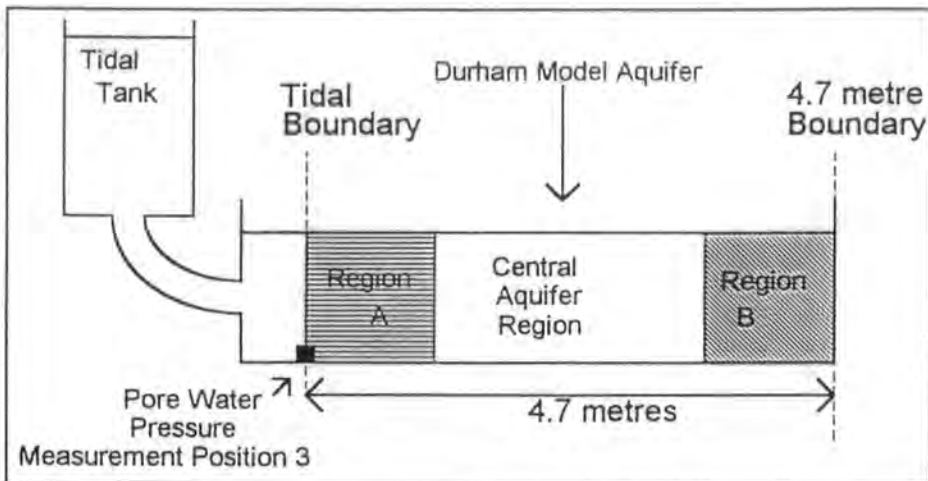
Figure 4.2. Schematic Diagram of Durham Model Aquifer Indicating Regions A and B in addition to the Central Aquifer Region.

For purpose of analysis of the aquifer without the reflective property, an aquifer length of 15 metres was defined, and observations of amplitude decay and time lag made over the first 4.7 metres of the model. It was assumed that this design would result in negligible reflective effects within the region of interest.

The dimensions of the numerical model aquifer were as follows:

Thickness of aquifer   0.25 metres

Width of aquifer   0.25 metres

Length   4.7 metres (incorporating reflective property)

                            15 metres (simulating no reflection)

The finite element model consisted of a specified number and arrangement of elements connected by nodes. The finer the mesh (i.e. larger number of elements), the more detailed the result, however the cost of this is run-time. It is useful to design the elemental mesh such that nodes fall close to physical positions of interest. The CVM software allows observation of results at six specified locations. It was decided that observation nodes, which are best equally spaced, should correspond to

positions 3, 4, 6, 9, 11 and 12 in the Durham Aquifer. The number of elements designed for the numerical model length of 4.7 metres was 94, whilst for the 15 metres long model, 150 elements were prescribed.

The software allows different materials types to be selected. This enables modelling of groundwater behaviour in areas comprising a variety of different soil materials with different aquifer properties. A numerical model of the physical Durham Aquifer was designed by Lourenco (1994) using CVM software and comprised two material types. These were prescribed as the tidal tank and the sand aquifer itself.

For the current analyses procedure, one material type was selected. This constituted the sand aquifer between position 3 and the boundary farthest from the tidal tank. It was assumed that aquifer properties remained constant within this region.

4.4.2. Tidal modelling

Tidal modelling was also designed to represent the tidal system used in conjunction the physical model aquifer.

The tidal boundary was corresponded with position 3 as was outlined in section 4.4.1. Although amplitude *decay* is independent of the original tidal amplitude, for purpose of analysis, a suitable amplitude had to be selected. The amplitude of the harmonic wave was specified based on laboratory results and wave spectra, in particular the primary constituent of the wave. The amplitude of the primary constituent of the wave at position 3 was used for numerical modelling purposes. Although the amplitude of the source wave varied slightly between laboratory results, an approximated value of 0.2 metres was concluded.

Several wave periods were considered for analysis. These are outlined in detail for each of the case studies.

The number of time steps was limited to 200 and linear time steps were chosen for easy analysis of output. The length of each time step was specified as 50 seconds. This was based on the amount of time the software required before a regular harmonic pattern was observed. An illustration of the output from running the tidal programme is illustrated in Figure 4.3. It was possible to view the data files

corresponding to these graphical results. From these files, amplitudes of the wave at each of the observation nodes could be calculated. In addition, the time lag of the wave at each observation node, with respect to the first, could be estimated. This could not be determined to any great degree of accuracy because the time steps were limited to 50 seconds. This resulted in errors in time lag estimates from the CVM model of approximately ± 25 seconds. Small values of time lag therefore incorporated a large percentage error.

4.5. Case Study A. Confined (Non-Leaky) Aquifer of Infinite Length.

Concepts of leakage and reflection were not included within the design of this particular numerical model.

4.5.1. Ferris Theory

Ferris' theory was outlined in section 1.4. of the thesis. The formulae Ferris developed for time lag and amplitude variation were applied for the case of the physical model, using estimates for parameters as explained in section 4.4. These are summarised below:

Coefficient of permeability, $K = 4 \times 10^{-3}$ m/s

Thickness of the aquifer, b = 0.25 metres

Width of Aquifer, w = 0.25 metres

Transmissivity, $T = Kb = 1 \times 10^{-3}$ m^2/s

Coefficient of storage, S = 0.1

The period of tidal wave selected for analyses was 1920 seconds. This period value was the most common from the laboratory work, and lay approximately in the middle of the range of other primary wave periods.

Equations 1.8 and 1.9 in chapter 1 were applied using the above parameters. Results of amplitude decay, h_x/h_0 and time lag, t_L, were calculated for various

105

horizontal distances from the tidal boundary. Hence, graphs were produced illustrating analytical results of amplitude decay and time lag of the tidal wave with horizontal distance. These are illustrated in Figures 4.4. and 4.5. respectively.

4.5.2. CVM solution

The model was designed as described in section 4.4. For this case study, the aquifer length was prescribed to be 15 metres. A wave period of 1920 seconds was selected for analysis, to comply with Ferris' method.

The software CVM was applied to the numerical model as described in section 5.2. Results of amplitude decay and time lag were calculated from the output data file. These results are illustrated in Figures 4.6. and 4.7. respectively.

4.5.3. Comparison of Results from CVM with Ferris Theory

The results from section 4.5.1 and application of Ferris theory were compared with CVM results from section 4.5.2. The comparisons of amplitude decay and time lag are shown in Figures 4.8. and 4.9. respectively.

It can be seen that results of amplitude decay from analytical theory compare well with the numerical solution. Figure 4.9. does not illustrate such a good comparison for the time lag results. This discrepancy is probably due to the inaccuracy in estimating time lag from the output files produced by CVM.

This work illustrated the suitability of applying the CVM model, and accuracy of the results it produced. It was concluded that amplitude decay results were highly accurate, whereas slight incorrections were inherent in determining time lag.

4.5.4. The Effects of Period Variation on Results

The effect of period variation on results of amplitude decay and time lag was investigated by application of Ferris theory. Three different tidal periods were considered and results of amplitude decay and time lag were deduced for each. The test periods were selected to correspond with the range of periods from the

experimental work, and were 1746s, 1920s and 2743s. Figures 4.10. and 4.11. illustrate the results. These Figures show that period has significant effect on amplitude decay and time lag. The extent of this effect decreases as period decreases.

The objective of this work, was to normalise data of amplitude decay and time lag so that results of different periods could be compared.

Results of work of other researchers were examined. Amplitude decay data of waves within the sea-bed has been plotted versus depth/wavelength (Thomas, 1990). Bearing this in mind, a corresponding graph of amplitude decay versus distance/wavelength was produced by applying Ferris theory to the Durham Model Aquifer.

The wavelength for the tidal period of 1920 seconds was calculated as follows:

$$\text{celerity} = \frac{\text{total length}}{\text{total time lag}} = \frac{4.7}{581} = 8 \cdot 1 \times 10^{-3} \text{ m/s}$$

wavelength = celerity × wave period = $8 \cdot 1 \times 10^{-3} \times 1920 = 15 \cdot 5$ metres

The wavelengths corresponding with the two other periods, 1746s and 2743s, were calculated following the same procedure, and found to be 14.8m and 18.6m respectively.

The data of amplitude decay for the three periods tested was found to converge. This is illustrated in Figure 4.12.

Time lag data was plotted versus distance/celerity. The celerity of the wave with period 1746s was 8.48 x 10^{-3} m/s, whilst that for period 2743s was 6.77 x 10^{-3} m/s. Figure 4.13 illustrates the convergence of the data for the three periods under investigation.

From Figures 4.12 and 4.13, it can be concluded that it is easily possible to normalise the wave period in a confined aquifer of infinite length.

For investigatory purposes, two graphs of amplitude decay and time lag versus distance/period were plotted. Results from different periods were not found to

converge. The parameters of distance/wavelength and distance/celerity were found to be unique for period normalisation of amplitude decay and time lag respectively.

4.6. Case Study B. Confined Aquifer of Finite Length

This section describes how the effects of reflection on amplitude decay and time lag were investigated. The CVM model was used to produce results incorporating the reflective boundary.

4.6.1. CVM Solution

As was explained in section 4.4. above, reflection was incorporated in the numerical model by the presence of a no-flow boundary at a distance of 4.7 metres from the tidal boundary. Leakage was not incorporated in the numerical model at this stage. The results from the numerical modelling for the three periods, 1746s, 1920s and 2743s are illustrated in Figures 4.14. and 4.15.

4.6.2. Comparison of Results from CVM with Ferris Theory

CVM results were then compared with results from Ferris work, to investigate the extent of the effect of reflection on amplitude decay and time lag. Figures 4.16 through to and including 4.21 illustrate this comparison. These figures clarify the extent of reflective effects and are discussed below.

4.6.3. Discussion of Reflection Effects

There will be several reflected waves due to the concept of Image Well theory. The real wave will be reflected from the 4.7 metre boundary. This primary reflected wave will be then reflected from the boundary where the tidal wave is initiated, to form a second reflected wave. This secondary reflected wave will then be reflected from the

aquifer boundary furthest from the tidal tank. This reflective process will continue *ad infinitum*. Decay of the waves as they are reflected will, however, mean that after a finite number of reflections their effects on water-level response will be negligible. Image well theory can be applied to predict reflective effects. Image well theory was developed by Ferris et al (1962) and is documented in several textbooks including Freeze and Cherry (1979). This theory applies to a confined aquifer bounded at one end by a hydro-geologic boundary, across which no flow can occur. The drawdown as a result of pumping, will be greater near this boundary. In order to predict these drawdowns, the method of images, a technique which is widely used in heat-flow theory, has been adapted to groundwater situations (Ferris et al., 1962). For purpose of analysis, boundaries are considered to be either recharge or barrier boundaries. Application of this theory to the Durham Model Aquifer is illustrated in Figure 4.22. Infinite images are considered for six reflections. In this diagram, h_f signifies the fixed amplitude of the tidal wave.
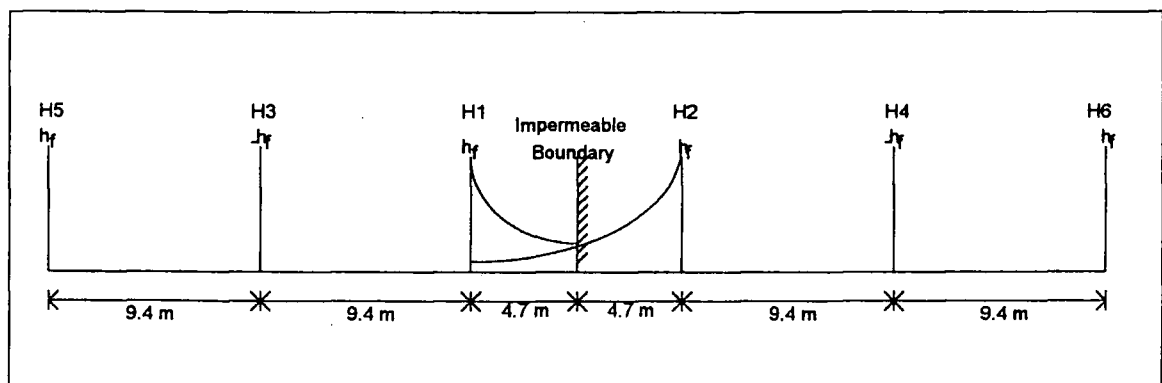
Figure 4.22. Image Well Theory Applied to the Durham Model Aquifer.

H1 represents the initial source of the real wave, with tidal amplitude, h_f. H2 represents an image tidal source, which causes the effect of the primary reflected wave in the region of interest (0 to 4.7 metres). The image tidal source produces waves also of amplitude, h_f, at a distance of twice the aquifer length (2L) from the real source. The effects of the third reflected wave can be represented by a second image source also 2L away, but in the opposite direction to real wave movement. This second image source produces a wave of amplitude $-h_f$. This negative

amplitude is brought about by the need to balance the overall system. Addition of the first image wave source with tidal amplitude, h_f, left the system out of balance. This effect therefore had to be compensated by a negative wave amplitude produced by the second image source. Further reflected waves were represented by image sources in the same manner to that described above.

The numerical magnitudes of the real wave from source H1 and the reflected waves from each of the sources H2 and H3 illustrated above were calculated. This computation was based on Ferris theory using the properties estimated initially for the Durham Model Aquifer. The result of this is shown in Figure 4.23. Superposition of each of these waves within the 0 to 4.7 metre range will produce an approximation of the actual wave. Superposition must incorporate the relative phases of the waves so that constructive and destructive interference effects are considered. Therefore, the magnitudes of the computed amplitude decays cannot simply be added together. Figure 4.23. does illustrate the reflected waves which significantly affect the resultant waveform. It can be clearly seen that the reflected wave from the H2 boundary is by far the most significant, with the wave from the H3 boundary also having a much smaller effect. The effects of further reflected waves appear negligible.

4.6.3.1.   Amplitude decay

It may be useful to refer to Figure 4.2. throughout this section which discusses Figures 4.16. to 4.21.

Reflective effects are particularly significant in aquifer region B. In this region, these effects approximately double the amplitude decay anticipated from Ferris theory due to the reflected wave from the H2 boundary.

From figures 4.16. to 4.21, it can be observed that some CVM values are lower than corresponding results from Ferris theory. There are two reasons for this phenomenon. Firstly, superposition of real and reflected waves results in constructive and destructive interference due to differences in phase. The effects of phase differences mean that some amplitude values are subtracted from the original wave, producing a lower value than might otherwise be anticipated. Secondly,

110

reflection from boundary H3 is equivalent to applying a *negative* fixed amplitude at a distance of 9.4 metres (twice the aquifer length) away from the tidal boundary, H1. The is the principle of image well theory which was illustrated in Figure 4.22.

4.6.3.2.   Time Lag

The wavelengths of the tidal waves of periods 1746s, 1920s and 2743s were calculated in section 4.5.4. above. The corresponding periods of all of these waves was at least three times the length of the aquifer. This implied that real and reflected waves would be notably out of phase with each other.

The time lag (or phase difference) of the superposed wave is significantly greater than Ferris solution in the central region of the aquifer. Values at the boundaries of the aquifer fall very close to those based on Ferris theory. Neglecting the small effects of reflection from boundary, H3, the reasons for similarities and discrepancies between the two solutions can be accounted for as follows.

Phase differences between the real and governing reflected wave (from the H2 boundary) will *increase* as the reflected wave progresses towards the tidal boundary, H1. In addition, the magnitude of the effect of the reflected wave *decreases* as the wave progresses towards the tidal boundary. Therefore in aquifer region B, farthest from the tidal tank, the phase difference between the real and reflected waves is minimal, resulting in little difference between CVM and Ferris solutions. In the central region of the aquifer, the phase difference between the real and governing reflected waves is greater, and therefore a large discrepancy between CVM and Ferris solutions is observed. In aquifer region A, the phase difference between real and reflected waves is highest, however, the reflected wave has decayed significantly by this time. This implies that the effect of the governing reflected wave on the real wave is marginal. Values from CVM and Ferris are therefore similar in the region of the aquifer close to the tidal tank.

4.6.3.3.   Conclusion

This work illustrated that reflective effects significantly influence amplitude decay and time lag. Therefore, it was concluded that application of Ferris theory to laboratory results from the Durham Model Aquifer would have the consequence of large inaccuracies in estimates of aquifer properties. These would occur due to the finite length of the Durham Model Aquifer.

4.7. Case Study C. Semi-confined Aquifer of Infinite Length.

This section describes how the effects of leakage on amplitude decay and time lag were investigated.   The CVM software was used to produce results for a semi-confined model aquifer.

4.7.1.   Comparison of Results from CVM with Ferris Theory

Initially, one tidal period of 1920 seconds was investigated. The numerical model was adjusted to incorporate leakage. For purpose of analyses, the value of leakage used was 2×10^{-5} s^{-1}. The reason for this prescribed value is outlined in section 5.2.1 above.   Results from application of the CVM software were compared with results derived from Ferris theory. Figures 4.24. and 4.25. illustrate amplitude decay and time lag comparisons from these two approaches.

4.7.2.   Discussion of Leakage Effects

Figures 4.24. and 4.25. illustrate that the prescribed leakage has little effect on results of amplitude decay and time lag. The numerical solution for amplitude decay is slightly lower than that derived from Ferris' analytical theory. This is to be expected since the leaked water will result in more rapid amplitude decay. There is a slight

discrepancy between the time lag results, although this may simply be due to the difficulty in determining time lag accurately from the CVM results. There is an error in each of the numerical values of approximately ± 25 seconds. Further numerical modelling with tidal waves of different periods was not performed since these results illustrated such small leakage effects.

In conclusion, the prescribed leakage has a very small effect on results of amplitude decay and time lag.

4.8. Case Study D. Semi-confined Aquifer of Finite Length.

This section describes how the effects of both reflection and leakage on amplitude decay and time lag were investigated. The CVM model was used to produce results incorporating both these concepts.

4.8.1. Comparison of Results from CVM with Ferris Theory

The numerical model data was modified to incorporate both leakage and reflection. Results of amplitude decay and time lag were computed for three periods, 1746s, 1920s and 2743s, based on application of CVM. These results were then compared with Ferris' theory. Figures 4.26. to 4.31. illustrate this comparison.

These figures illustrate a significant difference between numerical and analytical solutions, due to the combined effects of reflection and leakage.

4.8.2. Period Normalisation

From section 4.5.4, it was concluded that results of amplitude decay and time lag of varying periods could be easily normalised. This would enable easy comparison of results of different tidal period. The parameters determined for period normalisation of the analytical Ferris' theory were computed for numerical model results

incorporating leakage and reflection. This was done to observe the extent of any convergence. The normalisation parameters applicable to Ferris theory were, for time lag, distance/celerity (X/c), and for amplitude decay, distance/wavelength, (X/L). The wave properties were calculated in a similar manner to that outlined in section 4.5.4. These values of the wave properties did not differ significantly from those calculated earlier and based on Ferris theory, and the total time lag. Reflection and leakage do not significantly affect total time lag. These wave properties are summarised in table 4.1 below.

Period (s)	1746	1920	2743
Wavelength (m)	14.8 m	15.5 m	18.6 m
Celerity / Wave speed (m/s)	8.5×10^{-3}	8.1×10^{-3}	6.8×10^{-3}

Table 4.1. Summary of Wave Properties.

Time lag was plotted versus distance/celerity, as is shown in Figures 4.32. Amplitude decay was plotted versus distance/wavelength as illustrated in Figure 4.33.

From these figures, the data points are observed to be fairly scattered with no clear convergence of results from different periods. Therefore, the parameters, X/L, and X/c are not useful in providing results normalised for period effects. In order to determine the normalisation parameters for amplitude decay and time lag with leakage and reflection, analytical theory must be considered.

4.9. Conclusion

The numerical modelling illustrated that concepts of both leakage and reflection affected results of amplitude and time lag. Significant discrepancies were observed between numerical results and those based on Ferris' analytical theory. Reflection was found to influence amplitude decay and time lag results to a greater extent than

leakage. It was found possible to normalise data from Ferris theory so that results of different periods could be easily compared. Results from numerical modelling incorporating leakage and reflection were not normalised. It was concluded that analytical theory must be developed in order to investigate appropriate normalisation parameters.

In conclusion, Ferris theory cannot be directly applied to laboratory results to determine aquifer properties. New analytical theory must be developed to include these characteristics, from which aquifer properties may then be calculated.
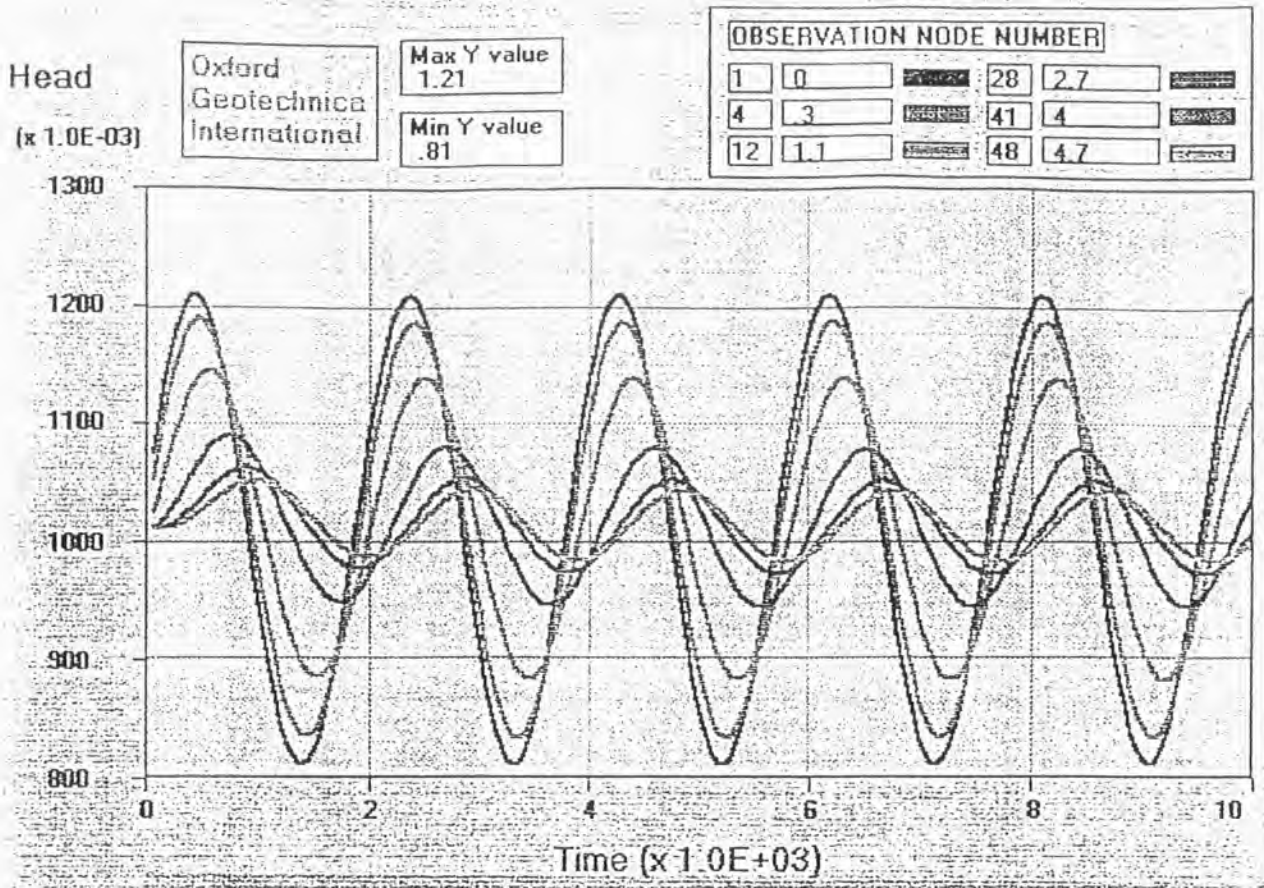
Figure 4.3. Output Format from Running CVMWAVE

Figure 4.4. Application of Ferris Theory to Determine Amplitude Decay, Period 1920s.
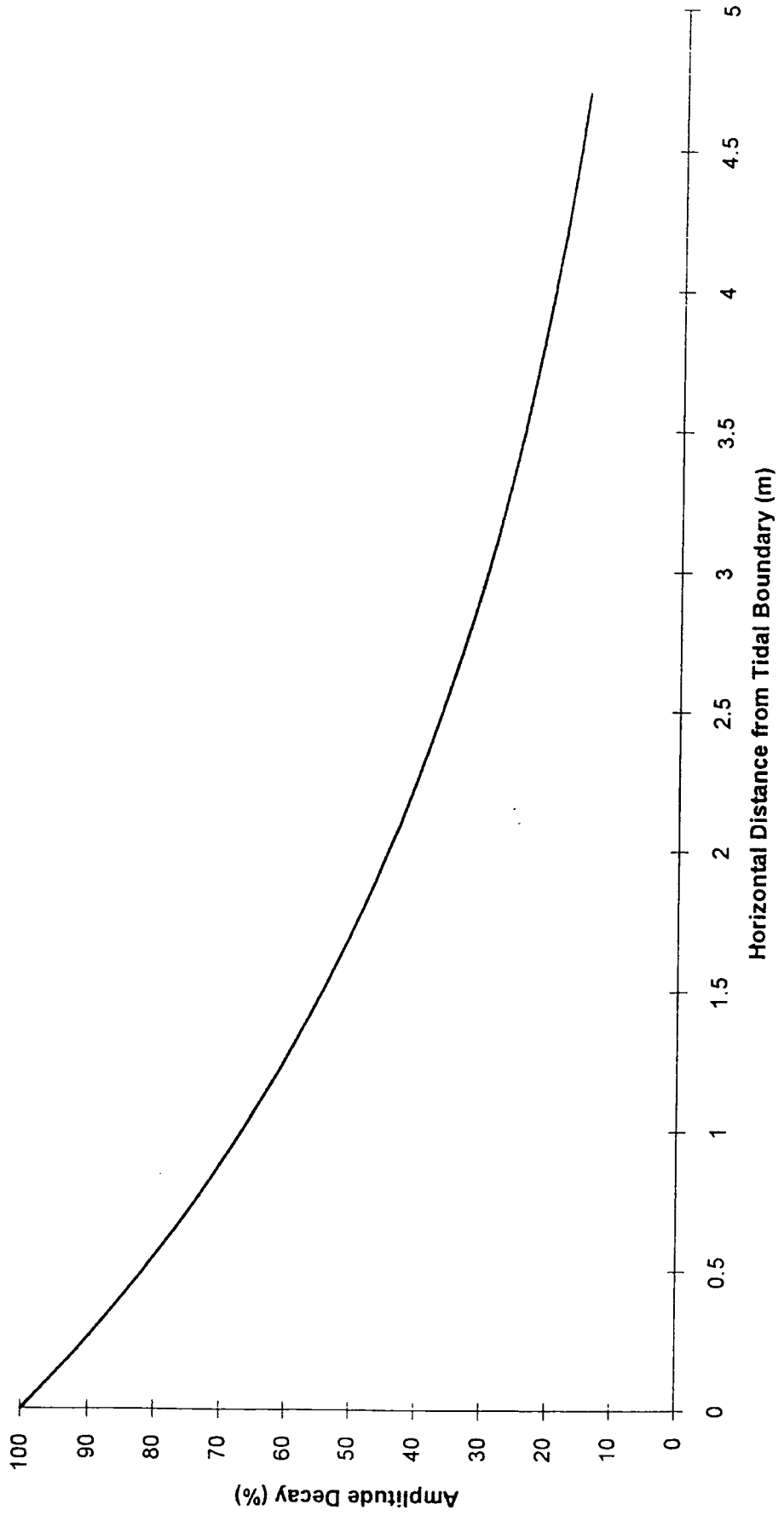
Figure 4.5. Application of Ferris Theory to Determine Time Lag. Period 1920s.
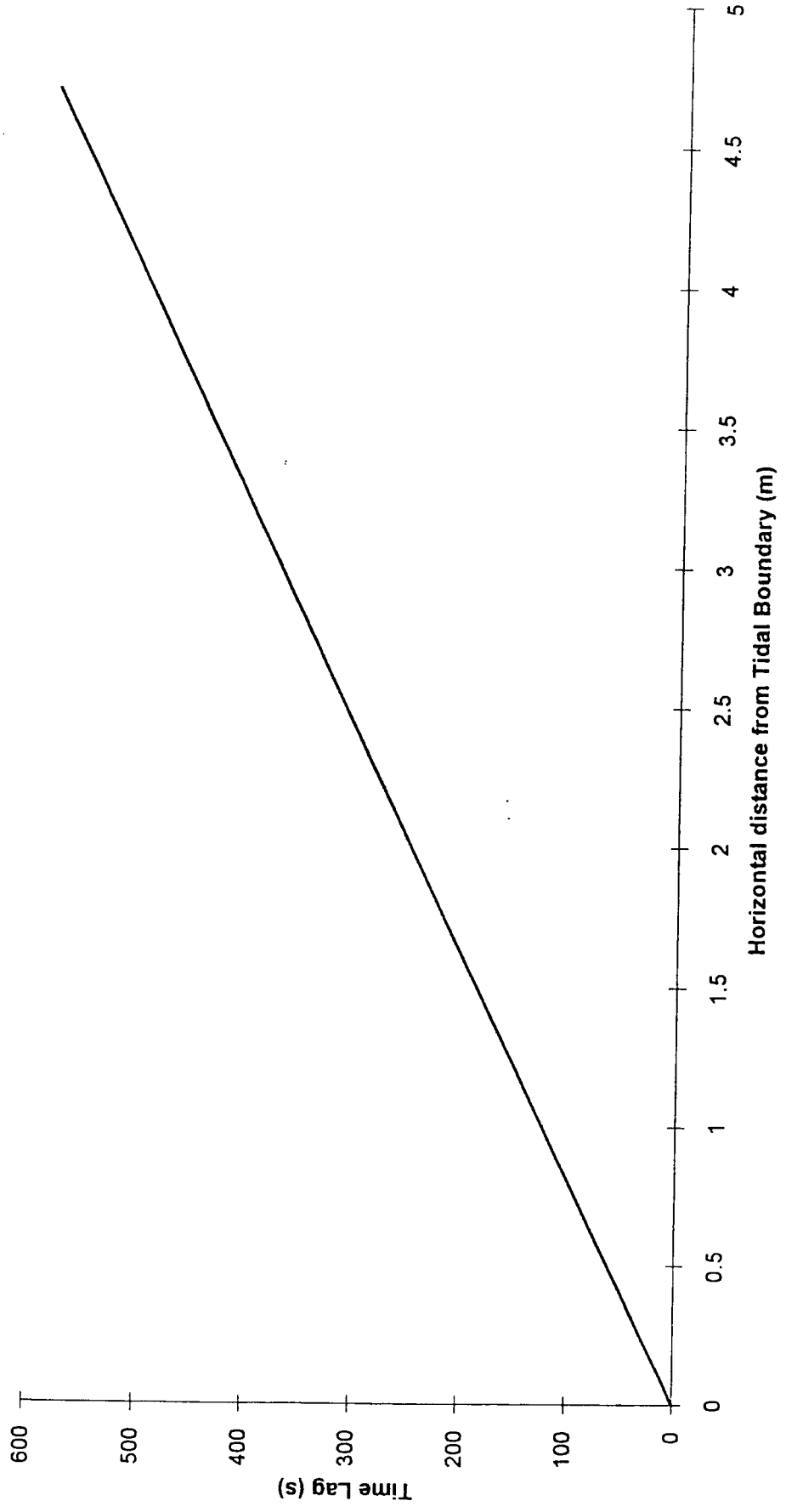
Figure 4.6. Amplitude Decay Results. CVM numerical modelling of Confined Aquifer of Infinite Length, Period 1920s.
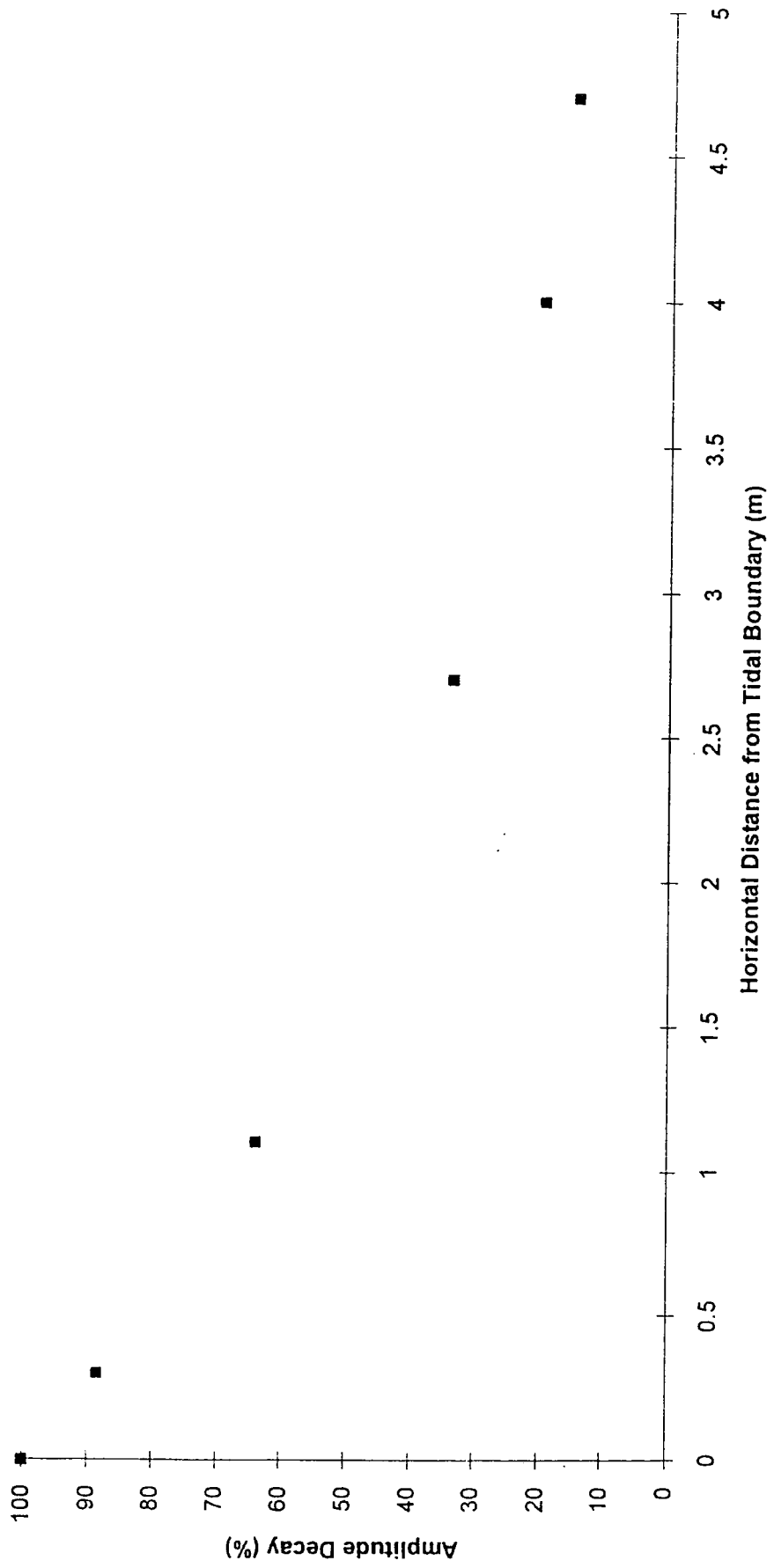
Figure 4.7. Time Lag Results from CVM numerical modelling of Confined Aquifer of Infinite Length. Period 1920s.
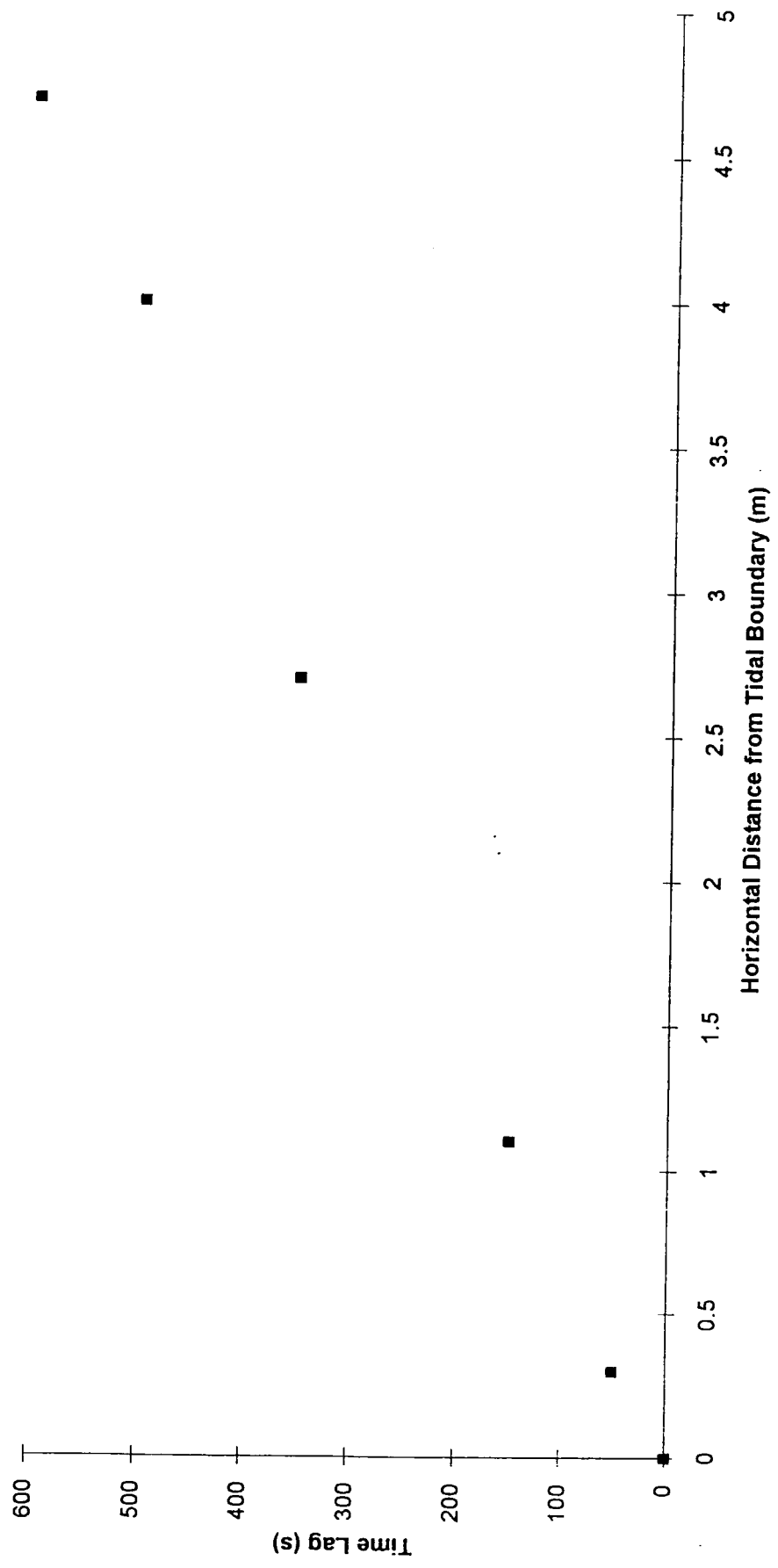
Figure 4.8. Comparison of Amplitude Decay Results from Ferris Theory and CVM. Confined Aquifer of Infinite Length. Tidal Period 1920s.
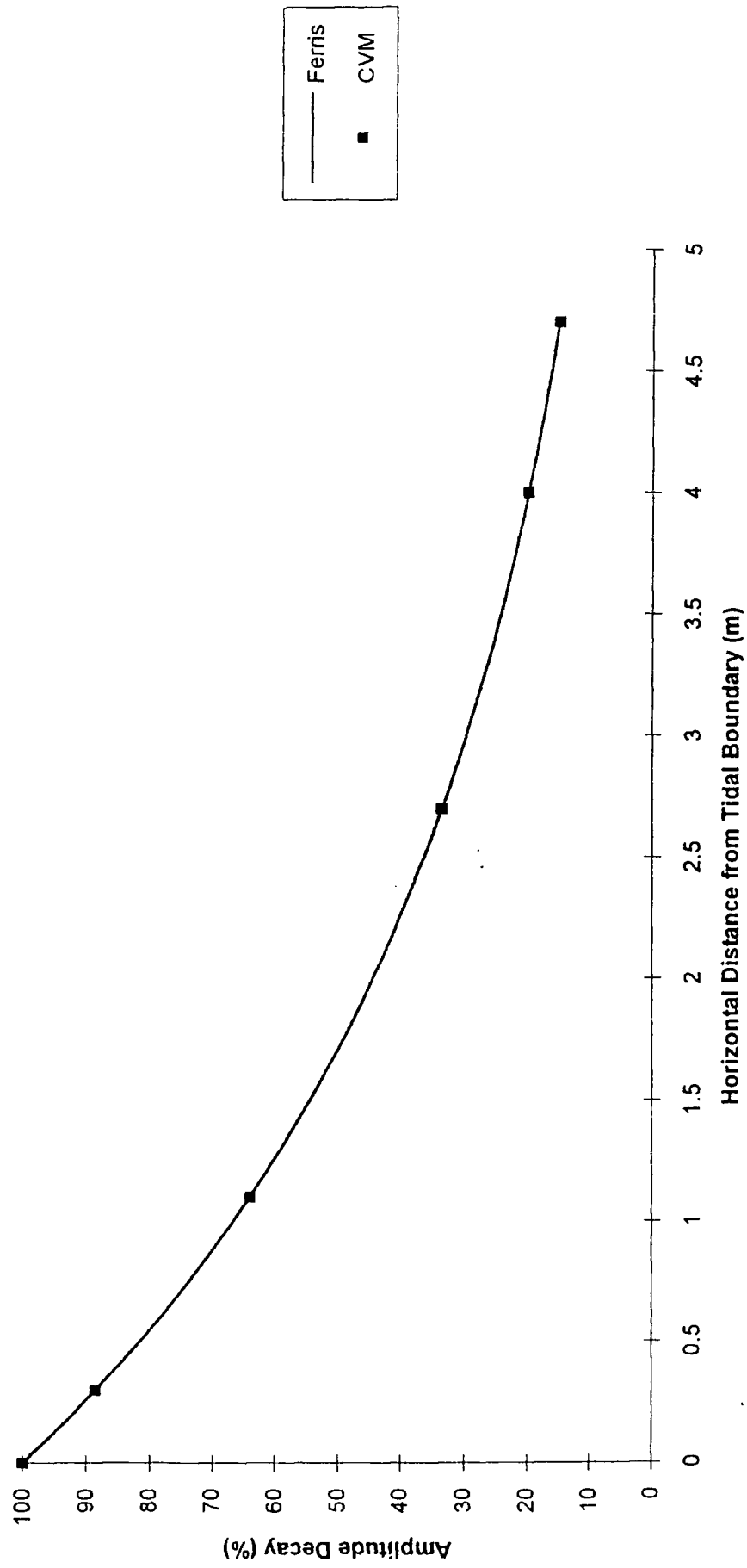
Figure 4.9. Comparison of Time Lag Results from Ferris Theory and CVM. Confined Aquifer of Infinite Length. Period 1920s.
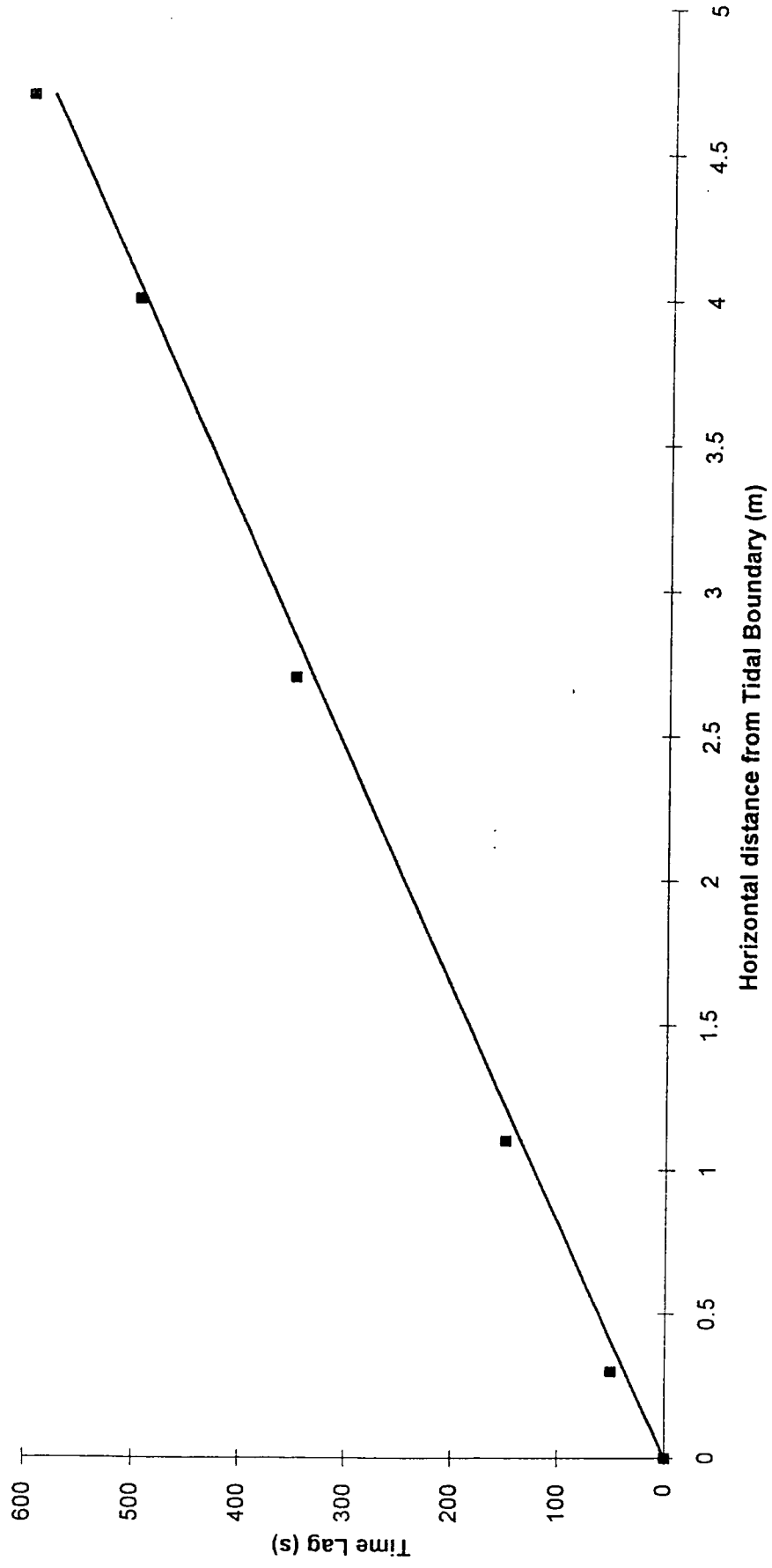
Figure 4.10. Amplitude Decay, Calculated from Ferris Theory, for Various Tidal Periods.
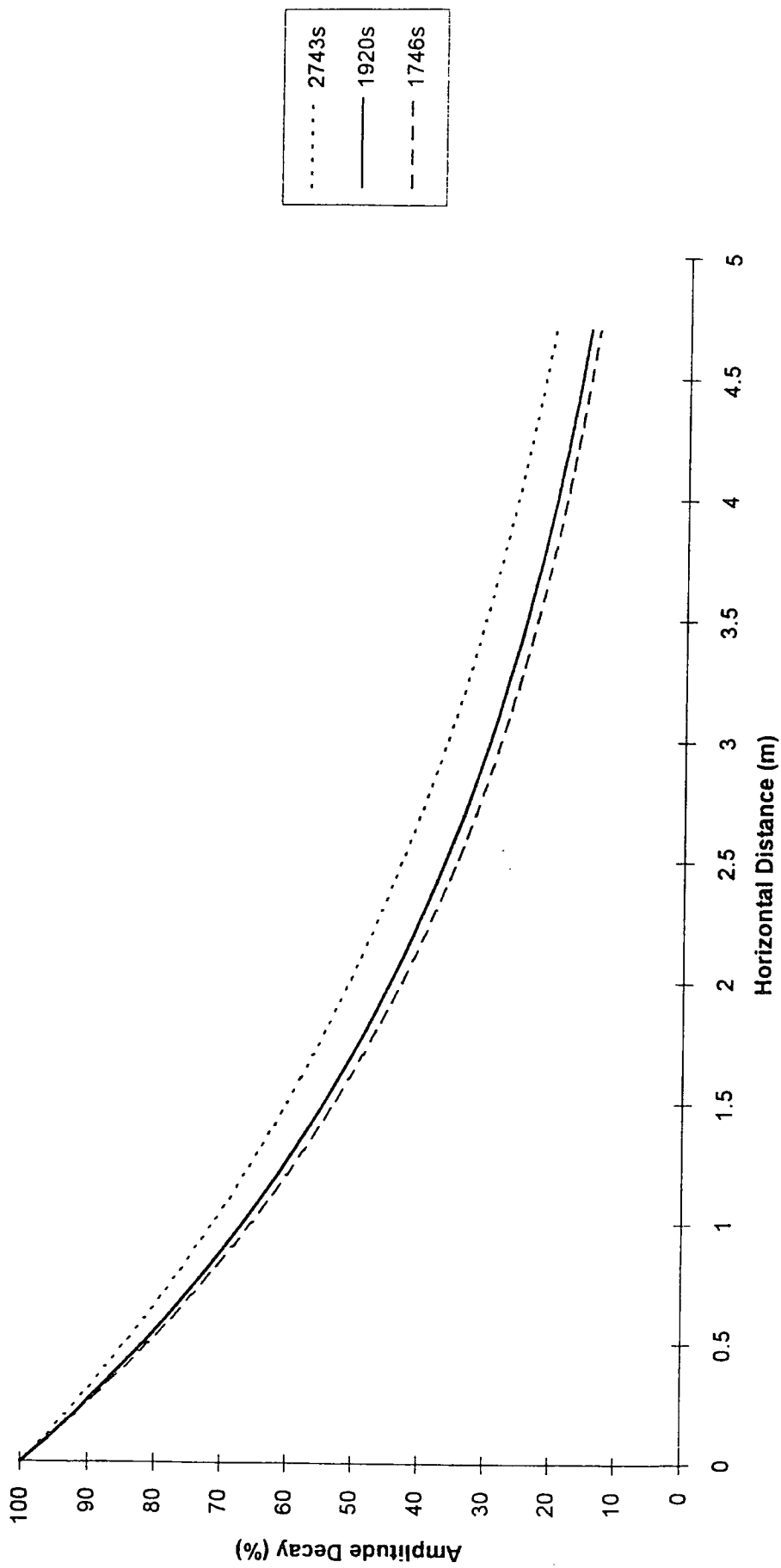
Figure 4.11. Time Lag, Calculated from Ferris Theory, for Various Tidal Periods.
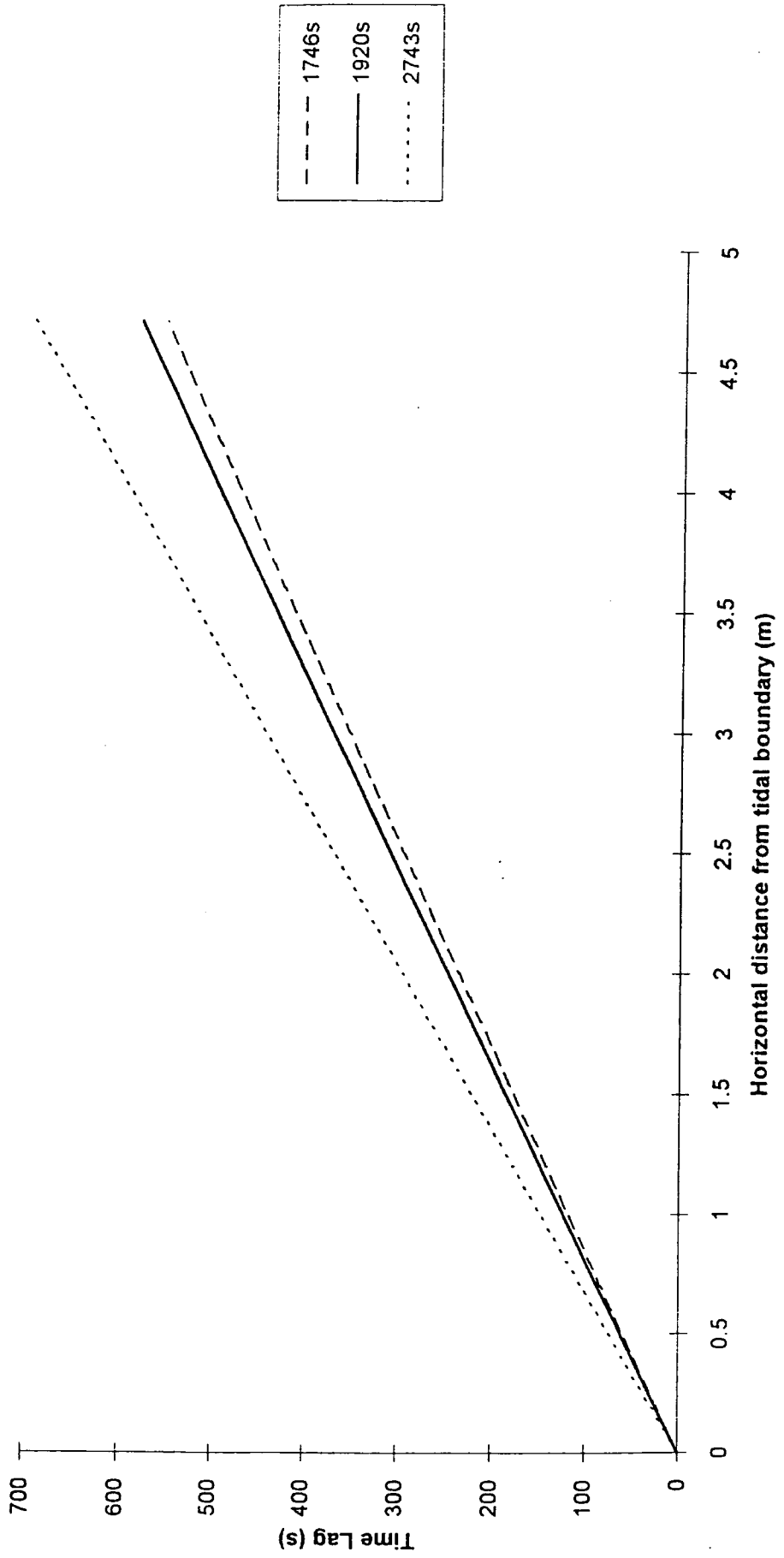
Figure 4.12. Period Normalisation of Amplitude Decay Results. Convergence of Data from Various Periods.
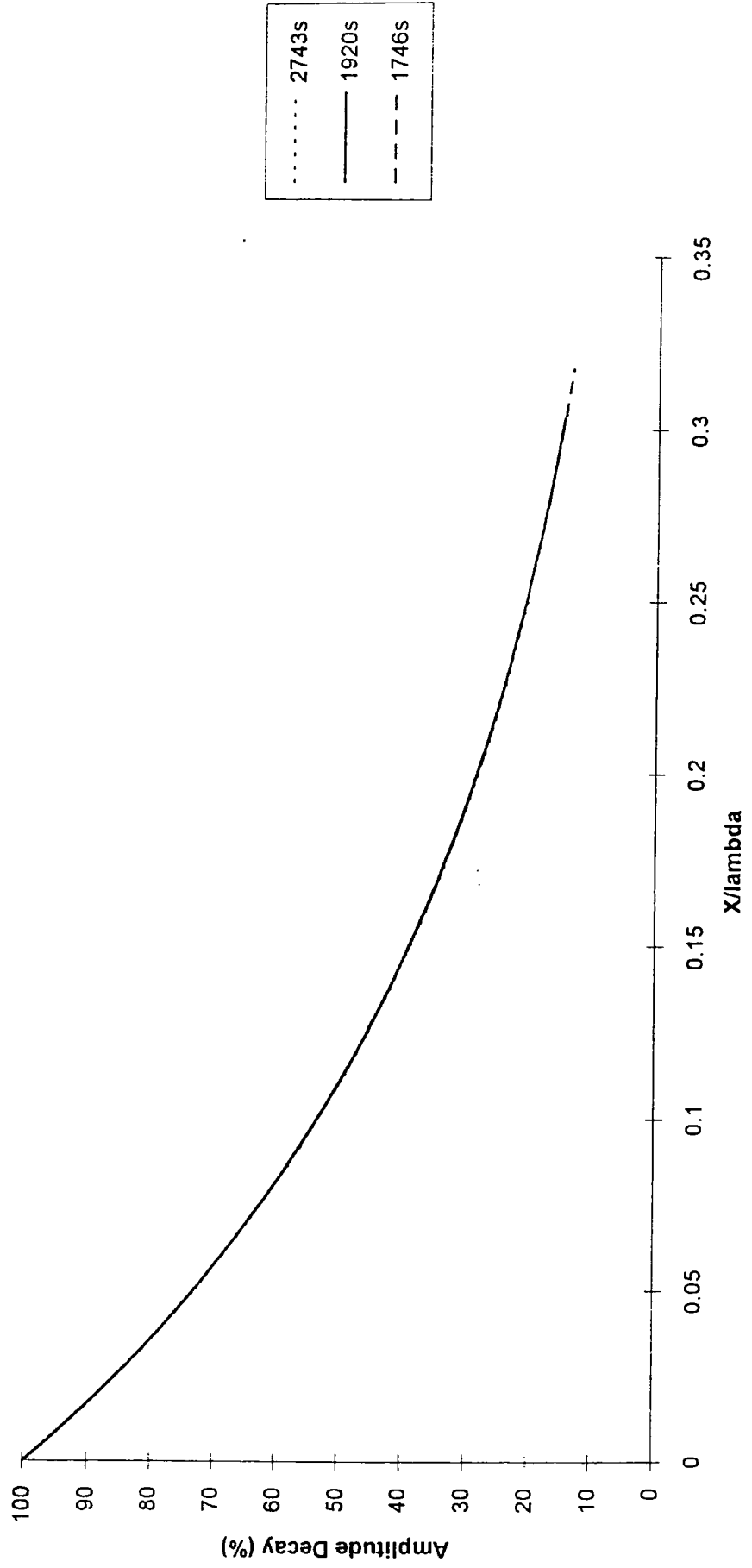
Figure 4.13. Period Normalisation of Time Lag Results. Convergence of data from various periods.

Legend:
- 2743s
- 1920s
- 1746s

Time Lag (s) vs Horizontal Distance/Celerity [s-1]
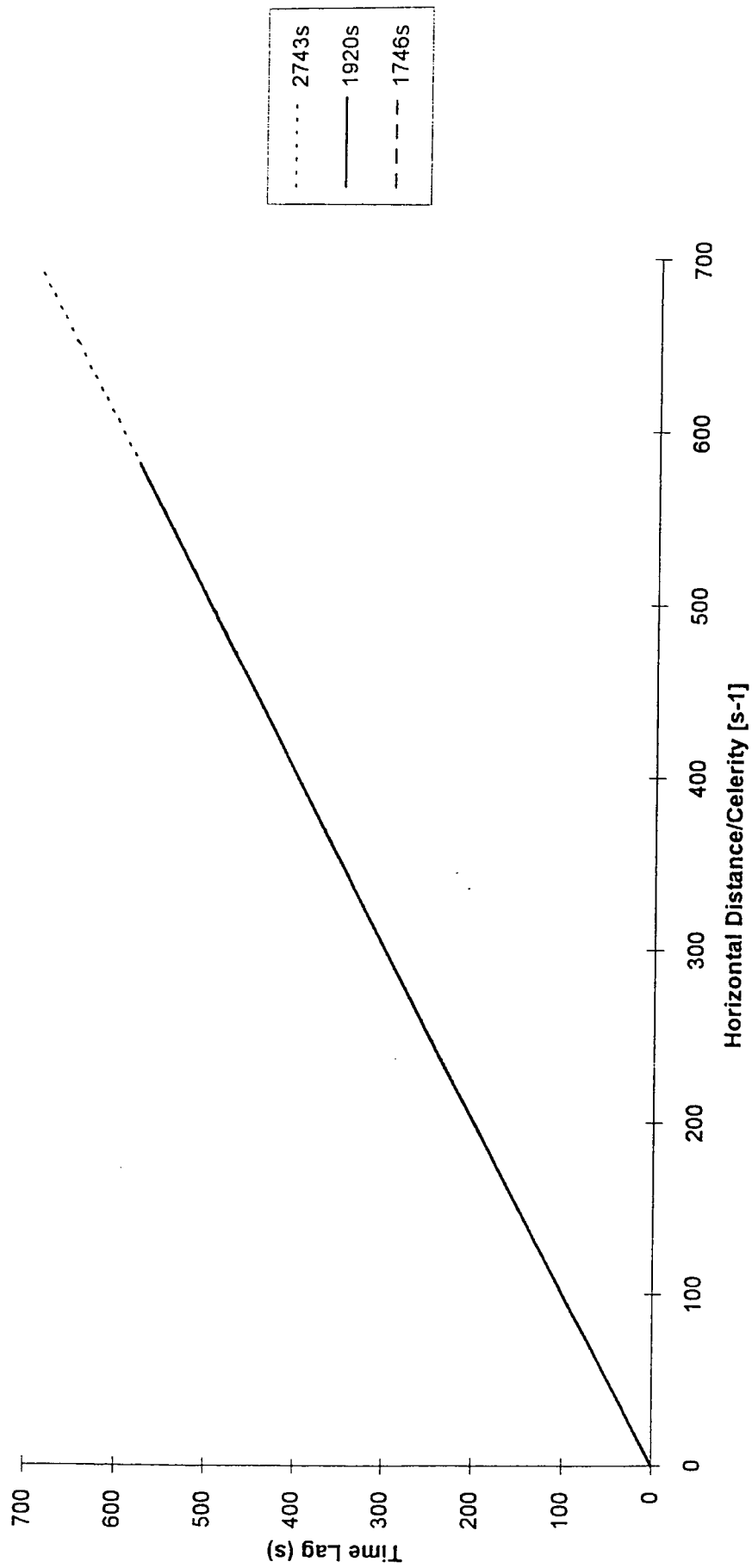
Figure 4.14. CVM Numerical Modelling Incorporating Reflection in a Confined Aquifer, Various Tidal Periods.
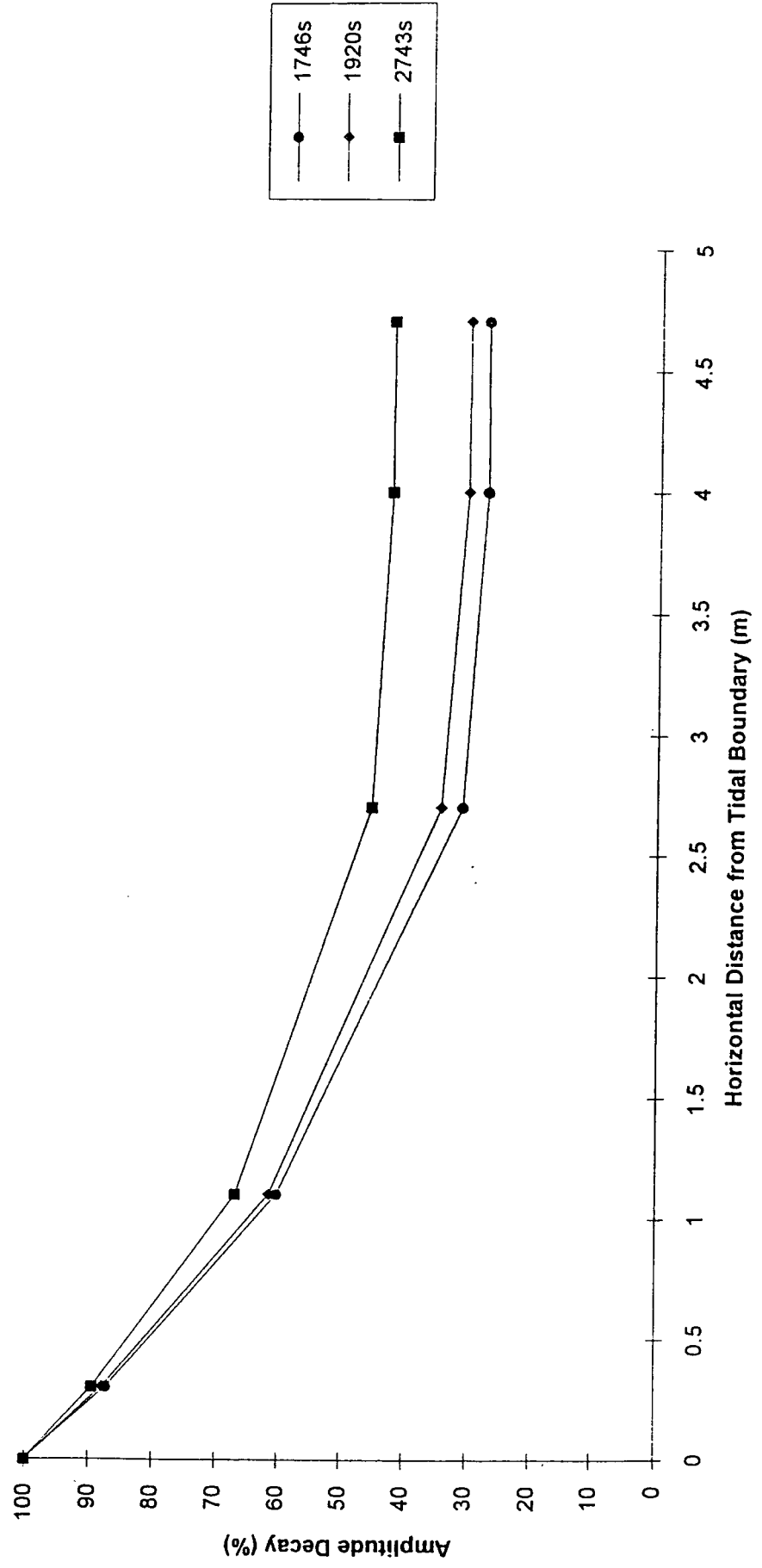
Figure 4.15. CVM Modelling Incorporating Reflection in a Confined Aquifer, Various Tidal Periods.
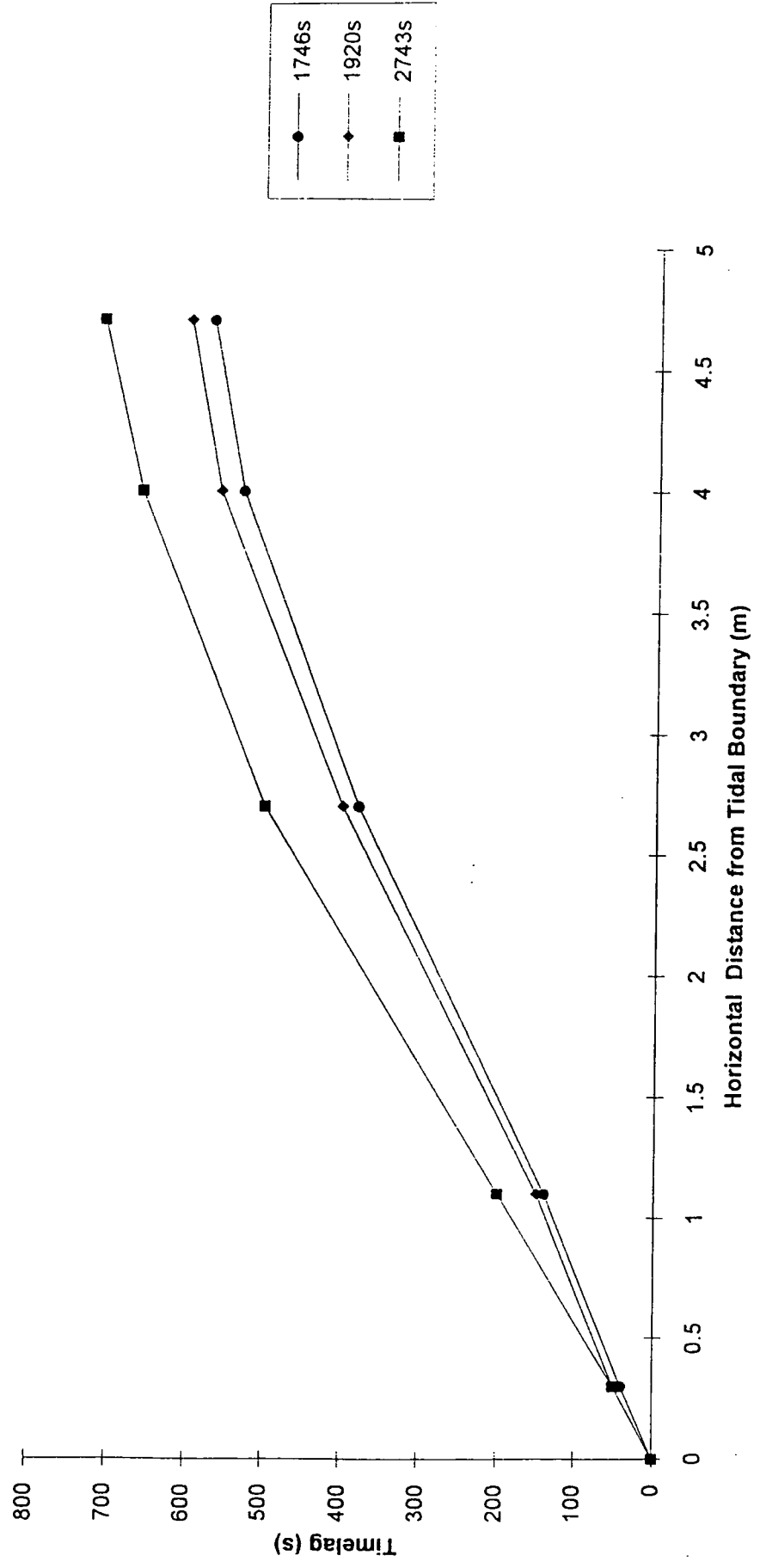
Tidal Period 1746 seconds
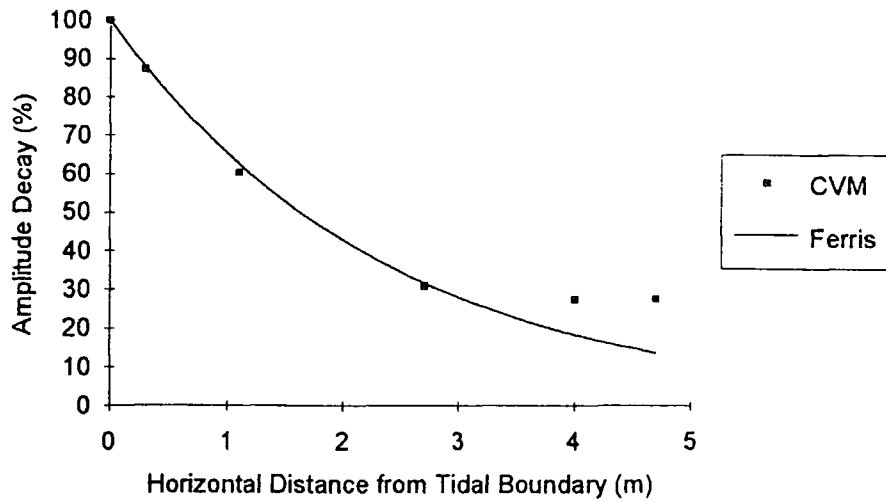
Figure 4.16. Amplitude Decay. Comparison of CVM, Incorporating Reflection, with Ferris Theory.
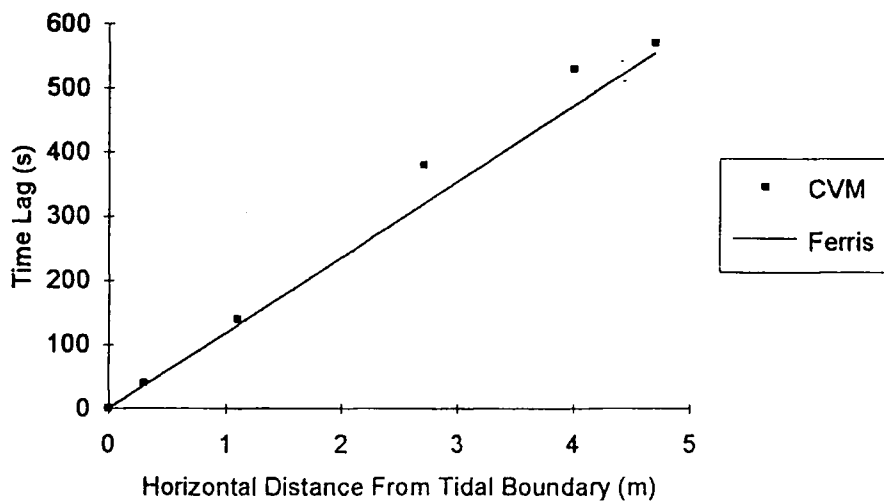
Figure 4.17. Time Lag. Comparison of CVM, Incorporating Reflection, with Ferris Theory.

Tidal Period 1920 seconds
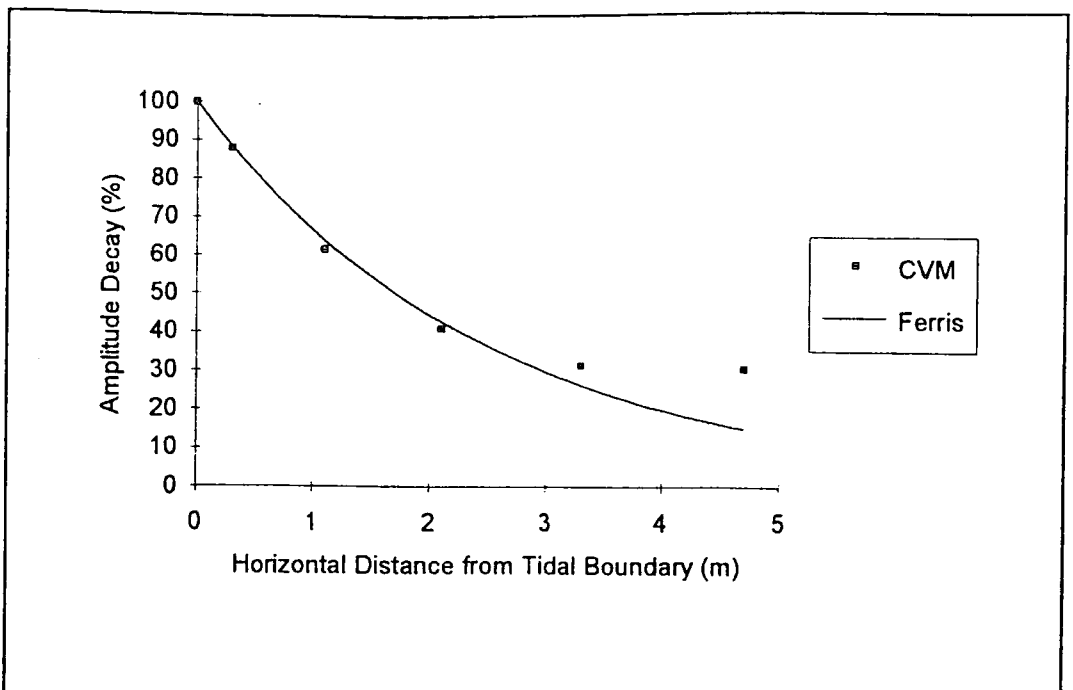
Figure 4.18. Amplitude Decay. Comparison of CVM, Incorporating Reflection, with Ferris Theory.
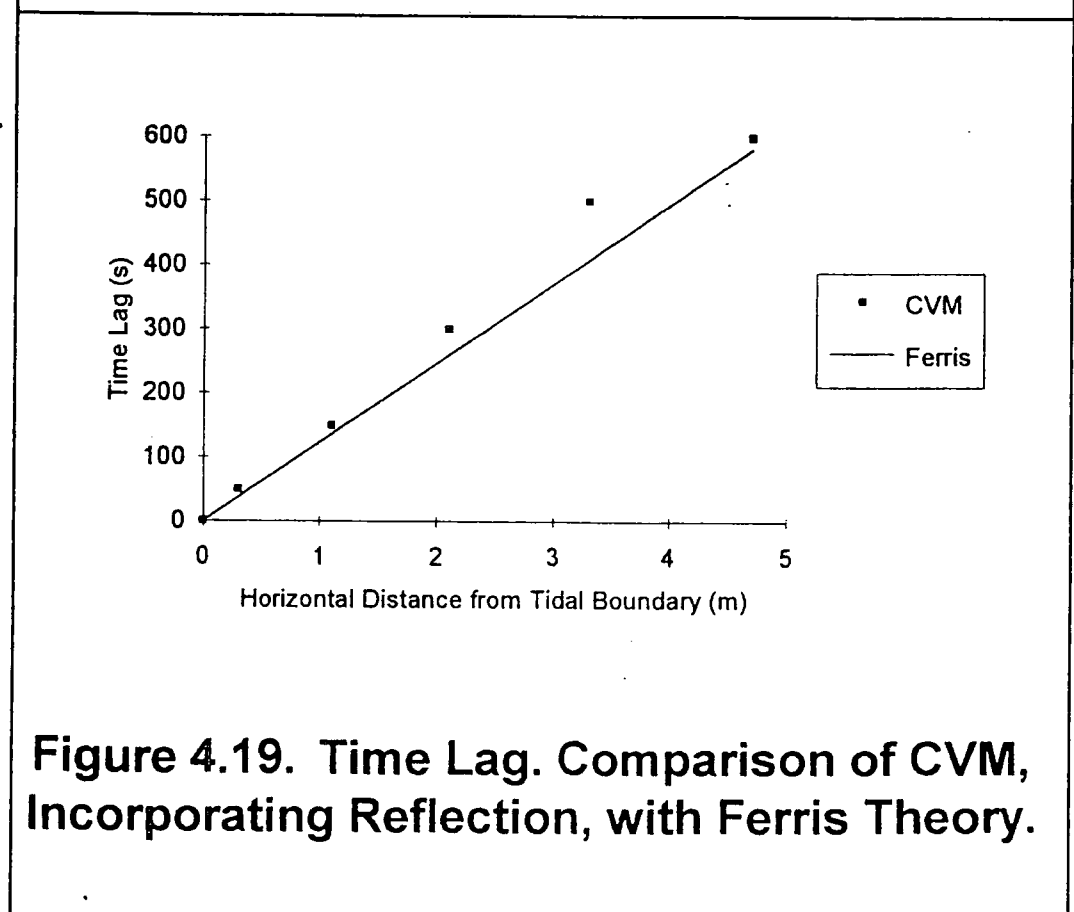
Figure 4.19. Time Lag. Comparison of CVM, Incorporating Reflection, with Ferris Theory.

Tidal Period 2743 seconds
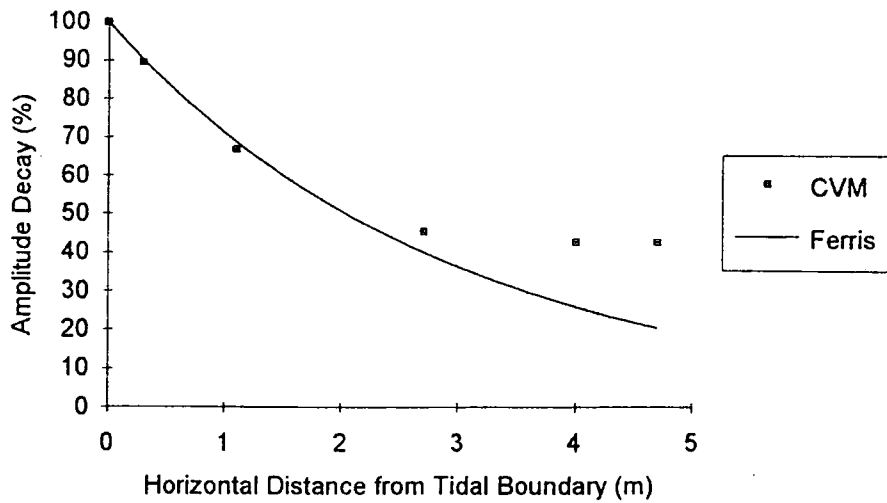
Figure 4.20. Amplitude Decay. Comparison of CVM, Incorporating Reflection, with Ferris Theory.
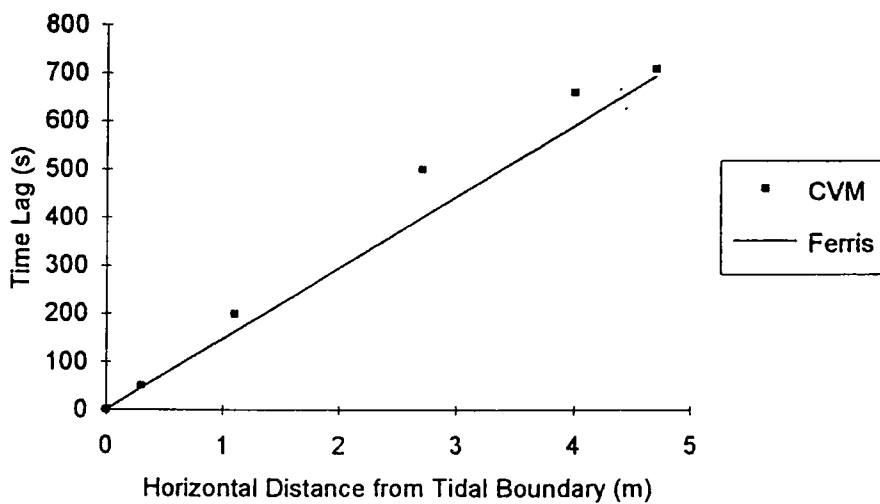
Figure 4.21. Time Lag. Comparison of CVM, Incorporating Reflection, with Ferris Theory.
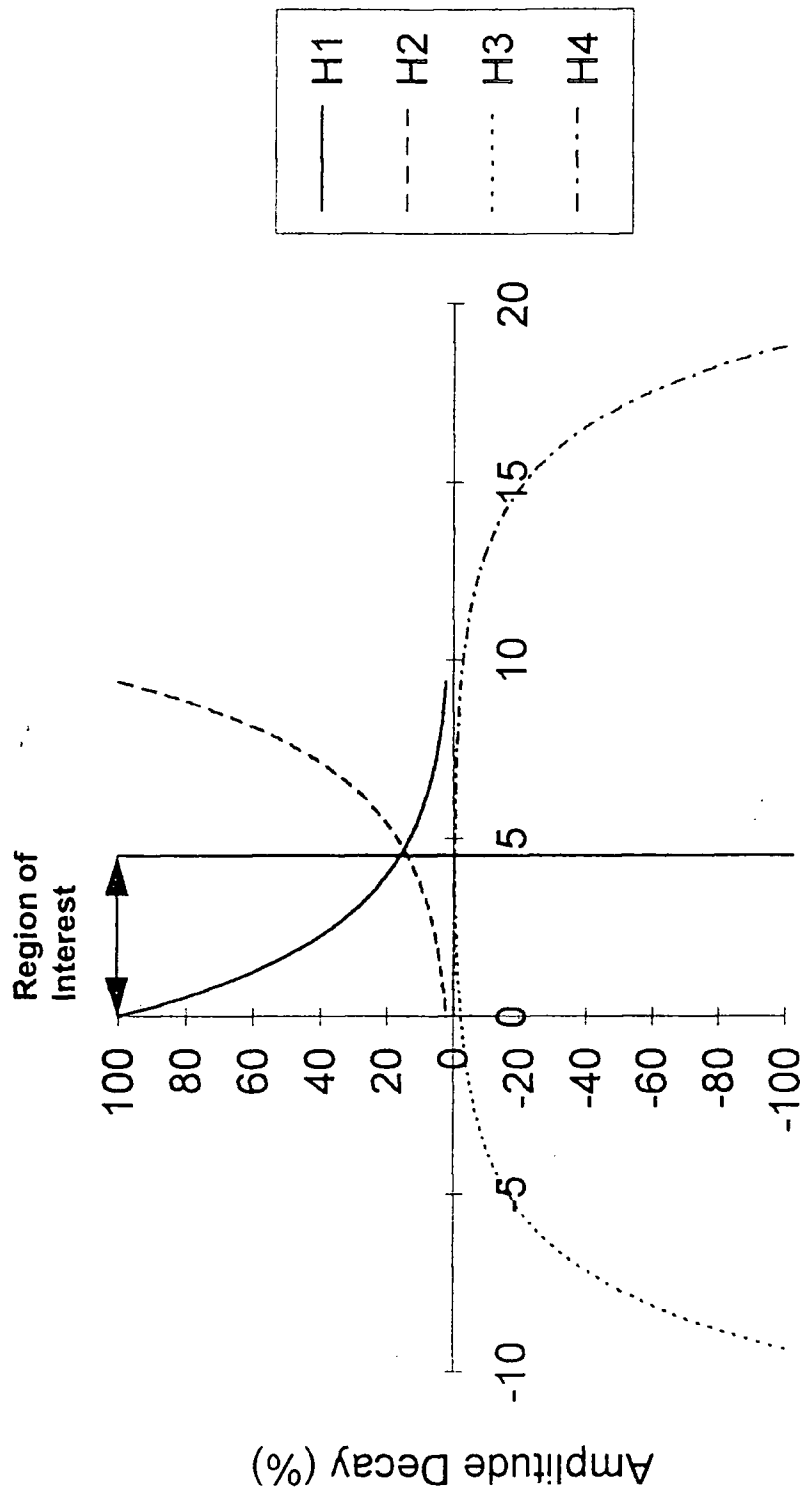
Figure 4.23. Image Well Theory Applied to the Durham Model Aquifer, Illustrating Amplitude Decay of Reflected Waves.

Tidal Period 1920 seconds
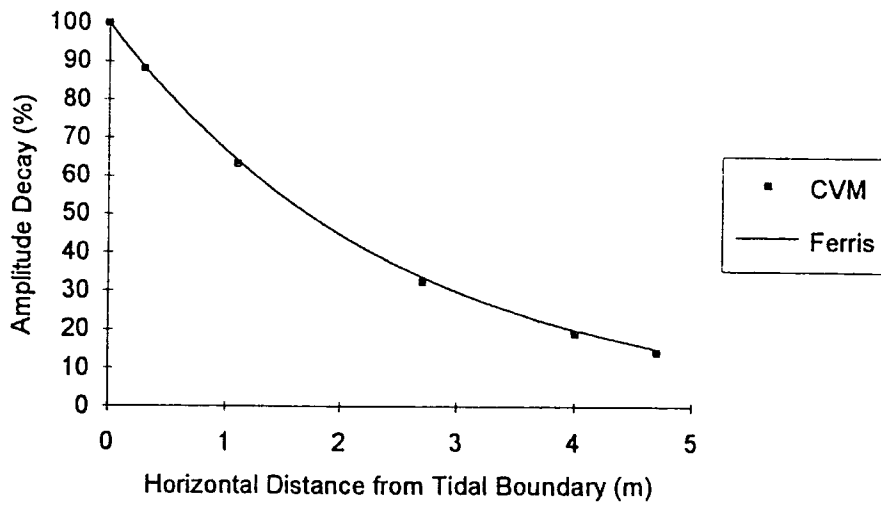
Figure 4.24. Amplitude Decay. Comparison of CVM, Incorporating Leakage, with Ferris Theory.
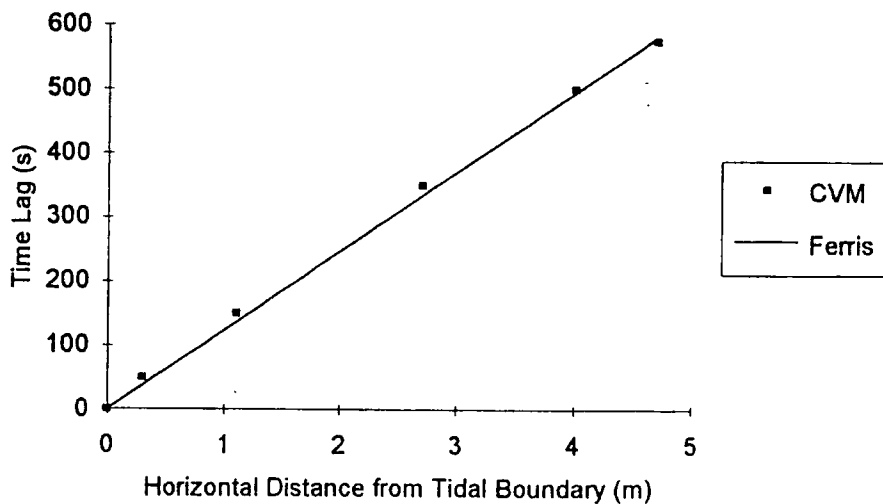
Figure 4.25. Time Lag. Comparison of CVM, Incorporating Leakage, with Ferris Theory.

Figure 4.26. Amplitude Decay. Comparison of CVM, Incorporating Leakage & Reflection, with Ferris Theory.
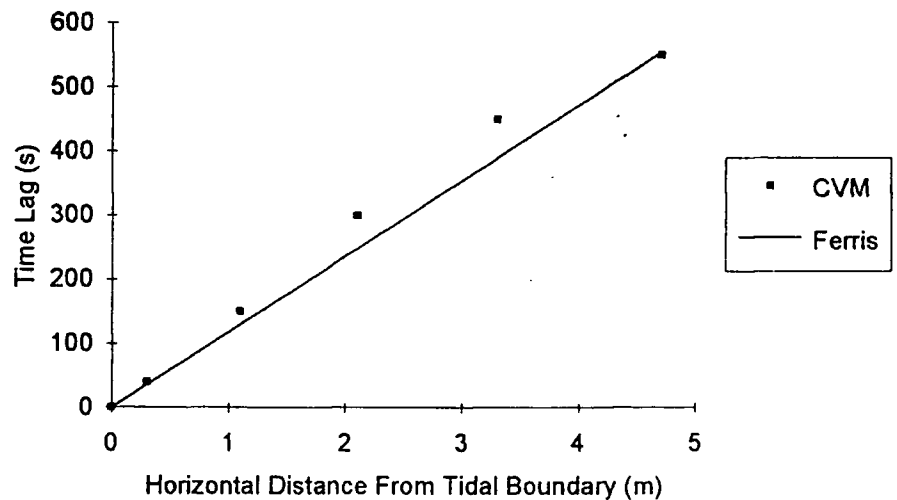
Figure 4.27. Time Lag. Comparison of CVM, Incorporating Leakage & Reflection, with Ferris Theory.

Figure 4.28. Amplitude Decay. Comparison of CVM, Incorporating Leakage & Reflection, with Ferris Theory.
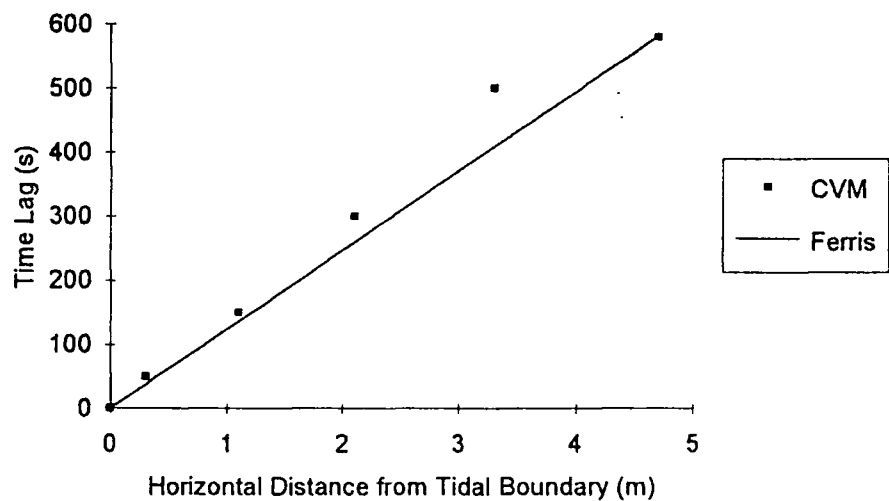
Figure 4.29. Time Lag. Comparison of CVM, Incorporating Leakage & Reflection, with Ferris Theory.

Tidal Period 2743 seconds
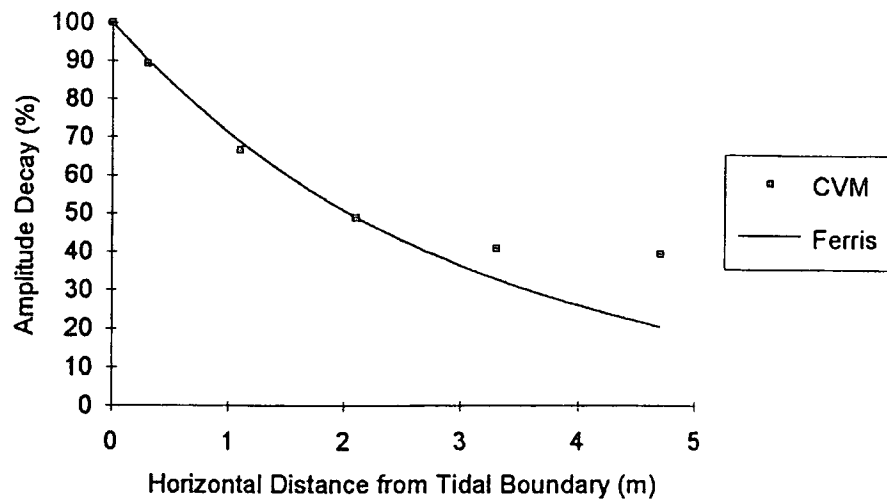
Figure 4.30. Amplitude Decay. Comparison of CVM, Incorporating Leakage & Reflection, with Ferris Theory.
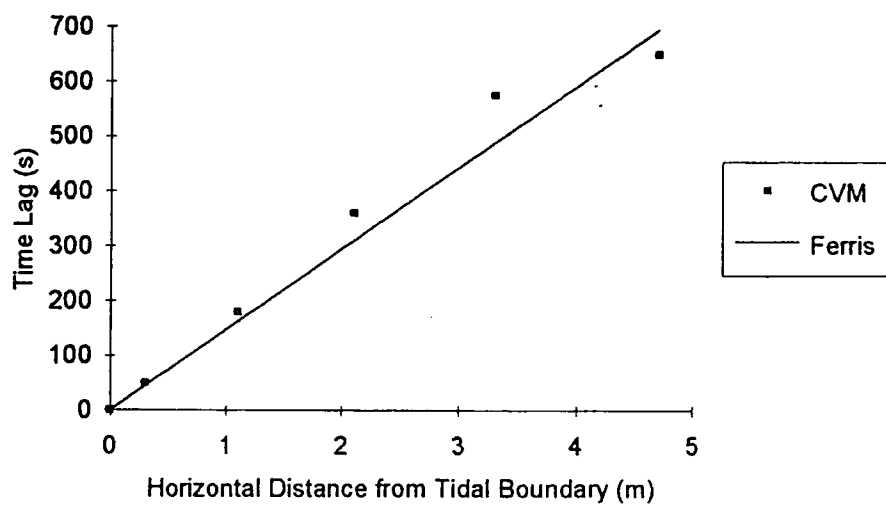
Figure 4.31. Time Lag. Comparison of CVM, Incorporating Leakage & Reflection, with Ferris Theory.
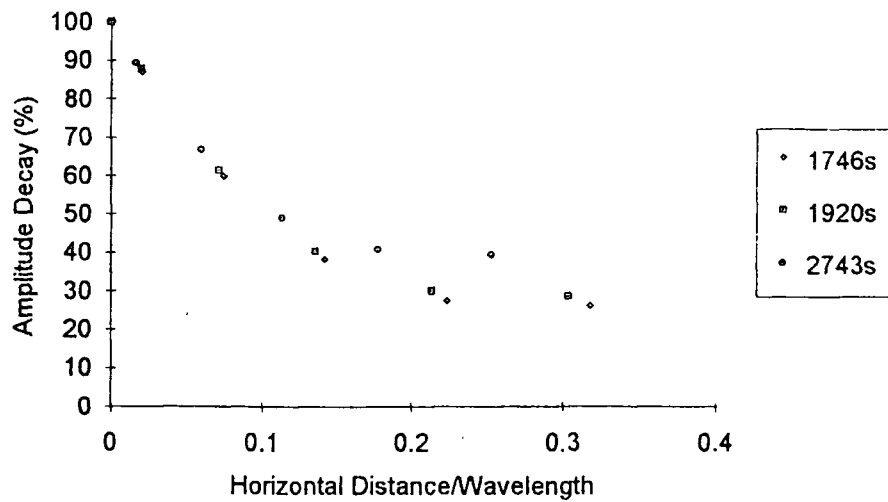
Figure 4.32. CVM Results for Amplitude Decay Incorporating Leakage and Reflection. Normalisation Attempt.
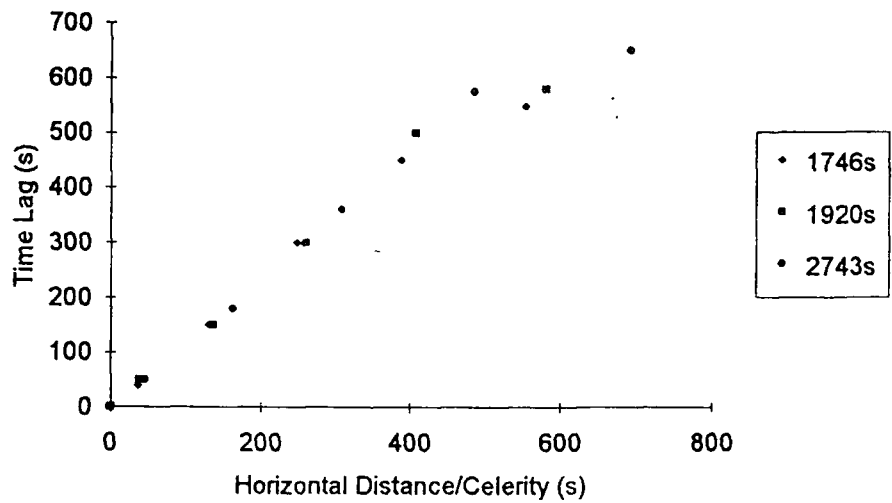
Figure 4.33. CVM Results for Time Lag Incorporating Leakage and Reflection. Normalisation Attempt.

Chapter 5

Development of Analytical Theory

5.1. Introduction

Following the numerical modelling simulating the Durham Model Aquifer and outlined in chapter 4, it was concluded that Ferris' theory was inapplicable to results from the Durham Model Aquifer. This was because two of the assumptions upon which the theory was based, were not valid for the Durham Model Aquifer. These assumptions were:

1. The aquifer is of infinite length/distance from the tidal boundary.

2. The aquifer is confined and therefore vertical flow is negligible.

The numerical model, CVM, illustrated the effects of reflection and leakage on results of amplitude decay and time lag. These effects were found to be significant for the case of the Durham Model Aquifer. Therefore, using Ferris theory to estimate aquifer properties would result in inaccuracies. In addition, the leakage coefficient cannot be determined by this method.

It was therefore decided to advance the theory developed by Ferris to include concepts of leakage and reflection. This chapter outlines the development of such analytical theory to describe the behaviour of groundwater in coastal areas. Three separate cases are considered. Firstly, Ferris' theory is developed to incorporate reflection from an impermeable boundary. Secondly, the concept of leakage is included in the theory, and finally, both leakage and reflection effects are incorporated in analytical theory. In summary, analytical theory is developed from Ferris theory to describe:

A. Groundwater behaviour in a confined coastal aquifer of finite length (i.e. incorporating reflective effects).

B. Groundwater behaviour in a semi-confined (leaky) coastal aquifer of infinite length.

C. Groundwater behaviour in a leaky coastal aquifer of finite length.

Analytical solutions were verified by comparison with numerical solutions produced using CVM.

5.2. Development of Ferris Theory to Incorporate Reflection

5.2.1. Concepts

The objective was to develop analytical theory for groundwater behaviour in a confined aquifer with

- Horizontal flow

- Periodic wave applied at one boundary

- Finite length, i.e. reflection from an impermeable boundary

5.2.2. Application of Image Well Theory

Image well theory was detailed in chapter 4.6.3. The primary reflected wave has a highly significant effect on water-level response. Therefore, initially only superposition of this primary reflected wave was considered. This was then compared with a numerical solution for a specific case.

5.2.2.1. Theory Incorporating One Reflective Boundary

Figure 5.1. below details the theoretical image source causing the effect of the primary reflective wave. This image source is located at a distance of twice the aquifer length (2L) from the real source. The amplitude of waves produced by the real source is denoted by h_x, whilst that produced as a result of the image source is h_{2L-x}. Amplitude is dependent on distance, x. This is illustrated in Figure 5.1. The

time lag as a result of the real wave affects a phase difference, phase0, with reference to the real source. The primary reflected wave incurs a time lag and phase difference, phase1, with reference to the image source. Again, this is illustrated in Figure 5.1 below.
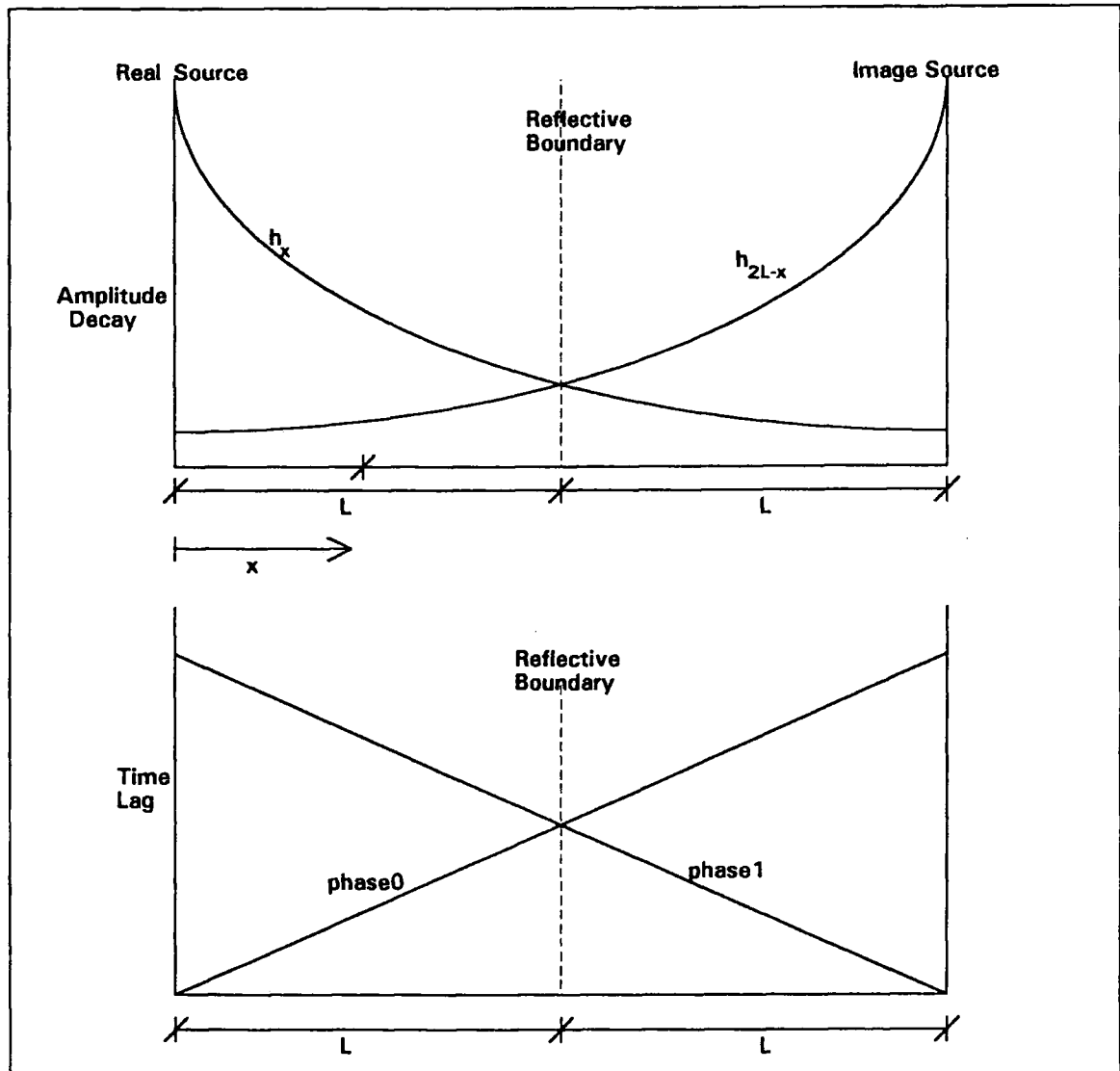
Figure 5.1. Image Well Theory, Considering Primary Reflective Effects.

For any point at a distance, x from the real source, the head, H(x,t), is given by:

$$H = h_{(x)} \sin(\omega t + \phi_0) \; + \; h_{(2L-x)} \sin(\omega t + \phi_1) \longrightarrow eqtn(5\cdot1)$$

where t = time

ω = angular velocity

ϕ_0 = phase0

ϕ_1 = phase1

140

It is assumed that the aquifer material is homogeneous for all values of x, and therefore the wavelength of both real and reflective waves is the same and constant. This implies that other wave parameters, wavelength and period, are also constant.

It is assumed that $0 \leq x \leq \lambda$ where λ is the wavelength, and that:

$$\omega = \frac{2\pi}{t_0} \longrightarrow eqtn(5 \cdot 2)$$

where t_0 is the wave period.

The phase differences phase0, ϕ_0, and phase1, ϕ_1, are given by eqtns (5.3) and (5.4) respectively.

$$\phi_0 = \frac{2\pi x}{\lambda} \longrightarrow eqtn(5 \cdot 3)$$

$$\phi_1 = \frac{2\pi(2L - x)}{\lambda} \longrightarrow eqtn(5 \cdot 4)$$

Substituting eqtns (5.2), (5.3) and (5.4) into eqtn (5.1) gives:

$$H = h_x \sin\left(\frac{2\pi t}{t_0} + \frac{2\pi x}{\lambda}\right) + h_{(2L-x)} \sin\left(\frac{2\pi t}{t_0} + \frac{2\pi(2L - x)}{\lambda}\right) \longrightarrow eqtn(5 \cdot 5)$$

Expanding eqtn(5.5)

$$H = h_x \left[\left(\sin\frac{2\pi t}{t_0}\cos\frac{2\pi x}{\lambda}\right) + \left(\cos\frac{2\pi t}{t_0}\sin\frac{2\pi x}{\lambda}\right)\right] +$$

$$h_{(2L-x)}\left[\left(\sin\frac{2\pi t}{t_0}\cos\frac{2\pi(2L - x)}{\lambda}\right) + \left(\cos\frac{2\pi t}{t_0}\sin\frac{2\pi(2L - x)}{\lambda}\right)\right] \longrightarrow eqtn(5 \cdot 6)$$

This can be simplified to

$$H = A(x)\sin\omega t + B(x)\cos\omega t \longrightarrow eqtn(5 \cdot 7)$$

Where

$$A(x) = h_x \cos\frac{2\pi x}{\lambda} + h_{(2L-x)}\cos\frac{2\pi(2L - x)}{\lambda} \longrightarrow eqtn(5 \cdot 8)$$

$$B(x) = h_x \sin\frac{2\pi x}{\lambda} + h_{(2L-x)}\sin\frac{2\pi(2L - x)}{\lambda} \longrightarrow eqtn(5 \cdot 9)$$

Figure 5.2. below illustrates the variation of the periodic wave with time, at distance x from the tidal source.
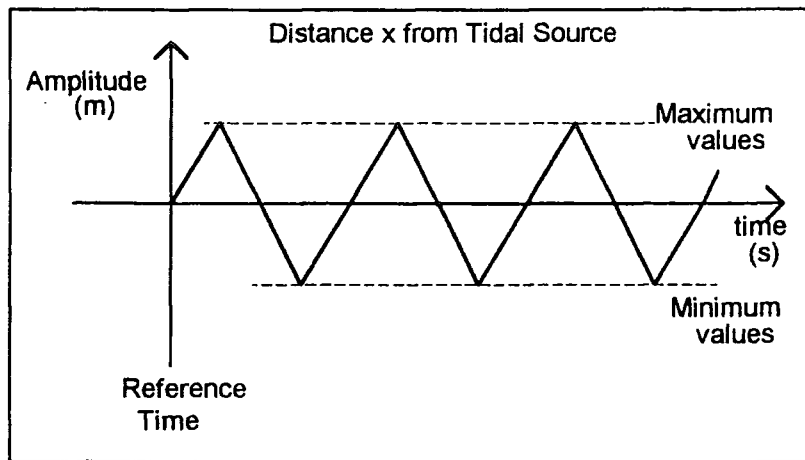
Figure 5.2. Harmonic Variation of Propagated Tidal Wave at Distance x from Source.

The objective was to determine the amplitude and time lag of the wave at various horizontal distances from the tidal source. The time of the occurrence of maximum or minimum value of the wave may be found by considering that, for a peak value:

$$\frac{dH}{dt} = 0$$

Therefore, in order to determine the time of occurrence of maximum/minimum values, the total head, H given by eqtn (5.7), was differentiated with respect to time, t. This is shown in eqtn (5.10) below.

$$\frac{dH}{dt} = A\omega\cos\omega t - B\omega\sin\omega t \longrightarrow eqtn(5\cdot10)$$

For a maximum or minimum value:

$$\frac{dH}{dt} = 0$$

Applying this to eqtn (5.15), implies that

$$A\omega\cos\omega t = B\omega\sin\omega t \longrightarrow eqtn(5\cdot11)$$

$$\Rightarrow \tan\omega t = \frac{A}{B} \longrightarrow eqtn(5\cdot12)$$

$$\Rightarrow \omega t = \tan^{-1}\left(\frac{A}{B}\right) + n\pi \longrightarrow eqtn(5\cdot13)$$

where n=0,1,2,3....

142

This incorporates the harmonic pattern of the wave with peaks/troughs at various late times with respect to a chosen reference time. This was illustrated in Figure 5.2 above.

The time of the occurrence of the first maximum/minimum value of the wave is given by eqtn (5.14) below.

$$t = \frac{1}{\omega}\tan^{-1}\left(\frac{A}{B}\right) \longrightarrow eqtn(5 \cdot 14)$$

The amplitude of the wave *at a specified horizontal position from the tidal source* does not change with time. Therefore eqtn (5.14) can be substituted into eqtn(5.7) to provide an equation for the amplitude of the superposed wave, H_{amp}.

$$\boxed{H_{amp} = A(x)\sin\left(\tan^{-1}\frac{A}{B}\right) + B(x)\cos\left(\tan^{-1}\frac{A}{B}\right) \longrightarrow eqtn(5 \cdot 15)}$$ **Amplitude Decay**

where A(x) and B(x) are defined in eqtns (5.8) and (5.9) above.

From Ferris Theory (1951), the wavelength and amplitude of the wave are defined as follows:

$$\lambda = \sqrt{4\pi t_0 \frac{T}{S}} \longrightarrow eqtn(5 \cdot 16)$$

$$h_x = h_0 \exp\left(-x\sqrt{\frac{\pi S}{t_0 T}}\right) \longrightarrow eqtn(5 \cdot 17)$$

Therefore

$$h_{2L-x} = h_0 \exp\left(-(2L-x)\sqrt{\frac{\pi S}{t_0 T}}\right) \longrightarrow eqtn(5 \cdot 18)$$

The time lag of the wave, with reference to the phase of the real source, at various horizontal distances was determined.

The time of occurrence of the first maximum/minimum value of the wave was defined in equation (5.14). The time lag was found by computing the times, with reference to the phase of the real source, at which this occurred for various values of x. The equation for time lag is therefore given by eqtn (5.19) below:

$$\boxed{t_L = \text{mod}\left[\left(\frac{1}{\omega}\right)\tan^{-1}\left(\frac{A}{B}\right) + timelag_{x=0}\right] \longrightarrow eqtn(5 \cdot 19)}$$ **Time Lag**

5.2.2.2. Comparison of Analytical and Numerical (CVM) Solutions for a Case Study. One Reflection.

In order to verify the developed analytical theory of chapter 5.2.2., a specific case study was defined and the analytical solution compared with a numerical solution produced using the software, CVM.

5.2.2.2.1. Outline of Case Study

The following parameter values were chosen (similar orders of magnitude to the laboratory aquifer):

Length of Aquifer, $L = 4.7m$

Transmissibility, $T = 0.001m^2/s$

Storage coefficient, $S = 0.1$

Period, $t_0 = 1920s$

Amplitude of harmonic wave at boundary (x=0), h0 = 0.2m

5.2.2.2.2. Analytical Solution

The analytical solutions for amplitude decay and time lag were produced with the mathematical and graphical assistance of the software, MATLAB[1].

A printout of the MATLAB file for this solution is provided in Appendix 5.1.

5.2.2.2.3. Comparison of Solutions

The graphs illustrating the comparison of the analytical and numerical solutions to this example are shown in Figures 5.3. and 5.4. for amplitude decay and time lag respectively.

For both amplitude decay and time lag, the analytical solution compares well with the numerical solution. There is discrepancy between numerical and analytical time lag

---

[1]MATLAB - A computer software package designed to solve complex mathematical formulae using matrix methods.

results. This was attributed to the errors in time lag data obtained from the numerical modelling approach. As was explained in chapter 4, accuracy of time lag results from CVM output files is only possible to the nearest ±25 seconds.

There is a discrepancy in values of amplitude decay at x=0. This may be because the analytical solution considers only one reflection.

5.2.2.3.   Theory Incorporating Two Reflections

Two reflections were considered to investigate whether this analytical theory matched the numerical solution more closely.

Figure 5.5. below illustrates how two reflections were incorporated in the theory. The concept of image well theory was applied. This was explained in detail in chapter 4.6.3.
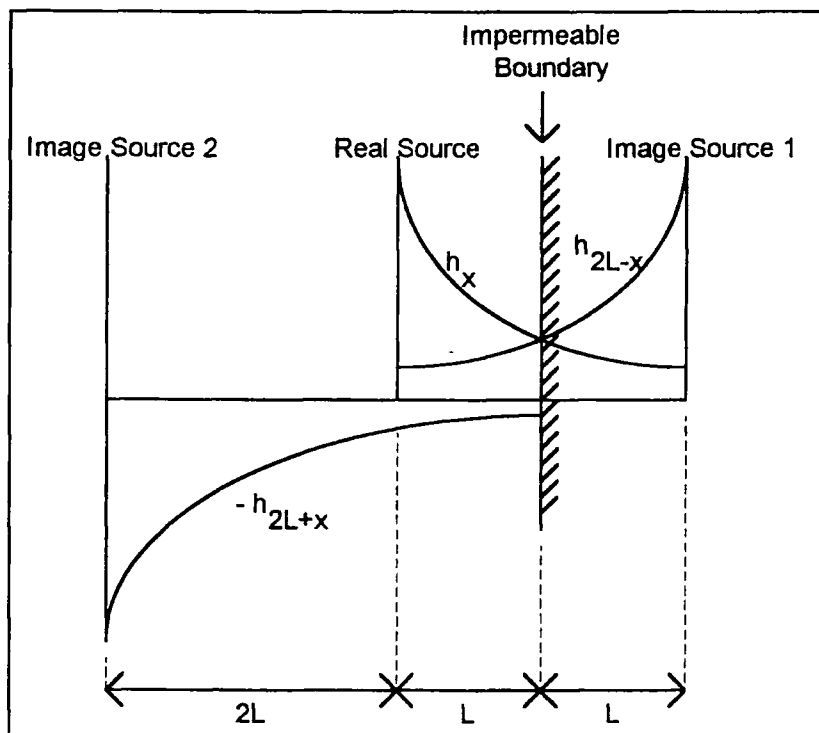
Figure 5.5. Image Well Theory, Considering Two Reflections.

Development of this analytical theory followed the same approach as for development of the theory with one reflection.

For any point at a distance, x from the real source, the head, H(x,t), is given by:

$$H = h_{(x)} \sin(\omega t + \phi_0) + h_{(2L-x)} \sin(\omega t + \phi_1) - h_{(2L+x)} \sin(\omega t + \phi_2) \longrightarrow eqtn(5 \cdot 20)$$

where ϕ_2 = phase2, the phase difference of the second reflected wave.

This phase difference is given by eqtn (5.21).

$$\phi_2 = \frac{2\pi(2L+x)}{\lambda} \longrightarrow eqtn(5 \cdot 21)$$

Incorporating this second reflective effect into eqtn (5.20)

$$H = h_x \left[\left(\sin\frac{2\pi t}{t_0}\cos\frac{2\pi x}{\lambda} \right) + \left(\cos\frac{2\pi t}{t_0}\sin\frac{2\pi x}{\lambda} \right) \right] +$$

$$h_{(2L-x)} \left[\left(\sin\frac{2\pi t}{t_0}\cos\frac{2\pi(2L-x)}{\lambda} \right) + \left(\cos\frac{2\pi t}{t_0}\sin\frac{2\pi(2L-x)}{\lambda} \right) \right] -$$

$$h_{(2L+x)} \left[\left(\sin\frac{2\pi t}{t_0}\cos\frac{2\pi(2L+x)}{\lambda} \right) + \left(\cos\frac{2\pi t}{t_0}\sin\frac{2\pi(2L+x)}{\lambda} \right) \right] \longrightarrow eqtn(5 \cdot 22)$$

This can be simplified to

$$H = A(x)\sin\omega t + B(x)\cos\omega t \longrightarrow eqtn(5 \cdot 23)$$

Where

$$A(x) = h_x \cos\frac{2\pi x}{\lambda} + h_{(2L-x)} \cos\frac{2\pi(2L-x)}{\lambda} - h_{(2L+x)} \cos\frac{2\pi(2L+x)}{\lambda} \longrightarrow eqtn(5 \cdot 24)$$

$$B(x) = h_x \sin\frac{2\pi x}{\lambda} + h_{(2L-x)} \sin\frac{2\pi(2L-x)}{\lambda} - h_{(2L+x)} \sin\frac{2\pi(2L+x)}{\lambda} \longrightarrow eqtn(5 \cdot 25)$$

The approach described in section 5.2.2.1 was followed to determine the amplitude and time lag. The time for maximum and minimum values to occur was calculated. The total head, H given by eqtn (5.23) was differentiated with respect to t. For a maximum/minimum

$$\frac{dH}{dt} = 0$$

Therefore:

$$\omega t = \tan^{-1}\left(\frac{A}{B}\right) + n\pi \longrightarrow eqtn(5 \cdot 26)$$

The first maximum/minimum value occurs at the time given by eqtn (5.27) below:

$$t = \frac{1}{\omega}\tan^{-1}\left(\frac{A}{B}\right) \longrightarrow eqtn(5 \cdot 27)$$

Substituting eqtn (5.27) into eqtn(5.23) to determine the amplitude of the superposed wave, H_{amp}

$$H_{amp} = A(x)\sin\left(\tan^{-1}\frac{A}{B}\right) + B(x)\cos\left(\tan^{-1}\frac{A}{B}\right)\longrightarrow eqtn(5\cdot28)$$ Amplitude Decay

where A(x) and B(x) are defined in eqtns (5.24) and (5.25) above.

where

$$h_{2L+x} = h_0 \exp\left(-(2L+x)\sqrt{\frac{\pi S}{t_0 T}}\right)\longrightarrow eqtn(5\cdot29)$$

The time lag of the wave, with reference to the phase of the real source, at various horizontal distances was determined.

The time of occurrence of the maximum/minimum value of the wave at various horizontal distances was defined in equation (5.27). The equation for time lag is hence:

$$t_L = \text{mod}\left(\frac{1}{\omega}\tan^{-1}\left(\frac{A}{B}\right) + timelag_{x=0}\right)\longrightarrow eqtn(5\cdot30)$$ Time Lag

5.2.2.4. Comparison of Analytical and Numerical (CVM) Solutions for a Case Study. Two Reflections.

In order to verify the developed analytical theory of chapter 5.2.2.3, the case study defined in section 5.2.3.1 was applied. The analytical solution incorporating two reflections was compared with the numerical solution produced using the software, CVM.

5.2.2.4.1. Analytical Solution

The printout of the MATLAB file for this solution is provided in Appendix 5.2.

5.2.2.4.2.   Comparison of Solutions

The graphs illustrating the comparison of the analytical and numerical solutions to this example are shown in Figures 5.6. and 5.7. for amplitude decay and time lag respectively.

The analytical solution for amplitude decay compares very well with the numerical solution.   There is discrepancy between values of time lag obtained from the numerical and analytical approaches. This was attributed to the accuracy of the CVM numerical solution, which was limited to ±25 seconds.

Incorporation of this second reflection in the analytical theory resulted in a closer match of numerical and analytical solutions for amplitude decay than was possible with theory incorporating one reflection. The theory was developed to include a third reflected wave and its effect on water-level response was also investigated for the above case study.   Inclusion of the third reflected wave was found to have a negligible effect.

5.2.3. Conclusion

Analytical was developed to describe water-level response in a coastal aquifer of finite length. Ferris' theory was developed to incorporate the effects of two reflective waves. Further reflected waves were found to have negligible effect on water-level response. The analytical solution was verified by computing results of amplitude decay and time lag for a specific case study. This was then compared with the numerical solution, produced by application of CVM software. Taking into account the errors in the numerical results, it was concluded that the analytical and numerical solutions compared very well.

Therefore, to summarise, the equations for amplitude decay and time lag in a confined, coastal aquifer of finite length are

$$H_{amp} = A(x)\sin\left(\tan^{-1}\frac{A}{B}\right) + B(x)\cos\left(\tan^{-1}\frac{A}{B}\right) \longrightarrow eqtn(5 \cdot 28)$$

$$t_L = \text{mod}\left(\frac{1}{\omega}\tan^{-1}\left(\frac{A}{B}\right) + timelag_{x=0}\right) \longrightarrow eqtn(5\cdot30)$$

where

$$A(x) = h_x \cos\frac{2\pi x}{\lambda} + h_{(2L-x)}\cos\frac{2\pi(2L-x)}{\lambda} - h_{(2L+x)}\cos\frac{2\pi(2L+x)}{\lambda} \longrightarrow eqtn(5\cdot24)$$

$$B(x) = h_x \sin\frac{2\pi x}{\lambda} + h_{(2L-x)}\sin\frac{2\pi(2L-x)}{\lambda} - h_{(2L+x)}\sin\frac{2\pi(2L+x)}{\lambda} \longrightarrow eqtn(5\cdot25)$$

and

$$\lambda = \sqrt{4\pi t_0 \frac{T}{S}} \longrightarrow eqtn(5\cdot16)$$

$$h_x = h_0 \exp\left(-x\sqrt{\frac{\pi S}{t_0 T}}\right) \longrightarrow eqtn(5\cdot17)$$

$$h_{2L-x} = h_0 \exp\left(-(2L-x)\sqrt{\frac{\pi S}{t_0 T}}\right) \longrightarrow eqtn(5\cdot18)$$

$$h_{2L+x} = h_0 \exp\left(-(2L+x)\sqrt{\frac{\pi S}{t_0 T}}\right) \longrightarrow eqtn(5\cdot29)$$
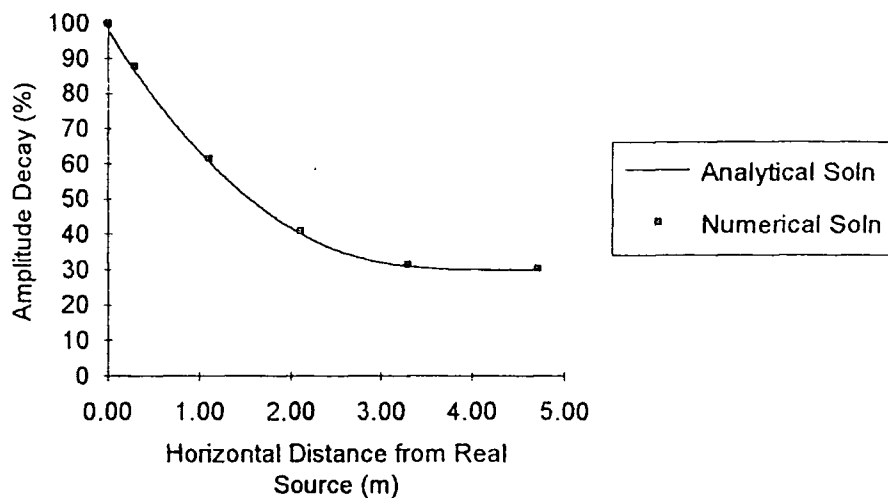
Figure 5.3   Amplitude Decay. Comparison of
Analytical Solution (Incorporating One
Reflections) with Numerical Solution for a
Confined Aquifer of Length 4.7 metres.
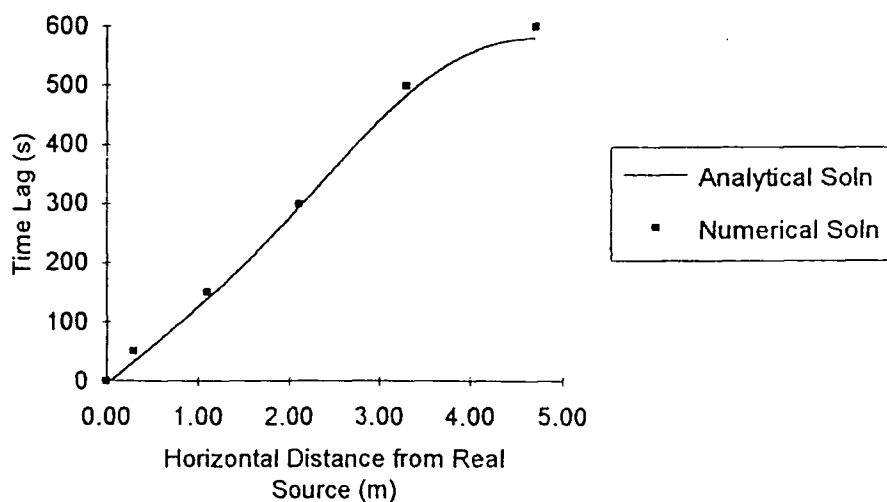
Figure 5.4. Time Lag. Comparison of
Analytical Solution (Incorporating One
Reflections) with Numerical Solution for a
Confined Aquifer of Length 4.7 metres.
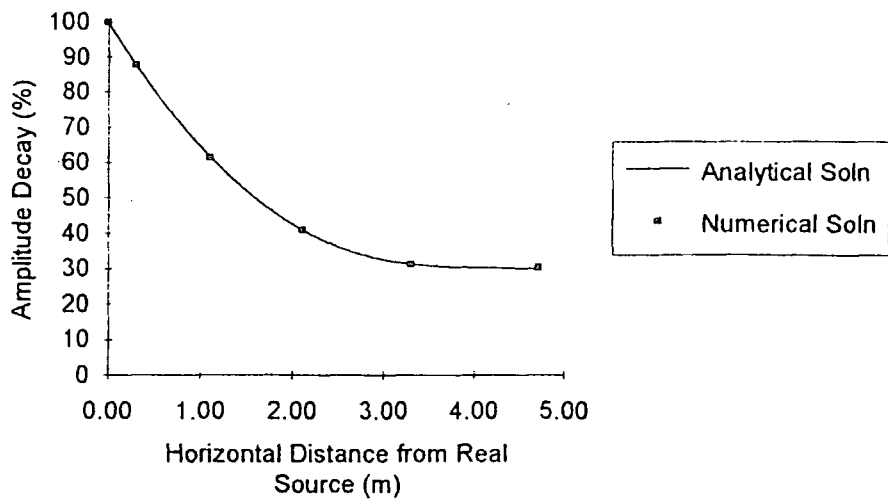
Figure 5.6. Amplitude Decay. Comparison of Analytical Solution (Incorporating Two Reflections) with Numerical Solution for a Confined Aquifer of Length 4.7 metres.
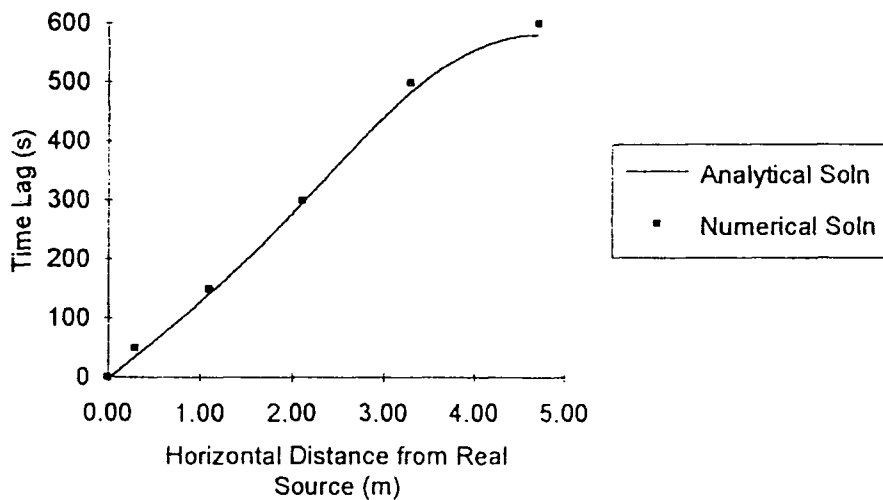
Figure 5.7 Time Lag. Comparison of Analytical Solution (Incorporating Two Reflections) with Numerical Solution for a Confined Aquifer of Length 4.7 metres.

5.3. Application of Angstrom Theory (Heat Conduction) to Groundwater Flow in a Leaky Aquifer System.

5.3.1. Concepts

The objective was to develop analytical theory for groundwater behaviour in a *semi-confined* aquifer with

- Horizontal flow

- Vertical flow (Leakage)

- Periodic wave applied at one boundary

- Infinite length

5.3.2. Heat Conduction Theory

Ferris based his theory on the heat conduction solution employed by Angstrom for the problem of potential distribution within a semi-infinite solid subjected to periodic variations of potential. This theory is documented in Carslaw (1945).

As part of this current programme of work, it was decided to investigate heat conduction theory further to see if a solution could be found to the problem of water-level response in a leaky, coastal aquifer.

5.3.3. Governing Groundwater Flow Equation

The governing equation describing flow in a one-dimension leaky aquifer system can be written in the form (Bear 1979):

$$S\frac{\partial h}{\partial t} = T\frac{\partial^2 h}{\partial x^2} - \beta(h - h^*) \longrightarrow eqtn(5\cdot31)$$

where h = Hydraulic head above datum, [L]

   h^* = Fixed hydraulic head in aquitard, [L]

   S = Storage coefficient ($bS_s + S_y$), [-]

   S_s = Specific storage, [1/L]

   S_y = Specific yield, [-]

T = Aquifer Transmissibility, $[L^2/T]$

x = Horizontal spacial co-ordinate, [L]

β = Leakage coefficient - this positive for water that passes through the aquitard (K'/b'), [1/T]

Equation(5.31) is known as the diffusion type equation and is derived by combining the mass conservation (water balance) and the effective momentum conservation (Darcy's Law) equations.

The following boundary conditions were applied to solve this equation:

- at x=0, the head varies periodically (h=Acoswt+Bsinwt)

Equation (5.31) can be rewritten as :

$$\frac{\partial h}{\partial t} = \frac{T}{S}\frac{\partial^2 h}{\partial x^2} - \frac{\beta}{S}\alpha \longrightarrow eqtn(5 \cdot 31b)$$

where α = (h-h*)

5.3.4. Application of Heat Conduction Theory

The current programme of work involved research into heat conduction theory to investigate if a problem similar to the above had been solved for heat flow. Angstrom's method for conductivity experiments upon bars under variable temperature was encountered. Angstrom employed long bars of small cross-section. The bar end, x=0, was subjected to periodic changes in temperature. After some time, the temperature within the bar will settle down to a periodic state. Angstrom investigated this periodic state. The bar is allowed to radiate into a medium at constant temperature, taken as the zero of the experiment. The length of the bar is such that the far end remains unaffected by alterations at x=0, so mathematical treatment assumes a bar of infinite length.

This theory is described in detail in Carslaw (1921). The equation for temperature is given by Carslaw (1921) as:

$$\frac{\partial v}{\partial t} = \kappa \frac{\partial^2 v}{\partial x^2} - \lambda v \longrightarrow eqtn(5 \cdot 32)$$

153

The heat conduction problem together with the governing equation (5.32) can be assimilated to groundwater-response in leaky coastal aquifers and equation (5.31b) above.

5.3.5. Development of Theory.

The solution derived by Angstrom and documented in Carslaw (1921) was applied to the governing equation (5.31b). This section explains development of analytical theory to solve equation (5.31b) in line with Angstrom's solution.

The head at x=0 varies periodically, thus the solution will be periodic with the same period, t_0, as that of the head at x=0, and will be of the form:

$$h = P\cos\omega t + Q\sin\omega t + h^* \longrightarrow eqtn(5\cdot33)$$

where $\omega = \dfrac{2\pi}{t_0}$ and given that $0 \le x \le \lambda$

where λ = Wavelength of the pressure wave, [L]

P and Q are functions of x.

Differentiating eqtn(5.33):

$$\frac{\partial^2 h}{\partial x^2} = \frac{\partial^2 P}{\partial x^2}\cos\omega t + \frac{\partial^2 Q}{\partial x^2}\sin\omega t \longrightarrow eqtn(5\cdot34)$$

$$\frac{\partial h}{\partial t} = -P\omega\sin\omega t + Q\omega\cos\omega t \longrightarrow eqtn(5\cdot35)$$

Substituting eqtns (5.34) and (5.35) into eqtn(5.31b)

$$-P\omega\sin\omega t + Q\omega\cos\omega t = \frac{T}{S}\left(\frac{\partial^2 P}{\partial x^2}\cos\omega t + \frac{\partial^2 Q}{\partial x^2}\sin\omega t\right) - \frac{\beta}{S}(P\cos\omega t + Q\sin\omega t) \longrightarrow eqtn(5\cdot36)$$

By equating the coefficients of sinωt and cosωt to zero in eqtn(5.36), this results in

quantities for P and Q which satisfy:

$$\frac{d^2P}{dx^2} - \frac{\beta}{T}P = \frac{\omega S}{T}Q \longrightarrow eqtn(5 \cdot 37)$$

$$\frac{d^2Q}{dx^2} - \frac{\beta}{T}Q = -\frac{\omega S}{T}P \longrightarrow eqtn(5 \cdot 38)$$

Thus we have:

$$\left(\frac{\partial^2}{\partial x^2} - a^2\right)^2 P + b^4 P = 0 \longrightarrow eqtn(5 \cdot 39)$$

where $a^2 = \frac{\beta}{T}$ and $b^2 = \frac{\omega S}{T}$

Therefore

$$P = A\exp^{-gx}\cos(g'x - \varepsilon) + A'\exp^{-gx}\cos(g'x - \varepsilon') \longrightarrow eqtn(5 \cdot 40)$$

where $g = \sqrt{\left\{\frac{a^2 + \sqrt{(a^4 + b^4)}}{2}\right\}}$; $g' = \sqrt{\left\{\frac{-a^2 + \sqrt{(a^4 + b^4)}}{2}\right\}}$

and A, A', ε and ε' are arbitrary constants.

Since P vanishes when x=∞ , it follows that A'=0, and our equation becomes:

$$P = A\exp^{-gx}\cos(g'x - \varepsilon) \longrightarrow eqtn(5 \cdot 41)$$

from which we obtain

$$Q = A\exp^{-gx}\sin(g'x - \varepsilon) \longrightarrow eqtn(5 \cdot 42)$$

Thus the solution to the governing eqtn(5.31b) is

$$h = A\exp^{-gx}\cos(g'x - \varepsilon)\cos\omega t + A\exp^{-gx}\sin(g'x - \varepsilon)\sin\omega t + h^* \longrightarrow eqtn(5 \cdot 43)$$

Differentiating the above eqtn (5.43) with respect to time, to find the amplitude of the wave at various distances from the end, x=0, subjected to periodic changes in temperature.

$$\frac{\partial h}{\partial t} = -A\omega \exp^{-gx} \cos(g'x - \varepsilon)\sin \omega t + A\omega \exp^{-gx} \sin(g'x - \varepsilon)\cos \omega t \longrightarrow eqtn(5 \cdot 44)$$

$$\frac{\partial h}{\partial t} = 0 \text{ for a peak.}$$

This implies

$$\cos(g'x - \varepsilon)\sin \omega t = \sin(g'x - \varepsilon)\cos \omega t \longrightarrow eqnt(5 \cdot 45)$$

$$\omega t = g'x - \varepsilon \longrightarrow eqtn(5 \cdot 46)$$

Substituting eqtn(5.46) back into eqtn(5.43):

$$h_{max} = A\exp^{-gx} \cos^2(g'x - \varepsilon) + A\exp^{-gx} \sin^2(g'x - \varepsilon) + h^* \longrightarrow eqtn(5 \cdot 47)$$

This can be simplified to

$$h_{max} = A\exp^{-gx} + h^* \longrightarrow eqtn(5 \cdot 48)$$

The amplitude of the periodic wave with relation to the horizontal distance, x, can be found be eliminating h^*, and is therefore given by:

$$h_{amp} = A\exp^{-gx} \longrightarrow eqtn(5 \cdot 49)$$

Applying boundary conditions to eqtn (5.49), to find a value for arbitrary constant, A.

At x=0, the amplitude of the wave is equal to h_0 (amplitude of the applied periodic wave). Therefore:

$$h_{max\,amp} = h_0 = A$$

Thus the solution to the governing equation for groundwater flow in a one-dimension leaky aquifer system with a periodic wave of amplitude h_0 applied at the boundary x=0 is

$$\boxed{h_{amp} = h_0 \exp^{-gx} \longrightarrow eqtn(5 \cdot 50)}$$ **Amplitude Decay**

$$\text{where } g = \sqrt{\left\{ \frac{(\beta/T) + \sqrt{(\beta^2/T^2) + (\omega^2 S^2/T^2)}}{2} \right\}}$$

156

The time lag can be determined from eqtn (5.46) above

$$t = \frac{1}{\omega}(g'x - \varepsilon) \longrightarrow eqtn(5 \cdot 51)$$

Applying boundary conditions to find constant, ε:

at x=0, $h = h_0 \cos \omega t + h^* \longrightarrow eqtn(5 \cdot 52)$

Substituting this into eqtn(5.43)

$h_0 \cos \omega t + h^* = A[\cos(-\varepsilon)\cos \omega t + \sin(-\varepsilon)\sin \omega t] + h^* \longrightarrow eqtn(5 \cdot 53)$

$h_0 \cos \omega t = A[\cos(\omega t - \varepsilon)] \longrightarrow eqtn(5 \cdot 54)$

This implies that $\varepsilon = 0$

Therefore:

$$\boxed{t = \frac{1}{\omega}(g'x) = t_L \longrightarrow eqtn(5 \cdot 55)}$$ **Time Lag**

$$\text{where } g' = \sqrt{\left\{ \frac{-(\beta/T) + \sqrt{(\beta^2/T^2) + (\omega^2 S^2/T^2)}}{2} \right\}}$$

Eqtn (5.55) gives the time for a peak to occur at various horizontal distances from x=0, and therefore provides an indication of the time lag, t_L. The equation illustrates that the time lag varies linearly with horizontal distance as expected from Ferris theory and illustrated in chapter 4, Figure 4.11.

5.3.6. Comparison of Analytical and Numerical Solutions for a Specific Case.

In order to verify the developed analytical theory of chapter 5.3.5, an approach similar to that outlined in chapter 5.2.2.2 was followed. A specific case was studied and the analytical solution compared with a numerical solution produced using the software, CVM.

5.3.6.1.   Outline of Specific Case

The following parameter values were chosen (similar orders of magnitude to the laboratory aquifer):

157

Length of Aquifer, L = 4.7m

Transmissibility, T = 0.001m²/s

Storage coefficient, S = 0.1

Period, t0 = 1920s

Amplitude of harmonic wave at boundary (x=0), h0 = 0.2m

The leakage coefficient of the Durham Model Aquifer was estimated to be 2×10^{-5} s^{-1}. The value of this parameter chosen for this case study was 6×10^{-5} s^{-1}. This larger coefficient would have a more significant effect on results of amplitude decay and time lag. Hence the theory could be more clearly verified by comparison with CVM.

5.3.6.2. Analytical Solution

The printout of the MATLAB file for this solution is provided in Appendix 5.3.

5.3.6.3. Comparison of Solutions

A comparison of the numerical and analytical solutions for the amplitude decay and time lag for this case study are illustrated graphically in Figures 5.8. and 5.9.

The analytical solution for amplitude decay compares very well with the numerical solution. Once again, there is discrepancy between values of time lag determined by the analytical and numerical methods. The numerical solution produces results with an error of ±25 seconds. Allowing for this error in the numerical solution, the analytical and numerical approaches compare well.

5.3.7. Conclusion

Analytical theory was developed for water-level response in a semi-confined coastal aquifer. This theory was applied to solve a specific case. Results of amplitude decay and time lag for this case were compared with a numerical solution to the problem. Analytical and numerical solutions compared well taking into consideration the errors in the results for time lag determined from the numerical solution. The analytical theory was hence verified.

Therefore, to summarise, the equations for amplitude decay and time lag of water-level response in a leaky coastal aquifer of infinite length are

$$h_{amp} = h_0 \exp^{-gx} \longrightarrow eqtn(5 \cdot 50)$$

$$t = \frac{1}{\omega}(g'x) = t_L \longrightarrow eqtn(5 \cdot 55)$$

where $g = \sqrt{\left\{ \dfrac{(\beta/T) + \sqrt{(\beta^2/T^2) + (\omega^2 S^2/T^2)}}{2} \right\}}$

and $g' = \sqrt{\left\{ \dfrac{-(\beta/T) + \sqrt{(\beta^2/T^2) + (\omega^2 S^2/T^2)}}{2} \right\}}$

159
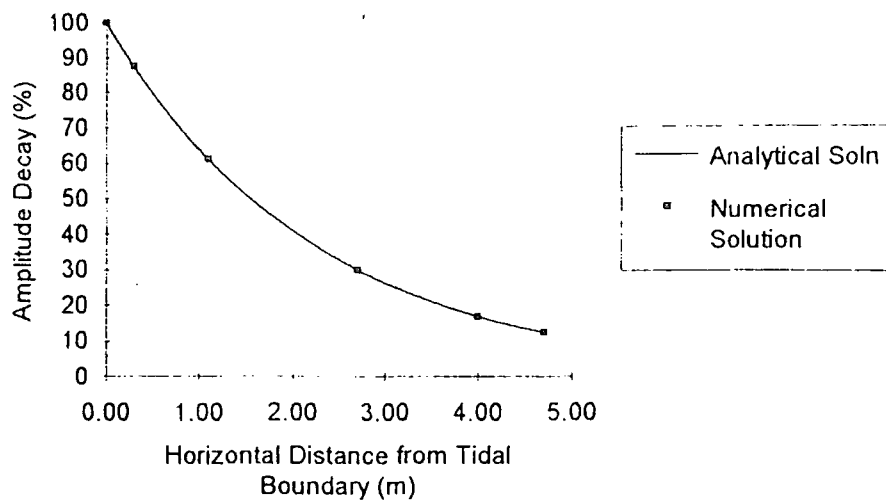
Figure 5.8. Amplitude Decay. Comparison of Analytical Solution (Incorporating Leakage) with Numerical Solution for a Leaky Aquifer of Infinite Length.
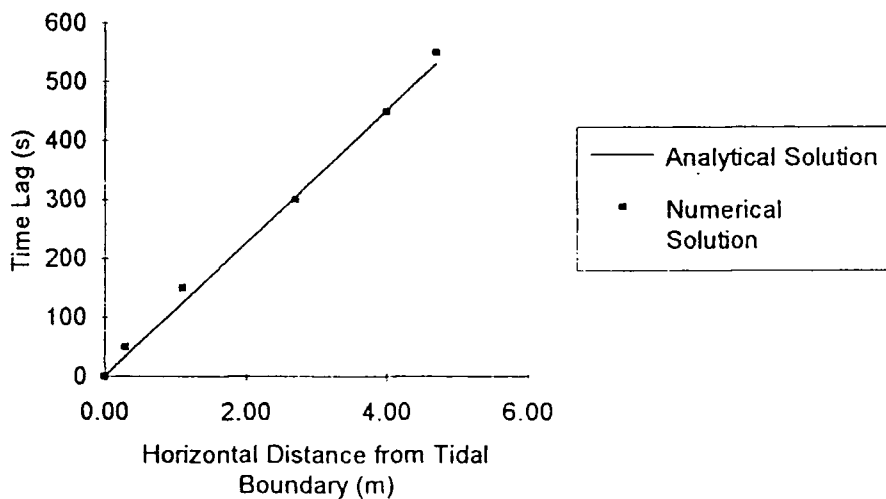
Figure 5.9. Time Lag. Comparison of Analytical Solution (Incorporating Leakage) with Numerical Solution for a Leaky Aquifer of Infinite Length.

5.4. Analytical Theory Describing Groundwater Behaviour with Leakage and Reflection

5.4.1. Concepts

The objective was to obtain two distinct equations incorporating aquifer parameters leakage, permeability and storage coefficient, together with terms describing the wave motion. The first equation would relate amplitude decay of the wave with horizontal distance, x. The second equation would provide an indication of the time lag of the wave, with respect to that at x=0, at various horizontal distances from this boundary.

Two mathematical approaches were investigated to achieve this objective. Firstly, analytical theory was derived combining the approaches of chapters 5.2 and 5.3. Secondly, a solution was derived using complex numbers. These two approaches resulted in the same solution. This section details this theory development and verification of concluded equations.

5.4.2. Combination Approach - Applying Theory of Chapters 5-2 and 5-3

The amplitude of the periodic wave at various horizontal distances, x, is given by eqtn(5.50) in chapter 5.3 and is recalled to be:

$$h_{amp} = h_0 \exp^{-gx} \longrightarrow eqtn(5 \cdot 56)$$

The equation of the wave is therefore:

$$H = h_0 \exp^{-gx} \sin(\omega t + \phi) \longrightarrow eqtn(5 \cdot 57)$$

where ϕ is the phase angle of the wave.

To incorporate reflection, image well theory was applied. The approach was similar to that described in chapter 5.2, the case for reflection without leakage.

Considering the main wave and two dominant reflections (described in chapter 5.2.2.3), the equation describing the resultant head is:

$$H_T = h_0 \exp(-gx)\sin(\omega t + ax) + h_0 \exp(-g(2L - x))\sin(\omega t + a(2L - x)) -$$
$$h_0 \exp(-g(2L + x))\sin(\omega t + a(2L + x)) \longrightarrow eqtn(5 \cdot 58)$$

where the wave number, a is defined as:

$$a = \frac{2\pi}{\lambda} \longrightarrow eqtn(5 \cdot 59)$$

Considering eqtn (5.55), the wavelength, λ can be defined as

$$\lambda = \frac{\omega t_0}{g'} \longrightarrow eqtn(5 \cdot 60)$$

From chapter 5.3 where

and $g' = \sqrt{\left\{ \dfrac{-(\beta/T) + \sqrt{(\beta^2/T^2) + (\omega^2 S^2/T^2)}}{2} \right\}}$

Expanding eqtn(5.58)

$$H_T = h_0 \exp(-gx)\{\sin \omega t \cos ax + \cos \omega t \sin ax\} +$$
$$h_0 \exp(-g(2L - x))\{\sin \omega t \cos a(2L - x) + \cos \omega t \sin a(2L - x)\} -$$
$$h_0 \exp(-g(2L + x))\{\sin \omega t \cos a(2L + x) + \cos \omega t \sin a(2L + x)\} \longrightarrow eqtn(5 \cdot 61)$$

Eqtn(5.61) can be simplified to

$$H_T = C(x)\sin \omega t + D(x)\cos \omega t \longrightarrow eqtn(5 \cdot 62)$$

where

$$C(x) = h_0 \exp(-gx)\cos(ax) + h_0 \exp(-g(2L - x))\cos(a(2L - x)) -$$
$$h_0 \exp(-g(2L + x))\cos(a(2L + x)) \longrightarrow eqtn(5 \cdot 63)$$

$$D(x) = h_0 \exp(-gx)\sin(ax) + h_0 \exp(-g(2L - x))\sin(a(2L - x)) -$$
$$h_0 \exp(-g(2L + x))\sin(a(2L + x)) \longrightarrow eqtn(5 \cdot 64)$$

Differentiating H_T [eqtn(5.62)] with respect to time, t, to find the amplitudes of the wave at various positions, x, from the sinusoidally varying boundary.

$$\frac{dH_T}{dt} = C\omega\cos\omega t - D\omega\sin\omega t \longrightarrow eqtn(5\cdot 65)$$

$$\frac{dH_T}{dt} = 0 \text{ for a maximum / minimum}$$

Applying this condition to eqtn (5.65) gives:

$$C\omega\cos\omega t = D\omega\sin\omega t \longrightarrow eqtn(5\cdot 66)$$

$$\omega t = \tan^{-1}\left(\frac{C}{D}\right) + n\pi \longrightarrow eqtn(5\cdot 67)$$

The time at which the *first* maximum/minimum value occurs for various horizontal distances is given by

$$t = \frac{1}{\omega}\tan^{-1}\left(\frac{C}{D}\right) \longrightarrow eqtn(5\cdot 68)$$

The amplitude decay of the wave is given by substituting eqtn(5.67) into eqtn(5.62):

$$H_{amp} = C(x)\sin\left\{\tan^{-1}\left(\frac{C}{D}\right)\right\} + D(x)\left\{\tan^{-1}\left(\frac{C}{D}\right)\right\} \longrightarrow eqtn(5\cdot 69)$$
Amplitude Decay

where C(x) and D(x) are given by eqtns(5.63) and (5.64) above.

The time lag of the wave at various horizontal positions with respect to x=0 is given by the modulus of equation (5.68)

$$timelag_{i\to L} = \text{mod}\left(\frac{1}{\omega}\tan^{-1}\left(\frac{C}{D}\right) - timelag_{x=0+i}\right) \longrightarrow eqtn(5\cdot 70)$$
Time Lag

where 0 < i < 0.1

This eqtn cannot be solved for x=0 because this results in a division by zero.

5.4.3. Complex Numerical Approach

A slightly different approach to the problem was taken in order to verify the solution given in chapter 5.4.1.

A complex numerical solution was investigated as a means of incorporating phase and time lag.

The amplitude of the periodic wave at various horizontal distances, x, is given by eqtn(5.50) in chapter 5.3 and is recalled to be:

$$h_{amp} = h_0 \exp^{-gx} \longrightarrow eqtn(5 \cdot 50)$$

The equation of the wave is therefore

$$H_A(x,t) = h_0 \exp^{-gx_A} \left[\cos \omega t_A + i \sin \omega t_A \right] \longrightarrow eqtn(5 \cdot 71)$$

But

$$c = \frac{x}{t} = \frac{\lambda}{t_0} \longrightarrow eqtn(5 \cdot 72)$$

Therefore

$$t = \frac{x t_0}{\lambda} \longrightarrow eqtn(5 \cdot 73)$$

and $\quad \omega t = \frac{2\pi}{t_0} * \frac{x t_0}{\lambda} = \frac{2\pi x}{\lambda} = \alpha x \longrightarrow eqtn(5 \cdot 74)$

Substituting this into eqtn(5.71) gives

$$H_A(x,t) = h_0 \exp^{-gx_A} \left[\cos \alpha x_A + i \sin \alpha x_A \right] \longrightarrow eqtn(5 \cdot 75)$$

Now, incorporating reflection, the equation of the first dominant reflective wave is

$$H_B(x,t) = h_0 \exp^{-gx_B} \left[\cos \alpha x_B + i \sin \alpha x_B \right] \longrightarrow eqtn(5 \cdot 76)$$

where

$$x_B = 2L - x_A \longrightarrow eqtn(5 \cdot 77)$$

The equation for the second dominant reflective wave is

$$H_C(x,t) = h_0 \exp^{-gx_B} \left[\cos \alpha x_C + i \sin \alpha x_C \right] \longrightarrow eqtn(5 \cdot 78)$$

where

$$x_c = 2L + x_A \longrightarrow eqtn(5 \cdot 79)$$

The total head, H_T by principal of superposition is therefore

$$H_T = H_A + H_B + H_C \longrightarrow eqtn(5 \cdot 80)$$

$$H_T = h_0 \exp(-gx_A) \left[\cos \alpha x_A + i \sin \alpha x_A \right] +$$
$$h_0 \exp(-gx_B) \left[\cos \alpha x_B + i \sin \alpha x_B \right] -$$
$$h_0 \exp(-gx_C) \left[\cos \alpha x_C + i \sin \alpha x_C \right] \longrightarrow eqtn(5 \cdot 81)$$

Collecting real and imaginary terms:

$$\text{Re}(H_T) = h_0 \exp(-gx_A)\left[\cos \alpha x_A\right] +$$
$$h_0 \exp(-gx_B)\left[\cos \alpha x_B\right] -$$
$$h_0 \exp(-gx_C)\left[\cos \alpha x_C\right] \longrightarrow eqtn(5\cdot82)$$

$$\text{Im}(H_T) = h_0 \exp(-gx_A)\left[\sin \alpha x_A\right] +$$
$$h_0 \exp(-gx_B)\left[\sin \alpha x_B\right] -$$
$$h_0 \exp(-gx_C)\left[\sin \alpha x_C\right] \longrightarrow eqtn(5\cdot83)$$

The absolute value of the complex numerical solution is the amplitude of the wave. This is given by

$$\boxed{H_{amp} = \sqrt{\left[\text{Re}(H_T)\right]^2 + \left[\text{Im}(H_T)\right]^2} \longrightarrow eqtn(5\cdot84)}$$ **Amplitude Decay**

The phase lag can be calculated from the argument of the complex solution. This is given by

$$Phase = \tan^{-1}\left(\frac{\text{Re}(H_T)}{\text{Im}(H_T)}\right) \longrightarrow eqtn(5\cdot85)$$

The time lag, t_L, is related to the phase the following equation:

$$t_L = \frac{t_0}{2\pi} * Phase \longrightarrow eqtn(5\cdot86)$$

The time lag of the sum of these waves for any value of x, with respect to the phase lag at x=0, is given by

$$\boxed{timelag = \frac{t_0}{2\pi} * \tan^{-1}\left(\frac{\text{Re}(H_T)}{\text{Im}(H_T)}\right) - timelag_{x=0} \longrightarrow eqtn(5\cdot87)}$$ **Time Lag**

5.4.4. Comparison of Analytical and Numerical Solutions for a Specific Case

In order to verify the analytical theory, an approach similar to that in chapters 5.2.2.2 and 5.3.6 was followed. A specific case was investigated and results of amplitude decay and time lag computed from application of analytical theory and numerical modelling.

5.4.4.1.   Outline of Specific Case

The case chosen for investigation was that outlined in section 5.3.6.1. The values for the parameters were as follows:

Length of Aquifer, $L = 4.7m$

Transmissibility, $T = 0.001m^2/s$

Storage coefficient, $S = 0.1$

Period, $t0 = 1920s$

Amplitude of harmonic wave at boundary (x=0), $h0 = 0.2m$

The leakage coefficient of the Durham Model Aquifer was estimated as $2 \times 10^{-5} s^{-1}$. The value of this parameter chosen for this case study was $6 \times 10^{-5} s^{-1}$. This larger coefficient would have a more significant effect on results of amplitude decay and time lag. Hence the theory could be more clearly verified by comparison with CVM.

5.4.4.2.   Analytical Solutions

Analytical solutions to the above problem were computed for both mathematical approaches.

The printouts of these two MATLAB files are provided in Appendices 5.4. and 5.5. Analytical solutions for one, two and three reflections were compared with numerical solutions. These comparisons are illustrated in Appendix 6.6.

5.4.4.3. Comparison of Solutions

The two analytical solutions for amplitude decay and time lag derived from the two mathematical approaches were compared. Graphs illustrating this comparison are shown in Figures 5.10. and 5.11. These graphs shown that the solutions from the two approaches exactly overlie.

A comparison of the numerical and analytical solutions for the amplitude decay and time lag for this case study are illustrated graphically in Figures 5.12 and 5.13.

The analytical solution for amplitude decay compares very well with the numerical solution. Once again, there is discrepancy between values of time lag determined by the analytical and numerical methods. The numerical solution produces results with an error of ±25 seconds. Allowing for this error in the numerical solution, the analytical and numerical approaches compare well.

5.4.5. Conclusion

Analytical theory was developed for water-level response in a semi-confined coastal aquifer of finite length. This theory was applied to solve a specific case. Results of amplitude decay and time lag for this case were compared with a numerical solution to the problem. Analytical and numerical solutions compared well, taking into consideration the errors in the results for time lag determined from the numerical solution. The analytical theory was hence verified.

Therefore, to summarise, the equations for amplitude decay and time lag of water-level response in a leaky coastal aquifer of finite length are

$$H_{amp} = C(x)\sin\left\{\tan^{-1}\left(\frac{C}{D}\right)\right\} + D(x)\left\{\tan^{-1}\left(\frac{C}{D}\right)\right\} \longrightarrow eqtn(5\cdot69)$$

$$timelag_{i\rightarrow L} = \text{mod}\left(\frac{1}{\omega}\tan^{-1}\left(\frac{C}{D}\right) - timelag_{x=0+i}\right) \longrightarrow eqtn(5\cdot70)$$

167

where

$$C(x) = h_0 \exp(-gx)\cos(ax) + h_0 \exp\bigl(-g(2L - x)\bigr)\cos\bigl(a(2L - x)\bigr) -$$
$$h_0 \exp\bigl(-g(2L + x)\bigr)\cos\bigl(a(2L + x)\bigr) \longrightarrow eqtn(5 \cdot 63)$$

$$D(x) = h_0 \exp(-gx)\sin(ax) + h_0 \exp\bigl(-g(2L - x)\bigr)\sin\bigl(a(2L - x)\bigr) -$$
$$h_0 \exp\bigl(-g(2L + x)\bigr)\sin\bigl(a(2L + x)\bigr) \longrightarrow eqtn(5 \cdot 64)$$
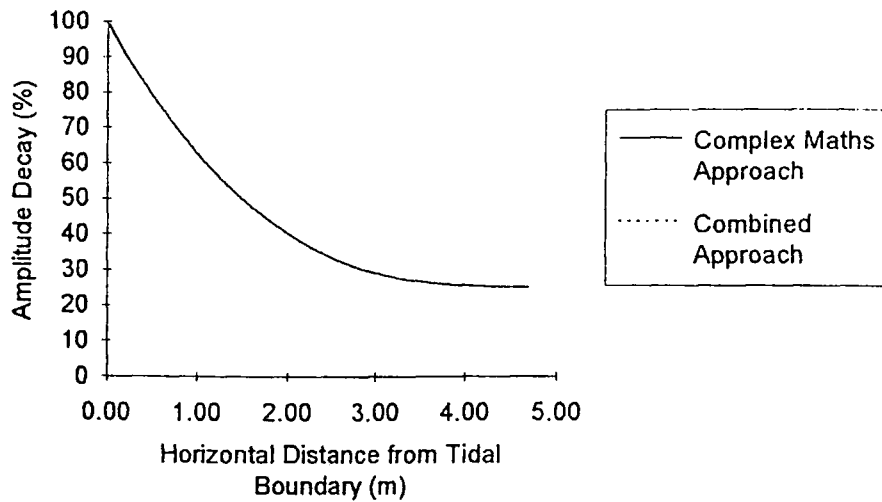
Figure 5.10 Amplitude Decay. Comparison of Two Analytical Solutions (Incorporating Leakage &Reflection) from two Different Mathematical Approaches.
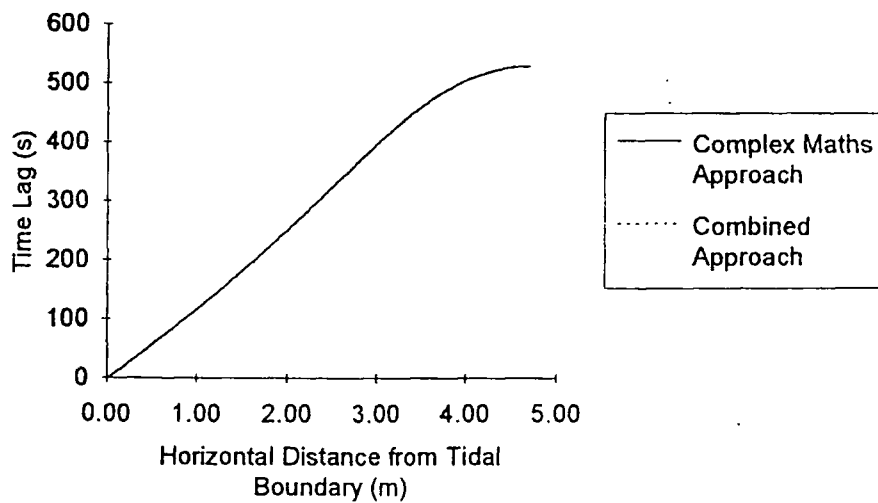
Figure 5.11. Time Lag. Comparison of Two Analytical Solutions (Incorporating Leakage &Reflection) from two Different Mathematical Approaches.
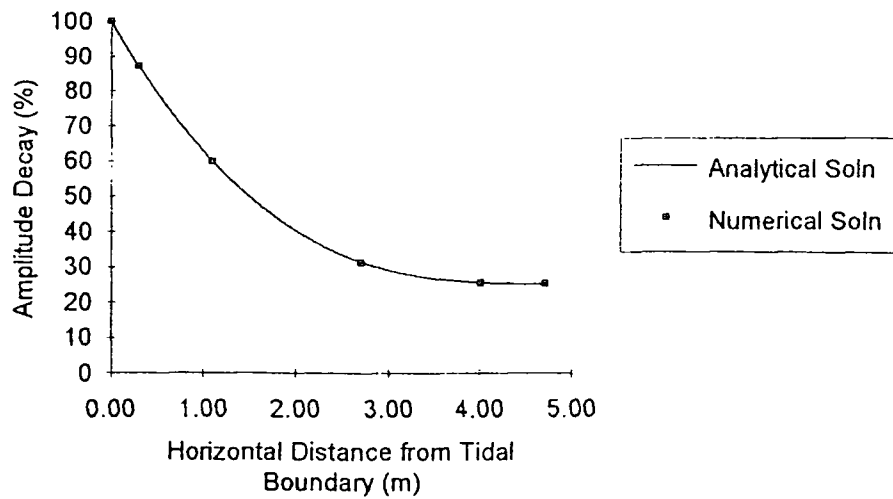
Figure 5.12 Amplitude Decay. Comparison of Analytical Solution (Incorporating Leakage & Reflection) with Numerical Solution for a Leaky Aquifer of Finite Length.
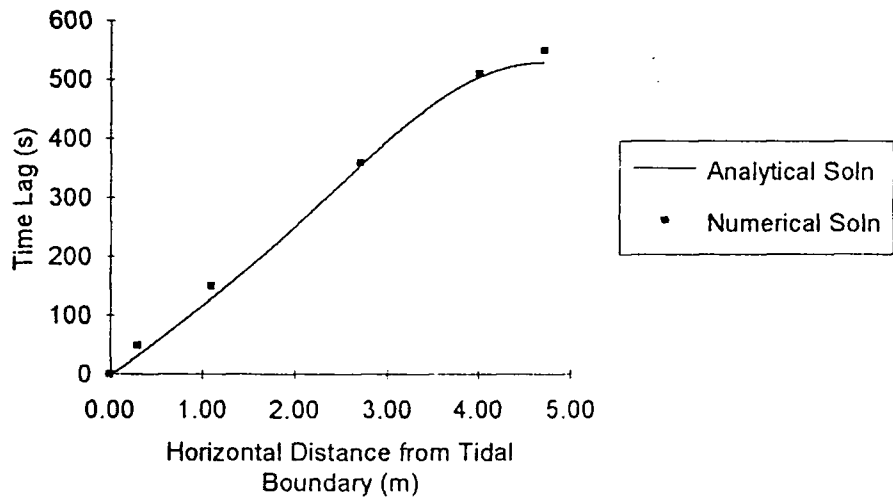
Figure 5.13 Time Lag. Comparison of Analytical Solution (Incorporating Leakage & Reflection) with Numerical Solution for a Leaky Aquifer of Finite Length.

Chapter 6

Application of Analytical Theory to Laboratory Results

6.1. Introduction

Chapter 5 concluded with two analytical equations for amplitude decay and time lag in a semi-confined aquifer of finite length. These formulae incorporate three aquifer properties, storage coefficient, transmissivity and coefficient of leakage.

The objective was to apply this newly developed theory to the results from experimental work performed using the Durham Model Aquifer. Aquifer properties for the laboratory model were determined from results of amplitude decay and time lag applying the theory of chapter 5.4. These values were then compared with estimates from preliminary experimental work.

6.2. Period Normalisation and Period Ranges - Investigation by Applying Analytical Theory.

In order to analyse the laboratory results of amplitude decay and time lag, it was necessary to normalise the data to eliminate variations due to differences in period between test series. As was discussed in chapter 4.8.2, period normalisation depended on the analytical theory. After much study of the equations outlined in chapter 5.4., it was concluded that period normalisation was complicated by the parameter, g (which incorporates all three aquifer properties).

The effects of period variation on amplitude decay and time lag were more closely investigated. Recalling tables 3.6 and 3.7, the primary periods ranged from 1600 seconds to 2743 seconds. The secondary periods ranged from 533 seconds to 1371

seconds. It was decided to prescribe period ranges, and investigate variations in results of amplitude decay and time lag based on analytical theory.

The first primary period range investigated was 1820 seconds to 2020 seconds. This range was selected since it contained a large number of experimental results. Once again, a specific case was outlined. Values for aquifer properties were based on earlier experimental work. These are summarised below.

Length of Aquifer, L = 4.7m

Transmissibility, T = 0.001m²/s

Storage coefficient, S = 0.1

Leakage coefficient, β = 2 x 10^{-5} s^{-1}

Amplitude of harmonic wave at boundary (x=0), h_0 = 0.2m

Three different periods were investigated within this range: 1820s, 1920s and 2020s. The analytical theory of chapter 5.4. was then applied and solutions of amplitude decay and time lag computed for the three periods under investigation. These are shown graphically in Figures 6.1 and 6.2. These figures illustrate that the greater the period, the larger the time lag and also the slower the rate of amplitude decay. The maximum difference in amplitude decay between period 1920s and the limits of the range was 3%, whilst that for time lag was 15s. As a percentage of the amplitude decay solution for a period of 1920s, this difference constituted 5%. The corresponding time lag difference constituted 3% of the time lag for the 1920s wave. These effects on amplitude decay and time lag were considered small, and it was therefore decided to group all laboratory results within this period range together. This included results from test Series 1, 9, 10, 12, 13, 14, 15. For purpose of analysis, these results were compared with theory of period 1920s, the central period within the range.

Following this work, three secondary periods were investigated, 620s, 790s and 960s. The reason for the selection of this period range, 620s to 960s, was to include secondary results which corresponded with primary results in the range 1820s to 2020s. Time lag was not investigated for variations in secondary periods because laboratory results for time lag were based on the period of the sawtooth waveform

172

(before fast fourier transform analysis). This was approximately equal to the period of the governing constituent waveform (the primary wave). Hence laboratory results for time lag were compared solely with time lag theory based on the primary period. The analytical solutions for secondary amplitude decay for each of the three periods were computed using the aquifer properties summarised above. Figure 6.3 illustrates these analytical solutions. The maximum difference in amplitude decay between the central period and limits of the range was calculated to be 3%. This constituted a maximum difference in amplitude decay of 20%. This percentage difference is large but this is because the values themselves are small.

Laboratory results from other test series were also grouped into period ranges. The size of the period ranges varied slightly due to the laboratory results available. In certain cases, period ranges encompassed only one series of laboratory results. This was because there was no other experimental data recorded for periods close to this value. This applied to series 6 and 8. Analytical solutions of amplitude decay, and for the cases of primary periods, time lag, were plotted graphically. The period ranges and their corresponding graphs are detailed in tables 6.1 and 6.2 below.

Primary Period Range Number	Period Range	Laboratory Results	Figure Numbers of Graphs (Analytical Solutions)
1	1820 s to 2020 s	Series 1, 9, 10, 12, 13, 14, 15.	6.1 & 6.2
2	2050 s to 2400 s	Series 2, 3, 4, 5, 7.	6.4 & 6.5
3	1600 s to 1800 s	Series manual, 8, 11.	6.6 & 6.7
4	2743s	Series 6.	6.8 & 6.9

Table 6.1. Primary Period Ranges. Analytical Solutions.

Secondary Period Range Numbers	Period Range	Laboratory Results	Figure Numbers of Graphs (Analytical Solutions)
5	533s	Series 8.	6.10
6	620s to 960 s	Series 1, 9, 10, 11, 12, 13, 14, 15.	6.3
7	1000 s to 1200s	Series 2, 3, 4, 5, 7.	6.11
8	1370 s	Series 6.	6.12

Table 6.2. Secondary Period Ranges. Analytical Solutions.

Thus, the variations in amplitude decay and time lag due to period differences were investigated by applying the analytical theory derived in chapter 5.4.

It was concluded that, for analyses purposes, laboratory results would be classified into the period ranges outlined above.

6.3. Laboratory Results Classified Within Period Ranges

The laboratory results of amplitude decay and time lag were arranged into graphical form according to the period ranges concluded following investigation of analytical solutions. These period ranges were defined in section 6.2 above. Results for each period range were plotted together on a single graph. Tables 6.3 and 6.4 below outline the period ranges and corresponding figures illustrating the spread of laboratory results within these ranges.

Primary Period Range Number	Period Range	Laboratory Results	Figure Numbers of Graphs (Laboratory Results)
1	1820 s to 2020 s	Series 1, 9, 10, 12, 13, 14, 15.	6.13 & 6.14
2	2050 s to 2400 s	Series 2, 3, 4, 5, 7.	6.15 & 6.16
3	1600 s to 1800 s	Series manual, 8, 11.	6.17 & 6.18
4	2743s	Series 6.	6.19 & 6.20

Table 6.3. Primary Period Ranges. Laboratory Results.

Secondary Period Range Numbers	Period Range	Laboratory Results	Figure Numbers of Graphs (Laboratory Results)
5	533s	Series 8.	6.21
6	620s to 960 s	Series 1, 9, 10, 11, 12, 13, 14, 15.	6.22
7	1000 s to 1200s	Series 2, 3, 4, 5, 7.	6.23
8	1370 s	Series 6.	6.24

Table 6.4. Secondary Period Ranges. Laboratory Results.

From observation of Figures 6.13 to 6.14, it can be seen that, for a number of period ranges, there is considerable amount of scatter of data. In particular, results from series 1, 9 and 10 appear to be quite different from others within the range. This is illustrated in Figures 6.13, 6.14 and 6.22. These differences may be attributed to variations in the amount of air within the system. Position 3 was selected as the

reference position (for reasons outlined in chapter 3). If air or silt becomes entrapped in the pore water pressure measurement system for this position, all the results of amplitude decay and time lag for that series will be affected. This is likely to be the reason why some of the results from measurement positions distant from the tidal tank exceed 100%.

These figures do, however, illustrate a general pattern of results of amplitude decay and time lag.

6.4. Analyses Procedure

6.4.1. Objective

A procedure had to be established to link analytical theory with experimental results. The analytical theory incorporated the parameter, g - a variable combining all three aquifer properties and the wave period.

$$g = \sqrt{\frac{-(\beta / T) + \sqrt{(\beta^2 / T^2) + (\omega^2 S^2 / T^2)}}{2}} \longrightarrow eqtn(6 \cdot 1)$$

One procedure that was considered involved determining, from analytical theory, a value for g which would lead to analytical solutions for amplitude decay and time lag similar to the experimental results. This procedure, however, would not lead to conclusions of individual aquifer properties, coefficients of leakage (β), storage (S) and permeability (K = T/aquifer width).

A procedure had to be established which separated out the three individual properties of interest.

6.4.2. Linking Pairs of Aquifer Properties to Aid Analysis.

The possibility of linking pairs of variables together was investigated with the objective of aiding the analysis procedure, and providing a clearer indication of

trends. The governing equation for flow in a one-dimensional leaky aquifer system is stated in eqtn (5.31) in chapter 5, and is recalled below:

$$S\frac{\partial h}{\partial t} = T\frac{\partial^2 h}{\partial x^2} - \beta(h - h^*) \longrightarrow eqtn(6 \cdot 2)$$

Dividing eqtn(6.1) by the storage coefficient, S:

$$\frac{\partial h}{\partial t} = \frac{T}{S}\frac{\partial^2 h}{\partial x^2} - \frac{\beta}{S}(h - h^*) \longrightarrow eqtn(6 \cdot 3)$$

From eqtn (6.3), it was thought that T/S and β/S may be linked pairs. The third linked pair would be T/β.

The parameter, g, defined in eqtn (6.1) comprises two unknowns, β/T and S/T, in addition to the angular velocity of the wave, ω. This equation provided an indication of linked pairs of aquifer properties.

Therefore, the analytical theory was applied to investigate whether solutions of amplitude decay and time lag for constant values of these variables assimilated, independent of the individual values of T, S and β themselves.

Appendices 6.1 and 6.2 show printouts of the MATLAB files for two case studies, the parameters of which are outlined below in Table 6.5.

Case 1 - Appendix 7.1	Case 2 - Appendix 7.2
T = 0.001 m^2/s	T = 0.02 m^2/s
S = 0.05	S = 0.1
β = 0.00001 s^{-1}	β = 0.00002 s^{-1}
T/S = 0.02 m^2/s	
T/β = 100 m^2	
L= 4.7 m	
t_0 = 1920 s	
h_0 = 0.2 m	

Table 6.5. Variables for Two Case Studies.

T/S and T/β were constant for both cases, although individual properties varied between the two. The solutions of amplitude decay and time lag for these two case studies are illustrated in Figures 6.25 and 6.26. These graphs illustrate that the two solutions for amplitude decay and time lag assimilate.

Two further case studies were prescribed. This time, T/S was constant, whilst T/β varied. Neither time lag nor amplitude decay solutions assimilated. The investigation is outlined in detail in Appendix 6.3.

For the final two case studies, T/β was constant, whilst T/S varied. Again, neither time lag nor amplitude decay solutions assimilated. This investigation is outlined in detail in Appendix 6.4.

Therefore, it was concluded that values of T/S and β/S had to be the constant for solutions of amplitude decay and time lag from separate case studies to assimilate. The fact that T/S and β/S were constant, implied that T/β was also constant.

6.4.3. Varying Linked Pairs of Aquifer Properties, T/S and T/β

It was concluded that for different case studies constant values of variables, T/S and T/β, provided unique solutions for amplitude decay and time lag. It was then decided to maintain one of these variables as a constant whilst varying the value of the other, and observe patterns in analytical solutions of amplitude decay and time lag. It was decided to maintain the variable T/S as a constant value, since the range of values of storage coefficient is small for a specified soil material. Leakage and permeability coefficients can vary to a more significant extent for a single soil material.

Therefore T/S was maintained as a constant whilst T/β was varied. This essentially involved varying the leakage coefficient, β. The solution for the following case study was determined from application of the analytical theory.

$T/S = 0.01$ m^2/s

$t_0 = 1920$ s

$h_0 = 0.2$ m

178

The leakage coefficient was varied. In order to indicate the solution for amplitude decay and time lag with no leakage, the inverse parameter β/T was selected. The leakage coefficient was altered to produce values of β/T of 0, 0.01m^{-2}, 0.02m^{-2} and 0.1m^{-2} for a constant value of T/S of $0.01\text{m}^2/\text{s}$. This implied that, assuming a value for transmissivity, T, of $0.001\text{m}^2/\text{s}$, the leakage coefficient, β varied between 0 and 10^{-4} s^{-1}. Figures 6.27 and 6.28 illustrate solutions of amplitude decay and time lag. It was found that the curves tended to an upper limit of T/β. This upper limit corresponded to the solution for a confined aquifer without leakage. The analytical theory of section 5.3 for a confined aquifer of finite length was applied to the above case study. Solutions of amplitude decay and time lag were compared with those from application of theory for a leaky aquifer of finite length with a leakage coefficient prescribed as zero (β = 0). These results are illustrated in Appendix 6.5. This work verified the two analytical theories.

It was observed that, as the leakage coefficient decreased ($\beta/T \rightarrow 0$), solutions of amplitude decay and time lag became increasingly similar.

Similar case studies to those outlined above were prescribed. The range of values of storage coefficient within a particular soil material is much smaller than the possible range of values of transmissibility. For this reason, transmissibility was varied, whilst the storage coefficient was maintained at a constant value of 0.1. The two case studies were prescribed values of T/S of $0.02\text{m}^2/\text{s}$ and $0.03\text{m}^2/\text{s}$. Values of leakage coefficient were varied to produce solutions for amplitude decay and time lag for values of β/T of 0, 0.01 m^{-2}, 0.02 m^{-2} and 0.1 m^{-2}. These solutions are shown in Figures 6.29 and 6.32.

6.4.4. General trends

From observation of Figures 6.27 and 6.32, general trends were noted. These are summarised in Figure 6.33 below.
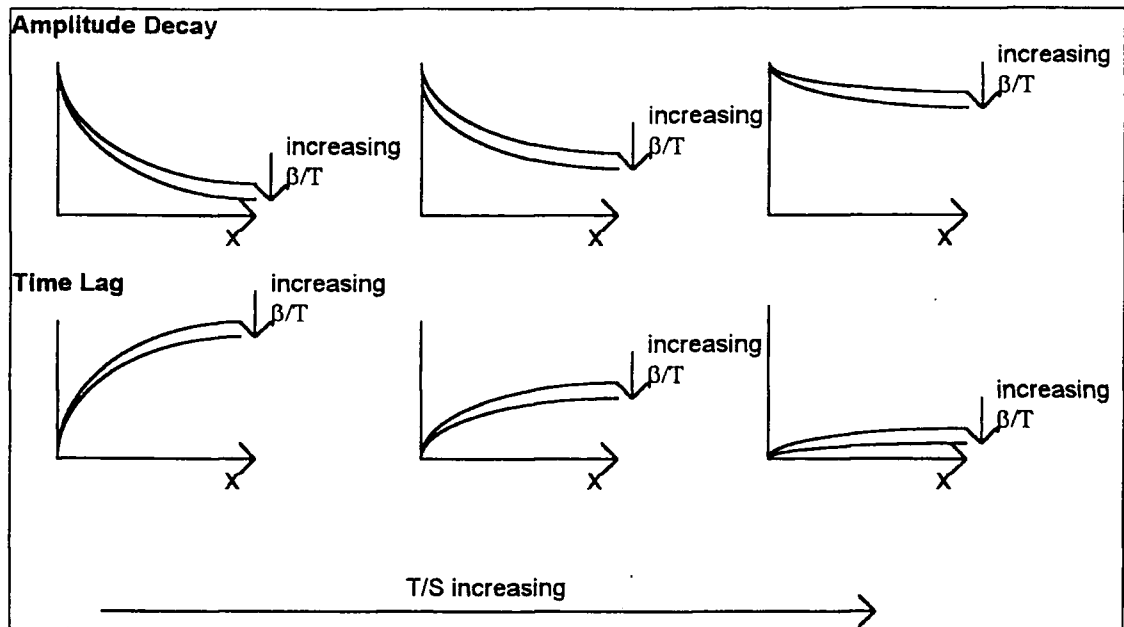
Figure 6.33. General Trends in Solutions of Amplitude Decay and Time Lag as Variables T/S and β/T are Altered.

It was noted that an increase in T/S of $0.01m^2/s$ lead to significantly less amplitude decay and, in addition, a significant reduction in the time lag. It was concluded that the theory was very sensitive to changes transmissivity.

This theory was not as sensitive to changes in leakage coefficient. For values of β/T in the order of $10^{-2}m^{-2}$ the variation in solutions of amplitude decay and time lag was small. Assuming a value for T of the order of $10^{-2}m^2/s$, this implies that when β is of the order of 10^{-4} s^{-1}, the leakage has little effect on solutions of amplitude decay and time lag. For values of β/T in the order of $10^{-1}m^{-2}$ the variation in solutions of amplitude decay and time lag was considerable. Assuming a value for T of the order of 10^{-2} m^2/s, this implies that when β is of the order of 10^{-3} s^{-1}, the leakage has significant effect on solutions of amplitude decay and time lag. Therefore, it was concluded that it would be difficult to determine accurately values of leakage coefficient less than 10^{-3} s^{-1}.

It was noted that solutions of amplitude decay and time lag were more affected by the leakage coefficient as distance from the tidal boundary increased. This can be explained by the fact water leaks continually from the upper surface of the aquifer,

and therefore an increasing amount of water is lost by leakage as distance from the tidal boundary increases.

6.5. Laboratory Results

This section discusses the assumptions made and arrangement of laboratory results in preparation for application of analytical theory.

6.5.1. Assumptions

In order to apply the analytical theory to the laboratory results, certain assumptions had to be made. These included establishing a region of study. Aquifer properties had to be assumed values as a starting point for analyses. Once again, the aquifer properties were assumed values based on the earlier experimental work performed on the Durham Model Aquifer under steady state conditions. These are summarised once more below:

Transmissibility, $T = 0.001 \text{m}^2/\text{s}$

Storage coefficient, $S = 0.1$

Leakage coefficient, $\beta = 2 \times 10^{-5} \text{ s}^{-1}$

The Durham Model Aquifer had been repaired following test series 4, before further tests were performed. This may have affected the leakage coefficient, however water leakage was not observed to have changed significantly as a result of these repairs. Comparison of results of amplitude decay and time lag from series 1 to 4 with those from later tests did not suggest greater leakage as a result of the repair work. In addition to this, from the application of the analytical theory in chapter 6.4.3. it was concluded that values of leakage coefficient of less than 10^{-4} s^{-1} would be difficult to determine accurately. Although this appeared unfortunate, since it was anticipated that β was of the order of 10^{-5} s^{-1} from earlier work, conversely it implied that variations in leakage coefficient during the experimental programme would not have significant affect on results of amplitude decay and time lag.

The leakage coefficient was therefore assumed to have remained constant throughout the duration of all the laboratory experiments.

For analyses purposes the aquifer was assumed to have a length of 4.7 metres. The analytical theory incorporated reflection from the boundaries at x=0 and x=4.7 metres. This was not strictly the case for the Durham Model aquifer[1].

It was decided to analyse results from primary period range 1 and secondary period range 6. These primary results corresponded exactly with the secondary results from range 6, however it was noted that series 11 was an addition to the secondary range. This additional information to the secondary series provided more accurate mean results. In addition, period ranges 1 and 6 encompassed the largest number of test series.

6.5.2. Arranging the Laboratory Results

The results were re-arranged for comparison with analytical theory. It was decided to calculate the mean value and also indicate maximum and minimum values. The mean values would provided average decay and time lag curves which could be easily compared with analytical theory. The maximum and minimum values would indicate spread.

Therefore, the mean value of results for amplitude decay and time lag for primary period range 1820s to 2020s was computed. These mean values were then plotted versus the horizontal distance from position 3. In addition, the maximum and minimum values of the results were also plotted on the graph to provide an indication of spread of the data. Figures 6.34 and 6.35 are graphs of amplitude decay and time lag indicating the mean values and spread of the data. The same statistical analysis procedure was also followed for secondary period range 620s to 960s. Figure 6.36

---

[1] The impermeable boundary was actually located at x=-0.145 metres. This distance was small, and therefore it was considered reasonable to assume an impermeable boundary at x=0 for analytical purposes.

illustrates the mean values and spread of amplitude decay results for this secondary period range.

There were three separate pieces of information available: primary amplitude decay, secondary amplitude decay and time lag. It was hoped that these pieces of information were sufficient to obtain distinct values of the three unknown aquifer properties, coefficients of leakage, storage and permeability.

6.6. Application of Analytical Theory to Laboratory Results

Laboratory results and analytical solutions were plotted simultaneously. As a starting point, the values of aquifer properties concluded from the earlier work were assumed. The objective was to conclude a suitable range of values of T/S and corresponding β/T values by application of analytical theory to results of primary amplitude decay, secondary amplitude decay and time lag. As explained above, primary period range 1 and corresponding secondary period range 6 were considered. Laboratory results were compared with the analytical solution of time lag computed for the primary period.

6.6.1. Primary Period Range 1

Three separate cases were studied. These are outlined below.

6.6.1.1. Case Study A

Firstly, a value of T/S from earlier work was considered. The earlier work concluded the following estimates for transmissivity and storage coefficient.

T = 0.001 m^2/s

S=0.1

Therefore, for application of analytical theory, an initial value of T/S of 0.01m^2/s was assumed. This provided a region of study. The period, t_0, was selected as 1920s for

application of analytical theory. This was the centre of the experimental results range 1820s to 2020s.

The tidal amplitude, h_0, was selected as 0.20 metres, based on the amplitude of the primary waveform determined by FFT analysis of laboratory results. This value of amplitude did vary slightly between tests. These variations occurred because the reference amplitude for calculation of amplitude decay results was position 3. The amplitude of the wave at position 1 was prescribed whilst the wave at position 3 was not, and was dependent on the prescribed wave. Variations may have occurred in the measured amplitude of the transmitted wave due to differences in the amount of air in the system. In addition, the fast fourier transform analyses concluded with constituent sinusoidal waveforms which varied slightly in amplitude. For comparison with analytical theory, a value of h_0 of 0.2 metres was assumed.

Analytical solutions of amplitude decay and time lag for four different values of β/T were computed. These were as follows:

$\beta/T = 0$

$\beta/T = 0.01$ m^{-2}

$\beta/T = 0.02$ m^{-2}

$\beta/T = 0.1$ m^{-2}

The analytical solutions of amplitude decay and time lag were plotted on a graph, together with the laboratory results (mean, and maximum and minimum values). These graphs are shown in Figures 6.37 and 6.38. From observation of Figure 6.36, it was concluded that the theoretical solution for amplitude decay with this T/S value was too low when compared with the laboratory results. Figure 6.38 illustrated that the theoretical solution for time lag for the value of T/S of 0.01m^2/s compared well with laboratory results. It was concluded that theoretical solutions for values of β/T ranging from 0.02m^{-2} to 0.1m^{-2} provided a satisfactory match with laboratory results.

6.6.1.2. Case Study B

The first case study concluded that application of theory for T/S of $0.01m^2/s$ provided results of amplitude decay which were generally lower than laboratory results. Earlier work investigating trends in the analytical solutions suggested that increasing the value of T/S reduced the rate of amplitude decay. Therefore, a value of T/S = $0.02m^2/s$ was substituted into the analytical theory for case study B. The same values of β/T were applied as for case study A.

Once again, the analytical solutions were plotted on a graph, together with the laboratory results. These graphs are shown in Figures 6.39 and 6.40. From observation of Figure 6.39, it was concluded that the theoretical solution for amplitude decay with this T/S value compared more closely with the laboratory results than in the previous case. For T/S of $0.02m^2/s$, it was concluded that an appropriate range of values for β/T, which matched the laboratory results of amplitude decay, was 0 to $0.02m^{-2}$. In addition, it was concluded that theoretical solutions of time lag for values of β/T ranging from 0 to $0.1m^{-2}$ provided a satisfactory match with laboratory results.

6.6.1.3. Case Study C

Finally, theoretical solutions for a value of T/S of $0.03m^2/s$ were computed. Once again, these solutions were plotted on a graph, together with the laboratory results. These graphs are shown in Figures 6.41 and 6.42. From observation of Figure 6.41, it was concluded that an appropriate range of values for β/T, which matched the laboratory results of amplitude decay, was 0.1 to 0.01 m^{-2}. In addition, it was concluded that the theoretical solution for time lag for values of β/T close to zero provided a satisfactory match with laboratory results.

6.6.2. Secondary Period Range 6

Similar cases to those outlined for primary period range 1 were studied. The wave period selected for investigation was 790s. This was the centre of the experimental

results range 620s to 960s. A tidal amplitude, h_0, of 0.03 was prescribed for purpose of analysis. This again was based on conclusions from FFT analysis of laboratory results. The case studies are outlined below.

6.6.2.1. Case Study A

For this case, a value of T/S of 0.01m^2/s was prescribed as before. Theoretical solutions of amplitude decay for four selected values of β/T were computed, and plotted graphically together with experimental results. These are shown in Figure 6.43. It was concluded that the theoretical solutions for amplitude decay were lower than experimental results.

6.6.2.2. Case Study B

Theoretical solutions for this case incorporated a value of T/S of 0.02m^2/s. Theoretical solutions of amplitude decay for four selected values of β/T were computed, and plotted graphically together with experimental results. These are shown in Figure 6.44. It was concluded that theoretical solutions of time lag for values of β/T ranging from 0 to 0.02m^{-2} provided a satisfactory match with laboratory results.

6.6.2.3. Case Study C

For this case, a value of T/S of 0.03m^2/s was prescribed. Theoretical solutions of amplitude decay for four selected values of β/T were computed, and plotted graphically together with experimental results. These are shown in Figure 6.45. It was concluded that theoretical solutions of time lag for values of β/T ranging from 0 to 0.02m^{-2} provided a satisfactory match with laboratory results.

6.7. Conclusions

From observation of Figures 6.27 to 6.45, ranges of values of β/T which contained the experimental results were concluded. The ranges of β/T for corresponding values of T/S from each of the three types of laboratory results are summarised in tables 6.6 to 6.8 below.

Primary Amplitude Decay	
T/S (m^2/s)	β/T (m^{-2})
0.01	NONE
0.02	$0 \rightarrow 0.02$
0.03	$0.01 \rightarrow 0.1$

Table 6.6. Primary Amplitude Decay. Range of Values of β/T for corresponding values of T/S.

Time Lag	
T/S (m^2/s)	β/T (m^{-2})
0.01	$0.02 \rightarrow 0.1$
0.02	$0 \rightarrow 0.1$
0.03	0

Table 6.7. Time Lag. Range of Values of β/T for corresponding values of T/S.

Secondary Amplitude Decay	
T/S (m^2/s)	β/T (m^{-2})
0.01	NONE
0.02	$0 \rightarrow 0.02$
0.03	$0 \rightarrow 0.02$

Table 6.8. Secondary Amplitude Decay. Range of Values of β/T for corresponding values of T/S.

The results of tables 6.6 to 6.8 are illustrated graphically in Figure 6.46.

The area of overlap of the results from the analysis of primary amplitude decay, time lag and secondary amplitude decay was concluded to be:

$T/S = 0.02 \ m^2/s$

β/T range $= 0 \rightarrow 0.02 m^{-2}$

The individual aquifer properties of T, S and β could not be determined solely from the above two conclusions. The range of values of storage coefficient is small compared to the range of values of the other aquifer properties, transmissivity and leakage coefficient. Therefore the storage coefficient, S, was assumed the value obtained from earlier work, S = 0.1. It was appreciated that this value was unusually high for sandy soil material, however this was attributed to the fact that the storage coefficient incorporates the compressibility of the water and soil matrix, and discounts the presence of any air within the soil strata. A significant amount of air bubbles were anticipated to be present in the Durham Model Aquifer, and this accounted for the unusually high estimate of storage coefficient of 0.1.

Therefore an assumption of storage coefficient, S=0.1 resulted in concluding the following estimates of aquifer properties:

Transmissivity, $T = 2 \times 10^{-3} \ m^2/s$

Coefficient of permeability, $K = T /$ thickness of aquifer $= 8 \times 10^{-3} \ m/s$

Leakage Coefficient, β ranging from $0 \rightarrow 4 \times 10^{-5} \ s^{-1}$

6.8. Discussion

The analysis procedure was applied to laboratory results from period ranges 1 and 6 i.e. test series 1, 9, 10, 11, 12, 13, 14 and 15.

An initial region of study was selected based on estimates of aquifer properties concluded from earlier experimental work using the Durham Model Aquifer. A region

of study had to be selected and assumptions for aquifer properties made before amplitude decay and time lag could be determined theoretically.

Based on the assumption that the storage coefficient was 0.1, tidal analyses concluded with an estimate for the coefficient of permeability of 8×10^{-3} m/s. In addition, the coefficient of leakage was estimated to lie in the range, $0 \rightarrow 4 \times 10^{-5}$ s^{-1}. Aquifer properties for the Durham Model Aquifer determined by preliminary work following alternative methods to tidal analysis, concluded with estimates for the coefficients of permeability and leakage of 4×10^{-3} m/s and 2×10^{-5} s^{-1} respectively. Estimates of aquifer properties determined by these alternative methods compared well with estimates based on tidal analyses. Estimates for the coefficient of permeability were of the same order of magnitude, which for such a wide-ranging parameter, illustrated a good comparison.

It could be argued, however, that since the region of study for tidal analyses was determined by the estimates of permeability based on the earlier work, that it was inevitable that results would compare well. This is partly true, but strictly speaking, theoretical solutions of amplitude decay and time lag *verified* the previous estimates of aquifer properties. The leakage coefficient was assumed to lie within the range 0 to 10^{-4} s^{-1}. A conclusive range for the leakage coefficient of $0 \rightarrow 4 \times 10^{-5}$ s^{-1} was of sufficient accuracy considering that the analyses procedure allowed detailed prediction of this parameter for values above 10^{-5} s^{-1}.

Assuming a value for the storage coefficient, S, is reasonable since this parameter has a smaller range of values than transmissivity (permeability). It is therefore more easily determined and to a higher degree of accuracy than transmissivity. Field tests may be used to provide an estimate of storage coefficient, S. Following this, tidal analyses may be applied to determine T/S and β/T and hence transmissivity and leakage coefficient can be estimated.

In summary, it was concluded that the results of the tidal analyses verified the earlier estimates of aquifer properties, permeability and leakage, for the case of the Durham Model Aquifer.
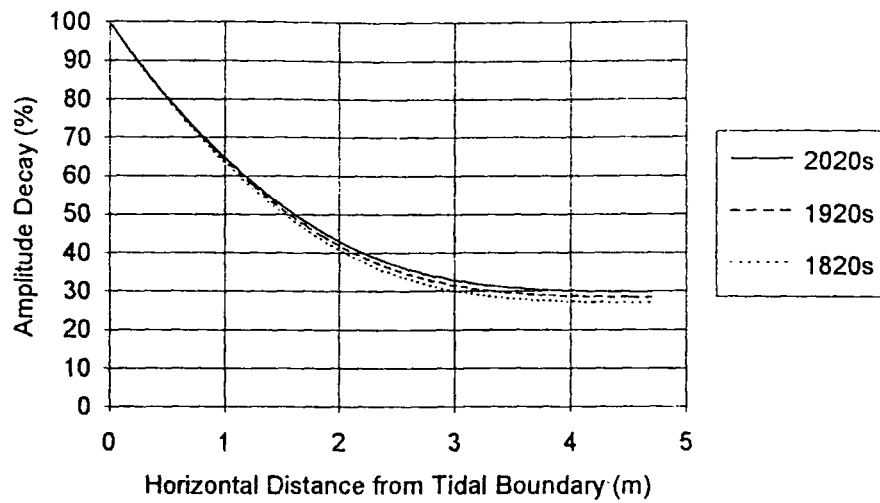
Figure 6.1. Amplitude Decay. Analytical Theory Illustrating Period Variation Within Specified Range.
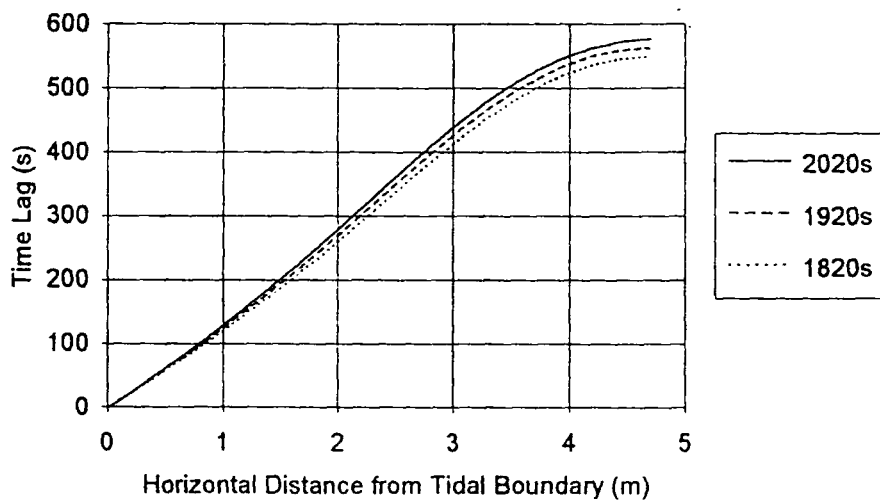
Figure 6.2. Time Lag. Analytical Theory Illustrating Period Variation Within Specified Range.
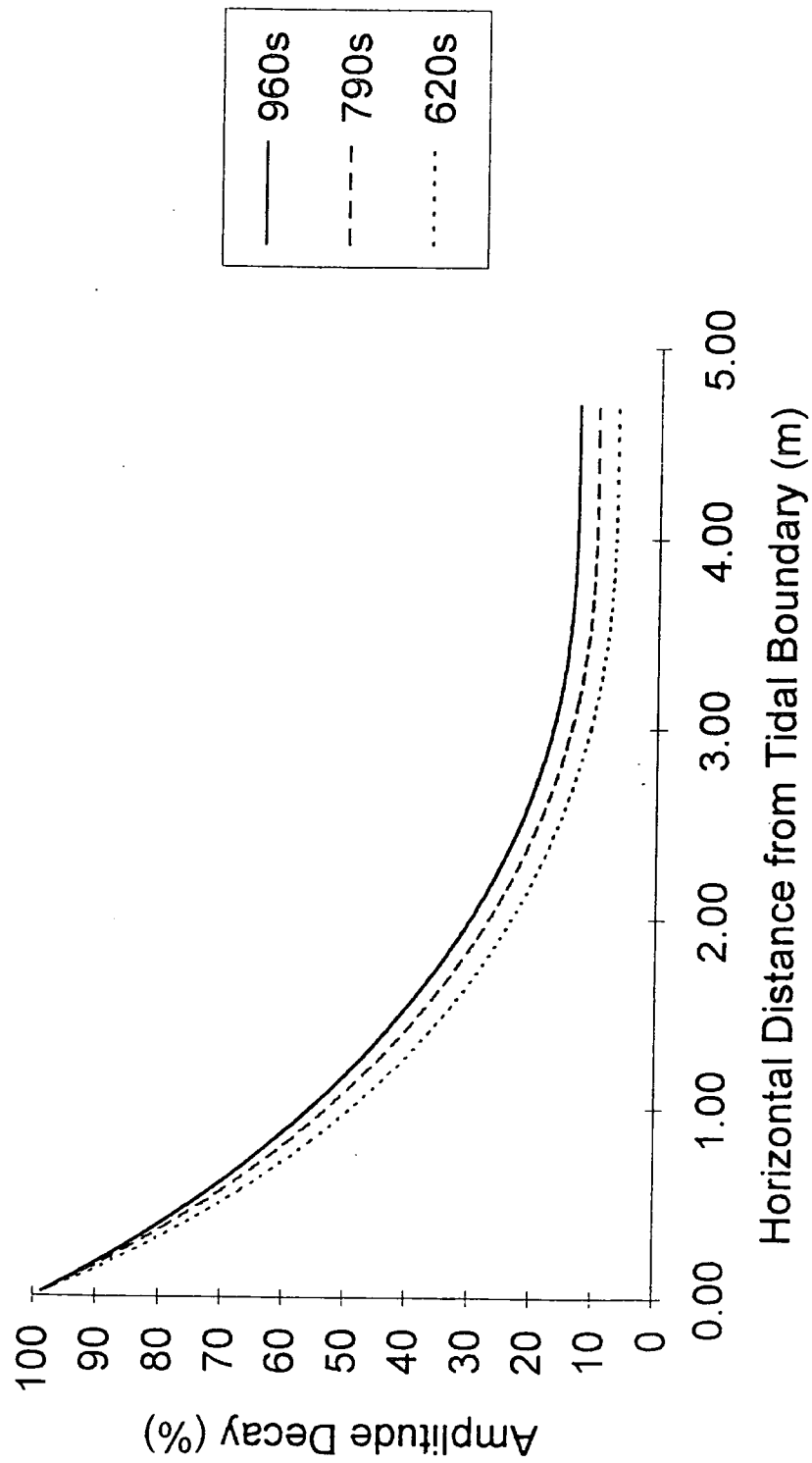
Figure 6.3. Amplitude Decay. Analytical Theory For Secondary Periods 620s, 790s, and 960s.
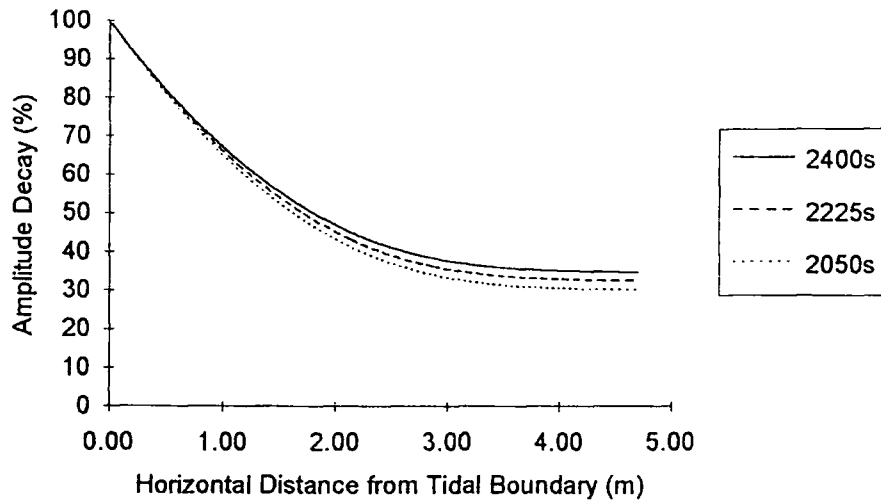
Figure 6.4. Amplitude Decay. Analytical Theory For Primary Periods 2050s, 2225s and 2400s.
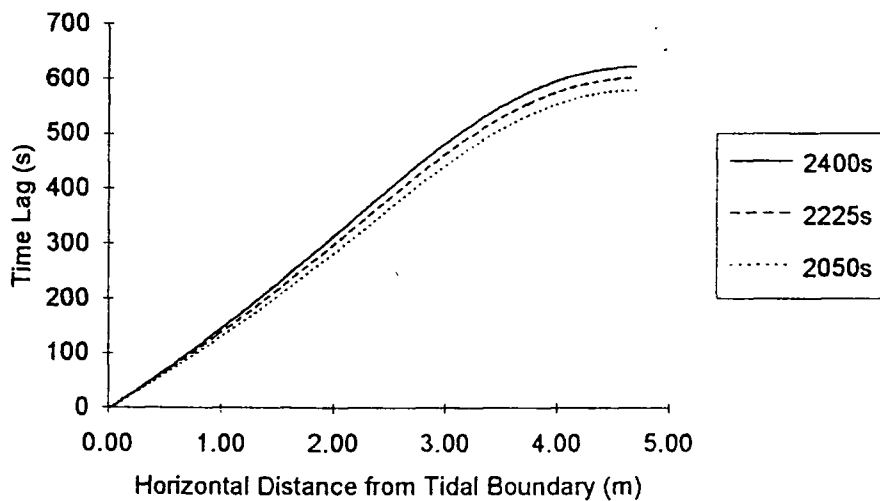
Figure 6.5. Time Lag. Analytical Theory For Primary Period 2050s, 2225s and 2400s.
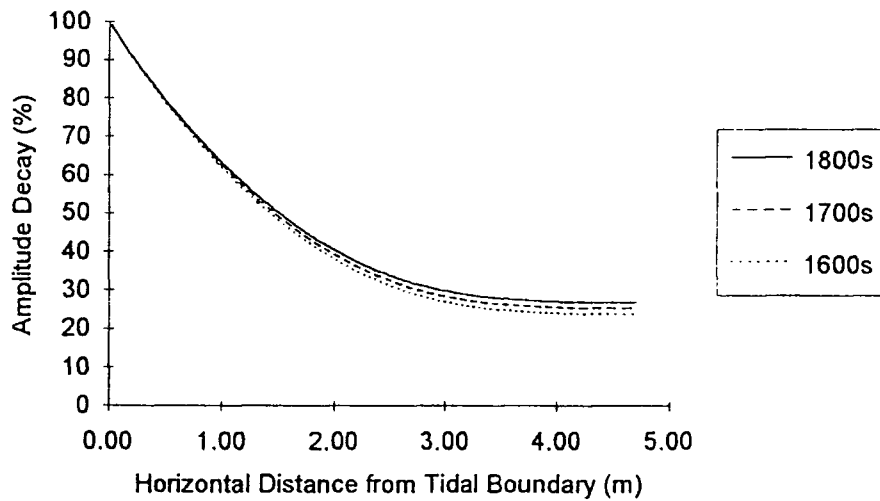
Figure 6.6.   Amplitude Decay. Analytical Theory For Primary Periods 1600s, 1700s and1800s.
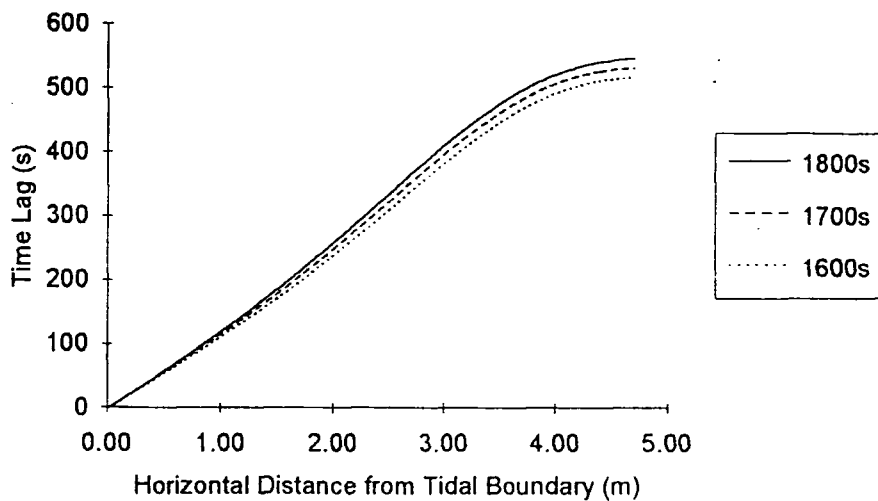
Figure 6.7.   Time Lag. Analytical Theory For Primary Periods 1600s, 1700s and1 1800s.

Period Range 2743 seconds
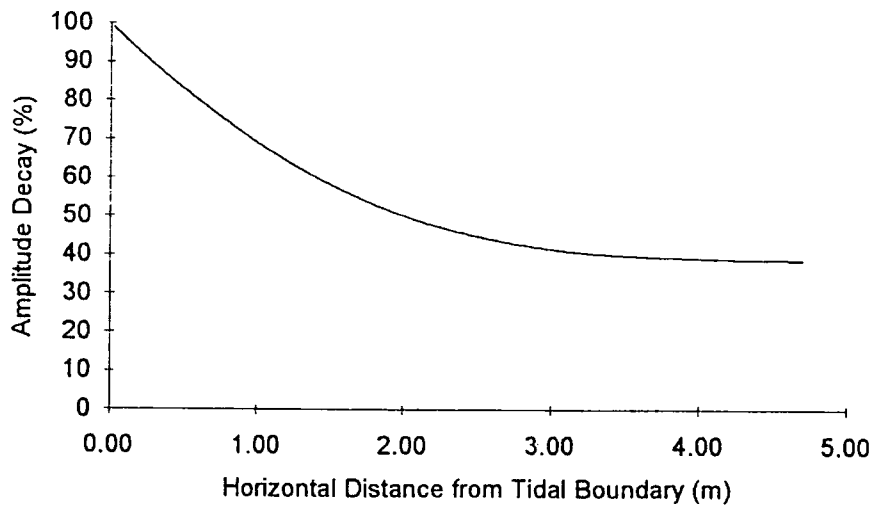
Figure 6.8. Amplitude Decay. Analytical Theory for Primary Period 2743s.
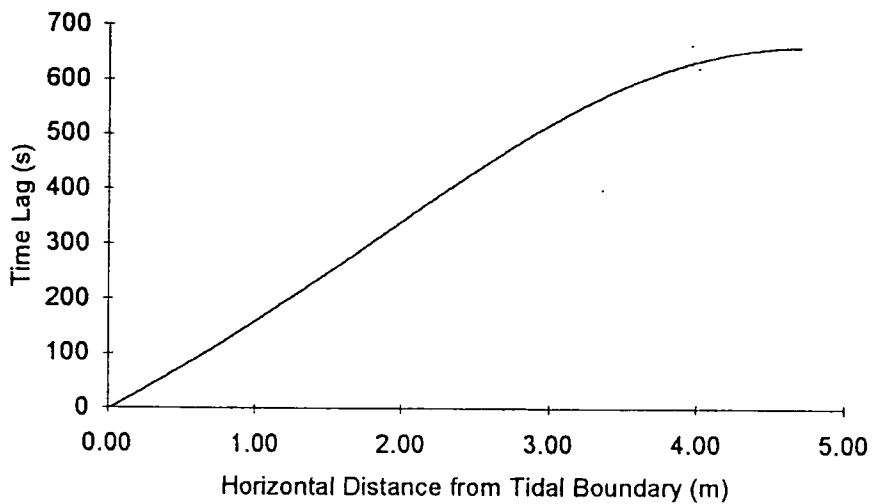
Figure 6.9. Time Lag. Analytical Theory for Primary Period 2743s.

Period Range 533 seconds

Amplitude Decay (%)

100 90 80 70 60 50 40 30 20 10 0

Horizontal Distance from Tidal Boundary (m)

0.00   1.00   2.00   3.00   4.00   5.00
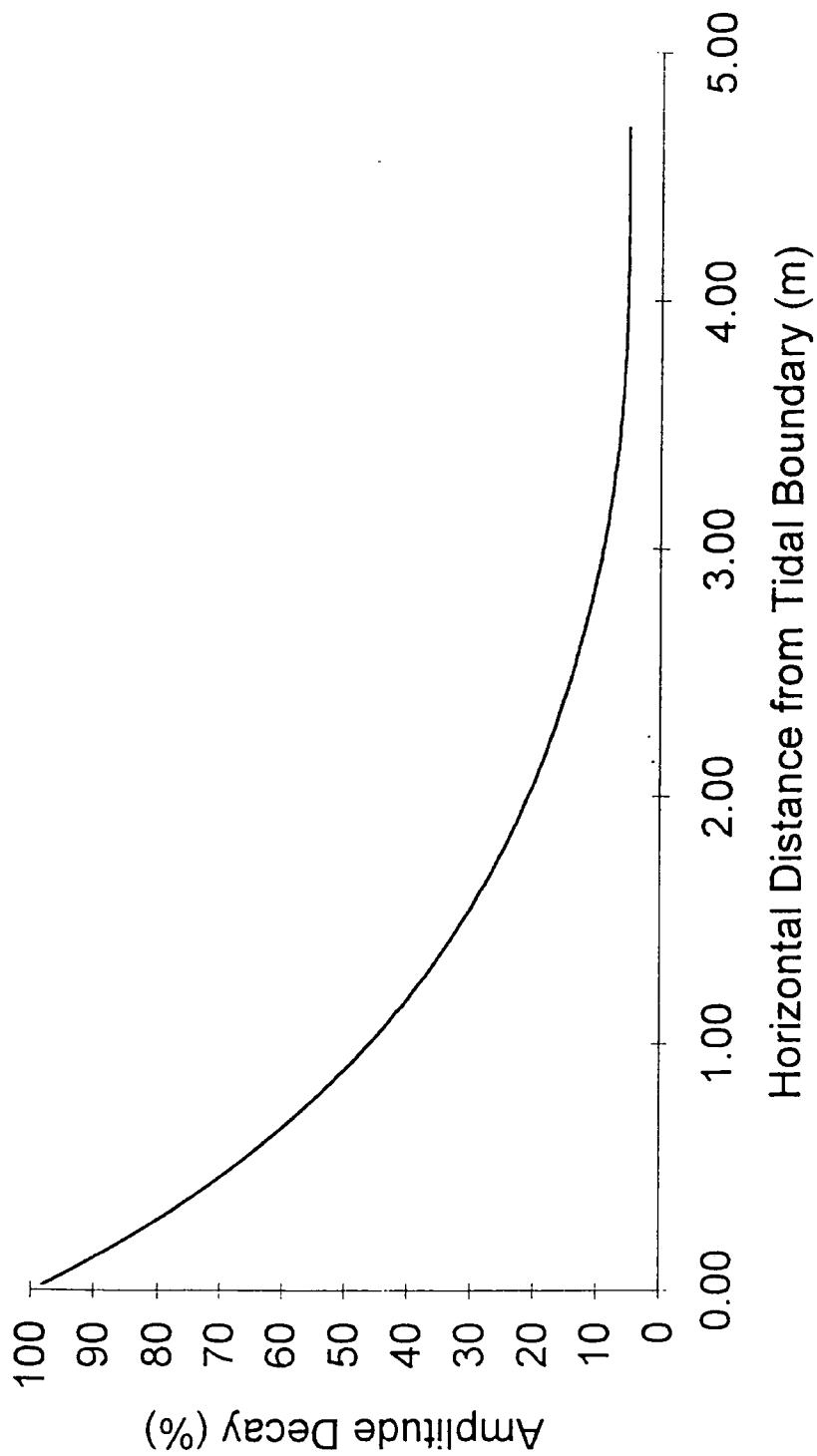
Figure 6.10. Amplitude Decay. Analytical Theory for Secondary Period 533 seconds.
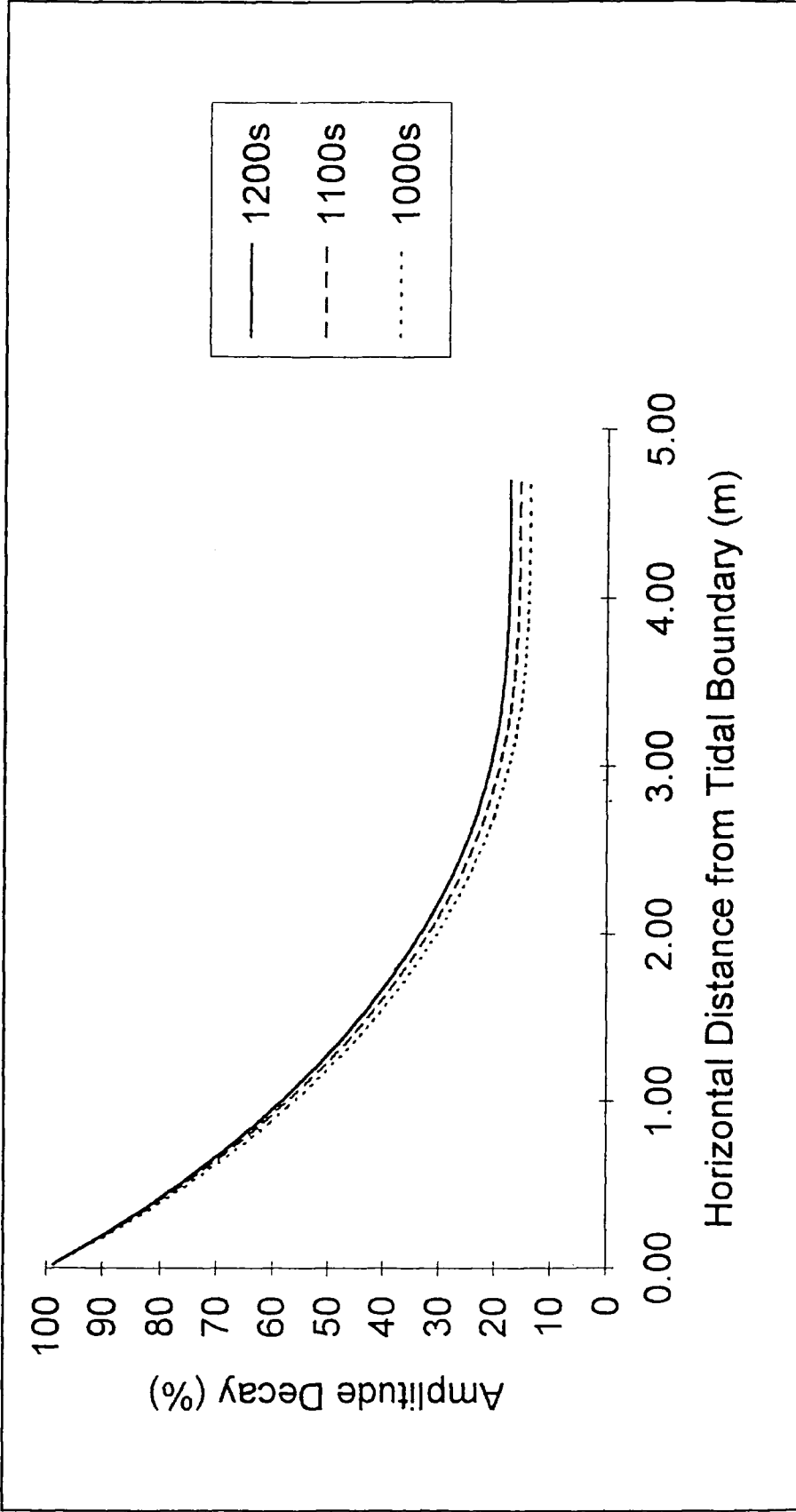
Figure 6.11. Amplitude Decay. Analytical Theory for Secondary Periods 1000s, 1100s and 1200s.

Period Range 1371 seconds

Amplitude Decay (%)

Horizontal Distance from Tidal Boundary (m)
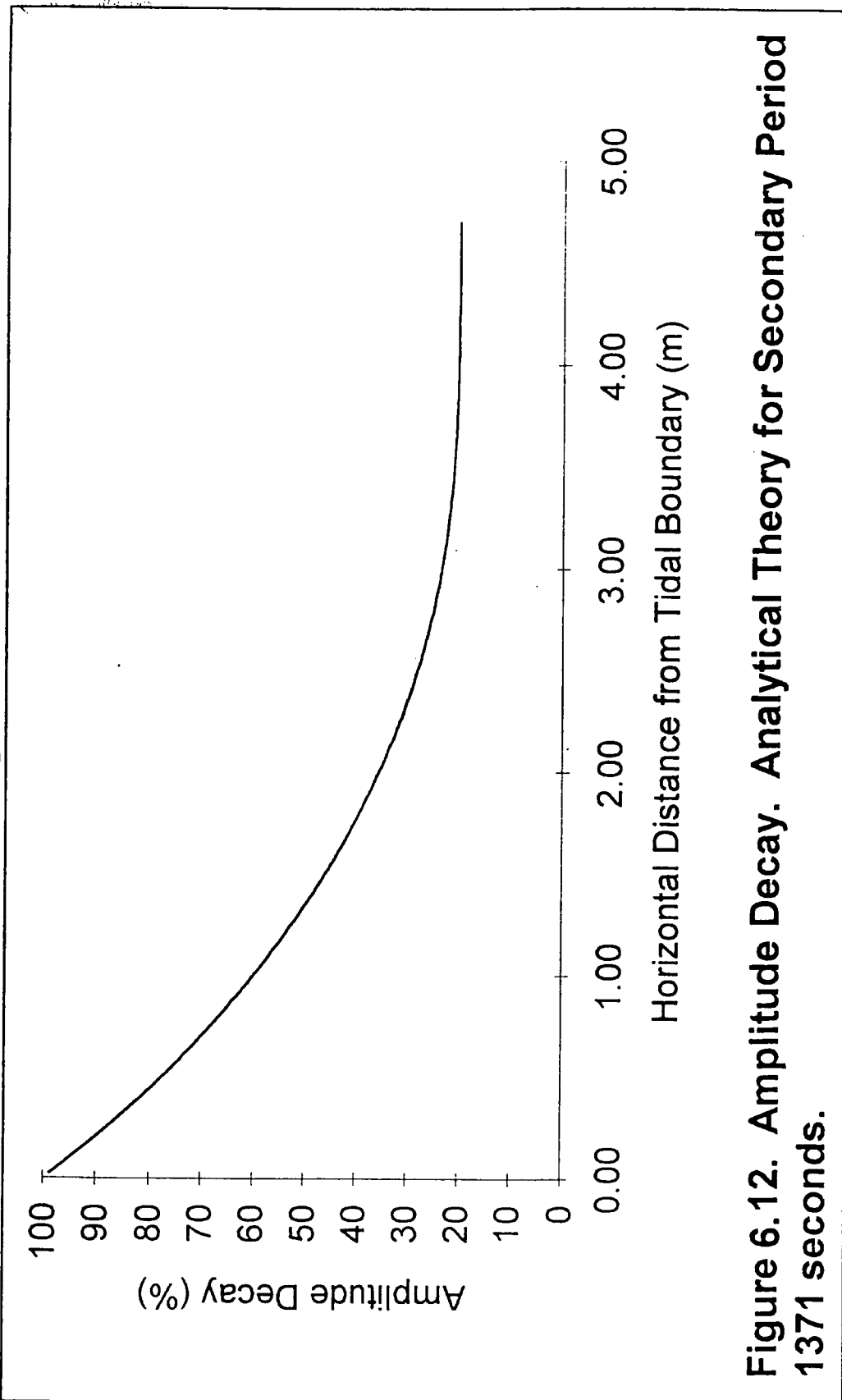
Figure 6.12. Amplitude Decay. Analytical Theory for Secondary Period 1371 seconds.
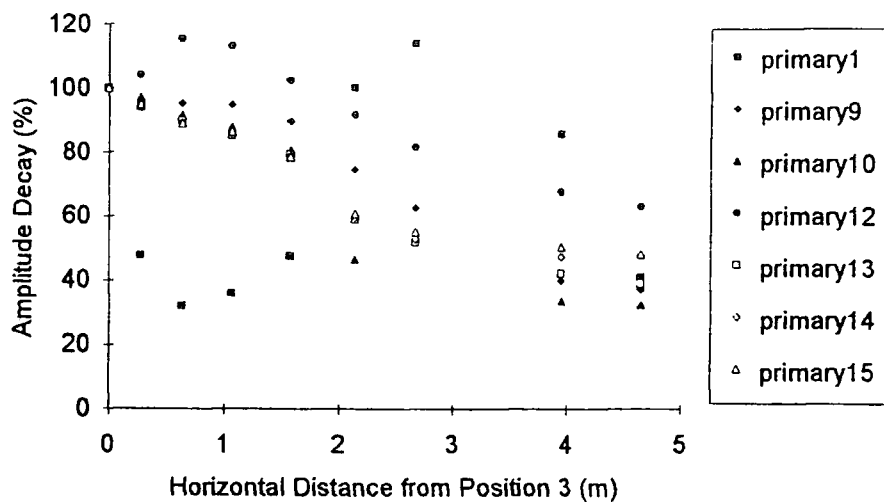
Figure 6.13. Amplitude Decay. Laboratory Results within Primary Period Range 1820s to 2020s.
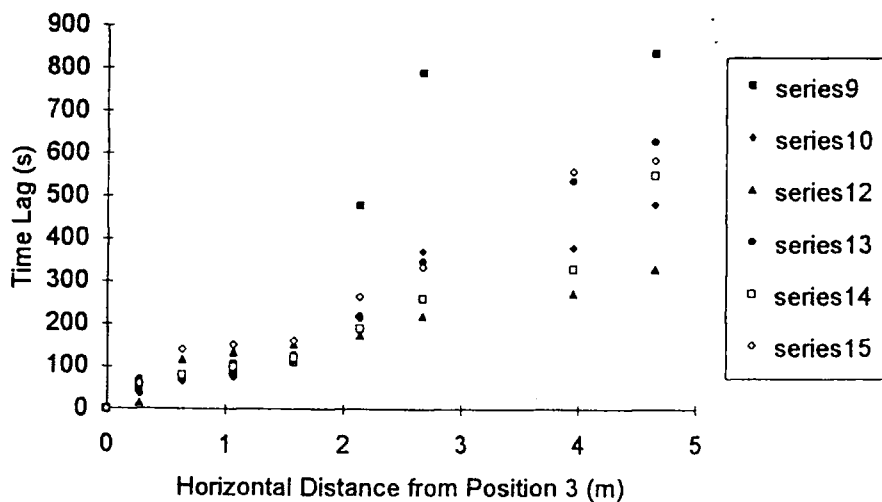
Figure 6.14. Time Lag. Laboratory Results within Period Range 1820s to 2020s.
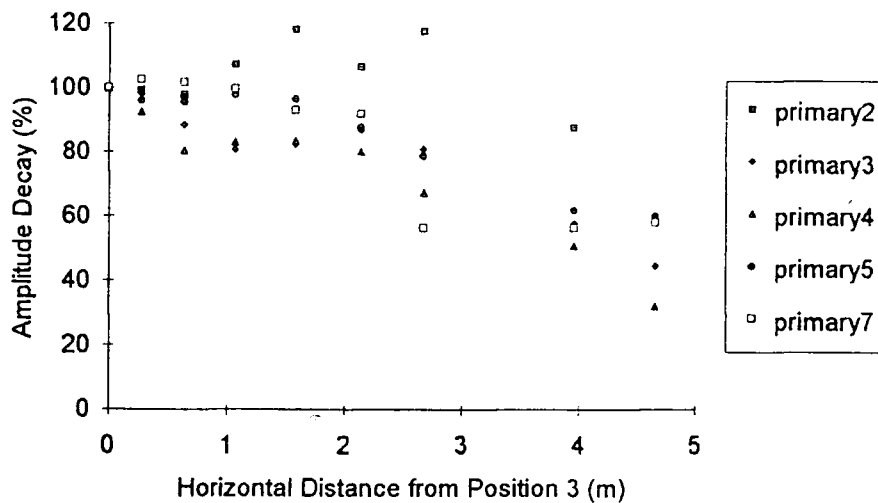
Figure 6.15. Amplitude Decay. Laboratory Results within Primary Period Range 2050s to 2400s.
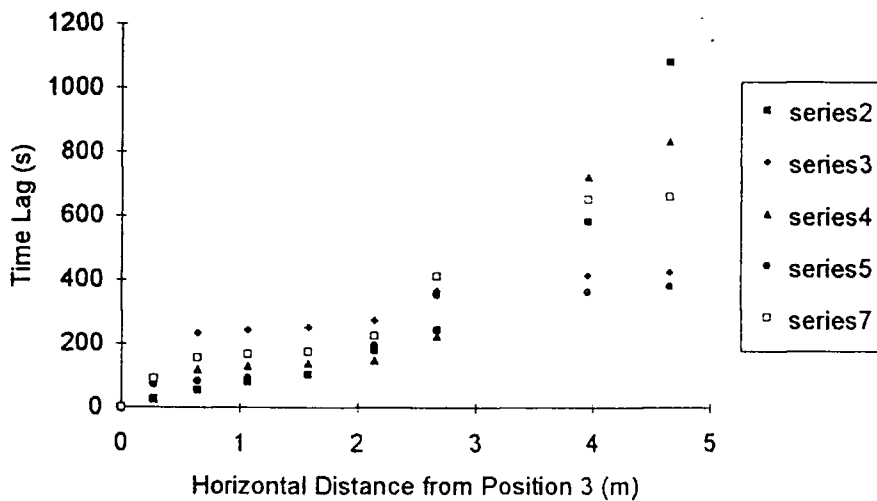
Figure 6.16. Time Lag. Laboratory Results within Period Range 2050s to 2400s.
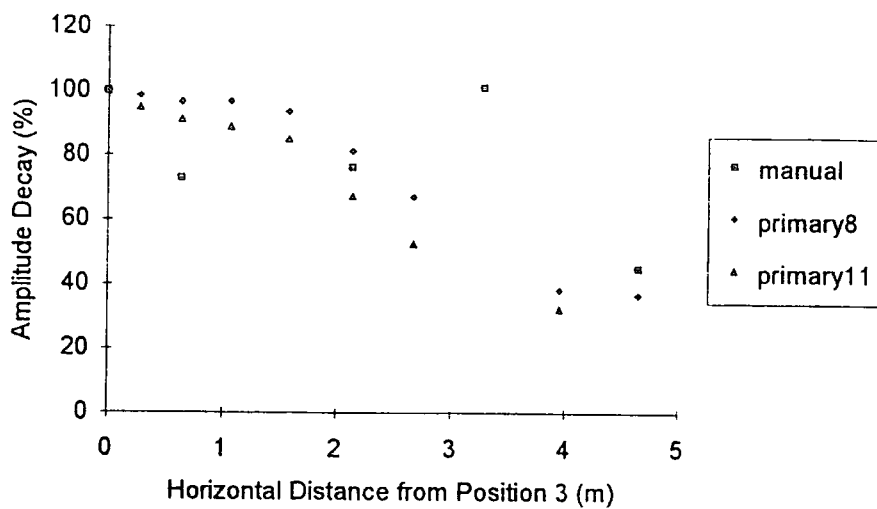
Figure 6.17. Amplitude Decay. Laboratory Results within Primary Period Range 1600s to 1800s.
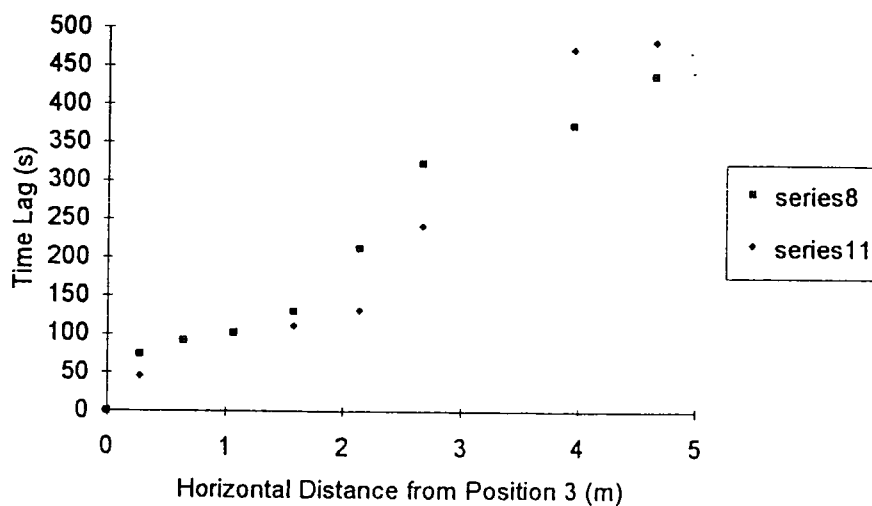
Figure 6.18. Time Lag. Laboratory Results within Period Range 1600s to 1800s.
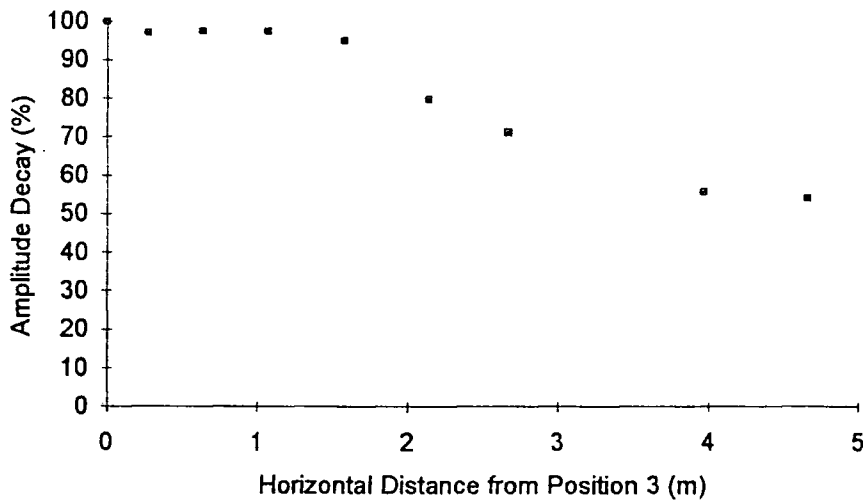
Figure 6.19. Amplitude Decay. Laboratory Results within Primary Period Range 2743s.
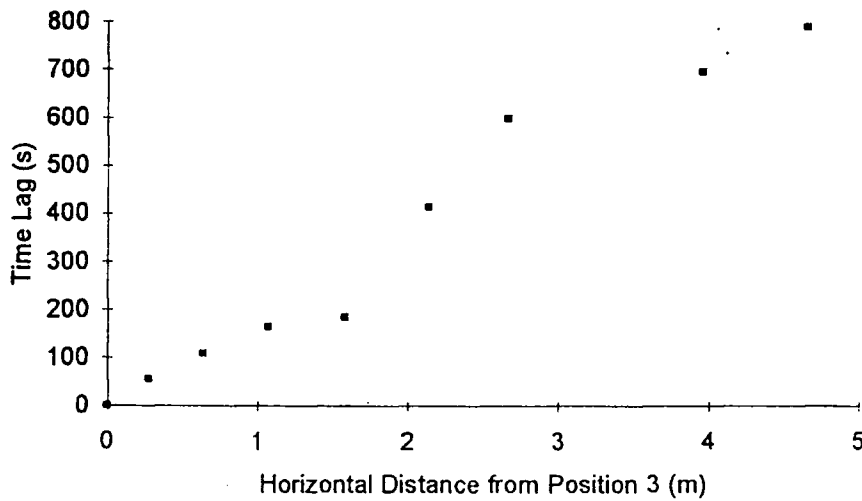
Figure 6. 20. Time Lag. Laboratory Results within Primary Period Range 2743s.
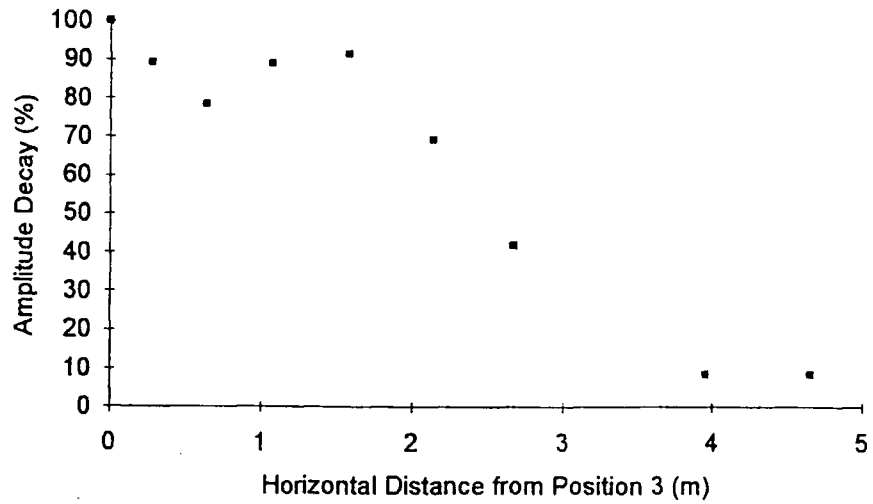
Figure 6.21. Amplitude Decay. Laboratory Results within Secondary Period Range 533s.
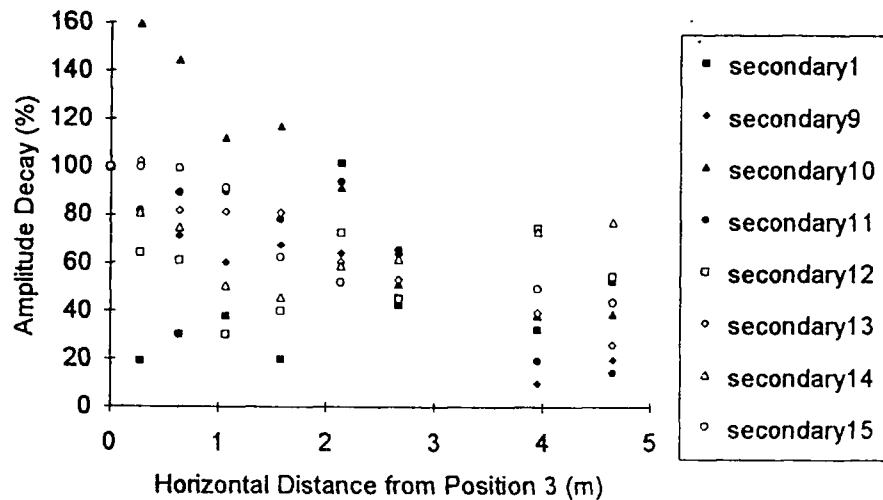
Figure 6.22. Amplitude Decay. Laboratory Results within Secondary Period Range 620s to 960s.
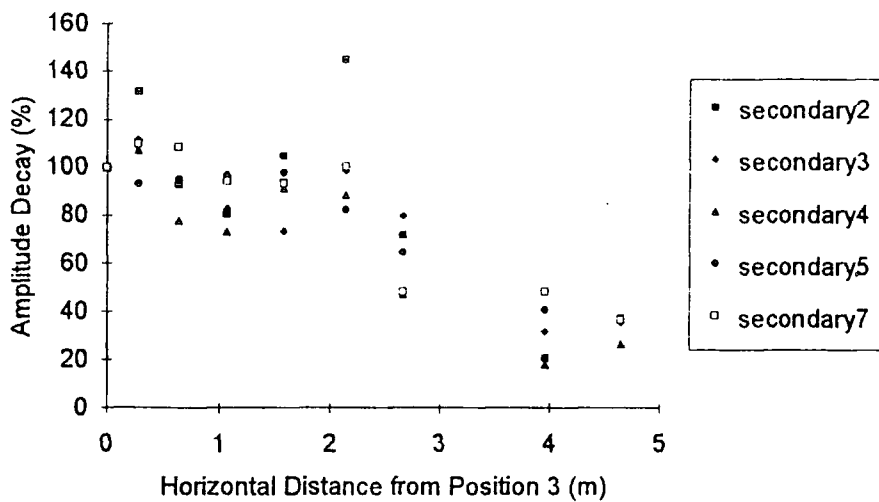
Figure 6. 23. Amplitude Decay. Laboratory Results within Secondary Period Range 1000s to 1200s.
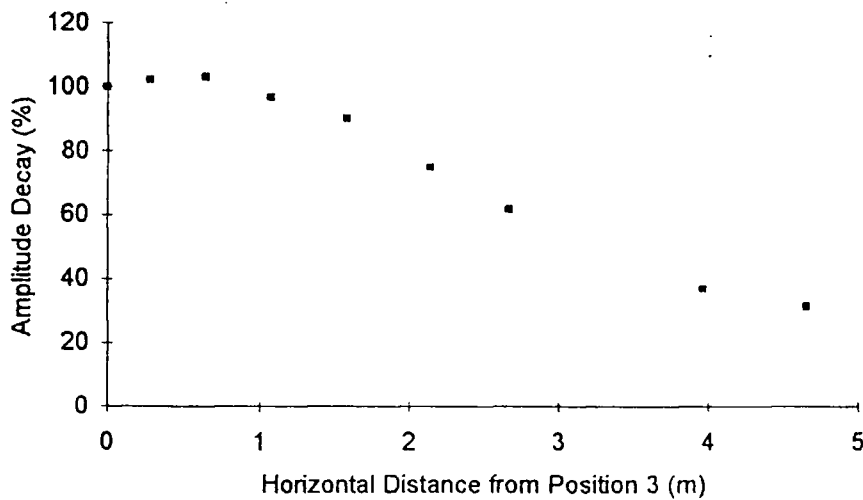
Figure 6. 24. Amplitude Decay. Laboratory Results within Secondary Period Range 1371s.
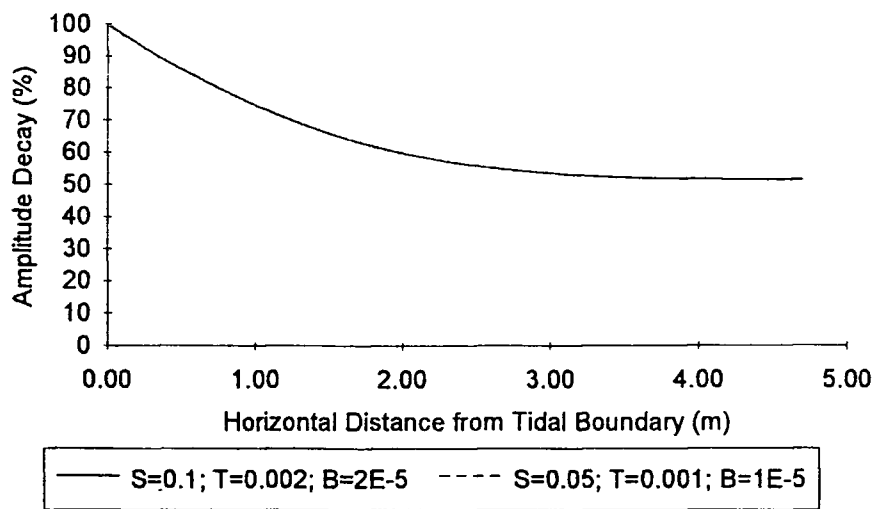
Figure 6.25. Amplitude Decay. Solutions from Application of Analytical Theory for Two Separate Case Studies. T/S and T/β constant.
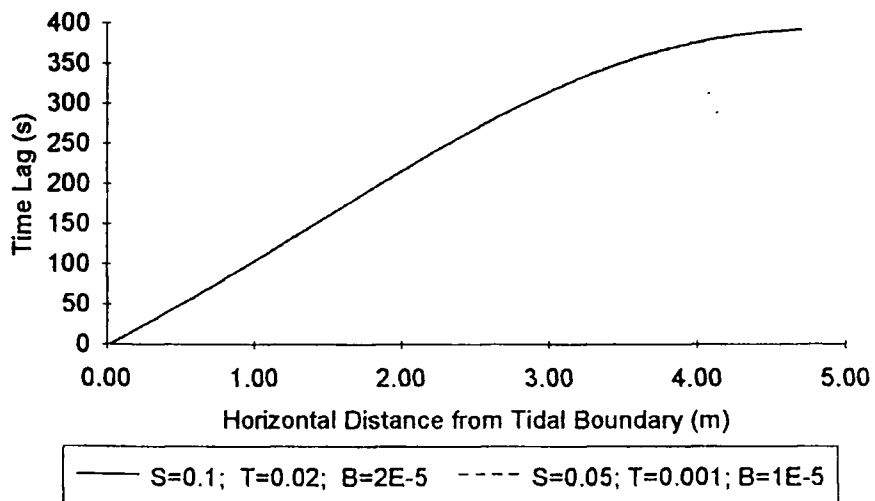
Figure 6.26. Time Lag. Solutions from Application of Analytical Theory for Two Separate Case Studies. T/S and T/β constant.
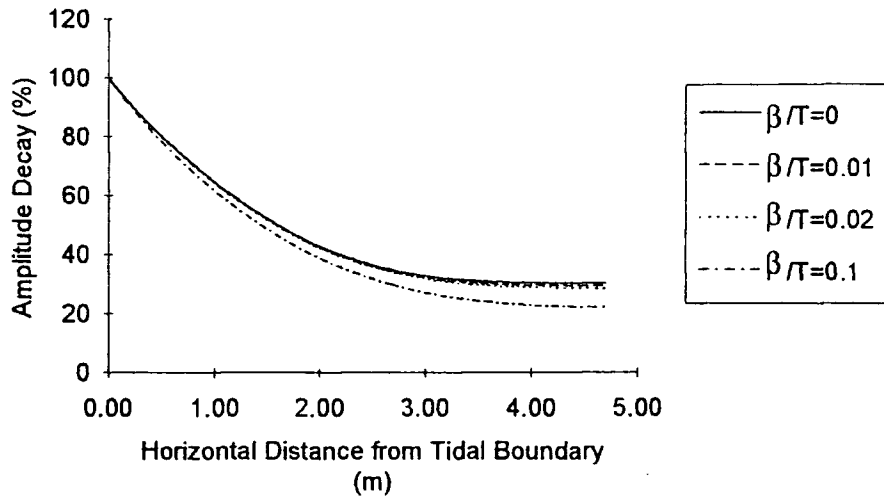
Figure 6.27. Amplitude Decay. Analytical Solution. T/S=0.01m²/s.
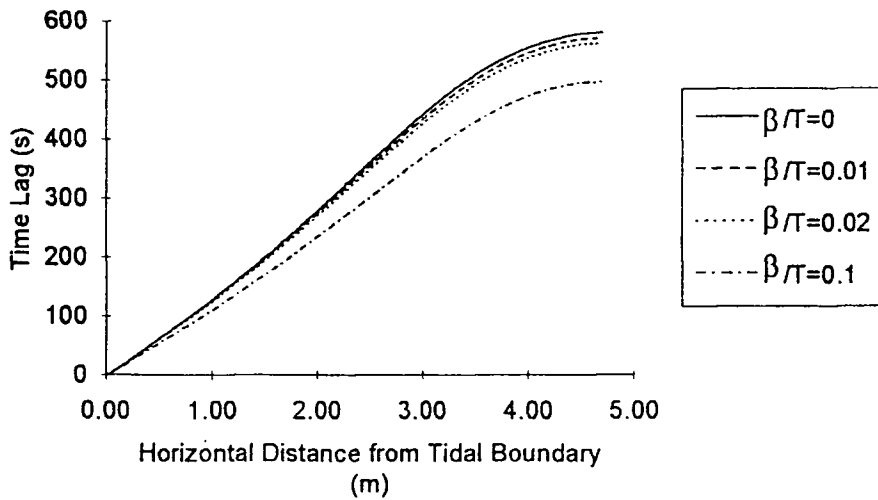
Figure 6.28. Time Lag. Analytical Solution. T/S=0.01m²/s.
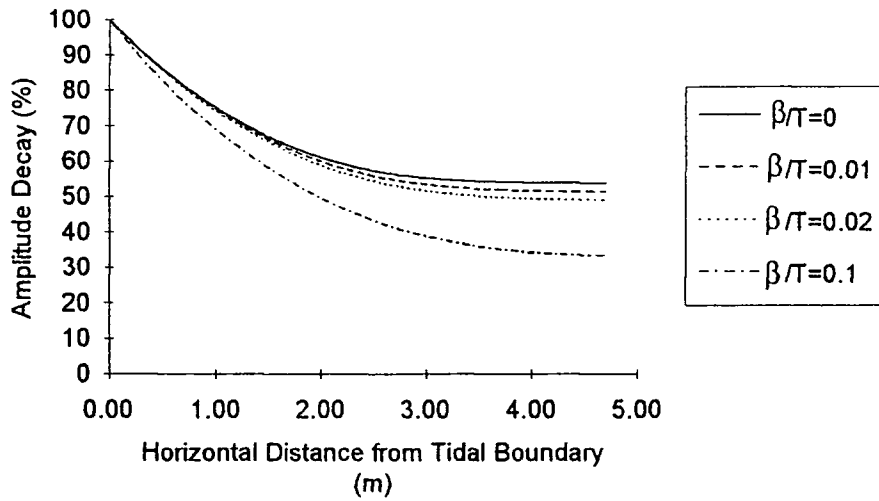
Figure 6.29. Amplitude Decay. Analytical Solution. T/S=0.02 m²/s.
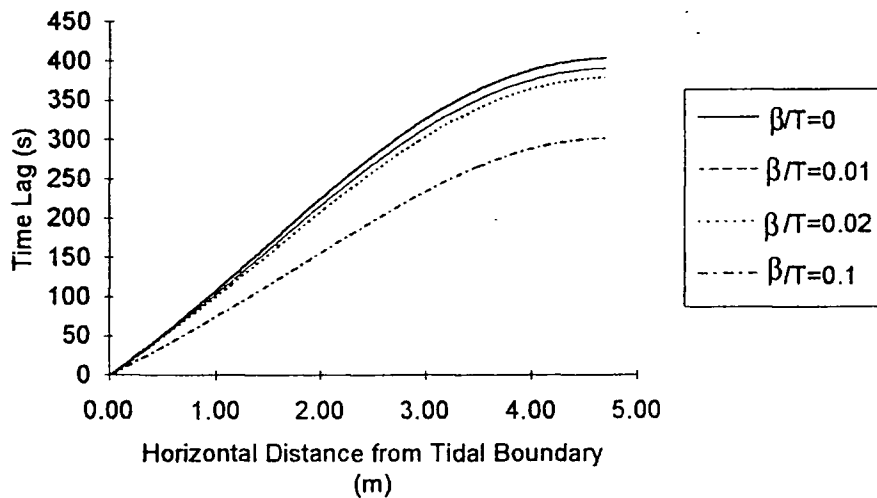
Figure 6.30. Time Lag. Analytical Solution. T/S=0.02m²/s.
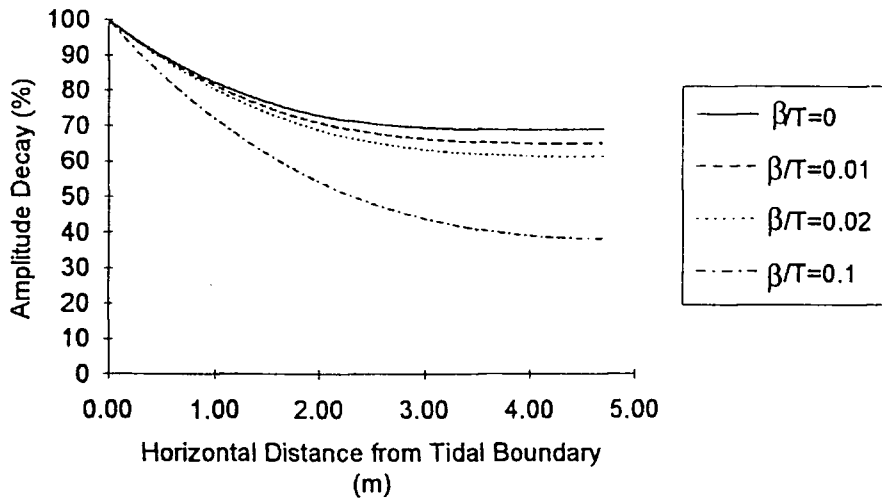
Figure 6.31. Amplitude Decay. Analytical Solution. T/S=0.03 m²/s.
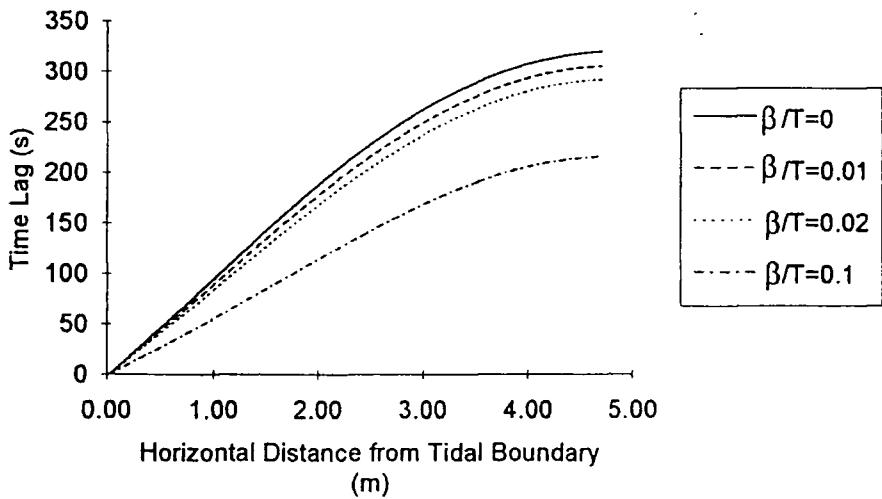
Figure 6.32. Time Lag. Analytical Solution. T/S=0.03m²/s.
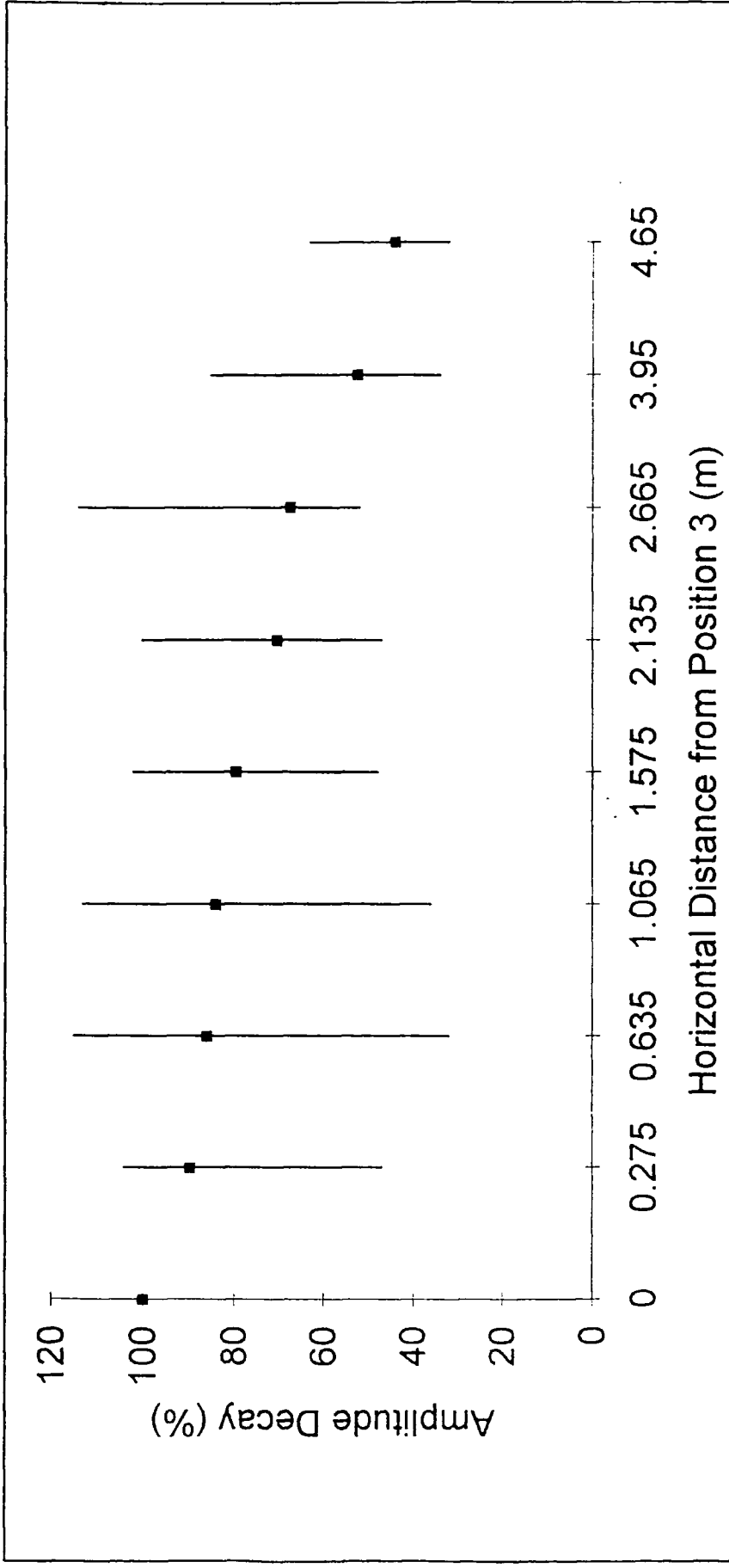
Figure 6.34. Amplitude Decay. Primary Period Range 1820s to 2020s. Mean Values and Spread of Data Indicated.
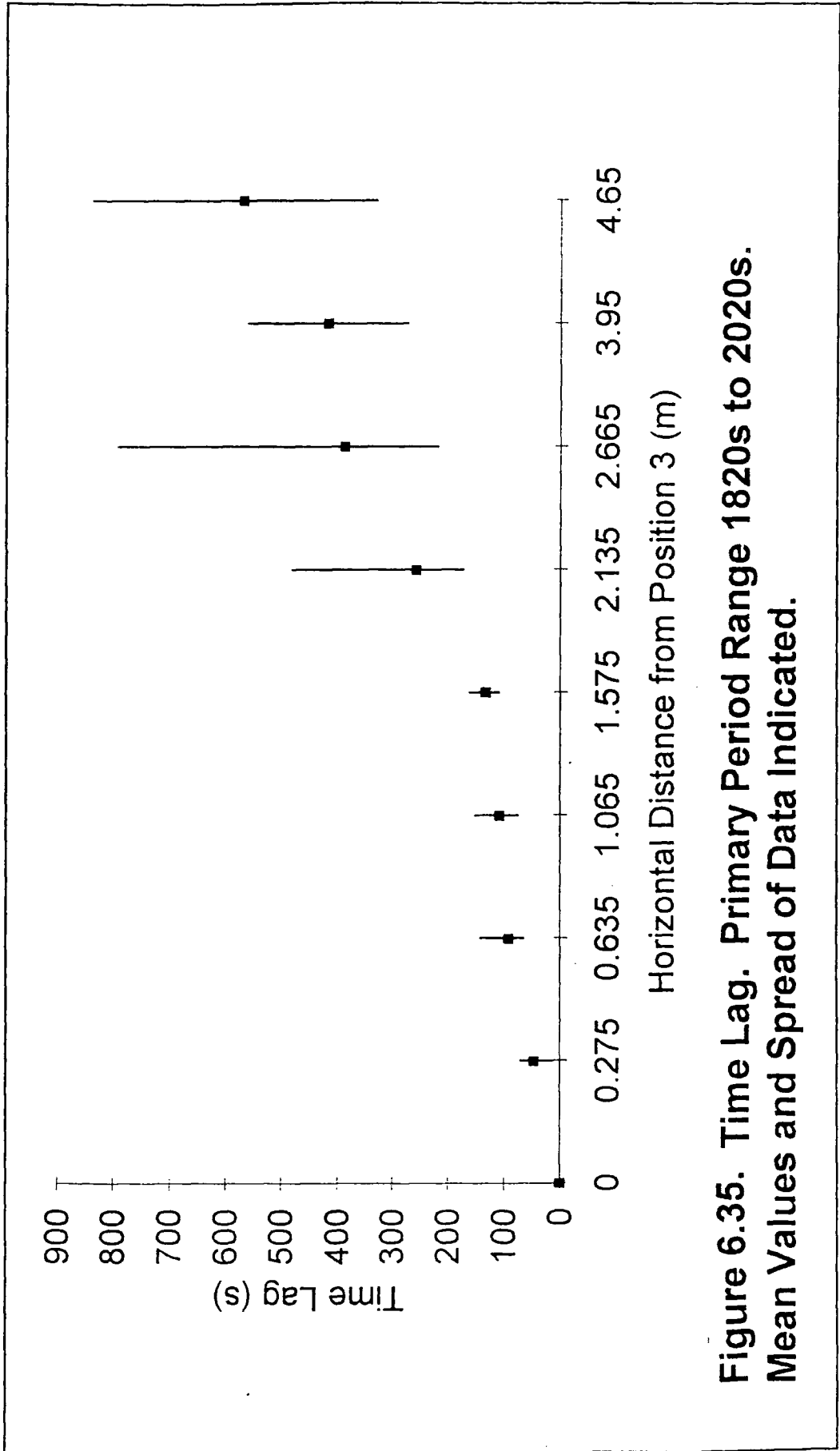
Figure 6.35. Time Lag. Primary Period Range 1820s to 2020s. Mean Values and Spread of Data Indicated.
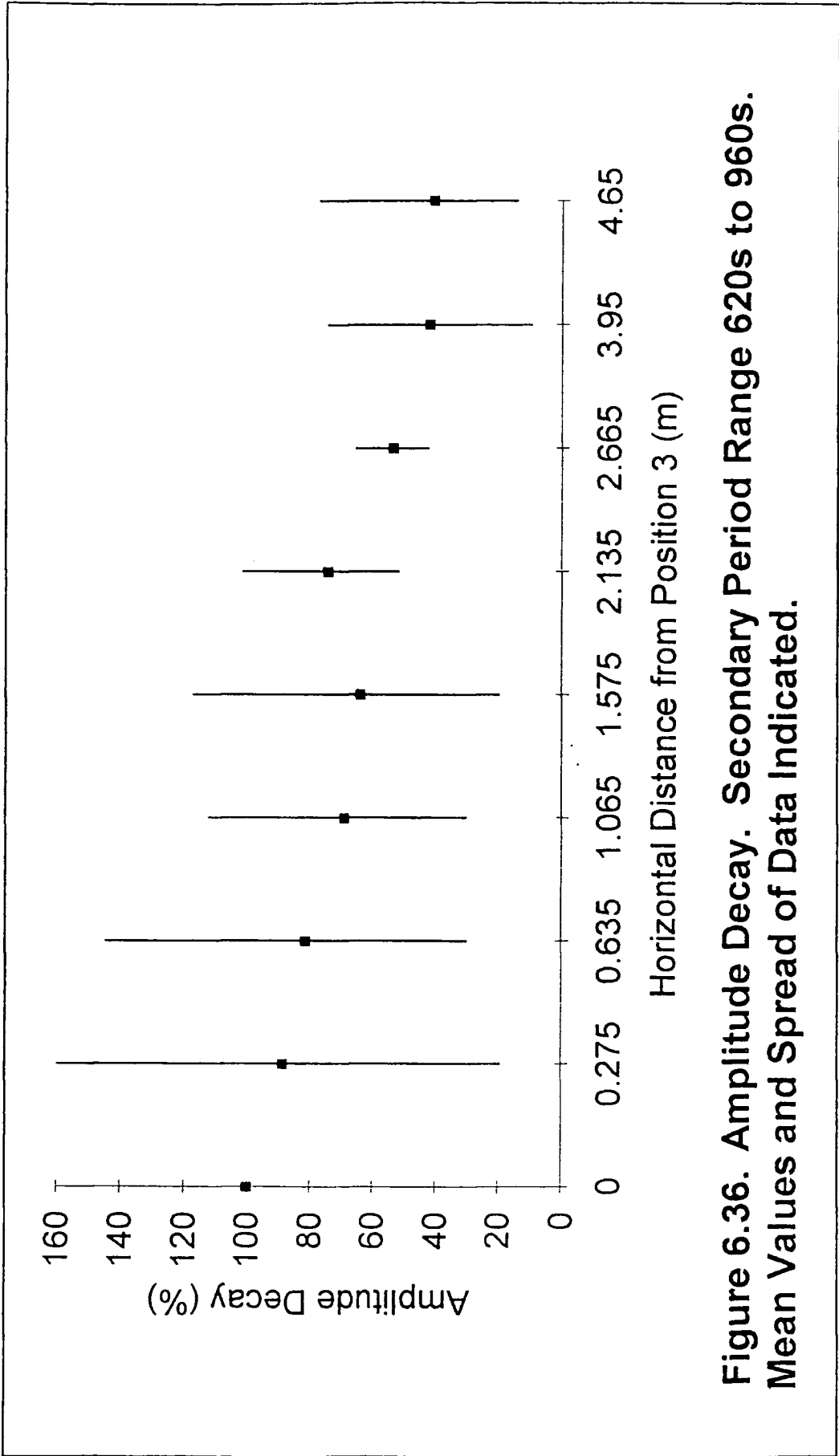
Figure 6.36. Amplitude Decay. Secondary Period Range 620s to 960s. Mean Values and Spread of Data Indicated.

Period Range 1820 to 2020 seconds. T/S = 0.01 m²/s.
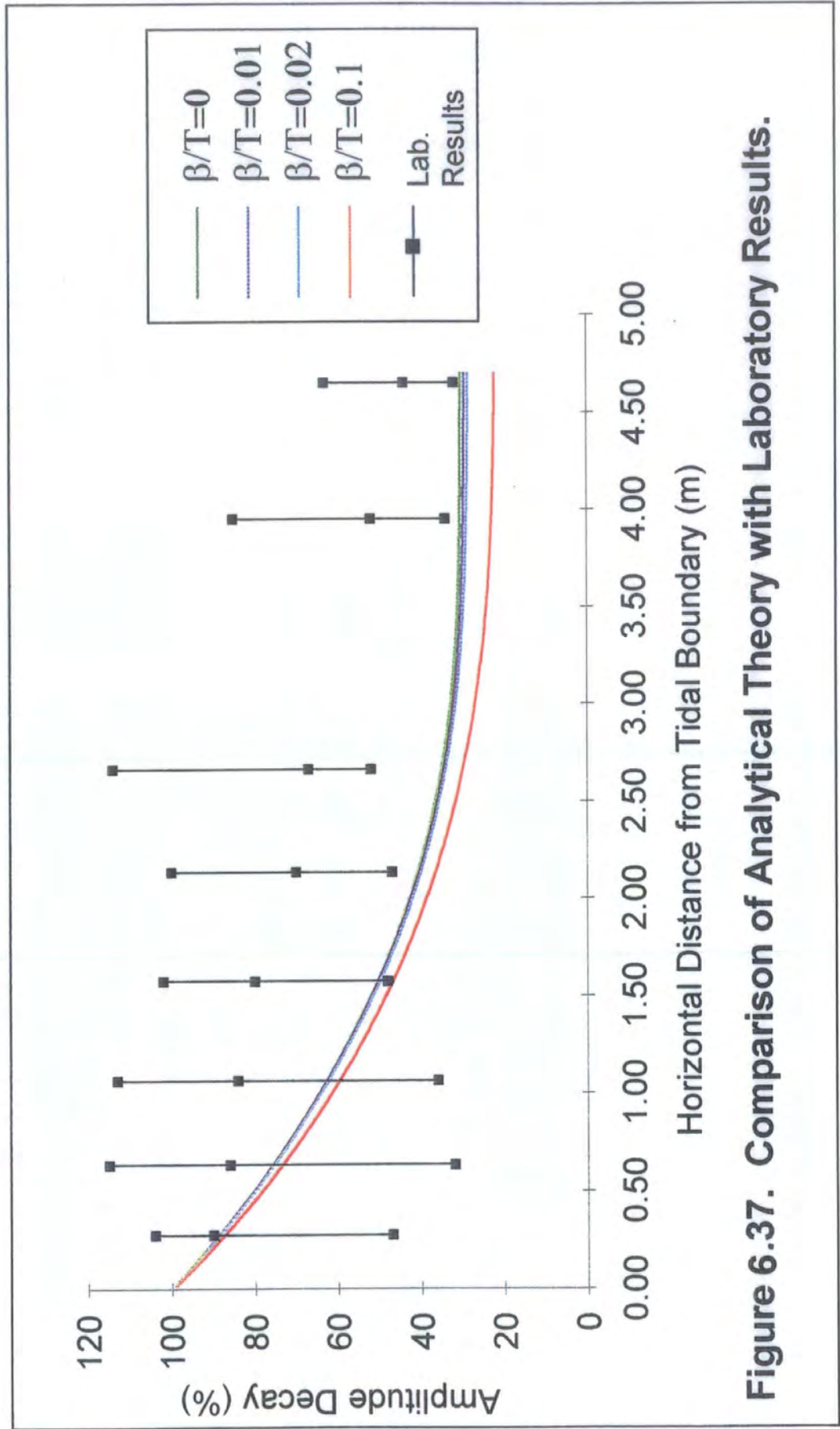
Figure 6.37. Comparison of Analytical Theory with Laboratory Results.

Period Range 1820 to 2020 seconds. T/S = 0.01 m²/s.

Legend:
- β/T=0
- β/T=0.01
- β/T=0.02
- β/T=0.1
- Lab. Results

X-axis: Horizontal Distance from Tidal Boundary (m)

Y-axis: Time Lag (s)
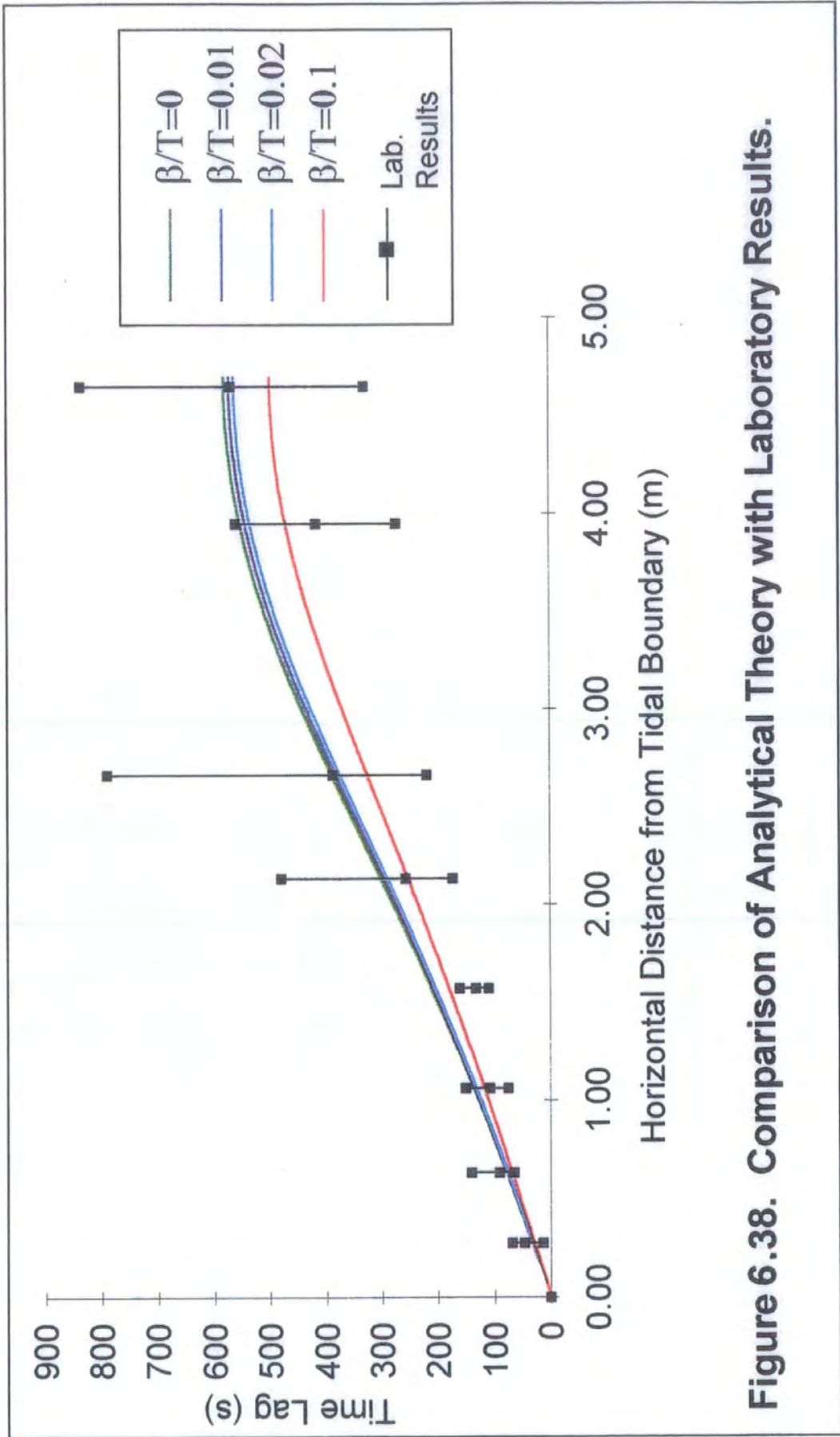
Figure 6.38. Comparison of Analytical Theory with Laboratory Results.

Period Range 1820 to 2020 seconds. T/S = 0.02 m²/s.
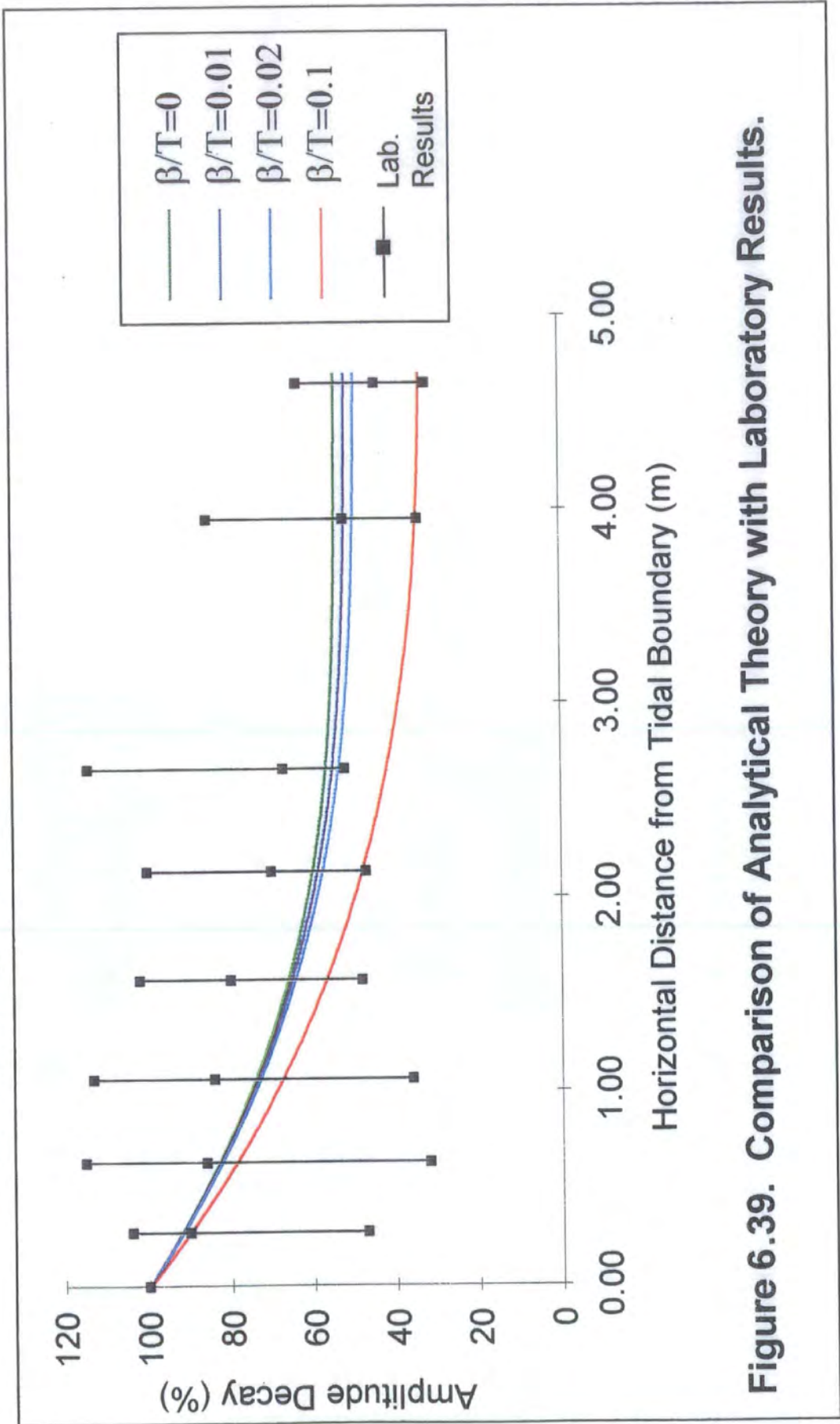
Figure 6.39. Comparison of Analytical Theory with Laboratory Results.
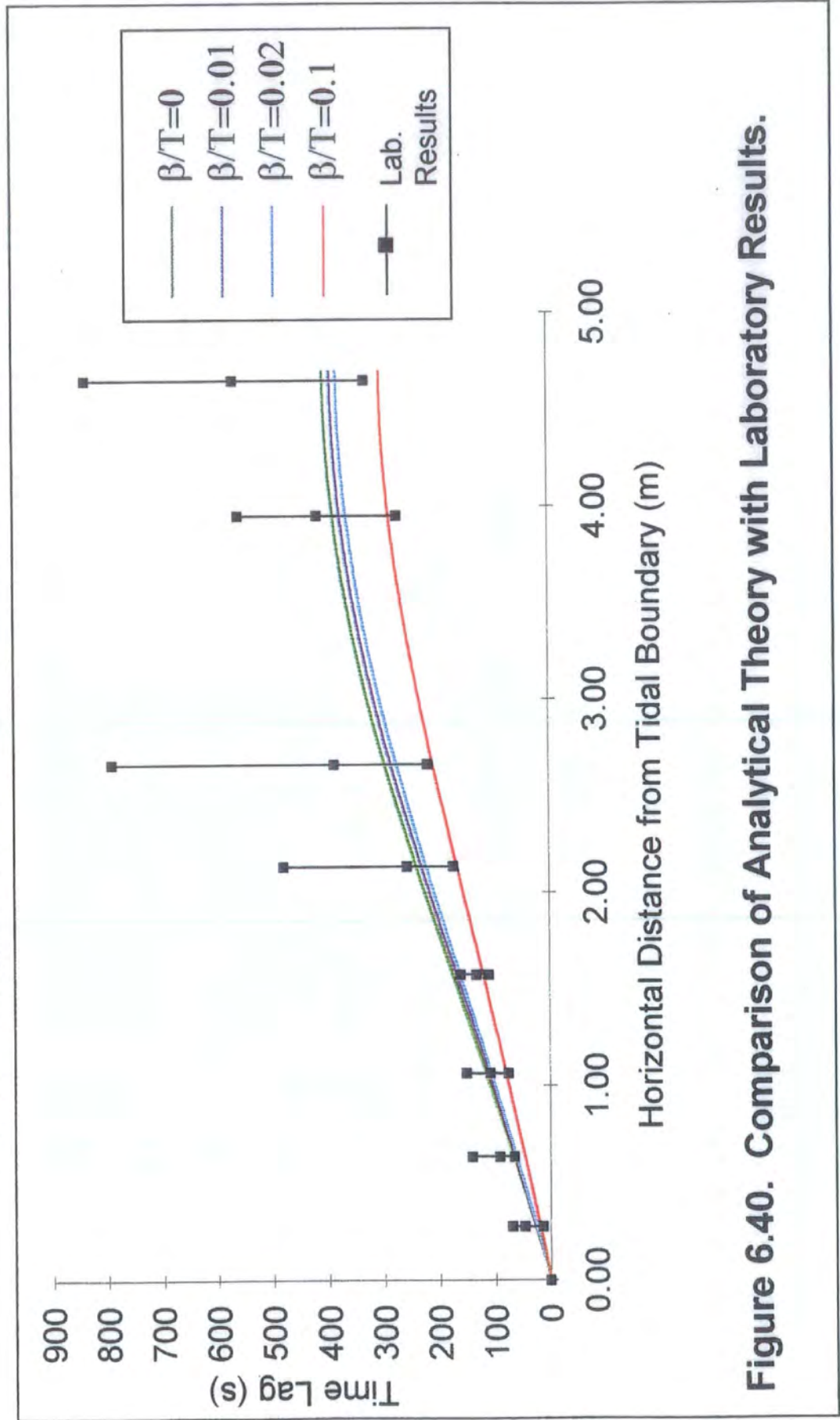
Figure 6.40. Comparison of Analytical Theory with Laboratory Results.
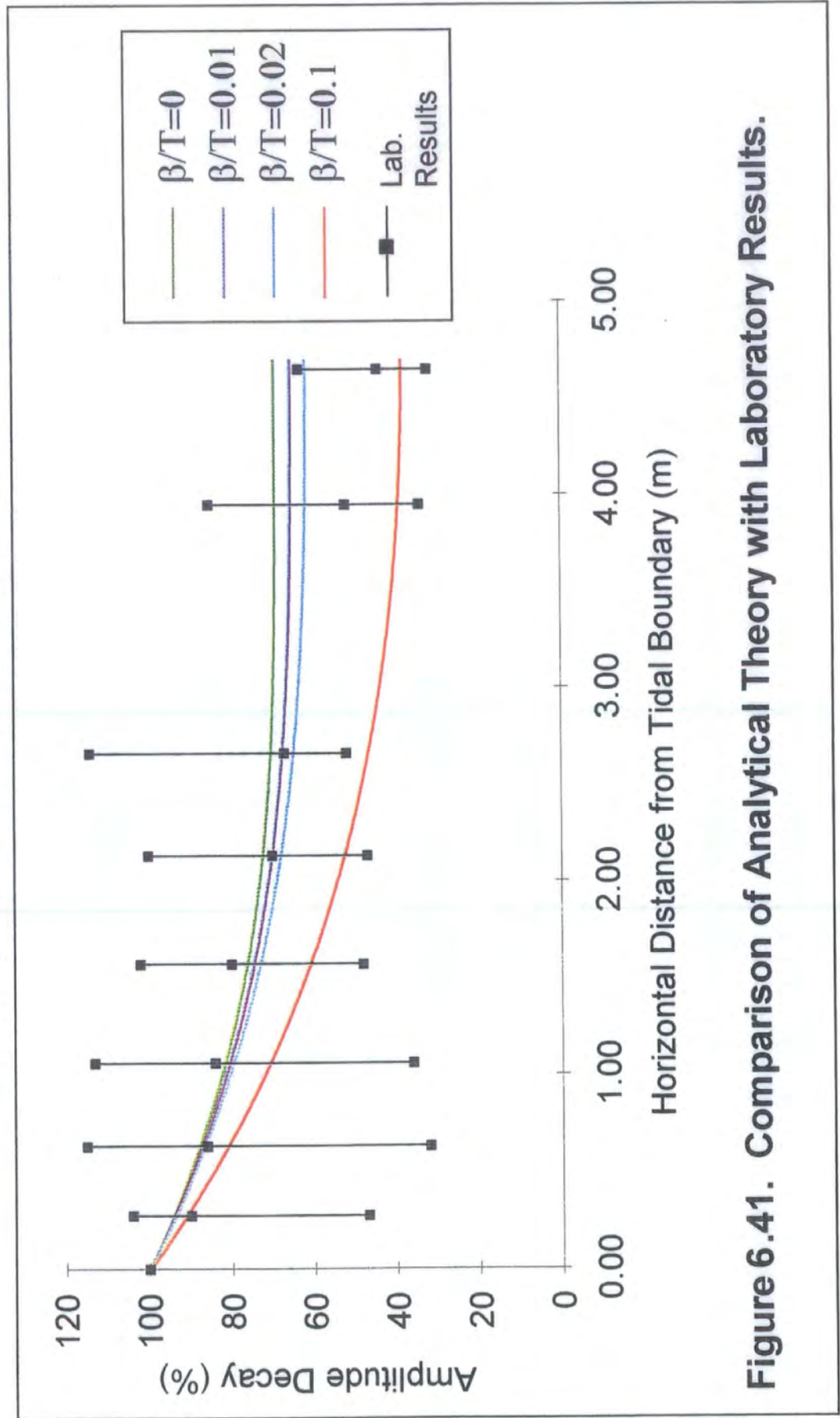
Figure 6.41. Comparison of Analytical Theory with Laboratory Results.

Period Range 1820 to 2020 seconds. T/S = 0.03 m²/s.
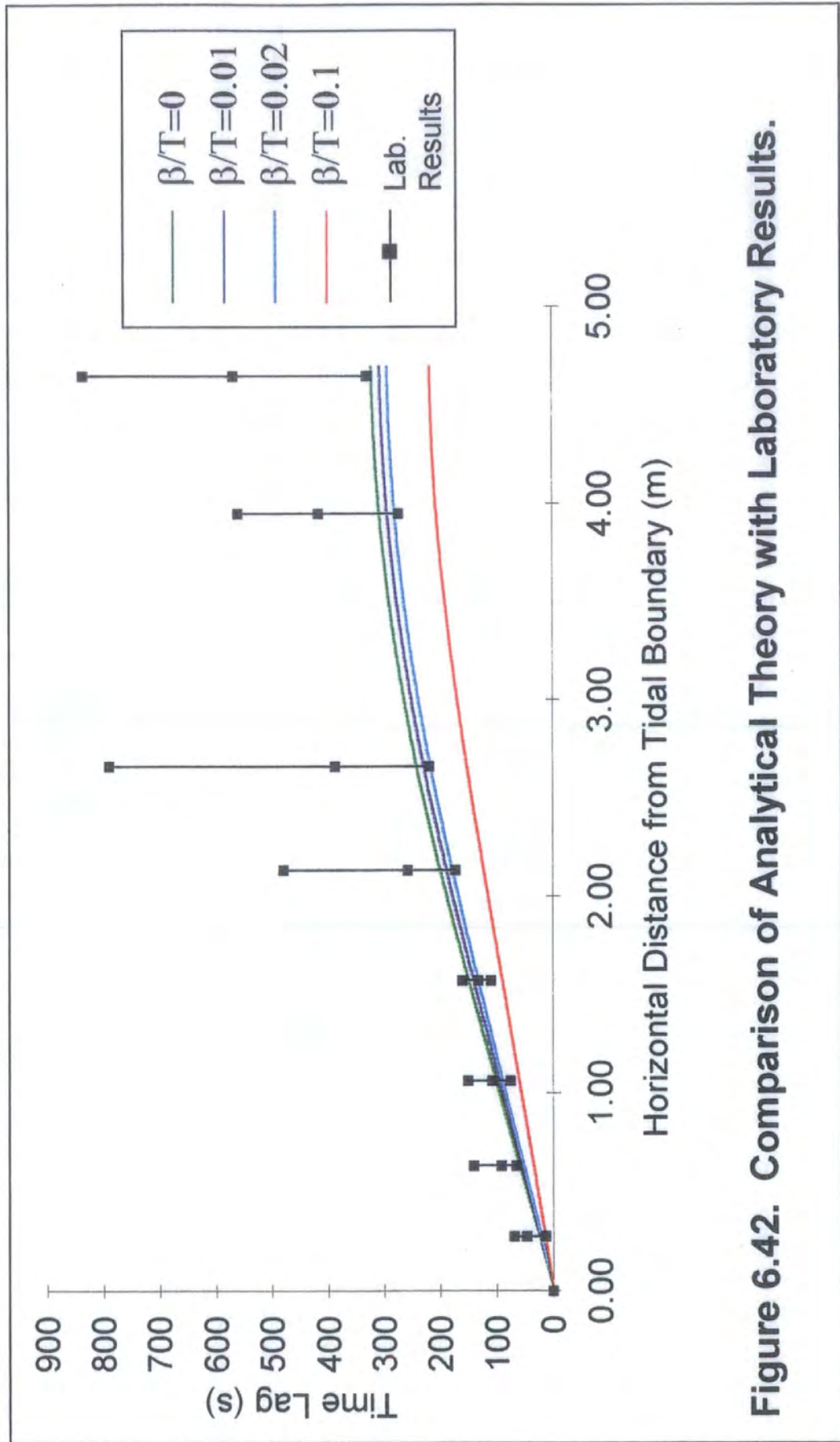
Figure 6.42. Comparison of Analytical Theory with Laboratory Results.

216

Figure 6.43. Comparison of Analytical Theory with Laboratory Results.

Period Range 620 to 960 seconds. T/S = 0.02 m²/s.
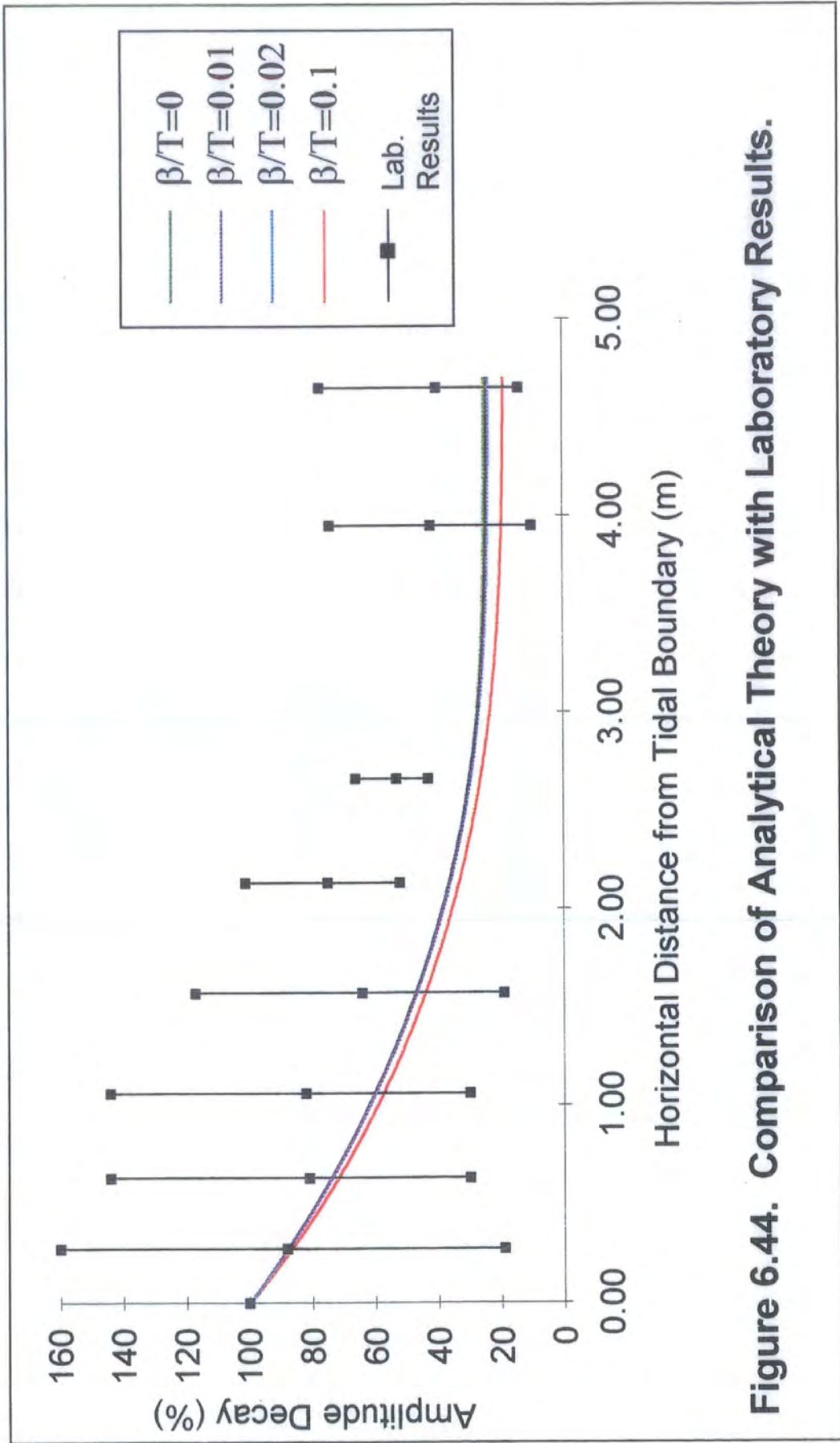
Figure 6.44. Comparison of Analytical Theory with Laboratory Results.
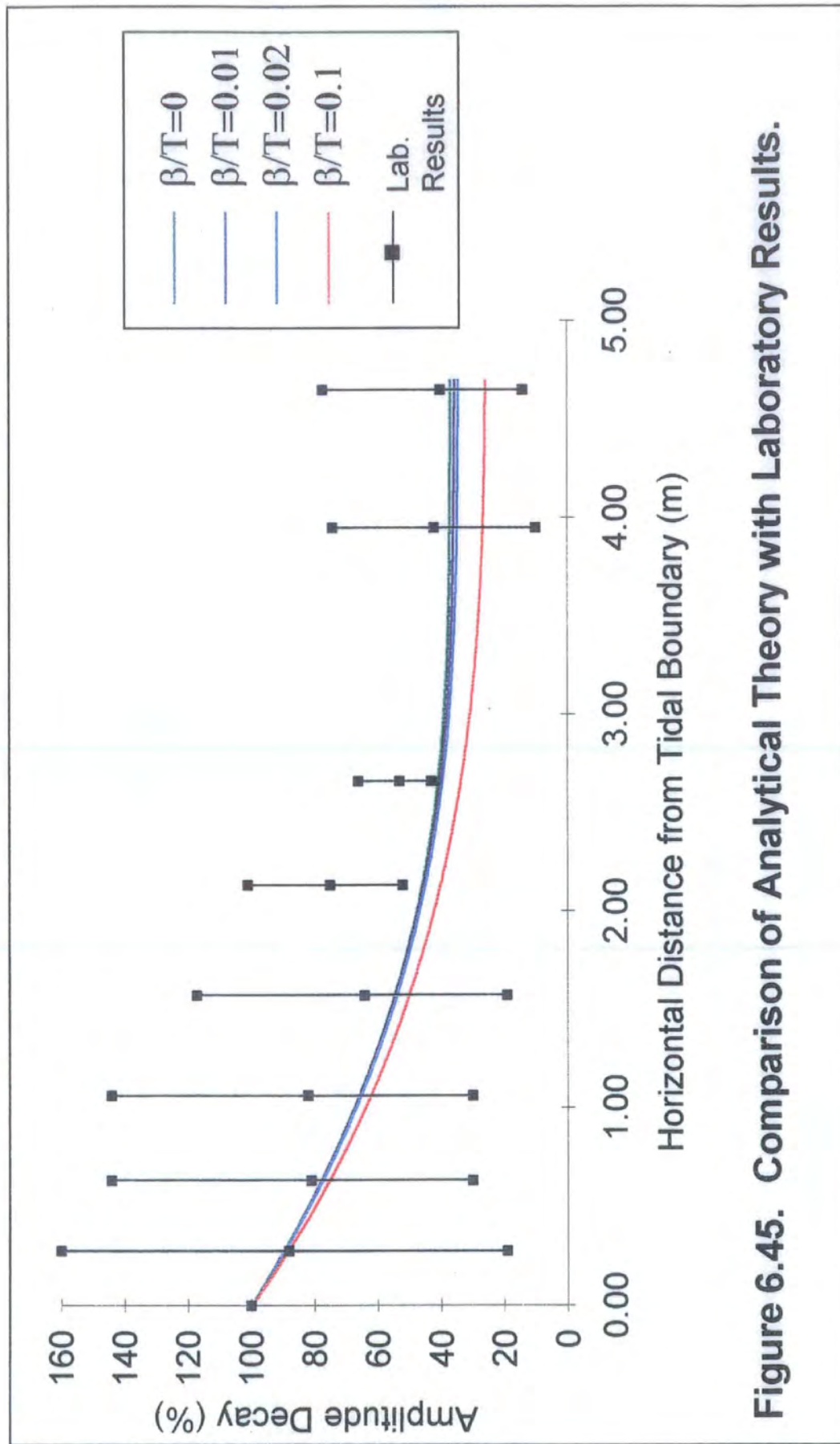
Figure 6.45. Comparison of Analytical Theory with Laboratory Results.
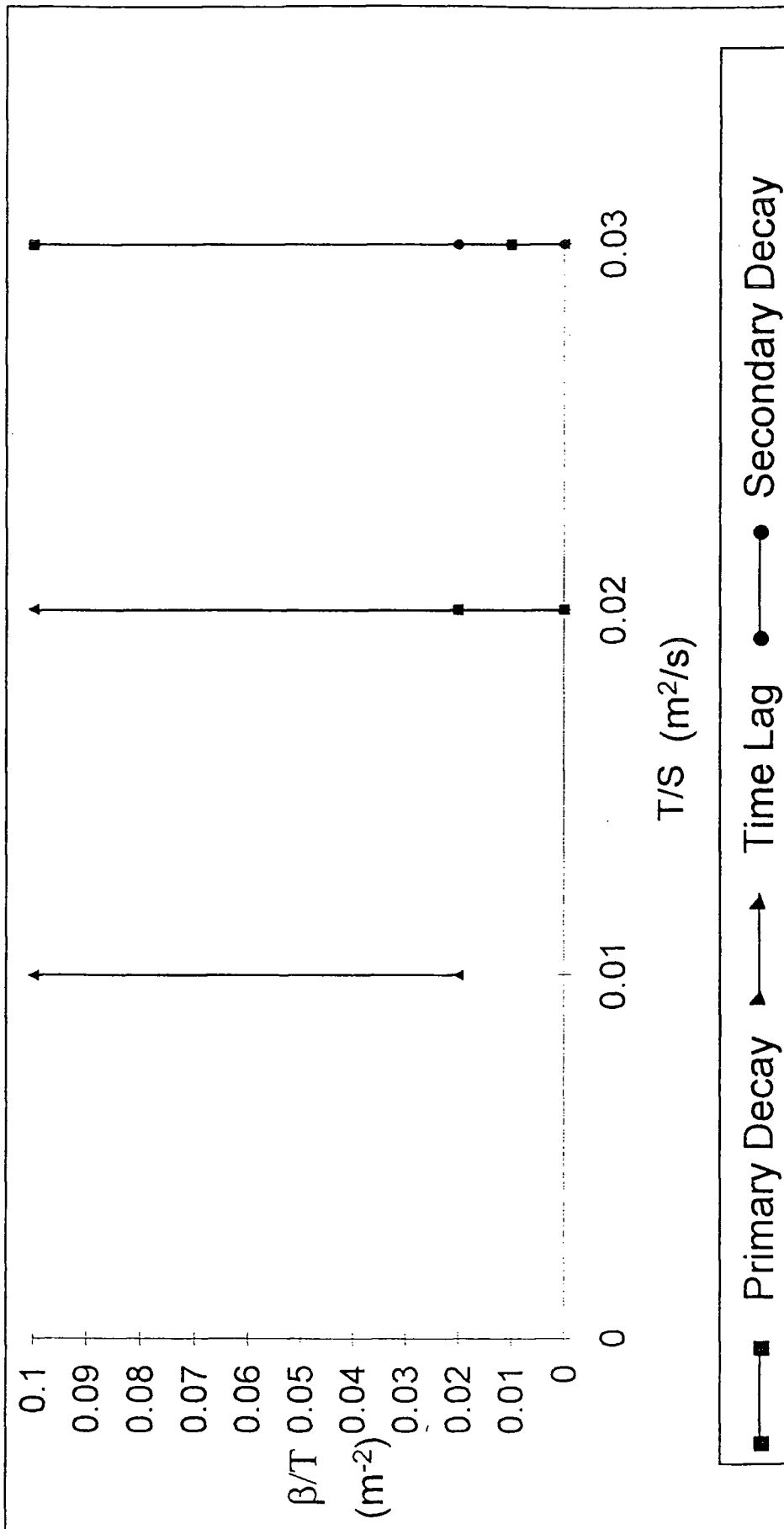
Figure 6.46. Ranges of Values of β/T for Corresponding Values of T/S.

Primary Decay ■—▲ Time Lag ●—● Secondary Decay

T/S (m^2/s)

β/T (m^{-2})

220

Chapter 7
Field Work

7.1. Introduction

The objectives of the field work were as follows:

- To measure and record changes in groundwater head / pore water pressure from a coastal aquifer at regular intervals for minimum periods of 24 hours.

- To investigate whether measurements illustrate tidal influences on groundwater behaviour.

- To determine aquifer properties (diffusivity, permeability, storage) from these results using the tidal analysis method where appropriate.

- To compare estimates of these properties based on alternative techniques with estimates formed as a result of tidal analysis.

- From this work, to discuss and conclude the viability of the tidal analysis technique for determining aquifer properties.

7.2. The Quayside, Newcastle-upon-Tyne

The site of the field work was on the Quayside of the tidally influenced River Tyne in Newcastle. Measurements of head changes with time were recorded from two boreholes (314 and 915) initially over a 24 hour period. Results from earlier monitoring of groundwater levels in Borehole 211 were also available for analysis. A schematic diagram illustrating the position of the boreholes with respect to each other and the River Tyne is given in Figure 7.1 below.
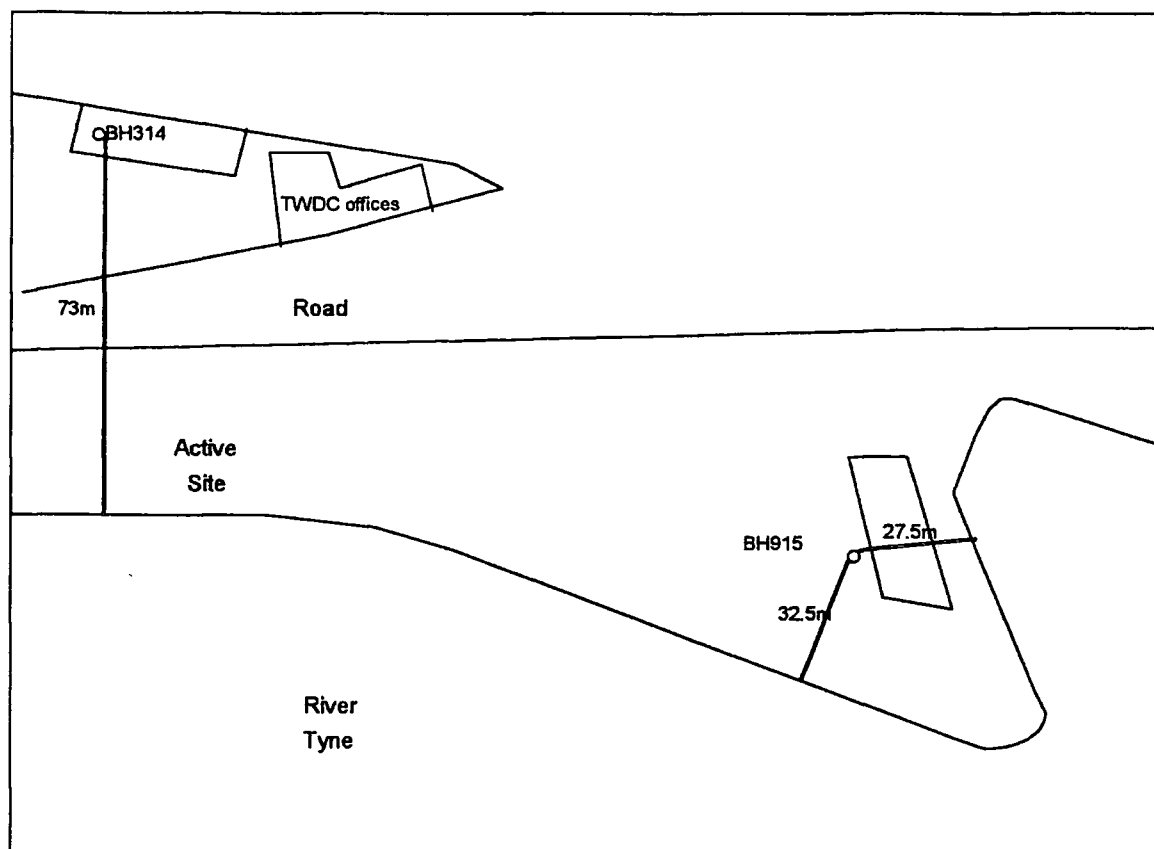
Figure 1. Schematic Diagram Illustrating Relevant Dimensions and Positions of Boreholes 314 and 915.

A more detailed scaled drawing showing positions of Boreholes 211, 911, and 915 is given in Figure 7.2.

7.2.1. Equipment and Instrumentation

The remote logging device used at the Quayside comprised a Druck pressure transducer (PDCR 800 series) linked to a Technolog digital logger. Two such systems were installed, one in each of boreholes 314 and 915. The Druck transducer/logging system provided a resolution of approximately 2mm. Information describing the logging equipment is presented in Appendix 7.1.

7.2.2. Borehole 314

7.2.2.1. Location of Piezometer

The piezometer tube was of diameter 19mm and was located in a clay soil at a distance of 73m from the River Tyne and at a depth of 19.50m.

7.2.2.2. Detailed Soil Description

Figure 7.3. below is a schematic diagram summarising the borehole records.
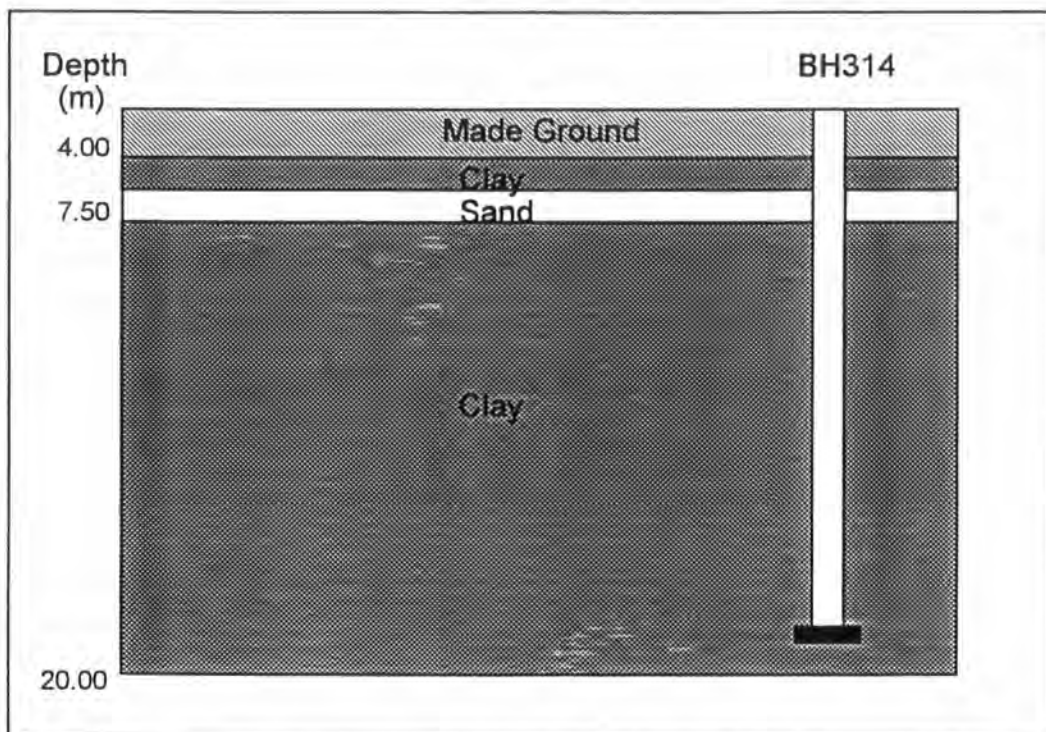
Figure 7.3. Schematic Diagram Illustrating Geological Strata Summarised from Borehole Records.

At a depth of 19.50m, the borehole record indicates a very stiff, dark grey brown, silty sandy CLAY, with gravels, occasional cobbles and rare boulders and with occasional sand lenses. The material is described as Pleistocene, glacial till.

7.2.2.3. Grading analysis

The particle size distribution of soil material found in borehole 314 at depth 20.50 metres is shown in Figure 7.4. below.

Grading Analysis of Borehole 314 at depth 20.50 metres
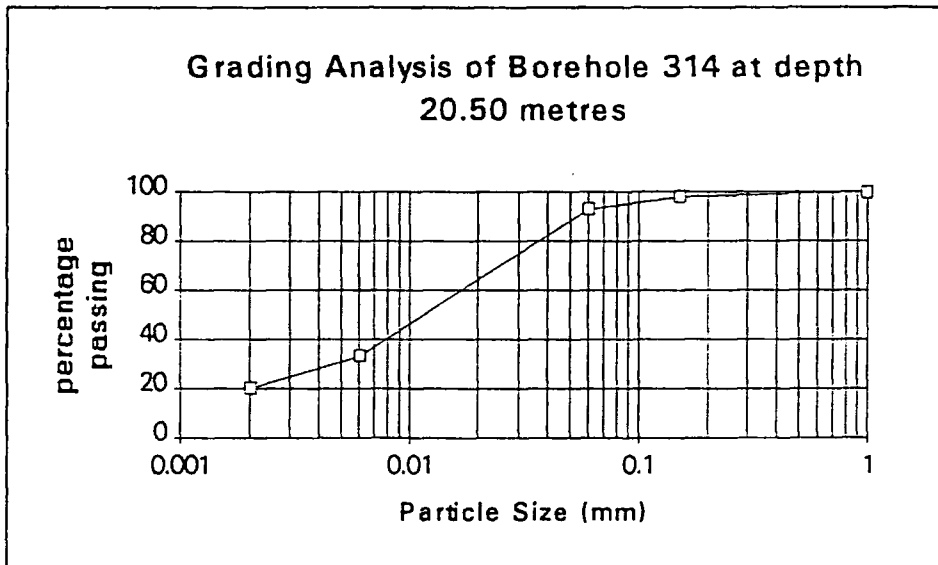
Figure 7.4. Particle Size Distribution of Soil Material in Borehole 314 at depth 20.50 metres.

7.2.2.4. Method

A suitable location for the logging box was found and a laptop computer was used to commence measurement and recording of data. Measurements of head were recorded every 15 minutes.

7.2.2.5. Results

A graphical illustration of the results is given in Figure 7.5. below.

Borehole 314. Head vs Time.
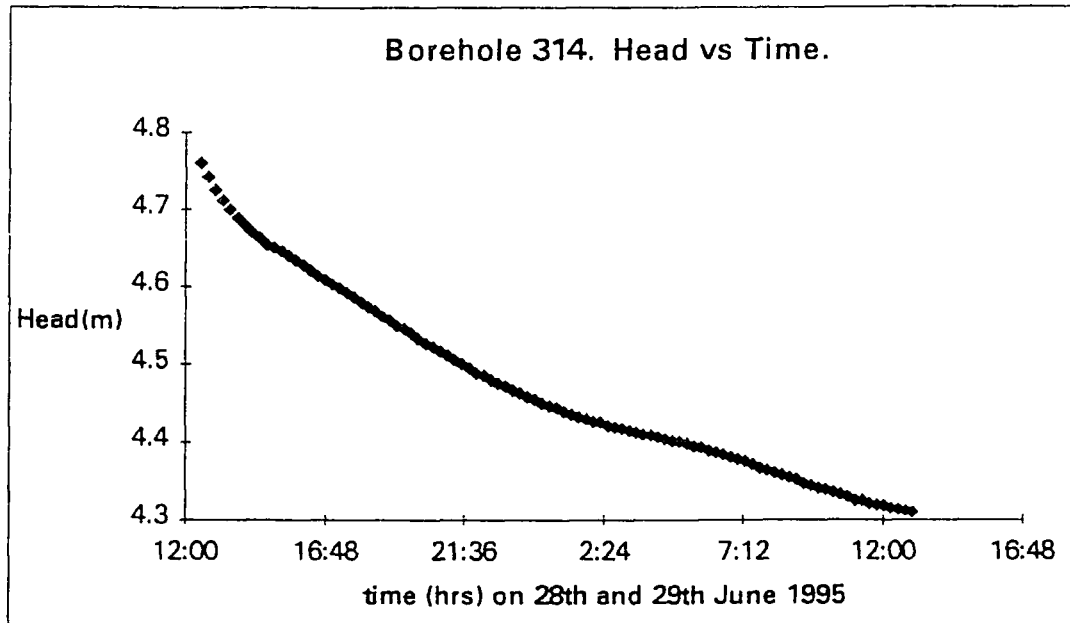
Figure 7.5. Graph of Groundwater Head vs.Time for Borehole 314.

7.2.2.6.   Discussion of Results

The presence of the pressure transducer and cable in borehole 314 appears to have caused a significant volume change and hence an increase in water level which then gradually dropped during the short time the logger was in place. The soil material (a high permeability clay) will ensure that a rise in head will take time to dissipate.

Fast Fourier Transform Analysis was performed using the data, however no major sinusoidal waveforms were observed. The groundwater behaviour appears to be governed by the falling head.

7.2.2.7.   Analysis of Results

The results were therefore analysed as a slug test. A slug test is used to determine *in situ* hydraulic conductivity using data from a single piezometer. The test is initiated by causing an instantaneous change in the water level in a piezometer tube by the sudden introduction of a known volume of water. It is also possible to create the same effect by introducing a cylinder of known volume (which in this case was the transducer and cable). The recovery of water level with time is then observed.

225

Hvorslev's method of analysis was used to interpret the results (Freeze and Cherry, 1979).

Figure 7.6 below is the graph of log(H-h/H-H$_0$) versus time which was plotted to determined T$_0$. The data was extrapolated to determine the value of T$_0$ when log(H-h/H-H$_0$)=0.37.
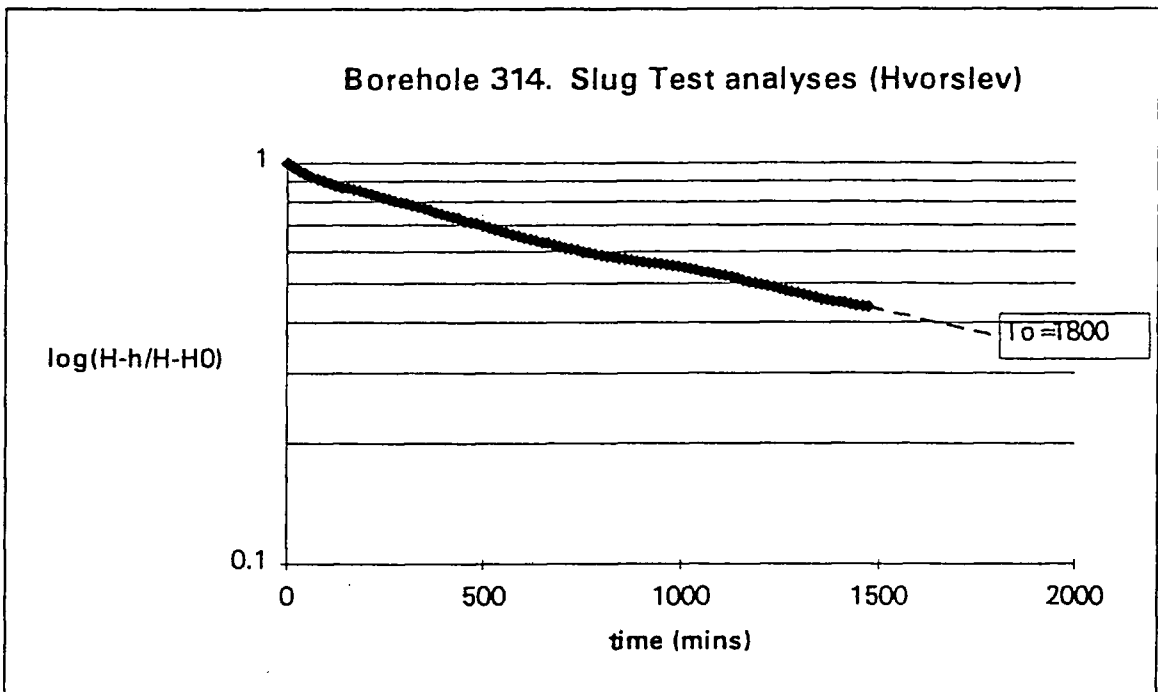
Figure 7.6. Graph of log(H-h/H-H$_0$) versus time to determine permeability using Hvorslev's technique.

From Figure 7.6. and the extrapolated data:

log(H-h/H-H$_0$)=0.37 corresponds to a value of T$_0$ = 1800 minutes

Applying Hvorslev's equation:

$$K = \frac{r^2 \ln(L / R)}{2LT_0} \longrightarrow eqtn(7 \cdot 1)$$

where K = coefficient of permeability [L/T]

     r = radius of piezometer tube [L]

     R = radius of piezometer intake [L]

     L = length of piezometer intake [L]

     T$_0$ = basic time lag [T]

Therefore:

$$K = \frac{(0.008)^2 \ln(0.2 / 0.008)}{(2 \times 0.2 \times 1800)} = 2.86 \times 10^{-7} \text{ m/ min} = 4.8 \times 10^{-9} \text{ m/}s$$

7.2.2.8. Conclusion and Discussion

The groundwater in borehole 314 was observed not to be influenced by tidal behaviour. The slug test method was used to analyse results. From this method, the coefficient of permeability of the material surrounding the piezometer in borehole 314 was estimated to be 4.8 x 10^{-9} m/s. This value of permeability suggests a glacial till or silt material (Freeze and Cherry, 1979), which agrees with borehole records and grading analysis results shown in Figure 7.4.

7.2.3. Borehole 915

7.2.3.1. Location of Piezometer

The piezometer tube was of diameter 19mm and was located in a gravel soil at a distance of approximately 30m from the River Tyne and at a depth of 17.90m.

7.2.3.2. Detailed Soil Description

Figure 7.7. below is a schematic diagram summarising the borehole records.
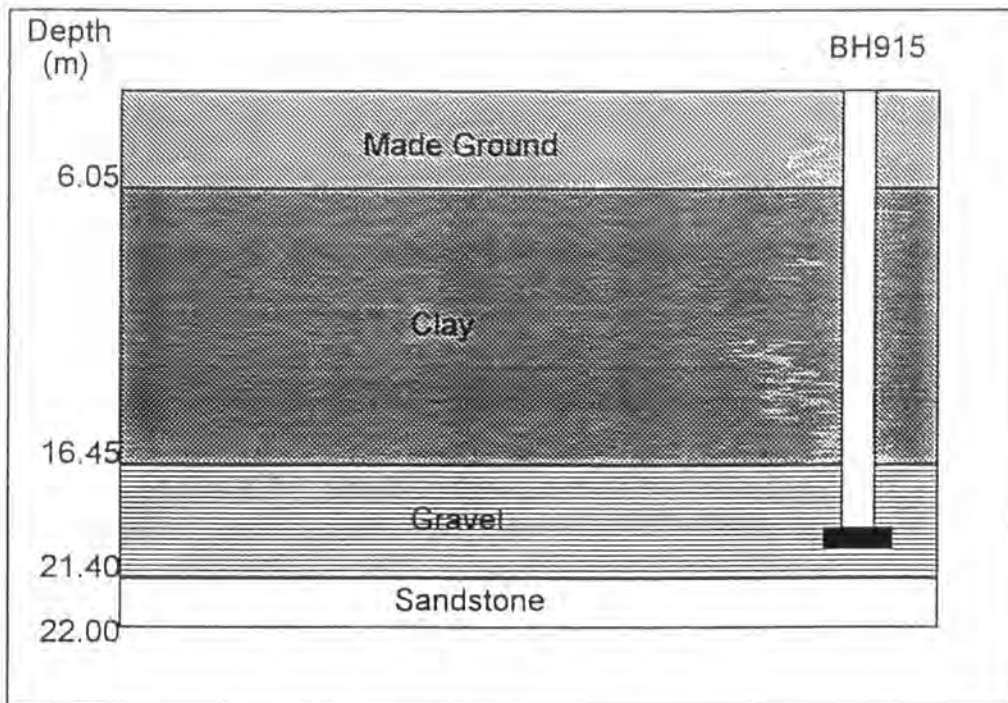
Figure 7.   Schematic Diagram illustrating Geological Strata Summarised from Borehole Records.

At a depth of 17.00m, the borehole record indicates a very dense brownish grey clayey fine to coarse sandy fine to coarse GRAVEL with some cobbles. The gravel and cobbles are described as rounded to angular comprising sandstone, siltstone, quartzite, quartz and some limestone. The soil becomes less clayey with depth.
A dark soft clay of high plasticity overlies the gravel layer.

7.2.3.3.   Grading Analyses

The particle size distribution of soil material found in borehole 915 at depth 16.60 metres is shown in Figure 7.8 below.
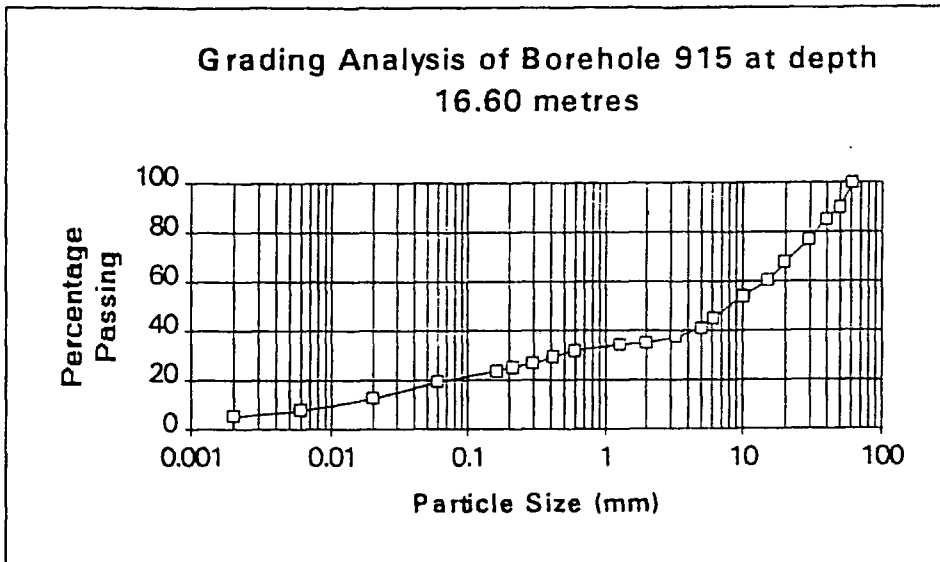
Figure 7.8. Particle Size Distribution of Soil Material in Borehole 915 at depth 16.60 metres.

The particle size distribution of soil material found in borehole 915 at depth 19.00 metres is shown in Figure 7.9. below.
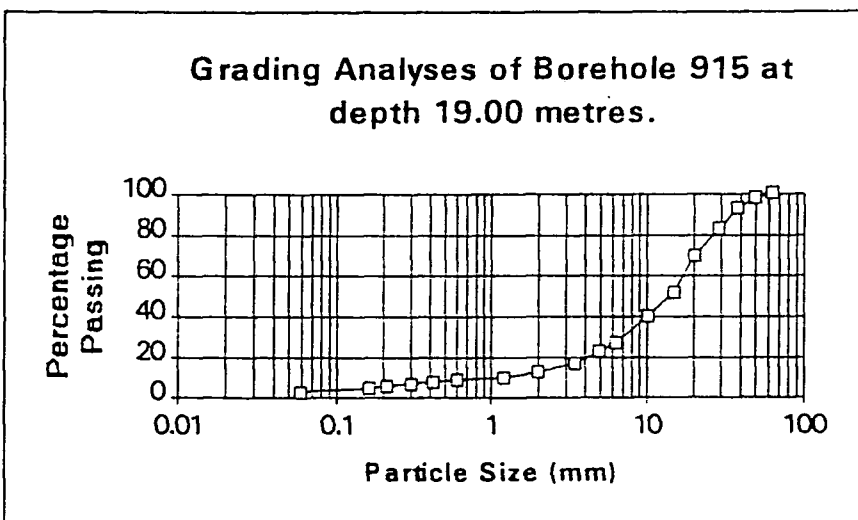
Figure 7.9. Particle Size Distribution of Soil Material in Borehole 915 at depth 19.00 metres.

The grading analyses show that the soil becomes less clayey with depth.

7.2.3.4.   Method

Once again, a suitable location for the logging box was found and a laptop computer was used to commence measurement and recording of data. An initial test, which lasted a period of 24 hours, illustrated tidal influence on groundwater in this area, however insufficient data was available for conclusive analysis. Therefore the test was repeated and data collected at 15 minute intervals for the period of a week.

7.2.3.5.   Water Level Variation During Test

The water level was measured before and after the test. The results are shown in Table 7.1. below.

Date	Water Level Beneath Ground Surface
25/7/95	3.55m
1/8/95	4.36m

Table 7.1. Water Level Variation in Borehole 915.

The results show that the piezometric level in BH915 fell by 0.81m during the test. This could be explained by the hot, dry weather during the test period. The catchment area of the aquifer may be significantly large, since it is near the coast (at the end of the groundwater journey) and therefore a large variance in groundwater level would be anticipated.

7.2.3.6.   Results

A graphic representation of the results from the borehole is illustrated in Figure 7.10. below. Times of high and low water for the area were available and are also plotted below. It was recognised that tidal tables discount effects of wind and atmospheric pressure on sea-water levels.
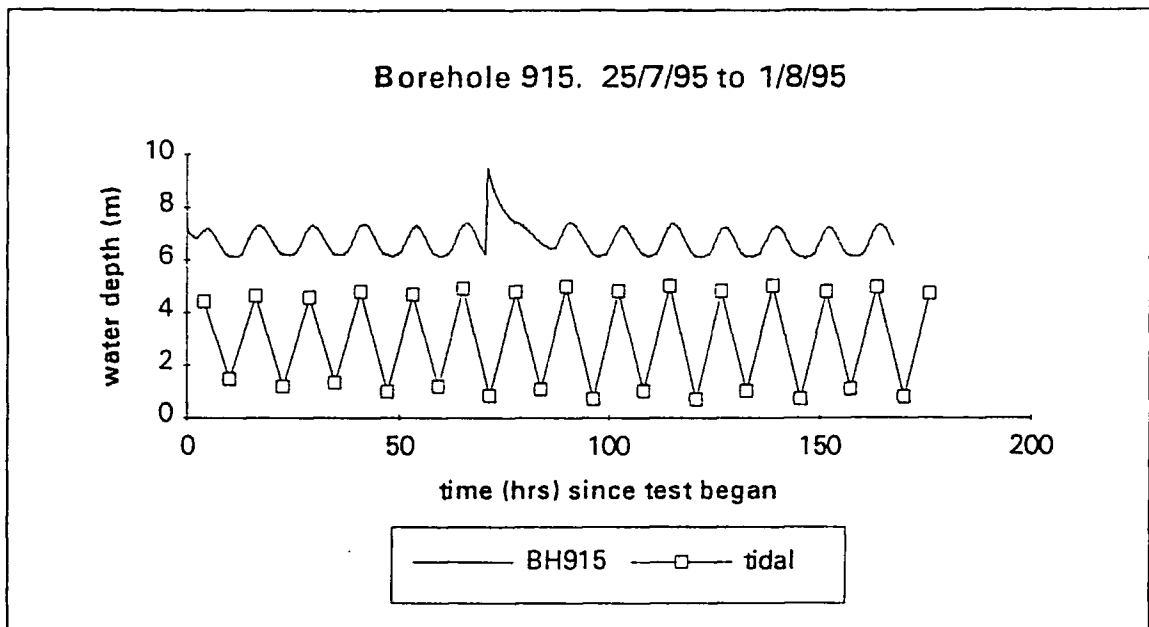
Figure 7.10. Borehole 915. Graph of Groundwater Head vs. Time Illustrating Tidal Data and Groundwater Fluctuations.

The graph illustrates the water changes in borehole 915 which are seen to vary harmonically with time, with a period of approximately 12 hours (suggesting tidal influence).

The data rises sharply approximately 70 hours after the test commenced. The reason for this sudden rise is unknown, however several possibilities are discussed below:

1. Sudden addition of water to the borehole. This could have been as a result of clearing the site (human interference) or a heavy rain storm. Close analysis of the data showed that this sudden rise took place over a 15 minute period between 10:30am and 10:45am on Friday 28/7/95. A heavy rainfall was not recorded in Newcastle during this period.

2. Sudden addition of water to another borehole in the vicinity. This could have occurred as work culminated on the active site.

3. Alteration of the depth of the instrumentation within borehole 915.

Whatever the reason for this sharp rise in water level, it was a unique event during the testing period and data prior to and after this time follows a distinct harmonic

231

pattern. The data was therefore split into 'early data' (prior to the sudden water level rise) and 'late data' (that recorded after the event).

Fast Fourier Transform (FFT) Analyses were performed on early and late data to investigate the major influencing sinusoidal waveforms. Figure 7.11 below provides a graphical illustration of the results of these analyses.

Wave Spectra. Borehole 915. Test 25/7/95 to 1/8/95
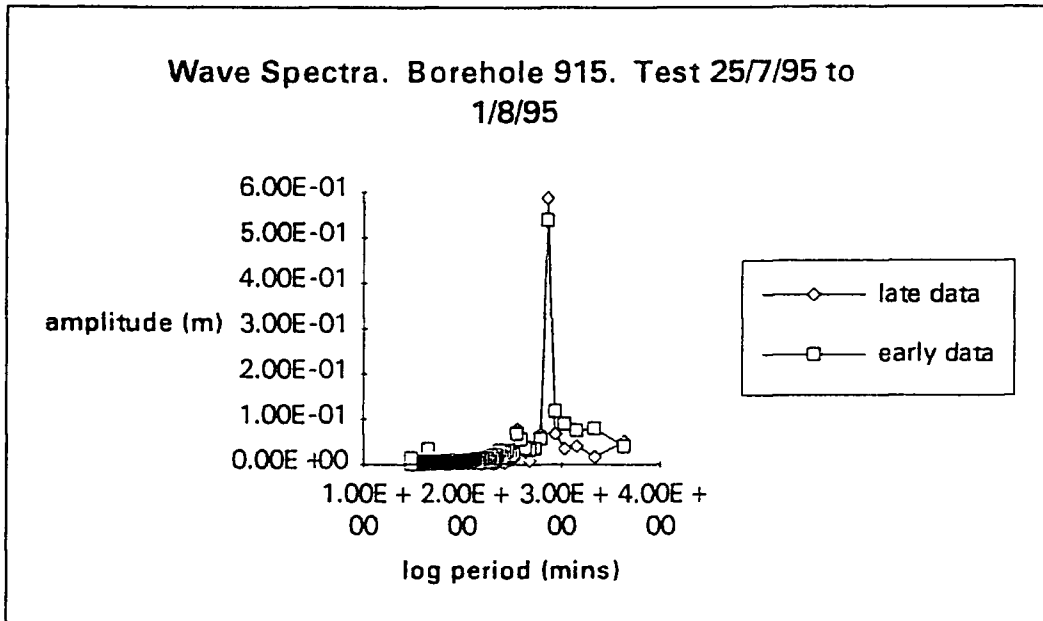
Figure 7.11. Wave Spectra following FFT analysis of early and late data.

The graph illustrates the three dominant waves which constitute the harmonic behaviour. Table 7.2. below summarises these three major constituents.

	Early Data		Late Data	
	Period	Amplitude (m)	Period	Amplitude (m)
Primary	12 hrs	0.539	12 hrs	0.587
Secondary	6 hrs	0.069	6 hrs	0.080
Tertiary	45mins	0.034	45 mins	0.032

Table 7.2. Major constituents of harmonic waveform recorded in Borehole 915.

The primary wave, and certainly the main constituent of the harmonic waveform, is characterised by a twelve hour period, the tidal period. It is interesting to note that

232

the primary, secondary and tertiary waves for both early and late data have approximately the same amplitude. This confirms that they are not caused by a random event, such as a thunderstorm.

7.2.3.7.   Analysis of the Tidal Cycle

Fast Fourier Transform analyses have been performed on tidal waveforms to establish the major tidal constituents (Crowe, 1994). His results identified that waveforms of periods of ½, 1 and 14 days were dominant and he proposed that, when considering a time scale of a week, it may be possible to ignore the 14 day cycle. Fourier analysis showed that the ½ day cycle was predominantly composed of a single sine wave.

Hence in the Tyneside area, it would be reasonable to model the tide as a single sine wave for the duration of a week.

7.2.3.8.   Atmospheric Pressure Influences

Atmospheric pressure was measured and recorded during the test. Results are shown in Figure 7.12 below.
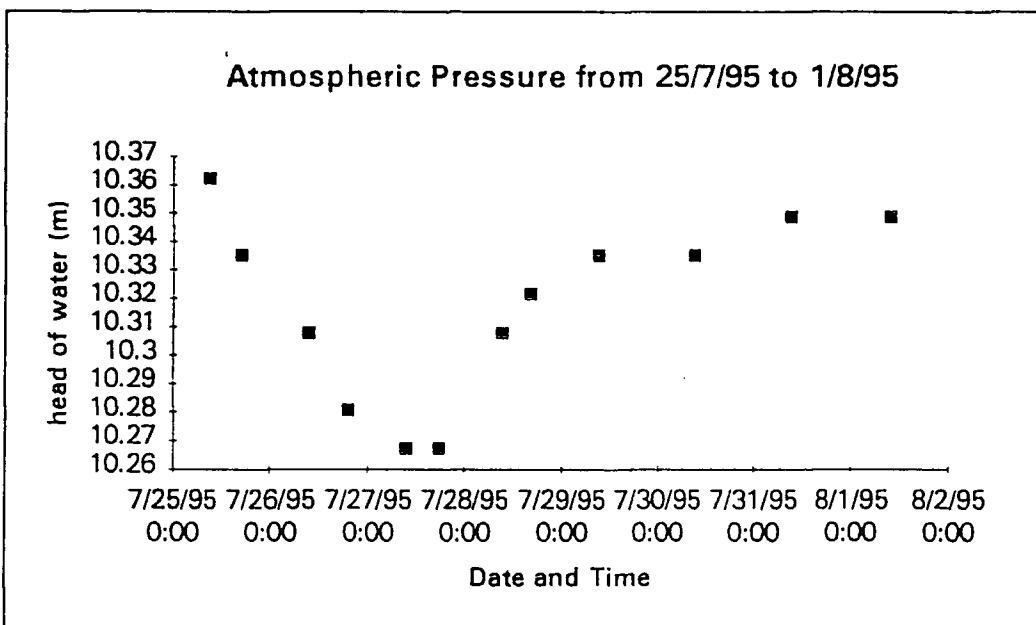
Figure 7.12. Atmospheric Pressure During Test Period.

It can be seen that the maximum change corresponds to approximately 100mm head of water. This compares well with a variation of 150mm recorded by Crowe (1994), from work in the Humberside area. The extent of the effect of atmospheric pressure on the results obtained from borehole 915 is questionable. Borehole records suggest the presence of a confining clay layer overlying the gravel aquifer, and atmospheric pressure is unlikely to have a significant effect on a confined aquifer, particularly compared with tidal effects. Also, if atmospheric changes did have a significant effect, the mean water level of the data would vary to a similar extent as the atmospheric pressure, however this was not observed.

7.2.3.9. Tidal Analyses of Data for Borehole 915

Ferris' theory does not incorporate leakage from or into the aquifer or reflection of the wave from a local impermeable boundary. As a separate part of my research work here at Durham University I have developed theory to incorporate effects of these two influences. The location of the piezometer in borehole 915 does not warrant application of the newly developed theory to the results. This is because:

1. The aquifer is overlain by a clay layer, a material of sufficiently low permeability to induce negligible leakage.

2. There are no clear impermeable boundaries within the vicinity of the borehole. The path of the groundwater flow to the River Tyne is most likely to be beneath the quayside wall.

From Ferris (1951):

$$t_L = x\sqrt{t_0 S / 4\pi T} \longrightarrow eqtn(7 \cdot 2)$$

$$h_x = h_0 \exp(-x\sqrt{\pi S / t_0 T} \longrightarrow eqtn(7 \cdot 3)$$

where t_L = the time lag of groundwater fluctuation compared with tidal fluctuation [T]

x = horizontal distance from tidal boundary [L]

t_0 = period of wave [T]

S = storage coefficient [non-dimensional]

234

T= transmissibility $[L^2 T^{-1}]$

h_0 = amplitude of tidal wave [L]

h_x = amplitude of groundwater wave at distance x inland [L]

Respective differences between times of maximum and minimum groundwater levels and times of high and low tide were calculated. An average value for the time lag was then estimated.

Amplitudes of groundwater levels were calculated from differences in groundwater level between maximum and minimum values. An average value of amplitude was then computed from this set of results. The amplitude of the tidal cycle was calculated in a similar manner.

Ferris' theory applies to two dimensional problems, the observation well located at a linear distance from the tidal boundary. Borehole 915 was located on a peninsula as can be seen in Figure 7.1. Groundwater flow is therefore complex and not a simple two dimensional situation. It was assumed, however, for purpose of analysis to resemble a two dimensional situation. The horizontal distance, x, was therefore computed as being the average of the two horizontal distances perpendicular to the shoreline, as shown in Figure 7.1.

Assuming the tidal period to be approximately 12 hours and applying this theory to the results which are summarised below:

$h_x = 0.563$ m
$h_0 = 1.901$ m
$t_L = 165$ mins
$x = 30$ m

7.2.3.9.1.   Timelag

$$t_L = (165 \times 60) = 30 \times \sqrt{(12 \times 3600) \times S / 4\pi T} \text{ seconds}$$

Therefore

$$\text{Diffusivity} = \frac{T}{S} = 3 \cdot 2 \times 10^{-2} \, \text{m}^2 / s$$

7.2.3.9.2. Amplitude Decay

$$\frac{h_x}{h_0} = \frac{0 \cdot 563}{1 \cdot 901} = \exp\left(-30 \times \sqrt{\pi S / (12 \times 3600)T}\right)$$

Therefore

$$\text{Diffusivity} = \frac{T}{S} = 4 \cdot 4 \times 10^{-2} \, \text{m}^2 / \text{s}$$

7.2.3.10.   Estimates of Aquifer Properties based on Alternative Techniques

Alternative techniques used to estimate aquifer properties are outlined below:

1. Hazen's Theory to estimate coefficient of permeability using Grading Analyses.

2. The Trilinear Diagram to estimate coefficient of permeability using Grading Analyses.

3. Estimate of Storage for Gravel Material.

7.2.3.10.1.   Hazen's Theory

Hazen's Theory was developed for single-size filter sands and gives a very approximate value for the coefficient of permeability. The sand is graded by particle size distribution tests in accordance with BS 1377. Further details regarding this theory are given by Somerville (1986).

Hazen's Formula:

$$K = \frac{C}{10^4} (D_{10})^2 \; \text{m} / \text{s} \longrightarrow eqtn(7 \cdot 4)$$

where: K = coefficient of permeability (m/s)

D_{10} = the sieve size through which 10% of the material passes (mm)

C = constant which varies from about 70 to 170 but for single-sized material, and for a first approximation of permeability, C is usually taken as equal to 100.

Applying this theory to results illustrated by the grading analyses for BH915:

Borehole 915. Depth 16.60 metres.

D$_{10}$ = 0.012 mm

C = 100

$$K = \frac{100}{10^4}(0.012)^2 = 1 \cdot 4 \times 10^{-6} \ m/s$$

Borehole 915. Depth 19.00 metres.

D$_{10}$ = 1.2 mm

C = 100

$$K = \frac{100}{10^4}(1 \cdot 2)^2 = 1 \cdot 4 \times 10^{-2} \ m/s$$

7.2.3.10.2.   Trilinear Diagram

The trilinear diagram (Summers and Weber, 1994) can be used to estimate permeability. Figure 7.13. shows the Trilinear Diagram, with isopleths of maximum value of permeability (m/day), for a variety of particle size distributions.

Table 7.3. below summarises the results of the grading analyses for borehole 915 at depths of 16.60 and 19.00 metres. The table also includes the corresponding ranges of permeability as determined by the trilinear diagram

	16.60 metres	19.00 metres
% Silt	20 %	2.5 %
% Sand	15 %	10 %
% Gravel	65 %	87.5 %
Permeability (m/s)	1 x 10^{-3} to 5 x 10^{-3}	5 x 10^{-3} to 1 x 10^{-2}

Table 7.3. Summary of Grading Analyses and Permeability for Borehole 915 from Trilinear Diagram.

237

7.2.3.10.3. Estimate of Storage for Gravel Material

For gravel material, values of specific storage, S_S are expected to range from:

$S_S = 1 \times 10^{-4}$ to 5×10^{-5} /m (Domenico, 1972)

Borehole records indicate an aquifer thickness, b, of 4.95 metres. An estimate of the range of values of storage, S, is:

$$S_{range} = S_s b = 5 \times 10^{-4} \rightarrow 2 \times 10^{-4}$$

An average value of Storage of 3.5×10^{-4} can be concluded.

7.2.3.11. Summary of Estimates of Aquifer Properties

Table 7.4. below summarises the results of aquifer properties determined by the various methods outlined above.

	Storage Coefficient	Permeability (m/s)	Diffusivity (m^2/s)
Tidal Analysis of BH915: Timelag Amplitude decay	N/A	N/A	3.2×10^{-2} 4.4×10^{-2}
Estimate of Storage Coefficient	3.5×10^{-4}	N/A	N/A
Hazen's Theory BH915 depth 16.6m BH915 depth 19m	N/A	1.4×10^{-6} 1.4×10^{-2}	N/A
Trilinear Diagram BH915 depth 16.6 m BH915 depth 19.0 m	N/A	2.5×10^{-3} 7.5×10^{-3}	N/A

Table 7.4. Summary of Results of Aquifer Properties Determined Using Variety of Methods.

Knowledge of soil material provides estimates for storage within a small range, as was illustrated above. This is unlike permeability which can vary much more significantly even for a specific soil material.

Therefore, the estimated value of storage coefficient was substituted into tidal analyses results of diffusivity (from timelag and amplitude decay) from borehole 915. This provided estimates of transmissivity and hence permeability, as shown below.

$S = 3.5 \times 10^{-4}$.

7.2.3.11.1.   Timelag

$T = 1.1 \times 10^{-5} \text{ m}^2/\text{s}$

$$K = \frac{T}{b} = 4 \times 10^{-5} \text{ m/s}$$

7.2.3.11.2.   Amplitude Decay

$T = 1.55 \times 10^{-5} \text{ m}^2/\text{s}$

$$K = \frac{T}{b} = 6 \times 10^{-5} \text{ m/s}$$

7.2.3.12.   Summary of Estimates of Permeability

Table 7.5. below summarises estimates of permeability considering the value of storage stated above.

	Permeability (m/s)
Tidal Analysis of BH915: Timelag Amplitude decay	 4×10^{-5} 6×10^{-5}
Hazen's Theory BH915 depth 16.6m BH915 depth 19m	 1.4×10^{-6} 1.4×10^{-2}
Trilinear Diagram BH915 depth 16.6 m BH915 depth 19.0 m	 2.5×10^{-3} 7.5×10^{-3}

Table 7.5. Summary of Estimates of Permeability.

7.2.3.13.   Discussion

The two estimates of permeability based on tidal analyses are of the same order of magnitude, yet are quite low for gravel soil. Although the borehole record indicates a largely gravel soil, it also details the presence of clay and sandy fines. This would have the effect of reducing permeability. Reasons for differences in estimates based on Ferris technique and alternatives could be due to a narrow zone of lower permeability material between the river and borehole. Ferris' technique would average out the effects of such material whereas alternative methods applied as above are localised to the borehole area. At a permeability of 10^{-6} m/s a 19mm diameter piezometer tube will tend to lead to an underestimate of tidal response by about 25% (White & Roberts 1994). This would lead to lower values of permeability than may otherwise be expected.

The coefficient of permeability is seen to vary significantly with depth. From application of Hazen's theory, it can be concluded that the coefficient of permeability around the piezometer (17.90 metres) lies within the range 10^{-2} m/s (16.60 metres) and 10^{-6} m/s (19.00 metres). The soil material at a depth of 16.60 metres is described as largely gravel, yet borders the clay layer. The soil material at a depth of 19.00 metres is well within the gravel layer. The borehole records and grading analyses indicated that, within the gravel layer, the soil became less clayey with depth. Therefore, it would be expected that permeability would *increase* with depth. Estimates of permeability from Hazen's theory increased with depth significantly, by four orders of magnitude. Estimates of permeability from tidal analyses were within the range of those calculated using Hazen's theory. From this it may concluded that Ferris' technique provided an estimate for permeability that compared well with those obtained from Hazen's theory.

Results from the trilinear diagram were higher than anticipated. The trilinear diagram provides a very approximate result for permeability. Estimates of permeability over the same range of depth as Hazen's theory were much less varied. The accuracy of the trilinear diagram was questioned. Both Hazen's theory and the trilinear diagram

were based on results from grading analyses. The larger variation in permeability found by Hazen's theory was thought to be more representative of the differences in soil material with depth than estimates from the trilinear diagram. It was therefore difficult to conclude the viability of the tidal technique when compared with such a general method.

Both Hazen's theory and the trilinear diagram provide a localised, rough estimate of permeability and are by no means rigorous methods, unlike pump tests (data of which was unavailable). It was found that Ferris technique compared well with estimates based on Hazen's theory, yet not so well with those based on the trilinear diagram approach. Therefore it was concluded that Ferris' technique provided an estimate of permeability that compared reasonably well with those obtained from alternative techniques.

7.2.4. Borehole 211

Results of groundwater variations with head were provided for borehole 211, therefore comparisons of aquifer properties from a variety of techniques were not as rigorous as for the case of borehole 915. The close proximity of BH915 to BH211 and general similarity of soil material, as illustrated by the grading analyses, will imply similar aquifer properties.

7.2.4.1. Location of Piezometer

The piezometer in borehole 211 was located in gravel soil at a distance of 17.5 metres from the River Tyne and at a depth of 21 metres.

7.2.4.2. Particle Size Distribution

The particle size distribution for borehole 211 for a sample depth of 21.50 to 21.60 metres is shown below in Figure 7.14.
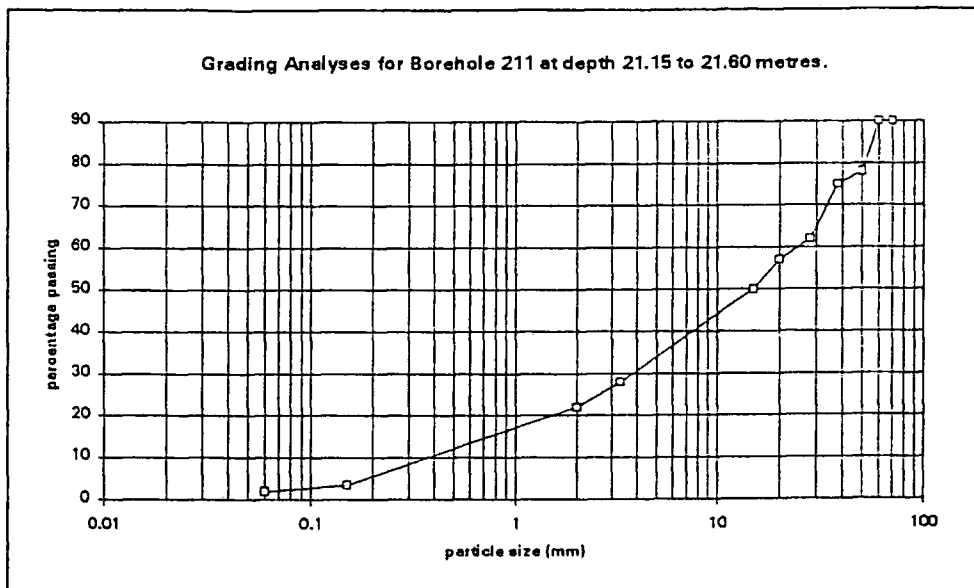
Figure 7.14. Particle Size Distribution of Soil Material in Borehole 211 at Depth 21.15 to 21.60 metres.

At a depth of 21 metres, the borehole record indicates a dense, dark brown/grey, sandy GRAVEL and cobble with occasional boulders. The material becomes more sandy (coarse) below 20.20 metres.

7.2.4.3.   Results

Results of groundwater changes in borehole 211 over a eight hour period were available. These results were recorded on 5th April 1989. The times of high and low water on this day were also available, however the actual tidal heights could not be obtained and therefore these were estimated based on tidal heights of 5th April 1995. A summary of the results is shown below.

$h_x = 1 \cdot 46 \text{ m}$

$h_0 = 1 \cdot 62 \text{ m}$

$t_L = 34 \ (\pm 10) \text{ mins}$

$x = 17 \cdot 5 \text{ m}$

7.2.4.4. Tidal Analyses of Data for Borehole 211

7.2.4.4.1. Timelag

$$t_L = (34 \times 60) = 17.5 \times \sqrt{(12 \times 3600)} \times S / 4\pi T$$

Therefore

$$\text{Diffusivity} = \frac{T}{S} = 0 \cdot 253 \text{ m}^2 / s$$

7.2.4.4.2. Amplitude Decay

$$\frac{h_x}{h_0} = \frac{1 \cdot 46}{1 \cdot 62} = \exp\left(-17 \cdot 5 \times \sqrt{\pi S / (12 \times 3600)T}\right)$$

Therefore

$$\text{Diffusivity} = \frac{T}{S} = 2 \text{ m}^2 / s$$

7.2.4.5. Estimates of Aquifer Properties based on Alternative Techniques

Once again, Hazen's theory was used to estimate the coefficient of permeability.

Applying this theory to results illustrated by the grading analyses for BH211:

D_{10} = 0.5 mm

C = 100

$$K = \frac{100}{10^4}(0 \cdot 5)^2 = 2 \cdot 5 \times 10^{-3} \text{ m} / s$$

The permeability is concluded to be 2.5 x 10^{-3} m/s.

7.2.4.6. Summary of Estimates of Aquifer Properties

Table 7.6. below summarises the results of aquifer properties determined above.

	Storage Coefficient	Permeability (m/s)	Diffusivity (m^2/s)
Tidal Analysis of BH211: Timelag Amplitude decay		N/A	3.95 0.50
Hazen's Theory BH211	N/A	2.5×10^{-3}	N/A

Table 7.6. Summary of Results of Aquifer Properties Determined Using Variety of Methods.

Assuming an estimate of storage coefficient = 3.5×10^{-4} as determined for similar soil material in borehole 915, and substituting this value into tidal analyses results of diffusivity (from timelag and amplitude decay), estimates of transmissivity and hence permeability can be determined. These calculations are shown below.

$S = 3.5 \times 10^{-4}$.

7.2.4.6.1.   Timelag

$T = 8.9 \times 10^{-5}$ m^2/s

$$K = \frac{T}{b} = 4 \times 10^{-4} \text{ m/s}$$

7.2.4.6.2.   Amplitude Decay

$T = 7 \times 10^{-4}$ m^2/s

$$K = \frac{T}{b} = 3 \times 10^{-3} \text{ m/s}$$

7.2.4.7.   Summary of Estimates of Permeability

Table 7.7 below summarises estimates of permeability considering the value of storage stated above.

	Permeability (m/s)
Tidal Analysis of BH211: Timelag Amplitude decay	 4×10^{-4} 3×10^{-3}
Hazen's Theory BH211	 2.5×10^{-3}

Table 7.7. Summary of Estimates of Permeability.

7.2.4.8.   Discussion

The two estimates of permeability based on tidal analyses are of similar orders of magnitude, and are satisfactory for gravel soils. Differences between time lag and amplitude decay methods may be due to leakage from the aquifer. It was thought that this may affect the amplitude result more significantly than those based on time lag. Leakage from the aquifer would cause more rapid decay in amplitude of the wave than if the aquifer were fully confined. The phase differences between tidal and groundwater fluctuations were thought to be largely unaffected by leakage effects. However, it was remembered that tidal times used in the analyses were not actual times but approximations based on more recent tidal tables. This is more likely to be the cause for discrepancy than leakage from the aquifer. A clay layer overlies the gravel in which the piezometer is situated. This was thought to have minimal permeability confining the aquifer and resulting in minimal leakage. It was therefore suggested that the estimate based on amplitude decay was more accurate.

Both estimates comply well with those based on Hazen's theory. The estimate based on amplitude decay is closer to that obtained by Hazen's theory than that based on time lag. The tidal analysis method provides an estimate of permeability incorporating ground conditions between the borehole and coast.

Hazen's theory provides an approximate and general, site-specific estimate of permeability. This method incorporates only the soil material in the immediate vicinity of the borehole. In addition to this, Hazen's formula includes a constant, the value of which may vary between 70 and 170. An approximation for this constant will also inherently lead to an approximate result for permeability.

Results from the tidal method will be affected by the piezometer. The time taken for the water level within the piezometer to respond to groundwater changes was not considered, nor was the damping effect of the piezometer on amplitude changes. These effects were outlined by Hvorslev (1951), and would lead to slight underestimates of permeability. Estimates of permeability based on Ferris' technique could be considered to be slightly lower than those based on Hazen's theory.

It was concluded that Ferris technique provided estimates of permeability that compared well with the estimate based on Hazen's theory. It was accepted however, that a comparison with a single general result was by no means definitively conclusive.

7.3. Conclusion

Data of groundwater levels in borehole 314 did not illustrate tidal behaviour, however the results were analysed using the slug test method. Application of this method concluded with an estimate for the coefficient of permeability of 4.8×10^{-9} m/s. This estimate was considered reasonable considering the glacial till and silt material detailed in borehole records.

Groundwater levels in boreholes 915 and 211 did illustrate tidal behaviour and therefore it was possible to analyse the data using Ferris' technique. Tidal analyses of borehole 915 provided an estimate for permeability of 5×10^{-5} m/s whilst from results for borehole 211, an estimate of 3×10^{-3} m/s was concluded. These values were based on an estimate for storage coefficient of 3.5×10^{-4}. For both boreholes

915 and 211, the estimates for permeability from tidal analyses were found to compare well with alternative and more localised methods.

Ferris' technique provides an average estimate of permeability of ground between the borehole and shoreline. It therefore provides a clearer indication of how groundwater flow may be affected over a wider area than localised tests using soil material information.

Figure 7.2.
Positions of Boreholes 211 and 915 - Quayside Site

BH915

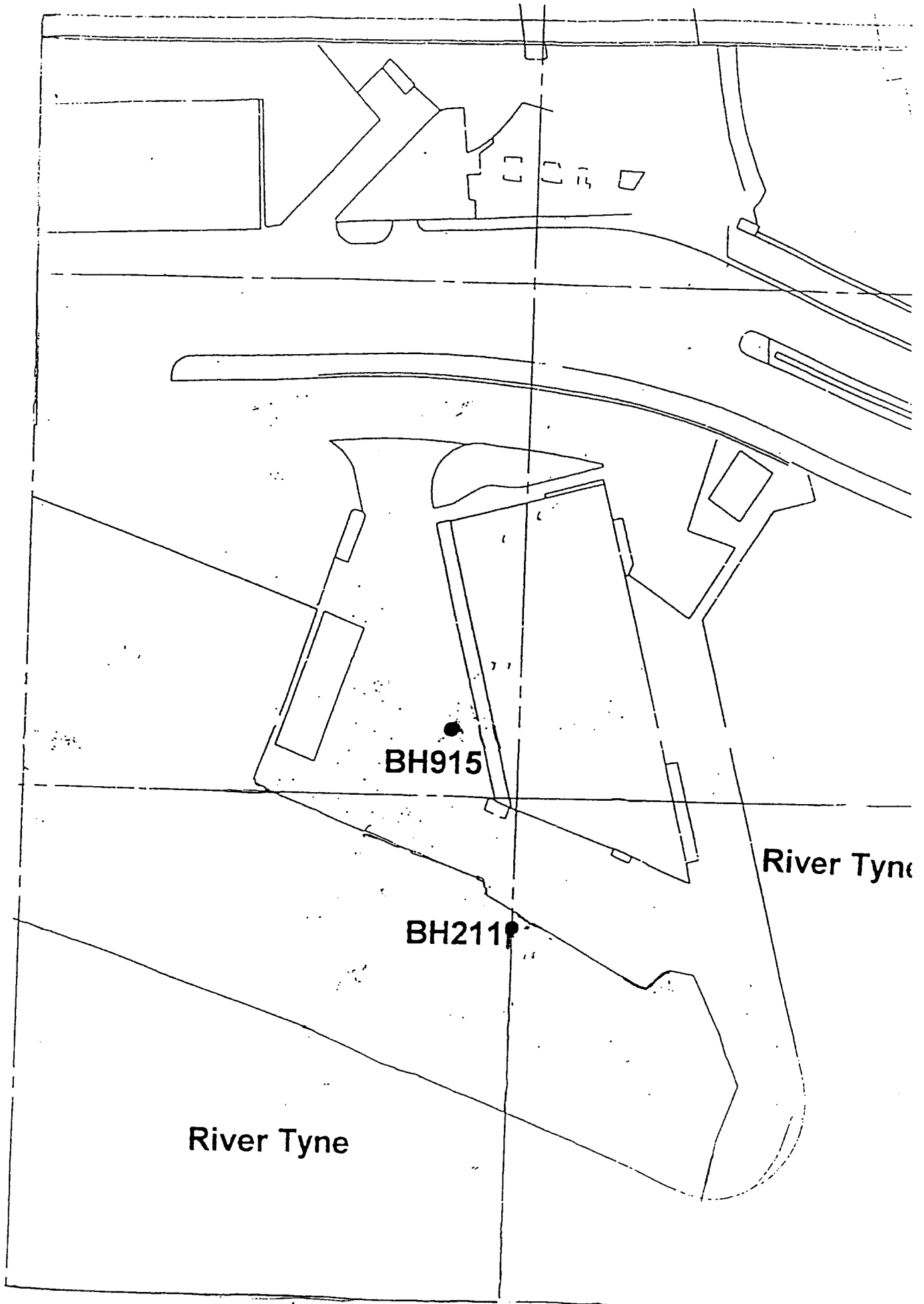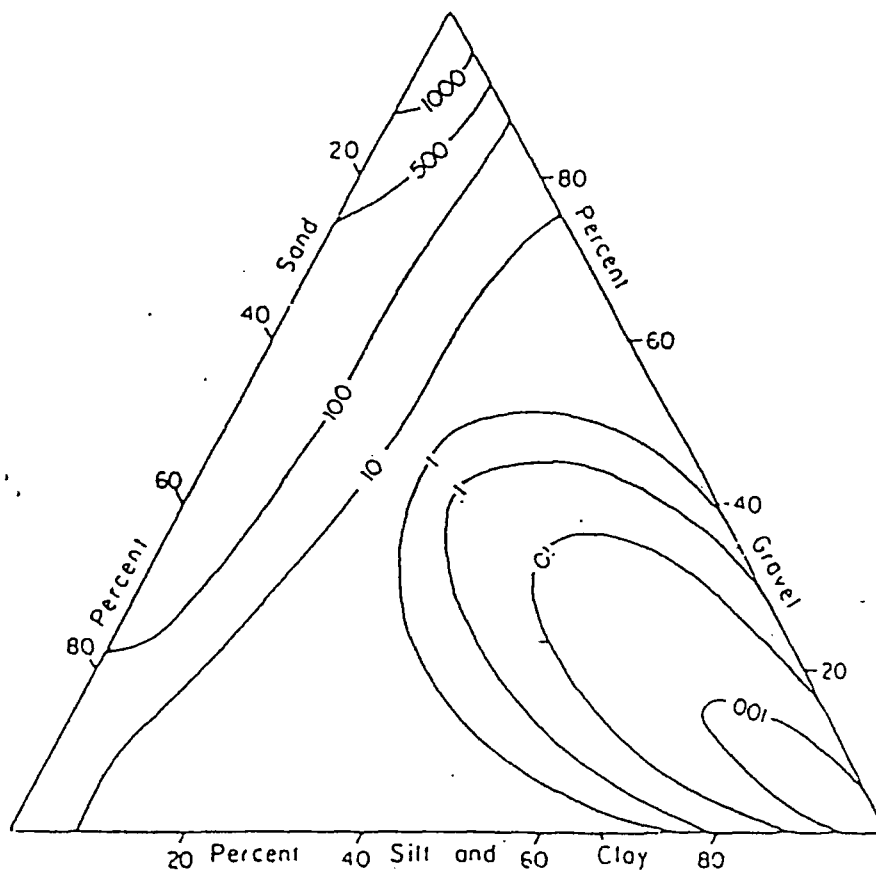River Tyne

BH211

River Tyne

Figure 7.13. Trilinear Diagram.

From Summers, W.K. and Weber, P.A. (1984).
The Relationship of Grain-size Distribution and
Hydraulic Conductivity - An Alternative
Approach. Ground Water, vol. 22 (4), pp 474 - 475.

Chapter 8

Discussion

8.1. The Importance of Determining Aquifer Properties

Determination of aquifer properties is important for evaluation of groundwater resources available, prediction of groundwater flow incurring migration of contamination and construction work below the water table. These aquifer properties include coefficients of permeability, leakage and storage. Accurate determination of each of these properties enables detailed predictive analysis of the effects on groundwater and the environment following human development. It is vital that this fresh-water resource is maintained as an investment for the future. In addition, induced alteration of water flowrates in surface and subsurface rivers alters the existing water table. The effects of this can be realised over hundreds of kilometres and can include settlement of soil, contaminant transport, flooding or conversely, drought. Detailed predictive analyses are required to avoid such disasters and this requires accurate estimation of aquifer properties.

Coastal regions are of particular concern since these areas are frequently densely populated. Two thirds of the world's population now inhabit coastal regions. Therefore even a small change in groundwater behaviour can have disastrous and expensive consequences by affecting thousands of people. In addition, the demand for fresh-water in such densely populated areas is high. Rivers are frequently polluted and therefore groundwater has become an important source of fresh-water supply. Excessive pumping can lead to drawdown and saline intrusion of the source. This then incurs the expense of desalination if the resource is to be further exploited. To avoid this expense, the effects of heavy pumping need to be predicted and this involves accurate determination of coastal aquifer properties.

250

8.2. Methods Available for Determining Aquifer Properties.

There are several methods available for determining aquifer properties. These include in situ tests such as pump tests, slug tests and tracer tests or soil sampling tests. The selection of a method depends on the accuracy required, options available at the site and the reason for determining aquifer properties. Pump tests are the most common and rigorous method. Analyses of these tests includes information from surrounding observation piezometers in addition to pumping details from the well. Therefore a large area of the aquifer is considered, however input information is localised.

An alternative method for determining aquifer properties in coastal areas was developed by Ferris (1951). This method considers fluctuations in groundwater levels due to tidal influence. Amplitude decay and time lag of the tidal wave as it propagates inland is used to determine diffusivity. Within a specified area, the range of values of aquifer properties obtained by analyses of tidal effects is much smaller than that obtained from several pump tests. Average estimates of aquifer properties are determined over a large region, between the coast and any number of observation wells. The impact of geological irregularities is therefore reduced.

Ferris method assumes an aquifer of finite length with negligible vertical flow. Work by past researchers has questioned the viability of these assumptions, and the reliability of results based on this technique.

8.3. Project Objective

The objective of this project was to further investigate the tidal analyses technique for determining aquifer properties. The approach included laboratory experimental work using the Durham Model Aquifer and field work at a site in Newcastle-upon-Tyne.

Tidal analyses were used to determine aquifer properties and these estimates were compared with those derived from alternative methods.

8.4. Achievements

Achievement of the project objective involved several distinct areas of work. These are summarised below.

8.4.1. Physical Modelling

Laboratory experimental work was performed using the Durham Model Aquifer. Preliminary work under steady state conditions, before application of the tidal system, concluded with the following estimates for aquifer properties:

Coefficient of permeability: 4×10^{-3} m/s

Coefficient of leakage: 2×10^{-5} s^{-1}

These estimates compared well with those concluded from results of a previous project. These previous results included an estimate for the storage coefficient of 0.1. Sixteen series of tidal tests were then performed using the Durham Model Aquifer. The tide was simulated by varying the head of water in a tank linked to the model aquifer by a length of pipe. Pore water pressure was measured and recorded from the base of the model aquifer at various horizontal distances from the tidal boundary. Fast fourier transform analyses were performed to determine the sinusoidal components of the simulated tidal wave. Two governing waveforms were concluded which constituted the tidal wave, primary and secondary. Results were arranged into graphs illustrating primary amplitude decay, secondary amplitude decay and time lag of the wave with respect to a selected reference position.

8.4.2. Numerical Modelling

Numerical modelling of the Durham Model Aquifer was carried out, applying the software CVM with the harmonic boundary modification. The reasons for the numerical modelling were to determine the suitability of applying Ferris theory, limited by assumptions of an aquifer of finite length with negligible vertical flow. In addition, the sixteen experimental tests were affected by simulated tides of varying periods, and the effect of period variation on results had to be investigated. Firstly, the objective was to investigate the reflection from the end of the aquifer farthest from the tidal boundary. The numerical solutions of amplitude decay and time lag, which incorporated reflection, were compared with solutions derived from Ferris' theory. Reflection was found to have a significant influence on results. The reflective effects increased as distance from the tidal boundary increased. The second objective was to determine the effects of leakage from the upper surface of the aquifer on results of amplitude decay and time lag. Again solutions of amplitude decay and time lag were compared with those derived from Ferris' theory. Leakage, at the rate specified, was found to have a small effect on results of amplitude decay and time lag. Finally, the effects of period variation were investigated. The numerical modelling work illustrated a marked difference in results of amplitude decay and time lag due to varying tidal periods.

From this work, it was anticipated that application of Ferris theory to laboratory results would imply significant inaccuracies in estimates of aquifer properties. Therefore it was concluded that Ferris' theory was unsuitable. Analytical theory would have to be developed which incorporated reflective and leakage effects.

It was also concluded that laboratory results from different periods could not be directly compared.

8.4.3. Development of Analytical Theory

The theory developed by Ferris theory was advanced to incorporate reflection by applying image well theory. Two principle reflective waves were considered. The

253

analytical theory was verified for a specific case study by comparing analytical and numerical solutions. The case study was prescribed based on parameters of the Durham Model Aquifer including previously estimated values for aquifer properties.

Heat conduction theory, Carslaw (1921), was related to groundwater behaviour. The solution employed by Angstrom for conductivity of bars, allowed to radiate into a medium under variable temperature, was assimilated to the problem of groundwater flow in a leaky aquifer. Hence, analytical theory was derived for an aquifer under tidal influence with leakage, otherwise known as vertical flow. Two equations were concluded for amplitude decay and time lag which incorporate the three aquifer properties, transmissivity (related to permeability), storage and leakage coefficients. This theory was verified by deriving solutions for a case study, and comparing these with numerical solutions.

Finally, analytical theory was derived which incorporated both reflection and leakage. This combined the theories of the earlier two derivations. The combined theory was verified by comparing analytical and numerical solutions for a specific case study.

8.4.4. Analysis of Results

The objective was to determine aquifer properties by applying the analytical theory, incorporating leakage and reflection, to the laboratory results of primary and secondary amplitude decay in addition to time lag. Numerical analysis had concluded that there was a marked difference in amplitude decay and time lag results due to period variation of the tidal wave. Therefore, experimental results were arranged into suitable period ranges for analyses purposes.

The analytical theory incorporated three unknown parameters, transmissivity, storage and leakage coefficients. These parameters were linked to form pairs to aid analyses by providing a clearer indication of trends. A region of study was established. This was based on estimates of aquifer properties from earlier work. Primary amplitude decay experimental results from one period range were considered together with the corresponding secondary period range. This encompassed results from eight series of tidal tests. The mean and spread of laboratory results for primary amplitude decay,

secondary amplitude decay and time lag were compared with analytical solutions. Aquifer properties were varied to produce a variety analytical solutions and hence a range of values of T/S[1] and β/T[2] were concluded which provided satisfactory matches with laboratory results.

The ranges of results from the three separate pieces of information (primary amplitude decay, secondary amplitude decay and time lag) were combined. The overlap of the ranges of T/S and β/T was concluded to be:

$T/S = 0.02$ m^2/s

$\beta/T = 0 \rightarrow 0.02$ m^{-2}

Assuming a value for the storage coefficient derived from previous work of 0.1, the following estimates of aquifer properties for the Durham Model Aquifer were concluded:

Transmissivity, $T = 2 \times 10^{-2}$ m^2/s

Coefficient of permeability = 8×10^{-3} m^2/s

Leakage coefficient, β ranging from $0 \rightarrow 4 \times 10^{-5}$ s^{-1}

These results compared reasonably well with those from earlier experimental work under steady state conditions, however, the region of study for tidal analyses was determined by the results from earlier experimental work. Therefore, it was concluded that the tidal analyses technique verified the results obtained from the earlier experimental work.

8.4.5. Field Work

The objective was to supplement the laboratory research and improve knowledge of the tidal analyses technique by application in the field.

The field work was performed at a site in Newcastle-upon-Tyne. Groundwater levels were monitored in two boreholes (BH915 and BH314) for periods of up to a week. Results from BH915 illustrated tidal influence on groundwater behaviour.

---

[1] Transmissivity / (Storage coefficient)

[2] (Leakage coefficient) / transmissivity

Groundwater levels were therefore monitored at this borehole for the duration of a week. The gravel aquifer layer was overlain by a confining clay layer and therefore negligible vertical flow was assumed. It was also deemed reasonable to assume the aquifer of infinite length since there were no clear, local impermeable boundaries. Therefore, Ferris theory was applied and values for diffusivity concluded for each of time lag and amplitude decay. The storage coefficient was assumed to be 3.5×10^{-4} based on the soil grading analyses. Therefore average values of transmissivity, and hence permeability were determined from the tidal analyses technique.

Transmissivity, $T = 1.25 \times 10^{-5} \ m^2/s$

Coefficient of permeability, $K = 5 \times 10^{-5} \ m/s$

These compared reasonably well with estimates based on application of Hazen's theory and the Trilinear diagram. It was difficult to definitively conclude the viability of the tidal technique compared to such general alternative methods.

Results from groundwater level monitoring in a clay layer at BH314, did not illustrate tidal behaviour. The groundwater level appeared to fall continually during the 24 hour test period. This was attributed to the additional volume of the transducer and cable in the piezometer tube, which caused a rise in head. This then dissipated during the course of the test. Considerable time was taken for a steady water level to be attained due to the fact that the piezometer was located in a relatively impermeable clay layer. These results were analysed as a slug test. A permeability of 4.8×10^{-9} m/s was concluded. This was deemed a reasonable estimate considering the soil material detailed in the borehole records in addition to grading analysis results.

Finally, results of groundwater levels at a third borehole, BH211, were also available. These results illustrated tidal influence. Ferris theory was applied and values for diffusivity concluded for each of time lag and amplitude decay. The storage coefficient was again assumed to be 3.5×10^{-4} since the location of this borehole was close to BH915 and in similar soil material. Therefore values of transmissivity, and hence permeability were determined from the tidal analyses technique. The values varied significantly between amplitude decay and time lag methods. The coefficients of permeability were as follows:

256

Amplitude Decay: 3×10^{-3} m/s

Time Lag: 4×10^{-4} m/s

The reason for the discrepancy was attributed to the fact that high and low tides were estimated. A variation of an order of magnitude may be considered to be reasonable for the coefficient of permeability which is known to be a very wide-ranging parameter. Estimates of permeability based on Hazen's theory were of the order of 10^{-3} m/s, comparing well with tidal analyses estimates.

8.5. Discussion of Achievements and Application of The Tidal Analyses Technique

8.5.1. Laboratory Experimental Work and Analyses of These Results

Analytical theory was derived which incorporated the effects of reflection and leakage from a coastal aquifer. This theory was verified by comparison with numerical solutions for a specific case study. Before analytical theory could be applied to laboratory results of amplitude decay and time lag, a region of study had to be established. This involved making assumptions of aquifer properties as an initial starting point for analysis. From this work, it was concluded that the tidal analyses technique supplemented and verified estimates of aquifer properties based on alternative methods. This agreed with the conclusion of White and Roberts (1994), who suggested that the tidal analyses technique could provide a useful supplement to a site investigation. Since the analyses procedure, defined within this programme of work, requires values of aquifer properties as a starting point for analyses, the technique could only be used to verify existing estimates.

The sensitivity of the solutions to changes in aquifer properties was noted. For the case of the primary period range, increasing the value of T/S from 0.01 m^2/s to 0.02 m^2/s reduced the rate of amplitude decay. The value of amplitude decay at the end of

the aquifer farthest from the tidal boundary rose from approximately 40% to 60%. Amplitude decay was therefore concluded to be highly sensitivity to changes in T/S. For a highly permeable material, it was anticipated that amplitude decay would be minimal.

Varying the value of β/T by an order of magnitude ($0.1m^{-2}$ to $0.01m^{-2}$) led to differences in amplitude decay. Variations in amplitude decay curves due to altering β /T were larger as T/S increased. For a value of T/S of $0.01m^2/s$, the amplitude decay varied by approximately 10% between values of β/T of $0.1m^{-2}$ and $0.01m^{-2}$. However, for a value of T/S of $0.03m^2/s$, the amplitude decay varied by approximately 40% between values of β/T of $0.1m^{-2}$ and $0.01m^{-2}$.

Time lag also varied significantly due to variations in T/S. Varying this parameter from $0.01m^2/s$ to $0.02 m^2/s$ for a period of 1920s, resulted in a decrease in the time lag by as much as 200s. Varying β/T by an order of magnitude resulted in a variation of time lag by approximately 100s. It was therefore concluded that time lag was highly sensitive to variations in T/S, whilst less sensitive to changes in the parameter, β/T.

The sensitivity of time lag and amplitude decay solutions to changes in parameters, T/S and β/T, implied that the values for aquifer properties were concluded to a high degree of accuracy.

Due to time constraints, results from only eight series of tidal tests were compared with analytical solutions. Further analyses incorporating the other experimental results is likely to have further verified the earlier estimates of aquifer properties.

Errors were inherent in the experimental results, particularly due to the following:

1. Leakage from the upper surface of the Durham Model Aquifer was unlikely to be uniform over the entire aquifer length.

2. Air entrapped within the aquifer and pipework systems.

Attempts were made to control and limit these effects as much as was physically possible.

8.5.2. Field Work

Tidal analyses of field work data concluded with estimates for the coefficient of permeability which compared well with estimates based on soil grading analyses. Soil grading analyses techniques for determining aquifer properties are not particularly accurate due to the fact that testing is not performed in situ. Material is disturbed during removal from the ground. In addition, Hazen's theory incorporates a constant, the exact value of which is uncertain. Comparison of estimates of aquifer properties from tidal analyses methods with pump test results would have provided a better indication of the accuracy of the tidal technique. Unfortunately, such information was unavailable.

Based on comparison with estimates for aquifer properties derived from soil grading analyses, the tidal analyses technique was considered to provide a viable indication of aquifer properties.

8.6. Comparison of this Research with Earlier Work Investigating the Tidal Analyses Technique

Two conclusions were drawn from this programme of research:

1.   Newly-developed analytical theory, incorporating leakage and reflective effects, may be used to supplement a site investigation by verifying estimates of aquifer properties derived from alternative methods.

2.   Application of Ferris' theory to field work data concluded estimates for aquifer properties that compared well with those derived from soil grading analyses.

Work of past researchers suggested that the tidal analyses technique did not provide such reliable estimates of aquifer properties as pump test methods. Erskine (1991)

259

and Crowe (1994) suggested that the application of the tidal technique may result in inaccuracies because of the assumption of a confined aquifer with negligible vertical flow. Crowe also suggested that the leakage may reduce apparent diffusivity as calculated by the amplitude method. Development of analytical theory which incorporates leakage, as derived in this programme of work, may improve the accuracy of estimates for aquifer properties based on tidal analyses.

Crowe also suggested, based on part of his work, that the period of the tidal wave may change as the wave progresses inland. This was not found to be the case for the Durham Model Aquifer. Fast fourier transform analysis illustrated that the period of the primary and secondary waves generally remained constant over the entire length of the Durham Model Aquifer.

It is interesting to note a similarity between Ferris' theory and the advanced theory outlined within this programme of work. Ferris' work concluded with two equations for time lag and amplitude decay incorporating two unknown parameters, transmissivity and storage coefficient. In order to apply this theory, an estimate for one of the properties had to be made by an alternative technique before the other property could be determined using the tidal analysis method. Similarly, the newly developed analytical theory, described within this thesis, incorporated three unknown parameters, transmissivity, coefficient of storage and leakage coefficient. The value of one of these properties had to be assumed in order to estimate values for the remaining properties using the tidal analysis technique. Assuming a value for the storage coefficient, S, based on an alternative method is most suitable since this parameter is not as wide-ranging as transmissivity and leakage coefficient, and is therefore more easily determined accurately.

8.7. Limitations

The analytical solution for the behaviour of semi-confined aquifers subject to a sinusoidal head boundary condition has been based on the equations developed by

Jacob (1946). Three assumptions were made when developing this analytical solution. These are as follows:

1. Leakage rate into or out of the aquifer is directly and instantaneously proportional to the fall or rise in hydraulic head.

2. The aquifer remains fully saturated.

3. The governing aquifer parameters of transmissivity and storage coefficient remain constant both with time and distance.

Furthermore, if the analytical solution is to be applied in practice, then in order to simulate natural tidal conditions, the principle of superpositions would need to be used to represent the appropriate non-sinusoidal boundary condition. Applying superposition, however, requires linear conditions. If this is not the case then a non-sinusoidal boundary conditions needs to be simulated which greatly adds to the complexity of the solution.

Despite these limitations, the governing equations for the groundwater flow in a semi-confined leaky aquifer are widely known in practice. In particular, the corresponding assumptions and limitations have nevertheless been incorporated and accepted in the development of numerous groundwater models such as USGS2D model (Trescott et al., 1976) or the VTT model (Reisenauer, 1979).

In terms of the validation of the solution developed in this thesis, this has been partly undertaken with the simulation of the results of the experimental aquifer. Whilst some simulation of field conditions has been attempted, it is recommended that a further study be undertaken to monitor tide induced hydraulic head response and to validate a number of equations and solutions against the observed responses.

8.8. Prospects for Further Work

The analytical theory, developed as part of this programme of work, has been verified by comparing results of amplitude decay and time lag with numerical solutions. In addition, theory was also compared with laboratory results, from physical modelling of a coastal aquifer.

The validity of the analytical theory would be further enhanced by field work. In particular, estimates based on pump tests may be compared with those based on application of this theory. The theory may then be applied to supplement site investigations by verifying estimates of aquifer properties derived from alternative techniques.

Chapter 9

Conclusions

Aquifer properties need to be determined accurately for predictive analysis of groundwater resources and behaviour. Particular properties of interest are the coefficient of permeability, the coefficient of storage, and the leakage coefficient. Various methods are available to estimate these properties. Pump testing is the most common and rigorous method. Results from these tests are localised to the borehole and subsequent observation wells. These site-specific tests do not incorporate the heterogeneity of the ground over a large aerial extent.

An alternative technique involves monitoring groundwater response to tidal behaviour. This tidal technique was developed by Ferris (1951) and provides a more accurate representation over a wider area than conventional methods. Ferris' theory is limited because it assumes an aquifer of finite length with negligible vertical flow.

The objective of this project was to further investigate the tidal method for determining aquifer properties. The approach included laboratory experimental work and development of analytical theory in addition to field work at a site in Newcastle-upon-Tyne.

The laboratory experimental work was performed using the Durham Model Aquifer. This five metre long physical model represented a semi-confined aquifer. Preliminary work under steady-state conditions concluded with the following estimates for aquifer properties:

Coefficient of permeability: 4×10^{-3} m/s

Leakage coefficient: 2×10^{-5} s^{-1}

Sixteen tidal experiments were performed. This work concluded with results of amplitude decay and time lag with respect to the simulated tidal boundary. Numerical

modelling was applied using software, CVM, to investigate the effects of leakage and reflection in addition to period variation of the tidal wave. This work proved that Ferris' theory was unsuitable for application to laboratory results. Therefore analytical theory, which incorporated reflection and leakage, was derived from Ferris' theory. This theory was validated by comparing solutions with numerical results. A region of study was prescribed based on estimates of aquifer properties from earlier work. The newly-developed theory was applied and solutions of amplitude decay and time lag compared with laboratory results. This work concluded with the following estimates for aquifer properties:

Coefficient of permeability: 8×10^{-3} m/s

Leakage coefficient range: $0 \rightarrow 4 \times 10^{-5}$ s^{-1}

It was concluded that estimates from tidal analyses verified those based on the preliminary work. The analytical theory, developed within this programme of work, incorporates three unknown parameters, permeability, leakage and storage. The value of one of these parameters must be assumed before the remaining two aquifer properties can be estimated.

The field work involved monitoring groundwater levels from two boreholes located adjacent to the tidally-influenced River Tyne. Groundwater in one of these boreholes was found to be influenced by the tide. Ferris theory was applied and a diffusivity of 3.7×10^{-2} m^2/s was concluded. A value for the storage coefficient of 3.5×10^{-4} was estimated from the grading analysis. Therefore, the coefficient of permeability was computed to be 5×10^{-5} m/s. This estimate was slightly lower than anticipated, but was within the range of values calculated using Hazen's theory. It was thought that the reason for this may be due to a narrow zone of lower permeability between the river and the borehole.

Records of groundwater level from previous monitoring were also available for another borehole. These were analysed by applying Ferris' theory. Assuming a value for the storage coefficient of 3.5×10^{-5}, the range of values for the coefficient of permeability concluded was 3×10^{-3} m/s to 4×10^{-4} m/s. Although this range spanned an order of

magnitude, it was realised that the coefficient of permeability is a very wide-ranging parameter, even within a specific soil material. Therefore estimates were considered of useful accuracy for site investigation purposes. The range of values for permeability based on tidal analyses compared well with an estimate from grading analysis.

Results from the third borehole did not illustrate tidal behaviour and were analysed as a slug test. An estimate for the coefficient of permeability of 4.8×10^{-9} m/s was concluded. This value compared well with grading analysis results.

This programme of work illustrated that estimates of aquifer properties from tidal analyses compared well with those from alternative methods. The tidal technique incorporates the heterogeneity of the ground between the observation boreholes and the coast. When a semi-confined aquifer is under investigation, application of the theory developed within this programme of work, rather than using the traditional Ferris' equations, leads to increased accuracy of aquifer properties. It was concluded that this method could be applied to supplement and verify estimates of aquifer properties derived from more rigorous techniques such as pump test methods.

Chapter 10

References

Carr, P.A. and Van Der Kamp, G.S. (1969). Determining Aquifer Characteristics by the Tidal Method. Water Resources Research. Vol. 5, No. 5, pp 1023-1031.

Carrington, R.E. (1994). Tidal Influence on Coastal Aquifers. Project submitted for the Degree of BSc (Hons) Engineering, University of Durham.

Carslaw, H.S. (1921). Mathematical Theory of The Conduction of Heat in Solids. MacMillan and Co, London.

Craig, R.F. (1992). Soil Mechanics. Fifth Edition. Chapman & Hall, London.

Crowe, C.G. (1994). Tidal Variations in Groundwater. University of Durham, Submission Thesis for the Degree of Master of Science.

Domenico, P. A. (1972). Concepts and Models in Groundwater Hydrology, McGraw-Hill, New York.

Erskine, A.D. (1991). The Effect of Tidal Fluctuations on a Coastal Aquifer in the U.K. Ground Water, Vol. 29, No. 4, pp 556-562.

Ferris, J.G. (1951). Cyclic Fluctuations of Water Level as a basis for Determining Aquifer Transmissibility. Int. Assoc. of Scientific Hydrology 33, 148-155.

Freeze, A.R. and Cherry, J.A. (1979). Groundwater. Prentice-Hall, New Jersey, U.S.A.

Gregg, D.O. (1966). An Analysis of Groundwater Fluctuation Caused By Ocean Tides in Glynn County, Georgia. Ground Water, Vol. 4, No. 3, pp 24-32.

Hantush, M.S. and Jacob, C.E. (1955). Non-steady Radial Flow in an Infinite Leaky Aquifer, Trans. Amer Geophysical Union, V.36, no. 1, pp 95-100.

Hvorslev, M.J. (1951). Time lag and Soil Permeability in Ground-water Observations. U.S. Army Corps Eng. Bull. No. 36.

Igarashi, G. and Wakita, H. (1991). Tidal Responses and Earthquake-Related Changes in the Water Level of Deep Wells. Journal of Geophysical Research, Vol. 96, No. B3, pp 4269-4278.

Ingersoll, L. R. and Zobel, O.J. (1913). An Introduction to the Mathematical Theory of Heat Conduction. Ginn and Company, The Anthenaeum Press, Boston, U.S.A.

Jacob, C.E. (1955). Radial Flow in a Leaky Artesian Aquifer. Trans. Amer. Geophysical Union, Vol. 27, No. 2, pp 198-208.

Lourenco, P.C.R.O. (1994). Fluctuations in Head due to Tides on Coastal Aquifers. Erasmus Project at University of Durham.

Money, M.S. (1986). Tidal Variations of Groundwater Level in an Estuarine Aquifer. Groundwater in Engineering Geology, London, pp 81-85.

Pandit, A., El-Khazen, C.C, Sivaramapillai, S.P. (1991). Estimation of Hydraulic Conductivity Values in a Coastal Aquifer. Ground Water, Vol. 29, No. 2, pp 175-180.

Pinder, G.F, Bredehoeft, J.D. and Cooper, H.H. (1969). Determination of Aquifer Diffusivity from Aquifer Response to Fluctuations in River Stage. Water Resources Research, Vol. 5, No. 4, pp 850-855.

Reisenauer, A.E. (1979). Variable Thickness Transient Groundwater Flow Model (VTT), Formulation, User's Manual and Program Listings. Pacific Northwest Laboratory Report PNL 3160-1, PNL 3160-2, PNL 3160-3.

Serfes, M.E. (1991). Determining the Mean Hydraulic Gradient of Ground Water Affected by Tidal Fluctuations. Ground Water, Vol. 29, No. 4, pp 549-555.

Shaw, E.M. (1994). Hydrology in Practice. Third Edition. Chapman & Hall, London.

Somerville, S.H. (1986). Control of Groundwater for Temporary Works. CIRIA Report 113, 1986.

Summers, W.K and Weber, P.A. (1984). The Relationship of Grain-size Distribution and Hydraulic Conductivity - An Alternative Approach. Ground Water, Vol. 22, No. 4, pp 474-475.

Theis, C.V. (1935). The Relation Between the Lowering of the Piezometric Surface and the Rate and Duration of Discharge of a Well Using Groundwater Storage. Trans. Amer. Geophysical Union, Vol. 16, pp 519-524.

Thomas, S.D. (1990). Analysis of Offshore Pore Pressure Data. University of Oxford. Soil Mechanics Report No. SM 107/90.

Thomas, S.D, Welch, J.P. & Castell, P.L. (1994). CVM: A Pragmatic Modelling Approach. *Hydroinformatics*: edited by Verwey, Minns, Babovic & Maksimovic. Published by A.A. Balkema, Netherlands.

Todd, D.K. (1980). Groundwater Hydrology. John Wiley & Sons, pp 242-247.

Trescott, P.C., Pinder, G.F. and Larsen, S.P. (1976). Finite-difference Model for Aquifer Simulation in Two Dimensions with Results of Numerical Experiments. U.S. Geological Survey, Techniques of Water-Resource Investigations, Book 7, Chapter C1.

Walton, W.C. (1970). Groundwater Resource Evaluation. McGraw-Hill Book Company, New York.

White, J.K. and Roberts, T.O.L. (1994). The Significance of Groundwater Tidal Fluctuations. Groundwater Problems in Urban Areas. Ed. W.B. Wilkinson. Thomas Telford, London.

Appendices

RS Programmable Timer Bases
Type 1 Stock No. 345-375
Type 2 Stock No. 345-369

Mounting

These timers should be mounted in one of three ways:—

)   Clip the base onto a 35mm DIN rail to EN50 022 — removal is achieved by use of the spring release tab.

i)   Surface mount the unit using the supplied hardware as follows:—

   a) Use the nut, screw, washer combination to replace the existing screw fitted through the central hole in the socket.

   b) Fit the pan head screw into the M3 threaded bush in the underside of the unit.

The chosen plug in relay will be held in place by the relay retention clip supplied.

Terminations

All terminations are onto the twelve screw clamp terminals — six at each end of the base moulding. Connections should be made as follows:
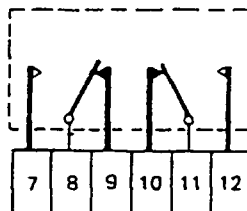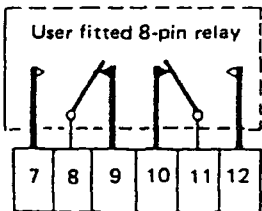
WARNING
(TYPE 1)
WHEN USED WITH A.C. MAINS,
TERMINALS 4 & 5 ARE AT A
HIGH POTENTIAL WITH RESPECT
TO EARTH. A VOLT-FREE
CONTACT MUST BE
PROVIDED FOR REMOTE
INITIATION
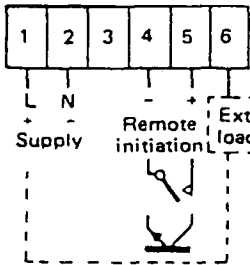
Total current of external load and plugged-in load, if used, 200mA maximum.

Type 1

User fitted 11-pin relay

Total current of external load and pluged-in load, if used, 200mA maximum.

Type 2

Dimensions

All dimensions are in mm.

8-pin socket on Type 1
11-pin socket on Type 2

Time range and function programming switches

101.5

Alternative surface mounting point using screw supplied with timer (replaces existing screw)

LED indicator

Set time

Mounting suitable for standard 35mm DIN rail

RS Plug-in relay not supplied

M3 bush for surface mounting with M3 pan head screw (supplied with timer)

54

30.85
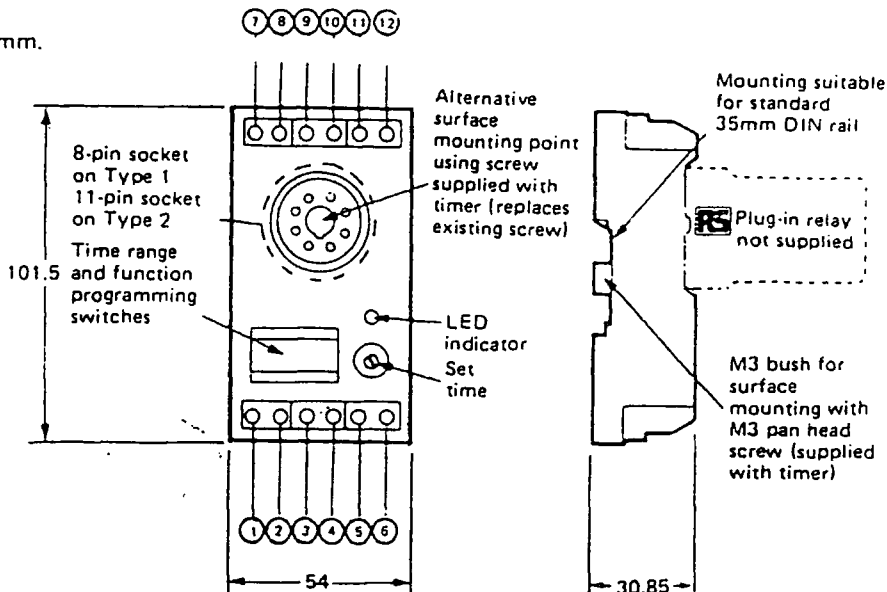
Specifications

Supply voltage :	12V to 120V d.c. N.B. ensure relay coil used is compatible with chosen supply.
	or 20V to 250V a.c.
Contact rating :	8A, 250V a.c./30V d.c.
(Limited by the timer terminations)	if used with **RS** relays.
Max. total load :	200mA (relay coil requirement plus any external load).
Time repeatability :	1%
Reset time :	50ms (the supply must be removed for this time to achieve a timer reset).
Terminations :	Screw clamp terminals.
Indicator :	A red L.E.D. is 'ON' when the relay (or external load) is energised.
Ambient temperature range :	−20°C to 50°C.

Time Setting

Four different time range settings are available on Type 1 timer (345−375) and seven on Type 2 (345−369). These are selected by using switches 3 and 4 on Type 1 and switches 3, 4 and 5 on Type 2. To obtain the required range use the switches in the positions as detailed below. Note that these time range top limits are guaranteed minimums — typically longer times may be achieved.

Type 1 Time Ranges		
t	SW. 3	SW. 4
5 sec.	A	B
20 sec.	B	A
2.5 min.	B	B
20 min.	A	A

Type 2 Time Ranges			
t	SW. 3	SW. 4	SW. 5
1 sec.	A	B	A
4 sec.	B	A	A
30 sec.	B	B	A
1 min.	A	B	B
4 min.	A	A	A
4 min.	B	A	B
30 min.	B	B	B
4 hr.	A	A	B

Adjustment of the time within these ranges can be made by using the potentiometer to the right of the switches.

Timing Modes

The modes of operation of these timer bases are determined by what combination of switch positions (A or B) have been selected. In the case of Type 2 only two switches (1 and 2) are used, with three switches (1, 2 and 5) being used for Type 1. Switch 5 on Type 1 selects remote control options.

Note : In all cases it is important to take into account the effect of the position of each of these switches to ensure that the desired operating mode has been selected.

The timing operations of these units are as follows :

Type 1 and Type 2

Switch Position

1A   PULSE — Immediately the supply is connected the relay will energise. The relay will de-energise after the set time and remain de-energised. Except when the cyclic (2A) mode has been selected (or the Type 1 timer is being used under remote control initiation) disconnection from the supply is necessary to reset the electronic circuit for the next operation.

or 1B   DELAY — Immediately the supply is connected a delay time as set will elapse, after which the relay will energise. Except when the cyclic (2A) mode has been selected (or the Type 1 timer is being used under remote control initiation) the relay will remain energised until the supply is disconnected. If the supply is disconnected before the set time has elaped the timing circuit will be reset without the relay energising. On subsequent reconnection of the supply timing will start again from zero.
(N.B. On the Type 1 timer, selection of the remote control initiation (5A) can be used to provide a type of "DELAY OFF" function (supply permanently connected), i.e. delay initiated when remote control contacts are opened).

Appendix 2.1.

and 2A   CYCLIC — When selected, this mode will provide a continuous relay energised / relay de-energised timing cyc. (total time 2t) with an equal mark/space ratio. When used with the PULSE mode (1A) the cycle will start with the relay energised and with DELAY mode (1B) with the relay de-energised.

or 2B   SINGLE OPERATION — With the switch in this position the timer operation is determined solely by the position of switch 1 (and also switch 5 when using the Type 1).

and for Type 1 only

5   REMOTE INITIATION — Using standard supply initiation of the timer, an open contact on the remote contol inputs will allow manual operation, as selected by switches 1 and 2 i.e. operation controlled by connection and dis-connection of the supply. With the supply permanently connected, the following remote initiations are obtained.

5A   SUSTAINED — Closing the contacts resets the timing circuit , which is the same as removal of the supply. Re-opening of the contacts initiates a new timing cycle, which is the same as connection of the supply.

or 5B   MOMENTARY — Closing the contacts resets the timing circuit momentarily and allows the next timing cycle to commence immediately, which is the same as briefly disconnecting the supply. Once timing has started the contacts can be re-opened without affecting operation.

Relay

These timer bases are designed to be used with standard octal, 2-pole (for Type 1) or 11-pin, 3-pole (for Type 2) plug in relays. For suitable **RS** relays refer to the Relay Section in the current **RS** catalogue (use octal types 348—756 (12V d.c.) etc. and 11-pin types 348—807 (12V d.c.) etc.).
It is very important to ensure the relay coil voltage used is the same as the supply to the timer. The wide operating voltage range available on the timer base enables operation from most supply rails, as long as a suitable relay is available. The chosen relay will be held in place by the relay retention clip provided.
Note : The terminations used on the base limit the relay contacts maximum load to 8A, 250V a.c./30V d.c. (resistive).

External Load

An external load requiring a maximum current of 200mA (resistive) at the supply voltage used, may be connected across terminals 1 (supply L or +) and 6. This load is usually in place of a plug in relay, although, if care is taken to ensure that the total load (external plus relay coil requirement) does not exceed 200mA, both may be used simultaneously.
Note : There is no short circuit or over-current protection when using these external load connections.

Appendix 3A Estimation of Leakage Coefficient.

Theory described in this section led to estimation of the leakage coefficient, β of the Durham Model Aquifer.

The leakage coefficient, β $= \dfrac{K}{b}$

where: K=hydraulic conductivity.

   b=aquifer thickness.

The leakage coefficient can be determined from the following:

$$q = \frac{Q}{A_s}$$

where: Q = flowrate (m^3 / s)

   A_s = area of leakage surface

$$\beta = \frac{q}{(h - h')}$$

where: h'= the level of the free water surface

   h = the piezometric level

Appendix 3B Leaky Aquifer Theory

Theory to describe leaky aquifer behaviour incorporating reflection was derived by Carrington and Thomas in May 1994 and is outlined in Carrington (1994). The derivation is as follows.

Figure 3B.1 illustrates the conceptual model of the Durham Model Aquifer. Analytical theory was derived to describe pressure head variations with horizontal distance, x. This incorporated dimensions of the aquifer and properties leakage and permeability. The governing equation describing groundwater flow in such a one-dimensional leaky aquifer is given by Bear (1979) as follows:

$$T\left(\frac{d^2h}{dx^2}\right) = \beta h \quad \text{...........................eqtn (3B.1)}$$

where T = transmissivity

      h = head of water

      x = horizontal distance

      ß = leakage coefficient

In an attempt to solve equation 3B.1, a solution of the form shown below was tried

$$h = \gamma \exp(\alpha x) \quad \text{.......................eqtn (3B.2)}$$

where γ and α are arbitrary constants.

Differentiating eqtn (3B.2) with respect to x:

$$\frac{dh}{dx} = \gamma\alpha \exp(\alpha x) \quad \text{..................eqtn (3B.3)}$$

$$\frac{d^2h}{dx^2} = \gamma\alpha^2 \exp(\alpha x) \quad \text{...............eqtn (3B.4)}$$

Substituting eqtns (3B.4) and (3B.2) into the governing equation (3B.1):

$$T\left(\gamma\alpha^2 \exp(\alpha x)\right) = \beta\left(\gamma \exp(\alpha x)\right) \quad \text{...................eqtn (3B.5)}$$

Therefore

$$T\left(\alpha^2\right) = \beta \quad \text{........................eqtn (3B.6)}$$

and

$$\alpha = \pm\sqrt{\frac{\beta}{T}}$$ ....eqtn (3B.7)

This was substituted back into eqtn (3B.2).

$$h = \gamma \exp\left(-\sqrt{\frac{\beta}{T}}x\right)$$ ....eqtn (3B.8)

It was noted that the following solution for α was correct considering pressure head, h

to be positive.

$$\alpha = -\sqrt{\frac{\beta}{T}}$$

Applying the following boundary conditions

$x = 0$ and $h = h_B =$ head of water in water tank

This results in $h_B = \gamma$ which when substituted into eqtn (3B.8) gives the following:

$$h = h_B \exp\left(-\sqrt{\frac{\beta}{T}}x\right)$$ ....eqtn(3B.9)

Also, boundary conditions at $x = 0$, $W = -K\dfrac{dh}{dx}$

where W = Darcy velocity

   K = hydraulic conductivity

Differentiating eqtn (3B.9)

$$\frac{dh}{dx} = h_B - \sqrt{\frac{\beta}{T}}\exp\left(-\sqrt{\frac{\beta}{T}}x\right)$$ ....eqtn (3B.10)

Applying boundary conditions to eqtn (3B.10) provides:

$$\left(-\frac{W}{K}\right) = -h_B\sqrt{\frac{\beta}{T}}$$ ....eqtn (3B.11)

Recalling eqtn (1.3) which relates transmissivity to permeability, K.

T=Kb....................eqtn (1.3) recalled

Also, the darcy velocity is defined as the flowrate of groundwater per unit area into

the aquifer face.

W=Q/A = Q/bw......................eqtn (3B.12)

where Q = flowrate

   A = area of aquifer face

w = width of the aquifer

Substitution of the above information into eqtn (3B.11) gives the following:

$$h = W\sqrt{\frac{b}{K\beta}}\,\exp\left(-\sqrt{\frac{\beta}{T}}x\right)$$ ....eqtn(3B.13)

Eqtn (3.13) provides the relationship between pressure head and horizontal distance a specific aquifer with given properties, permeability and leakage.

In order to apply this equation to the Durham Model Aquifer, the effects of a single reflection from the end of the aquifer were considered. This is illustrated in Figure 3B.2. where Q_1 and Q_2 represent the two finite volumetric flow rates into the system, whilst h_1 and h_2 represent the resulting heads.

Considering an aquifer of finite length, L, the effects of two finite flow rates applied at opposite ends of an aquifer of length 2L were combined using image well theory to incorporate reflection.

$$h_1 = \frac{Q_1}{A}\sqrt{\frac{b}{K\beta}}\,\exp\left(-\sqrt{\frac{\beta}{T}}x\right)\ \text{where } x = 0;$$

$$\Rightarrow h_1 = \frac{Q_1}{A}\sqrt{\frac{b}{K\beta}}$$ ....eqtn(3B.14)

$$h_2 = \frac{Q_1}{A}\sqrt{\frac{b}{K\beta}}\,\exp\left(-\sqrt{\frac{\beta}{T}}x\right)\ \text{where } x = 2L$$

$$\Rightarrow h_2 = \frac{Q_1}{A}\sqrt{\frac{b}{K\beta}}\,\exp\left(-2\sqrt{\frac{\beta}{T}}L\right)$$ ....eqtn(3B.15)

Applying the principal of superposition, adding eqtn(3B.14) and eqtn(3B.15), and designating h_B as the sum of the two heads, h_1 and h_2

$$h_B = h_1 + h_2 = \frac{Q}{A}\sqrt{\frac{b}{K\beta}}\left\{1 + \exp\left(-2\sqrt{\frac{\beta}{T}}L\right)\right\}$$ ....eqtn(3B.16)

There are several reflections similar to those described above extending an infinite distance from the aquifer in both directions. The actual theoretical value of volumetric flow rate at each point must be thereofore be 2Q. This is illustrated in Figure 3B.3. At the boundary where the flow rate is applied, the *total* head realised is the sum of all waves produced from boundaries distances 2L, 4L, 6L....away, together with the

head induced by the applied flow rate. Obviously, these boundaries will occur in both directions from the position under question, and therefore a multiplication of two will be involved.

Recalling eqtn (3B.16) above, and arranging this to incorporate the above reflections

$$h_1 = \frac{Q}{A}\sqrt{\frac{b}{K\beta}}\left\{1 + 2\exp\left(-2L\sqrt{\frac{\beta}{T}}\right) + 2\exp\left(-4L\sqrt{\frac{\beta}{T}}\right) + 2\exp\left(-6L\sqrt{\frac{\beta}{T}}\right) + 2\exp\left(-8L\sqrt{\frac{\beta}{T}}\right) + \dots\right\} \dots \text{eqtn(3B.17)}$$

where h_1 is the head of water above the datum (defined as the phreatic surface of leaked water overlying the aquifer) at the position where volumetric flow rate, Q, is applied.

Similarly, the theory can also be applied to head of water, h_2 above datum at the end of the aquifer as shown by the dashed line in Figure 3B.3. At this boundary, the *total* head realised will be the sum of volumetric flow rates produced at boundaries of distances L, 3L, 5L....away. A flow rate is not applied at this boundary and therefore consideration need only be given to reflected effects.

$$h_2 = \frac{2Q}{A}\sqrt{\frac{b}{K\beta}}\left\{\exp\left(-L\sqrt{\frac{\beta}{T}}\right) + \exp\left(-3L\sqrt{\frac{\beta}{T}}\right) + \exp\left(-5L\sqrt{\frac{\beta}{T}}\right) + \exp\left(-7L\sqrt{\frac{\beta}{T}}\right) + \dots\right\} \dots\dots \text{eqtn(3B.18)}$$

This analytical solution was verified using the computer finite element model, Curved Valley Model (CVM), and found to be correct. Details of this verification are given in Carrington (1994).
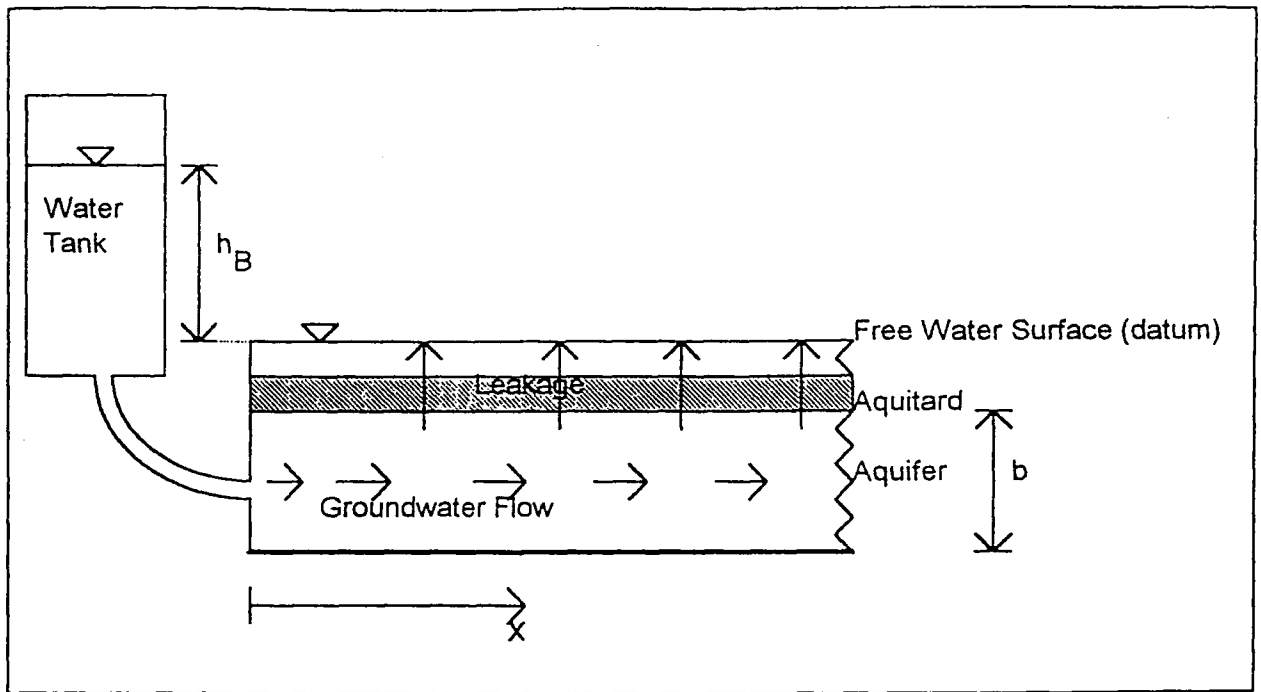
Figure 3B-1. Flow in the Durham Model Aquifer (a leaky aquifer system).
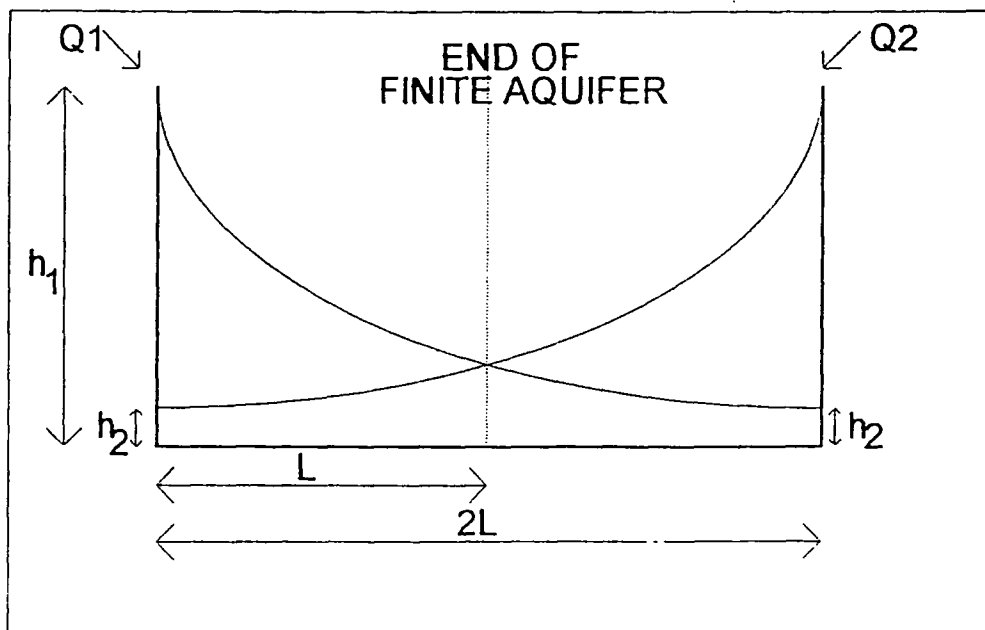
Figure 3B-2. Image Well Theory
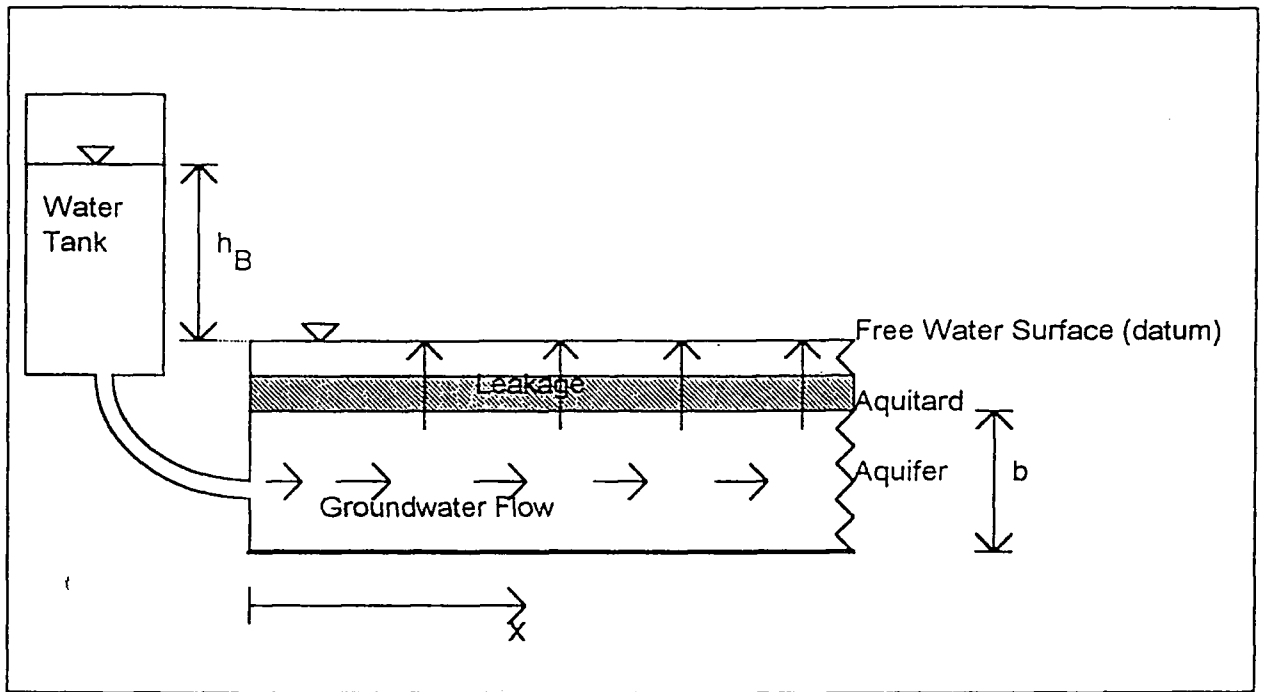
Figure 3B-1. Flow in the Durham Model Aquifer (a leaky aquifer system).
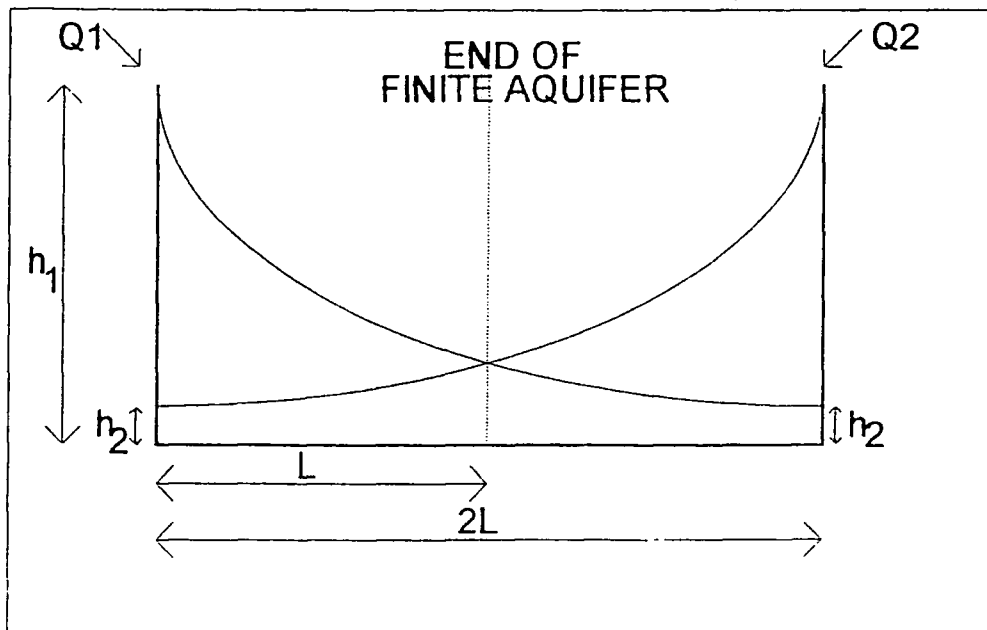
Figure 3B-2. Image Well Theory
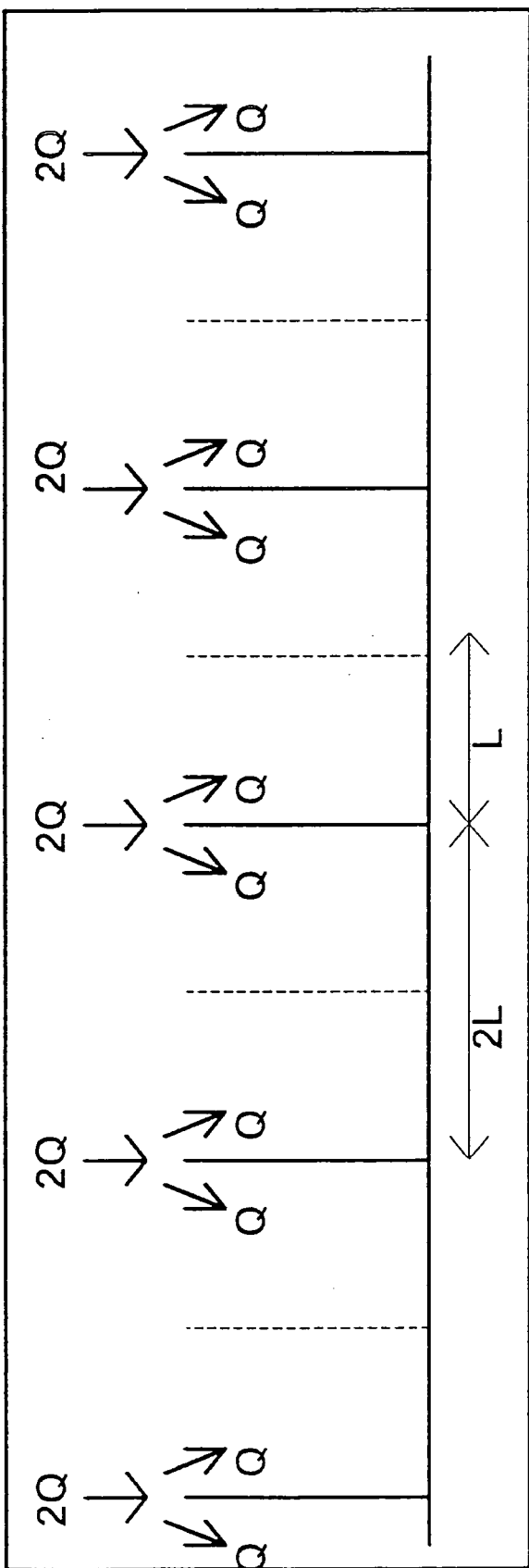
Figure 3B-3. Infinite Image Well Theory

Appendix 3C-1. Manual Tidal Simulation. Wave Spectra from Fast Fourier Transform Analysis. Position 3.
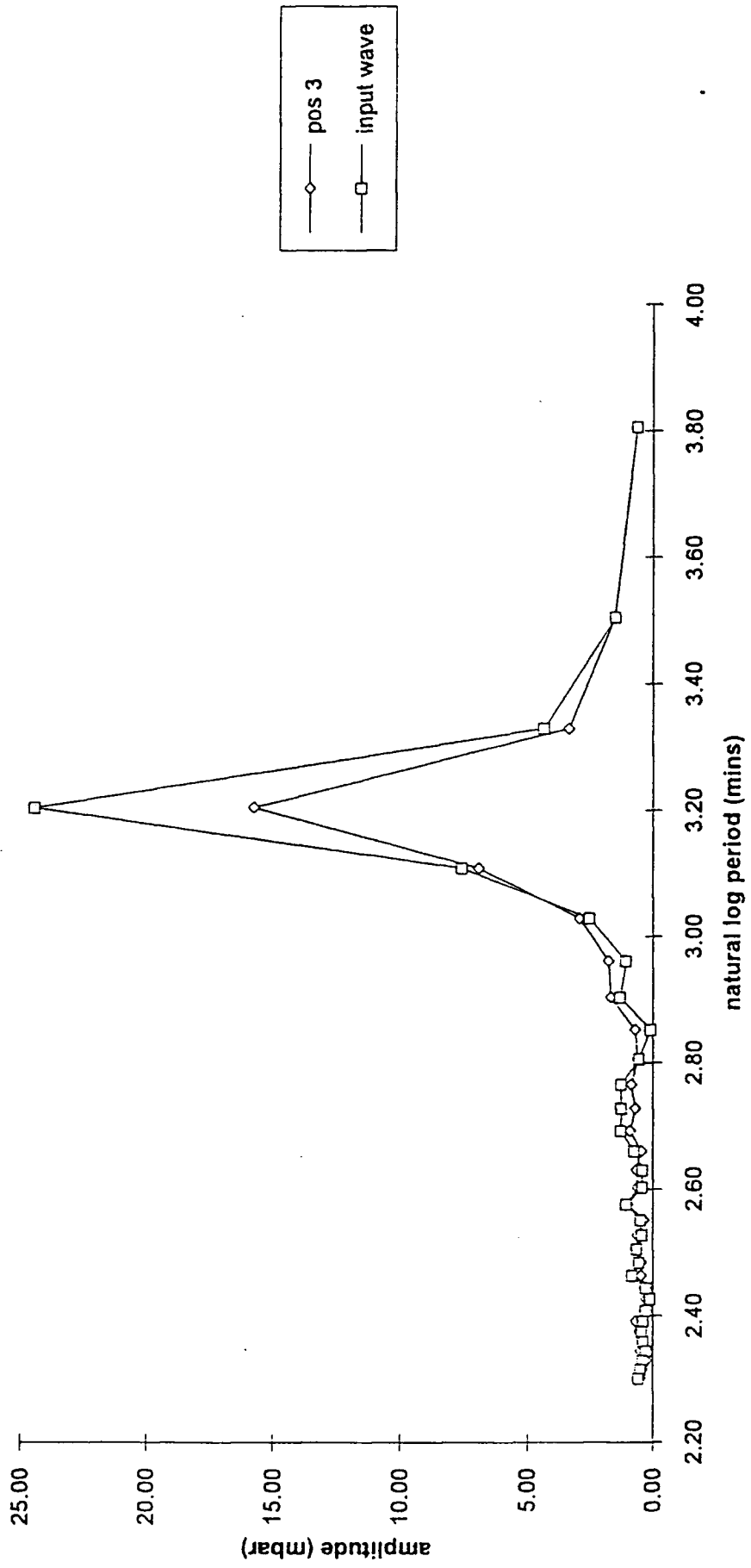
Appendix 3C-2. Manual Tidal Simulation. Wave Spectra from Fast Fourier Transform Analysis. Position 5.
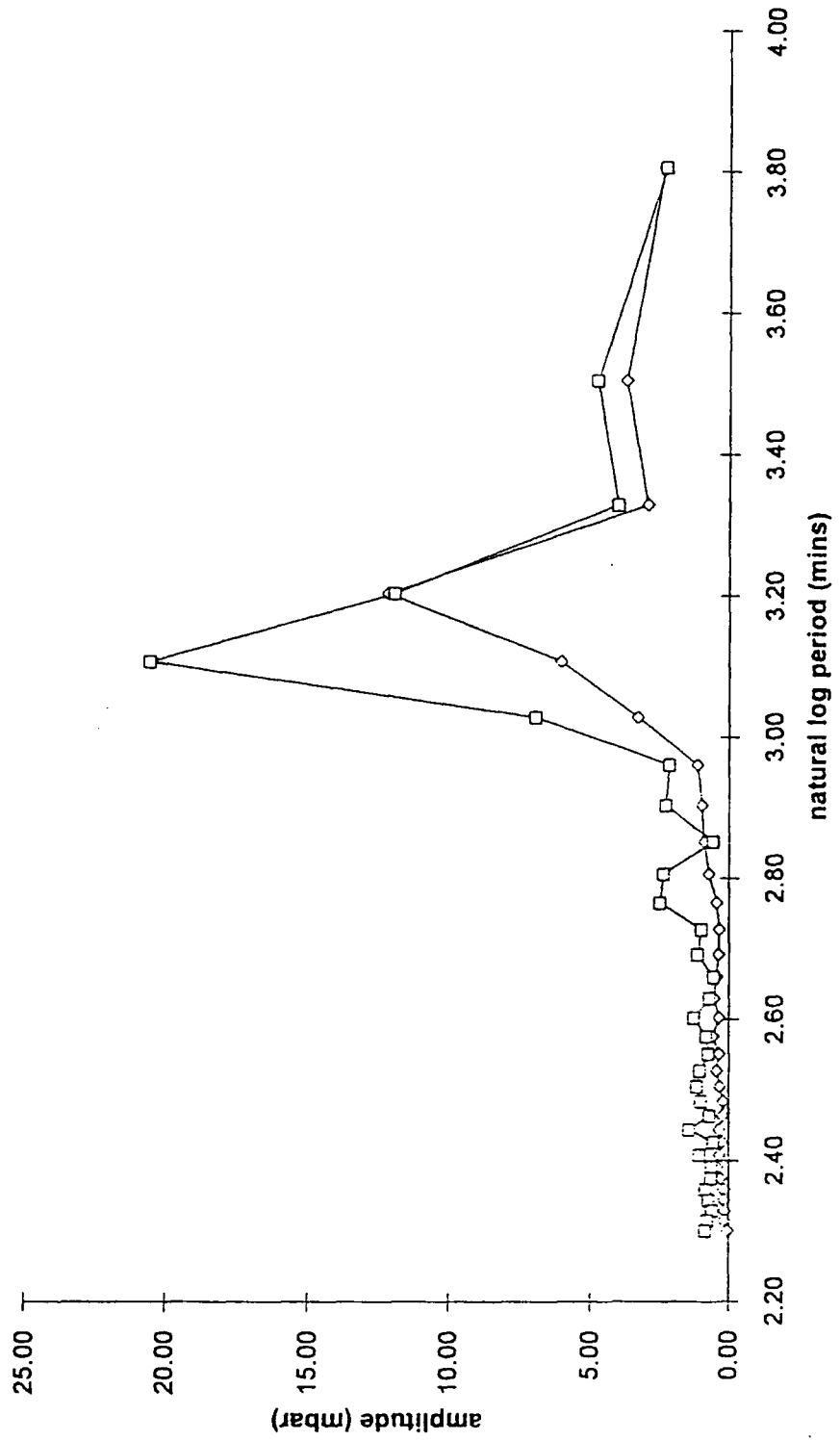
Appendix 3C-3. Manual Tidal Simulation. Wave Spectra from Fast Fourier Transform Analysis. Position 8.
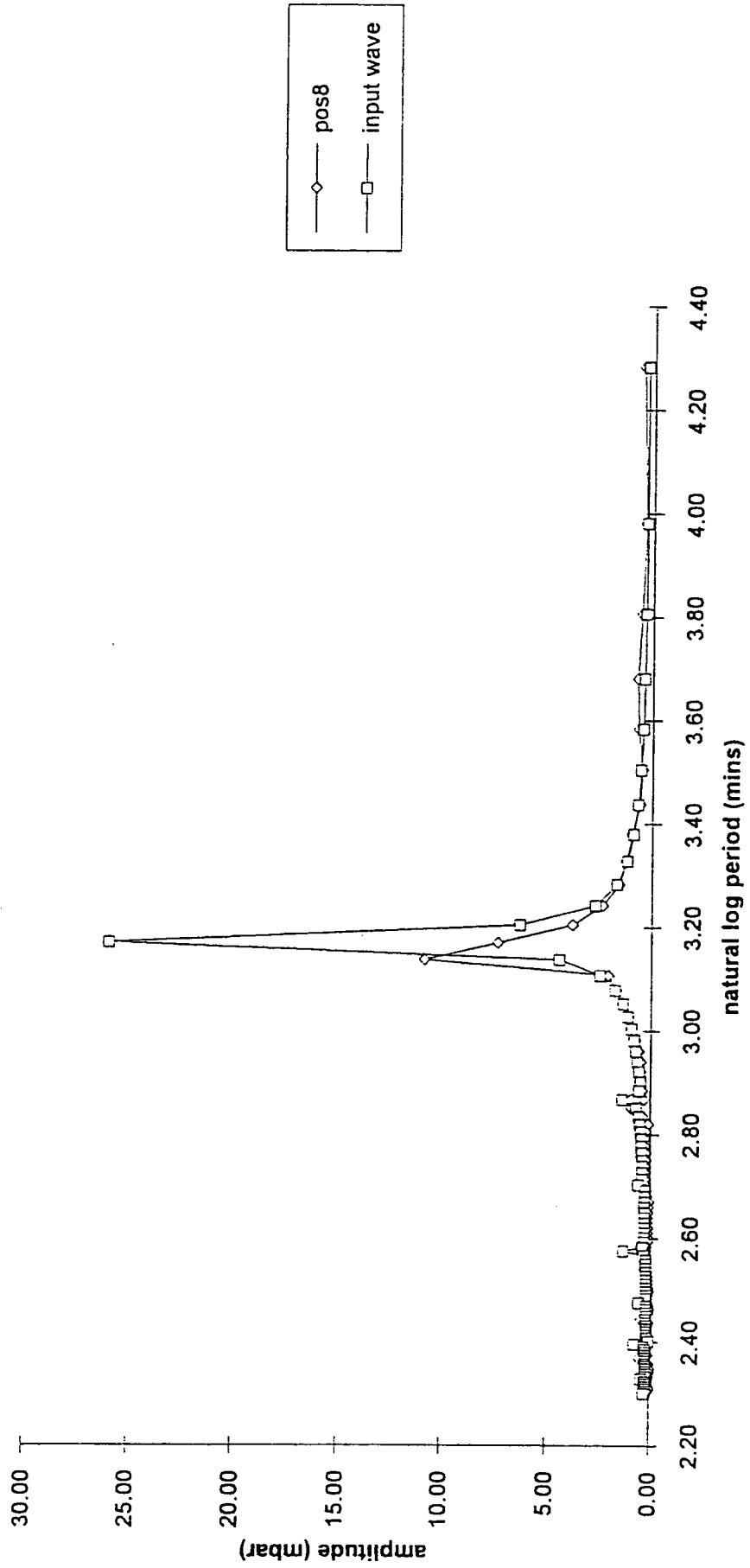
Appendix 3C-4. Manual Tidal Simulation. Wave Spectra from Fast Fourier Transform Analysis. Position 10.
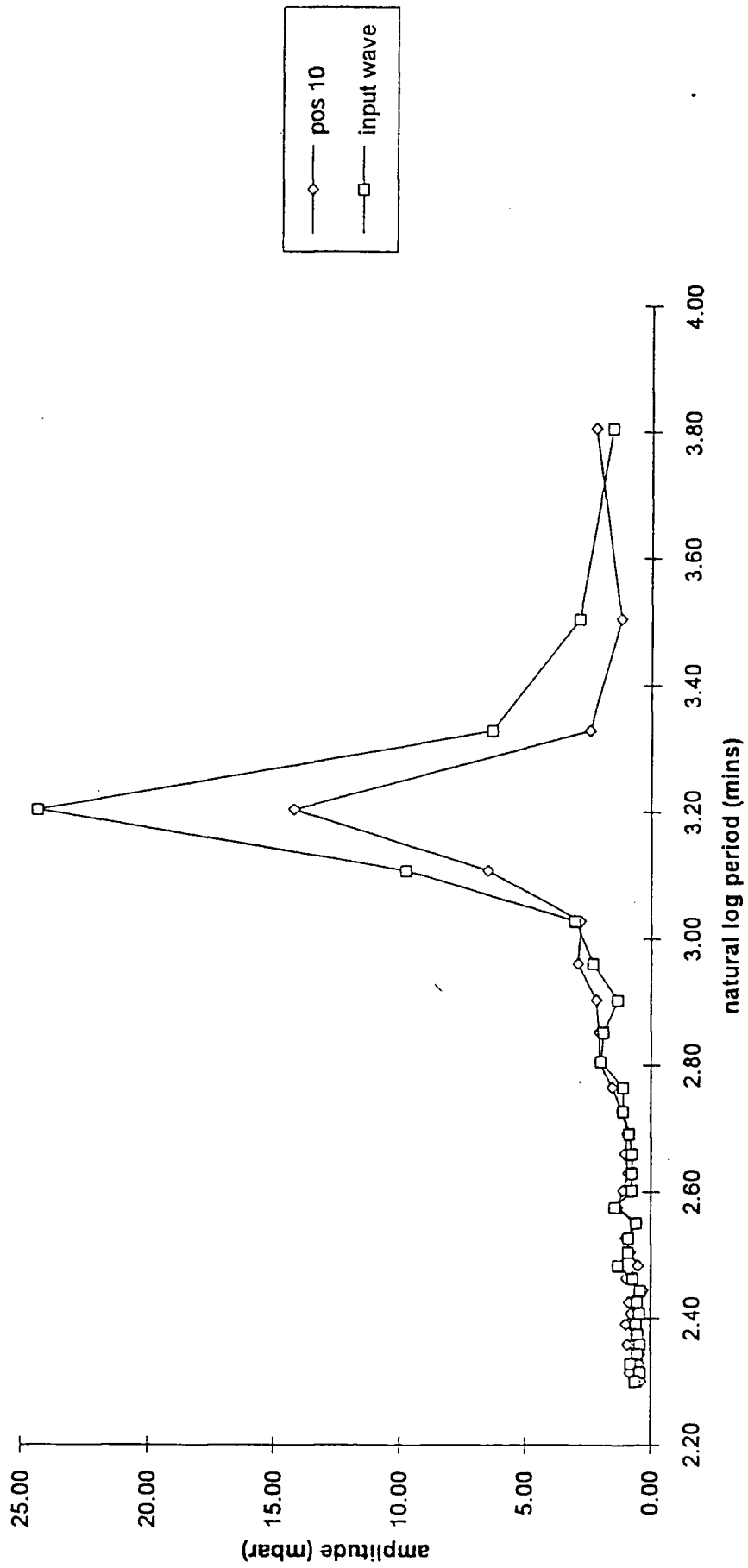
Appendix 3C-5. Manual Tidal Simulation. Wave Spectra from Fast Fourier Transform Analysis. Position 12.
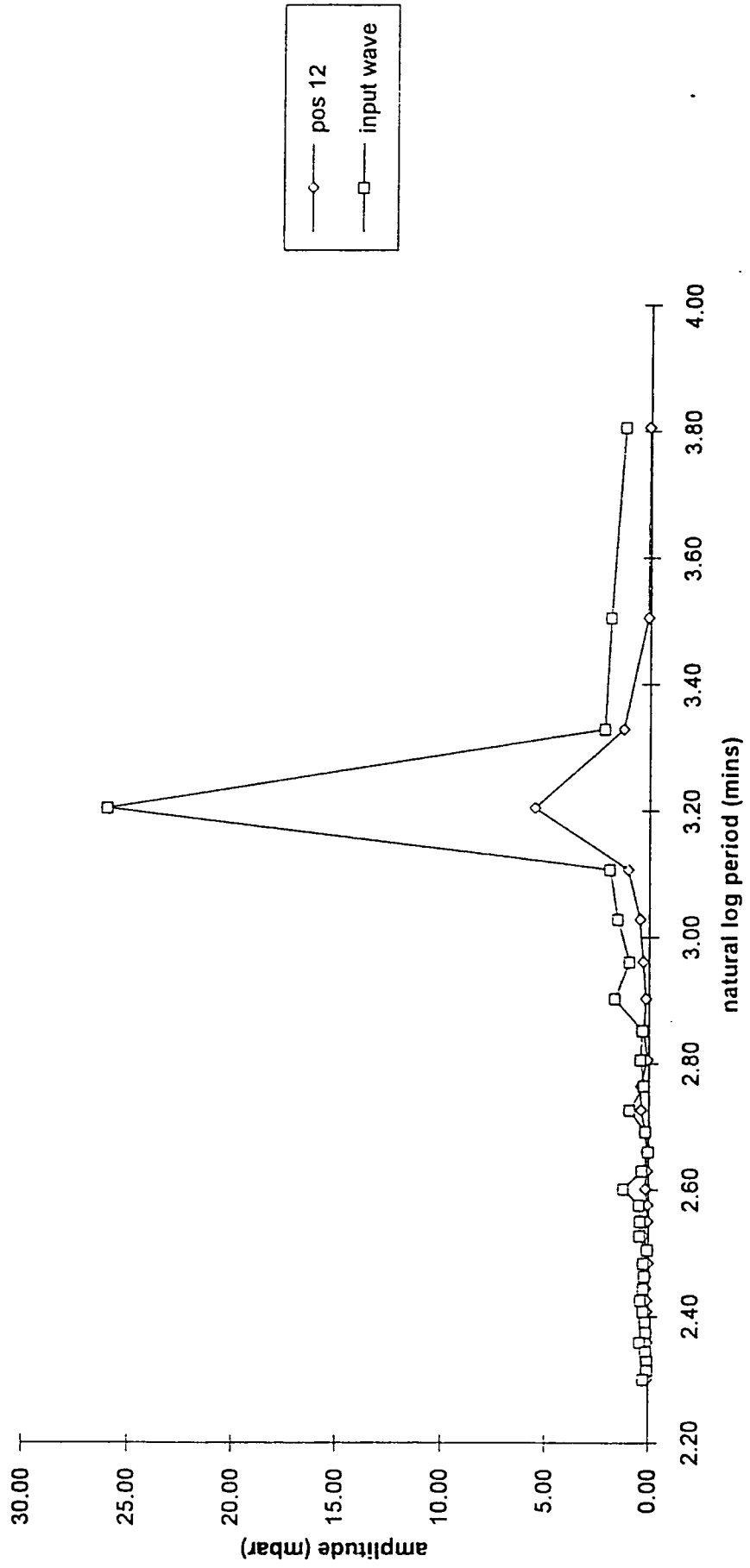
Appendix 3D

## Pore Water Pressure Results from Electrical Tidal Simulation

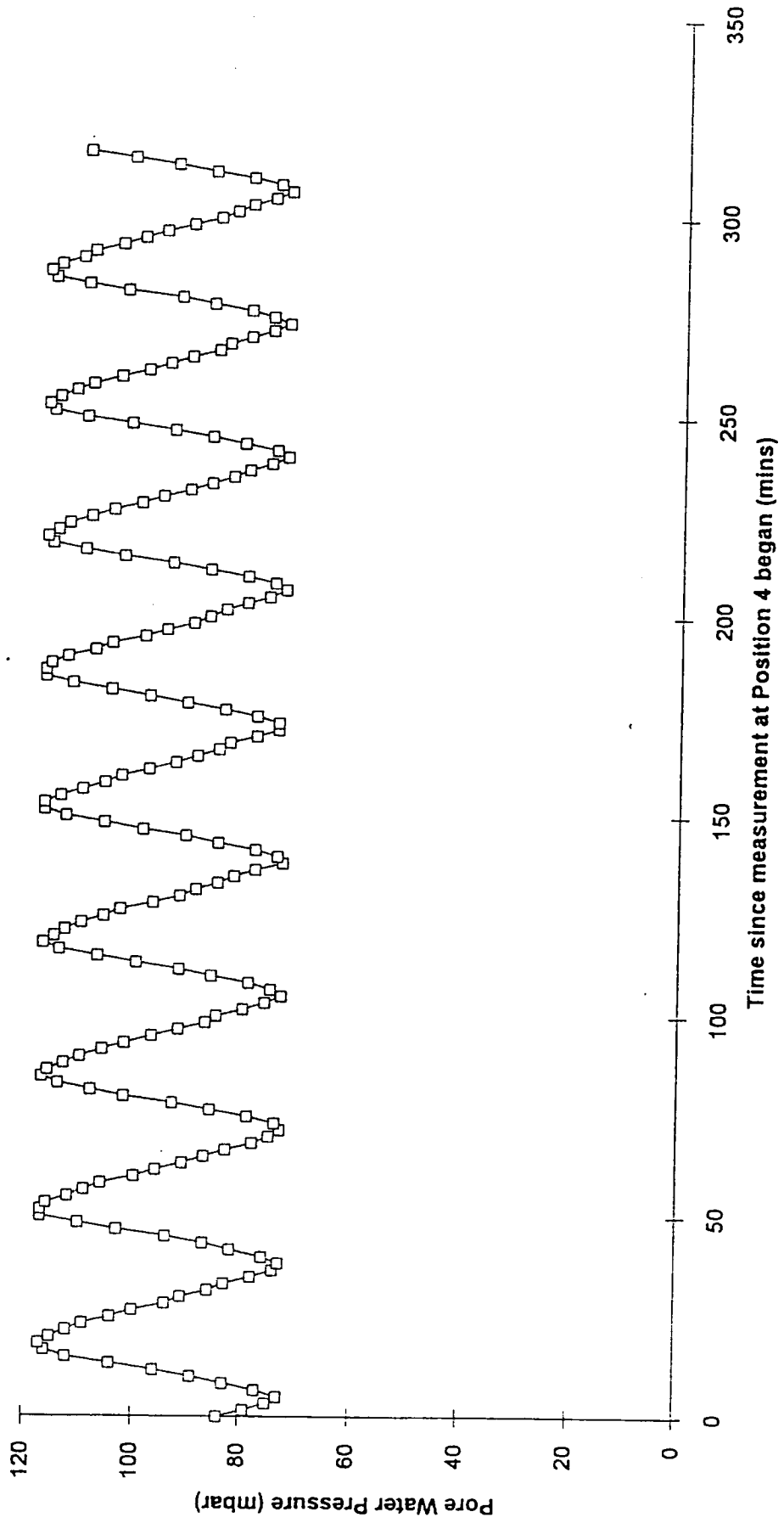**Appendix 3D-1. Series 1. Pore Water Pressure Variations at Position 1 (in base of tidal tank).**
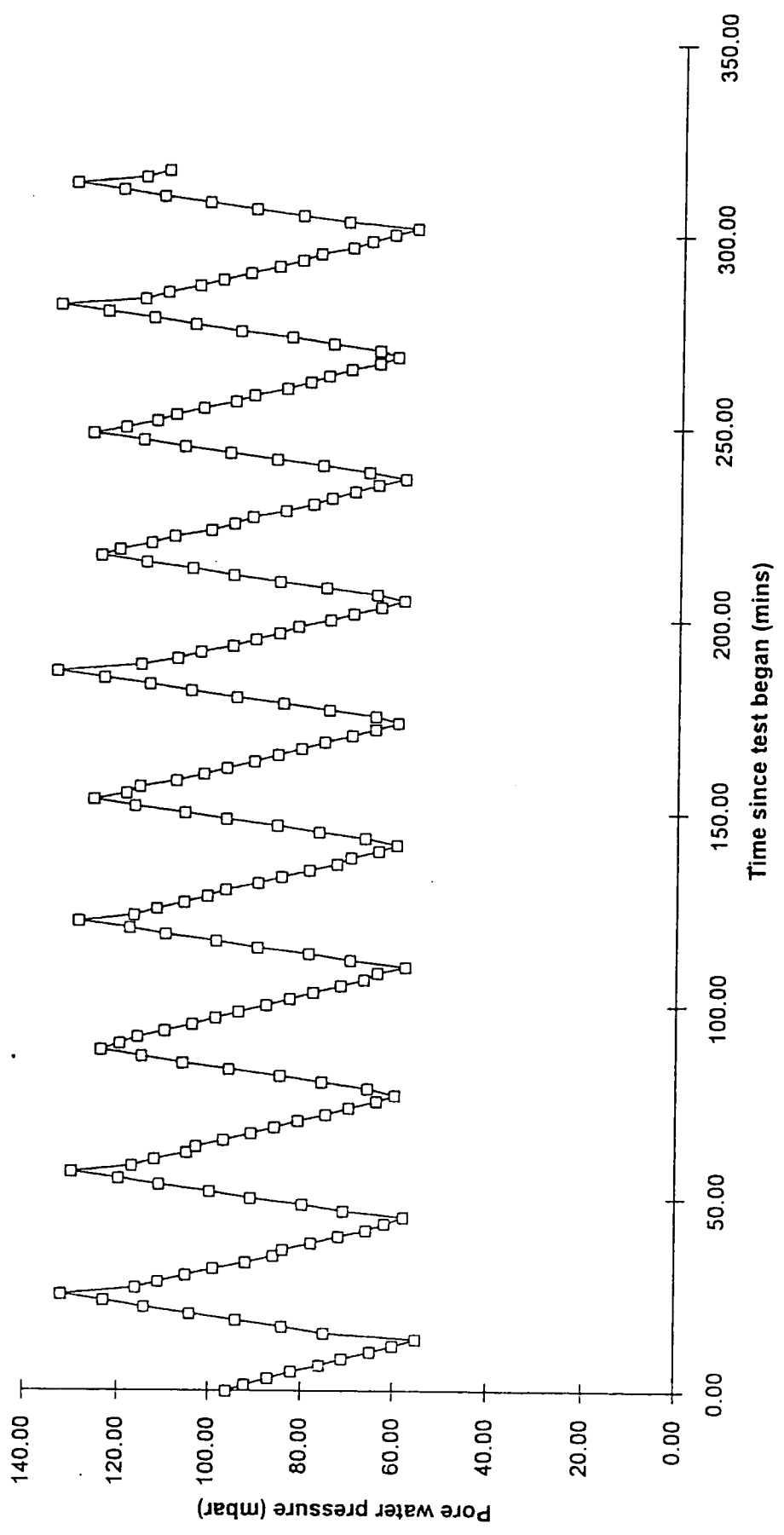
Appendix 3D-2. Series 1. Pore Water Pressure Variations at Position 2.
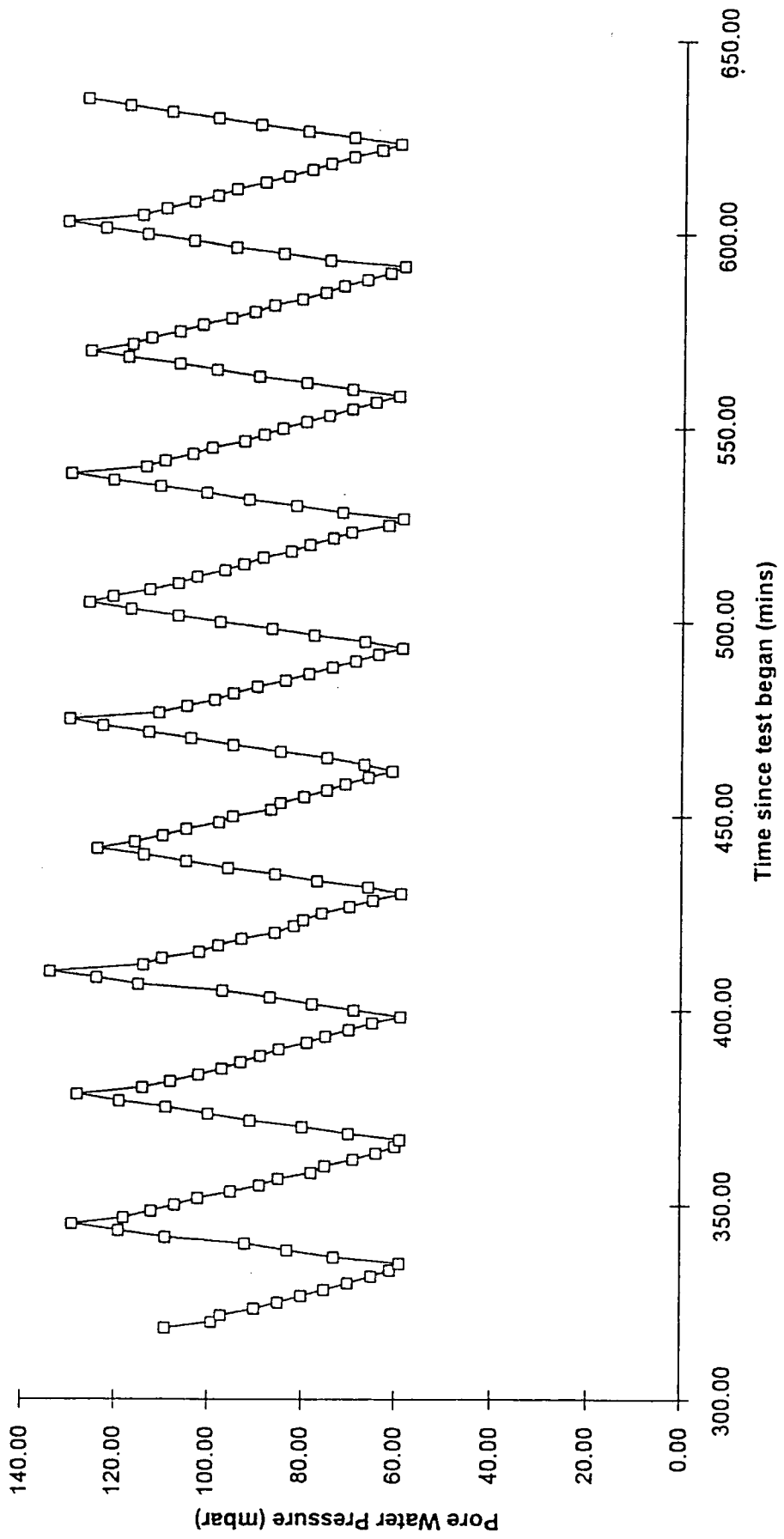
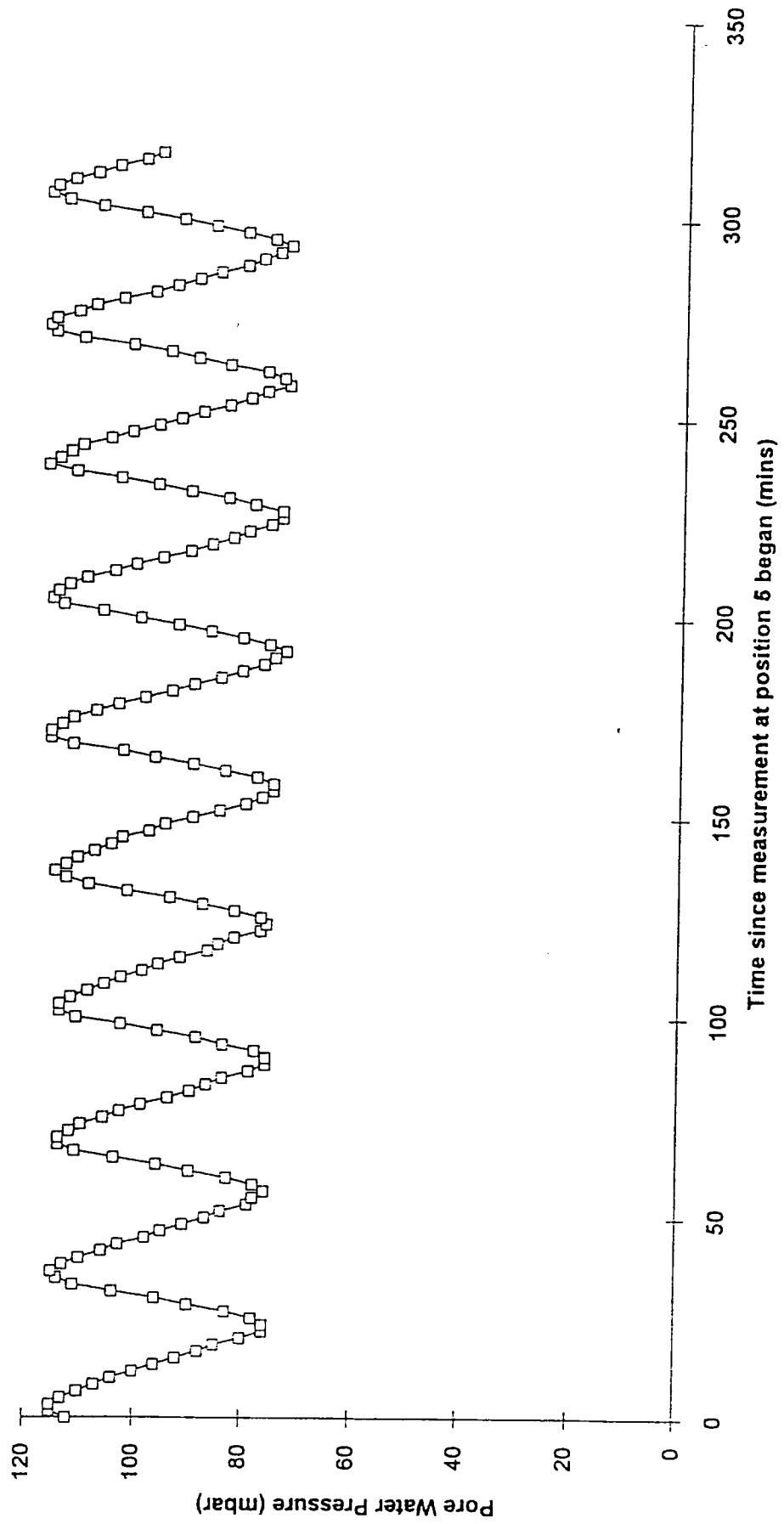Appendix 3D-3. Series 1. Pore Water Pressure Variations at Position 3.
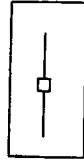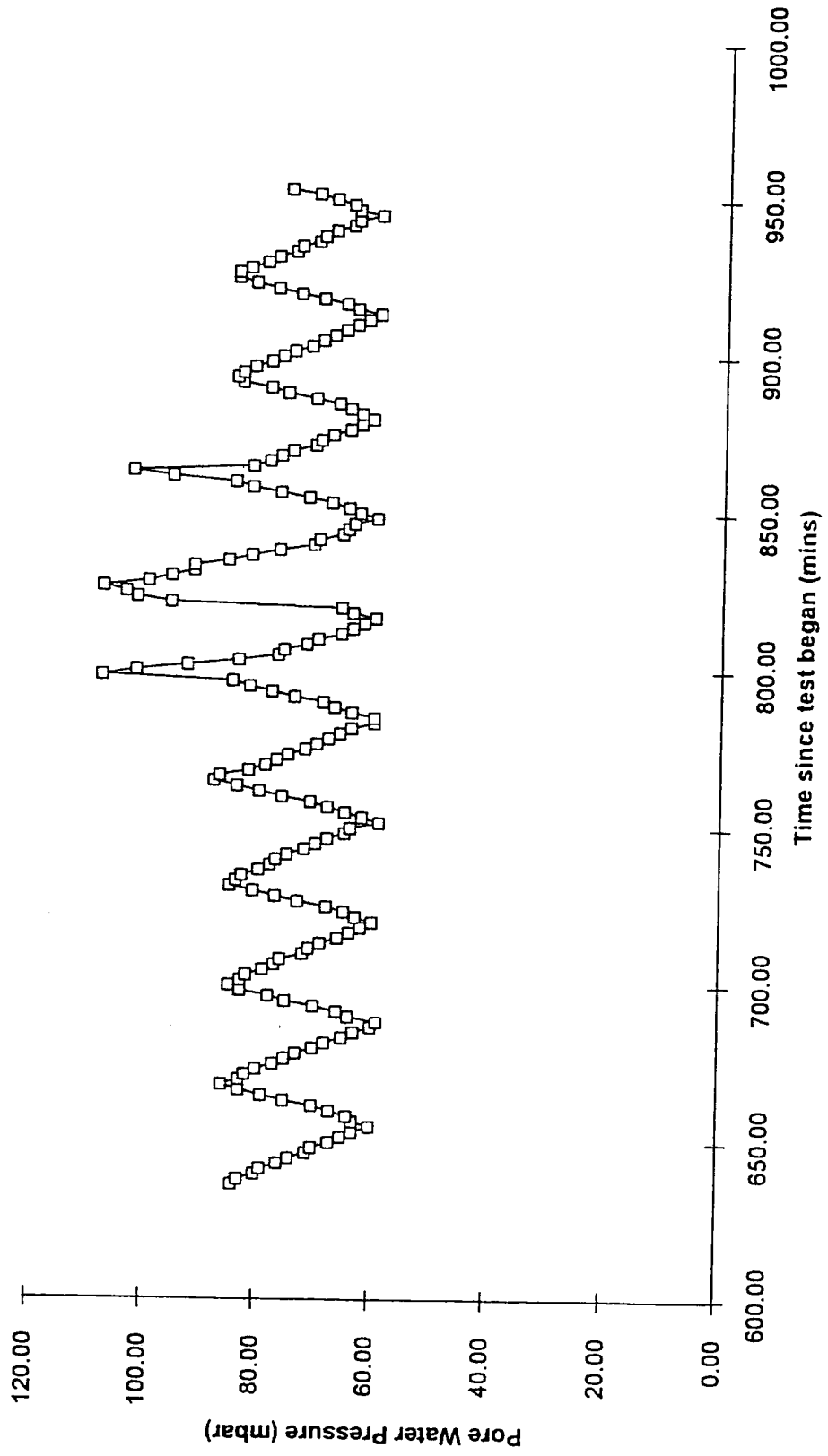
Appendix 3D-5. Series 1. Pore Water Pressure Variations at Position 5.

Time since test began (mins)

Pore water pressure (mbar)
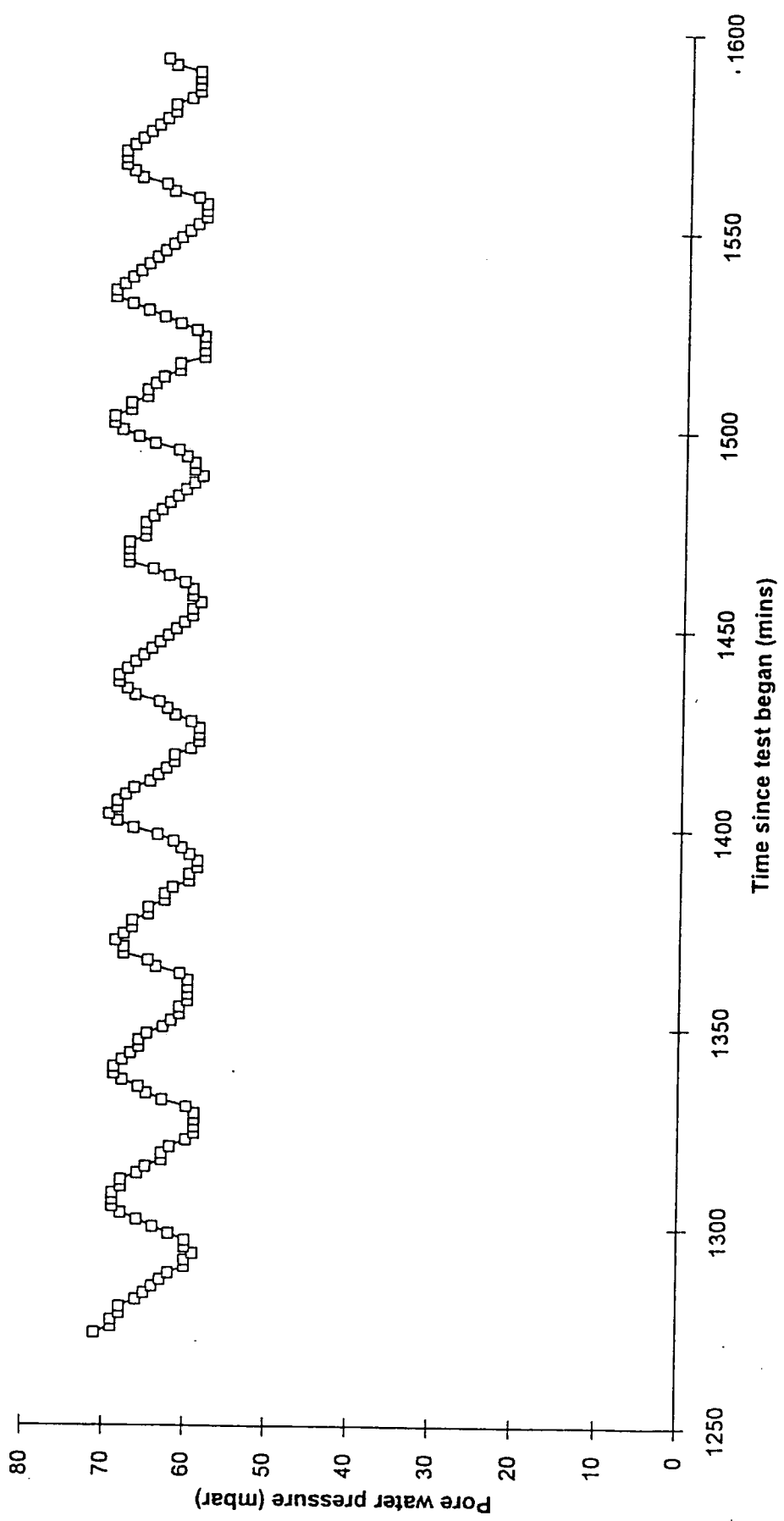
Appendix 3D-6. Pore Water Pressure Variations at Position 6. Series 1.
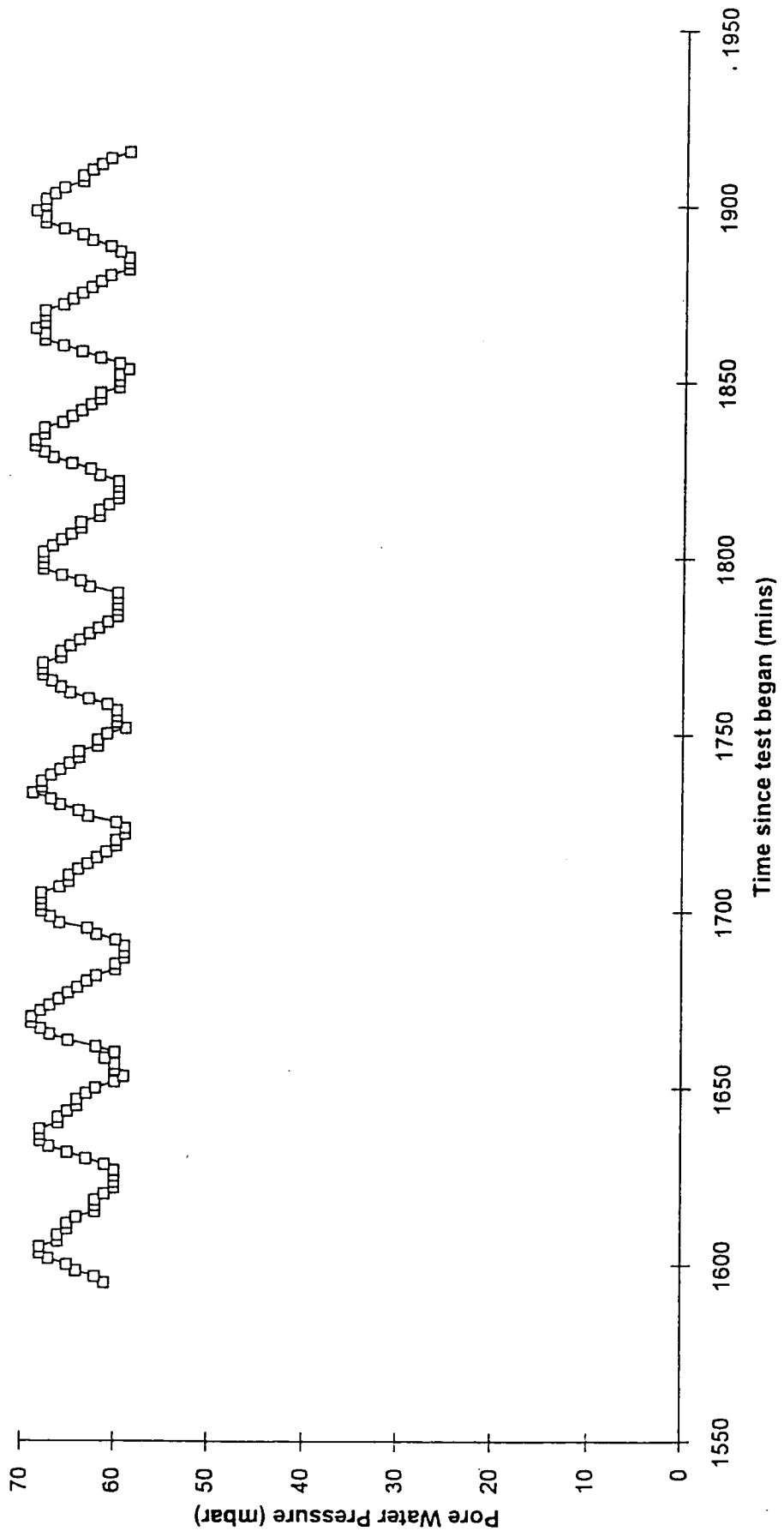
Appendix 3D-7. Pore Water Pressure Variations at Position 7. Series 1.
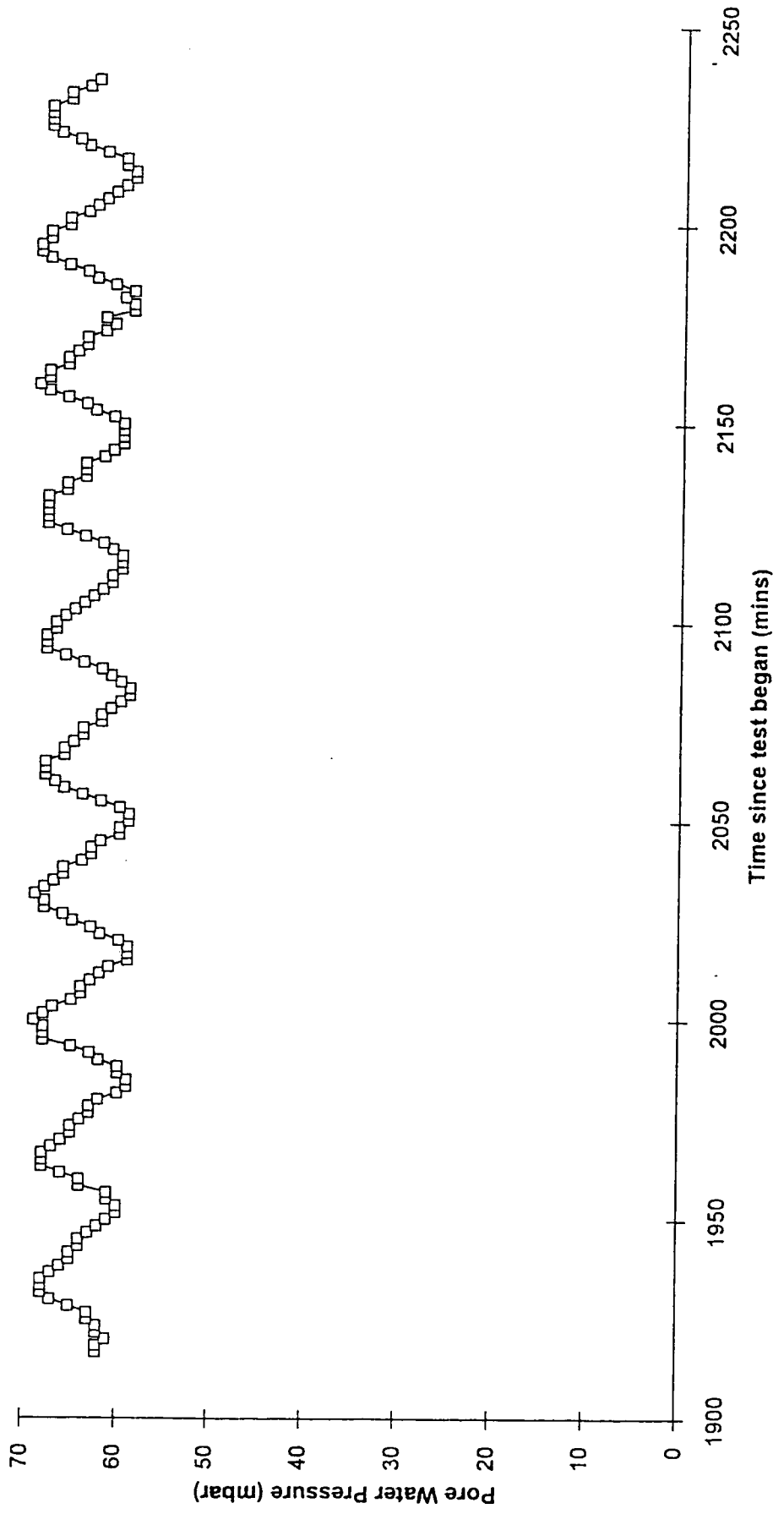
Appendix 3D-8. Pore Water Pressure Variations at Position 8. Series 1.
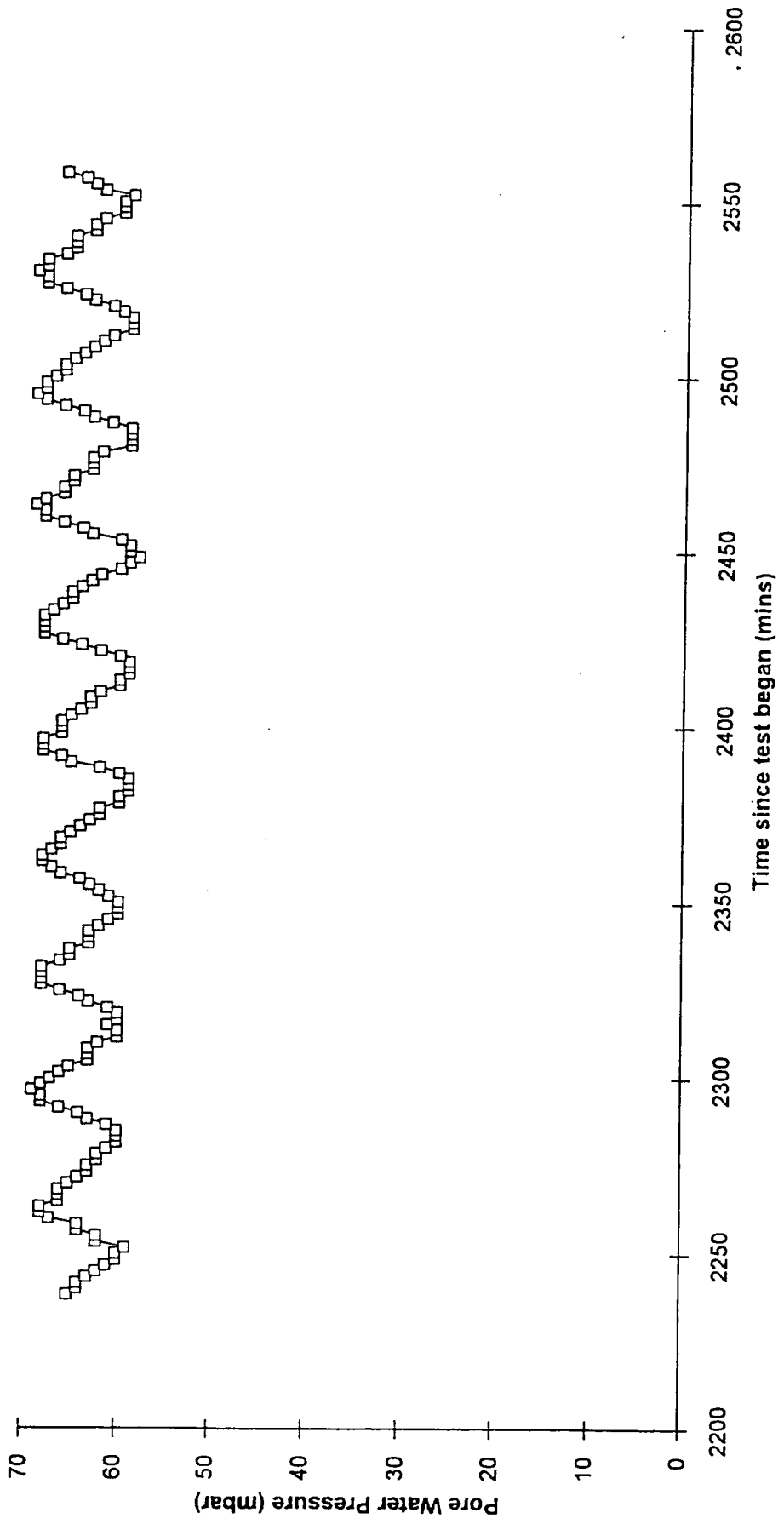
Appendix 3D-9. Series 1. Pore Water Pressure Variations at Position 9.
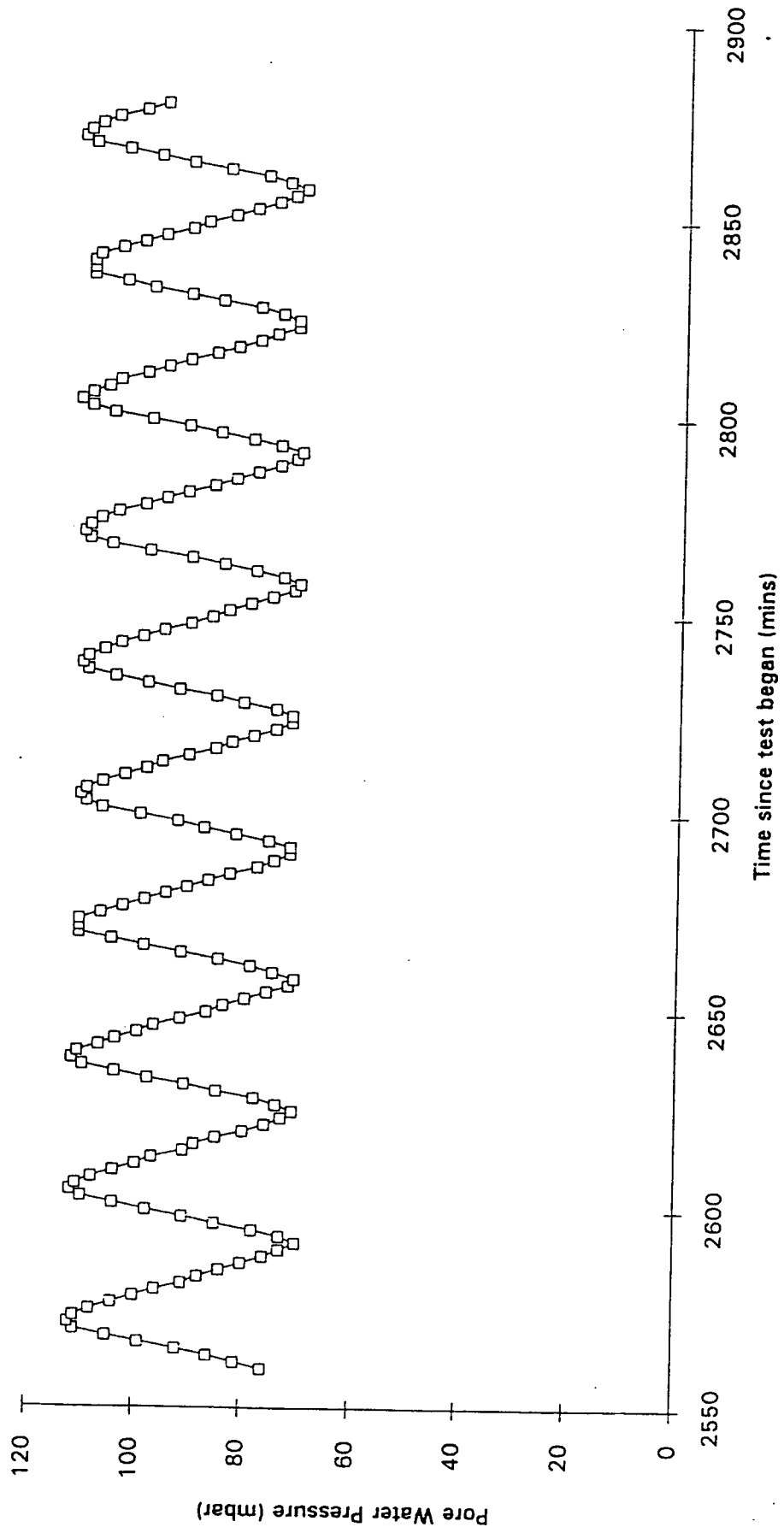
Appendix 3D-10. Series 1. Pore Water Pressure Variations at Position 10.
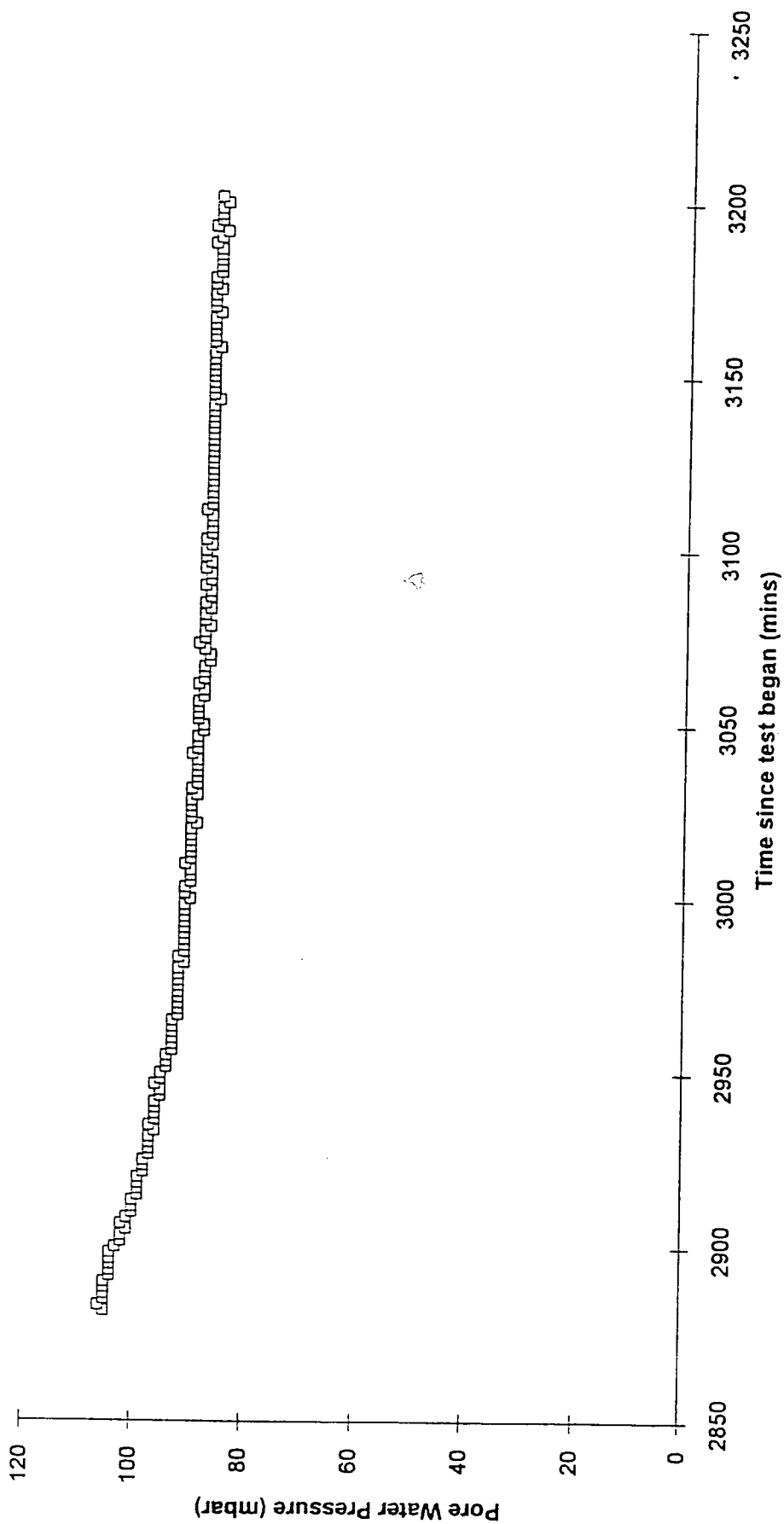
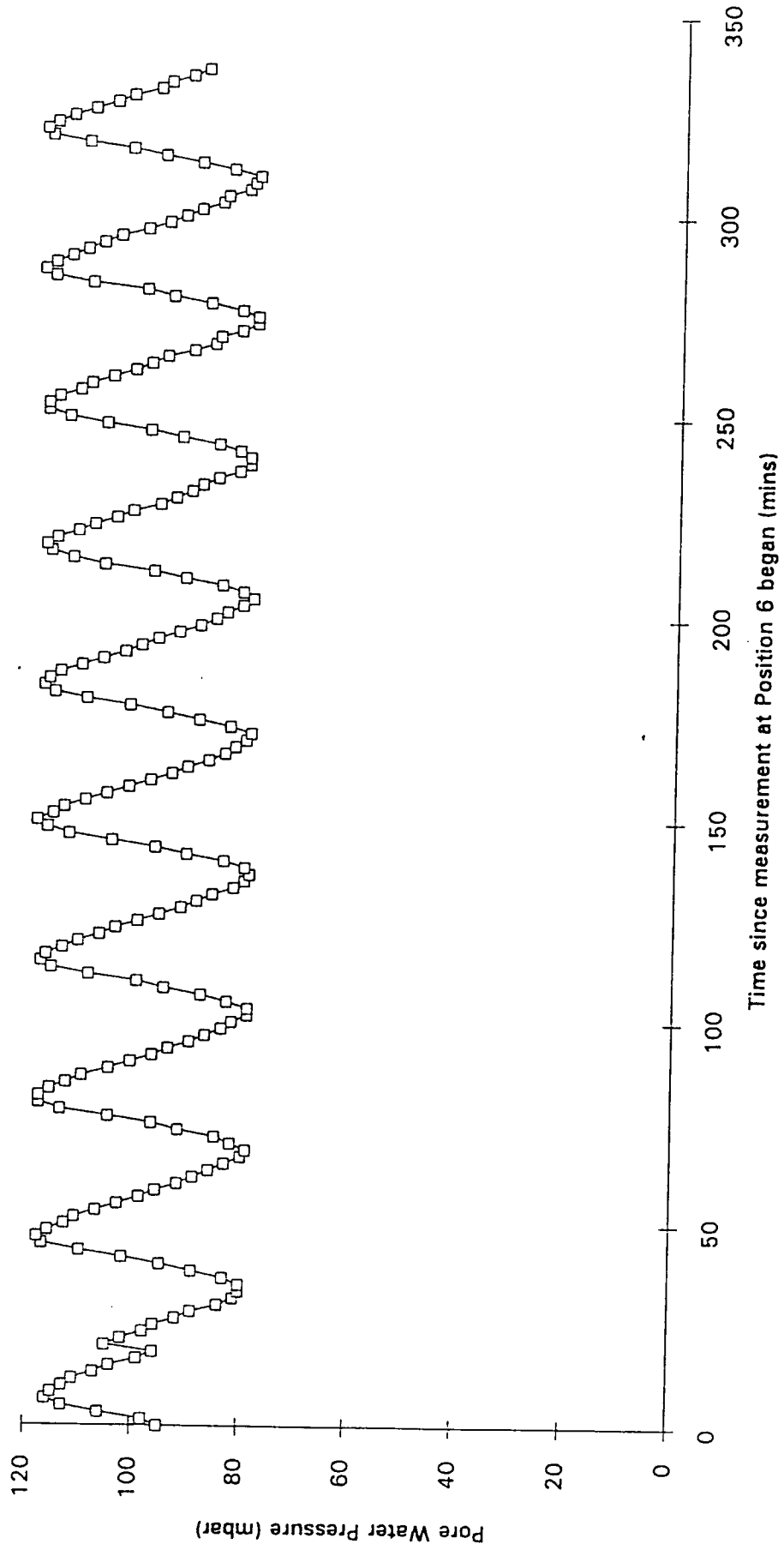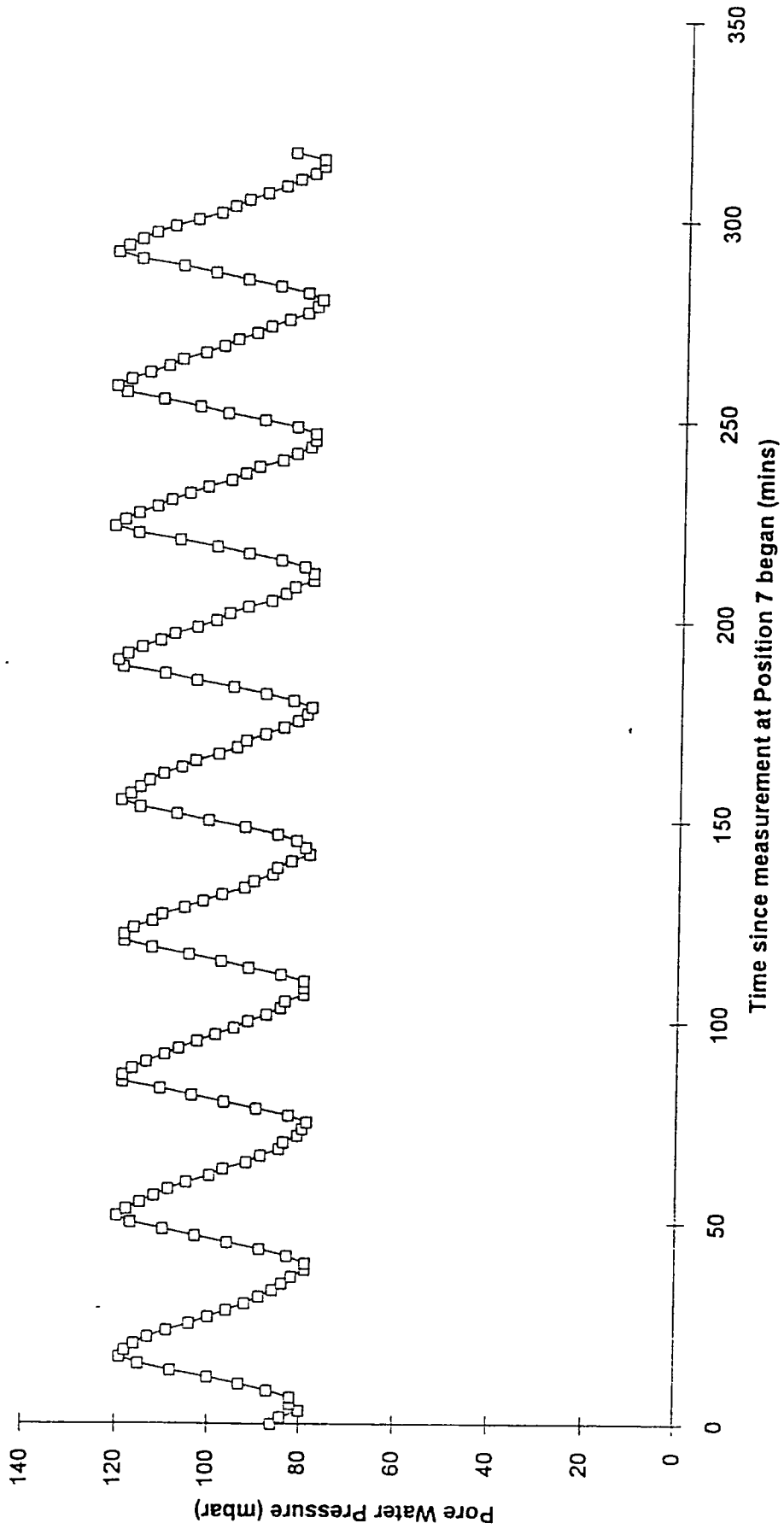Appendix 3D-11. Series 1. Pore Water Pressure Variations at Position 11.
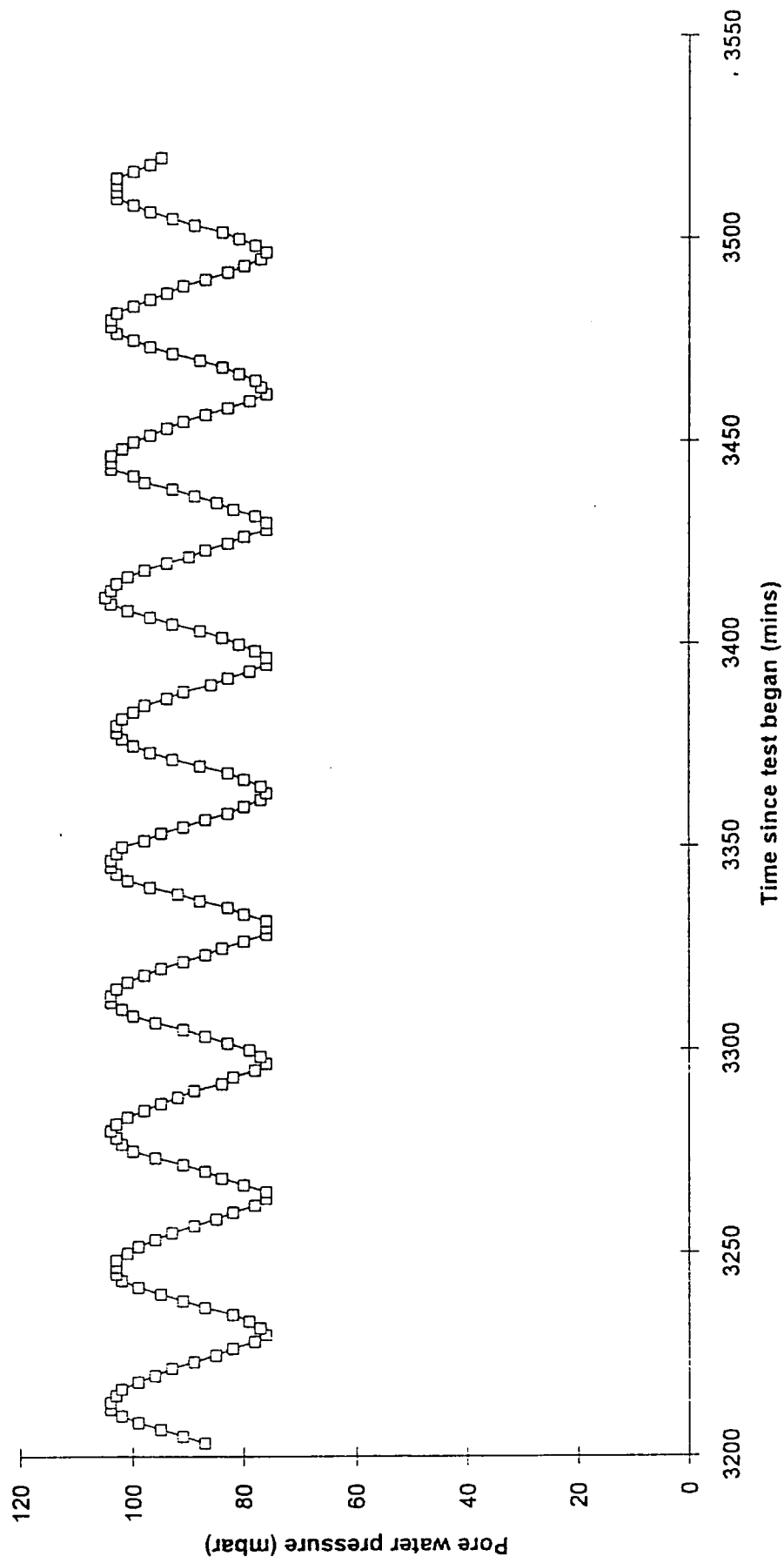
Appendix 3D-12. Series 1. Pore Water Pressure Variations at Position 12.
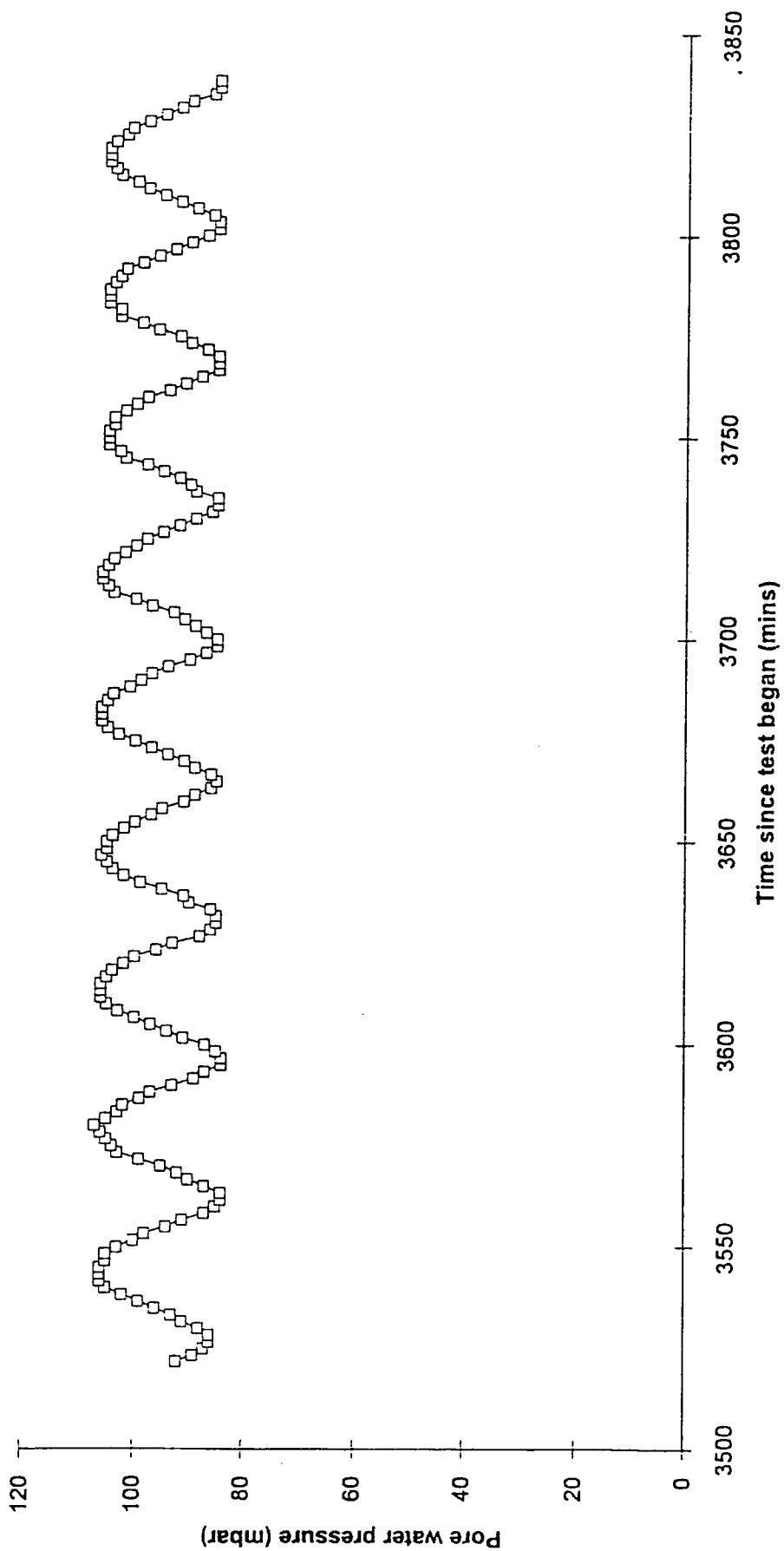
Appendix 3D -13. Series 2. Pore Water Pressure Variations at Position 1 (in base of tidal tank).
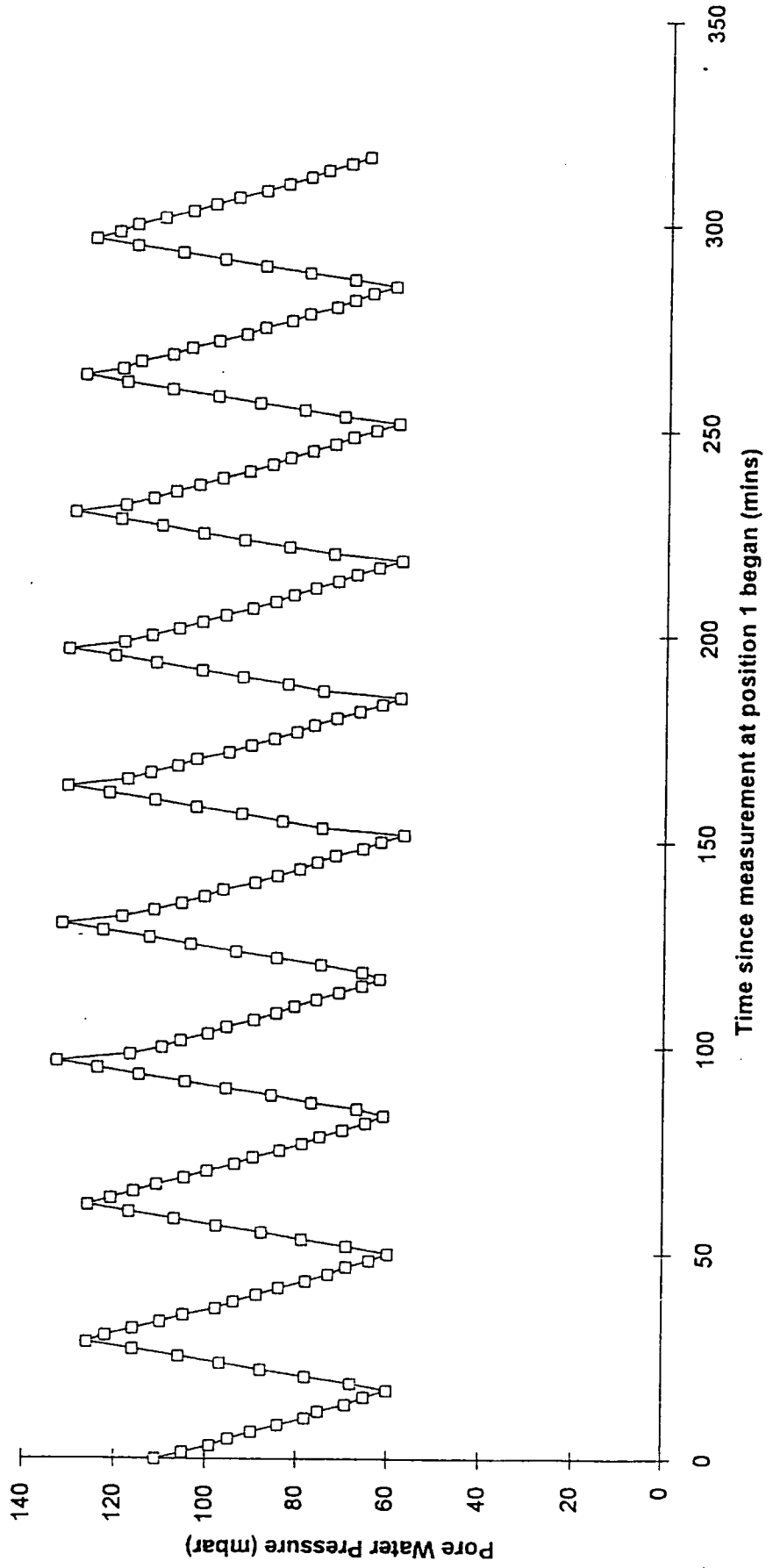
Appendix 3D-14. Series 2. Pore Water Pressure Variations at Position 2.
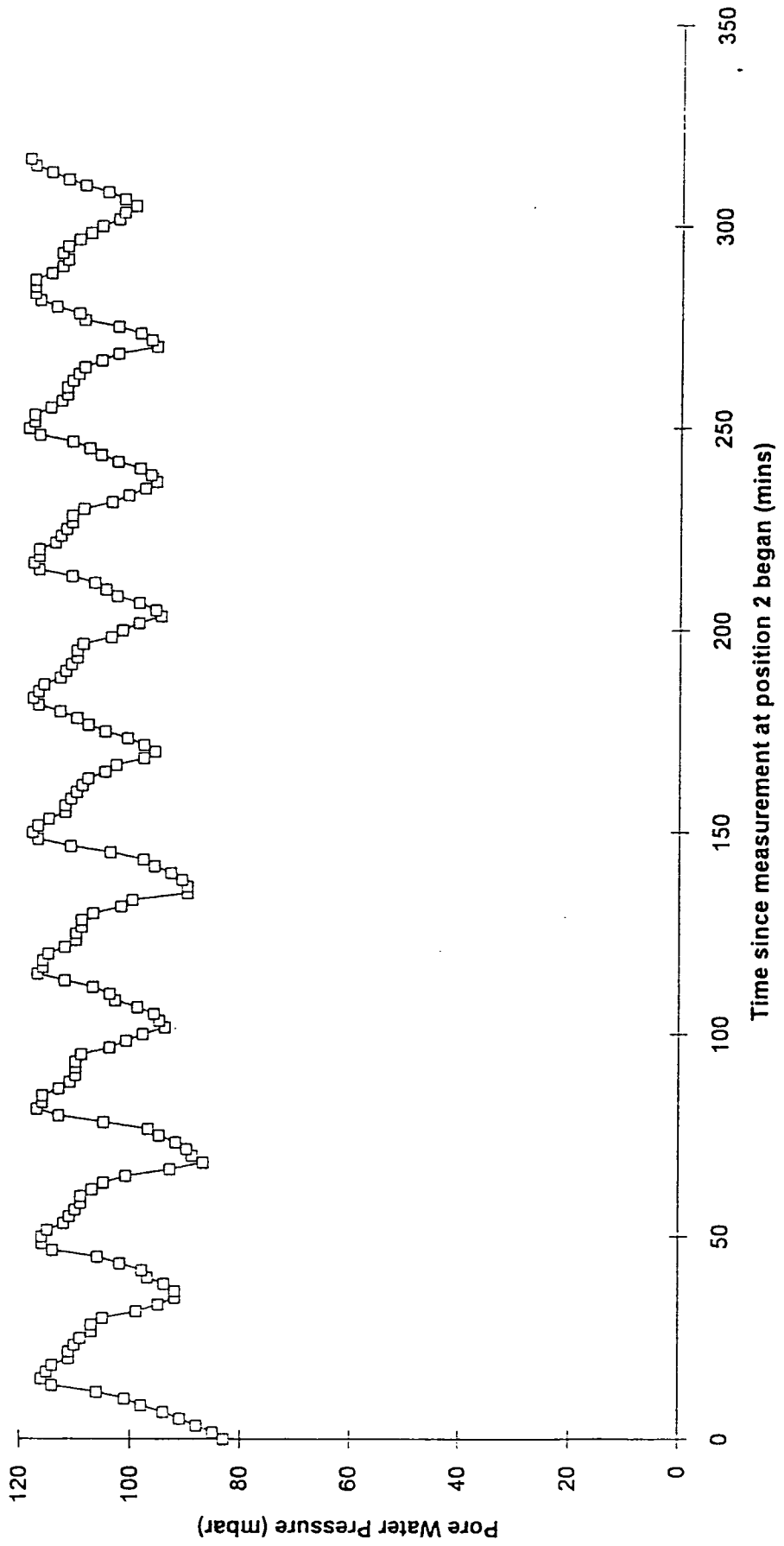
Appendix 3D-15. Series 2. Pore Water Pressure Variations at Position 3.
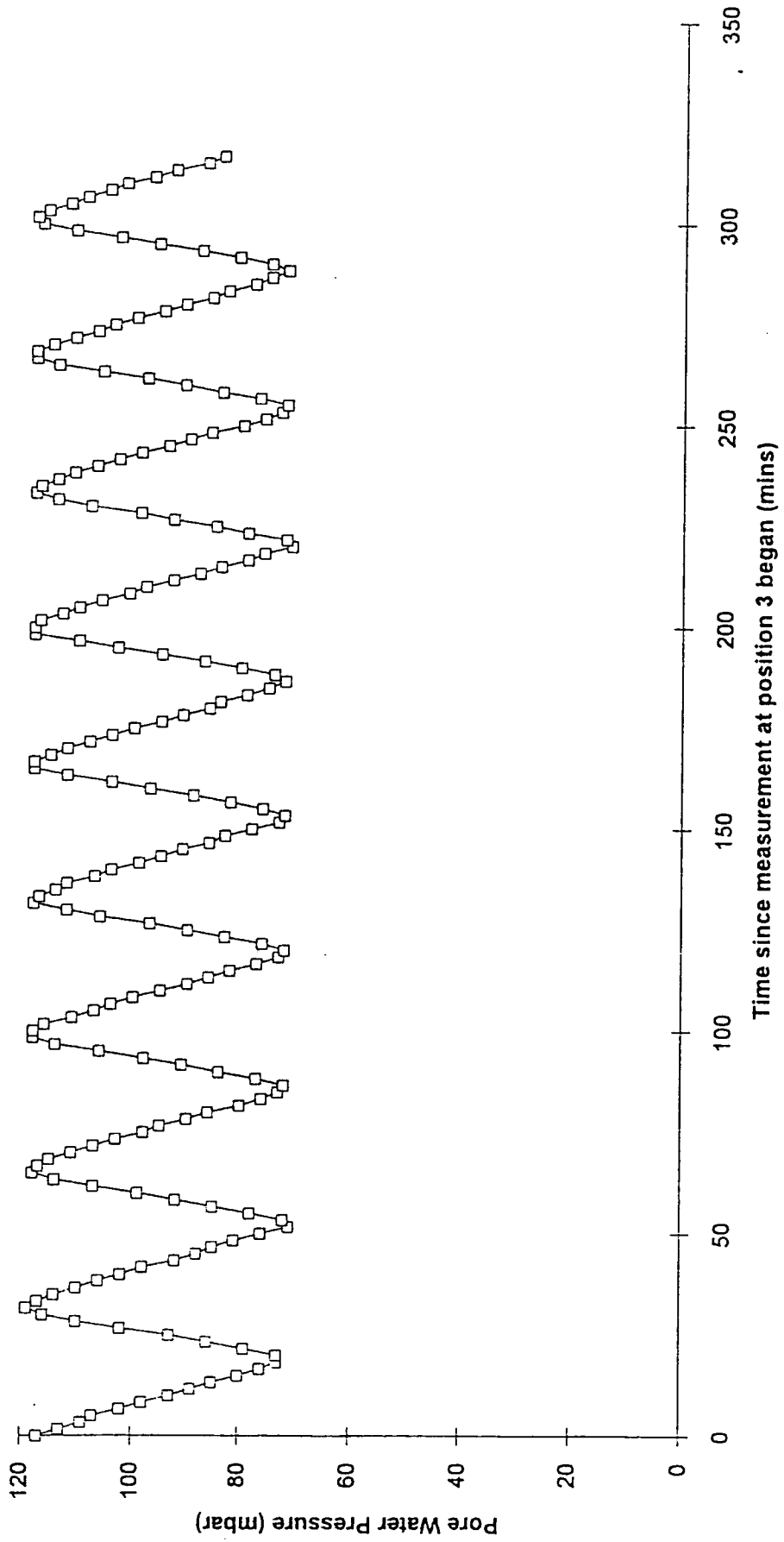
Appendix 3D-16. Series 2. Pore Water Pressure Variations at Position 4.

Appendix 3D -17. Series 2. Pore Water Pressure Variations at Position 5.

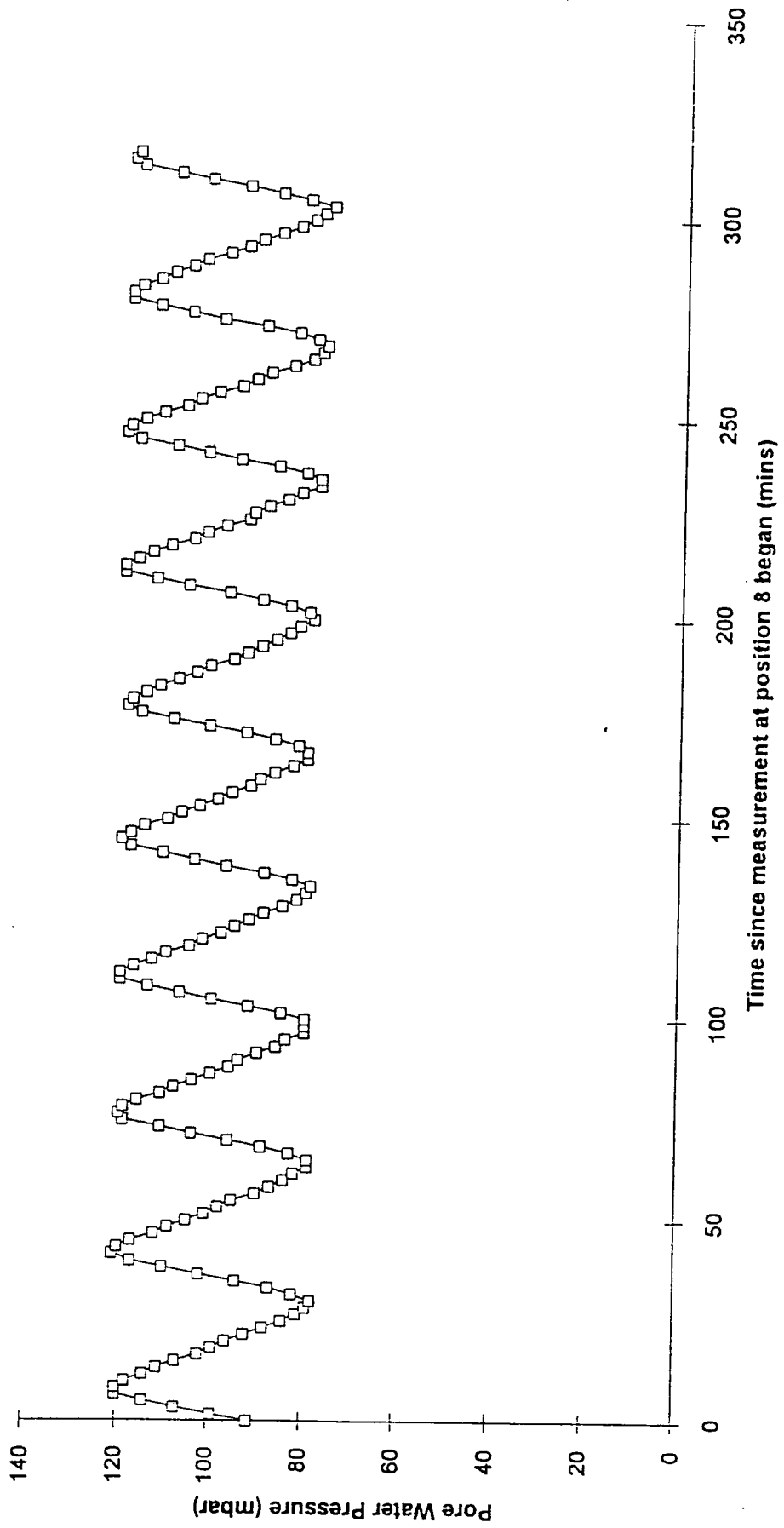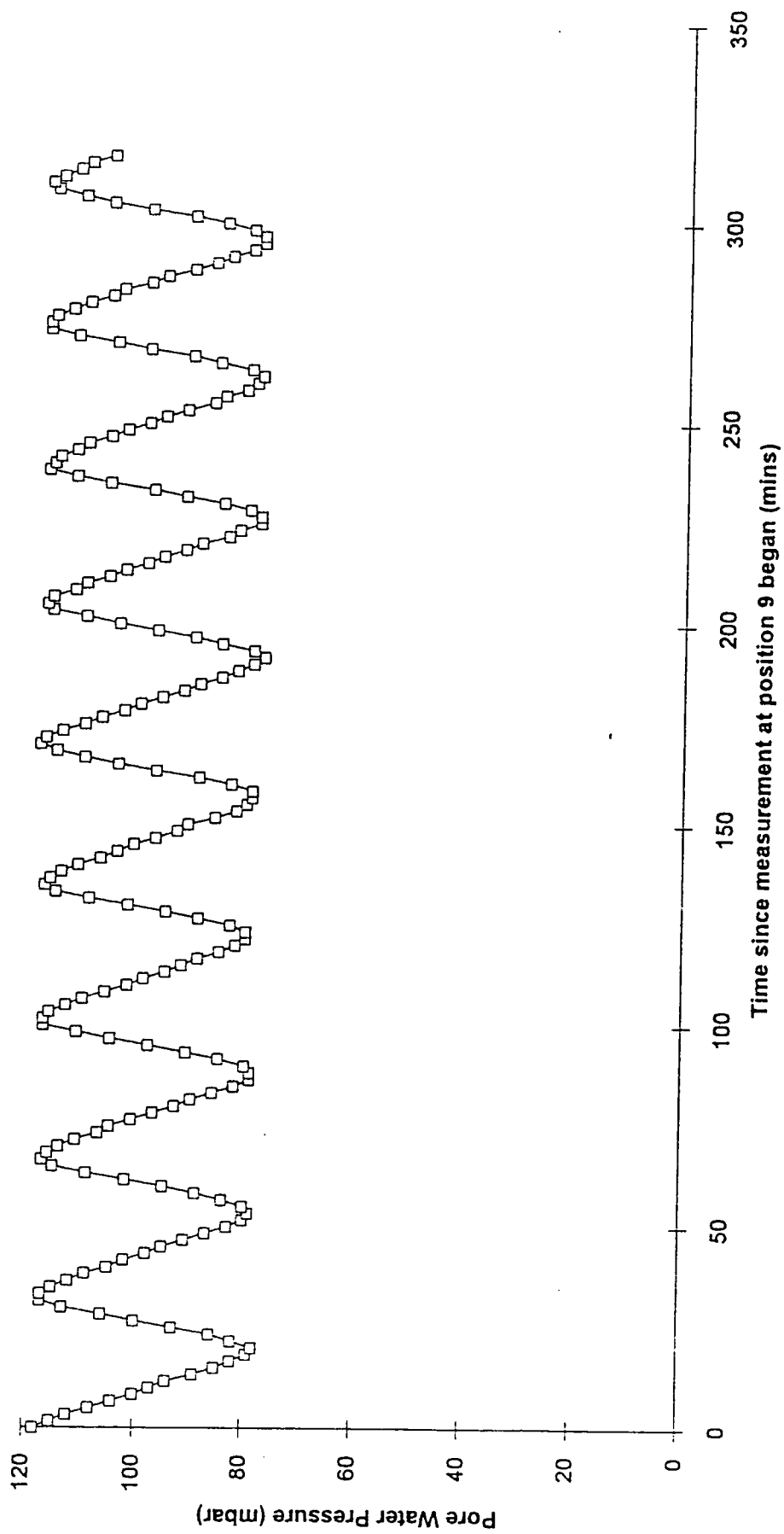Appendix 3D-18. Series 2. Pore Water Pressure Variations at Position 6.

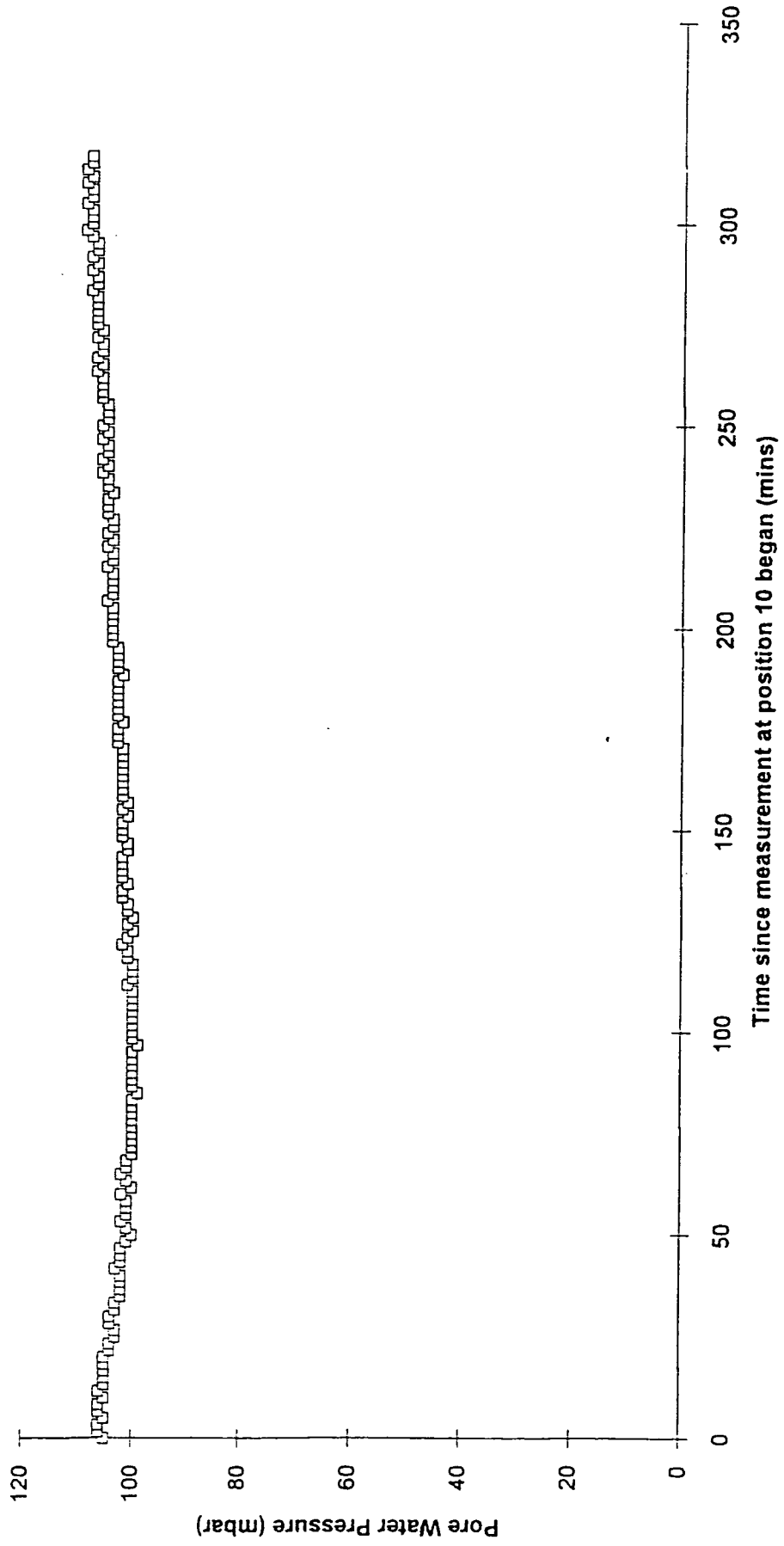Appendix 3D-19. Series 2. Pore Water Pressure Variations at Position 7.

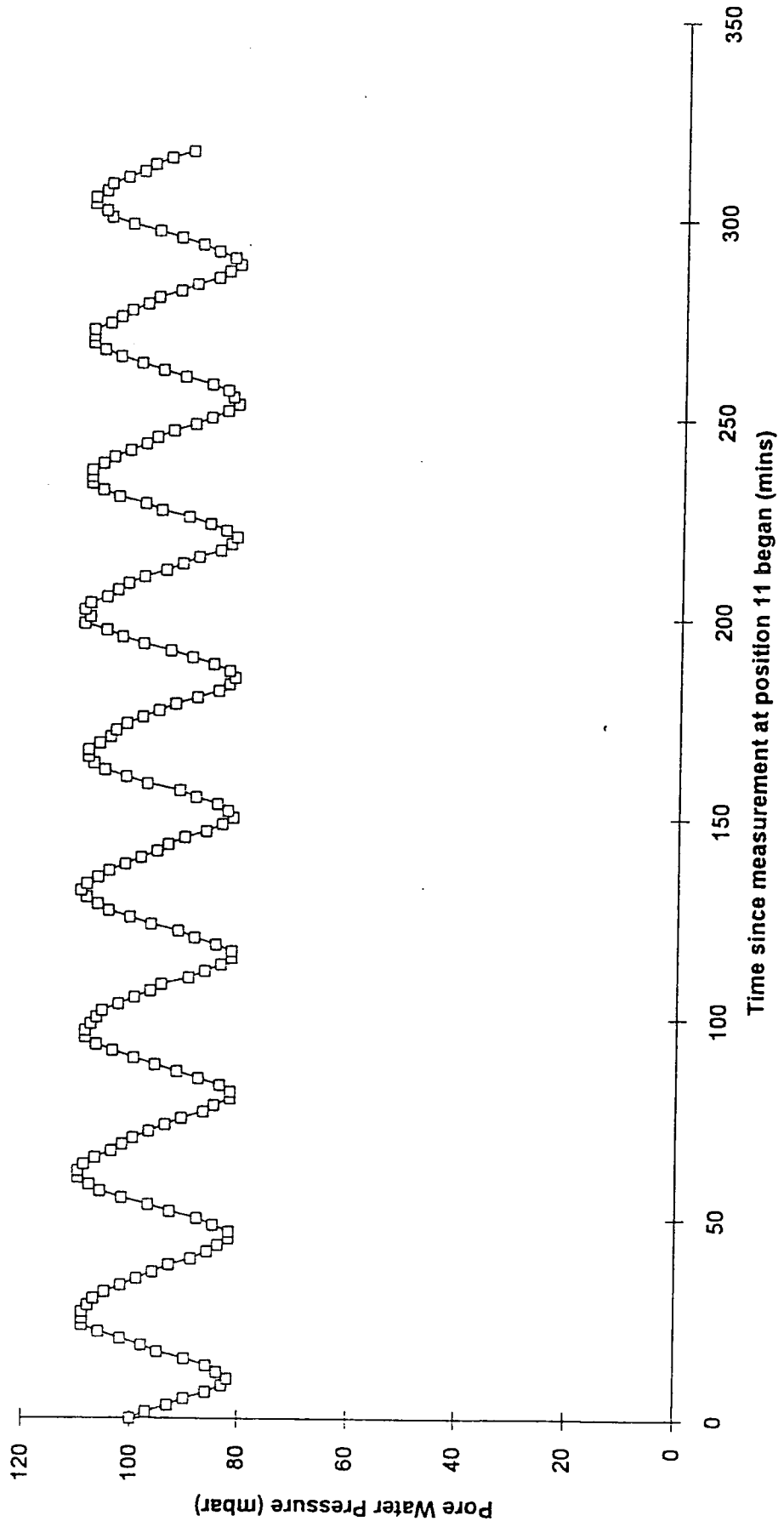Appendix 3D-20. Series 2. Pore Water Pressure Variations at Position 8.

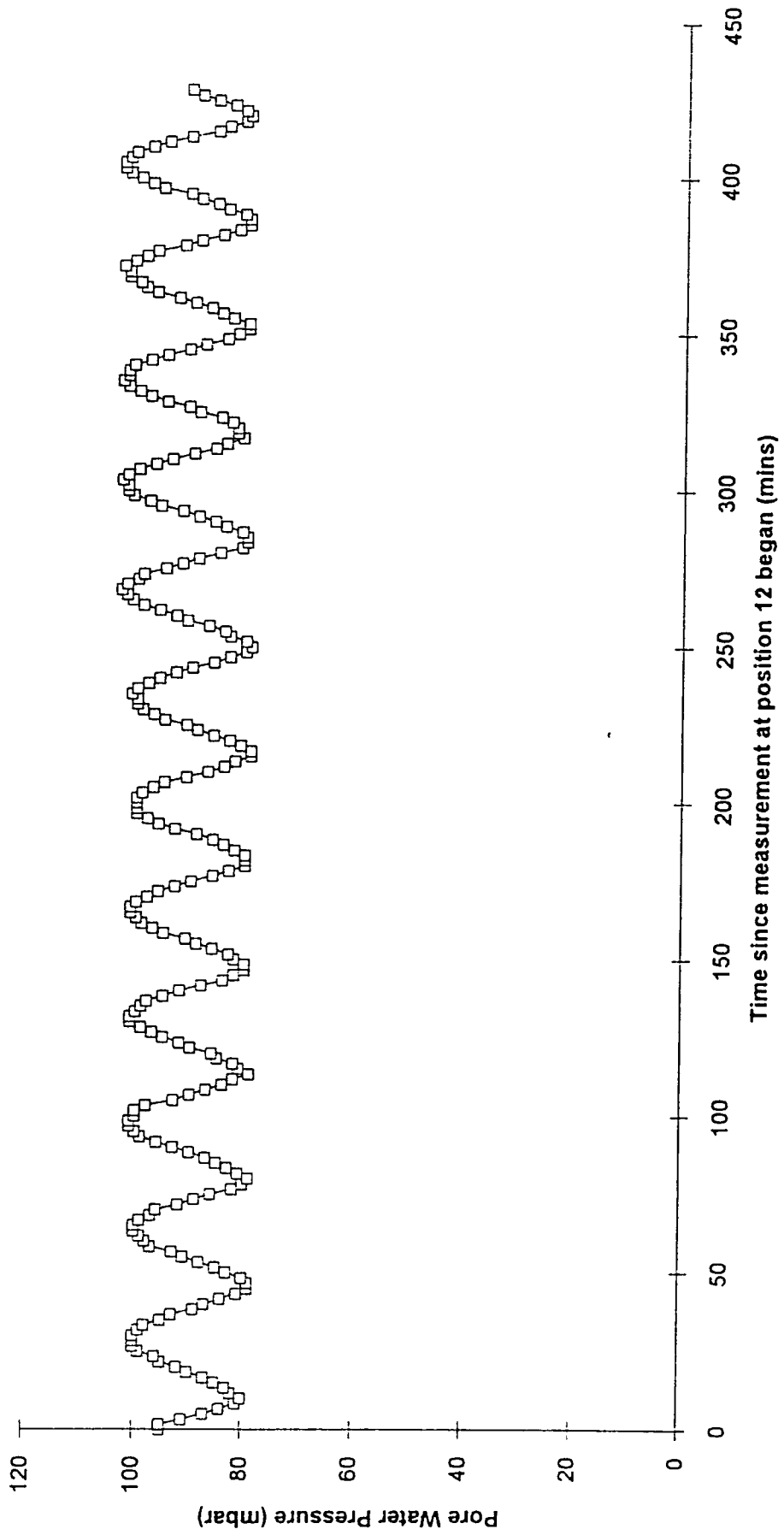Appendix 3D-21. Series 2. Pore Water Pressure Variations at Position 9.

Appendix 3D-22. Series 2. Pore Water Pressure Variations at Position 10.

Appendix 3D-23. Series 2. Pore Water Pressure Variations at Position 11.
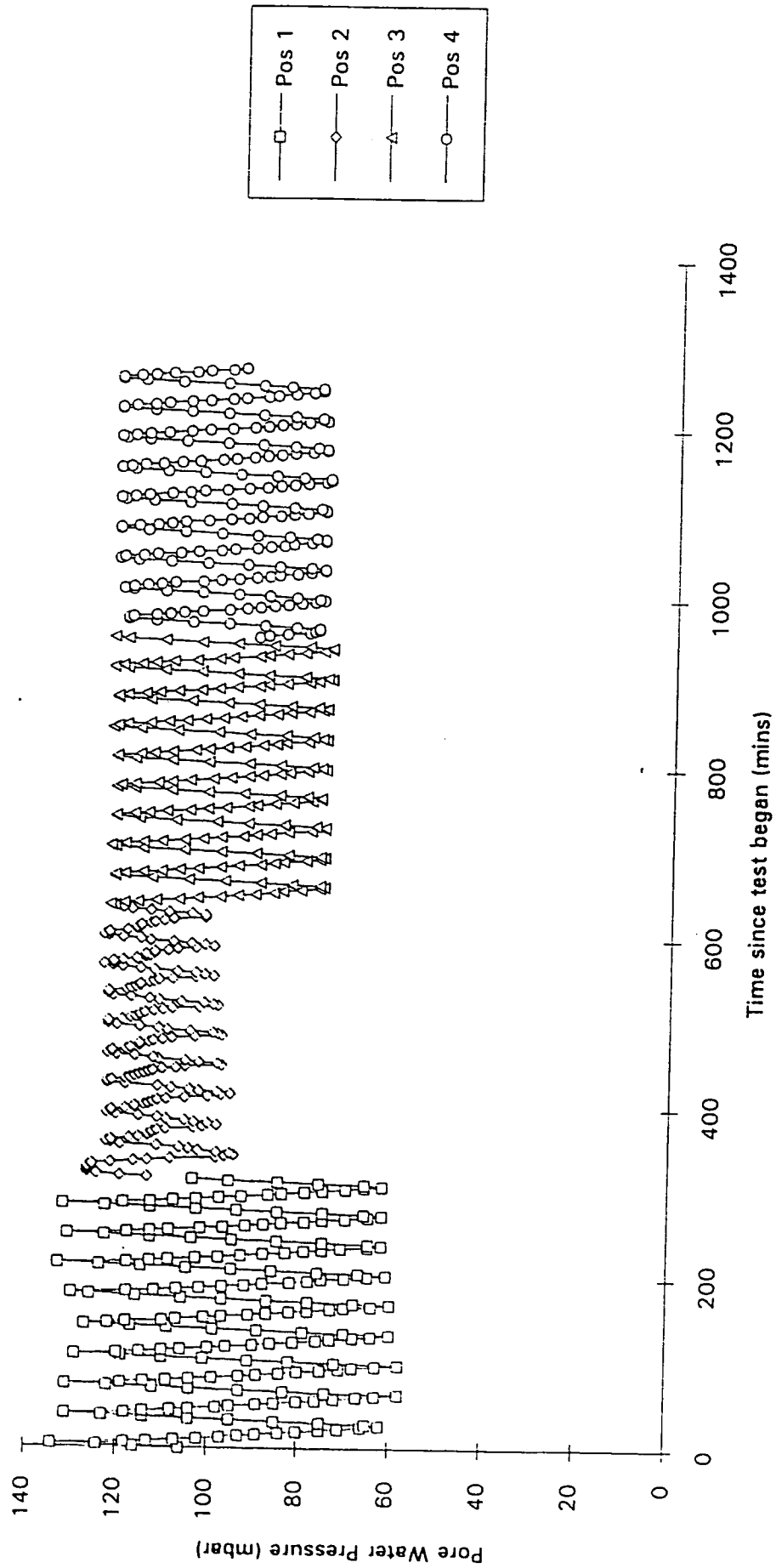
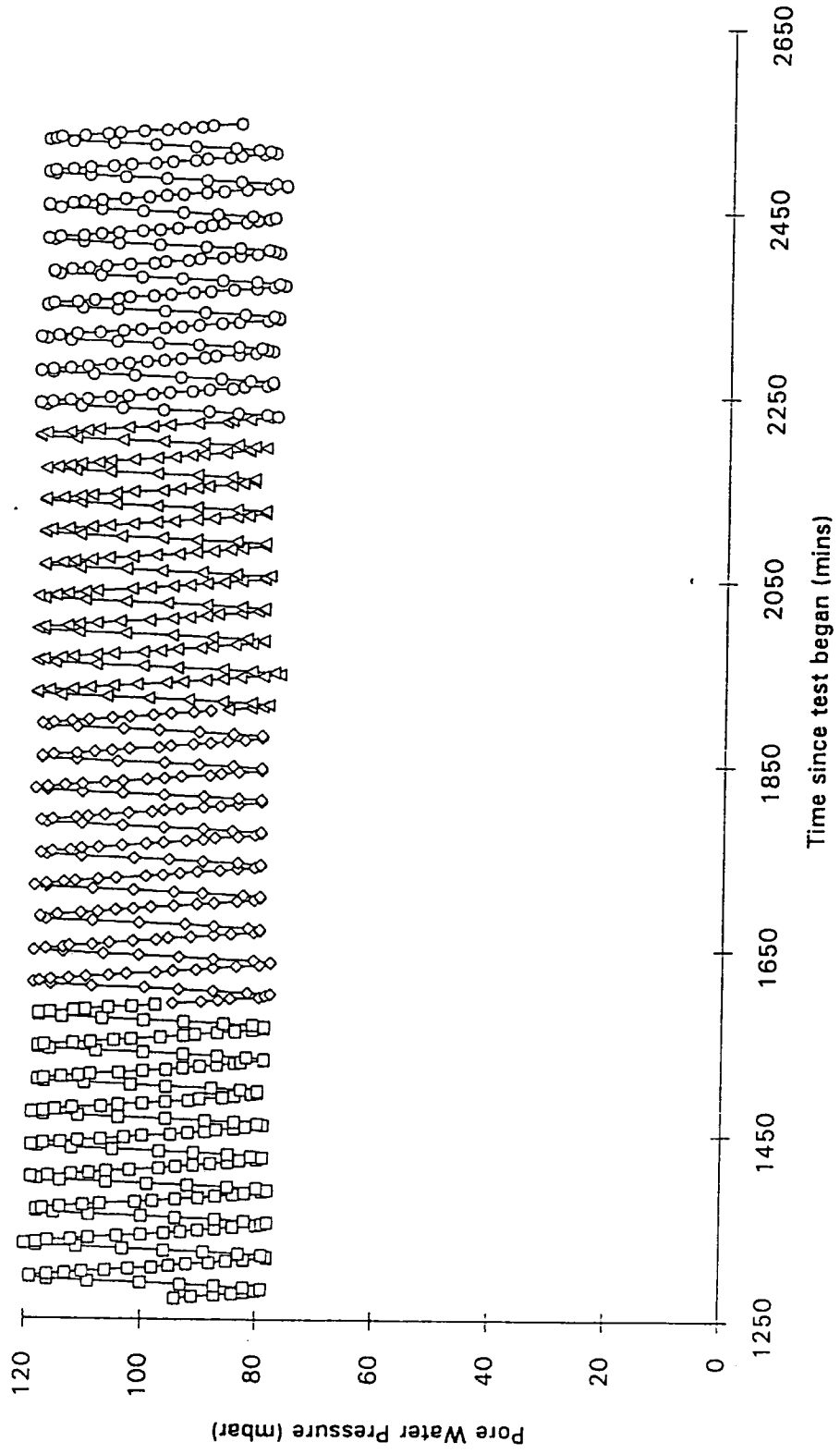Appendix 3D-24. Series 2. Pore Water Pressure Variations at Position 12

Appendix 3E
Series 3 and 4
Pore Water Pressure
Variations

Appendix 3E-1. Series 3. Pore Water Pressure Variations at Positions 1 to 4.

Appendix 3E-2. Series 3. Pore Water Pressure Variations at Positions 5 to 8.

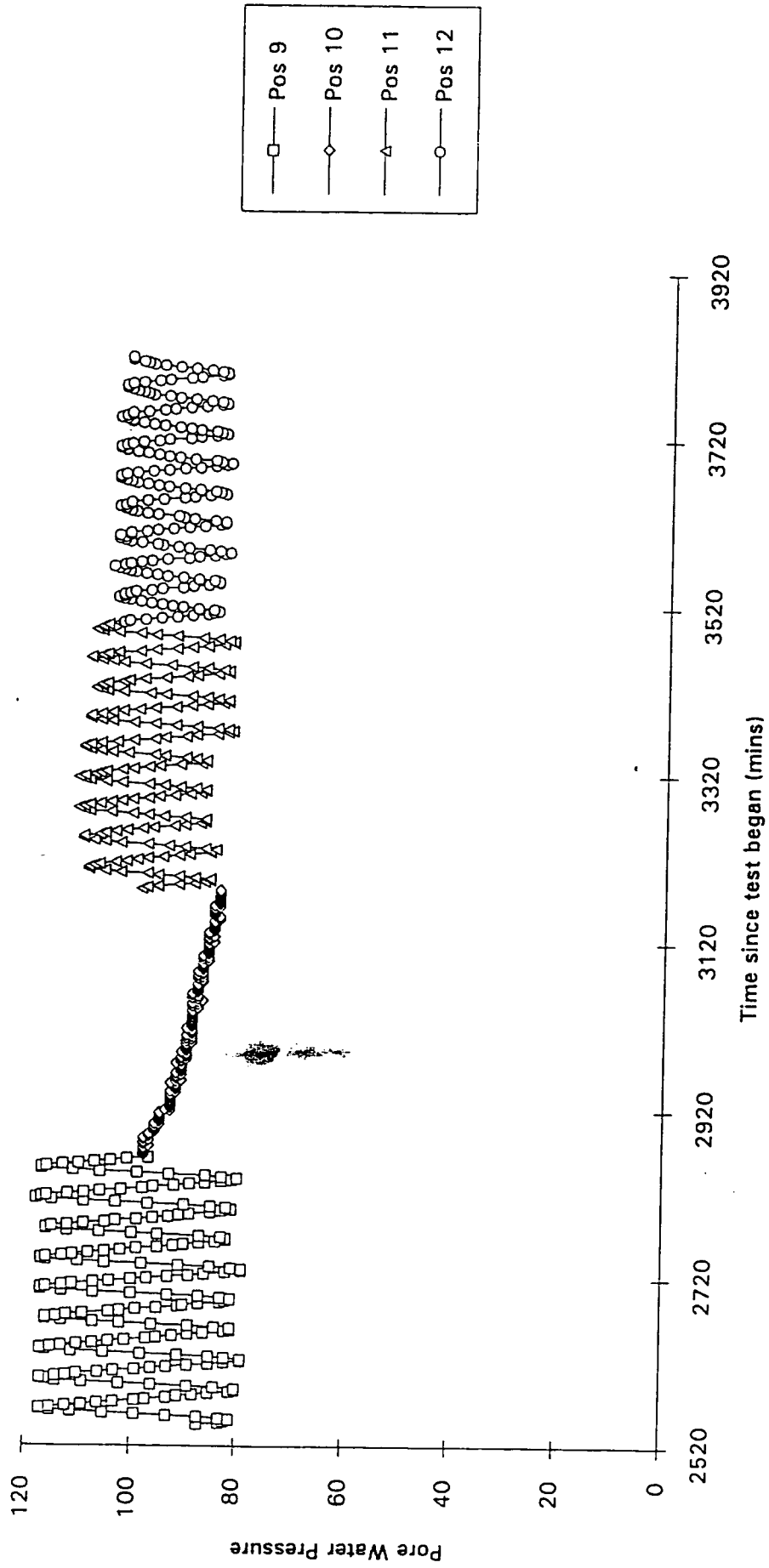Appendix 3E-3. Series 3. Pore Water Pressure Variations at Positions 9 to 12.

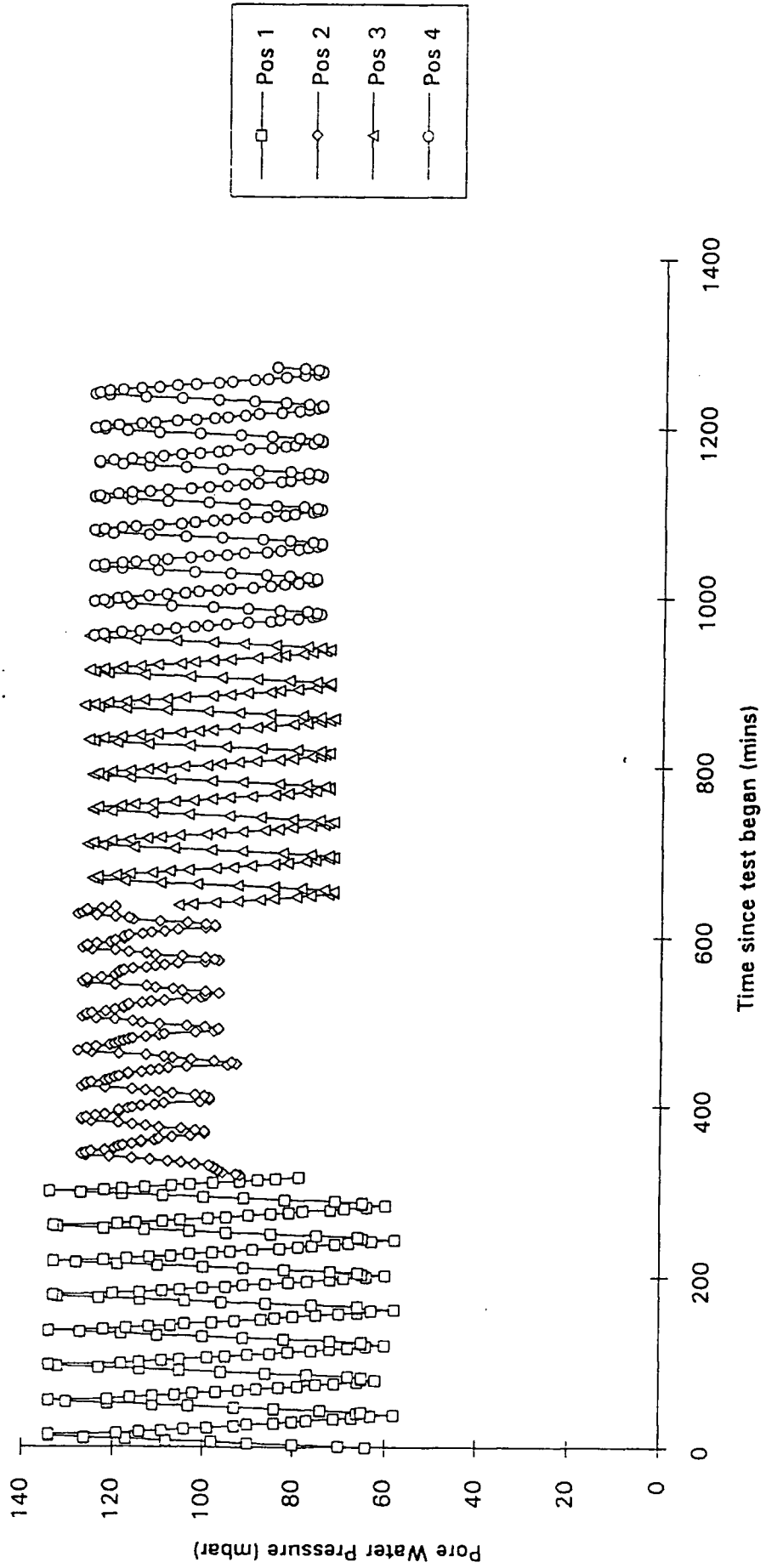Appendix 3E-4. Series 4. Pore Water Pressure Variations at Positions 1 to 4.

Appendix 3E-5. Series 4. Pore Water Pressure Variations at Positions 5 to 8.

Legend:
- Pos 5 (□)
- Pos 6 (◇)
- Pos 7 (△)
- Pos 8 (○)

Y-axis: Pore Water Pressure (mbar)
X-axis: Time since test began (mins)
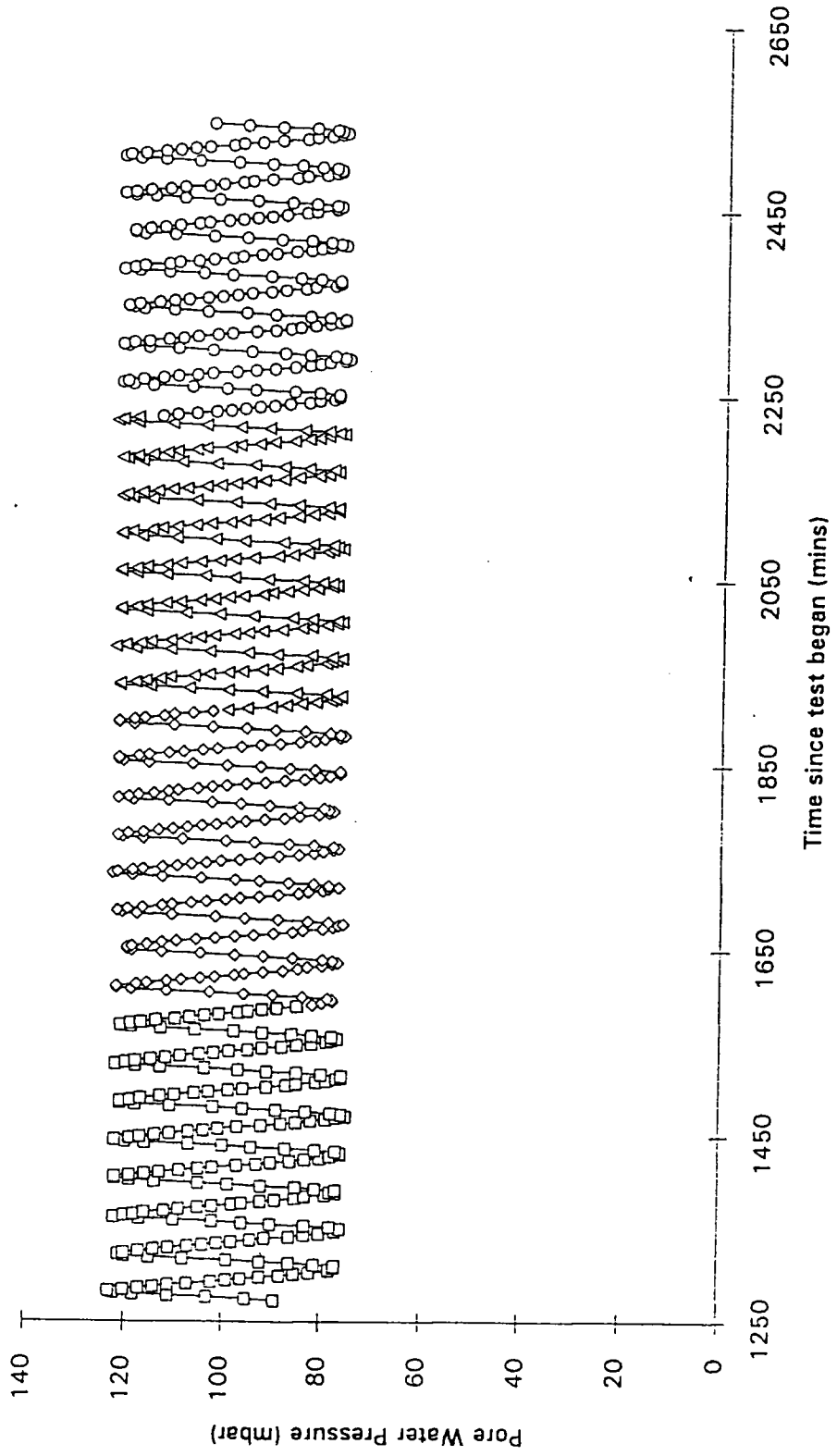
Appendix 3E-6. Series 4. Pore Water Pressure Variations at Positions 9 to 12 (excluding 10).
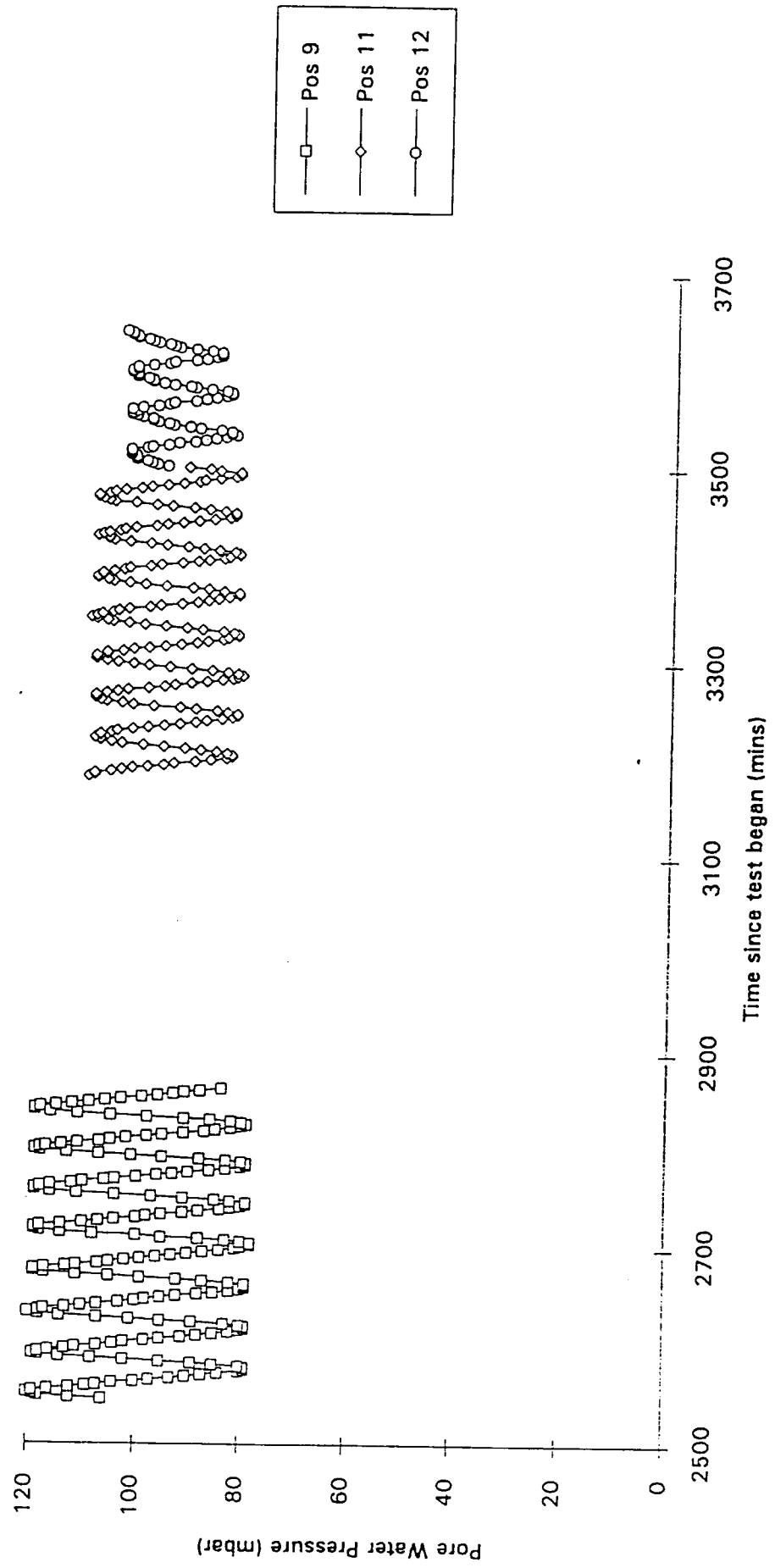
Appendix 3F
Series 1 to 4
Wave Spectra

Appendix 3F-1. Series1. Electrical Tidal Simulation. Wave Spectra from Fast Fourier Transform Analysis. Positions 1 to 4.
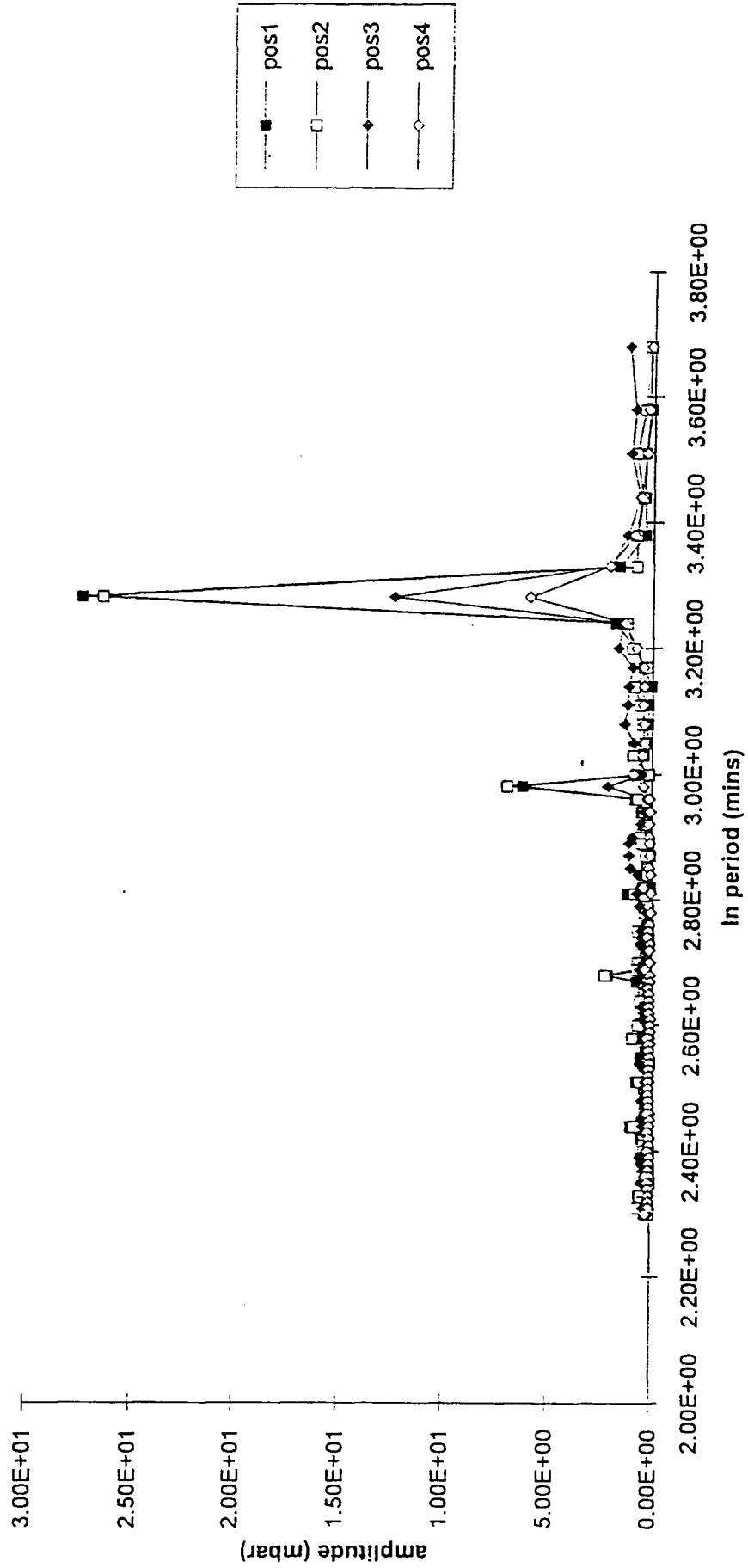
Appendix 3F-2. Series 1. Electrical Tidal Simulation. Wave Spectra from Fast Fourier Transform Analysis. Positions 5 to 8.

Appendix 3F-3. Electrical Tidal Simulation. Wave Spectra from Fast Fourier Transform Analysis. Positions 9 to 12. Series 1.

Appendix 3F-4. Series 2. Electrical Tidal Simulation. Wave Spectra from Fast Fourier Transform Analysis. Positions 1 to 4.

Appendix 3F-5. Series 2. Electrical Tidal Simulation. Wave Spectra from Fast Fourier Transform Analysis. Positions 5 to 8.

Appendix 3F-6. Series 2. Electrical Tidal Simulation. Wave Spectra from Fast Fourier Transform Analysis. Positions 9 to 12.
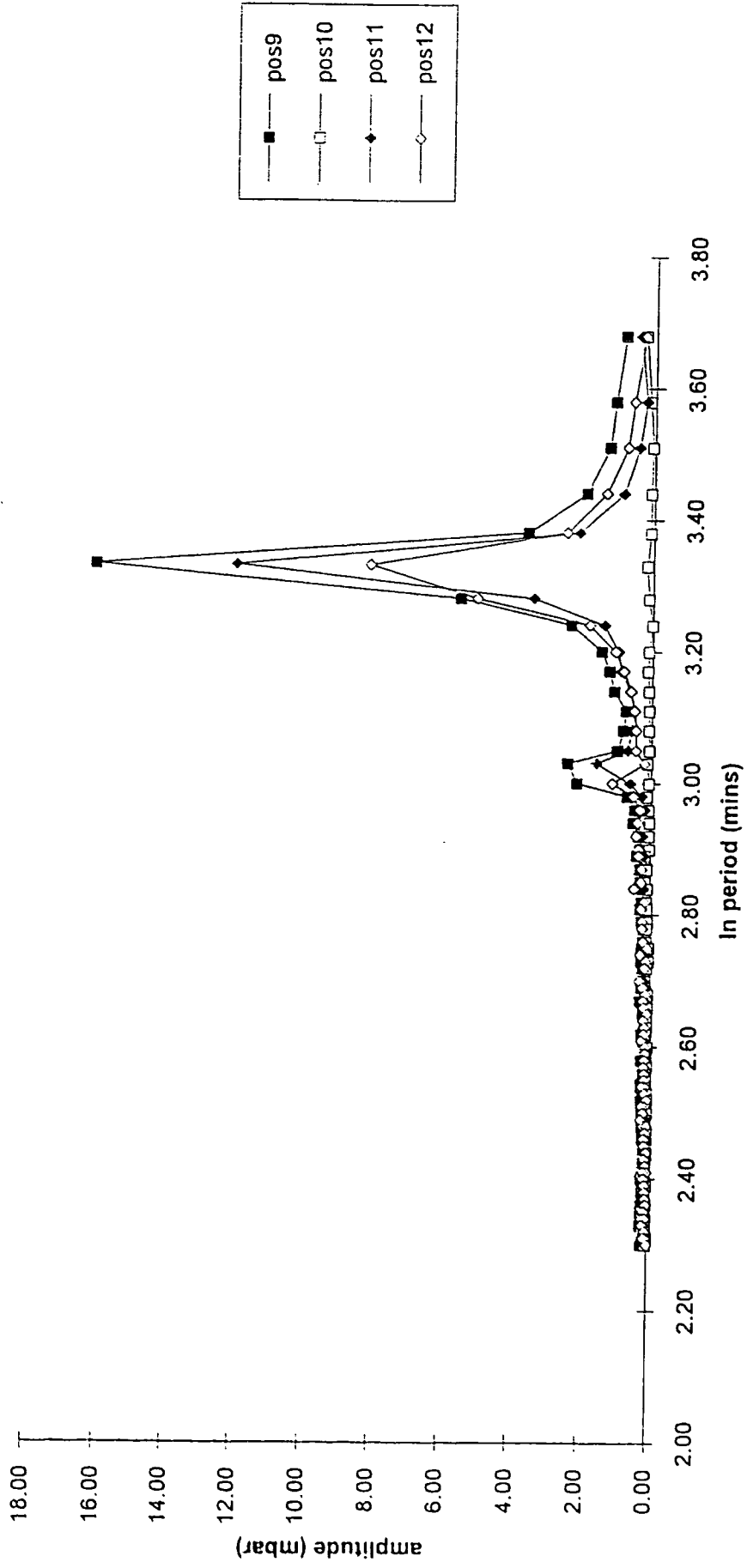
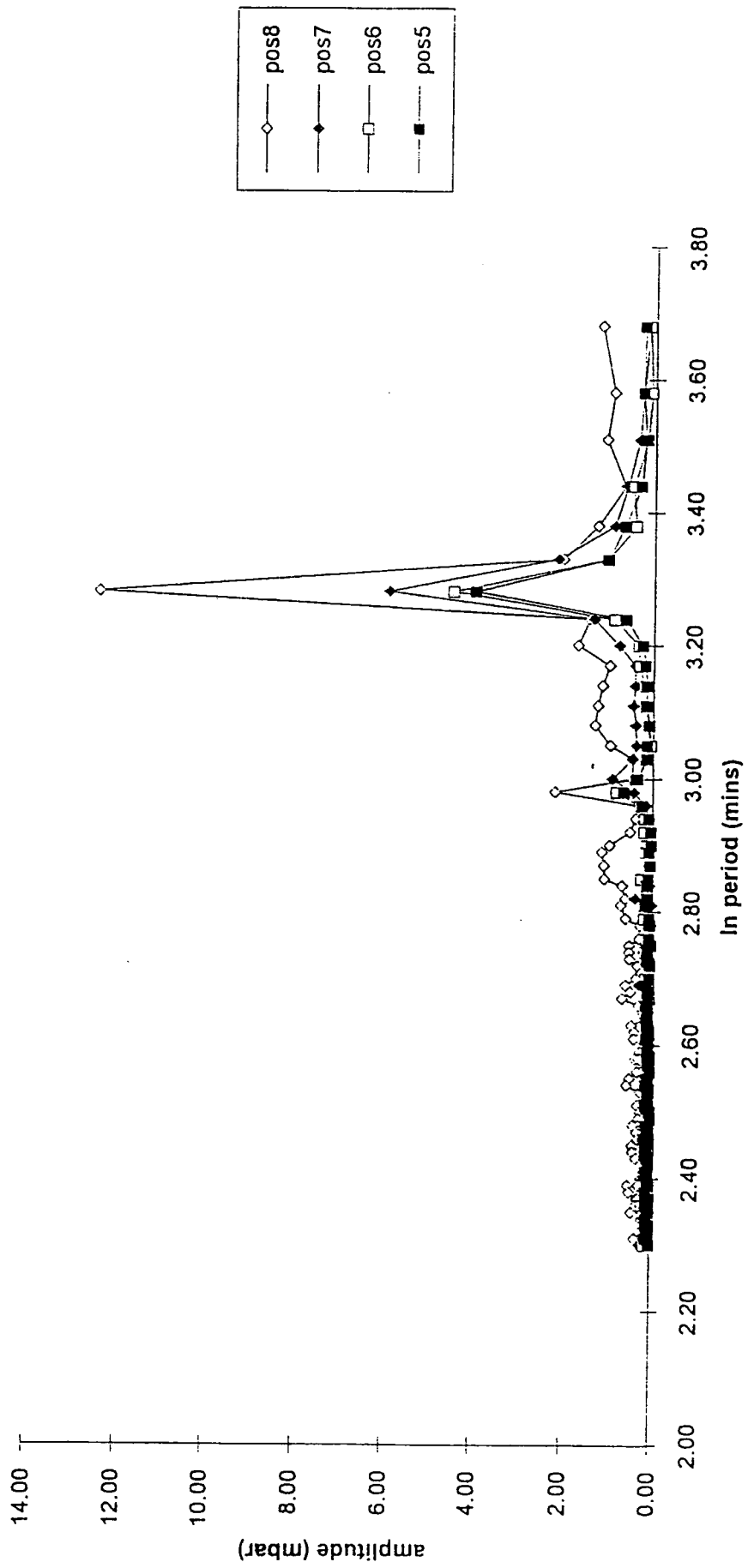Appendix 3F-7. Series 3. Electrical Tidal Simulation. Wave Spectra from Fast Fourier Transform Analysis. Positions 1 to 4.
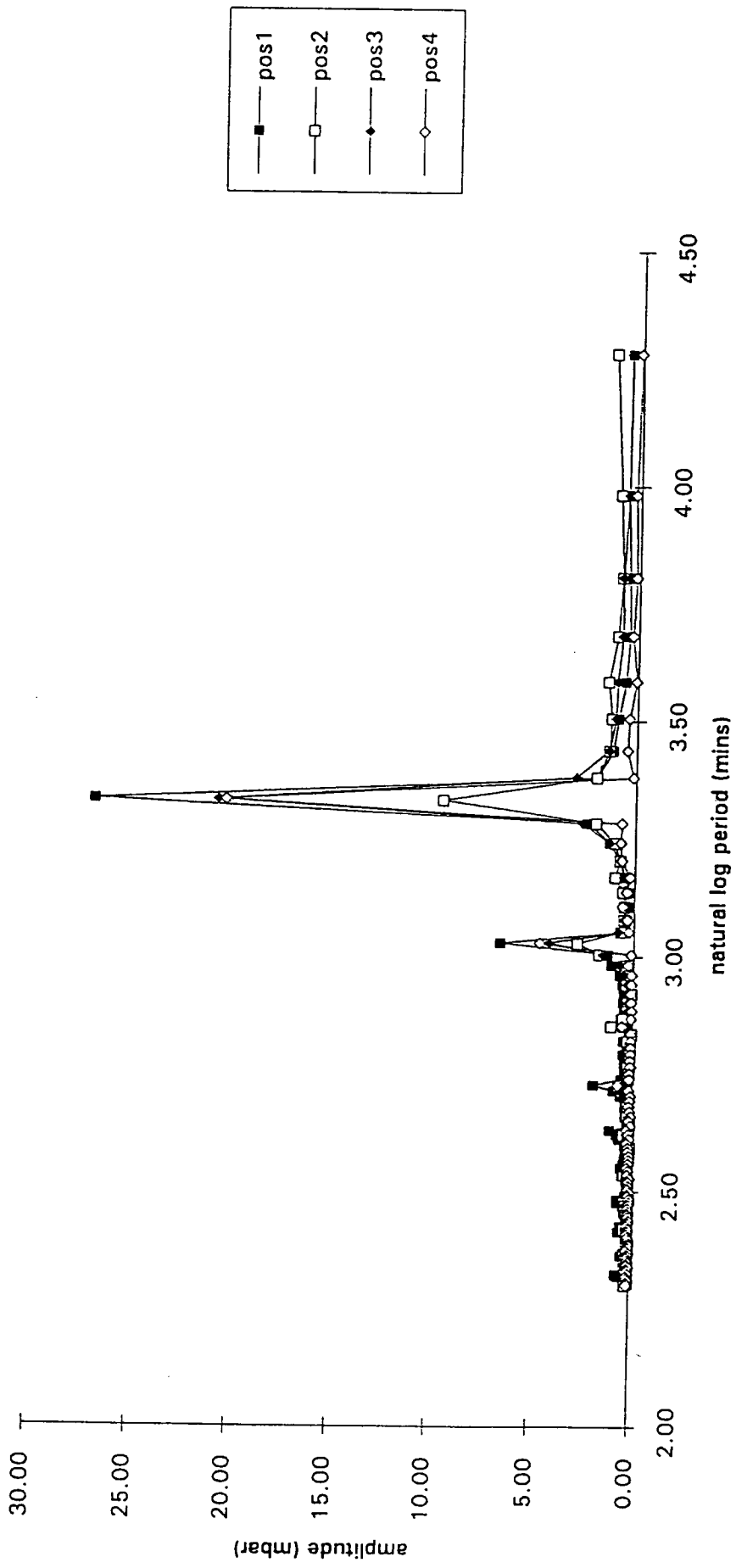
Appendix 3F-8. Series 3. Electrical Tidal Simulation. Wave Spectra from Fast Fourier Transform Analysis. Positions 4 to 7.
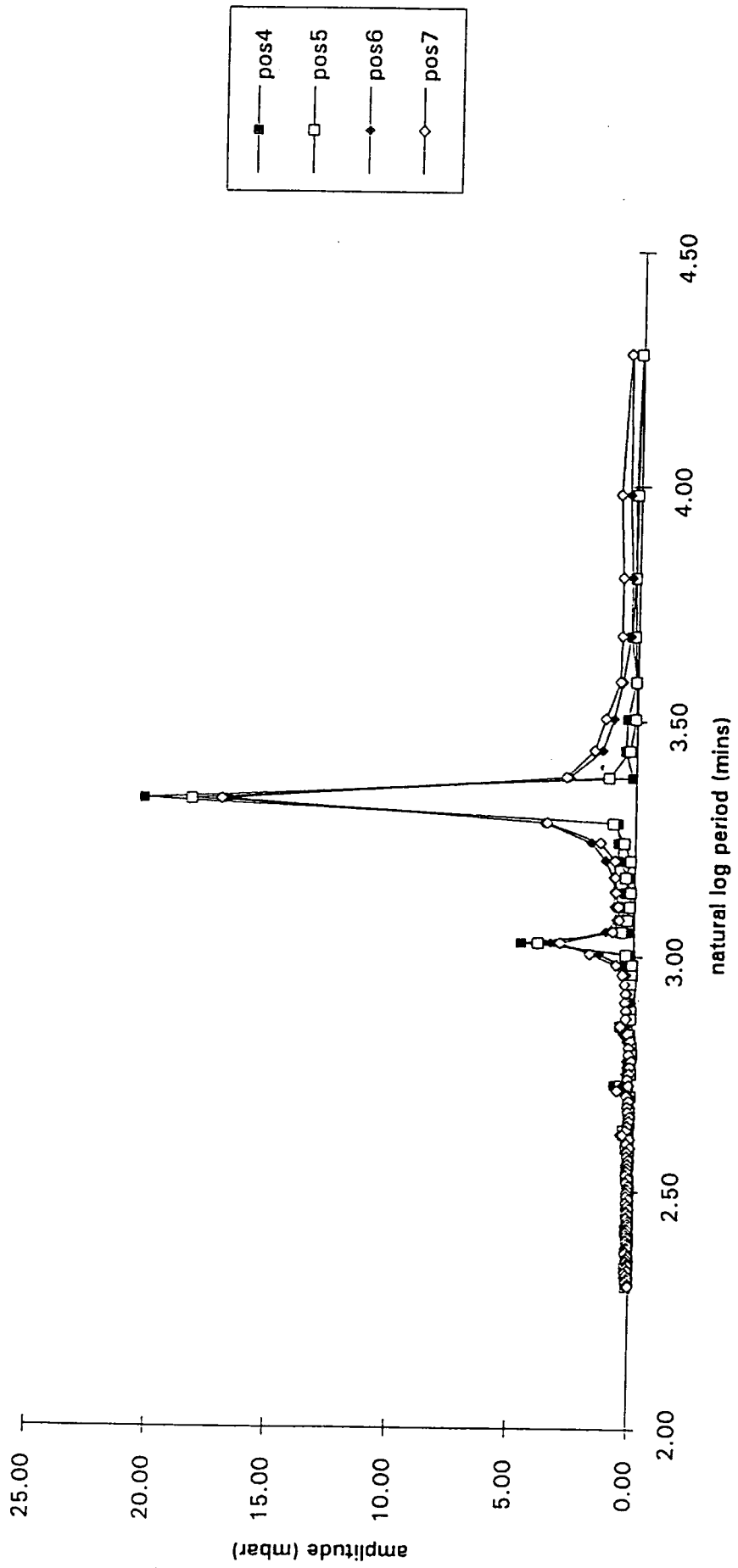
Appendix 3F-9. Electrical Tidal Simulation. Wave Spectra from Fast Fourier Transform
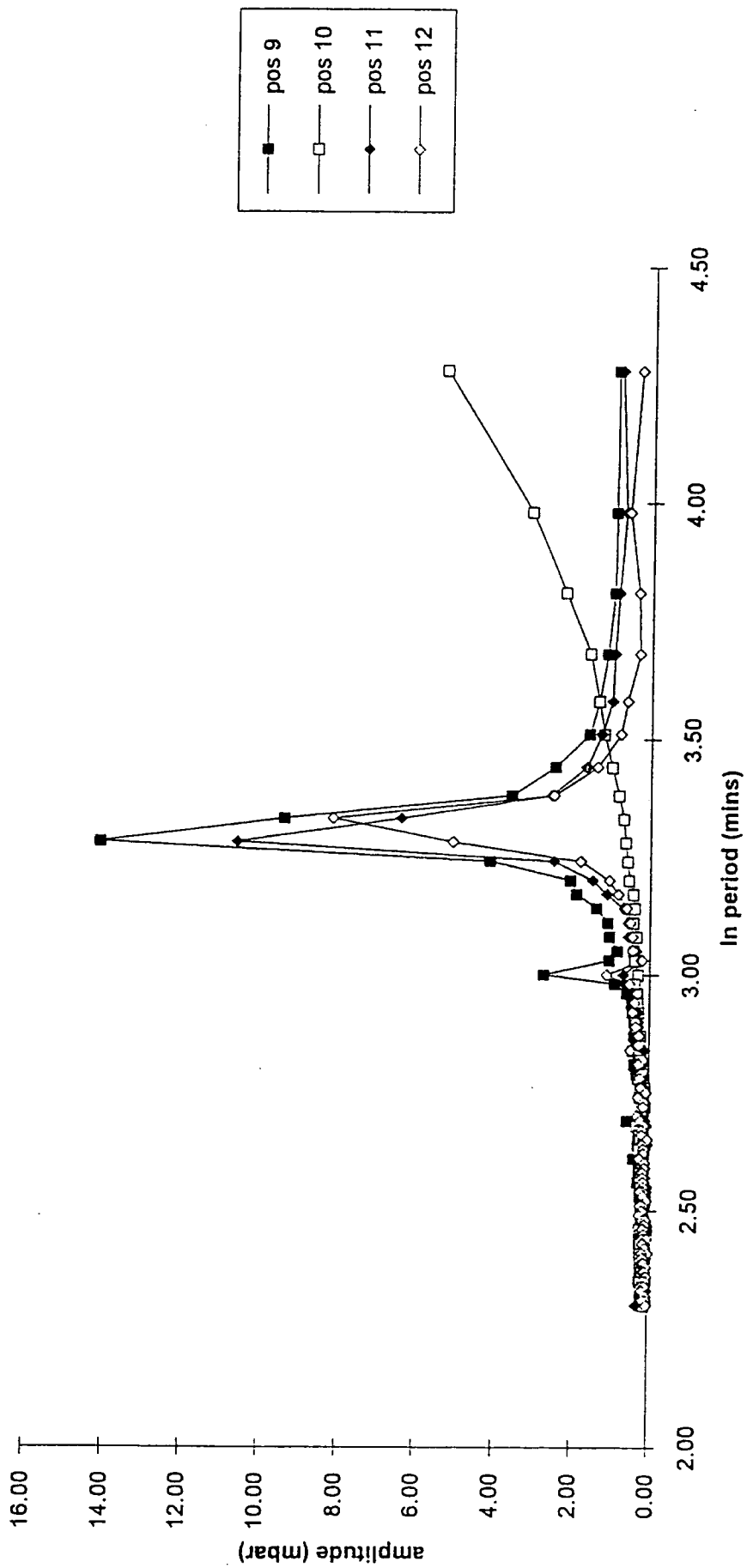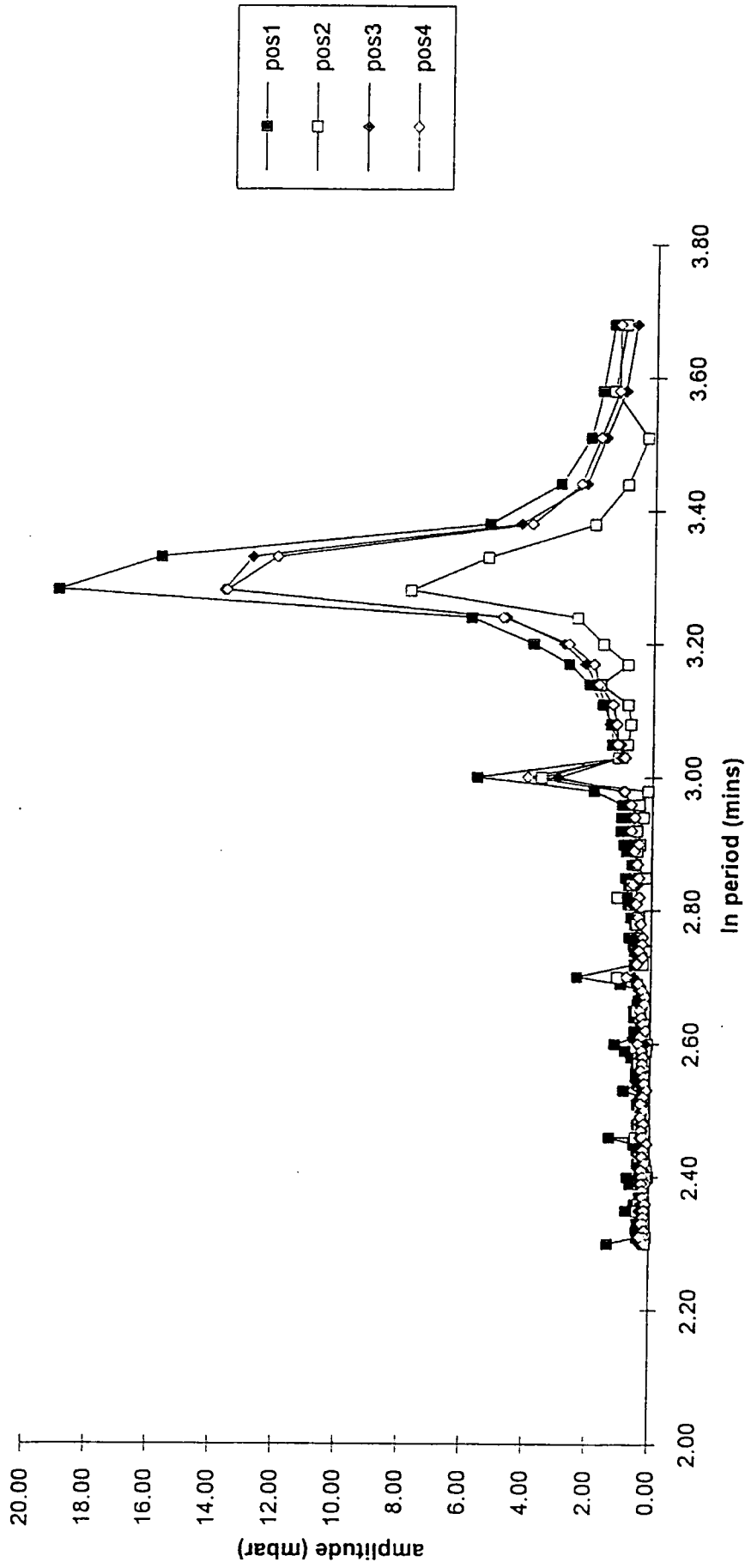Analysis. Positions 8 to 12.
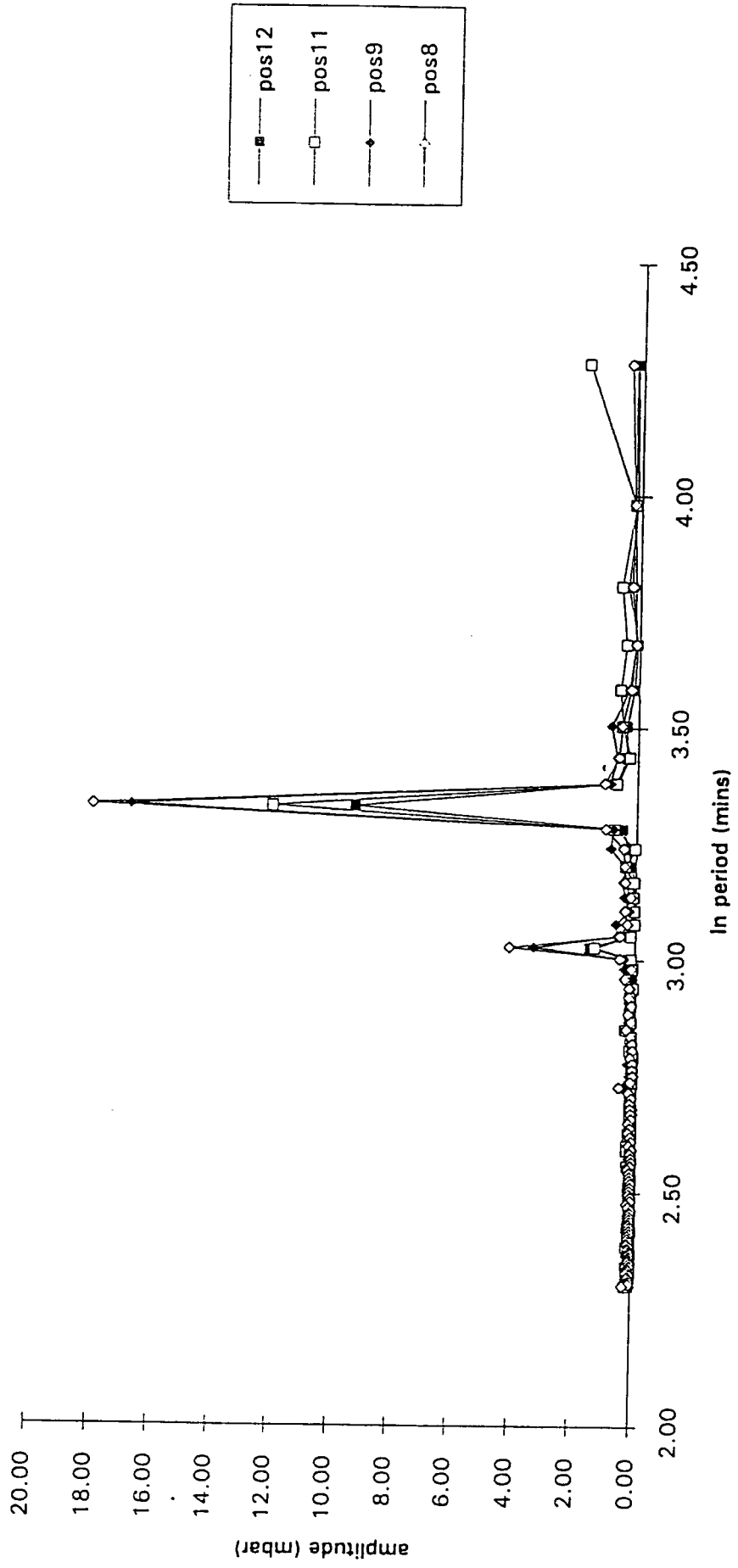
Appendix 3F-10. Series 4. Electrical Tidal Simulation. Wave Spectra from Fast Fourier
Transform Analysis. Positions 1 to 4.
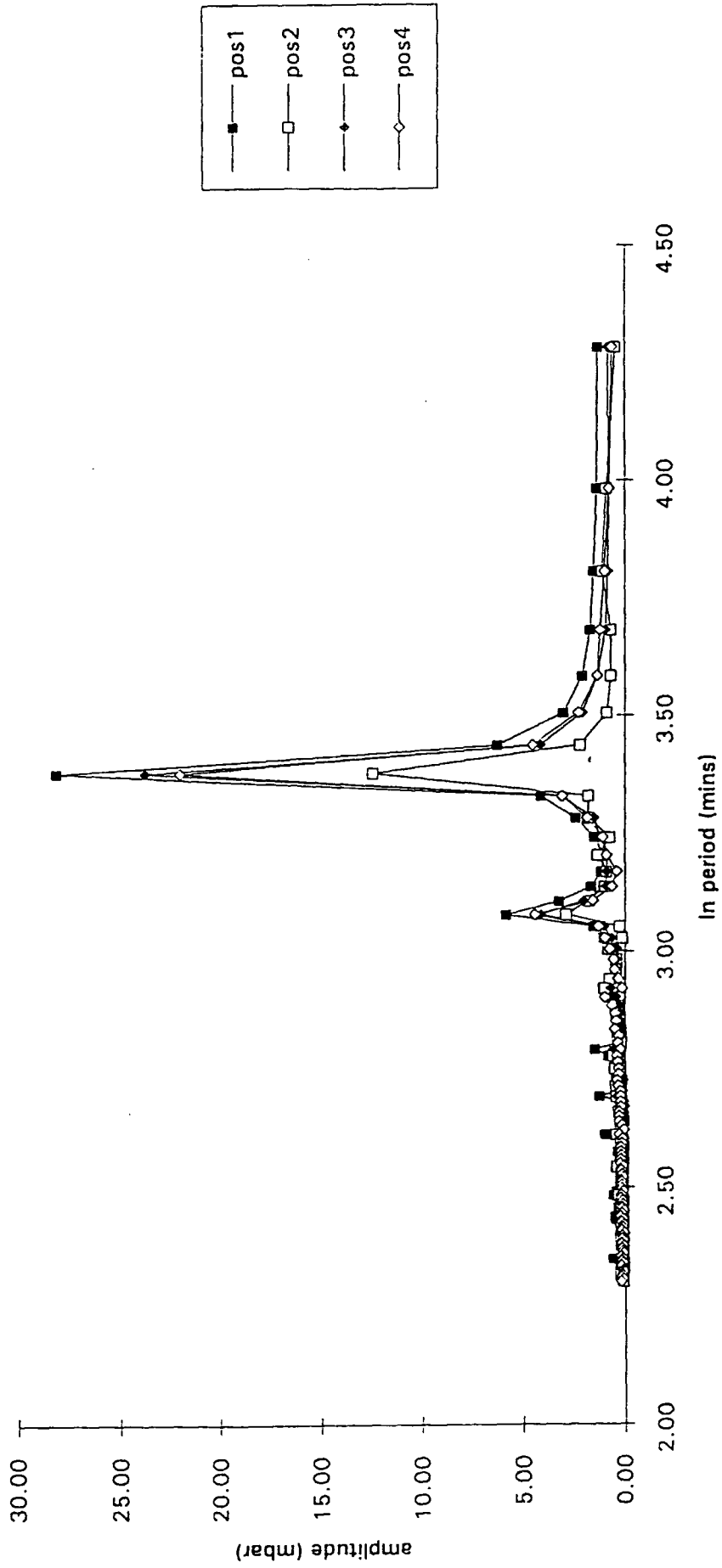
Appendix 3F-11.   Series 4.   Electrical Tidal Simulation.   Wave Spectra from Fast Fourier
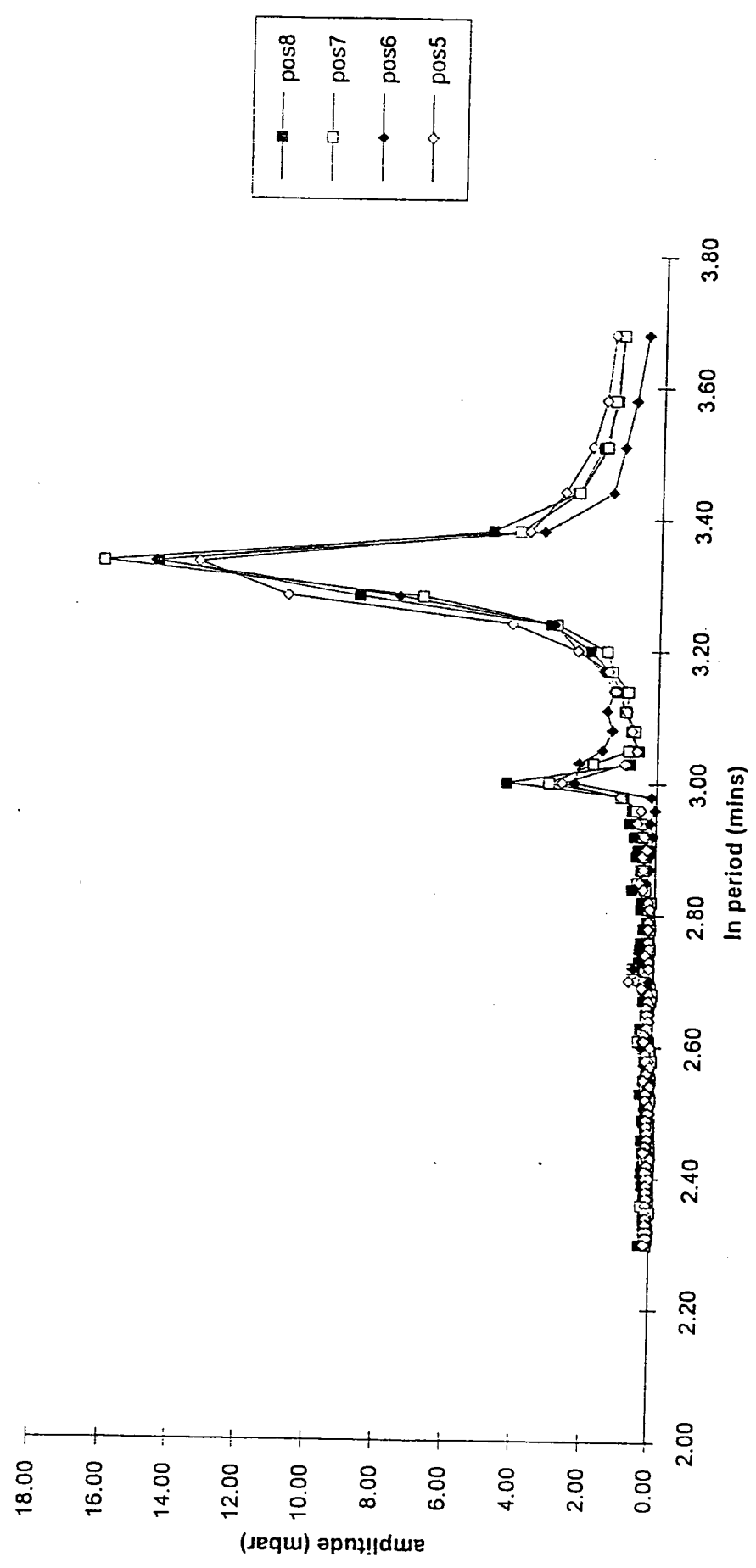Transform Analysis.   Positions 5 to 8.

Page 1
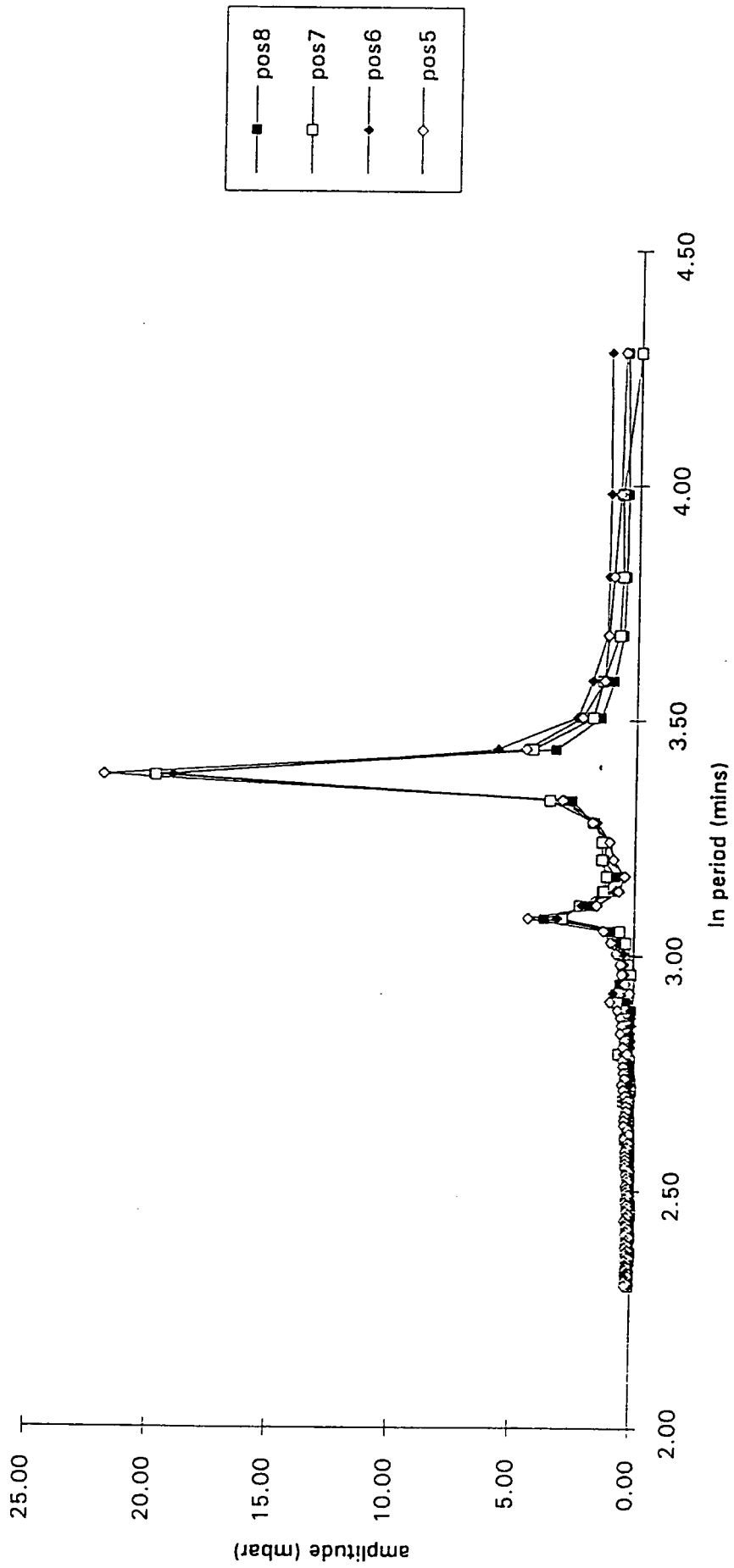
Appendix 3G

Series 2

Time Lag Calculations

Appendix 3G-1

Calculation of Time Lag Series 2. Positions 3 and 4
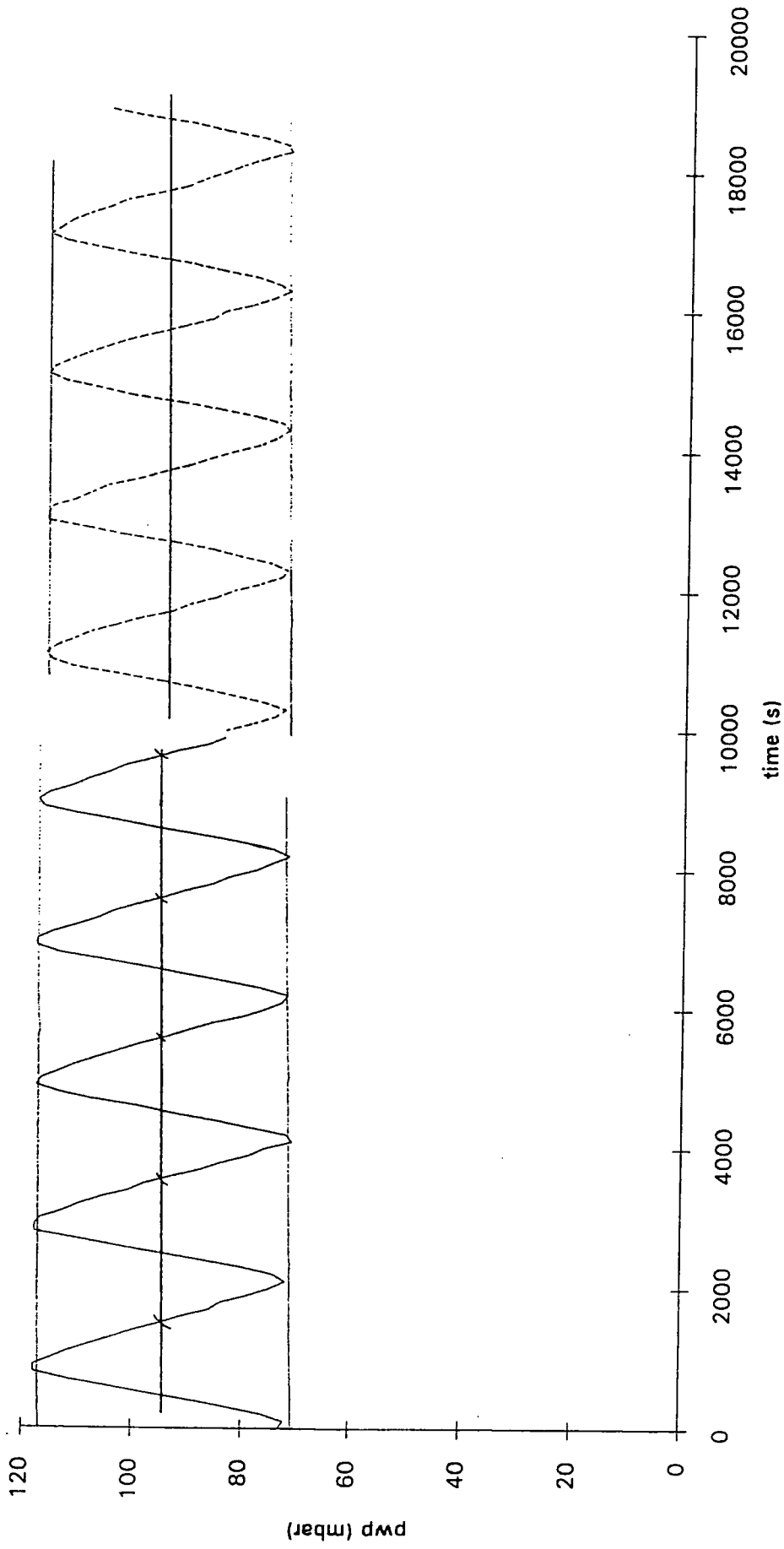
Appendix 3G-2
Calculation of Time Lag   Series 2. Positions 4 and 5
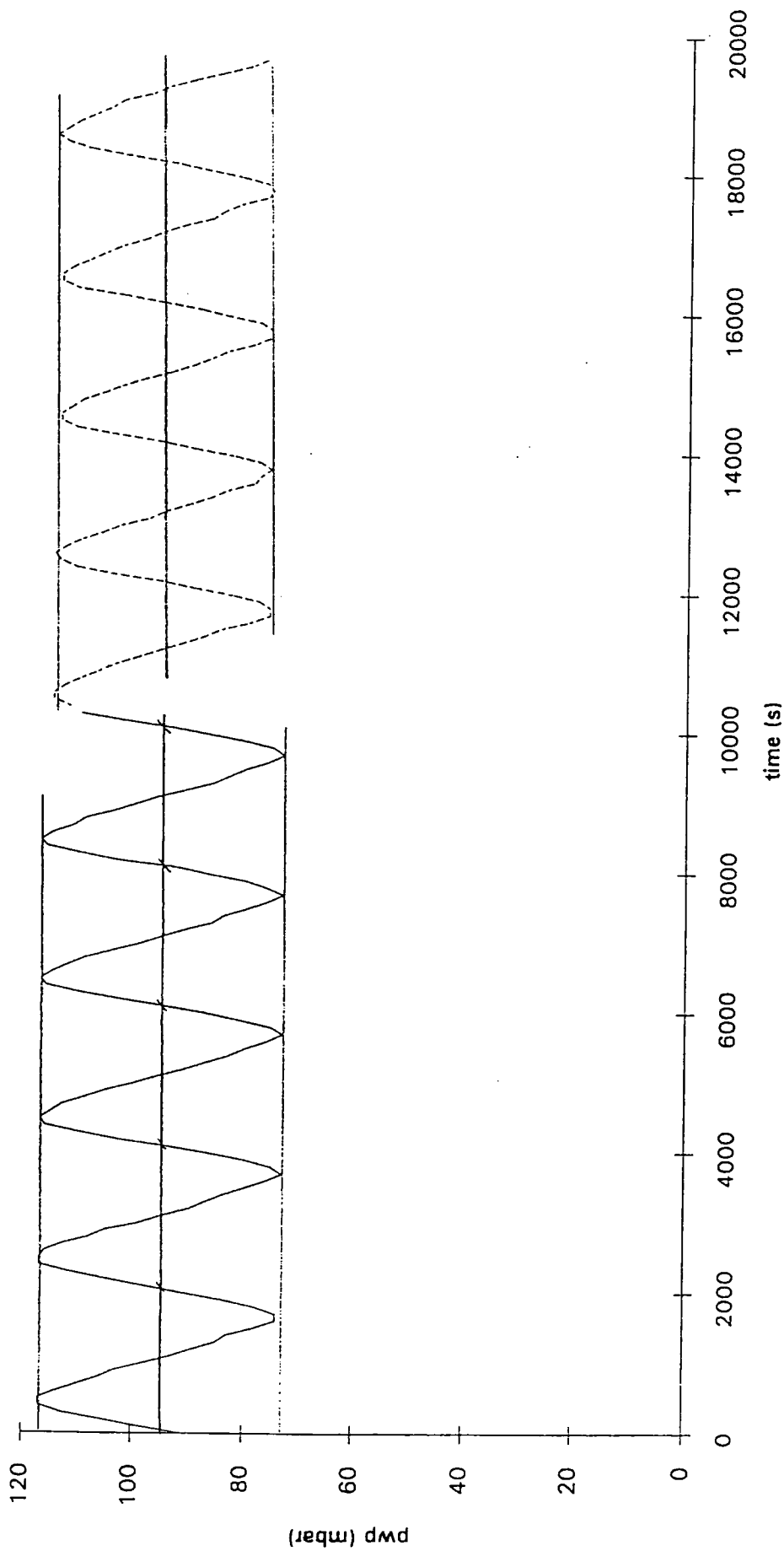
Appendix 3G-3
Calculation of Time Lag   Series 2. Positions 5 and 6
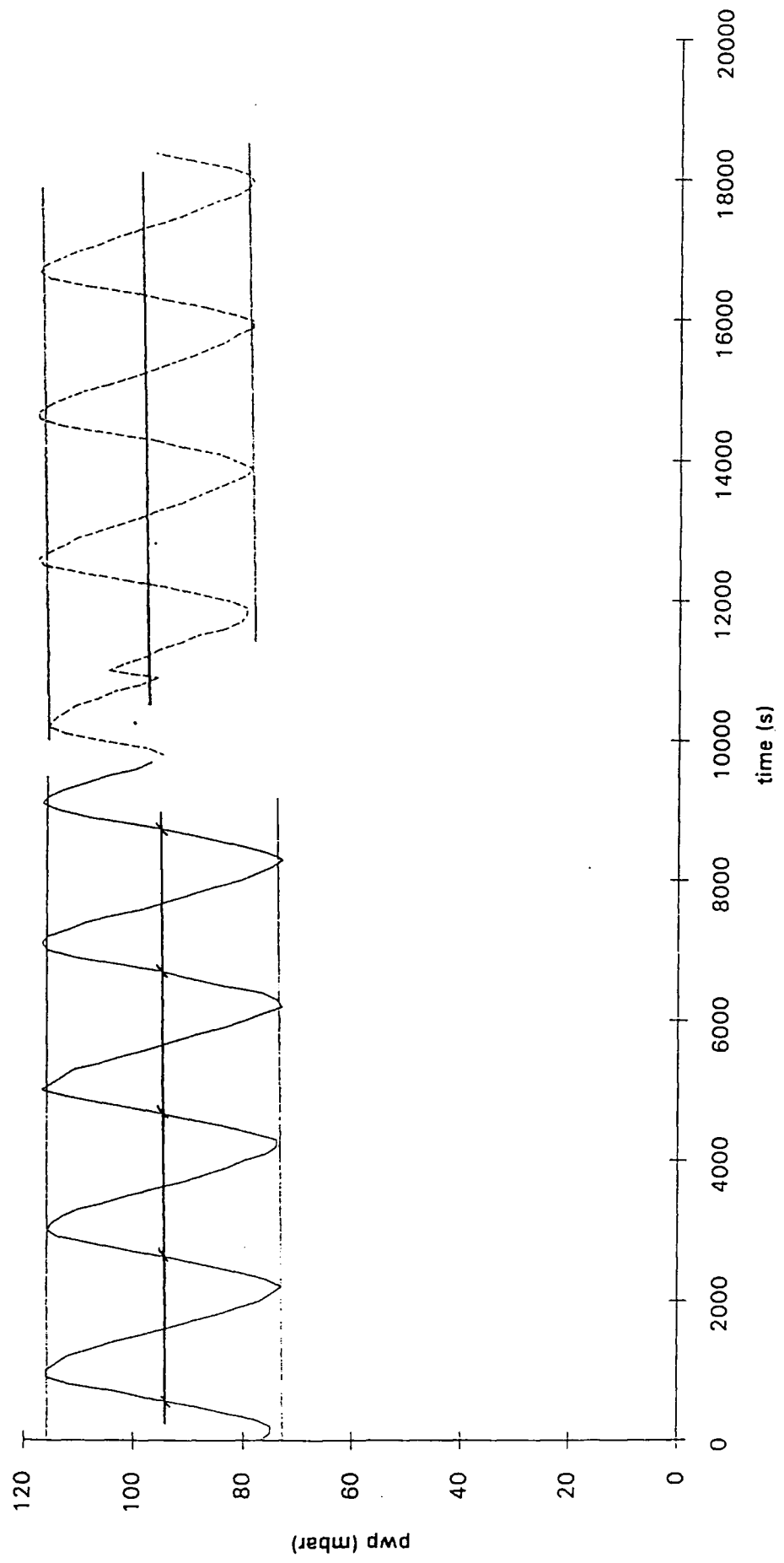
Appendix 3G-4
Calculation of Time Lag   Series 2. Positions 6 and 7

pwp (mbar)

time (s)
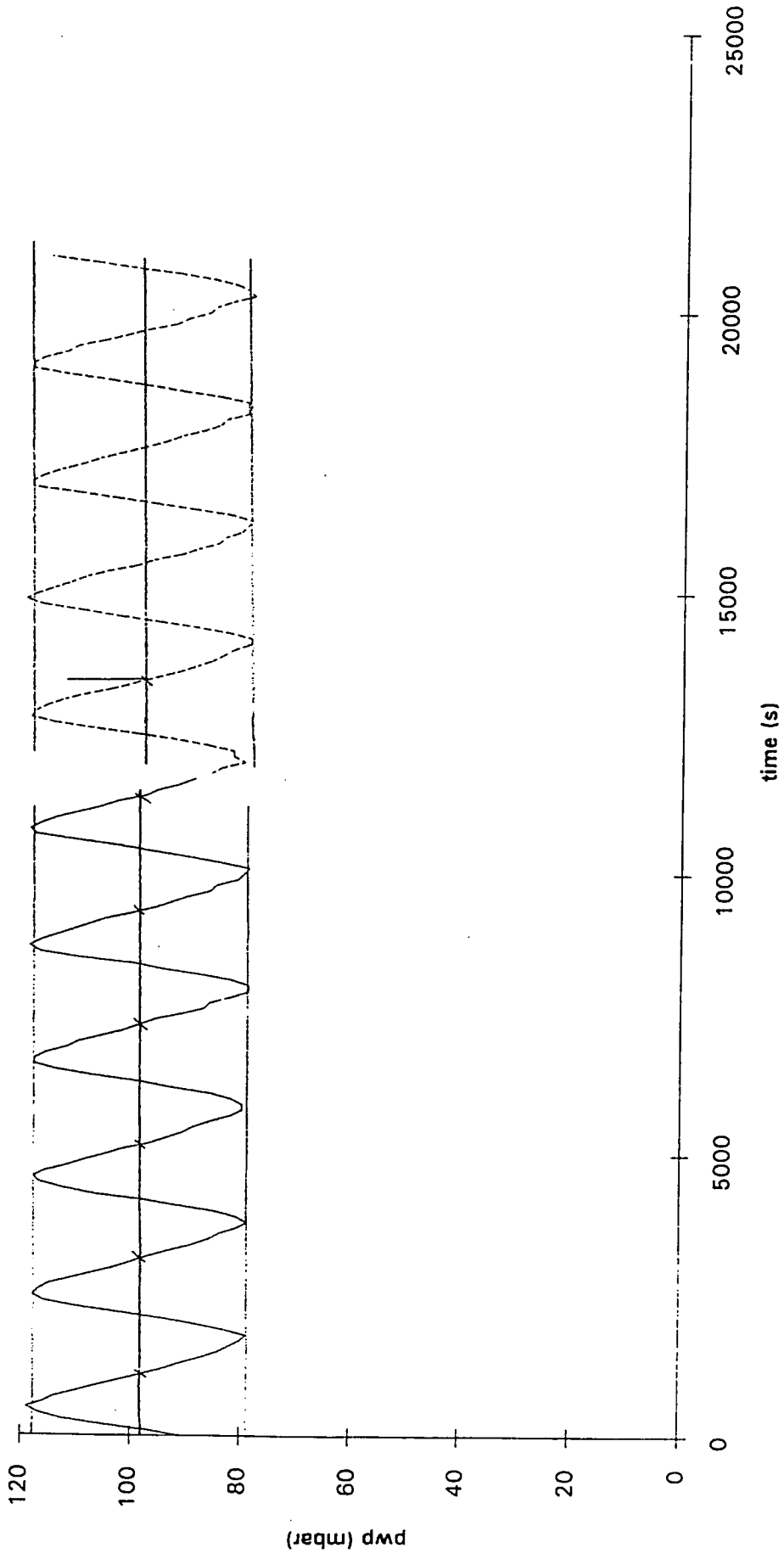
Appendix 3G-5
Calculation of Time Lag   Series 2. Positions 7 and 8
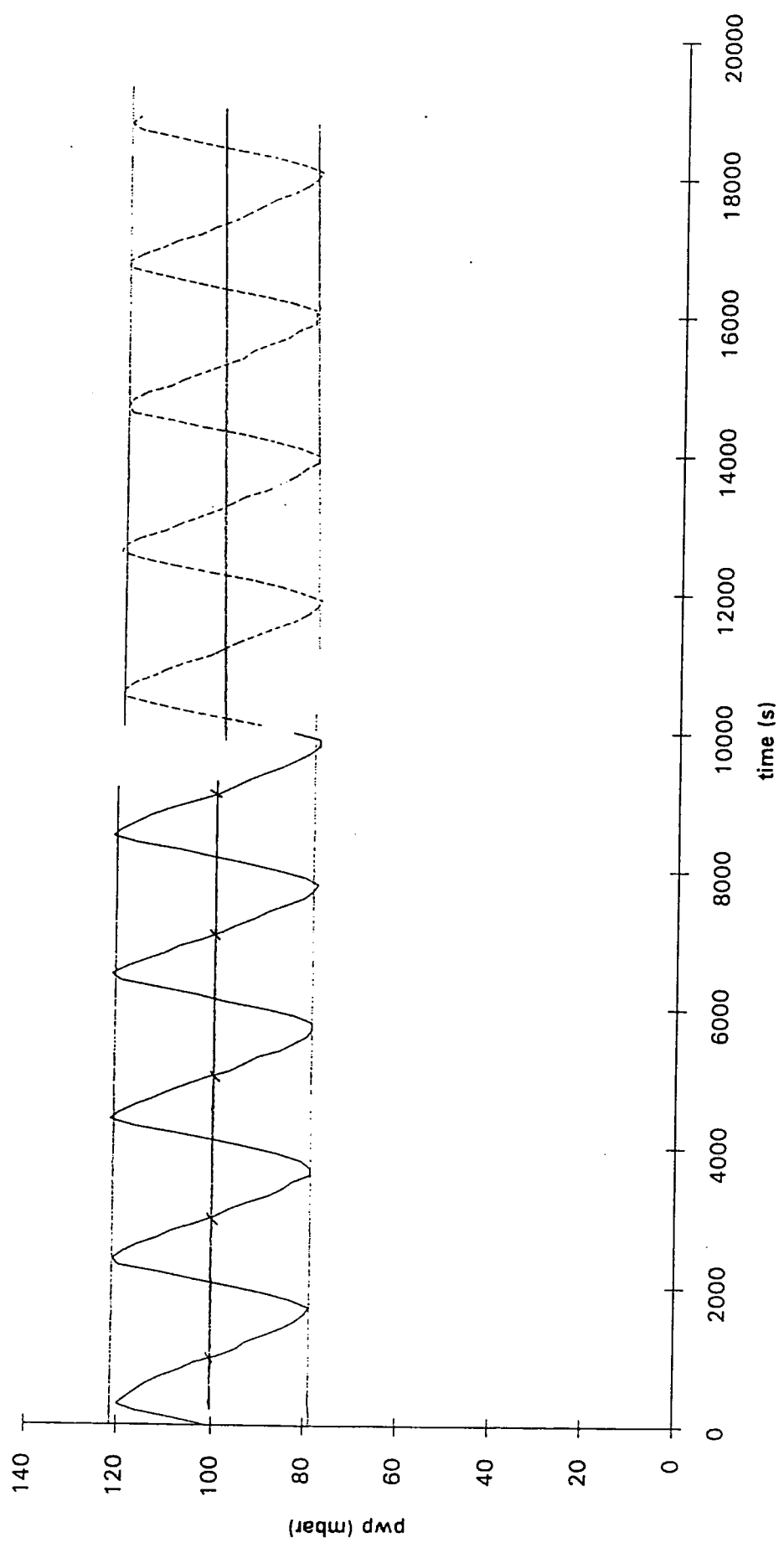
Appendix 3G-6
Calculation of Time Lag   Series 2. Positions 8 and 9
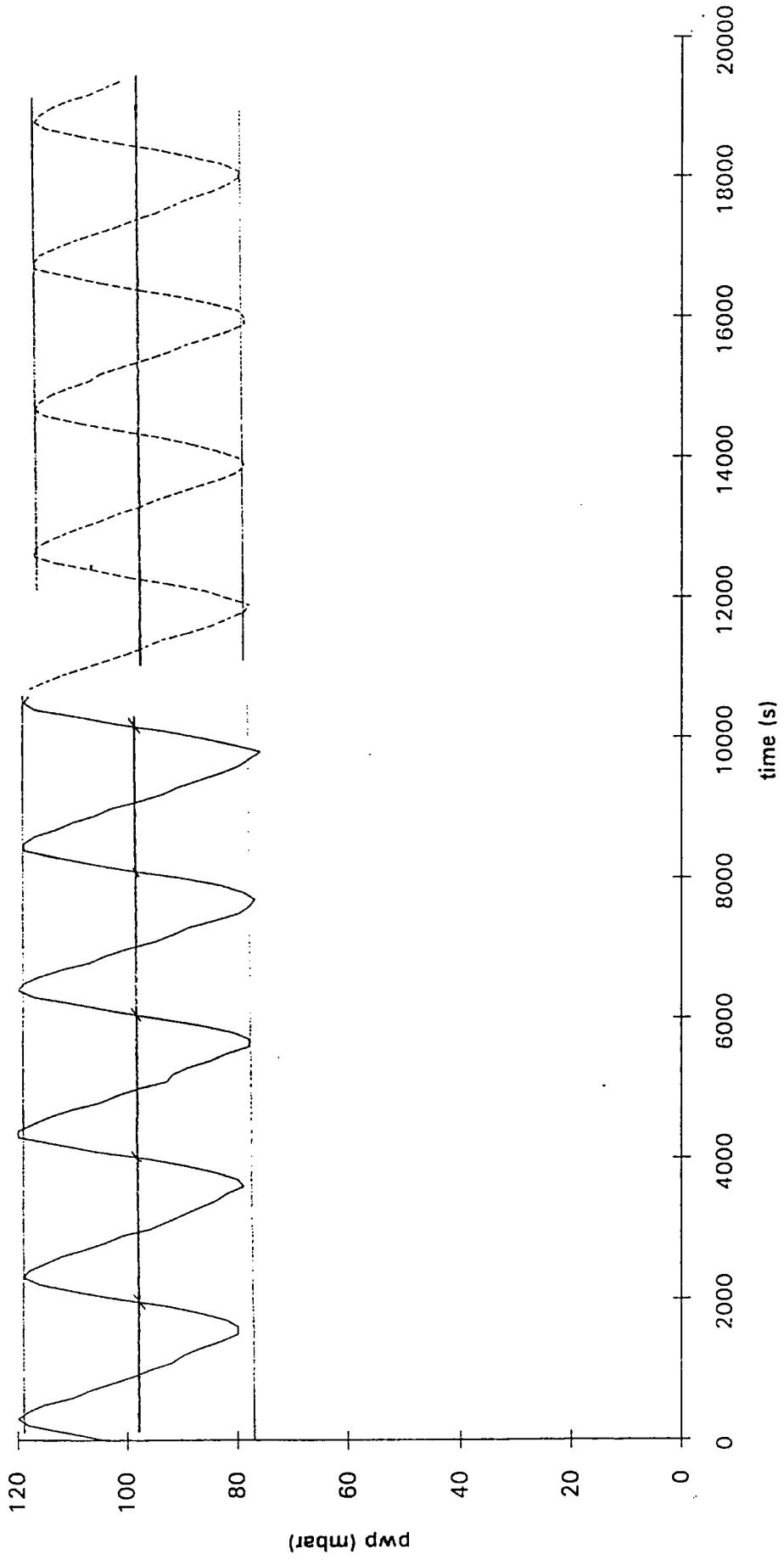
Appendix 3G-7
Calculation of Time Lag   Series 2. Positions 9 and 11
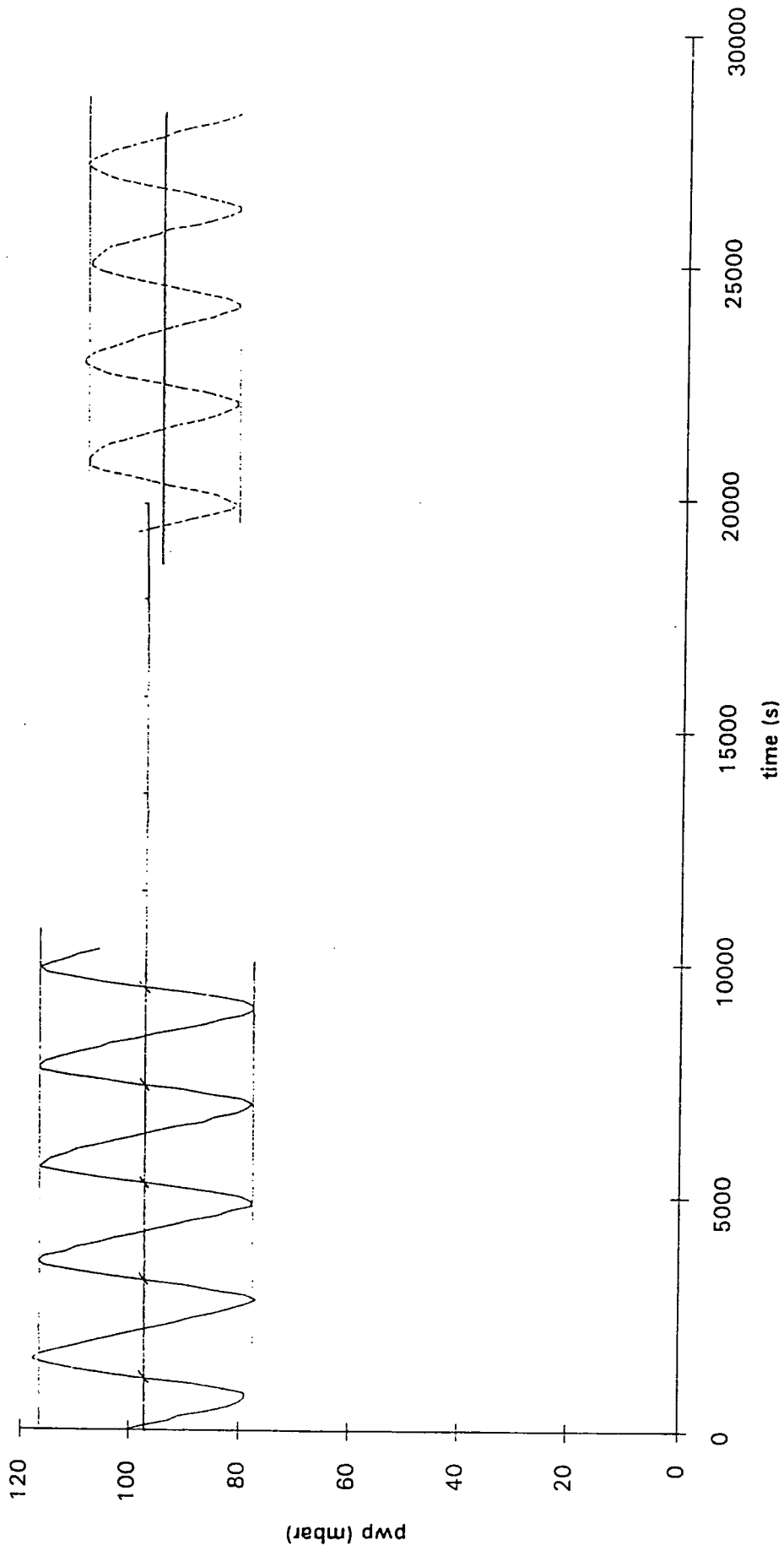
Appendix 3G-8
Calculation of Time Lag Series 2. Positions 11 and 12
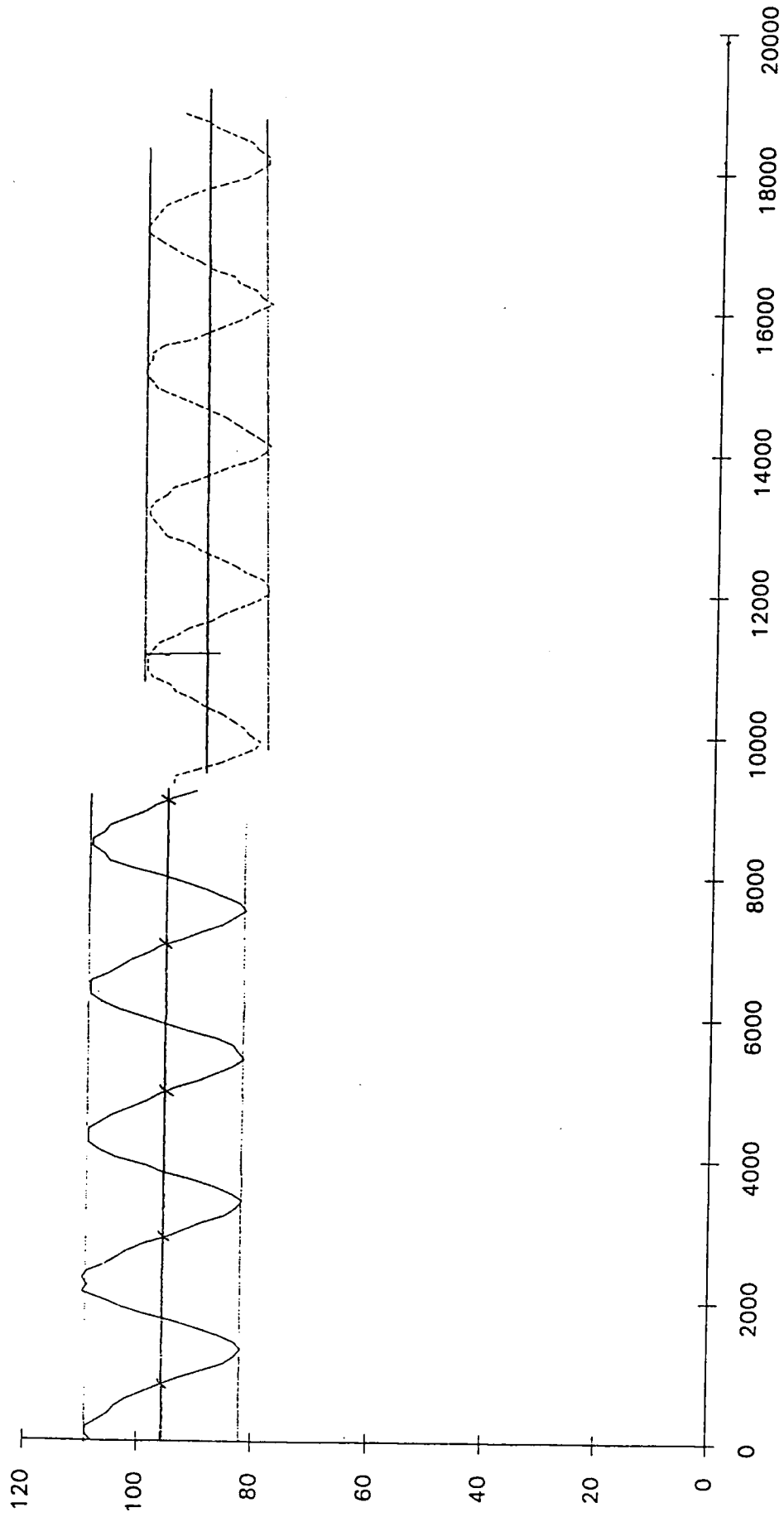
Appendix 5.1.

```
%
%Ferris incorporating one reflection - one image source
%
N=200;
H=zeros(N,1);
hadd=zeros(N,1);
L=4.7;
T=0.001;
S=0.1;
t0=1920;
h0=0.2;
lambda=sqrt(4*pi*t0*T/S);
w=2*pi/t0;
xrangea=[0+L/N:L/N:L];
xrange=xrangea';

for     i=1:N
        hx=h0*exp( -i*(L/N) * sqrt(pi*S/(t0*T)) );
        h2Lx=h0*exp( -((2*L)-i*(L/N)) * sqrt(pi*S/(t0*T)) );
        amp1=(2*pi*i*(L/N))/lambda;
        amp2=2*pi* ((2*L)-(i*L/N)) / lambda;
        A=(hx*cos(amp1)) + (h2Lx*cos(amp2));
        B=(h2Lx*sin(amp2)) + (hx*sin(amp1));
        angle=atan(A/B);
        H(i)=abs(A*sin(angle) + B*cos(angle));
        hx0=h0*exp( -(L/N) * sqrt(pi*S/(t0*T)) );
        h2Lx0=h0*exp( -((2*L)-(L/N)) * sqrt(pi*S/(t0*T)) );
        amp10=(2*pi*(L/N))/lambda;
        amp20=2*pi* ((2*L)-(L/N)) / lambda;
        A0=(hx0*cos(amp10)) + (h2Lx0*cos(amp20));
        B0=(h2Lx0*sin(amp20)) + (hx0*sin(amp10));
        angle0=atan(A0/B0);
        timelag0=((1/w)*angle0);
        timelag(i)=-((1/w)*angle+timelag0);

end
```

Appendix 5.2.

```
%Ferris incorporating two reflections - two image sources
%
N=200;
H=zeros(N,1);
timelag=zeros(N,1);
decay=zeros(N,1);
L=4.7;
T=0.001;
S=0.1;
t0=1920;
h0=0.2;
lambda=sqrt(4*pi*t0*T/S);
xrangea=[0+L/N:L/N:L];
xrange=xrangea';
w=2*pi/t0;
for i=1:N
    hx=h0*exp( -i*(L/N) * sqrt(pi*S/(t0*T)) );
    h2Lx=h0*exp( -((2*L)-i*(L/N)) * sqrt(pi*S/(t0*T)) );
    h3Lx=h0*exp( -((2*L)+(i*(L/N))) * sqrt(pi*S/(t0*T)) );
    amp1=(2*pi*i*(L/N))/lambda;
    amp2=2*pi* ((2*L)-(i*L/N)) / lambda;
    amp3=2*pi* ((2*L)+(i*L/N)) / lambda;
    A=( (hx*cos(amp1)) + (h2Lx*cos(amp2)) - (h3Lx*cos(amp3)) );
    B=( (hx*sin(amp1)) + (h2Lx*sin(amp2)) - (h3Lx*sin(amp3)) );
    angle=atan(A/B);
    H(i)=abs(A*sin(angle) + B*cos(angle));
    decay(i)=H(i)/h0;
    hx0=h0*exp( -(L/N) * sqrt(pi*S/(t0*T)) );
    h2Lx0=h0*exp( -((2*L)-(L/N)) * sqrt(pi*S/(t0*T)) );
    h3Lx=h0*exp( -((2*L)+((L/N))) * sqrt(pi*S/(t0*T)) );
    amp10=(2*pi*(L/N))/lambda;
    amp20=2*pi* ((2*L)-(L/N)) / lambda;
    amp30=2*pi* ((2*L)+(L/N)) / lambda;
    A0=(hx0*cos(amp10)) + (h2Lx0*cos(amp20)) - (h3Lx*cos(amp30)) ;
    B0=(h2Lx0*sin(amp20)) + (hx0*sin(amp10)) - (h3Lx*sin(amp30)) ;
    angle0=atan(A0/B0);
    timelag0=((1/w)*angle0);
    timelag(i)=-(1/w)*angle+timelag0;

end
```

Appendix 5.3.

```
% Application of Angstrom Theory to Leaky Coastal Aquifers
%
N=200;
amp=zeros(N,1);
timelag=zeros(N,1);
L=4.7;
T=0.001;
S=0.1;
t0=1920;
h0=0.2;
B=0.00006;
hstar=0.44;
W=2*pi/t0;
xrangea=[0+L/N:L/N:L];
xrange=xrangea';


for      i=1:N
         asquare=B/T;
         bsquare=W*S/T;
         gsquare=(asquare+sqrt((asquare*asquare)+(bsquare*bsquare)) )/2;
         g=sqrt(gsquare);
         gdashsquare=(-asquare+sqrt((asquare*asquare)+(bsquare*bsquare)) )/2;
         gdash=sqrt(gdashsquare);
         A=h0;
         hmax=(A*exp(-g*i*L/N)) + hstar;
         amp(i)=hmax-hstar;
         timelag(i)=(1/W)*(gdash*i*(L/N));

end
```

Appendix 5.4.

```
% Combination Approach - leakage and refl - two reflected waves
%
N=200;
l=zeros(N,1);
timelag=zeros(N,1);
L=4.7;
T=0.001;
S=0.1;
t0=1920;
h0=0.2;
B=0.00006;
w=2*pi/t0;
asquare=B/T;
afour=asquare*asquare;
bsquare=w*S/T;
bfour=bsquare*bsquare;
gsquare=(asquare+sqrt(bfour+afour))/2;
g=sqrt(gsquare);
gdashsq=(-asquare+sqrt(bfour+afour))/2;
gdash=sqrt(gdashsq);
lambda=w*t0/gdash;
xrangea=[0+L/N:L/N:L];
xrange=xrangea';

for      i=1:N
         hx=h0*exp( -i* (L/N) * g );
         h2Lx=h0*exp( -((2*L)-i* (L/N)) * g );
         h3Lx=h0*exp( -((2*L)+i* (L/N)) * g );
         amp1=(2*pi*i* (L/N))/lambda;
         amp2=2*pi* ((2*L)-(i*L/N)) / lambda;
         amp3=2*pi* ((2*L)+(i*L/N)) / lambda;
         A=(hx*cos(amp1)) + (h2Lx*cos(amp2)) - (h3Lx*cos(amp3));
         B=(h2Lx*sin(amp2)) + (hx*sin(amp1)) - (h3Lx*sin(amp3));
         angle=atan(A/B);
         H(i)=abs(A*sin(angle) + B*cos(angle));
         hx0=h0*exp( -(L/N) * g );
         h2Lx0=h0*exp( -((2*L)-(L/N)) * g );
         h3Lx0=h0*exp( -((2*L)+(L/N)) * g );
         amp10=(2*pi* (L/N))/lambda;
         amp20=2*pi* ((2*L)-(L/N)) / lambda;
         amp30=2*pi* ((2*L)+(L/N)) / lambda;
```

Appendix 5.4. cont.

```
A0=(hx0*cos(amp10)) + (h2Lx0*cos(amp20)) - (h3Lx0*cos(amp30));
B0=(h2Lx0*sin(amp20)) + (hx0*sin(amp10)) - (h3Lx0*sin(amp30));
angle0=atan(A0/B0);
timelag0=abs((1/w)*(angle0));
timelag(i)=abs(((1/w)*(angle))-timelag0);

end
```

Appendix 5.5

```
% complex mathematical approach - two reflected waves
%
N=200;
H=zeros(N,1);
timelag=zeros(N,1);
L=4.7;
T=0.001;
S=0.1;
t0=1920;
h0=0.2;
B=0.00006;
w=2*pi/t0;
asquare=B/T;
afour=asquare*asquare;
bsquare=w*S/T;
bfour=bsquare*bsquare;
gsquare=(asquare+sqrt(bfour+afour))/2;
g=sqrt(gsquare);
gdashsq=(-asquare+sqrt(bfour+afour))/2;
gdash=sqrt(gdashsq);
lambda=w*t0/gdash;
xrangea=[0+L/N:L/N:L];
a=(2*pi)/(lambda);
xrange=xrangea';

for     i=1:N
        hx=h0*exp( -i*(L/N) * g );
        h2Lx=h0*exp( -((2*L)-(i*(L/N))) * g );
        h3Lx=h0*exp( -((2*L)+(i*(L/N))) * g );
        reala=hx*cos(-a*i*L/N);
        ima=hx*sin(-a*i*L/N);
        realb=h2Lx*cos(-a*((2*L)-(i*L/N)) );
        imb=h2Lx*sin(-a*((2*L)-(i*L/N)) );
        realc=h3Lx*cos(-a*( (2*L)+(i*(L/N)) ) );
        imc=h3Lx*sin(-a*( (2*L)+(i*(L/N)) ) );
        H(i)=sqrt( ((reala+realb-realc)*(reala+realb-realc)) + ((ima+imb-imc)*(ima+imb-imc)) );
        decay(i)=H(i)/h0;
        phase=atan((reala+realb-realc)/(ima+imb-imc));

%phase zero
        hx0=h0*exp( (L/N) * g );
        h2Lx0=h0*exp( -((2*L)-((L/N))) * g );
```

Appendix 5.5. cont.

```
h3Lx0=h0*exp( -((2*L)+((L/N))) ^ g );
ima0=hx0*sin(-a*L/N);
reala0=hx0*cos(-a*L/N);
realb0=h2Lx0*cos(-a*((2*L)-(L/N)) );
imb0=h2Lx0*sin(-a*((2*L)-(L/N)) );
realc0=h3Lx0*cos(-a*( (2*L)+((L/N)) ) );
imc0=h3Lx0*sin(-a*( (2*L)+((L/N)) ) );
phase0=atan((reala0+realb0-realc0)/(ima0+imb0-imc0));
time0=(phase0*t0)/(2*pi);

timelag(i)=(phase*t0)/(2*pi)-time0;
```

end

Appendix 5.6   Amplitude.   Analytical Solution (Incorporating Leakage & Reflection) compared with Numerical Solution.

Legend:
- ■ Numerical Soln
- Analytical Soln - 1 refl
- Analytical Soln - 2 refls
- Analytical soln - 3 refls

X-axis: Horizontal distance from Tidal Boundary (m)

Y-axis: Amplitude (m)

Appendix 6.1.

```
% T/S=0.02; T/E=100
N=200;
H=zeros(N,1);
timelag=zeros(N,1);
L=4.7;
T=0.001;
S=0.05;
t0=1920;
h0=0.2;
B=0.00001;
w=2*pi/t0;
asquare=B/T;
afour=asquare*asquare;
bsquare=w*S/T;
bfour=bsquare*bsquare;
gsquare=(asquare+sqrt(bfour+afour))/2;
g=sqrt(gsquare);
gdashsq=(-asquare+sqrt(bfour+afour))/2;
gdash=sqrt(gdashsq);
lambda=w*t0/gdash;
xrangea=[0+L/N:L/N:L];
a=(2*pi)/(lambda);
xrange=xrangea'/(lambda);

for      i=1:N
      hx=h0*exp( -i*(L/N) * g );
      h2Lx=h0*exp( -((2*L)-(i*(L/N))) * g );
      h3Lx=h0*exp( -((2*L)+(i*(L/N))) * g );
      reala=hx*cos(-a*i*L/N);
      ima=hx*sin(-a*i*L/N);
      realb=h2Lx*cos(-a*((2*L)-(i*L/N)) );
      imb=h2Lx*sin(-a*((2*L)-(i*L/N)) );
      realc=h3Lx*cos(-a*( (2*L)+(i*(L/N)) ) );
      imc=h3Lx*sin(-a*( (2*L)+(i*(L/N)) ) );
      H(i)=sqrt( ((reala+realb-realc)*(reala+realb-realc)) + ((ima+imb-imc)*(ima+imb-imc)) );
      decay(i)=H(i)/h0;
      phase=atan((reala+realb-realc)/(ima+imb-imc));

%phase zero
      hx0=h0*exp( (L/N) * g );
```

Appendix 6.1. cont.

```
h2Lx0=h0*exp( -((2*L)-((L/N))) * g );
h3Lx0=h0*exp( -((2*L)+((L/N))) * g );
ima0=hx0*sin(-a*L/N);
reala0=hx0*cos(-a*L/N);
realb0=h2Lx0*cos(-a*((2*L)-(L/N)) );
imb0=h2Lx0*sin(-a*((2*L)-(L/N)) );
realc0=h3Lx0*cos(-a*( (2*L)+((L/N)) ) );
imc0=h3Lx0*sin(-a*( (2*L)+((L/N)) ) );
phase0=atan((reala0+realb0-realc0)/(ima0+imb0-imc0));
time0=(phase0*t0)/(2*pi);

timelag(i)=(phase*t0)/(2*pi)-time0;
```
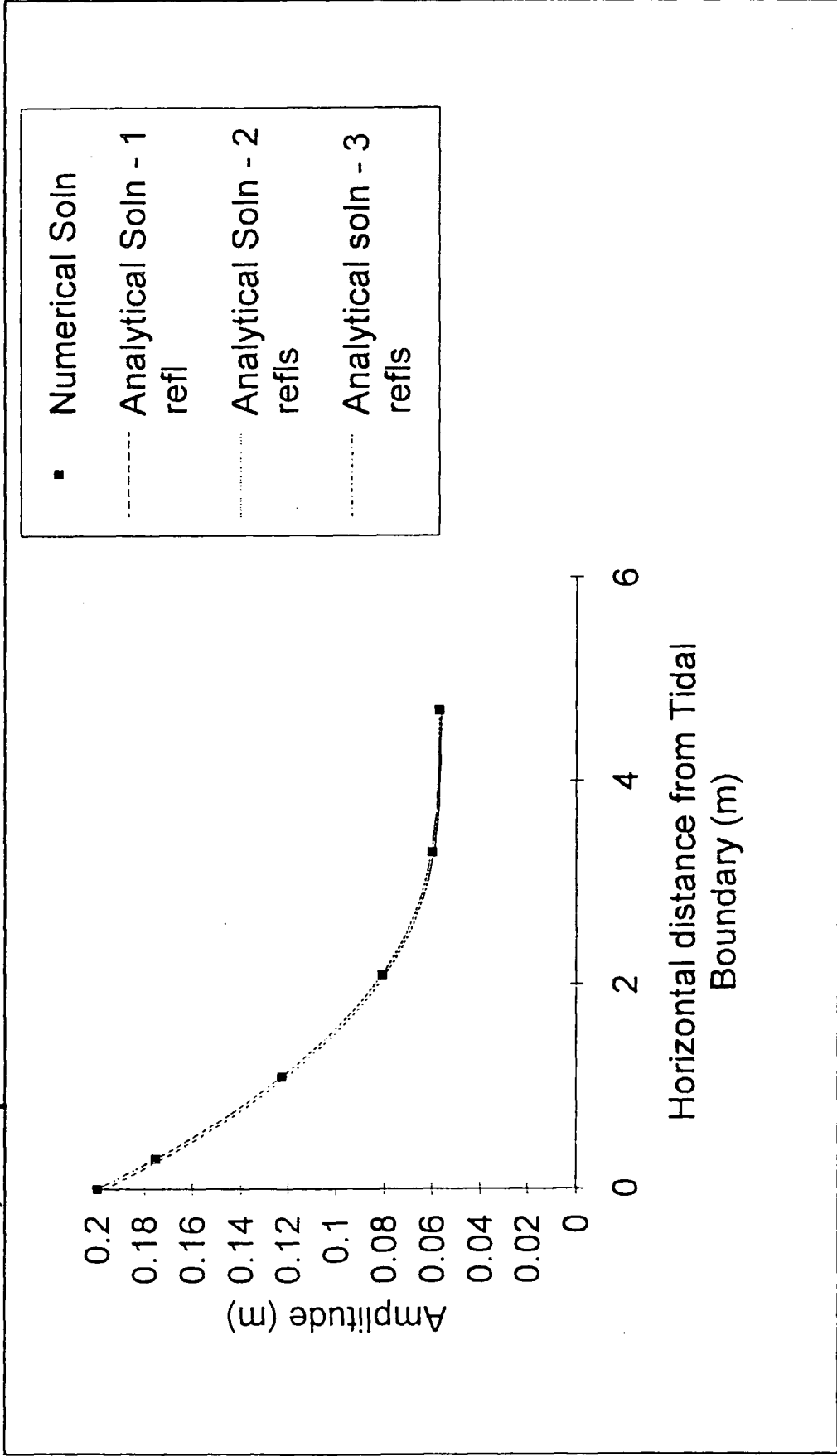
end

Appendix 6.2.

```
% T/S=0.02;  T/B=100
%
N=200;
H=zeros(N,1);
timelag=zeros(N,1);
L=4.7;
T=0.002;
S=0.1;
t0=1920;
h0=0.2;
B=0.00002;
w=2*pi/t0;
asquare=B/T;
afour=asquare*asquare;
bsquare=w*S/T;
bfour=bsquare*bsquare;
gsquare=(asquare+sqrt(bfour+afour))/2;
g=sqrt(gsquare);
gdashsq=(-asquare+sqrt(bfour+afour))/2;
gdash=sqrt(gdashsq);
lambda=w*t0/gdash;
xrangea=[0+L/N:L/N:L];
a=(2*pi)/(lambda);
xrange=xrangea'/(lambda);

for     i=1:N
        hx=h0*exp( -i*(L/N) * g );
        h2Lx=h0*exp( -((2*L)-(i*(L/N))) * g );
        h3Lx=h0*exp( -((2*L)+(i*(L/N))) * g );
        reala=hx*cos(-a*i*L/N);
        ima=hx*sin(-a*i*L/N);
        realb=h2Lx*cos(-a*((2*L)-(i*L/N)) );
        imb=h2Lx*sin(-a*((2*L)-(i*L/N)) );
        realc=h3Lx*cos(-a*( (2*L)+(i*(L/N)) ) );
        imc=h3Lx*sin(-a*( (2*L)+(i*(L/N)) ) );
        H(i)=sqrt( ((reala+realb-realc)*(reala+realb-realc)) + ((ima+imb-imc)*(ima+imb-imc)) );
        decay(i)=H(i)/h0;
        phase=atan((reala+realb-realc)/(ima+imb-imc));

%phase zero
        hx0=h0*exp( (L/N) * g );
```

Appendix 6.2. cont.

```
h2Lx0=h0*exp( -((2*L)-((L/N))) * g );
h3Lx0=h0*exp( -((2*L)+((L/N))) * g );
ima0=hx0*sin(-a*L/N);
reala0=hx0*cos(-a*L/N);
realb0=h2Lx0*cos(-a*((2*L)-(L/N))) );
imb0=h2Lx0*sin(-a*((2*L)-(L/N)) );
realc0=h3Lx0*cos(-a*( (2*L)+((L/N)) ) );
imc0=h3Lx0*sin(-a*( (2*L)+((L/N)) ) );
phase0=atan((reala0+realb0-realc0)/(ima0+imb0-imc0));
time0=(phase0*t0)/(2*pi);

timelag(i)=(phase*t0)/(2*pi)-time0;

end
```

Appendix 6.3.

Two further investigatory case studies were prescribed to investigate solutions of amplitude decay and time lag for constant values of T/S but varying values of T/β. The parameters of these two case studies are outlined below:

Case 7.3a	Case 7.3b
$T = 0.002$ m^2/s	$T = 0.002$ m^2/s
$S = 0.1$	$S = 0.1$
$\beta = 0.00001$ s^{-1}	$\beta = 0.00002$ s^{-1}
$T/\beta = 200$ m^2	$T/\beta = 100$ m^2
$T/S = 0.02$ m^2/s	
$L = 4.7$ m	
$t_0 = 1920$ s	
$h_0 = 0.2$ m	

The solutions for amplitude decay and time lag for these two case studies are shown overleaf.

Appendix 6.3. cont.

```
% T/S=0.02;  T/B=200
%
N=200;
H=zeros(N,1);
timelag=zeros(N,1);
L=4.7;
T=0.002;
S=0.1;
t0=1920;
h0=0.2;
B=0.00001;
w=2*pi/t0;
asquare=B/T;
afour=asquare*asquare;
bsquare=w*S/T;
bfour=bsquare*bsquare;
gsquare=(asquare+sqrt(bfour+afour))/2;
g=sqrt(gsquare);
gdashsq=(-asquare+sqrt(bfour+afour))/2;
gdash=sqrt(gdashsq);
lambda=w*t0/gdash;
xrangea=[0+L/N:L/N:L];
a=(2*pi)/(lambda);
xrange=xrangea';

for     i=1:N
        hx=h0*exp( -i*(L/N) * g );
        h2Lx=h0*exp( -((2*L)-(i*(L/N))) * g );
        h3Lx=h0*exp( -((2*L)+(i*(L/N))) * g );
        reala=hx*cos(-a*i*L/N);
        ima=hx*sin(-a*i*L/N);
        realb=h2Lx*cos(-a*((2*L)-(i*L/N)) );
        imb=h2Lx*sin(-a*((2*L)-(i*L/N)) );
        realc=h3Lx*cos(-a*( (2*L)+(i*(L/N)) ) );
        imc=h3Lx*sin(-a*( (2*L)+(i*(L/N)) ) );
        H(i)=sqrt( ((reala+realb-realc)*(reala+realb-realc)) + ((ima+imb-imc)*(ima+imb-imc)) );
        decay(i)=H(i)/h0;
        phase=atan((reala+realb-realc)/(ima+imb-imc));

%phase zero
        hx0=h0*exp( (L/N) * g );
```

Appendix 6.3. cont.

```
h2Lx0=h0*exp( -((2*L)-((L/N))) * g );
h3Lx0=h0*exp( -((2*L)+((L/N))) * g );
ima0=hx0*sin(-a*L/N);
reala0=hx0*cos(-a*L/N);
realb0=h2Lx0*cos(-a*((2*L)-(L/N))) );
imb0=h2Lx0*sin(-a*((2*L)-(L/N)) );
realc0=h3Lx0*cos(-a*( (2*L)+((L/N)) ) );
imc0=h3Lx0*sin(-a*( (2*L)+((L/N)) ) );
phase0=atan((reala0+realb0-realc0)/(ima0+imb0-imc0));
time0=(phase0*t0)/(2*pi);

timelag(i)=(phase*t0)/(2*pi)-time0;

end
```

Appendix 6.3. cont.

```
% T/S=0.02;  T/B=100

N=200;
H=zeros(N,1);
timelag=zeros(N,1);
L=4.7;
T=0.002;
S=0.1;
t0=1920;
h0=0.2;
B=0.00002;
w=2*pi/t0;
asquare=B/T;
afour=asquare*asquare;
bsquare=w*S/T;
bfour=bsquare*bsquare;
gsquare=(asquare+sqrt(bfour+afour))/2;
g=sqrt(gsquare);
gdashsq=(-asquare+sqrt(bfour+afour))/2;
gdash=sqrt(gdashsq);
lambda=w*t0/gdash;
xrangea=[0+L/N:L/N:L];
a=(2*pi)/(lambda);
xrange=xrangea';

for     i=1:N
   hx=h0*exp( -i*(L/N) * g );
   h2Lx=h0*exp( -((2*L)-(i*(L/N))) * g );
   h3Lx=h0*exp( -((2*L)+(i*(L/N))) * g );
   reala=hx*cos(-a*i*L/N);
   ima=hx*sin(-a*i*L/N);
   realb=h2Lx*cos(-a*((2*L)-(i*L/N)) );
   imb=h2Lx*sin(-a*((2*L)-(i*L/N)) );
   realc=h3Lx*cos(-a*( (2*L)+(i*(L/N)) ) );
   imc=h3Lx*sin(-a*( (2*L)+(i*(L/N)) ) );
   H(i)=sqrt( ((reala+realb-realc)*(reala+realb-realc)) + ((ima+imb-imc)*(ima+imb-imc)) );
   decay(i)=H(i)/h0;
   phase=atan((reala+realb-realc)/(ima+imb-imc));

%phase zero
   hx0=h0*exp( (L/N) * g );
```
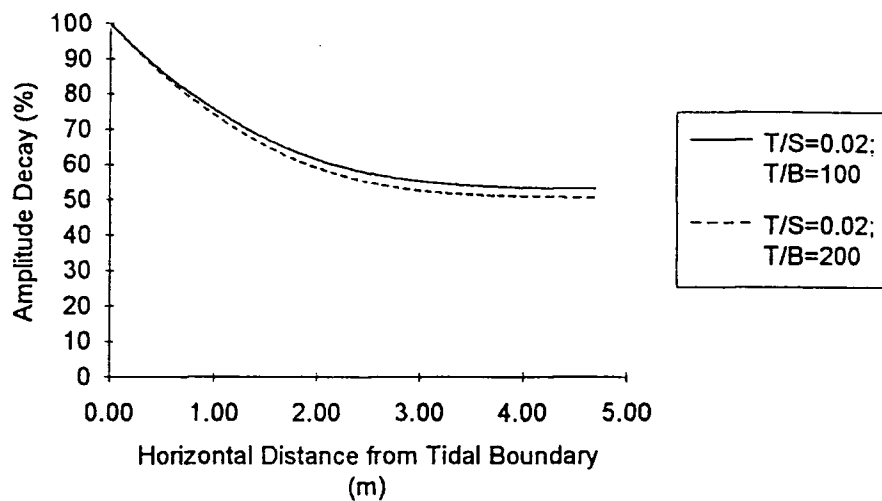
Appendix 6.3. cont.

```
h2Lx0=h0*exp( -((2*L)-((L/N))) * g );
h3Lx0=h0*exp( -((2*L)+((L/N))) * g );
ima0=hx0*sin(-a*L/N);
reala0=hx0*cos(-a*L/N);
realb0=h2Lx0*cos(-a*((2*L)-(L/N)) );
imb0=h2Lx0*sin(-a*((2*L)-(L/N)) );
realc0=h3Lx0*cos(-a*( (2*L)+((L/N)) ) );
imc0=h3Lx0*sin(-a*( (2*L)+((L/N)) ) );
phase0=atan((reala0+realb0-realc0)/(ima0+imb0-imc0));
time0=(phase0*t0)/(2*pi);

timelag(i)=(phase*t0)/(2*pi)-time0;

end
```
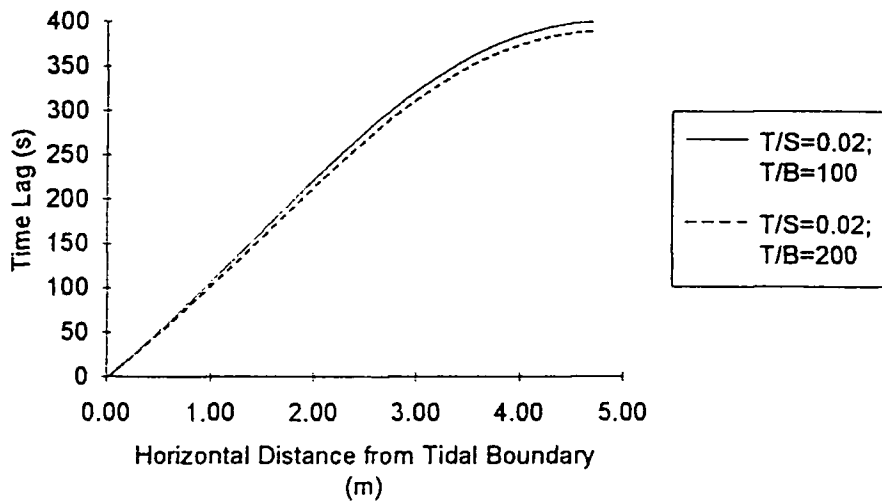
Appendix 6.3

Appendix6. 3.1. Amplitude Decay.
T/S Constant, whilst T/β Varied for Two Cases.

Appendix6. 3.2. Time Lag.
T/S Constant, whilst T/β Varied for Two Cases.

Appendix 6.4.

Two further investigatory case studies were prescribed to investigate solutions of amplitude decay and time lag for constant values of T/β but varying values of T/S. The parameters of these two case studies are outlined below:

Case 7.4a	Case 7.4b
$T = 0.001$ m^2/s	$T = 0.002$ m^2/s
$S = 0.1$	$S = 0.1$
$\beta = 0.00001$ s^{-1}	$\beta = 0.00002$ s^{-1}
$T/S = 0.01$ m^2/s	$T/S = 0.02$ m^2/s
$T/\beta = 100$ m^2	
$L = 4.7$ m	
$t_0 = 1920$ s	
$h_0 = 0.2$ m	

The solutions for amplitude decay and time lag for these two case studies are shown overleaf.

Appendix 6.4. cont.

```
% T/S=0.01;  T/B=100
%
N=200;
H=zeros(N,1);
timelag=zeros(N,1);
L=4.7;
T=0.001;
S=0.1;
t0=1920;
h0=0.2;
B=0.00001;
w=2*pi/t0;
asquare=B/T;
afour=asquare*asquare;
bsquare=w*S/T;
bfour=bsquare*bsquare;
gsquare=(asquare+sqrt(bfour+afour))/2;
g=sqrt(gsquare);
gdashsq=(-asquare+sqrt(bfour+afour))/2;
gdash=sqrt(gdashsq);
lambda=w*t0/gdash;
xrangea=[0+L/N:L/N:L];
a=(2*pi)/(lambda);
xrange=xrangea';

for    i=1:N
       hx=h0*exp( -i*(L/N) * g );
       h2Lx=h0*exp( -((2*L)-(i*(L/N))) * g );
       h3Lx=h0*exp( -((2*L)+(i*(L/N))) * g );
       reala=hx*cos(-a*i*L/N);
       ima=hx*sin(-a*i*L/N);
       realb=h2Lx*cos(-a*((2*L)-(i*L/N)) );
       imb=h2Lx*sin(-a*((2*L)-(i*L/N)) );
       realc=h3Lx*cos(-a*( (2*L)+(i*(L/N)) ) );
       imc=h3Lx*sin(-a*( (2*L)+(i*(L/N)) ) );
       H(i)=sqrt( ((reala+realb-realc)*(reala+realb-realc)) + ((ima+imb-imc)*(ima+imb-imc)) );
       decay(i)=H(i)/h0;
       phase=atan((reala+realb-realc)/(ima+imb-imc));

%phase zero
       hx0=h0*exp( (L/N) * g );
```

Appendix 6.4. cont.

```
h2Lx0=h0*exp( -((2*L)-((L/N)))  * g );
h3Lx0=h0*exp( -((2*L)+((L/N)))  * g );
ima0=hx0*sin(-a*L/N);
reala0=hx0*cos(-a*L/N);
realb0=h2Lx0*cos(-a*((2*L)-(L/N)) );
imb0=h2Lx0*sin(-a*((2*L)-(L/N)) );
realc0=h3Lx0*cos(-a*( (2*L)+((L/N)) ) );
imc0=h3Lx0*sin(-a*( (2*L)+((L/N)) ) );
phase0=atan((reala0+realb0-realc0)/(ima0+imb0-imc0));
time0=(phase0*t0)/(2*pi);

timelag(i)=(phase*t0)/(2*pi)-time0;
```

end

Appendix 6.4. cont.

```
% T/S=0.02; T/B=100
%
N=200;
H=zeros(N,1);
timelag=zeros(N,1);
L=4.7;
T=0.002;
S=0.1;
t0=1920;
h0=0.2;
B=0.00002;
w=2*pi/t0;
asquare=B/T;
afour=asquare*asquare;
bsquare=w*S/T;
bfour=bsquare*bsquare;
gsquare=(asquare+sqrt(bfour+afour))/2;
g=sqrt(gsquare);
gdashsq=(-asquare+sqrt(bfour+afour))/2;
gdash=sqrt(gdashsq);
lambda=w*t0/gdash;
xrangea=[0+L/N:L/N:L];
a=(2*pi)/(lambda);
xrange=xrangea';

for    i=1:N
       hx=h0*exp( -i*(L/N) * g );
       h2Lx=h0*exp( -((2*L)-(i*(L/N))) * g );
       h3Lx=h0*exp( -((2*L)+(i*(L/N))) * g );
       reala=hx*cos(-a*i*L/N);
       ima=hx*sin(-a*i*L/N);
       realb=h2Lx*cos(-a*((2*L)-(i*L/N)) );
       imb=h2Lx*sin(-a*((2*L)-(i*L/N)) );
       realc=h3Lx*cos(-a*( (2*L)+(i*(L/N)) ) );
       imc=h3Lx*sin(-a*( (2*L)+(i*(L/N)) ) );
       H(i)=sqrt( ((reala+realb-realc)*(reala+realb-realc)} + ((ima+imb-imc) * (ima+imb-imc)) );
       decay(i)=H(i)/h0;
       phase=atan((reala+realb-realc)/(ima+imb-imc));

%phase zero
       hx0=h0*exp( (L/N) * g );
```
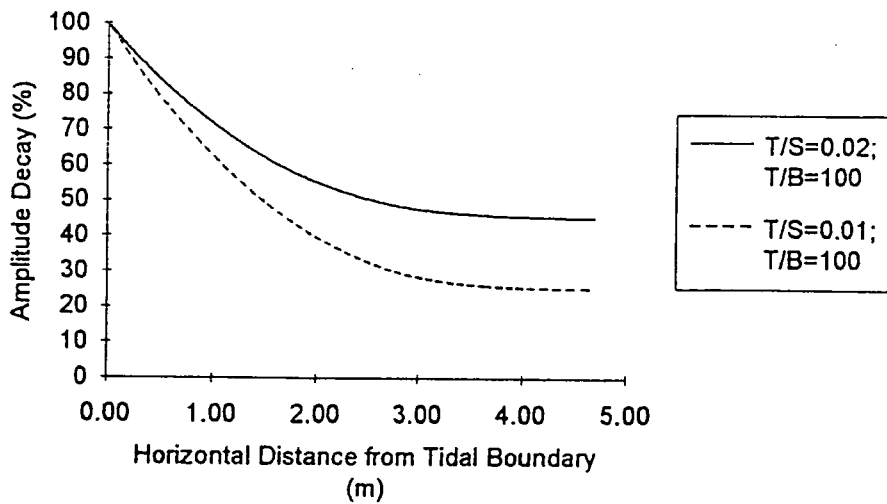
Appendix 6.4. cont.

```
h2Lx0=h0*exp( -((2*L)-((L/N))) * g );
h3Lx0=h0*exp( -((2*L)+((L/N))) * g );
ima0=hx0*sin(-a*L/N);
reala0=hx0*cos(-a*L/N);
realb0=h2Lx0*cos(-a*((2*L)-(L/N)) );
imb0=h2Lx0*sin(-a*((2*L)-(L/N)) );
realc0=h3Lx0*cos(-a*( (2*L)+((L/N)) ) );
imc0=h3Lx0*sin(-a*( (2*L)+((L/N)) ) );
phase0=atan((reala0+realb0-realc0)/(ima0+imb0-imc0));
time0=(phase0*t0)/(2*pi);

timelag(i)=(phase*t0)/(2*pi)-time0;

end
```
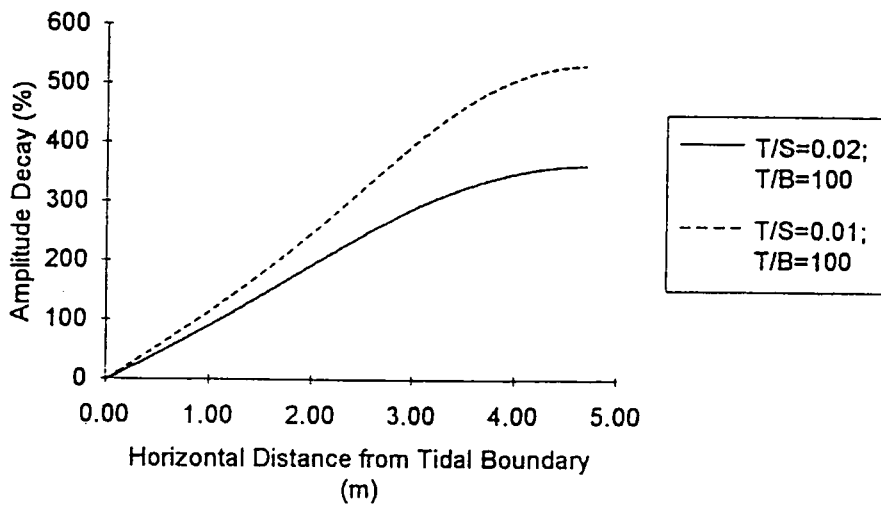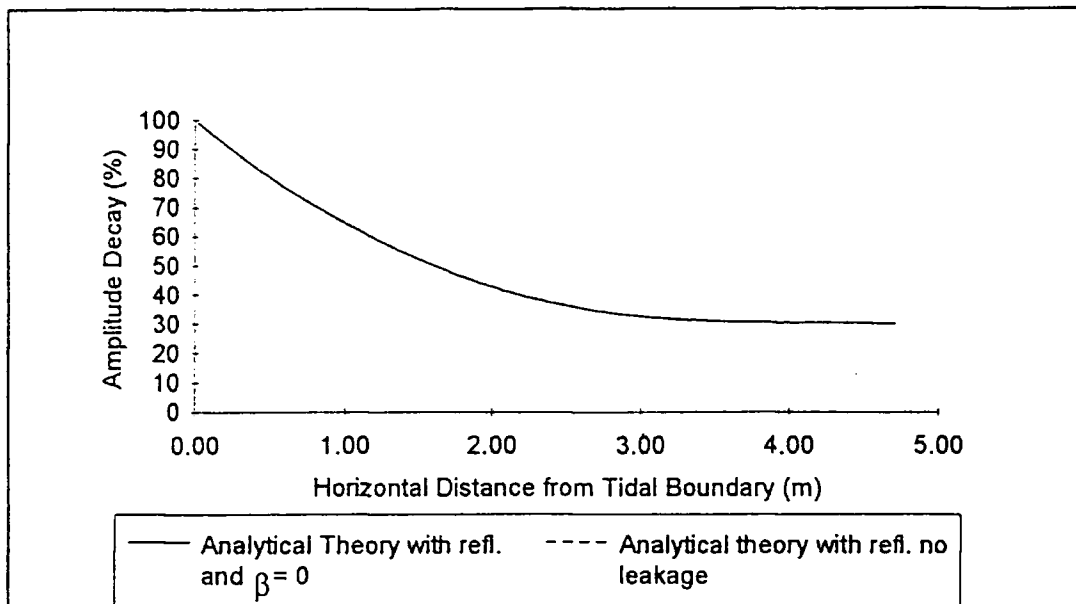
Appendix 6.4

Appendix 6. 4.1. Amplitude Decay.
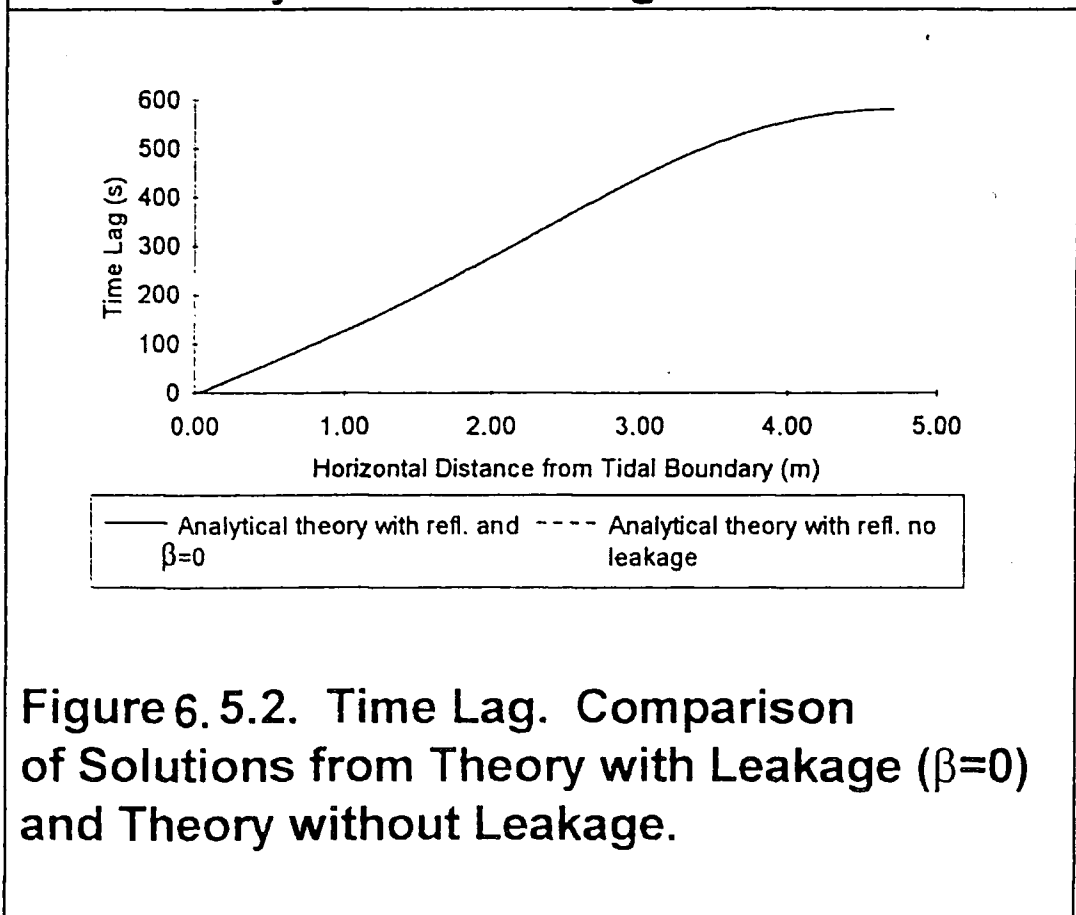## T/S Constant, whilst T/β Varied for Two Cases.

Appendix 6.4.2. Time Lag.
T/S Constant, whilst T/β Varied for Two Cases.

Figure 6.5.1. Amplitude Decay. Comparison of Solutions from Theory with Leakage (β=0) and Theory without Leakage.

Figure 6.5.2. Time Lag. Comparison of Solutions from Theory with Leakage (β=0) and Theory without Leakage.

Druck

PDCR 800 SERIES

General Purpose Pressure Transducers

- Excellent linearity and hysteresis
  ±0.1% B.S.L. for ranges to 60 bar

- High overload capability

- Rationalized outputs

- Good thermal stability
  ±1.5% total error band −20° to +80°C

- Parameter selection available